Titre: Title:	Slope Stability Analyses of Waste Rock Piles Under Unsaturated Conditions Following Large Precipitations
Auteur: Author:	Maryam Maknoon
Date:	2016
Type:	Mémoire ou thèse / Dissertation or Thesis
Référence: Citation:	Maknoon, M. (2016). Slope Stability Analyses of Waste Rock Piles Under Unsaturated Conditions Following Large Precipitations [Thèse de doctorat, École Polytechnique de Montréal]. PolyPublie. https://publications.polymtl.ca/2345/

Document en libre accès dans PolyPublie
Open Access document in PolyPublie

URL de PolyPublie: PolyPublie URL:	https://publications.polymtl.ca/2345/
Directeurs de recherche: Advisors:	Michel Aubertin
Programme: Program:	Génie minéral

UNIVERSITÉ DE MONTRÉAL

SLOPE STABILITY ANALYSES OF WASTE ROCK PILES UNDER UNSATURATED
CONDITIONS FOLLOWING LARGE PRECIPITATIONS

MARYAM MAKNOON

DÉPARTEMENT DES GÉNIES CIVIL, GÉOLOGIQUE ET DES MINES
ÉCOLE POLYTECHNIQUE DE MONTRÉAL

THÈSE PRÉSENTÉE EN VUE DE L'OBTENTION

DU DIPLÔME DE PHILOSOPHIAE DOCTOR

(GÉNIE MINÉRAL)
SEPTEMBRE 2016

UNIVERSITÉ DE MONTRÉAL

ÉCOLE POLYTECHNIQUE DE MONTRÉAL

Cette thèse intitulée :

SLOPE STABILITY ANALYSES OF WASTE ROCK PILES UNDER UNSATURATED
CONDITIONS FOLLOWING LARGE PRECIPITATIONS

présentée par : MAKNOON Maryam

en vue de l'obtention du diplôme de : Philosophiae Doctor

a été dûment acceptée par le jury d'examen constitué de :

M. PABST Thomas, Ph. D., président

M. AUBERTIN Michel, Ph. D., membre et directeur de recherche

M. JAMES Michael, Ph. D., membre

M. SIMMS Paul H., Ph. D., membre externe

DEDICATION

To my dear family

ACKNOWLEDGEMENTS

RÉSUMÉ

Les roches stériles sont extraites des mines pour accéder aux zones minéralisées. Le traitement de cette roche n'est   pas économiquement rentable. Les roches stériles sont habituellement transportées par camions (ou convoyeurs) et disposées en haldes à la surface. Ces haldes doivent être conçues de manière à assurer leur stabilité géotechnique pendant que la mine est en opération et après sa fermeture. La construction optimale de ces haldes à stériles requiert une bonne planification. La présente thèse traite de l'analyse de la stabilité des haldes de grande taille.

Les principaux objectifs du travail présenté dans cette thèse consistent à i) enrichir les connaissances sur le comportement géotechnique des haldes à stériles de grande taille, ii) étudier l'effet des propriétés mécaniques des matériaux sur la stabilités des haldes, iii) améliorer la capacité d'évaluer la stabilité de la pente des haldes selon différentes configurations internes et externes, iv) étudier les effets de l'infiltration d'eau et des fluctuations des pressions interstitielles négatives (succion matricielle) sur la stabilité des pentes des haldes à stériles en conditions non saturéessur le facteur de sécurité, et v) étudier l'influence de la variabilité spatiale des propriétés mécaniques des matériaux dans les haldes sur leur stabilité.

Même si elles se basent sur des situations typiques, les analyses n'ont pas été menées pour simuler en détail un cas spécifique, mais plutôt pour mettre en application une procédure d'évaluation systématique de la stabilité des haldes à stériles non saturées, en tenant compte des paramètres qui l'influencent.

Ces analyses ont été menées en appliquant la méthode de l'équilibre limite à partir de l'état des contraintes obtenu d'une analyse par la méthode des éléments finis, et utilisé pour évaluer le facteur de sécurité (FS). L'écoulement de l'eau et la répartition de l'humidité dans les haldes ont également été pris en compte. Les analyses ont été réalisées à l'aide du groupe de logiciels de la suite Geostudio 2007 (i.e. SEEP/W, SIGMA/W et SLOPE/W; GeoSlope International Ltd, 2008).

Une analyse de sensibilité relativement exhaustive a également été menée pour étudier les facteurs qui inflencent la stabilité de la pente des haldes à stériles. Les résultats indiquent que leur stabilité peut être affectée par différentes caractéristiques, incluant la configuration géométrique (c.-à-d. angle d'inclinaison des pentes et la présence de bancs et de couches internes), ainsi que

par les propriétés géotechniques (tels que l'angle de friction interne et la cohésion apparente des stériles miniers et de la fondation).

Un autre aspect spécifique de cette recherche consistait à investiguer le rôle de la succion matricielle à l'intérieur des halde sur la stabilité de la pente. Les résultats montrent les impacts positifs de cette cohésion apparente générée par la succion matricielle (dans des conditions non saturées) sur le facteur de sécurité. L'analyse a pris en compte différents flux hydriques (recharges) en fonction de leur intensité et de leur durée, sur la circulation et la distribution de l'eau (et des succions) dans les haldes non saturées et l'effet sur la stabilité. Divers scénarios ont été considérés dans cette étude pour évaluer comment les précipitations affectent la succion (de même que la cohésion apparente) et le facteur de sécurité.

Ce projet de recherche inclus aussi différentes analyses probabilistes. L'impact du coefficient de variation et de la variabilité spatiale a été pris en compte afin d'évaluer leur influence sur la stabilité de la pente des haldes selon les valeurs du facteur de sécurité, de l'index de fiabilité et de la probabilité de défaillance.

ABSTRACT

Waste rock is extracted from mines to reach the ore zones and is not economically valuable. They are usually transported by truck (or conveyor) and placed in waste rock piles on the ground surface. Waste rock piles must be designed to ensure their geotechnical stability during mine operations and after closure. The optimal construction of a pile requires detailed planning. This thesis deals with the stability analysis of large waste rock piles.

The main objectives of the work presented in this thesis were to i) increase the knowledge of the geotechnical behaviour of large waste rock piles, ii) investigate the effect of material properties on waste rock pile stability, iii) improve the ability to estimate the slope stability of waste rock piles of different internal and external configurations, iv) investigate the contribution of water infiltration and change in the matric suction (negative pore water pressure) on the slope stability of unsaturated waste rock piles and the related changes in the factors of safety, and v) study the influence of spatial variability of the waste rock mechanical properties on stability.

This study used numerical analysis to assess the behaviour and stability of unsaturated waste rock piles. Although based on typical situations, these analyses were not intended to simulate particular cases in detail, but rather to apply a systematic procedure to evaluate the stability of unsaturated waste rock piles and investigate the influencing parameters.

The analyses were conducted by applying the limit equilibrium method based on the state obtained from finite element analyses to assess the factor of safety (FS). Internal water flow and moisture distribution in the piles were also taken into account. The commercial software package Geostudio 2007 (SEEP/W, SIGMA/W, and SLOPE/W; GeoSlope International Ltd, 2008) was used for these analyses.

A comprehensive sensitivity analysis was completed to investigate the factors that influence the slope stability of waste rock piles. The results indicate that waste rock pile stability can be affected by different parameters including geometric configuration (i.e. local and global slope angles, the presence of benches and internal layers) and geotechnical parameters (such as internal friction angle and apparent cohesion of the waste rock and foundation).

Another specific aspect of this research was to investigate the role of matric suction distribution inside the waste rock piles and its effect on slope stability. The results indicate the positive

contribution of apparent cohesion generated by matric suction (under unsaturated conditions), on the slope stability and factor of safety. An extensive parametric study was conducted for different applied water flux (recharge) rates (intensity and duration) to obtain a better understanding of the water movement within the unsaturated piles and its effects on pile stability. Different scenarios were considered in this study to evaluate how rainfall infiltration affects the suction (and apparent cohesion) and the factor of safety.

Probabilistic analyses were also included in this research project. The impact of the coefficient of variation (COV) and spatial variability was studied, and their influence on slope stability of waste rock piles was assessed on the factor of safety, reliability index (RI) and the probability of failure (PoF).

TABLE OF CONTENTS

LIST OF TABLES

LIST OF FIGURES

LIST OF SYMBOLS AND ABBREVIATIONS

AEV   Air Entry Value $[ML^{-1}T^{-2}]$

{A}   Vector of actions at the nodes

a, n, m   Fitting parameters (model from Fredlund and Xing, 1999)

b   ln (10^6) $[ML^{-1}T^{-2}]$, model from Fredlund et al. (1994)

c   Cohesion $[ML^{-1}T^{-2}]$

c'   Effective cohesion $[ML^{-1}T^{-2}]$

c_{app} Apparent cohesion $[ML^{-1}T^{-2}]$

C   Capacity

C_G Constant material parameter (KCM method, =0.1)

C_U Uniformity coefficient (D_{60}/D_{10}) [-]

COV   Coefficient of variation

D   Demand

D_{50} Mean particle diameter [L]

D_r (or G_s)   Specific gravity [-]

D_5 Sieve size that 5% of the particles (by size) passes it [-]

D_{10} Sieve size that 10% of the particles (by size) passes it [-]

D_{60} Sieve size that 60% of the particles (by size) passes it [-]

[D]   Drained constitutive matrix

e   Void ratio[-]

e   Natural logarithmic constant (model from Fredlund and Xing, 1999)

E   Young's modulus $[FL^{-2}]$

F   Fitting equations (Table 2-7)

FS   Factor of safety [-]

FEM	Finite element method
g	Gravitational acceleration $[LT^{-2}]$
h	Hydraulic head $[L]$
h_c	Distance from water table to the point of interest $[L]$
h_{co}	Equivalent capillary rise
H, H_t	Total height of waste rock pile $[L]$
H_f	Foundation height $[L]$
$\{H\}$	The vector of nodal heads
i	Slope angle
I_D	Relative density $[-]$
$k, k_w, k(\psi), k(\theta)$	Hydraulic conductivity $[LT^{-1}]$
k_r	Relative hydraulic conductivity $[-]$
k_{sat}, k_s	Saturated hydraulic conductivity $[LT^{-1}]$
k_x, k_y	Hydraulic conductivity in x and y-direction $[LT^{-1}]$
K_0	Coefficient of lateral stress
$[k_{w,\ sat}]$	Hydraulic conductivity matrix
$[K]$	Matrix of coefficients related to geometry and materials properties
$[L]$	Coupling matrix
L_f	Foundation length $[L]$
L_t	Layer thickness $[L]$
$[M]$	Element mass matrix
MP	Morgenstern-Price method
m^2_w	Slope of WRC $[-]$, equation [2-7]
M-C	Mohr-Coulomb

n_v, m_v	Fitting parameter – Model from van Genuchten (1980) [-]
n	Porosity
P	Predicting equation (Table 2-7)
PMP	Probable maximum precipitation
PoF, P_f	Probability of failure
PWP	Pore water pressure
Q	Volume of discharge [L^{-3}]
Q	Boundary flux [LT^{-1}]
{Q}	Flow quantities at the node
R	Particle shape – Roundness [-]
RI	Reliability index (or β)
S	Equivalent strength related to USC, Figure 2-6
S_c	Capillary component of the degree of saturation [-]
S_r	Residual degree of saturation [-]
S_r	Total shear resistance
S_s	Specific surface [L^2M^{-1}]
S_m	Total mobilized (imposed) shear [$ML^{-1}T^{-2}$]
t	Time [T]
u_a	Pore air pressure [$MT^{-2}L^{-1}$]
u_w	Pore water pressure [$MT^{-2}L^{-1}$]
UCS	Uniaxial compressive strength [$MT^{-2}L^{-1}$]
VWC	Volumetric water content
W	Total weight of a soil slice
WEV	Water Entry Value [$ML^{-1}T^{-2}$]

WRC	Water retention curve
{X}	Vector of field variables
y	Dummy variable of integration representing ln (ψ) (Fredlund 1994)
z_w	Ground water level [L]
α	Fitting parameter - Van Genuchten (1980) equation [$M^{-1}LT^2$] or [L^{-1}]
α	Global slope angle for waste rock pile
α	Angle between the base of the slice and the horizontal
β	Local slope angle for waste rock pile
β	Angle of repose
γ_{sub}	Submerged soil weight [$MT^{-2}L^{-2}$]
γ_{total}	Wet unit weight [$MT^{-2}L^{-2}$]
γ_w	Water unit weight [$MT^{-2}L^{-2}$]
ρ_w	Density of water [ML^{-3}]
σ, σ_{FS}	Standard deviation
σ_y	Total vertical stresses [$ML^{-1}T^{-2}$]
σ, σ_n	Normal stress [$ML^{-1}T^{-2}$]
σ'_y	Vertical effective stress [$ML^{-1}T^{-2}$]
ε	Normal strain [$ML^{-1}T^{-2}$]
τ, τ_{xy}	Shear strength [$ML^{-1}T^{-2}$]
ψ_a, ψ_{aev}	Air Entry Value [$ML^{-1}T^{-2}$]
ψ_d	Dilatation angle
ψ_0	Pressure corresponding to zero water content [$ML^{-1}T^{-2}$]
Ψ	Matric suction [$ML^{-1}T^{-2}$]
ψ_r	Pressure corresponding to the residual water content [$ML^{-1}T^{-2}$]

θ, θ_w	Volumetric water content [-]
θ_r	Residual volumetric water content [-]
θ_s	Saturated volumetric water content [-]
λ	Pore size distribution index – Brooks and Corey [-]
$\lambda_{c\phi}$	Cousins's (1978) charts parameter [4-2]
ϕ	Friction angle [-]
ϕ^b	Friction angle with respect to matric suction [-]
ϕ'	Effective internal friction angle [-]
ϕ_b	Basic angle of friction [-],Barton (1981), Equation 4-2
ϕ_c	Minimum friction angle for soils [-]
Θ	Normalized water content [-]
Θ^q	Correction factor for tortuosity (Fredlund et al (1994) Model, equation [2-5]
μ_w	Dynamic viscosity [$ML^{-1}T^{-1}$]
μ, μ_{FS}	Mean
υ	Poisson's ratio
Δ	Increment
∇h	Hydraulic head gradient [-]

LIST OF APPENDICES

CHAPTER 1   INTRODUCTION

Waste rock from hard rock mines is produced by the blasting and extraction process Waste rock, which lacks sufficient value for treatment (Tachie-Menson, 2006), is usually transported by trucks (or conveyors) and disposed of in waste rock piles (sometimes called dumps) for long-term disposal. These are among the largest types (by volume, weight or height) of man-made constructions (Robertson, 1982; Wickland and Wilson, 2005; McLemore et al., 2009). Waste rock piles are typically designed and constructed on the ground surface to prevent the retention of water behind or above the pile surface. As a result, most of the piles are unsaturated (Nelson and McWhorter, 1985).

The behaviour and the stability of waste rock piles have not been studied extensively, in part due to their lack of economic significance in the mining process. The most important aspects considered for their design are the general location (preferably near the mine site), transport, placement (based on available equipment), and other short-term economic factors. A few decades ago (starting mainly in the 1980s), environmental organisations and governmental agencies started demanding improvement in the design of waste rock piles on safety and reclamation (Klohn Leonoff Ltd., 1991; Piteau Associates Engineering, 1991). This thesis pursues this line of work by extending the investigation of the slope stability of piles, taking into account the consequences of internal and external structures, hydro-geotechnical properties and rainfall patterns.

This dissertation addresses the issue of slope stability of waste rock piles having characteristics fairly similar to those constructed at various mine sites. The main objective is to develop and apply a general approach to the assessment of the stability of unsaturated waste rock piles under various conditions. The investigation takes into account several influencing factors including internal features and external geometry of the pile, distribution of pore water pressures before, during and after rainfall, and the spatial variability of important geotechnical properties. The study uses numerical simulations as the main tool in the analytical process.

The specific objectives of the thesis can be summarised as:

i. Assess the basic physical and geotechnical characteristics of waste rock and waste rock piles.

ii. Develop (partly) coupled analytical models to investigate the sensitivity of different parameters, including the pile internal features and external geometry (i.e. height, slope angle, compacted layers, the number of benches, etc.), and material properties (i.e. geotechnical and hydrogeological).

iii. Develop models to simulate pore water distribution and stress-strain behaviour, and then assess slope stability analysis of unsaturated waste rock piles under various rainfalls (i.e. recharge conditions).

iv. Implement stochastic analysis of the main input parameters and apply to pile slope stability.

v. Investigate ways to improve slope stability.

vi. Recommend practical means to improve stability and also topics for future research.

This thesis consists of seven chapters. The organisation and the content of each chapter are summarised as follows:

Chapter 1 (current chapter) provides a short introduction to the project and briefly describes the content of the thesis.

Chapter 2 presents a literature review of relevant knowledge on waste rock piles. The chapter starts by presenting different methods for the construction of waste rock piles. This is followed by a description of the geometric configuration of waste rock piles. Previous investigations indicate that the degree of compaction and material (particles) segregation creates internal features within piles. The literature review also includes a summary of the main properties of waste rock, such as grain size distribution, the angle of repose, and initial friction angle. The unsaturated behaviour of granular materials is also addressed in this chapter, and typical hydraulic properties of waste rock (i.e. volumetric water content, hydraulic conductivity) are presented. The influence of negative pore water pressures on strength (i.e. apparent cohesion) is also reviewed, together with seepage flow in the unsaturated zone. The last sections contain a review of slope stability analysis. It includes different methods of slope stability and recalls

factors that affect stability. Previous studies have shown that the flow and water distribution within waste rock piles are difficult to measure or predict due to the complex internal structure and material characteristics. This chapter finishes with a review of probabilistic analysis, with a definition of the main input and output parameters related to Monte-Carlo analysis. A single factor of safety may not be enough to discuss the stability of a waste rock pile and other parameters (such as the reliability index RI and the probability of failure PoF) can be used to obtain a more complete assessment, these tools are applied later in the thesis.

Chapter 3 describes the approach used for the modelling and the methodology applied for conducting the stability analyses on waste rock piles under unsaturated conditions. The chapter includes a basic description of the problem and presentation of the calculation tools, including the fundamentals of numerical modelling with the finite element combined with limit equilibrium methods. Also, some of the main challenges related to the stability analyses of waste rock piles under unsaturated conditions are briefly addressed.

Chapter 4 presents preliminary results from slope stability analyses for constant conditions in the piles (mainly for dry cases). The effects of apparent cohesion (produced by the matric suction) on the stability of unsaturated waste rock pile are also investigated. The results serve to illustrate the influence of different factors such as pile geometry, waste rock properties and matric suction on the stability of the waste rock pile. These results are obtained by a coupled approach using SIGMA/W and SLOPE/W.

Chapter 5 presents the calculations results on the effect of relatively short and heavy rainfalls on the stability of unsaturated waste rock piles. The results show that the shear strength produced from matric suction can change over time and location due to the evolution of the water distribution. These results are obtained from an (indirect) coupled approach using SEEP/W, SIGMA/W, and SLOPE/W, starting with the pore water pressures, and the stress distributions, which are then used to assess the factor of safety and the critical slip surfaces. The chapter provides specific details on seepage modelling and slope stability analyses for transient conditions. Different rainfall patterns were applied as boundary conditions to evaluate time-dependent phenomena. The presence of loose and compacted waste rock layers was also taken into account. Chapter 6 presents the results related to uncertainties on the stability (and reliability) of waste rock piles. The results demonstrate the effect of having non-unique values for

different parameters through probabilistic analyses, using the Monte-Carlo approach as implemented in SLOPE/W. This last section summarises and discusses the main results of the research project. Limitations of this study are addressed at the end of this chapter.

Chapter 7 presents the conclusion with key findings and recommendations for further work.

Supplementary information and results are presented in the appendices.

CHAPTER 2   LITERATURE REVIEW

Waste rocks produced by mining operations are not sufficiently economically valuable for processing. They are usually transported by trucks (or conveyors) and disposed of in waste rock piles, which are among the largest (by volume, weight or height) man-made structures (Robertson, 1982; Wickland and Wilson, 2005; Tachie-Menson, 2006; McLemore et al., 2009).

Waste rock typically includes a very wide range of particle sizes, from fine-grained particles (µm) to cobbles and boulders (m). The piles can form massive structures that may contain more than 500 million cubic meters of waste rock with heights of up to 300 m (McCarter, 1990; Fala, 2002).

This chapter begins by reviewing the different methods for site selection and construction of waste rock piles. Then it presents a literature review of the properties of waste rock (i.e., mechanical, geotechnical and hydraulic). Next a background of the slope stability analysis is presented, and different methods are briefly reviewed. The topics reviewed here include factors affecting the stability, rainfall infiltration, and probabilistic analysis. The information presented in this chapter will provide the reader the necessary background to understand the methodology and analysis undertaken in this research project.

2.1   Site selection and construction of waste rock piles

The characteristics of the site should be comprehensively investigated in the process of site selection (Klohn Leonoff Ltd., 1991; Piteau Associates Engineering, 1991). It is often preferable to select a location close to the mine site to minimize transportation, although other issues may favor more distant sites (i.e. the watershed and reclamation scenarios).

Different factors including geological, geotechnical, hydrogeological, hydrological, topographical, climatic, environmental, economic and operational parameters can influence the selection of an appropriate site for a waste rock pile (Aubertin et al., 2002a). Due to the many different factors, this selection process can be quite a challenge (Hustrulid et al., 2000).

The short or long term geotechnical stability of piles must also be considered in this process. As will be shown later, the pile stability can be influenced by various factors such as geometry,

properties of the materials, methods of construction, foundation conditions, climate, and hydrology.

The most suitable method for construction of a waste rock pile should be evaluated based on the topography of the area, foundation conditions, available equipment, and overall pile design (Piteau Associates Engineering Ltd., 1991). The five main types of pile configurations are described below (Aubertin et al., 2002a; Fala, 2002; Tachie-Menson, 2006; Fala, 2008); either one or a combination of them can be considered.

Figure 2-1 (a) shows a schematic view of the valley fill type pile. The waste rock fills the valley partially or entirely. Issues such as disruption of stream flow, the creation of a large pond upstream and the potential of overtopping due to a large flood should be avoided. As these may result in slope failure (Claridge et al., 1986). The construction should begin at the upstream end of the valley with dumping proceeding along the downstream face while the surface is sloped and graded prevent water ponding at the head of a valley. Construction of culverts or diversion ditches may be needed (Tachie-Menson, 2006).

Figure 2-1 (b) shows a cross-valley fill type pile that starts from one side and crosses the valley without filling the upstream end. There is a need for diversion elements (ditches or culverts) to transport water around or through the pile to avoid impounding water upstream.

Figure 2-1 (c) presents a schematic view of the side hill fill type pile. These piles are constructed on sloping terrain with the slope in the same direction as the foundation. The pile lies along the side of the hill without crossing the valley or blocking any major drainage courses (Tachie-Menson, 2006).

Figure 2-1 (d) shows a pile that links the crest of a ridge (ridge-crest fill type). The waste rock material is placed along both sides of the area, and the fill is sloped on both sides of the crest.

The heaped fill type is a pile on level terrain. It consists of a waste rock with slopes on all sides (Figure 2-1 (e)). These are constructed on the flat or moderately inclined terrain and typically surface of these piles is flat.
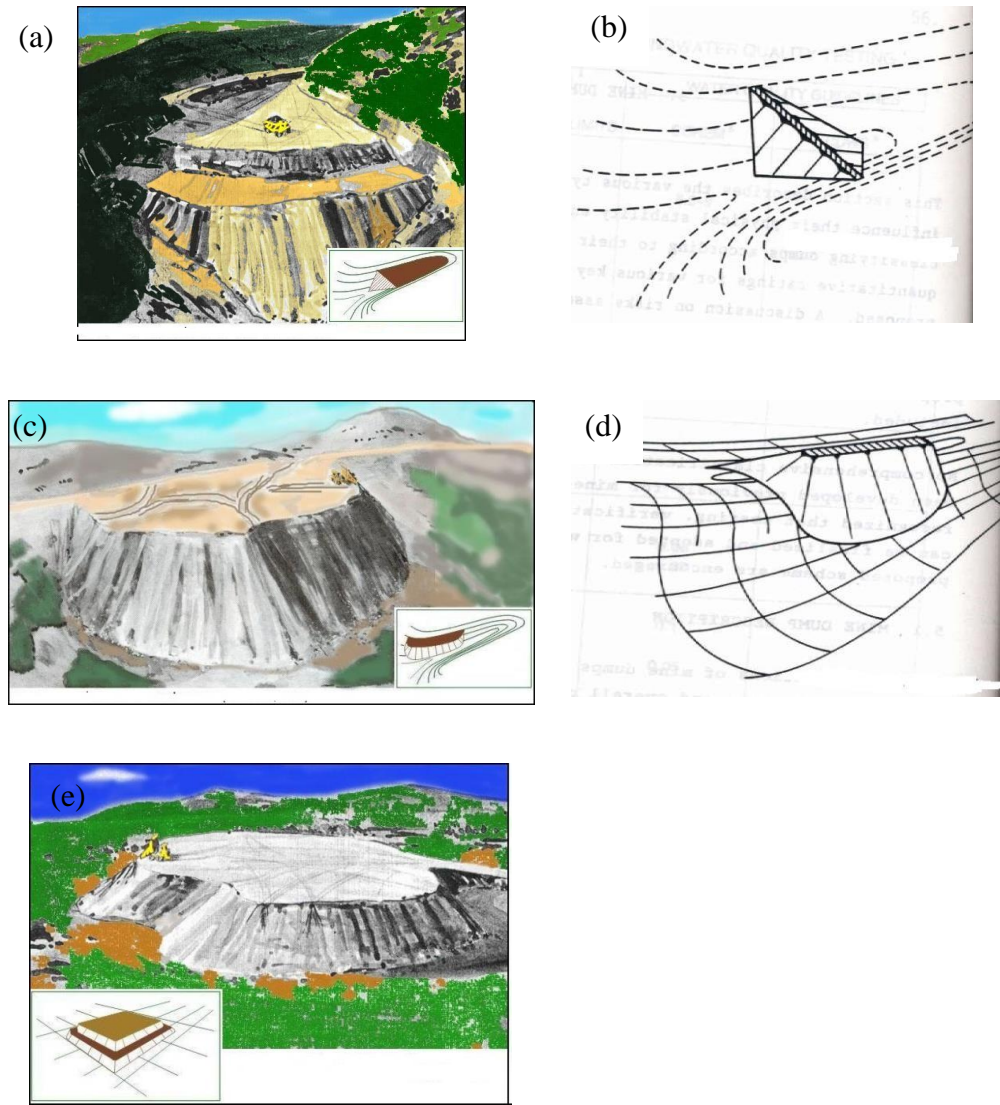
Figure 2-1: Different construction types, a) Valley fill pile; b) Cross-valley fill; c) Sidehill fill pile; d) Ridge crest pile; e) Heaped pile (a, c and e adapted from McCarter (1990), taken from Aubertin et al., (2002a); b and d taken from Wahler (1979))

2.1.1 Construction methods

The construction method depends on the selected site particularly the topography, equipment available for transportation and physicochemical characteristics of the waste rock (Burnley, 1993). Each of the methods leads to a different degree of compaction and segregation that may

impact water movement in a pile (Morin et al., 1991; Fala, 2002). Four main construction methods are summarized below.

End dumping

The waste rock is directly dumped from the trucks along the crest of the pile and tumbles down the slope due to an initial velocity and gravity. The coarser particles tend to come to rest near the toe due to higher momentum and finer particles usually come to rest near the crest due to lower momentum, creating segregation. Lower piles may result in less segregation than higher piles (McLemore et al., 2009).

The resulting surface takes the angle of repose of the waste rock, sub-parallel to the initial slope, resulting in successive layers of segregated materials (Robertson, 1982, 1985; McLemore et al., 2005). The dozers then rework the surface to keep it clear from boulders and try to create a positive slope outward (to the crest). Compacted layers are created over larger boulders and cobbles. Gradually, as the pile is extended, the overall configuration (with compacted layers over coarse layers) can change depending on whether this extension is horizontal or vertical (built on several levels) (Burnley, 1993). These features have a major influence on water flow inside the pile (Fala, 2002, 2008).

There usually exist three particle size zones along the slope for this method; the fine-grained particles near the top, the coarser particles at the base and intermediate particles in a transitional zone as shown in Figure 2-2.
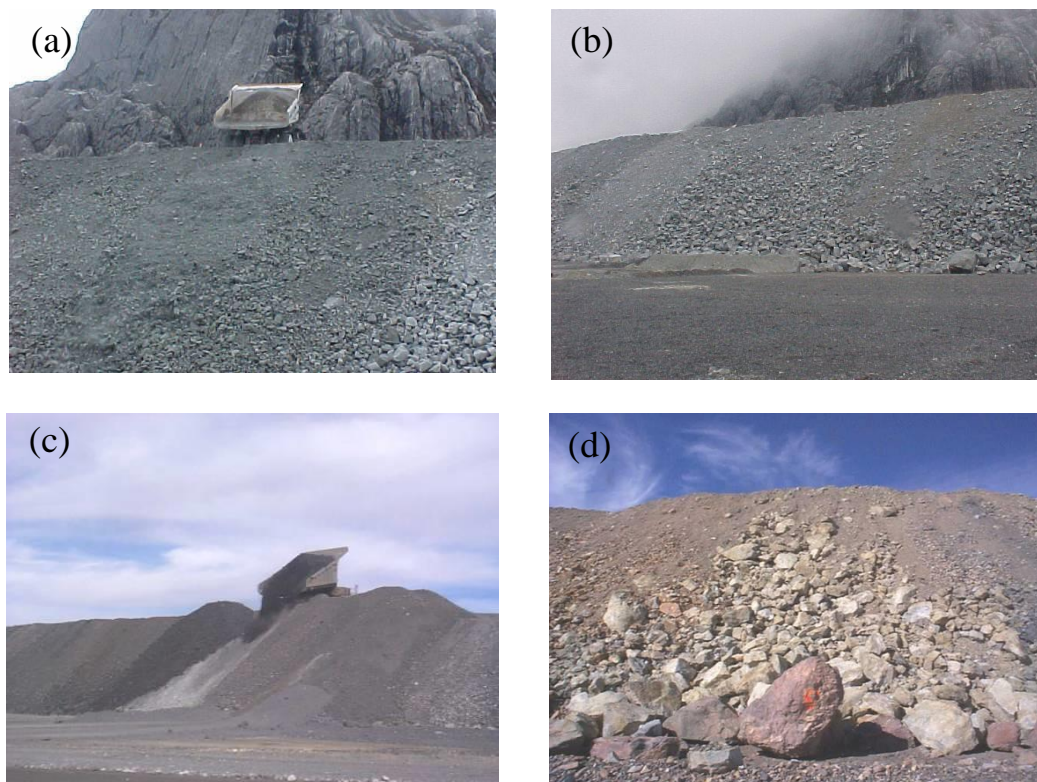
Figure 2-2: Construction of waste rock piles using end dumping; during (a) and after (b) McLemore et al. (2009); during (c), after (d) Martin (2004)

Push dumping

The waste rock is dumped into the surface, near the crest, and bulldozers push the waste rocks deposited near the crest by trucks off the slope. Compared to the end-dumping method, the initial velocity is lower here. The smaller momentum results in less segregation (Fala, 2002; McLemore et al., 2009). In the push dumping method, only about 40% of coarse particles reach the base of the slope, while this proportion is about 75% with end-dumping (Nichols, 1986).

Free dumping

Small embankments (heaps) are deposited on the pile surface, as individual stacks with a height of about 2 m. This method is typically used early in the project and later replaced by end-dumping or push dumping methods. The surface is then leveled and compacted (Aubertin et al., 2002b), achieving more compaction and less segregation (Quine, 1993; Tachie-Menson, 2006).

The resulting layers can differ in the degree of compaction when the method involves the movement of heavy machinery on the surface.

Dragline

This approach used a dragline for transport and handling of waste rock, which is relatively common in the large-scale mining of flat deposits near the surface (such as coal). The segregation is rather limited, and the material is less dense (less compacted) compared to other methods (Aubertin et al., 2002a; McLemore et al., 2009).

2.1.2 **Geometric configuration**

The geometric configuration of piles can be described based on the internal and external geometry. The internal geometry relates to features within the pile (including their number, thickness, inclination and degree of compaction), while the external geometry relates to its external characteristics (circular, long, with or without benches). The main influencing the internal structure are material properties, mineral composition, blasting and sequencing, transportation and dumping, and climatic conditions (Azam et al., 2007). These characteristics may change over time.

Different geometric features of piles have been described in the literature (Smith et al., 1995; Herasymuik, 1996; Wilson, 2000; Aubertin et al., 2005). Figure 2-3 illustrates the typical internal structure of a pile constructed by an end-dumping or push-dumping method on a relatively flat surface. In this schematic view, the sub-horizontal layers are formed by the passage of heavy equipment on each bench. Movements of heavy equipment create denser layers on the surface (crushed and compacted materials, up to 1 m in thickness; Martin, 2004). The side zones are affected by the graded bedding and inclined stratification on the slope. Such stratification and heterogeneity have important effects on the fluid flow behavior (Fala, 2002; 2005) and the geotechnical and geochemical responses of waste rock piles (Aubertin et al., 2005; Molson et al., 2005; Fala et al., 2006).
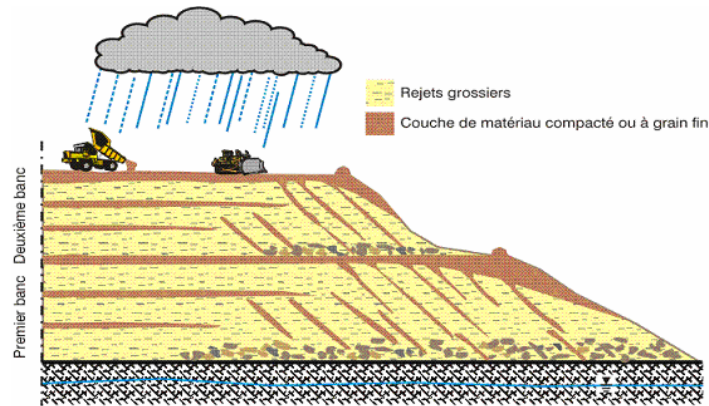
Figure 2-3: Sectional view of a waste rock pile with segregation along the slope (Aubertin et al., 2005)

2.2 Waste rock properties (mechanical, geotechnical)

Particle size distribution

It is not easy to obtain accurate gradations of waste rock in piles (Fala, 2008). As material heterogeneity, segregation, and the presence of large boulders make measurement difficult (or inaccurate). Different methods such as sampling and laboratory measurements, in situ determination and image analysis of photographs, can be used to estimate the particle size distribution (McLemore et al., 2009).

Typical waste rock shows a wide gradation curve (from silt to boulders size); with a coefficient of uniformity C_U (= D_{60}/D_{10}; ratio of the sieve size that permits the passage of 60% of the particles and of 10% of the particles by weight) of 20 or more (Barbour, SL et al., 2001; Aubertin et al., 2002a; Gamache-Rochette, 2004).

For such well-graded (or widely graded) materials ($C_U \gg$ 5-6), the main construction method (end-dumping or push dumping) results in segregation. The grain size distribution curve can be used to identify the characteristics and behavior of water flow within a waste rock pile. For example, the proportion of fine and coarse material affects the hydraulic properties of the soil.

Some grain size distributions of different waste rock that have been measured (laboratory or in situ) and reported in the literature are presented in Figure 2-4; the origin of the curves is given in Table 2- 1.
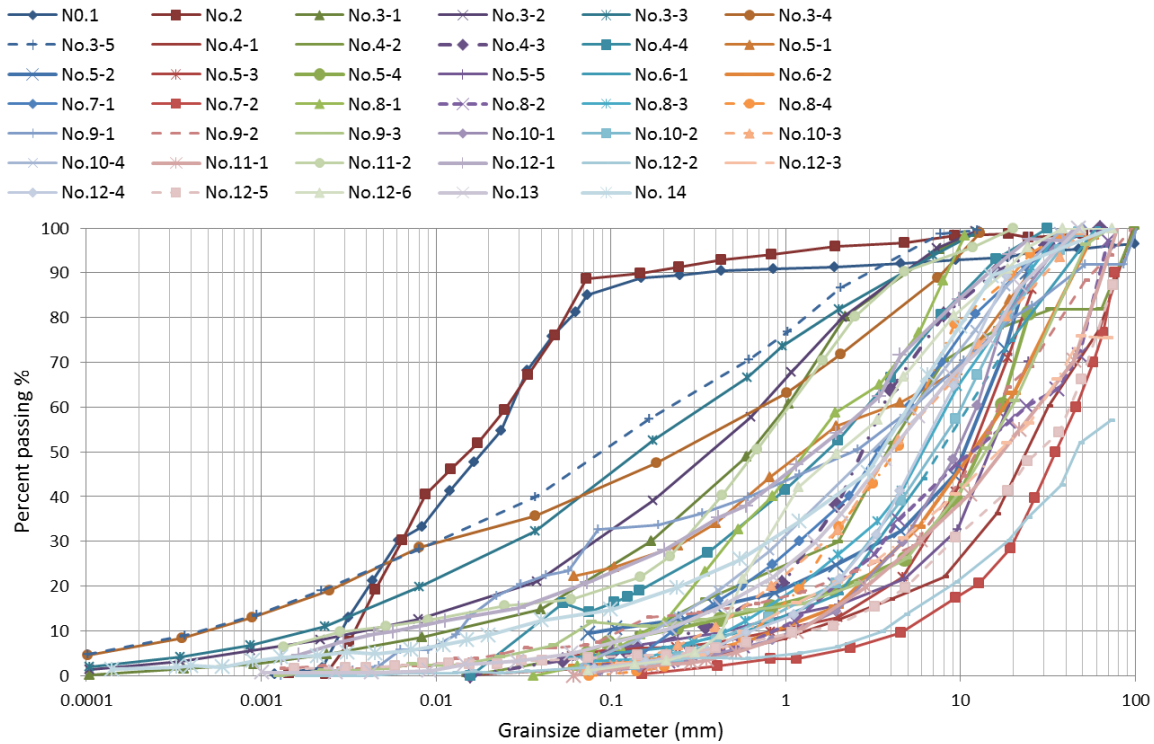
Figure 2-4: Grain size distribution curves from literature- see details in Table 2-1

The distributions shown in Figure 2-4 indicate that bulk of the grain size curves are often in the sand and gravel range (from 75 µm to about 4.5 mm to about 10 cm and more).

Table 2-1: Identification of the gradation curves shown in Figure 2-4

Curve No.	Reference
No.1, No.2	B-zone waste rock pile at Rabbit Lake mine in Canada (Ayres et al., 2006)
No. 3-1 to No.3-5	Golden sunlight mine, Montana (Azam et al., 2007)
No. 4	Libiola Fe-Cu sulfide mine, eastern Liguria, Italy (Marescotti et al., 2008)
No.5-1 to No. 5-5	Bonner mine, Colorado (Stormont and Farfan, 2005)
No.6-1, No. 6-2	Stockpile in the Ruhr district, Germany(Neumann-Mahlkau, 1993)
No.7	Range of four rock piles from Carlin deposits, Nevada (Quine, 1993)
No.8 -1 to No. 8-4	Questa rock piles (Nunoo, 2009)
No. 9-1, to No. 9-3	(Gamache-Rochette, 2004; Aubertin et al., 2005)
No. 10-1 to No. 10-4	Field samples were chosen for large diameter pressure plate testing (after Herasymuik (1996)
No. 11 (1-2)	Samples from the GHN rock pile (Gutierrez, 2006)
No.12-1 to No. 12-6	(Boakye, 2008)
No.13	(Peregoedova, 2012)
No. 14	Goldstrike Mine (Martin, 2004)

Density and specific gravity

The in Situ density of waste rock can range from 1600 to 2200 kg/m^3 (Williams, 2000). The specific gravity of particles (G_s or D_r), can vary between about 2.6 to 4.8 and more (e.g. (Kesimal et al., 2004; Bussière, 2007). Table 2-2 presents some values of density and specific gravity for waste rock material from the literature.

Table 2-2: Summary of various parameters of waste rock

Mine	Dry density kg/m^3 (mean)	Density in situ (wet density) kg/m^3 (mean)	Specific Gravity (mean)	References
Davis mine	2650	-	-	Adams et al. (2007)
Ajo, Arizona	1943	-	-	Savci and Williamson (2002)
Golden sunlight Montana	1900 to 1990	-	-	Azam et al. (2007)
Lichtenberg pit Germany	2100	-	2.75	Hockley et al. (2003)
Changi	-	-	2.66	Na et al. (2005)
Middle rock pile	2220	2600	2.74	Boakye (2008)
Sugar shack west	1920	2150	2.78	
Spring Gulch rock pile	1760	2010	2.74	
Sugar shack south	1890	2100	2.82	
Pit alteration scar	1800	2010	2.76	
Debris flow	2020	2120	2.71	

Angle of repose (β)

The angle of repose (β) is relevant in assessing pile stability. Quine (1993) measured the angle of repose of several waste rock piles and obtained 37° ± 3. Burnley (1993) reported two different piles with overall slopes of32º to 37° for one and 28º to 38° for the other.

Baumer (1973) indicated that angles of repose approaching 37° were likely as a result of push and end dumping in waste rock piles (based on the Bougainville copper project). An average angle of repose for free-dumped or end-dumped cohesionless rockfill within the range of 35 to 40° (typically very close to 37°) is also reported in the literature (Piteau Associates Engineering, 1991; Williams and Rohde, 2008).

Internal friction angle ϕ'

The internal friction angle (ϕ') is a measure of the frictional strength of the material the particles. Its value can be determined experimentally using different tests (such as direct shear or triaxial

tests), depending on the grain size. Different parameters may affect the internal friction angle (Hustrulid et al., 2000).

i. Particle size distribution

In relatively fine-grained soils, an increasing amount of coarse particles typically results in an increase of the internal friction angle (Leps, 1970; McLemore et al., 2009). The values of ϕ' typically decrease with decreasing the coefficient of uniformity, C_U (Hawley, 2000; Holtz et al., 2010); adding finer particles and filling the voids between coarser particles can increase the friction angle by as much as 10° (Statham, 1974).

Figure 2-5 shows the general relationship between the internal friction angle ϕ', density (and density index I_D) and soil classification for cohesionless soils. Well-graded soils typically have a greater friction angle (Holtz et al., 2010). This angle also increases when going from a fine-grained soil (silt) to a coarser material (sand and gravel).
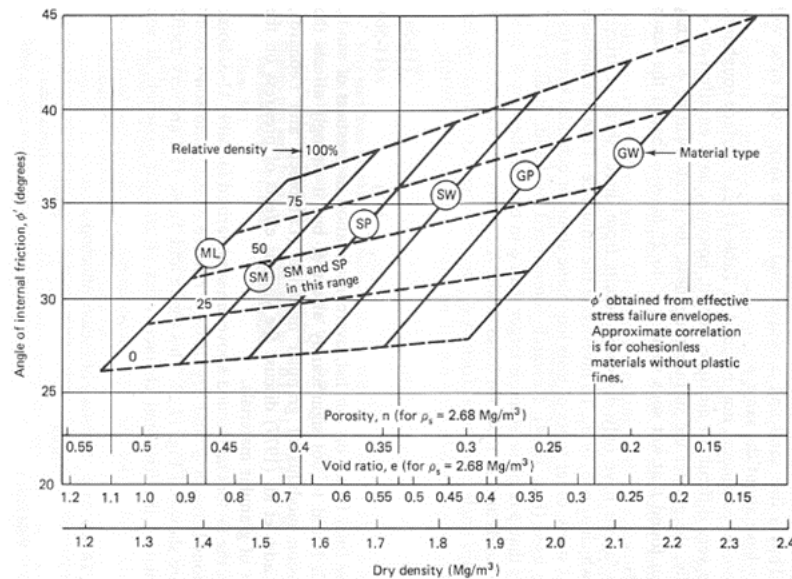
Figure 2-5: Correlations between the internal friction angle and density for different soil types; adapted from Navfac (1982) and Holtz et al. (2010)

Typical internal friction angle values for medium-dense sand can range from 32º to 38º and for medium-dense sandy gravel the range is from 34º to 48º (Das, 1983), which gives an indication of what can be expected for waste rock, as their grain size is often dominated by the sandy and gravelly fractions (between 75 μ, and 10 cm approximately) (Aubertin, 2013).

Figure 2-6 was obtained from published rockfill test data. It estimates the S-value as a function of UCS (σ_c) (equivalent strength) based on rockfill particle size (d_{50}) (Barton and Kjaernsli, 1981). The reduction of particle strength due to mean particle size decrease is more pronounced under triaxial conditions compare to plane strain conditions. Friction angles are typically several degrees higher (e.g. about 2° to 4°) when plane strain tests are compared with triaxial tests on the same material. There is noticeably less crushing of particles in the former case (Barton, 2008).
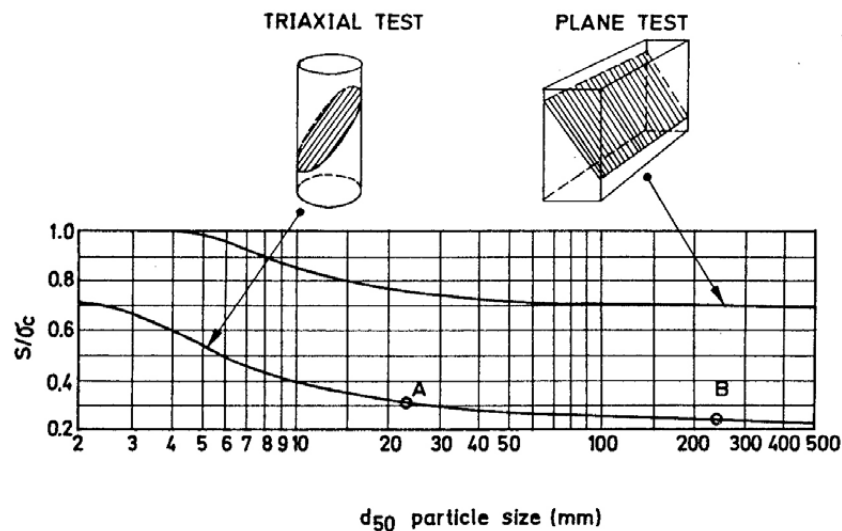
Figure 2-6: Estimation of equivalent strength (S) of rockfill based on D_{50} value (cited by Barton, 2008)

ii.   Particle characteristics (i.e. shape, surface roughness)

The angularity and surface roughness of particles have a direct impact on the internal friction angle (Barton, 2008; Holtz et al., 2010). A comparison between angular and sub-round particles showed a difference in the value of ϕ' as large as 7.5°, at a void ratio of 0.80 (Vallerga et al., 1957).

Barton (1981) presented R (equivalent roughness) as a function of porosity of the rockfill and particle origin (Figure 2-7, a). He found that increasing the rockfill particle angularity results in a higher equivalent roughness and internal friction angle.
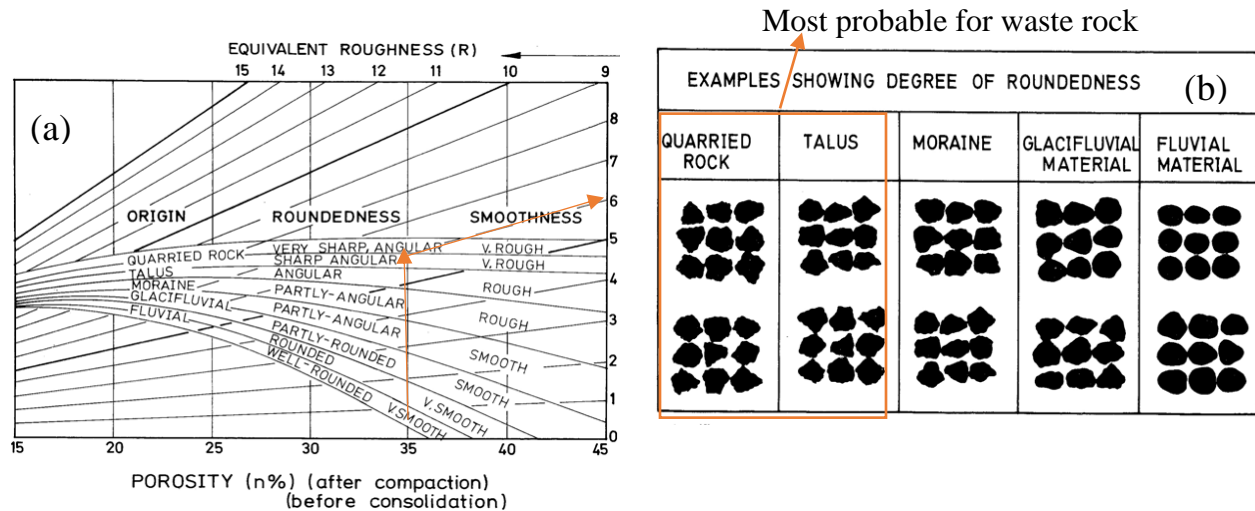
Figure 2-7: Empirical method to estimate the equivalent roughness R of rockfill as a function of porosity and particle origin, roundness and smoothness (adapted from Barton and Kjaernsli, 1981)

Figure 2-8 illustrates the relationship between roundness (i.e. average radius of curvature of surface features about the radius of the maximum sphere which can be inscribed in the particle) and critical state friction angle (ϕ_c, the minimum friction angle for soils) (based on the experimental data). The results show that an increase of roundness from 0.1 (very angular) to 1 (well rounded) produces a decrease of the critical state friction angle ϕ' of sandy soils from 40º to 28º approximately (Cho et al., 2006).
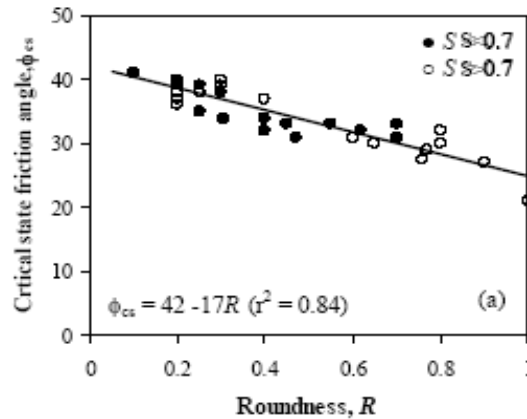
Figure 2-8: Effect of particle shape on critical state friction angle for sand; adapted from Cho et al. (2006)

iii.   Confining stress level

There is an inverse relation between the internal friction angle and the confining pressure (Marachi et al., 1969; Anderson and Anderson, 1970; Leps, 1970; Becker et al., 1972; Skempton, 1975; Hribar et al., 1986; Hawley, 2000; Linero et al., 2007; Holtz et al., 2010). As confining pressure increases, the tendency of particles to crush under pressure increases (Quine, 1993). Leps (1970) studied the results from (Marasal, 1965) and indicated adding 10 psi (69 kPa) may decrease ϕ' by 3 or 4°. Billam (1971) mentioned a decrease of friction angle from 58.4° to 36.9° while the pressure is increased from 3 kPa to 10 MPa on a limestone sand (Billam, 1971). Charles (1990) also reported a decrease of internal friction angle (rockfill) from 62° to 36° when the confining stress increased from 20 to 500 kPa (Charles, 1990) cited by Quine (1993)).

The internal friction angle typically increases with increasing density or decreasing void ratio (Holtz et al., 2010). Figure 2-9 illustrates the relation between void ratio, effective normal stress, and shear test results for Ottawa sand. For both loose and dense sand, an increase of effective normal stress results in a reduction of friction angle (Das, 1983). Denser sands nonetheless remain stronger (higher value of ϕ') than loose sands.
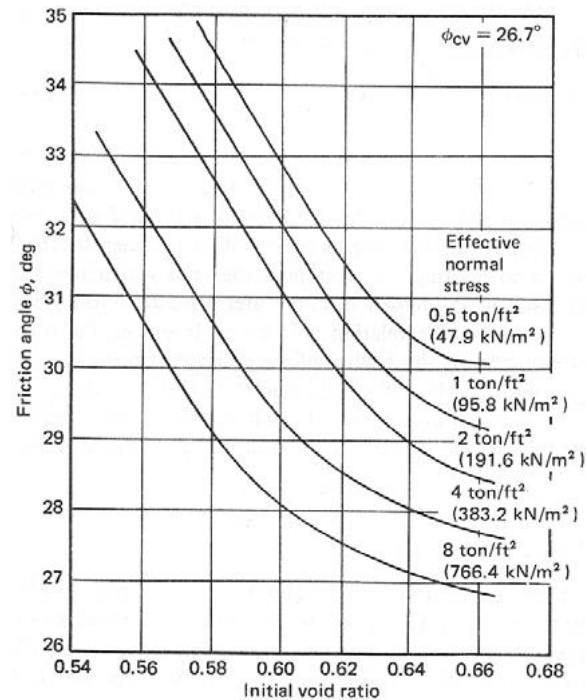
Figure 2-9: Variation of peak internal friction angle with effective normal stress for direct shear tests on standard Ottawa sand; adapted from Das (1983)

Leps (1970) presented Figure 2-10 based on a large number of large-scale triaxial shear test data for rockfills of various types (cited by (Barton, 2008). It presents a relationship between the friction angle and normal stress for different density of rockfills. The lines semi-log plot indicates that there can be a large variation in friction angle ϕ' with the confining pressure and density.
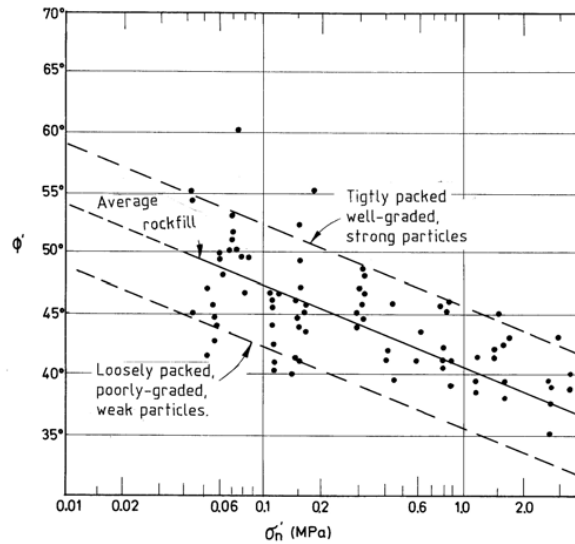
Figure 2-10: Peak shear strength data for rockfills from Leps (1970); adapted from Barton (2008)

Published results from different authors have shown that the typical internal friction angle φ', which controls the shear strength of waste rock (under effective stresses), can vary between 21º (for softer rock) and 62º, with usual values for hard rocks ranging between 34º and 45º (Quine, 1993; URS Corporation., 2003; Gutierrez, 2006; Boakye, 2008; McLemore et al., 2009; Nunoo, 2009)

2.3 Behaviour of unsaturated soils

Waste rock piles are usually under unsaturated conditions (Nelson and McWhorter, 1985). Figure 2-11 presents a schematic overview of the natural hydrologic cycle. The precipitation, evaporation, and evapotranspiration are important natural mechanisms that influence the depth and extent of the unsaturated zones (Lu and Likos, 2004).
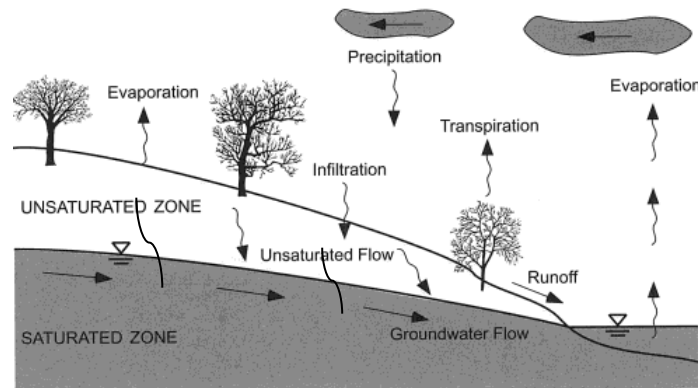
Figure 2-11: The unsaturated zone and the natural hydrologic cycle (Lu and Likos, 2004)

The water from several sources (rainfall, snowmelt or runoff) can come into contact with a pile and infiltrates through it to the underlying soil or drain from the toes of the piles (Morin et al., 1991; Wilson, 2003). Below the phreatic surface, the pore water pressure in soils for both saturated and unsaturated hydrostatic conditions can be expressed as follow (Fredlund and Rahardjo, 1993):

$$u_w = -\rho_w g h_c \qquad\qquad [2\text{-}1]$$

Where

ρ_w: water density $[ML^{-3}]$

g: gravitational acceleration $[LT^{-2}]$

h_c: vertical distance from the surface of the water table to the point of interest $[L]$

A typical pore water pressure distribution (at steady-state) below and above the water table (horizon of zero pore pressure) is presented in Figure 2-12. The positive pore water pressure increases hydrostatically with depth below the water table. Above it, water rises through the spaces of the soil due to capillary action (Fredlund and Rahardjo, 1993), and negative pore pressures are created due to surface tension in the water. This negative pore pressure (suction) increases uniformly (linearly) from the water table up to the top of the saturated capillary zone

under steady-state conditions. The capillary zone can be large (thick) for finer grained soils (i.e. silt and clay) or small for coarse soils (i.e. sand, waste rock).
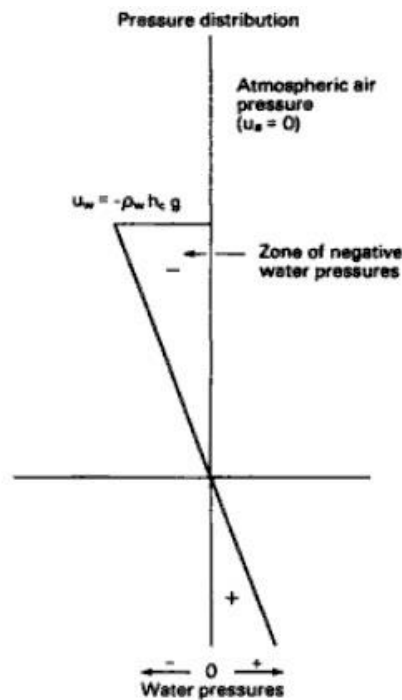
Figure 2-12: Typical soil profile showing positive and negative pore pressures distribution (Fredlund and Rahardjo, 1993)

Matric pressure is the suction created by capillary forces and the interaction of water, air, and solid surfaces. The matric suction is defined as the difference between air pressure and water pressure.

$$\Psi = \text{Matric suction} = u_a - u_w \qquad\qquad [2\text{-}2]$$

The matric suction can be measured by both direct and indirect methods. In direct methods, high air entry ceramic disks are often used whereas in indirect methods, different types of porous sensors are utilized (Fredlund and Rahardjo, 1993).

The hydrogeological behavior of waste rock can be evaluated by a combination of laboratory tests, site observations and measurements, theoretical work, and numerical analyses (Aubertin et al., 2005, , 2008; Bussière et al., 2011). Experimental results can be used to extend and calibrate

predictive models and assess hydrogeological properties (Aubertin et al., 1996, 1998, 2003; Mbonimpa et al., 2002; Chapuis and Aubertin, 2003). In that regard, specific laboratory testing protocols have been developed to study the hydraulic properties (i.e. water retention curve and hydraulic conductivity) of waste rock at an intermediate scale (Hernandez, 2007; Peregoedova, 2012). Field measurements have also been conducted to obtain representative results under *in situ* conditions, on a larger scale (e.g. Gamache-Rochette, 2004; Fala, 2008; Lessard, 2011). These are needed to take into account the important effect of scale on waste rock properties and behavior; this in fact is part of ongoing work within RIME (Research Institute on Mines and the Environment) at Polytechnique and UQAT. Some of the specific approaches developed and results obtained are summarized in the followings.

2.3.1 **Water retention curve (WRC)**

The water retention curve (WRC) is the function that illustrates the evolution of the water content with the matric suction. It depends on many factors such as particle size distribution, porosity, and of the material (Freeze and Cherry, 1979; Kovacs, 1981; Aubertin et al., 1996; Dye et al., 2009).

This WRC is often used for predicting the soil capacity for water storage. Figure 2-13 shows a schematic view of a water retention curve (WRC). It is similar to the water capillary rise curve in a homogeneous soil above the water table (Freeze and Cherry, 1979; Kovacs, 1981).
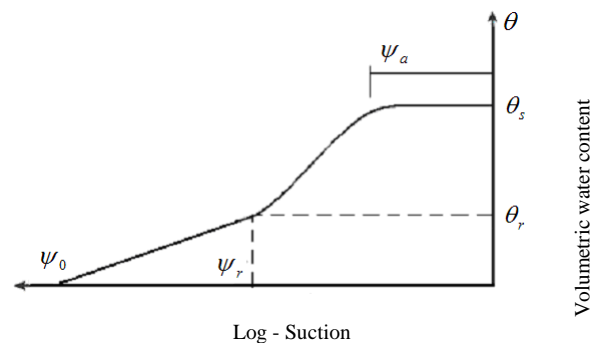
Figure 2-13: Schematic representation of a water retention curve for soil (Fala 2008)

In this figure, the key parameters are:

θ_r [-] = residual water content

ψ_0 [L] = pressure corresponding to zero water content

ψ_r [L] = pressure corresponding to the residual water content

ψ_a [L] = (AEV- air entry value), the suction where the material starts to desaturate

θ_s [-] = water content at saturation, equals to the porosity

The air-entry value is a commonly used parameter that corresponds to the suction at which the air starts to enter the largest pores (de-saturation starts). The air entry value and residual water content can be estimated graphically on the water retention curve by pairs of tangent lines from inflection points (Fredlund and Xing, 1994; Lu and Likos, 2004).

The WRC can be obtained either in the laboratory or by various predictive models (such as the MK model; (Aubertin et al. 1998, 2003). Table 2-3 presents some of the fitting and prediction equations for water retention curve.

Table 2-3: Conditions and formulations of different fitting and prediction methods for the WRC

Method		Conditions	Equations
Brooks and Corey (1964)	Fitting	ψ_a: air-entry value λ: pore size distribution index	$\theta = \begin{cases} \theta_s & \text{for} & \frac{\psi}{\psi_a} < 1 \\ \theta_r + (\theta_s - \theta_r)\left(\frac{\psi_a}{\psi}\right)^{\lambda} & \text{for} & \frac{\psi}{\psi_a} \geq 1 \end{cases}$
Van Genuchten (1980)	Fitting	a_v: fitting parameter, $[M^{-1}LT^2]$ or $[L^{-1}]$ n_v and m_v: fitting parameters, related to soil pore size distribution and the overall symmetry of the characteristic curve respectively	$\Theta = S_e = \left[\dfrac{1}{1 + (\alpha_v \psi)^{n_v}}\right]^{m_v}$ $m_v = 1 - \dfrac{1}{n_v}$ or $m_v = 1 - \dfrac{1}{2n_v}$
Fredlund and Xing (1999)	Fitting	e: natural logarithmic constant a, n and m: fitting parameters C (ψ): correction factor	$\theta = C(\psi)\theta_s \left[1/\ln\left[e + \left(\psi/a\right)^n \right] \right]^m$
Modified Kovács (MK) model (Aubertin et al., 1998; Aubertin et al., 2003)	Prediction		$S_r = \dfrac{\theta}{n} = 1 - \langle 1 - S_a \rangle (1 - S_c)$ $\langle y \rangle = 0.5(y + |y|)$ $S_c = 1 - \left[\left(h_{co}/\psi\right)^2 + 1 \right]^m \exp\left[-m\left(h_{co}/\psi\right)^2 \right]$ $S_a = a_c \left[1 - \dfrac{\ln\left(1 + \psi/\psi_r\right)}{\ln\left(1 + \psi_0/\psi_r\right)} \right]\left(\left(h_{co}/\psi_n\right)^{2/3} / e^{1/3} \left(\psi/\psi_n\right)^{1/6} \right)$ $h_{co,G} = \dfrac{0.75}{[1.17\log(C_U) + 1]e\, D_{10}}$

The grain size distribution and density (void ratio, compaction) influence the WRC. The smaller pores retain more water. The AEV increases as the soil pore size decreases (Powrie, 2004). Figure 2-14 illustrates WRC of sand and silt; these curves show that coarser grain soils desaturate faster compared with fine-grained soils (Aubertin et al., 2002a).

Log - Suction
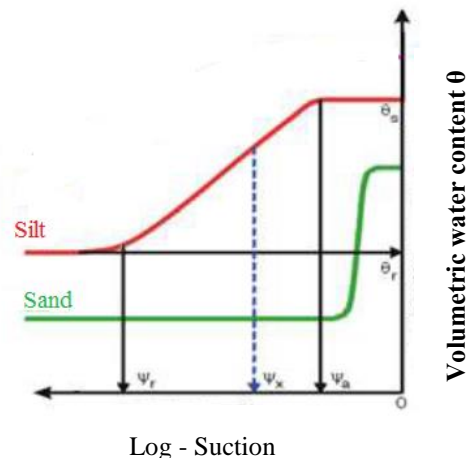
Figure 2-14: Schematic presentation of water retention curve for two types of soil, modified by Aubertin et al. (2002a)

Peregoedova (2012) showed that the water retention curve obtained experimentally for waste rock material has a low AEV (<10 cm) and a residual volumetric water content (θ_r) relatively high (0.06 to 0.08). Table 2-4 presents different parameters related to WRC, obtained by different authors.

Table 2-4: Measured values for WRCs parameters (van Genuchten (1980) equation), based on the literature

Method	Material	θ_r	θ_s	α (m)	L	n	k_{sat} (ms^{-1})	References
VG	GRV	0	0.39	14960	0.5	1.45	4.7×10^{-3}	Bussière and Aubertin (1999)
	SBL	0.01	0.29	3	0.5	3.72	5.1×10^{-5}	
VG	Well-graded sand with fines and gravel	0.06	0.23	0.7519 (cm^{-1})	0.5	2.68	1×10^{-3}	Peregoedova (2012)

2.3.2 **Hydraulic conductivity**

Saturated hydraulic conductivity

The saturated hydraulic conductivity (k_{sat}) tends to increase with the average particle size. The value of the saturated hydraulic conductivity can be measured by either laboratory or in situ tests, or it can be estimated from predictive models (Peregoedova, 2012).

Different predictive methods exist, and each method has its specific features and range of application. For waste rock, the predictive Kozeny-Carman (KC, Chapuis and Aubertin, 2003) and Kozeny-Carman modified (KCM, Mbonimpa et al. 2002) models have been applied (with some adjustments) with relative success to estimate the value of k_{sat} (Hernandez, 2007; Peregoedova, 2012).

Table 2- 5 presents different equations available to estimate the saturated hydraulic conductivity.

Table 2-5: Conditions and formulations of various prediction methods for saturated hydraulic conductivity

Method	Conditions	Equations
Hazen and Tayler Taken from Chapuis (2004)	Void ratio close to e_{max} (loose soil) $C_u < 5$ 0.1mm $\leq d_{10} \leq 3$ mm Reference temperature 20 °	$$k\left(\frac{cm}{s}\right) = 1.157d_{10}^2(mm)[0.7 + 0.03T°]$$
Navfac (1974) taken from Chapuis et al. (1989b)	$0.3 \leq e \leq 0.7$ (sands and mixtures of sand and gravel) $2 \leq C_U \leq 12$ 0.1mm $\leq d_{10} \leq 2$ mm $d_{10}/d_5 \leq 1.4$ mm	$$k\left(\frac{cm}{s}\right) = 10^{1.291e-0.6435}(d_{10})^{10^{0.5504-0.2987e}}$$
Kozeny-Carman taken from Chapuis and Aubertin (2003)	Covers a wide range of plastic or non-plastic soils needs the specific surface of the soil	$$\log(k) = \log\left[\frac{e^3}{D_R^2 S_s^2(1 + e)}\right]$$
KCM (Aubertin et al., 1996; Mbonimpa et al., 2002)	Most often used to estimate k_{sat} of mine wastes	$$ksat\left(\frac{cm}{s}\right) = C_G \frac{\gamma_w}{\mu_w}\frac{e^{(3+x)}}{(1 + e)}C_U^{1/3}D_{10}^2$$

Where

C_U: Uniformity coefficient (D_{60}/D_{10})

C_G: Constant material parameter (MKC method, =0.1)

D_{10}: Sieve size that 10% of the particles (by size) passes it

D_5: Sieve size that 10% of the particles (by size) passes it

k_{sat}: Saturated hydraulic conductivity [LT^{-1}]

e: Void ratio [-]

S_s: Specific surface [L^2M^{-1}]

D_r: Specific gravity (or Gs) [-]

Different values of saturated hydraulic conductivity (k_{sat}) are presented in the literature, for various waste rock materials, Table 2-6 shows some of these results.

Table 2-6: Values of hydraulic conductivity from literature

Location	k_{sat} (cm/s)	References
Health steel mine, Cu, Zn, Ag	5.2×10^{-4}	Li (2000)
Quirke mine, Uranium	5×10^{-2}	Barbour, S.L et al. (2001)
Golden sunlight mine, Or	3.4×10^{-3}-1×10^{-4}	Herasymuik (1996)
KCM model KC model Labo (constant head) Labo (variable head) Labo (triaxial)	6.61×10^{-4}, 9.67×10^{-4}, 2.38×10^{-4} 3.38×10^{-4}, 6.58×10^{-4}, 4.46×10^{-4} 2.96×10^{-3}, 3.74×10^{-3}, 1.73×10^{-4} 2.54×10^{-4}, 1.34×10^{-3}, 2.34×10^{-4} 1.2×10^{-4}, 2.98×10^{-4}, 1.92×10^{-5}	Gamache-Rochette (2004); Aubertin et al. (2005)
various waste rock materials	10^{-7} to 1	Morin et al. (1991)
	4×10^{-3} to 3×10^{-1}	Lessard (2011)
Loose waste rock Compacted waste rock	4.7×10^{-1} 5.1×10^{-3}	Bussière and Aubertin (1999)
Loose waste rock	Up to 10^{-1}	Peregoedova (2012).

Unsaturated hydraulic conductivity

The theory of flow in unsaturated media shows that the hydraulic conductivity is not constant. It depends on volumetric water content (or matric suction), which also affects geotechnical properties. The variation of hydraulic conductivity is commonly represented by the relative hydraulic conductivity (k_r) function. It is the ratio of the unsaturated hydraulic conductivity to saturated hydraulic conductivity k_{sat} (Espinoza, 1999)

$$k_r(\psi) = \frac{k(\psi)}{k_{sat}} = \frac{k(\theta)}{k_{sat}} \qquad [2\text{-}3]$$

The range for the relative hydraulic conductivity varies between 1 and a very low value (close to 0). Figure 2-15 shows that the hydraulic conductivity decreases gradually when the soil de-saturates due to the presence of air in the mass. Testing results on different types of materials indicates that, saturated fine-grained soils have a lower hydraulic conductivity compared to saturated coarser grained soils. However, coarse materials desaturate faster (at lower ψ) compared to fine-grained soils, so their hydraulic conductivities decrease more rapidly (compared to fine-grained soils). In the unsaturated zone, a coarser material can have a lower conductivity than a finer material (Figure 2-15) (Aubertin et al., 2002a).
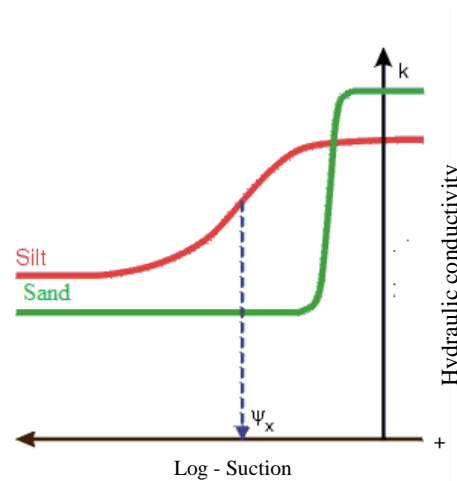
Figure 2-15: Schematic presentation of hydraulic conductivity curve for two types of soil, modified by Aubertin et al. (2002a)

Empirical models

Simple mathematical equations are used to predict the hydraulic conductivity function with empirical models. Numerous models have been proposed to represent the hydraulic conductivity in a variety of functional forms (Richards, 1931; Brooks and Corey, 1964; Campbell, 1974). Some of these are recalled below.

Statistical models are based on the assumption that the soil matrix is a network of capillary tubes of various sizes, where the flow through the network occurs only through the liquid-filled tubes. The controlling parameters for the overall hydraulic conductivity are the statistical distribution of tube sizes and their connectivity across a given plane in the soil mass. Some of the proposed models are:

van Genuchten (1980)- (Mualem, 1976) method (cited by Lu and Likos (2004):

$$k_r(\psi) = \frac{[1-(\alpha\psi)^{n-1}[1+(\alpha\psi)^n]^{-m}]^2}{[1+(\alpha\psi)^n]^{m/2}}$$
[2-4]

Fredlund et al. (1994) method

$$k_r(\psi) = \Theta^q(\psi)\frac{\int_{\ln(\psi)}^{b}\frac{\theta(e^y)-\theta(\psi)}{e^y}\theta'(e^{\acute{y}})dy}{\int_{\ln(\psi_{aev})}^{b}\frac{\theta(e^y)-\theta_s}{e^y}\theta'(e^{\acute{y}})dy}$$
[2-5]

Where:

y: dummy variable of integration representing ln (ψ)

b: ln (10^6)

ψ_{aev}: air entry pressure

θ': derivative of equation

Θ^q: correction factor for tortuosity (q=1)

The hydraulic conductivity in unsaturated conditions varies with θ_w (or ψ) nonlinearly.

The hydraulic properties of materials are expected to vary within a waste rock pile. For instance, the phenomenon of stratification, produced by either equipment movement or material

segregation, can create areas with higher or lower conductivity in the piles (Smith et al., 1995; Li, 2000; Zhan, 2000).

2.3.3 **Water flow in the unsaturated zone**

Darcy's law is commonly used to describe water flow in saturated soils. It was modified by Richards (1931) to express water movement through the unsaturated zone, considering the degree of saturation. Richards (1931) equation of transient unsaturated flow gives the relationship between the change in water pressure head and change in volumetric water content, considering the principle of continuity. This equation can be expressed as (Richards, 1931; Fredlund et al., 1978):

$$\frac{\partial}{\partial x}\left(k_x \frac{\partial h}{\partial x}\right) + \frac{\partial}{\partial y}\left(k_y \frac{\partial h}{\partial y}\right) + q = \frac{\partial \theta_w}{\partial t} \qquad [2\text{-}6]$$

With

θ_w: volumetric water content

h: hydraulic head [L]

k_x, k_y: conductivity of soil [LT^{-1}]

For unsaturated materials, the pore water pressure distribution and seepage pathways transient seepage can be described as:

$$\frac{\partial}{\partial x}\left(k_x \frac{\partial h}{\partial x}\right) + \frac{\partial}{\partial y}\left(k_y \frac{\partial h}{\partial y}\right) = -m_w^2 \gamma_w \frac{\partial h}{\partial t} \qquad [2\text{-}7]$$

With

m^2_w: slope of WRC [-]

γ_w: water unit weight [MT^{-2}L^{-2}]

k_x, k_y: hydraulic conductivity in x and y-direction [LT^{-1}]

h: hydraulic head [L]

The water distribution within waste rock piles is complex due to factors such as internal structure, and particles and pore size distribution and it is not easy to measure or predict (Molson et al.,

2005). A broad range of behavior can be observed in unsaturated materials (Fredlund, 2000a), with the range of negative pore pressure and degree of saturation (from near 100% in the capillary fringe to near zero near the surface).

2.3.4 **Apparent cohesion (c_{app})**

Effective cohesion c' of dry or saturated waste rock from hard rock mines is usually close to zero in the absence of cementing minerals (Aubertin, 2013)

In unsaturated soil, the capillary forces resulting from suction contribute cohesion between particles. This component is commonly called apparent cohesion (c_{app}). It reflects the effect of suction (u_a - u_w) on the effective stress and thus the shear strength (Ward and Robinson, 1967; Fredlund and Rahardjo, 1993; Lu and Likos, 2004), which can have a significant impact on the mechanical behavior of unsaturated soil. The total cohesion then becomes

$$C = c' + c_{app} \qquad [2\text{-}8]$$

Where c' is the effective cohesion [$ML^{-1}T^{-2}$] (c' ~ 0 for waste rock from hard rock mines).

The apparent cohesion c_{app} can be measured, e.g. (Narvaez, 2013) or it can be predicted using different formulations such as (Vanapalli et al., 1996):

$$c_{app} = (u_a - u_w) \tan \phi' \frac{(\theta - \theta_r)}{(\theta_s - \theta_r)} \qquad [2\text{-}9]$$

In these equations (u_a - u_w) is the matric suction (u_a and u_w are pore air pressure and pore water pressure respectively [$ML^{-1}T^{-2}$]); θ is volumetric water content; θ_s and θ_r are the saturated and residual volumetric water contents respectively. Other expressions have also been proposed to represent c_{app}, using different suction functions (e.g. (Öberg and Sällfors, 1997; Lu and Likos, 2004; Narvaez, 2013). Eq. 2-9 is used in this project, as it is already integrated in the numerical codes applied for the simulations and slope analyses (see below).

As a result of infiltration, the volumetric water content may change in the waste rocks, hence affecting the value of the apparent cohesion (c_{app}). It is considered conservative to neglect this apparent cohesion in the initial stability analyses, as its value is difficult to estimate or control and it may change over time. This aspect will be considered in this project.

2.3.5 **Unsaturated shear strength**

The main difference between slope stability analysis of saturated and unsaturated soils lies in the definition of shear strength.

The Mohr-Coulomb theory defines the failure (or yield) strength of soils with two parameters: cohesion within the soil and the internal friction angle (Holtz et al., 2010). It has long been used to represents the shear strength of saturated soil, using the effective stress in 2D (e.g. McCarthy, 2007)

The shear strength of unsaturated soil typically involves two independent stress state variables: the net normal stress and the matric suction which are introduced in the extended Mohr-Coulomb failure criterion (Fredlund, 1995, 2000a).

Different equations have been proposed to estimate the shear strength of unsaturated soils (Fredlund et al., 1978; Lee et al., 2005). The shear strength equations could either be a fitting type or prediction type, based on their nature. For the fitting type, the measurements of unsaturated shear strength at different matric suctions are needed (Fredlund et al., 1978; 1996; Shen and Yu, 1996; Vanapalli et al., 1996; Rassam and Cook, 2002; Lee et al., 2005; Vilar, 2006). Parameters correlated with the WRC are needed for the prediction type (Fredlund et al., 1996; Vanapalli et al., 1996; Öberg and Sällfors, 1997; Bao et al., 1998; Khalili and Khabbaz, 1998; Tekinsoy et al., 2004; Garven and Vanapalli, 2006; Guan et al., 2010). This method usually provides a good first approximation of unsaturated shear strength (Guan et al., 2010). Some of these equations are presented in Table 2-7.

Table 2-7: Equations for shear strength in unsaturated soils (different authors)

Author	Equation type	Equation
Fredlund et al. (1978)	F	$\tau = c' + (\sigma - u_a) \tan \phi' + (u_a - u_w) \tan \phi^b$
Fredlund et al. (1996)	F	$\tau = c' + (\sigma - u_a) \tan \phi' + (u_a - u_w)[\Theta(u_a - u_w)]^k \tan \phi'$
Shen and Yu (1996)	F	$\tau = c' + (\sigma - u_a) \tan \phi' + (u_a - u_w) \left(\dfrac{1}{1 + (u_a - u_w)d} \right) \tan \phi'$
Vanapalli et al. (1996)	F	$\tau = c' + (\sigma - u_a) \tan \phi' + \left[(u_a - u_w)\Theta^k \right] \tan \phi'$
Vanapalli et al. (1996)	P	$\tau = c' + (\sigma - u_a) \tan \phi' + (u_a - u_w) \left[\tan \phi' \left(\dfrac{\theta_w - \theta_r}{\theta_s - \theta_r} \right) \right]$
Öberg and Sällfors (1997)	P	$\tau = c' + (\sigma - u_a) \tan \phi' + (u_a - u_w)[\tan \phi' (S)]$
Khalili and Khabbaz (1998)	P	$\tau = c' + (\sigma - u_a) \tan \phi' + (u_a - u_w)[\tan \phi' (\lambda')]$ $\lambda' = \left[\left(\dfrac{(u_a - u_w)}{(u_a - u_w)_b} \right) \right]^{-0.55}$

Where

F: fitting equations; and P: predicting equations
c, c': cohesion, effective [ML^{-1}T^{-2}]
u_a, u_w: pore -air and pore-water pressure [ML^{-1}T^{-2}]
(u_a-u_w): matric suction [ML^{-1}T^{-2}]
$(u_a-u_w)_b$: air entry value [ML^{-1}T^{-2}]
Θ: normalized water content [-]
θ_r, θ_s, θ_w: residual, saturated and volumetric water content [-]
σ, $(\sigma-u_a)$: normal and net normal stress [ML^{-1}T^{-2}]
τ: shear strength [ML^{-1}T^{-2}]
ϕ': effective internal friction angle of saturated soil [-]
ϕ^b: internal friction angle with respect to matric suction [-]

The failure envelope intersects the shear stress versus matric suction plane as shown in Figure 2-16. The equation for the line of intercept is the total cohesion, which can be defined as Equation 2-8 (Rahardjo et al., 1996):

$$C = c' + (u_a - u_w) \tan \phi^b \qquad\qquad [2\text{-}10]$$
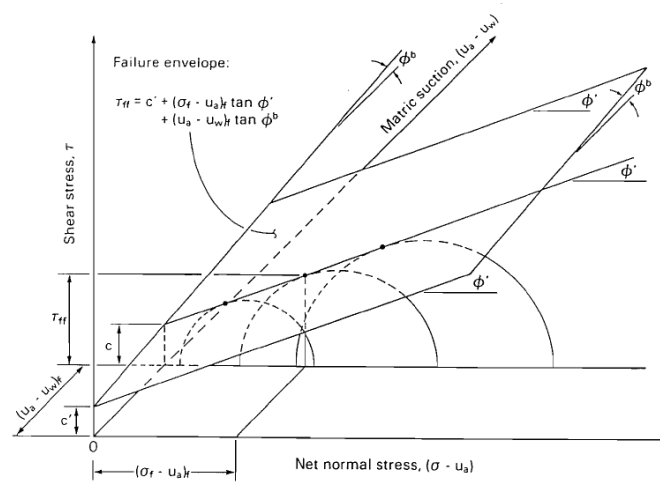
Figure 2-16: Extended Mohr-Coulomb failure envelope for soils with matric suction

 (Rahardjo et al., 1996)

The equations presented in Table 2-7 implies that the total cohesion C depends on apparent cohesion generated by the matric suction and effective cohesion c'.

For points with suction lower than AEV ($\psi < \psi_0$), there is usually a linear relationship between shear strength and matric suction, whereas the strength between the AEV (ψ_0) and residual matric suction (ψ_r) obeys a nonlinear relationship (Vanapalli et al., 1996; Bao et al., 1998; Rassam and Williams, 1999; Lee et al., 2005). Beyond the residual matric suction, the shear strength of an unsaturated soil is not well defined (Vanapalli et al., 1996; Guan et al., 2010).

2.4 Slope stability analysis

Slope failures happen worldwide and may result in considerable loss of lives and damages. A slope failure is a complex process which is determined by internal and external factors, with gravity as the main force (Terzaghi, 1950; Selby, 1982). Stability of waste rock piles can be a major concern because of the risks involved such as human and financial damages (e.g., waste rock pile failure in Jade mine Kachine state, Myanmar in May 2916 lead to the death of at least 12 people (Adamczyk, 2016); failure in Gold Quarry Mine (Nevada) in February 2005 (Sheets and Bates, 2008)).

A slope failure can result from two processes: increased shear stresses (such as: removal of support, overloading, earthquakes, decrease in lateral pressure) or decreased shear strength of the soil (such as: stratification, hydration of minerals, of pore pressure due to rainfall event or melting snow) (Abramson et al., 2002).

The stability of a slope is assessed using the factor of safety FS (= Capacity/Demand). There exist different definitions for the factor of safety, and all involve the shear strength of the soil. The basic method is to define the factor of safety based on the ratio of the moments resisting sliding (or the resisting shear force) to the moments causing sliding (or driving shear force); FS can also be expressed as the ratio of soil shear stress to soil shear strength imposed along a slip surface (considering a constant factor of safety along the potential failure surface) (Cheng and Lau, 2014).

A factor of safety of unity theoretically means that the failure mass is on the verge of sliding (Gofar and Kassim, 2007). It is necessary to provide a reasonable value for the factor of safety that satisfies both safety and economic conditions. Table 2-8 presents minimum values of FS proposed by different authors. A long term FS equal to 1.5 is often recommended in the literature.

For waste rock piles, the value of FS for slope stability should be between 1.3 and 1.5 during mining operation; FS = 1.5 is recommended for the long-term behavior upon closure. This means that α (global slope) $\leq 26°$ for piles constructed on most hard rock mine sites, with $\phi = 37°$ (Aubertin, 2013).

Table 2-8: Relative importance of different factors of safety (based on literature, for relatively large structure, obtained from different methods)

Factor of safety	Significance	References
Less than 1	Failure	Cheng and Lau (2014)
1.0-1.2	Questionable safety	
1.3-1.4	Satisfactory for cuts questionable for dams	
1.5-1.75	Safe for dams	
FS < 1.07	Unstable slope	Bowles (1984)
1.07 < FS < 1.25	Critical slope	
FS > 1.25	Stable slope	
FS < 1	unstable	Modified from Ray and de Smedt, (2009)
1 < FS < 1.25	Quasi stable	
1.25 < FS < 1.5	Moderately stable	
FS > 1.5	Theoretically stable	

The analysis of slopes often distinguishes between infinite (very long) and finite slopes. Infinite slopes extend over a considerable distance within the soil mass, whereas finite slopes are characterized by a limited height with a base and a top surface. From the stability point of view, these two types of slopes are treated differently.

2.4.1 Methods of slope stability analysis

Infinite slope stability analysis

The critical slip surface (related to the lowest factor of safety), for slopes composed of cohesionless materials and without seepage forces, is typically shallow, planar, and parallel to the inclined slope surface. The factor of safety can then be evaluated using infinite slope stability analysis (Cornforth, 2005; McCarthy, 2007).

Simple equations can be used to calculate the factor of safety (FS= C/D) for different conditions related to infinite slopes; the most commonly used ones are listed in Table 2-9:

Table 2-9: Simplified Methods of Analysis for Waste Dumps from Caldwell and Moss (1981)

Soil type	Mode	Factor of safety	Parameters
Cohesionless soil	Dry condition	$$FS = \frac{\tan \phi}{\tan i}$$	i: slope angle ϕ: angle of friction of pile material
Cohesionless soil	Submerged, subject to groundwater flow	$$FS = \frac{\gamma_{sub}(\tan \phi')}{\gamma_{total}(\tan i)}$$	i: actual slope angle ϕ': angle of friction of pile material γ_{total}: wet soil unit weight above water γ_{sub}: submerged soil weight
Cohesive soil	Dry	$$F = \frac{c}{\gamma Z \sin i \cos i} + \frac{\tan \phi}{\tan i}$$	i: actual slope angle ϕ: angle of friction of pile material
Cohesive soil	Submerged, subject to groundwater flow	$$F = \frac{c'}{\gamma Z \sin i \cos i} + \frac{\gamma_{sub}(\tan \phi')}{\gamma_{total}(\tan i)}$$	i: actual slope angle ϕ': angle of friction of pile material γ_{total}: wet soil unit weight above water γ_{sub}: submerged soil weight

Finite slope analysis

The critical slip surfaces for slopes composed of cohesive soil or affected by seepage are often (quasi) circular. This assumption is based on various observations of failed slopes, which usually show that the failure mass moves downward and outward. In most designs or slope failure investigation, a 2D analysis is used as it gives reasonable results that stand on the safe side (Sun et al., 2012).

Slope stability analysis is typically conducted with the limit equilibrium method (first applied in geotechnical problems by Coulomb, 1773). This has led to the development of the method of slices for slopes. The main advantages of this method are the simplicity and long history of use. It can also handle relatively complex slope geometries, variable soil conditions, and the influence of external boundary loads (Abramson et al., 2002).

In its basic form, this approach assumes a failure surface and implicitly considers the stresses on the failure planes are limited by the strength parameters C and ϕ'. The soil mass above the slip surface is divided into several vertical slices (with the number of slices defined by slope geometry and soil profile). Each slice is considered as a single element for limit equilibrium. The

total weight of each slice (plus the weight of water or any other forces acting on the surface) is considered. Equilibrium is analyzed in terms of the sum of the forces and/or moments acting on the slices (Nash, 1987; Duncan and Wright, 2005). The principle of limit equilibrium states that the sum of the driving forces (or moments) are equal to the resisting forces (or moments) for a factor of safety against slope failure equal to unity (FS = C/D = 1). The actual value of FS for a specific slope is then given by calculating the capacity (resisting forces/moments) and demand (driving forces/demand), for the critical slip surface (with minimum FS).

Applying this method requires iterative techniques. In this process, a possible slip surface is assumed and is divided into several slices. The equilibrium of forces acting on this surface is studied, and the process is repeated until the critical slip surface (with a minimum factor of safety) is found.

Different methods based on limit equilibrium techniques have been developed to evaluate the stability of slopes. The differences between these equations mainly on the inter-slice forces and shape of the slope surface and the assumed relationship between the inter-slice shear and normal forces (Krahn, 2007c). These methods assume that pore water pressures are positive or zero along the slip surface (Bishop, Allan W, 1954; Morgenstern and Price, 1965; Spencer, 1967; Duncan, 1996).

Many different types of failure analysis with the method of the slices are presented in the literature. A summary of these methods with description and different types of calculation approaches is presented in Table 2-10.

There are also slope stability charts developed by different authors that can be used for solving the stability problems, (e.g. Taylor, Bishop-Morgenstern, Barens and Spencer and Cousins charts).

Table 2-10: Some methods for slope failure analysis, adopted from McCarthy (2007)

Failure analysis method		Typical applications and limitations
Bishop method (Bishop, AW, . 1954)	$$FS = \frac{\sum \frac{1}{m_a}[c'b + (W - ub)\tan\varphi]}{\sum W \sin\alpha}$$ • Unrealistic high FS when (α) approaches a value of about 30° • Less conservative compared to Fellenius method	• Circular failure surfaces • all soil types • consider force equilibrium • less conservative compared to Fellenius method • Rigorous method
Simplified Bishop method	• Inter-slice forces are horizontal • No inter-slice shear forces	• Circular failure surfaces, all soil types • Semi-rigorous method
Morgenstern-Price method (Morgenstern and Price, 1965)	• Considers the normal and shear force on the slice side including the water pressure • Satisfies the equilibrium of forces and moments • Direction of the resultant inter-slice defined using arbitrary function	• Circular and noncircular failure surfaces • all soil types • Rigorous method
Spencer method (Spencer, 1967)	• Assume the forces on the sides of slices are parallel • Satisfy the equilibrium of forces and moments. • Resultant inter-slice forces are of constant slope throughout the sliding mass	• Circular and noncircular failure surfaces • all soil types • Rigorous method
Noncircular slip surface method (Janbu, 1959, 1975)	$$FS = \frac{f_0 \sum[c'b + (W - ub)\tan\varphi]\frac{1}{\cos\alpha\, m_a}}{\sum(W \tan\alpha)}$$	• Considers the slices and forces on them as for force and moment equilibrium in horizontal and vertical direction. • The inter-slice forces are neglected initially • Calculated FS is modified by applying an empirically determined correction factor

In real situations, the pore water pressure and degree of saturation can be highly variable along the slip surface (negative and positive) (Godt et al., 2009; Borja and White, 2010; Buscarnera and Whittle, 2012). This analysis needs more advanced methods to assess slope stability (Duncan, 1996; Dawson et al., 1999; Lu and Likos, 2004; Song et al., 2016). In recent years methods such as "gravity increase method," "strength reduction method" are developed for a more accurate calculation of factor of safety and the failure surface (Dawson et al., 1999; Griffiths and Lane, 1999; Krahn, 2007c; Lu et al., 2012). Such an approach is used in the following chapters of this thesis.

2.4.2 **Factors affecting slope stability**

There have been several examples of waste rock pile instability around the world which resulted in failure and loss of life and/or other damages (Caldwell and Moss, 1981; Upadhyay et al., 1990; Bian et al., 2009; Yellishetty and Darlington, 2011).

The stability analysis of unsaturated slopes is a complex problem. It can be evaluated by a broad range of approaches, from simple limit equilibrium solutions to advanced finite element method analyses (Gavin and Xue, 2010).

Failure of a pile is associated with the uncontrolled release of pile materials beyond its confines (Robertson and Clifton, 1987). Many factors such as the properties of the waste rock, geometry of the pile (i.e. angle of slope, height), foundation conditions (i.e. weaker materials compared to the pile), topography, seepage and pore pressures (Piteau Associates Engineering Ltd., 1991; Moffitt, 2000; Walker and Johnsonf, 2000; Aubertin et al., 2002a; McLemore et al., 2009) and seismicity may also impact the stability of a waste rock pile (Piteau Associates Engineering Ltd., 1991; Hustrulid et al., 2000).

The method and rate of construction and the resultant stratification may also have an impact on the waste rock pile stability. The internal structure of pile influences the water flow within the pile and also the shear strength distribution. As mentioned in section 2-1-4, the end-dumping or push-dumping methods result in an accumulation of coarser particles at the toe (at the angle of repose) and the presence of finer particles at the crest creating inclined stratification on the slope. On the other hand, the movements of heavy equipment on the surface form sub-horizontal

(denser) layers within the pile (crushing and compacting). The horizontal and inclined stratification and heterogeneity influences the water flow inside the piles.

Materials with a high percentage of fine grains or a rapid rate of dumping may increase the possibility of pile failure due to the generation of excess pore water pressure (Caldwell and Moss, 1981).

The failure can happen in either sudden or slow modes. The sudden modes usually follow extreme events such as large precipitations, earthquakes or volcanic activity. The slow modes are mainly due to factors such as seepage, wind/water erosion, material degradation, chemical and biological reactions (Hutchinson, 1988; Tachie-Menson, 2006). Human activities (such as loading on the slope or excavating of the toe) can also play a role (Anderson and Sitar, 1995; Iverson, 2000; Sassa et al., 2007).

The stability of waste rock piles depends specifically on the strength distribution within the pile, which may be affected by local pore water pressures (Caldwell and Moss, 1981; Robertson, 1985; Basile et al., 2003). Water movement within the pile should be considered as part of the stability analysis process as it controls the water distribution and pore water pressure which in return, influences the stability (Wilson, 2000).

Hence, the knowledge of the internal structure and hydraulic properties of waste rock materials is required. Some of these factors are discussed in more details in the following.

Observations of waste rock piles instabilities indicate that multiple failure modes should be considered. The four main types of sudden (intense) failures in waste rock piles are (Pernichele and Kahle, 1971):

- Debris flow (flow slide)
- Foundation failure (for piles on relatively weak soils)
- Edge slump
- Blowout (when elevated hydraulic pressures in some layers result in decreasing effective internal stress and stability)

Specific observations about the various modes of failure occurring in waste rock piles are described in Table 2-11 (Caldwell and Moss, 1981).

Table 2-11: Different modes of failure in waste rock piles, adopted from Caldwell and Moss (1981)

Failure mode	Initiating causes	Consequences
Surface or edge slides	• In crest tipped piles • Over steeping due to accumulation of fines or temporary cohesion	• Movement of material down the slope considering the foundation inclination and embankment area
Shallow flow slide	• Infiltration of rain or snowmelt results in flow parallel to the face	• Substantial damage • Failure can cover large distances rapidly
Base failure	• Coverage of flat ground by a thin layer of weak material • Excessive pore pressure • Excessive height • Decay of organic matter • Earthquakes	• Disturbance initially limited to immediate vicinity of slope • Progressive movements if dumping continues • Intermediate suspension of dumping operations • Piles on flat ground the least likely to fail
Block translation	• End-dumped or layer placed construction method • Pile on inclined ground with thin/weak soil cover • Melting snow or groundwater • Decay of organic matter • Earthquakes	• Suspension of dumping operations dependent on natural ground slope
Circular arc failure	• High water tables • Earthquakes • Decay of organic material beneath the pile • Excessive height (cohesive material) • Reduction in toe support	• Partial loss of dump • Common in piles with high percentage of fine grain soil
Foundation circular failure	• Weak foundation materials • Excessive pore pressure	• Major disturbance • Loss of dump
Toe spreading	• Weak foundation materials • Excess pore pressure in foundation	• Signals on-set of base failure or block translations

Rainfall infiltration and the stability of slopes

Many authors have studied the stability of unsaturated slopes by including matric suction (negative pore water pressure) in stability analyses (Cho and Lee, 2001; Rahardjo et al., 2007; Muntohar and Liao, 2009). The effect of rainfall on slope stability has also been frequently investigated (Ng and Shi, 1998; Rahardjo et al., 2005; Huat et al., 2006; Guzzetti et al., 2007; Xue and Gavin, 2008; Rahimi et al., 2010; Kim et al., 2012; Tang et al., 2015). These investigations cover a wide variety of parameters including different soil types, rainfall duration and intensity, initial conditions and location of the phreatic surface (Gasmo et al., 2000; Rahardjo et al., 2001; Cai and Ugai, 2004; Rahardjo et al., 2010; Napolitano et al., 2015).

During the process of infiltration (highly complicated due to nonlinearity of water retention and hydraulic conductivity curves) a transformation in the strength profile within a slope can occur due to the variation of pore water pressures (Igo, 2006; Indrawan et al., 2006) (Mukhlisin et al., 2006; Yang et al., 2006; Lee et al., 2011). The rate and depth of infiltration depends on the initial soil condition (i.e. water content or suction) and hydraulic conductivity (Rahardjo et al., 2007; Fala et al., 2008; Rahimi et al., 2010), slope angle, vegetation and also the rainfall intensity and duration (Gavin and Xue, 2010; Pirone et al., 2015)..

Coarse materials (i.e. gravel, sand) usually have higher infiltration rates compared to fine materials (i.e. clay, silt). Soils with uniform particle sizes show higher infiltration rate compared to well-graded particle sized materials. A common assumption for geotechnical studies of sloped surfaces is that on a sloped surface, all precipitation more than the immediate infiltration capacity becomes runoff, and surface storage is assumed to be negligible (O'Kane et al., 2002).

The failure process due to infiltration can be classified into two types: generation of positive pore water pressure and dissipation of matric suction (Au, 1998; Chen et al., 2004; Collins and Znidarcic, 2004; Zhang et al., 2011). These are described briefly below.

Infiltration and groundwater level

Rainfall can influence the piezometric level. The infiltration into the ground surface and groundwater seepage may raise the groundwater table (or develop a perched water table) resulting in a reduction of effective stresses and a corresponding decrease of soil strength (Jones et al., 1961; Moregenstern, 1963; Lane, 1966; Deng et al., 2000; Lane and Griffiths, 2000; Dai et al., 2004; Zhan et al., 2006; Jia et al., 2009; Zhou et al., 2009).

Infiltration and wetting front

The negative pore water pressures distribution is dynamic and changes with time. Rainfall on a pile usually flows downward (and partly sideways) and may lead to a decrease of matric suction with wetting that results in the reduction of shear strength of the material (WANG and CAO; Fredlund and Rahardjo, 1993; Li et al., 2005; Rahardjo et al., 2005; Guan et al., 2010). Such infiltration may lead to either shallow slides in the slope or deep-seated failures depending on hydraulic conductivity and the intensity and duration of rainfall (Laloui et al., 2010).

Traditional slope stability analysis usually considers the main effect of infiltration as increasing of groundwater level; however there exist many real slope failure cases with no evidence of groundwater level increasing but the development of wetting front and the reduction of shear strength due to the matric suction has been observed (Fredlund and Rahardjo, 1993; Rahardjo et al., 1996). For the cases of unsaturated slopes with a deep water table that usually stays stable, failures (mostly shallow landslides) are typically related to infiltration and advancement of wetting front (Selby, 1982; Kirkby, 1987; Benda and Cundy, 1990; Lim et al., 1996; Toll et al., 1999; Williams, 2000; Rahardjo et al., 2005).

Rainfall pattern

For materials with a high hydraulic conductivity (e.g. waste rock), the water infiltration and evolution of pore water pressures can be relatively rapid, even during an intense rainfall. The majority of slope failures for such type of materials seems to be due to high-intensity rainfalls, with little effect of antecedent rainfalls (Gerscovich et al., 2006). In these cases, both intensity and duration of the rainfall may have important contributions to potential instability (Lumb, 1975; Fourie, 1996).

One of the parameters that can be estimated and used in the design of large constructions such as waste rock piles is the Probable Maximum Precipitation (PMP). PMP is defined as "theoretically the greatest accumulation of precipitation for a given duration that is physically possible over a given size storm area at a particular geographical location at a certain time of year" (WMO, 1986).

The PMP for a particular geological zone can be estimated using different methods for duration of 24 hours (but can vary from 6 to 72 hours). Table 2-12 shows different estimations of PMPs related to various locations by different authors.

Table 2-12: Different PMPs estimation for different regions

PMP (24 hrs)	Location	References
65-310 cm	Sri Lanka	Wickramasuriya (2011)
31- 49 cm	Malaysia (region of Selangor)	Noriah and Rakhecha (2001)
30-110 cm	India (region of the Godavari river basin)	Kulkarni (2002)
50-100 cm	India (different location)	Rakhecha and Clark (1999)
13-48 cm	Thailand (heavy storm data from 1972 to 2000)	Kingpaiboon S.; Netwong T. (2004)
58-125 cm	Hong Kong	Wang (1998)
102-112 cm	Hainan coast	
77-98 cm	Hawaii	
370 mm	southern Quebec	ASCE (1996), SNC-LAVALIN (2004)
350 mm	Abitibi (Rouyn-Noranda, Val Golden)	SNC-LAVALIN (2004)
300 mm	North Shore (Sept-Îles)	

2.4.3 **Probabilistic stability analysis**

Soil structures (e.g., slopes) are usually formed from different layers (zones) of materials. Each zone may consist of soil with relatively uniform property distribution, which can be presented by a single value for each characteristic. This assumption usually leads to a deterministic slope stability analysis, resulting in a single factor of safety.

In reality, soil property values are not constant even within a given zone (or layer). They may change from one point to another leading to a heterogeneous distribution. Hence, a deterministic

factor of safety is not sufficient in these cases. The uncertainty in input parameters should be considered in the analysis to determine the risk of slope failure (Li and Lumb, 1987; Haldar and Mahadevan, 2000). Such uncertainty may be due to different factors such as insufficient tests, natural spatial variability, or human error (El-Ramly, 2001). These may affect the performance of the slope and the analysis.

Monte-Carlo simulation-based probabilistic analysis is a powerful method that can help with the evaluation of slope stability, by considering the uncertainties of input parameters (Alonso, 1976; Vanmarcke, 1977b; Li and Lumb, 1987; Gui et al., 2000; El-Ramly, 2001; El-Ramly et al., 2002; Christian, 2004). The output of probabilistic analysis usually provides more information about slope performance than just a unique factor of safety (in the form of the reliability index and probability of failure). These aspects are briefly reviewed in the following.

2.4.3.1 Sources of uncertainty

Different types of uncertainty may affect slope stability. These uncertainties may be divided into three main categories including parameter uncertainty, model uncertainty and human uncertainty (Tang, 1984; Kulhawy, 1993; Morgenstern, 1995).

Parameter uncertainty can be categorized in different ways (Vanmarcke, 1977a; Tang, 1984; Phoon and Kulhawy, 1999; Gui et al., 2000; Baecher and Christian, 2003; Zhang, 2005). These uncertainties may be due to different factors such as spatial variability, bias in measurements and sampling with field or laboratory techniques, limitation due to number of samples, difference between the actual behaviour and the mechanical model (Christian et al., 1994; Phoon and Kulhawy, 1999; Baecher and Christian, 2003). Uncertainties in input parameters can lead to uncertainties in output parameters (e.g. factor of safety) and the probability of failure. Soil properties uncertainties may be represented by data statistics (such as mean value and standard deviation). Model uncertainty relates to the limitation and simplification in the selected theory and simulation tools used in predicting the slope performance (Krahn, 2007c). Human uncertainties are related to mistakes and errors made by humans.

Monte-Carlo method

In this research project, the Monte-Carlo method implemented in SLOPE/W (Krahn, 2007c) is used to conduct probabilistic analyses and evaluate the factor of safety, reliability index and the probability of failure.

Such probabilistic analysis has been considered for several years to assess the effect of uncertainty in slope stability (Li and Lumb, 1987; Oka and Wu, 1990; Duncan, 2000; Whitman, 2000; Duncan and Wright, 2005; Griffiths et al., 2009; Duncan et al., 2014).

The Monte-Carlo method is effective, and common method to perform a probabilistic analysis (El-Ramly, 2001; El-Ramly et al., 2002; Cho, 2007; Griffiths et al., 2009; Cho, 2010). In Monte-Carlo simulations, the stochastic process is simulated by the random selection of input variables (with statistical distribution). Random numbers are generated, and the deterministic analysis is performed for each set of values (for the properties distributed in the soil mass). The analysis of all the results from multiple calculations represents the probability density function of output parameters (e.g. factor of safety FS) based on the probability distribution of input parameters (such as internal friction angle and cohesion). The output results can be analyzed to determine the probability of failure PoF and the reliability index. This method of simulation is powerful and suitable for both linear and non-linear problems. A reliable distribution of outputs usually requires a significant number of simulations with different sets of random numbers (characteristics).

The Monte-Carlo simulation technique is implemented in some commercial slope stability analysis software such as SLOPE/W, which is used in this study. SLOPE/W is first used to perform a typical deterministic slope stability analysis, with representative values of input parameters (e.g. internal friction angle, cohesion). This gives a single value of factor of safety and the related critical slip surface. This critical slip surface is then used to perform probabilistic analysis with the statistical distribution of input variables as described below.

Monte-Carlo input parameters

One approach to generating a probabilistic analysis for slope stability is to "sample" the soil properties. For this purpose, the proper mean values for input parameters are selected. The probability distribution function is then defined based on the former. Another approach is to consider at the onset spatial variability of input parameters (El-Ramly et al., 2002; Griffiths and Fenton, 2004; Cho, 2007). The total uncertainty for each variable is represented by the sum of two types of uncertainties, related to the statistical distribution and the spatial variability of the input variable, as described below.

- Uncertainty of input parameters

Soil properties can be defined as random variables using the mean value and standard deviation (or coefficient of variation) and a probability distribution function.

Figure 2-17 (a) and (b) present a soil property defined deterministically and with its uncertainty respectively. The appropriate deterministic value can be selected based on the available data (number of tests, expected a range of values, etc.), the type of problem and past experiences.
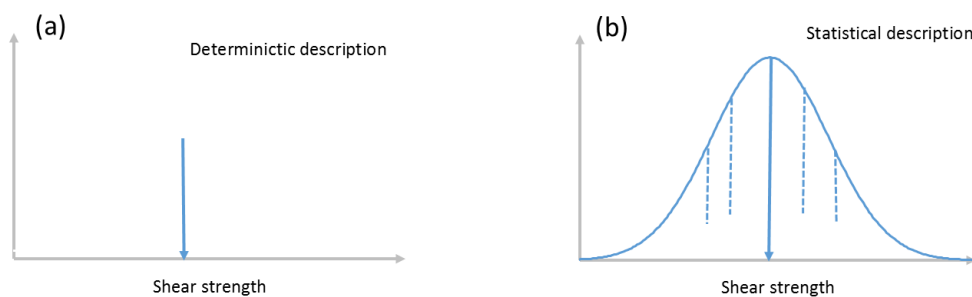
Figure 2-17: Deterministic and statistical description of soil property (taken from Griffiths, 2007)

The coefficient of variation (COV) is a standardized measure of the dispersion of a probability distribution. It is usually expressed as a percentage that represents the ratio of the standard deviation (σ) to the mean (μ):

$$COV\% = \frac{\sigma}{\mu} X100 \qquad\qquad [2\text{-}11]$$

The COVs values are different from one site to another and for different properties. Representative values of COV have been given in the literature for different materials and properties. Usually, there is no need to consider all the parameters variability. Only the parameters whose variability has a significant effect on the analysis need to be modeled as random variables.

The coefficient of variation for soil properties measured in the field can be as large as 100%; although values of 30-50% are more common (Agaiby et al., 1996; Phoon and Kulhawy, 1996). Most geotechnical parameters have COVs within the range of 0 to 68% (Duncan, 2000). Table 2-13 gives some typical values for ϕ' from various sources.

Table 2-13: COV for the internal friction angle ϕ' of different soils submitted to various engineering tests

Material type	Reported COV (%)	Source
Sand	5-15 5-11 (mean value 37.6) 13-14 (mean 14) 2-5 12 5-15 15-25	Singh (1972); Höeg and Murarka (1974); Lumb (1974); Schultze (1975) from Lee et al. (1983) Phoon and Kulhawy (1996) Phoon and Kulhawy (1999) Lacasse (1996) Harr (1987) Becker (1997); Cherubini (1997) from Cherubini (2000) Barker et al. (1991) from Becker (1997)
Clay, silt	12-56 10-50 (mean value 15.3) 4-12 (mean value 33.3) 7-56 (mean 24) 3-29 (mean 13) 6-20 10-50 5-25	Singh (1972); Lumb (1974); Schultze (1975) from Lee et al. (1983) Phoon and Kulhawy (1996) Phoon and Kulhawy (1999) Phoon and Kulhawy (1999) Phoon (1995) Becker (1997); Cherubini (1997) from Cherubini (2000)
Various soils (Laboratory measured)	9	Lumb (1966)
Compacted fill	20	White et al. (2005)
alluvium	21	
Highly weathered shale	38	
Moderately weathered shale	44	
Slightly weathered shale	48	
Gravel	7	Harr (1987)
Different material From laboratory test	5-25	Manoliu and Marcus; Cherubini et al. (1993); Kulhawy (1993); Meyerhof (1995) from Becker (1997)

Based on extensive studies, three ranges for the effective internal friction angle ϕ' will be considered in this project: the low COVs (5%-10%), medium COVs (10%-15%) and high COVs (15%-20%) (based on Phoon, 1995).

As stated above, SLOPE/W is used for a deterministic failure surface and then performs a probabilistic analysis on this same surface (slip surface does not vary). In SLOPE/W, the input parameters can be presented by various probability distribution functions, such as normal, lognormal, and uniform functions; the normal and lognormal are the most widely used distributions (El-Ramly, 2001). In this thesis, the normal distribution is used. The probability distribution of the resulting factor of safety is calculated by using a Monte-Carlo method and SLOPE/W (Krahn, 2007c)

- Uncertainty and spatial variability

To define the spatial variation of soil properties at a site, one needs to perform characterization tests. Such spatial variability represents the variation of soil properties from one point to another, even within a so-called homogeneous zone (Lacasse, 1996).

A large amount of data is usually needed to evaluate the spatial variability of geotechnical engineering properties. The spatial variability may be affected by different factors such as in situ variability (due to variation in mineralogy), deposition condition, physical and mechanical decomposition process or measurement errors due to sample distribution, limited availability of in-situ information and stress history, test imperfection and human factors (Vanmarcke, 1977a; Lacasse and Nadim, 1997). It is usually requested by the correlation length, describing the distance over which the spatially random values will tend to be significantly correlated (Vanmarcke, 1983). The evaluation of this length is often difficult due to a large amount of data needed. Extensive literature reviews on the values of correlation length indicate that depending on the geological history and composition, the length in horizontal direction typically varies between 10 to 40 m while it may be between 0.5 to 3 m in the vertical direction (Phoon and Kulhawy, 1996; El-Ramly, 2001; Hicks and Samy, 2002).

The spatial variability (defined as *sampling distance* in SLOPE/W) may have a significant effect on the probability of the failure, especially when the length of potential slip surface is larger in

one material. Numerical studies have shown that ignoring the spatial variation of soils properties often lead to an overestimated factor of safety and by an over or underestimation of the probability of failure (Griffiths et al., 2009; Wang et al., 2010).

SLOPE/W uses limit equilibrium methods to analyze the stability. The factor of safety calculations considers the strength at the mid-point of each slice. The uncertainty of the average shear strength along the slip surface appears to be an appropriate measure of uncertainty (Anderson et al., 1984; Baecher, Gregory, 1987; Li and Lumb, 1987).

SLOPE/W tracks the slip surface for each trial as a part of a spatial variability analysis. The statistical parameters are sampled where the horizontal distance along slip surface exceeds the pre-defined sampling distance or where the slip surface enters new materials.

SLOPE/W proposes three options for including spatial variability along the slip surface, based on the number of times the statistical soil properties are sampled. The first option is sampling the probabilistic data only once for the entire slip surface; such one-time sampling usually gives the highest probability of failure, due to the larger trial runs with a factor of safety smaller than one. This option does not seem appropriate (Krahn, 2007c). The second option is sampling the probabilistic data for each slice along the slip surface, which results in a lower probability of failure due to the significant fluctuation of soil properties within the slip surface and the tendency towards an average condition. This may not be realistic (Krahn, 2007c).The third option (used here) is to sample properties at a specific horizontal distance along the slip surface (as recommended by Krahn (2007c).

Monte-Carlo Output parameters

Probabilistic slope stability analyses are based on the same principles as deterministic methods (e.g. limit equilibrium) with the advantage of considering the uncertainties of selected parameters. The factor of safety indicates the relative stability of a slope, but it does not directly provide information on the actual risk of slope failure. The outputs of probabilistic analyses provide additional information about slope performance. The analysis can be used to evaluate two useful indices, i.e. reliability index RI and the probability of failure PoF (El-Ramly, 2001). These can help quantify the risk of a slope failure. It is also possible to calculate the mean factor of safety and its related variance.

The probability density function for the factor of safety follows the same probability density function as the input parameters, which is usually the Normal (Gaussian) distribution for simplicity. This Normal distribution is the most common function used for probabilistic studies in geotechnical engineering (Krahn, 2007c). It represents the factor of safety with a mean value (μ) and a standard deviation (σ).

- Reliability index RI

A method has been developed to evaluate the stability of geotechnical structures (such as slope) and the related risk of instability, by calculating a parameter known as the reliability index RI (or β). It is related to the probability that the slope remains stable under a specific set of conditions (Duncan and Wright, 2005).

The values of RI (or β) are based on the margin of safety MS = C-D (instead of FS = C/D). RI is related to the mean (μ) and the standard deviation (σ) of MS. The value of RI gives the number of standard deviations that separates the mean factor of safety from FS=1.

The Reliability Index is usually defined as the ratio of the mean factor of safety minus one is the related standard deviation (Alonso, 1976; Bergado and Anderson, 1985; Christian et al., 1994):

$$\text{Reliability Index } (\beta \text{ or RI}) = \frac{\mu_{FS} - 1}{\sigma_{FS}} \qquad [2\text{-}12]$$

The Reliability Index reflects both the mechanics of the problem and the uncertainty of the input parameters. The combination of a factor of safety and reliability index helps identify which failure has the lower amount of uncertainty related to input parameters.

USACE (1997) made recommendations for the acceptable value of the reliability index (RI) in geotechnical projects. It suggested that a value of RI of 3 or more is needed for an above average performance. For major structures such as dams, it should be closer to 5. Table 2-14 presents the ranges for reliability index and the probability of failure indicated by U.S. Army Corps of Engineering.

Table 2-14: Expected levels of performance regarding probability of failure and corresponding reliability indexes (U.S. Army Corps of Engineers, 1999)

Expected performance level	Reliability index (β)	Probability of failure (PoF)
High	5.0	0.0000003
Good	4.0	0.00003
Above average	3.0	0.001
Below average	2.5	0.006
Poor	2.0	0.023
Unsatisfactory	1.5	0.07
Hazardous	1.0	0.16

- Probability of failure

The probability (likelihood) of failure represents the probability of having a factor of safety less than one, or the ratio of the number of calculation with a factor of safety less than one to the total number of iterations in the calculations.

The probability of failure can be obtained by calculating the area under the PDF curve that is less than the value of the limit state (FS=1) (see Figure 2-19). The probability of failure (PoF or P_f) can be determined as:

$$P_f \text{ (PoF)} = 1 - \psi(\text{RI}) \qquad\qquad [2\text{-}13]$$

This probability of failure shows the likelihood of slope failure without any consideration of time effect.

There is no direct relation between the factor of safety and the probability of failure of a slope (e.g. a slope with a higher FS may be more stochastically vulnerable to failure compare to a slope with lesser FS). Figure 2-18 represents two different probability analysis for a pile foundation (Lacasse, 1996). It indicates the normal distribution for the factor of safety. The original design showed an FS of 1.79 with a probability of failure (PoF= P_f) of 5×10^{-3}. An updated analysis gave FS=1.4 with $P_f = 1\times10^{-4}$. This comparison indicates that the higher FS may have a higher probability of failure.

A probabilistic analysis can provide a consistent measure of safety; hence, designs with equal probabilities of failure (or reliability index) would have a more uniform level of safety compare to designs with an equal factor of safeties. Baecher (1987) indicated that the targeted probability of failure should be around 0.0001 as an acceptable probability of failure for large geotechnical engineering structures (Baecher, Gregory B, 1987).
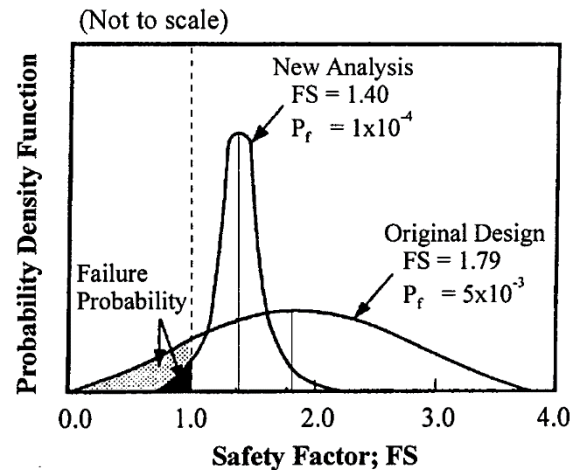
Figure 2-18: Comparison of two probabilistic analysis of a deep pile foundation (adopted from El-Ramly (2001) modified from Lacasse (1996)

The probability of failure is sensitive to sampling distance, especially when there are few probabilistic input variables. When the shape of the probability distribution of the factor of safety is known, the reliability index can be related to the probability of failure. Figure 2-20 shows the probability of failure for a normal distribution of the factor of safety. It is seen that as the probability of failure decreases, the reliability index increases. Table 2-14 can explain figure 2-19. For instance, moving from PoF (0.6) with RI zero to PoF (0.0001) with RI 3.7 put the hazardous structure in good performance level.
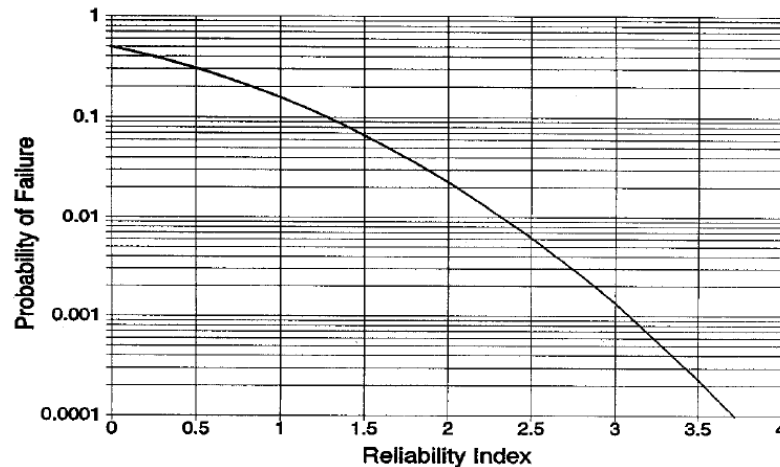
Figure 2-19: Nominal probability of failure for normally distributed FS as function of reliability index; adapted from Christian et al. (1994)

The Monte-Carlo method implemented in SLOPE/W allows numerical sampling of the statistical variables considering the spatial variability of input materials. Then, the output can give the reliability index (RI or β) and the probability of failure (PoF), which can help evaluate the risk of failure. This approach has been used here for some of the slope stability analyses (see Chap. 6)

The summary of the literature review explains the need for the development of analytical models to investigate the importance of the parameters (e.g. material properties, pile internal and external geometry) affecting the waste rock pile stability. More detailed modeling is required to understand the mechanism of rainfall infiltration through waste rock piles (based on different rainfall intensity and duration, pile geometry, initial hydraulic condition) and their impact on unsaturated waste rock pile stability. To obtain a more realistic understanding of the actual material properties distribution inside the pile (due to internal geometry and method of construction) stochastic analysis is required.

CHAPTER 3   NUMERICAL MODELING APPROACH

The main objective of this chapter is to describe the methodology that has been used to conduct the stability analyses of waste rock piles under unsaturated conditions. The approach presented here is being applied for the first time (to the author's knowledge) to address this issue. The chapter covers several areas, including a basic description of the problem, a presentation of the calculation tools, and the application of the model validation and verification procedure. Some of the main challenges related to the stability analyses of waste rock piles under unsaturated conditions (with/without rainfall) are also briefly addressed.

3.1 Stability analysis procedure

Water from different sources (such as rainfall) can enter and infiltrate within a waste rock pile. The material properties and internal structure of each pile influence the water movement and the distribution of pore water pressures, which are also affected by duration/intensity of the recharge.

The stability of a waste rock pile is dependent on the strength distribution within the pile, which in turn can be affected by pore water pressure (positive or negative) development. For instance, during a rainfall, the downward movement of the wetting front may affect the suction in the unsaturated material. The increase in water level at the base or the accumulation of a large amount of water within the pile as a result of climatic events (such as rainfall) may have an adverse impact on the pile stability.

The slope stability analysis aims to define the critical slip surface that coincides with the lowest factor of safety, FS. A sequentially coupled seepage - stress distribution - slope stability procedure has been adopted here to assess the stability of a pile for various conditions. The analysis consists of three steps: i) simulate the rainfall infiltration and flow into the waste rock pile; ii) evaluate the stresses within the pile following the rainfall; iii) analyze the stability conditions resulting from the rainfall and stress state. These stages are described in the following sub-sections.

3.1.1 **Simulation of rainfall infiltration and water flow**

Darcy's law is used to analyze the water movement within soil under saturated conditions. Richards' (1931) equation (a modified version of Darcy's Law) is commonly used to represent the water flow in unsaturated soil (Fredlund et al., 1978; Fredlund and Rahardjo, 1993).

The hydraulic conductivity (k_s) remains constant in the saturated zone, whereas it varies under unsaturated conditions with the volumetric water content k (θ) (or k (ψ)). Comprehensive formulations give nonlinear relations between k, the volumetric water content θ and the pore water pressure (suction ψ) in the unsaturated zone (see Section 2-3-2 for more details).

Several functional relationships are proposed that relate water retention curve to unsaturated hydraulic conductivity curve including (Brooks, 1964; Van Genuchten, 1980; Fredlund and Xing, 1994). These equations are typically expressed as a function of the volumetric water content θ (L^3/L^3), hydraulic head H [L], elevation z [L], and time t [T]. Unsaturated hydraulic conductivity k_w (LT^{-1}) is expressed as a function of suction (ψ) or water content (θ) [Equation 2-3]

The water retention curve presents the volumetric water content as a function of the matric suction (Aubertin et al., 1996; Dye et al., 2009) which is used for predicting the soil capacity for water storage. The flow equations can be express in 2D by Richards' equation [Equation 2-9].

The process of solving theses equations can be complex because of the high nonlinearity of the water retention function (θ versus ψ) and the hydraulic conductivity curve (k_w versus ψ). These are mainly solved using numerical methods.

One of the numerical analysis techniques for solving these types of equations is the finite element method (FEM) based on continuity equations. The FEM divides the model body into smaller regions or elements to seek an approximate solution. The divisions allow the analyses of the distribution of pore water pressure (or displacement) in the body. The discretized body, divided into mesh with several elements with the properties stored at the nodes (used for connection with adjacent elements).

The FEM processes the behavior of each element with some interpolation functions (Huyakorn, 2012). The key to this method is the principle of minimization to limit errors. It then combines all of the regions/elements together to represent the behavior of a unit body (Strang and Fix, 1973; Zienkiewicz et al., 1977; Hughes, 2012)

The basic simplified finite element equation is usually expressed as follows (Krahn, 2007b):

$$[K]\{X\} = \{A\} \qquad\qquad [3\text{-}1]$$

Where [K] represents a matrix of coefficients (related to geometry and material properties), {X} represents the vectors in field variables and {A} are the vectors of actions at the nodes.

For seepage analyses, {X} is usually considered equal to {H} (i.e. total pore water pressure heads at the nodes) and {A} equals {Q} (flow quantities at the node). Equation (3-2) can then be written as follows for seepage analyses:

$$[K]\{H\} = \{Q\} \qquad\qquad [3\text{-}2]$$

More generally for transient flow, the FE seepage equation is expressed as (Krahn, 2007b):

$$[K]\{H\} + [M]\{H\}, t = \{Q\} \qquad\qquad [3\text{-}3]$$

Where [M] is the element mass matrix and t is time.

In a seepage analysis, the first primary unknown is usually the total head at each node. The specified H or Q at some nodes is used to compute the detailed values. The specified H or Q is presented as boundary conditions in the model, which can also be defined as a gradient.

The process to solve Richard's equation is iterative. In the first step, the total H is defined at each node. In successive iterations, the value of H is updated taking into consideration the values of H from previous iterations. For transient simulations, the average head between two successive time steps is considered (the past and current: the midpoints of time intervals). The iterations continue until the convergence criteria is met, i.e., when the calculated results do not change by more than a specified amount between two successive iterations. More details on these analyses can be found in the references (e.g. (Krahn, 2007b).

3.1.2 **Analysis of the stress-strain behavior**

In unsaturated soils, the transient flow of water can change the stress state in the soils. The soil structure can deform following these changes and reach a new equilibrium state. The related stresses change the space available for the flow of water, resulting in new hydraulic properties for

the soil. The transient process of water flow is thus highly non-linear. Two constitutive relationships can describe a volume change of an unsaturated soil. One relationship for the soil structure (concerning volumetric strains) and another for the water phase (concerning degree of saturation or volumetric water content).

The relation between water flow and deformation process can be evaluated through the coupling of mechanical equilibrium equations and water continuity equations.

The equilibrium equations and water continuity equations can be considered at the same time (coupled approach), or considered independently (uncoupled approach).

An elastic-plastic model is used here to describe the geomechanical behavior of the waste rock. Figure 3-1 presents a typical stress-strain curve for the elastic-plastic model. It shows that the stresses are proportional to strains until the yield point; beyond that, the stress-strain follows a horizontal line. The Mohr-Coulomb yield criterion can be used as the yield function for the elastic-plastic model (Section 2-3-4).
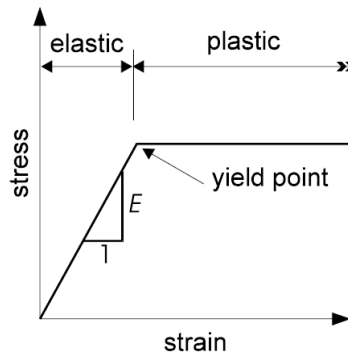
Figure 3-1: Elastic-perfectly plastic constitutive relationship (GeoSlope International Ltd, 2008)

With the coupled approach, the water continuity equations are solved separately from the equilibrium equations in an iterative manner. The flow formulation is solved first then the subsequent pore water pressure (PWP) changes are used as input for a stress-deformation analysis that provides displacement and induced stresses due to applied boundary conditions (e.g. PWP changes).

To perform a stress-strain analysis, the geometry and the boundary conditions applicable to the pile and the material behavior (elastic - plastic) and geotechnical parameters of the waste rock (and foundation soils) must be specified.

The dependent variables for the stress-deformation analysis are horizontal and vertical displacement.

The finite element code represents the field variables for stress-strain analysis as incremental displacements at the nodes, whereas in the finite element code for unsaturated seepage, the field variables are hydraulic heads at the nodes (Wong et al., 1998).

The FEM deals with the incremental analysis of the stress – strain behavior. It uses this process with the boundary conditions for each step. As an example, the forces are obtained as:

$$\Delta F = F_i - F_{i-1} \qquad\qquad [3\text{-}4]$$

Where i represents the time step number; Both F_i and F_{i-1} are calculated based on boundary conditions for that time step. An initial boundary condition must be defined for the first step. Hence, it is necessary to define in-situ conditions for a waste rock pile stress distribution analysis.

The incremental form of the stress – strain relationship can be defined as (Fredlund and Rahardjo, 1993):

$$
\begin{Bmatrix} \Delta(\sigma_x - u_a) \\ \Delta(\sigma_y - u_a) \\ \Delta(\sigma_z - u_a) \\ \Delta\tau_{xy} \end{Bmatrix}
= \frac{E(1-v)}{(1+v)(1-v)}
\begin{bmatrix} 1 & 0 & 0 & 0 \\ 0 & 1 & 0 & 0 \\ 0 & 0 & 1 & 0 \\ & & & \dfrac{1-2v}{2(1+v)} \end{bmatrix}
\begin{Bmatrix} \Delta\left(\varepsilon_x - \dfrac{u_a - u_w}{H}\right) \\ \Delta\left(\varepsilon_y - \dfrac{u_a - u_w}{H}\right) \\ \Delta\left(\varepsilon_z - \dfrac{u_a - u_w}{H}\right) \\ \Delta\gamma_{xy} \end{Bmatrix}
\qquad [3\text{-}5]
$$

Where Δ symbolizes increments; ε, σ ($ML^{-1}T^{-2}$) and τ ($ML^{-1}T^{-2}$) represent the normal strains, normal stresses, and shear stresses; u_a and u_w are pore air and pore water pressures. E is elastic modulus for the soil structure and H is unsaturated soil modulus on matric suction; υ is the Poisson's ratio. The air pressure is the atmospheric condition. The equation can then be simplified as:

$$\{\Delta\sigma\} = [D]\{\Delta\varepsilon\} + [D]\{m_H\}(u_w) \qquad\qquad [3\text{-}6]$$

With [D] as a drained constitutive matrix and $\{m_H\}^T = \left\langle \dfrac{1}{H}\, \dfrac{1}{H}\, \dfrac{1}{H}\ 0 \right\rangle$ (Krahn, 2007d)

The additional displacement for each time step is calculated based on the previous time step displacement:

$$\sigma_{step2} = \sigma_{step1} + \Delta\sigma_{new} \qquad [3\text{-}7]$$

It should be noted that time is a relevant parameter where the dissipation/change of pore water pressure depends on time (such as during consolidation).

The following is a simplified coupled equation where the top half represents the equilibrium equation and bottom half represents the seepage continuity equation (Krahn, 2007b).

$$\begin{bmatrix} [K]_s & [L] \\ [L]^t & [K]_w \end{bmatrix} \left\{ \begin{matrix} \Delta d \\ \Delta u \end{matrix} \right\} = \left\{ \begin{matrix} F \\ Q \end{matrix} \right\} \qquad [3\text{-}8]$$

Where

[L]: coupling matrix

Δd: incremental displacement

Δu: incremental change in pore water pressure

If Δu is obtained from another source (from the code SEEP/W for instance), it becomes a known condition for this equation, which gives the volume change calculated from the previously computed Δu. This leads to strains and stresses at any location.

3.1.3 **Evaluation of the stability and safety factor of the slope**

In a slope stability analysis, the slope can be either infinite or finite. Different solutions have been proposed to assess infinite slope stability. For finite slope, it has been observed that a failed slope moves downward and outward along a curved plane with an approximately circular shape (at least initially).

The basic method of stability analysis defines the factor of safety FS as the ratio of the moments or forces resisting the sliding to the moments and forces causing the sliding, or the ratio of the shear stress applied to the shear strength of the soil.

The main method used for slope stability analysis is the limit equilibrium method. It is a widely used technique for solving factor of safety equations. The process starts with the selection of a potential sliding mass and dividing it into slices of varying widths. An assumption must be made regarding the inter-slice forces, then, equilibrium of the potential sliding mass is evaluated based on the terms of forces acting on the slices and the moment about an assumed center of rotation through one of the computational methods (see details in section 2-4-1).

This process is systematically repeated for a great number of possible slip surfaces to determine the most critical surface location (the minimum factor of safety FS). This application of the limit equilibrium method does not give any information on the stress-strain behavior leading to failure.

Limit equilibrium methods use vertical slices to divide the sliding mass. The acting forces and/or moments are analyzed for each slice. The sum of the driving forces (or moments; i.e. demand D) is compared to the resisting force (or moments; i.e. capacity C)), to determine the Factor of safety against slope failure (FS $= \frac{C}{D}$) (see section 2-4).

It is also possible to compute the distribution of stresses with the finite element method within the slope (as explained below, in section 3.2) and then implement these stresses inside a limit equilibrium framework to analyze the stability. In this case, there are usually no interslice forces.

3.2 Calculation tools

The codes from GeoStudio (GeoSlope International Ltd, 2008) have been used to perform the analyses of the waste rock piles. These are described in the followings:

3.2.1 SEEP/W

In this study, SEEP/W (version 7.23) is used to assess the pore water pressures distribution within the waste rock piles. SEEP/W is a finite element program that can simulate seepage within the soil (Krahn, 2007b). It is capable of modeling different types of material and boundary conditions in two-dimensions, for either a steady-state or transient analysis, under saturated or unsaturated conditions. It has been widely used for seepage modeling by different authors; e.g. (Chapuis et al., 2001; Fala, 2002).

The code requires the water retention curves (WRC) and hydraulic conductivity functions (which are highly nonlinear in unsaturated soils) of the materials as inputs to solve the flow equations (based on Richard's, Equation 2-9).

Three fundamental steps are needed to use the software (Krahn, 2007b)

  i)   Discretization to divide the model domain into small areas (called elements)
  ii)   Specify and implement material properties
  iii)   Define the boundary conditions

The geometry of the model is first defined in two dimensions. The material properties (established directly from measurements, taken from the literature, or generated by predictive methods) are then implemented.

The constitution of the model must also include the initial conditions and the boundary conditions (which may vary over time). The external environment is usually considered to define the boundary conditions for the models, in the form of constant head or time-variable continuous flow (includes rainfall with various levels of intensity or duration). These boundary conditions are applied on the element's edges or nodes.

Two assumptions (simplifications) have been adopted to conduct this part of the study with SEEP/W; i) the effect of evaporation are neglected; ii) the hysteresis of the water retention and k function is not taken into account.

3.2.2 **SIGMA/W**

The code SIGMA/W (version 7.23) is also based on the finite element method. It can simulate problems with boundary conditions that change over time. It can be used to model a variety of stress-strain and deformation problems in soils such as consolidation problems and stress-strain analyses (Pedroni, 2011; El Mkadmi, 2012; L-Bolduc, 2012).

It includes various formulations for the constitute equations, from a simple linear elastic model to highly nonlinear elastoplastic models. It can be used to compute stresses and deformations with or without changes in pore-water pressures. SIGMA/W can also be coupled with SEEP/W for the interactive analysis of changes in pore pressures and deformations.

Material properties used in SIGMA/W can be either effective stress parameters for drained conditions or total stress parameters for undrained conditions.

Two methods can be used in SIGMA/W to solve the seepage and the related stress distribution. The first one is a fully coupled consolidation type, which calculates both pore water pressures and the displacements simultaneously. In this case, both hydraulic and displacement boundary conditions are added for the SIGMA/W calculations.

The second method is partially coupled. The changes in pore water pressure are calculated first by software like, SEEP/W. Then SIGMA/W takes the pore water pressure for each step as an input for the deformation analysis. The related effective stresses and volume changes due to pore water pressure changes are then computed.

In partially coupled simulation, the boundary conditions for the stress-deformation analyses can be either of the displacement or load type.

For the relatively complicated seepage analyses conducted here, it is recommended to use the partially coupled procedure (Krahn, 2007a). The transient flow equation is solved first, and then the results are used to obtain the related stresses. The stress-deformation analyses give the displacements and stresses due to applied boundary conditions and changes in matric suction.

3.2.3 **SLOPE/W**

The code Slope/W (version 7.23) uses the limit equilibrium theory to compute the factor of safety for slope stability (Krahn, 2007c). It can analyze the slope stability for saturated/unsaturated zones by computing the factor of safety as a function of the input parameters. SLOPE/W is capable of modeling heterogeneous soil types and complex slip surface geometry with variable pore pressure conditions (Krahn, 2007c)

Various methods of slices, including Bishop, Janbu, and Morgenstern-Price, are available in code to evaluate the factor of safety FS of the slope (see section 2-4 for more details about the methods). It also provides a choice of probabilistic inputs for soil parameters.

The stress distribution obtained with the limit equilibrium methods does not typically represent the actual stress field along a slope (Griffiths and Lane, 1999; GeoSlope International Ltd, 2008). Adding the stress-strain relationship (from SIGMA/W) to the stability analysis results in a stress

distribution that is more accurate and closer to field conditions. Here the stresses were first computed by SIGMA/W. The results were then used in a conventional limit equilibrium framework by SLOPE/W to calculate the factor of safety based on input provided by SIGMA/W (which gives σ_x, σ_y and τ_{xy} within each element).

The stresses are known for each element from the SIGMA/W calculations, so the normal and mobilized shear stresses are calculated for each slice (at the base mid-point of each slice) with the following process:

- The stresses at each node (σ_x, σ_y, and τ_{xy}) give stresses at any point within the element (including the base mid-point of each slice)

- The limit equilibrium discretization provides the inclination angle (α) at the base of the slice

- Having α and using the Mohr circle gives the base normal and shear stress

- The frictional shear strength is calculated from the normal stress

- These stresses are then converted to forces by multiplying the former by the length of the slice

- This process is repeated for all of the slices.

The critical factor of safety is then calculated:

$$FS = \frac{\sum S_r}{\sum S_m} = \frac{C}{D} \qquad [3\text{-}9]$$

where

S_r: total shear resistance
S_m: the total mobilized (imposed) shear

There is the added possibility of checking the local factor of safety for each slice with this method; No assumption is needed about the interslice forces, and the displacement compatibility is always satisfied.

Slip surface

The primary goal of the slope stability analyses is to determine the potential slip surface that has the overall minimum factor of safety. In SLOPE/W, the slip surface may be circular, composite or take on other shapes defined by a series of straight lines.

Several search methods are available in SLOPE/W to identify either circular or non-circular slip surfaces (identified as Grid and Radius, Entry and Exit methods, etc.). The method of Grid and Radius, which is commonly used for slope stability analyses, includes defining a grid of points (representing the potential centers) and a range of tangent lines to the circular slip surface (representing the radius of the slip surfaces). For Entry and Exit method, the location where the trial slip surfaces enter the ground surface and where they exit the ground surface need to be identified.

In the literature, it has been reported that the failure surface of slopes is often non-circular due to different soil characteristics such as hydrological or geotechnical heterogeneity (Brooks et al., 1993).

Recent studies have shown that circular slip surfaces do not necessarily give the minimum factor of safety (Krahn, 2007a, 2007c). Refinement of the slip surface shape may lead to a non-circular slip surface with the lowest factor of safety. The process of defining a non-circular slip surface is available in SLOPE/W under the *optimization* option (Krahn, 2007c).

Figure 3-2 illustrates a typical optimization process for a non-circular slip surface. The critical circular slip surface is obtained first, and then the optimization process starts.

The slip surface is divided into several straight line segments. Then the point where slip surface enters the ground is moved backward and forward randomly along the ground surface to obtain the lowest factor of safety. Adjustments are then made to the next point along the slip surface to reach the lowest factor of safety again. This process is repeated for many points along slip surface. Then the longest line segment is divided into two parts by adding a new point, and this process is repeated until the process reaches specified limits (e.g. maximum number of optimization trials). The results present the critical *Optimized* (non-circular) slip surface. In this study, both circular and non-circular (*Optimized*) slip surfaces are shown.
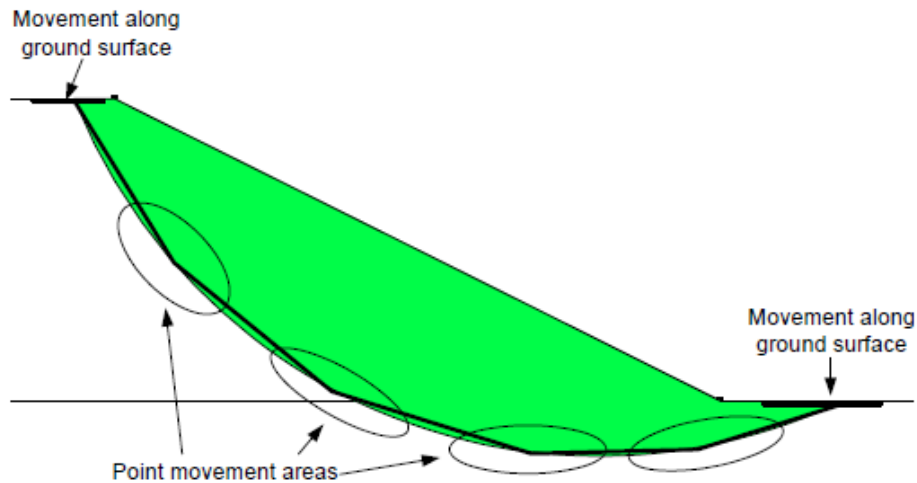
Figure 3-2: Movement areas of points in the optimization procedure, taken from Krahn (2007c)

The minimum depth of a slip surface can enter into SLOPE/W. This option expresses the minimum depth of a slip surface through the minimum depth of at slice along the slip surface. This feature can be defined for all the methods presented in SLOPE/W, for any slip surface shape (circular or *Optimized*).

3.3 Details on the analysis procedure and parameters selection

The stability of a waste rock pile depends on the stresses and strength distribution within the pile, which is influenced by the pore water pressure. The slope geometry and initial pore water pressure are first defined in the model. Then the seepage due to infiltration (rainfall) is analyzed with SEEP/W. The resulting PWP distribution becomes the input for the SIGMA/W simulation. The stress distribution in a pile calculated with SIGMA/W is used as input for SLOPE/W to determine the critical slip surface (either circular or *Optimized*) and the minimum factor of safety. Additional information is presented in the following sections.

3.3.1 SEEP/W model characteristics

Different piles with two-dimensional geometries have been considered for the simulations. The details of these geometries are presented in Chapter 4 (Tables 4-4 and 4-5).

The hydraulic properties of the materials were established directly from experimental measurements (Aubertin et al., 1996; Fala, 2002; Gamache-Rochette, 2004; Aubertin et al., 2005; Aubertin et al., 2008; Bussière et al., 2011; Peregoedova, 2012). The details are presented in Chapter 4.

The boundary conditions were defined based on the purpose of the simulations. As an example, for cases dealing with unsaturated waste rock with an apparent cohesion, the initial negative pore water pressures are used to define the expected value of c_{app} (see Section 4-6). For transient analyses, various rainfalls with different durations/intensities are defined as boundary conditions (see Section 5-4).

For all cases, the water table was defined at a selected depth, and a drainage point was added (at the very right end of water table surface) to make sure that the water table was not significantly raised during and after the rainfall (see section 5-3, Figure 5-2).

The mesh size is an important parameter that affects the accuracy of FEM calculations. These can be advantageous to choose a fine mesh taking into consideration the software capacity and computing time limitations (Delleur, 2006). However, there are few rules for selecting the mesh size (specially for waste rock), and it should be considered case by case. Typically the mesh is a function of material properties; for example, the air entry value and slope of the WRC may have an influence on mesh size (Aubertin et al., 1996; Fala, 2002). Aside from these, it is also important to consider the model size, material properties, time steps and boundary conditions (Chapuis et al., 2001).

An extensive mesh study is presented in Appendix B (section B-1), section Figure 3-3 presents a typical mesh configuration for Case S21 (see Tables 4-4 and 4-5). The unstructured mesh type is used to evaluate the effect of infiltration. Element size, located on the slope surface, is selected to be close to the waste rock AEV (about 12 cm, see Figure 3-3). Along the interface between two materials (e.g. loose and compacted waste rock, loose waste rock, and silty sand foundation), finer meshes are defined to limit the fluctuations due to the sudden changes of hydraulic properties.
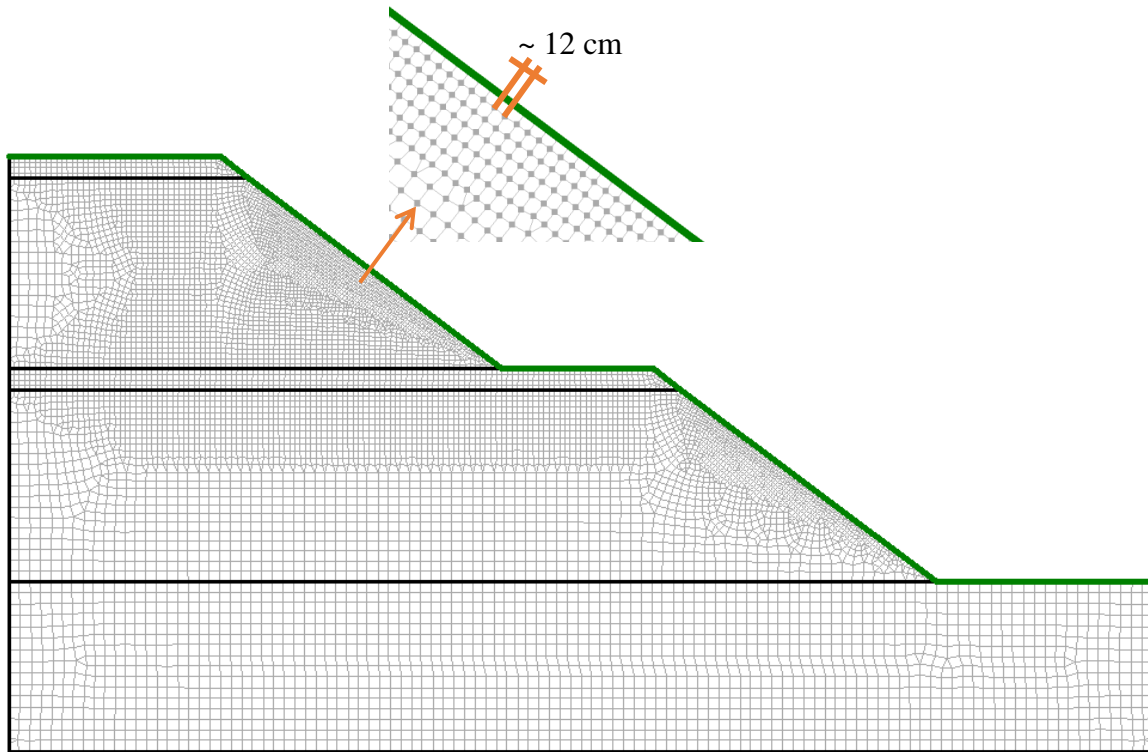
Figure 3-3: Typical mesh configuration for a typical model simulation (in SEEP/W and SIGMA/W), Case S21

For transient analyses, a constant time step was used (a constant value of ~100 sec for short-term - 24 hours – recharge, and 10 000 sec for long-term - 365 days- analyses). This time step is the smallest possible that leads to valid results (obtained by comparing results for varying time steps).

Rainfall is a boundary condition defined in SEEP/W. This boundary condition is defined without ponding on the crest and slope surfaces during the rainfall. This means that the model does not allow a pore water pressure at the surface greater than 0 (kPa). In this case, the excess water is removed from the surface as runoff without further infiltration.

3.3.2 **SIGMA/W model characteristics**

The geometry, boundary conditions, material behavior (nonlinear elastic-plastic) and geotechnical parameters must be specified to perform the stress analyses of waste rock piles.

The geometry of the pile and the mesh properties used in the SIGMA/W models are identical to these used for the SEEP/W simulations. Un-coupled analyses were used with SIGMA/W in this study. Hence, the hydraulic conditions are transferred from SEEP/W to SIGMA/W for the simulations.

The displacement boundary conditions at the base were "Fixed X/Y" (i.e. the displacements in X and Y directions are not allowed at the base). For the sides (right and left), displacements along X are not allowed (Fixed X). The elastic-plastic model with the Mohr-Coulomb yield criterion was used. Details with other geotechnical parameters are presented in section 4-3.

3.3.3 **SLOPE/W model characteristics**

The Grid and Radius method was mainly used, with the possibility of evaluating both circular and non-circular (*Optimized*) critical slip surface. For some cases, the Entry and Exit method is used to search for specific critical slip surfaces (e.g. section 5-5).

A few simulations are presented to compare the values of FS, and the shape of slip surface from different methods of calculations, including the Bishop, simplified, Morgenstern-Price and *FE stress-based* (circular and non-circular) methods in Chapter 4.

3.4 **Validation and verification of the models**

The improper use of Numerical models can provide results that are unrealistic or meaningless. Therefore, it is necessary to verify the validity of results of the calculations obtained with numerical codes. In cases where analytical solutions are known, one can compare results for simple models to verify if the results are the same (Chapuis et al., 2001). However, analytical solutions usually require simple geometries, initial and boundary conditions and homogeneous properties. Numerical methods can deal with heterogeneity, anisotropy, asymmetrical geometries and mixed boundary conditions, which are usually too complicated for analytical solutions. In such cases, the results provided by the code can be compared to experimental results or the results provided by other (better known) and already validated codes (Chapuis et al., 2001).

In the literature, there are very few numerical simulations dealing with the unsaturated flow in waste rock piles or similar structures (Fala, 2002, 2008; Dawood and Aubertin, 2009; Dawood and Aubertin, 2012). One of the main numerical issues is simulation convergence. Different factors may influence the convergence of the simulations calculated with a code like SEEP/W including the convergence criteria, the mesh characteristics, and material properties.

Convergence of finite element calculations can be improved by (Chapuis et al., 2001; Fala, 2002):

- Reducing the size of the elements

- Reducing the time interval increasing the number of iterations

- Adjusting the hydraulic functions

The residuals (i.e. the difference between Gauss point conductivity) obtained as the solver iterates can be checked to evaluate the convergence. A smaller residual indicates a better convergence.

Due to the coarse-grained nature of the waste rock, the hydraulic conductivity function becomes a critical factor. The convergence is usually not achieved easily because of the steep slope of this function, together with the low air entry value at the WRC. This means that a very small change in suction may result in a large change (by order of magnitudes) to the hydraulic conductivity due to changes in θ (or S_r).

The main method of checking the convergence of simulations with SEEP/W is by comparing the hydraulic conductivity ($k_w - \psi$) function and water retention curve (volumetric water content versus suction) in successive iterations with the initial curves implemented into the model. Convergence is usually achieved when these graphs coincide (Fala, 2002).

For each simulation, the time step is constant. The time step value may change from simulation to simulation, as a function of the boundary conditions and the duration of transient analyses. The time steps are kept as small as possible; values in the range of 100 to 200 seconds are used for different simulations considering short term analyses.

3.5 Types of problems and main challenges

Various parameters were implemented for the simulations to obtain adequate convergence. As was stated earlier, the mesh was designed to have a small size, i.e. close to the AEV of waste rock (~ 12 cm; see also Appendix B – section B-1)

Smoothing the WRC and imposing a limit to the lower hydraulic conductivity limit (i.e. 10^{-13} m/s) may also help improve numerical stability in some calculations (Fredlund et al., 1994; Mbonimpa et al., 2006).

Despite this precaution and measure, some convergence issues were encountered during the simulations. These issues are mainly related to the waste rock pile with compacted waste rock layers within the pile. For example, Figure 3-4 presents a waste rock pile with compacted waste rock layers and a silty sand foundation (Case S21 described in Chapter 4). The boundary condition is based on rainfall (recharge) of $5.78\text{x}10^{-7}$ m/s with 24 hr duration. The initial suction is 1 kPa (= $c_{app)}$ through the pile. The water table is located 7 m below the ground surface.
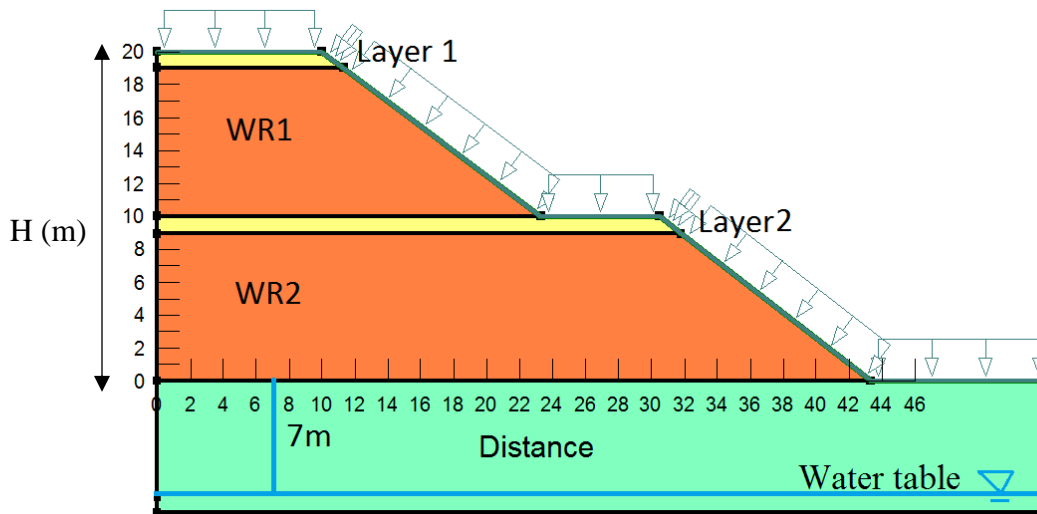
Figure 3-4: Geometry and regions for the simulated waste rock pile (Case S21) under transient conditions (rainfall of 5.78×10^{-7} m/s, duration of 24 hrs; c_{app}=1 kPa) to evaluate numerical convergence issues.

The convergence was assessed for four different regions: Layer1, WR1, Layer2, and WR2. These regions are shown in Figure 3-5. After the rainfall, each region is checked for convergence. For

that purpose, the value of volumetric water content θ and its related suction ψ for all the nodes in that region was retrieved. Figure 3-5 presents a portion of layer 1 with its nodes (in blue).
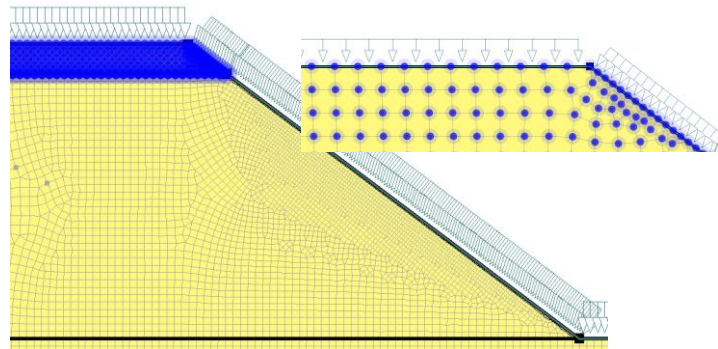
Figure 3-5: Points representing the nodes in Layer 1 for convergence issues

Figure 3-6 presents the volumetric water content versus suction for all the nodes in Layer 1 and the water retention curve of the compacted waste rock material. It is observed that almost all of the nodes show a behavior similar to the curve (more than 80%), but a few of them are not located on the WRC. The points that are not on the curve are located at H = 19 m, with varying values of x. This means they are all located very near the interface between the compact and loose waste rock materials; at these locations, the extracted data for each element gives a value, for both the volumetric water content and suction, between the WRC of these two materials (see also below).
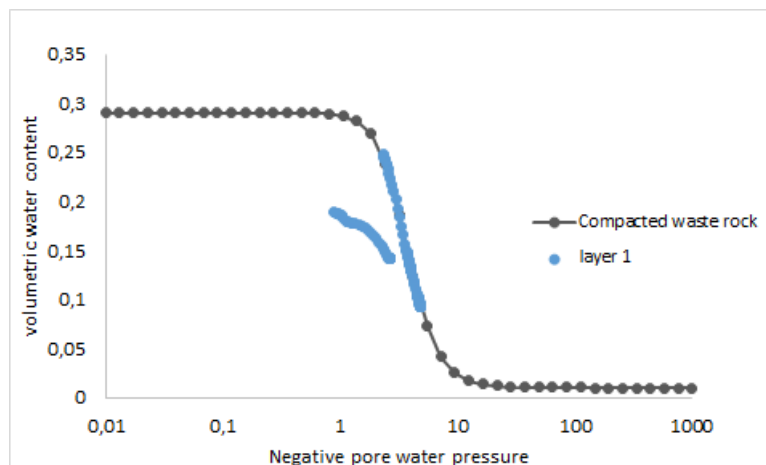
Figure 3-6: Volumetric water content versus suction for nodes in Layer 1 after rainfall 5.78×10^{-7} m/s with 24 hr duration compared to the imposed water retention curve

Figure 3-7 presents similar results for Layer 2. After locating the nodes that are not placed on the water retention curve of compacted waste rock material, it was observed that these nodes are located at H=9 m. This means these nodes located near the interface of Layer 2 and WR2.
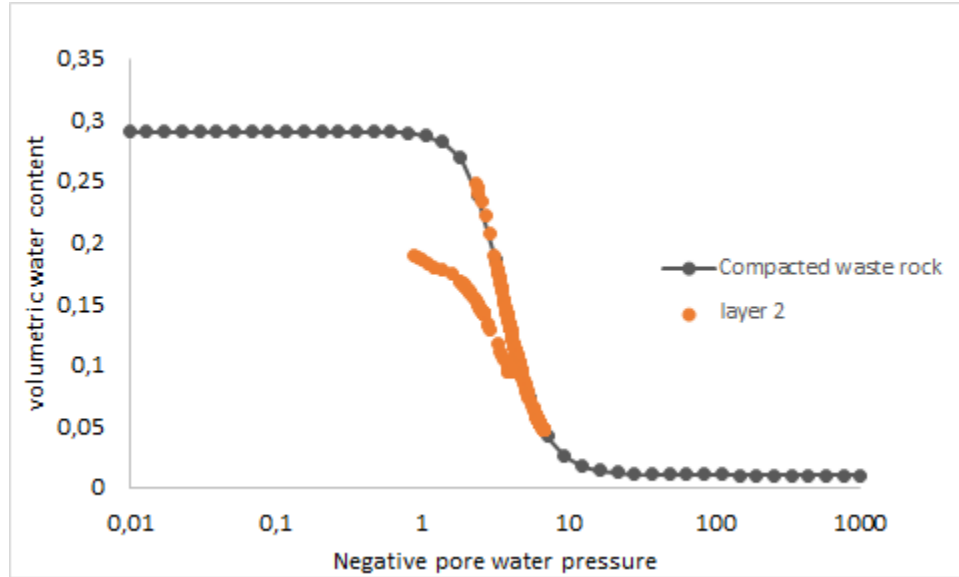
Figure 3-7: Volumetric water content versus suction for nodes in Layer 2 after rainfall $5.78e \times 10^{-7}$ m/s with 24hr duration compared to the water retention curve of the compacted waste rock

Figure 3-8 shows a part of WR1 with the nodes that are used for assessing convergence. For each node, the value of volumetric water content and its related suction are retrieved from SEEP/W results, and they are compared with the water retention curve of the waste rock material.
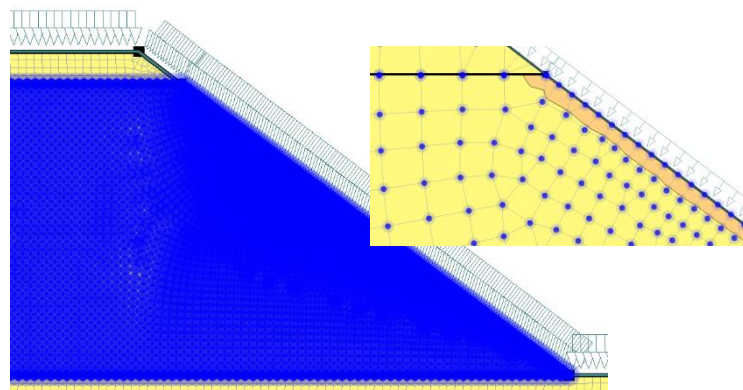
Figure 3-8: Points representing the nodes in WR1 to be checked for convergence issues

Figure 3-9 (a) and (b) illustrate the volumetric water content vs. negative pore water pressure for all of the nodes in WR1 and WR2.

It is observed that for both cases a significant number of the nodes volumetric water content are located on the water retention curve (the total number of nodes is approximately 2900 and 3800 for WR1 and WR2, respectively).

For WR2, the nodes with different volumetric water content are located on the waste rock pile. It is observed that nodes are located at different heights (H), including H=0 to 0.3 m (interface of WR1 and foundation), H=9 m (interface of WR2 and Layer 2) along the x axis.

For WR1, the nodes with volumetric water content different are located on the waste rock pile. It is observed that nodes are located at different heights (H), including H=10 to 10.3 m (the interface of WR1 and Layer 2), H=19 (interface of WR1 and Layer 1) along x axis.

Figure 3-9 presents the volumetric water content of nodes in WR1 and WR2 compared with both the water retention curve of loose and compacted waste rock material.

It is shown that the nodes which have a volumetric water content not located on the water retention curve of the waste rock, have volumetric water content closer to the compacted waste rock material.
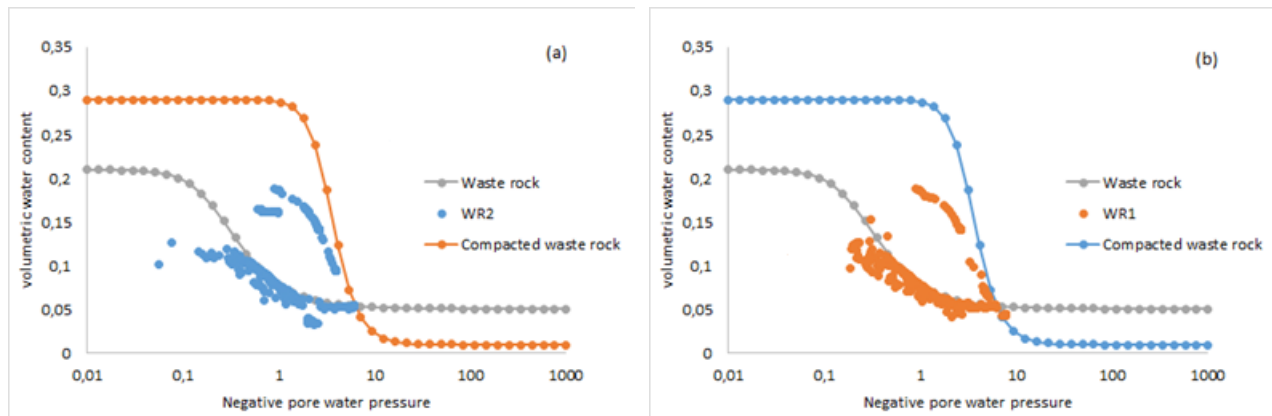
Figure 3-9: Volumetric water content versus suction for nodes in WR1 (a) and WR2 (b) after a rainfall of 5.78×10^{-7} m/s with 24 hr duration compare to WRC of the loose and compacted waste rocks

Due to the difference in hydraulic conductivity and water retention curve of the loose and compacted waste rock (specifically the air entry value and the curve slope), there is an issue for

the nodes that are located at the interface of two materials. The value of the volumetric water content for these elements may not be calculated correctly as it is computed at the element Gauss points and is then projected to the nodes for contouring purposes (in SEEP/W). Large changes in the values at the Gauss points within an element may lead to imprecise estimates in such cases (Krahn, J., 2007b). Also for the nodes located on (or very near) the interface of two materials the parameter values at the Gauss points may vary widely (for three or four Gauss points adjacent to the node). The projection of these points to the nodes (average) can result in an over-shoot for the projected nodal water contents (i.e. beyond the range of the volumetric water content function; see SEEP/W Manual).

The issue is associated with the change of material from one point to another (from a higher saturated hydraulic conductivity to a lower saturated hydraulic conductivity and vice versa), and the software does not correctly calculate the local properties (and response). However, these nodes should not have a significant influence on the outcomes of these simulations, which is the extension of a wetting front in the slope due to rainfall and changes in a factor of safety as a result of that. Hence, this aspect is not expected to affect the accuracy of the calculations.

CHAPTER 4   STABILITY ANALYSIS OF WASTE ROCK PILES UNDER STABLE, DRY OR HUMID, CONDITIONS

4.1 Introduction

As stated earlier, mining operations often produce large amounts of non-economical, coarse-grained waste rocks. These are typically disposed of as piles on the surface above the water table, under unsaturated conditions (Aubertin et al., 2002a; Fala et al., 2005; Aubertin et al., 2008; McLemore et al., 2009; Blight, 2010). The local slope angle of these piles is mainly controlled by the natural deposition (repose) angle β of the waste rock, dumped from trucks or pushed by dozers. The value of β is usually close to the internal friction angle ϕ' of the waste rock (i.e. around 37° for hard rock mines). As the local factor of safety FS is small (close to 1), slope stability of piles can be a concern for mine operators (Piteau Associates Engineering, 1991; Aubertin et al., 2002a; Aubertin, 2013)

The shear strength of unsaturated waste rock can be affected by various factors (see section 2-3-4), including the apparent cohesion produced by matric suction within an unsaturated pile. This apparent cohesion, which affects the factor of safety, FS, can change with time and location due to the evolution of water distribution. This aspect is investigated in a preliminary manner in this chapter through slope stability analyses, for constant and uniform conditions in the piles. The calculations are performed according to the procedure described in section 3-3. The influence of different factors, including the pile geometry and properties of the waste rock is considered.

4.2 Methodology

The behavior of waste rock piles depends on the pile geometry, boundary conditions, and geotechnical parameters. Numerical simulations were used to evaluate their stability considering different values of apparent cohesion, internal friction angle, pile geometry (both internal and external), and foundation properties. As discussed earlier, the stability of a waste rock pile depends on the strength distribution within the pile, which may be influenced by pore water pressure. For cases where there is infiltration, the pore water pressure is first defined using

SEEP/W. SIGMA/W was then used to calculate the stress distribution, and SLOPE/W used to determine the critical slip surface and the minimum factor of safety. SEEP/W was not used for idealized cases where there is no infiltration; in such cases, the PWP (or VWC) are imposed as an initial (constant) condition in the models.

The geometry and initial boundary conditions (including the imposed apparent cohesion) were defined for SEEP/W and SIGMA/W to evaluate the PWP and stress state in a pile. The code SLOPE/W (Geoslope International Ltd; Krahn, 2007c) was used for the slope stability analyses using the method of slices (e.g. simplified Bishop Method, MP method, *FE stress-based* method with the circular and *optimized* surface). For *FE stress-based* method (circular and *Optimized*) the critical slip surface and the matching factor of safety were determined from the computed stresses obtained with the finite element (stress-based) method (with SIGMA/W). With this procedure, calculated values of σ_x, σ_y, and τ_{xy} at the Gauss numerical integration point for each element is projected to the nodes, giving the stresses at each node of the FE mesh. The shear stresses (normal and mobilized) were obtained for each slice at mid-point of its base.

The stability analysis with SLOPE/W provides a factor of safety FS, and the location and shape of the critical slip surface (circular or non-circular).

These results were used to assess the stability of waste rock piles as a function of different factors including pile geometry and material properties.

4.3 Materials characteristics

Four different materials were considered in constructing the conceptual and numerical models of the unsaturated waste rock piles. A gravelly material (coarse waste rock), a crushed (sandy) waste rock (which represents the finer material layers, with a lower saturated hydraulic conductivity and higher internal friction angle, as mentioned in sections 2-1-2 and 2-2), as well as a silty sand and a clayey sand (for foundation soil).

4.3.1 Hydraulic properties

Waste rock from the Tio mine site has been characterized by (Peregoedova, 2012). The properties of compacted waste rock layer were taken from (Bussière, 1999) based on the characterization of

a sandy material (which represents the finer-grained, compacted layers). The water retention curves for these materials were obtained laboratory data interpreted using Van Genuchten (1980), Table 2-3. The hydraulic conductivity was then derived from the Mualem (1976) analytical model as developed by van Genuchten (1980) (more details are given in sections 2-3-1 and 2-3-2). The corresponding parameters are provided in Table 4-1. The hydraulic properties of the silty sand and silty clay (foundation soils) are based on typical values for the hydraulic conductivity and WRC for these types of soils (Chapuis, 2010).

The coarse and compacted (sandy) waste rocks show relatively high values for the saturated hydraulic conductivity k_{sat}, with a low water retention capacity (i.e. low air entry value, AEV).

The silty sand and silty clay foundation materials have much lower saturated hydraulic conductivity and higher AEV compared to the waste rock materials.

Table 4-1: The van Genuchten (1980) model (see Table 2-3) parameters for the coarse and compacted fine waste rock materials, silty sand and silty clay foundation materials

Material	θ_r	θ_s	α_v (cm^{-1})	n_v	k_s (m/s)	AEV (kPa)	WEV (kPa)	D_{10} (mm)	D_{60} mm
Coarse waste rock	0.051	0.21	0.419	2.194	1×10^{-3}	0.12	1.2	0.22	67
Compacted waste rock	0.01	0.29	0.03	3.72	5.1×10^{-5}	2	7	0.12	0.5
Silty sand	0.11	0.51	0.0075	N/A	5×10^{-7}	13	50	N/A	N/A
Silty clay	0.13	0.49	0.0019	N/A	3×10^{-8}	50	250	N/A	N/A

θ_r = residual volumetric water content

θ_s = saturated volumetric water content

α_v, n_v = van Genuchten fitting parameters

k_s = saturated hydraulic conductivity

Figure 4-1 presents the water retention curves based on the van Genuchten (1980) (see Table 2-3) for the coarse and compacted waste rock material and those adopted for the silty sand and silty clay foundation soils.
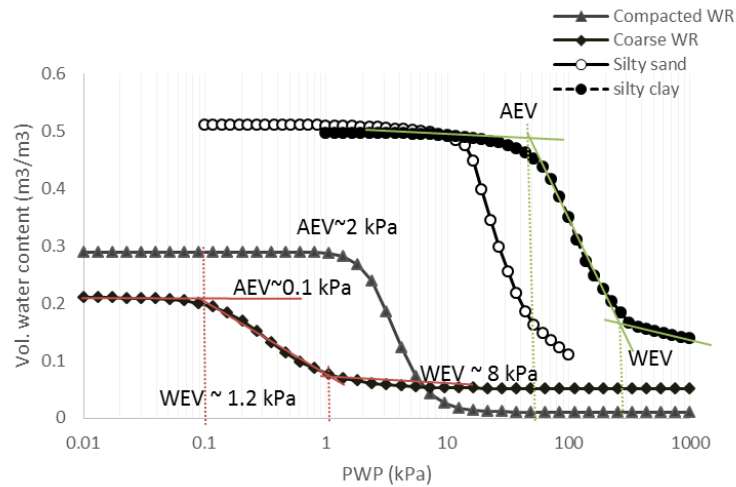
Figure 4-1: Water retention curves for the four materials (compacted and coarse WR, silty sand and silty clay) used in the analyses

Figure 4-2 presents the hydraulic conductivity functions (based on the Mualem (1976) van Genuchten (1980) Equation 2-5) for these same materials.
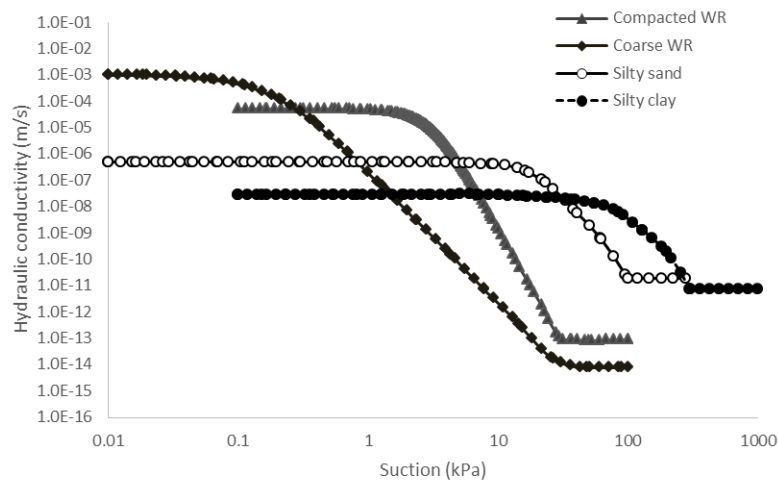
Figure 4-2: Hydraulic conductivity functions used in the analyses for the four materials (compacted and coarse WR, silty sand, and silty clay)

4.3.2 **Geotechnical properties**

As already mentioned, the internal friction angle ϕ' of coarse waste rock is often close to the angle of repose of waste rock in piles, while the value of the effective c' cohesion is zero. For other parameters such as dilatation angle ψ_d and Poisson ratio υ, the values mentioned in Table 4-3 are used; these values of the dilatation angle and Poisson's ratio are a function of the internal friction angle ϕ'.

There is a paucity of results available to assess the modulus of elasticity (Young's modulus) E $[FL^{-2}]$ of waste rock, which is related to the material stiffness and its resistance to straining. The value of E is expected to depend on various factors, including material density and effective confining stresses. The Young's modulus (kPa) is used as input parameters in SIGMA/W. Table 4-2 presents some E modulus values for granular soils (pavement materials) that can be considered fairly similar to waste rock (Sveinsdóttir, 2011). These values correlate fairly well with recent laboratory measurements on a waste rock which indicates that Young's modulus E can exceed 100 MPa (see Appendices A).

Table 4-2: Typical values of the Young's modulus (E) for granular materials

Materials	E modulus (MPa)	Reference
Uncrushed base - Clean, well-drained gravel	70 - 400	Sveinsdóttir (2011)
Uncrushed base - Clean, poorly-drained gravel	20 – 100	
Gravelly and/or sandy soil	70 - 400	
Gravel/sand well-graded	30 – 80 (Loose)	based on Obrzud and Truty (2012) taken from Kézdi and Rétháti (1974) and Prat et al. (1995)
	80-160 (Medium)	
	160-320 (Dense)	
Sand and gravel	70-170	Das (2003)
Sand and gravel	50 – 150 (Loose)	Bowles (1996)
	100 – 200 (Dense)	

The geotechnical characteristics of the four materials used in the analyses are presented in Table 4-3. The waste rock is cohesionless (c' = 0), and its internal friction angle (ϕ') is 37° (in a relatively loose state). The relationships given in Table 4-3 give the value of the dilation angle

(ψ_d) and Poisson's ratio (ν) (more analyses have been conducted with a dilatation angle of zero, presented in Appendix A; these analyses indicate that dilatation angle has no significant role in these type of simulations). The geotechnical characteristics of silty sand and silty clay material are taken from the literature referencing typical properties for these materials.

Table 4-3: Geotechnical parameters of the different materials used for the analyses (basic values)

Material	Cohesion c' (kPa)	Internal friction angle ϕ' (°)	Unit weight γ (kN/m³)	Young modulus (MPa)	Dilation angle (°) [1]	Poisson ratio [2]
Coarse waste rock	0[3]	37 [3]	19.5	80	24.8	0.29
Compacted waste rock	0[3]	45[3]	19.5	240	22.0	0.23
Silty sand	15[4]	30[4]	17.0[4]	20	20.0	0.33
Silty clay	60[4]	20[4]	18.0[4]	150	13.4	0.39

[1] Dilation angle $\psi_d = 0.67 \phi'$ (McCarthy, 2007)

[2] Poisson's ratio ν based on Jaky's relationship for K_o (McCarthy, 2007) $\nu = \frac{1 - \sin \varphi}{2 - \sin \varphi}$

[3] Typical for waste rocks from metal mines (Aubertin et al., 2002a; Aubertin et al., 2008; McLemore et al., 2009; Aubertin, 2013)

[4] Typical for silty sand and clayey soils (McCarthy, 2007)

4.4 Geometry of waste rock piles with foundation

4.4.1 Pile Models

Different scenarios have been considered in the simulations by varying the piles internal and external geometry. All of the models in this study were defined in two dimensions (2D) under plane strain conditions.

Nine groups with different geometries are presented in Tables 4-4 and 4-5. The foundation material is a coarse waste rock, silty sand or a silty clay soil.

The simulations in Group 1 (Cases S1 to S4, H_t = 20, 40, 80, and 120 m respectively; S5, S6, H_t = 40 m) consider waste rock piles without a bench. Table 4-5 presents the details of the geometry regarding the height H_t (m), the length of the base L_{b1} (m) and length at the top L_s (m) (Tables 4-4 for other details and the geometry). Cases S1 to S4 have slope angles of 37° ($\alpha = \beta = 37°$ with α and β representing the global and local slope angles respectively; see Table 4-4) and Case S5 and S6 $\alpha = \beta = 26°$ and 30°, respectively. The body of the pile consists of homogenous coarse waste rock while the foundation is either coarse waste rock, silty sand or clayey soil.

Group 2 (Cases S11 to S14, H_t = 20 m to 120 m; and S18, H_t = 20 m) and Group 3 (Cases S15 to S17, Ht = 40 m to 120 m; S19, H_t = 80 m) represent homogenous waste rock piles with 2 or 3 benches (see Tables 4-4 and 4-5). The geometry is defined in terms of heights H_t, H_{i1}, H_{i2}, H_{i3} (m), lengths at the base of the benches L_{b1}, L_{b2}, L_{b3} (m); length at the top L_s (m) and the global and local angles (with $\beta = 37°$ for all cases and $\alpha = 26°$ for all cases except S18 $\alpha = 30°$ These parameters are defined in Table 4-5.

Group 4 (Cases S21 to S24, H_t = 20 m to 120 m) and Group 5 (Cases S25 to S27, H_t = 40 m to 120 m) correspond to waste rock piles with 2 or 3 benches, with 2 or 3 horizontal (compacted) waste rock layers within the pile. The pile body is made of coarse waste rock, and the layers are made of compacted (fine) waste rock. The geometry is defined in terms of heights H_t, H_{i1}, H_{i2}, H_{i3} (m), lengths at the base L_{b1}, L_{b2}, L_{b3} (m), length at the top L_s (m), thickness of layers L_t (m), and the angles (with $\beta = 37°$ for all cases and $\alpha = 26°$ for all cases except S19 $\alpha = 30°$ see Tables 4-4 and 4-5).

Group 6 (Cases S31 to S34, H_t = 20 m to 120 m) and Group 7 (Cases S35 to S38, H_t = 20 m to 120 m) represent waste rock piles with two benches and compacted layers placed with an inclination of 1% or 5%. The geometry is defined based on heights H_t, H_{i1}, H_{i2}, H_{i3} (m), length at the base L_{b1}, L_{b2}, L_{b3} (m) and length at the top L_s (m), thickness of layer L_t (m), inclination of layers and the angles ($\alpha = 26°$ and $\beta = 37°$) (see Table 4-3 and 4-4).

Groups 8 and 9 represent waste rock piles with alternate layers parallel to the pile external slope (Tables 4-4 and 4-5). Group 8 (Cases S41 to S44, H_t = 20 m to 120 m) represents waste rock piles with two benches, with horizontally compacted layers in the pile and alternate layers parallel the slope. Group 9 (Cases S51, H_t = 20 m) represents waste rock pile with two benches,

5% inclined compacted layers and alternate layers parallel to the external slope. The geometry of Groups 8 and 9 is defined based on height H_t, H_{i1}, H_{i2} (m), length at the base L_{b1}, L_{b2} (m) and length at the top L_s (m), thickness of layer L_t (m) and the angles ($\alpha = 26°$ and $\beta = 37°$).

Table 4-4: Geometric configuration of the waste rock piles used for the stability analysis

Materials	Geometric configuration	Cases
Coarse WR — Foundation		Group 1 S1: H_t=20m S2: H_t=40m S3: H_t=80m S4: H_t=120m $\alpha=\beta=37°$ S5: Ht=40m $\alpha=\beta=26°$ S6: Ht=40m $\alpha=\beta=30°$
Coarse WR — Foundation		Group 2 S11: H_t=20m S12: H_t=40m S13: H_t=80m S14: Ht=120m $\alpha= 26°$, $\beta=37°$ S18: $H_t = 20$m $\alpha= 36°$, $\beta=37°$
Coarse WR — Foundation		Group 3 S15: H_t=40m S16: H_t=80m S17: Ht=120m $\alpha= 26°$, $\beta=37°$ S19: $H_t = 80$m $\alpha= 30°$, $\beta=37°$

Table 4-4: Geometric configuration of the waste rock piles used for the stability analysis (continued)

Materials	Geometric configuration	Cases
		Group 4 S21: H_t=20m S22: H_t=40m S23: H_t=80m S24: Ht=120m L_t=1 m α= 26° β=37°
		Group 5 S25: H_t=40m S26: H_t=80m S27: Ht=120m L_t=1 m α= 26° β=37°
		Group 6 S31: H_t=20m S32: H_t=40m S33: H_t=80m S34: Ht=120m Inclination 1%
		Group 7 S35: Ht=20m S36: Ht=40m S37: Ht=80m S38: Ht=120m Inclination 5%
		Lt=1 m α= 26° β=37°

Table 4-4: Geometric configuration of the waste rock piles used for the stability analysis (continued)

Materials	Geometric configuration	Cases
Coarse WR Compacted WR Foundation		Group 8 S41: Ht=20 m S42: Ht=40 m S43: Ht=80 m S44: Ht=120m α= 26° β=37° L_t = 1 m
Coarse WR Compacted WR Foundation		Group 9 S51: Ht=20 m inclination: 5% α= 26° β=37° L_t = 1 m

The detailed dimensions used in the simulation for Groups 1 to 9 are presented in Table 4-5.

Table 4-5: Additional details on Groups 1 to 9 (Cases S1 to S51)

Group	Cases	H_t (m)	Lb_1 (m)	Lb_2 (m)	Lb_3 (m)	L_s (m)	Hi_1 (m)	Hi_2 (m)	Hi_3 (m)	L_t (m)	Inclination CL
1	S1	20	36.5	-	-	10	-	-	-	-	-
	S2	40	73.1	-	-	20	-	-	-	-	-
	S3	80	146.2	-	-	40	-	-	-	-	-
	S4	120	219.2	-	-	60	-	-	-	-	-
	S5	40	102	-	-	20	-	-	-	-	-
	S6	40	89.3	-	-	20	-	-	-	-	-
2	S11	20	43.8	23.3	-	10	10	-	-	-	-
	S12	40	77.5	36.5	-	10	20	-	-	-	-
	S13	80	155	73	-	20	40	-	-	-	-
	S14	120	232.6	109.6	-	30	60	-	-	-	-
	S18	20	40.77	23.3	-	10	10	-	-	-	-
3	S15	40	78.7	51.8	24.8	6.75	13	13.5	13.5	-	-
	S16	80	158.5	104.13	49.35	13.5	26.5	26.5	27	-	-
	S17	120	237.4	155.1	73	20	40	40	40	-	-
	S19	80	141	94.2	49.3	13.5	26.5	26.5	27	-	-
4	S21	20	43.8	23.3	-	10	10	-	-	1	-
	S22	40	77.5	36.5	-	10	20	-	-	1	-
	S23	80	155	73	-	20	40	-	-	1	-
	S24	120	232.6	109.6	-	30	60	-	-	1	-
5	S25	40	78.7	51.8	24.8	6.75	13	13.5	13.5	1	-
	S26	80	158.5	104.13	49.35	13.5	26.5	26.5	27	1	-
	S27	120	237.4	155.1	73	20	40	40	40	1	-
6	S31	20	43.8	23.3	-	10	10	-	-	1	1%
	S32	40	77.5	36.5	-	10	20	-	-	1	1%
	S33	80	155	73	-	20	40	-	-	1	1%
	S34	120	232.6	109.6	-	30	60	-	-	1	1%
7	S35	20	43.8	23.3	-	10	10	-	-	1	5%
	S36	40	77.5	36.5	-	10.71	20	-	-	1	5%
	S37	80	155	73	-	21.4	40	-	-	1	5%
	S38	120	232.6	109.6	-	32.1	60	-	-	1	5%
8	S41	20	43.8	23.3	-	10	10	-	-	1	-
	S42	40	77.5	36.5	-	10	20	-	-	1	-
	S43	80	155	73	-	20	40	-	-	1	-
	S44	120	232.6	109.6	-	30	60	-	-	1	-
9	S51	20	43.8	23.3	-	10	10	10	-	1	5%

4.4.2 **Characteristics of the pile foundation**

Three different materials and various geometries have been considered for the foundation below the pile in the numerical analyses. The foundation dimensions in the calculations are defined with the value of L_F and H_F (m) shown in Figure 4-3.
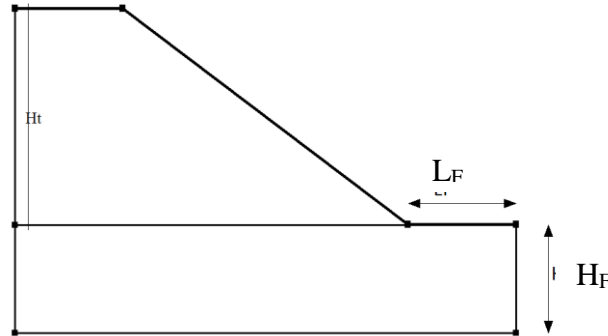
Figure 4-3: Dimensions of the foundation used for the simulations performed with GeoStudio (SEEP/W, SIGMA/W, and SLOPE/W; see text for details)

Different values of LF and HF were initially considered, based on the ratio of the total pile height Ht (m). LF (= 0.4, 0.5, 1, 2 Ht m) and HF (= 0.25, 0.5, 1, 1.5, 2 Ht m). The effect of these sizes on the values of FS for two types of geometry (Case S1 and S11) is presented in Figure 4-4 for two foundation materials, i.e., waste rock and silty sand. The geometric characteristics are presented in Table 4-3; $c_{app} = 0$ for these simulations.

Figure 4-4 demonstrates that changing the two sizes HF; LF does not have a significant impact on the value of FS (with SLOPE/W). The change in FS is between 0.3 to 0.6 % when the length goes from 0.4 H to 2 H (m). It was decided to use a value of LF = 0.5 Ht or0.8 Ht (m) in the different simulations (i.e. 0.5 H_t for smaller piles, 0.8 H_t for larger piles). The changes in FS are between 0.4 to 5 % (FS increases as the depth of foundation is increased) when the foundation H (H_f) changes from 0.25 Ht to 1.5 H_t. Following this preliminary evaluations, it was decided to fix the value of H_F at 0.4 H_t (m) in all simulations.
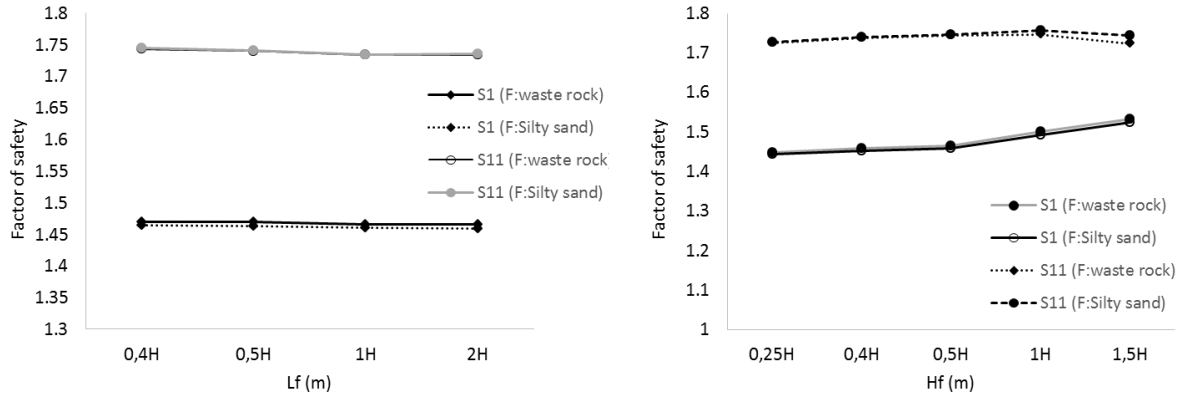
Figure 4-4: Effect of the model foundation size (length L_F and height H_F see Figure 4-3) on the factor of safety of waste rock pile for Cases S1 and S11 (with $c_{app} = 0$); Foundation material: waste rock or silty sand; simulation with SIGMA/W and SLOPE/W

4.5 Boundary conditions

For the simulations where there is no rainfall (or infiltration), only SIGMA/W and SLOPE/W were used. In this case, two types of boundary conditions were defined, i.e. the displacement and the hydraulic conditions.

Figure 4-5 presents a typical of displacement conditions for a single bench waste rock pile (Case S1, left) and a two bench waste rock pile (Case S11, right) simulated with SIGMA/W. In these two cases (and other cases not shown here), the movement is blocked in the horizontal (x) direction on both vertical sides (left and right) of the model. The movement is blocked along x and y directions at the base of the foundation. This type of boundary condition is imposed for all the simulations conducted with SIGMA/W.
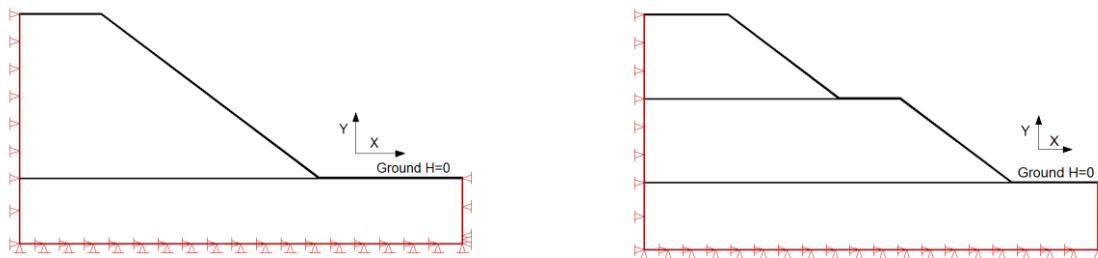
Figure 4-5: Displacements boundary conditions for simulations with SIGMA/W (Cases S1 left and S11 right)

The initial hydraulic condition is based on an initial negative pore water pressure (suction) distribution within the pile, established as a function of the specific apparent cohesion (as described in section 4-6).

4.6 Apparent cohesion in the waste rock

The factor of safety (FS) of geotechnical works is controlled by the material strength and induced loading (stress) state. The shear strength is influenced by different factors, including particle shape, porosity, natural stresses, pore water pressures and degree of saturation.

The shear strength of unsaturated soils and similar materials (such as waste rock, see Section 2-3-4) can be defined using the extended Mohr-Coulomb criterion (i.e. Table 2-7, (Fredlund et al., 1978; Vanapalli et al., 1996; Khalili and Khabbaz, 1998).

The apparent cohesion c_{app} can then be expressed from this formulation. Equation [4-1] is available in SIGMA/W (Vanapalli et al., 1996):

$$C = c^{'} + (u_a - u_w)\left[\tan \phi^{'}\left(\frac{\theta_w - \theta_r}{\theta_s - \theta_r}\right)\right] \qquad [4-1]$$

In this study, the material properties (i.e. internal friction angle, ϕ') are defined as effective parameters in SIGMA/W simulation, and also suction is considered in the process of simulating of the unsaturated waste rock. SIGMA/W then uses the volumetric water content function and Equation 4-1 to generate the value of c_{app}. It considers that the saturated volumetric content θ_s is related to the lowest suction; it then calculates residual water content θ_r as 5% of saturated water content θ_s. For any other suction, it retrieves the volumetric water content from the water retention curve and calculates the apparent cohesion from Equation 4-1.

In these calculations, the suction values and the related specific volumetric water content in the material were adjusted to obtain targeted values for the apparent cohesion.

As an example, Figure 4-6 presents two sample function generated by SIGMA/W, showing the relationship between c_{app} and suction for loose and compacted waste rock material with an internal friction angles ϕ' of 37° (Fig. 4-6 a) and 45° (Fig. 4-6 b) (based on Equation 4-1 used by

SIGMA/W). The water retention curves were retrieved from Figure 4-1. The values of c_{app} were calculated for each θ and related suction $(u_a - u_w)$; for instance, when $\psi = 6$ kPa, $c_{app} = 1$ kPa; for $\psi = 60$ kPa, $c_{app} = 10$ kPa (a).
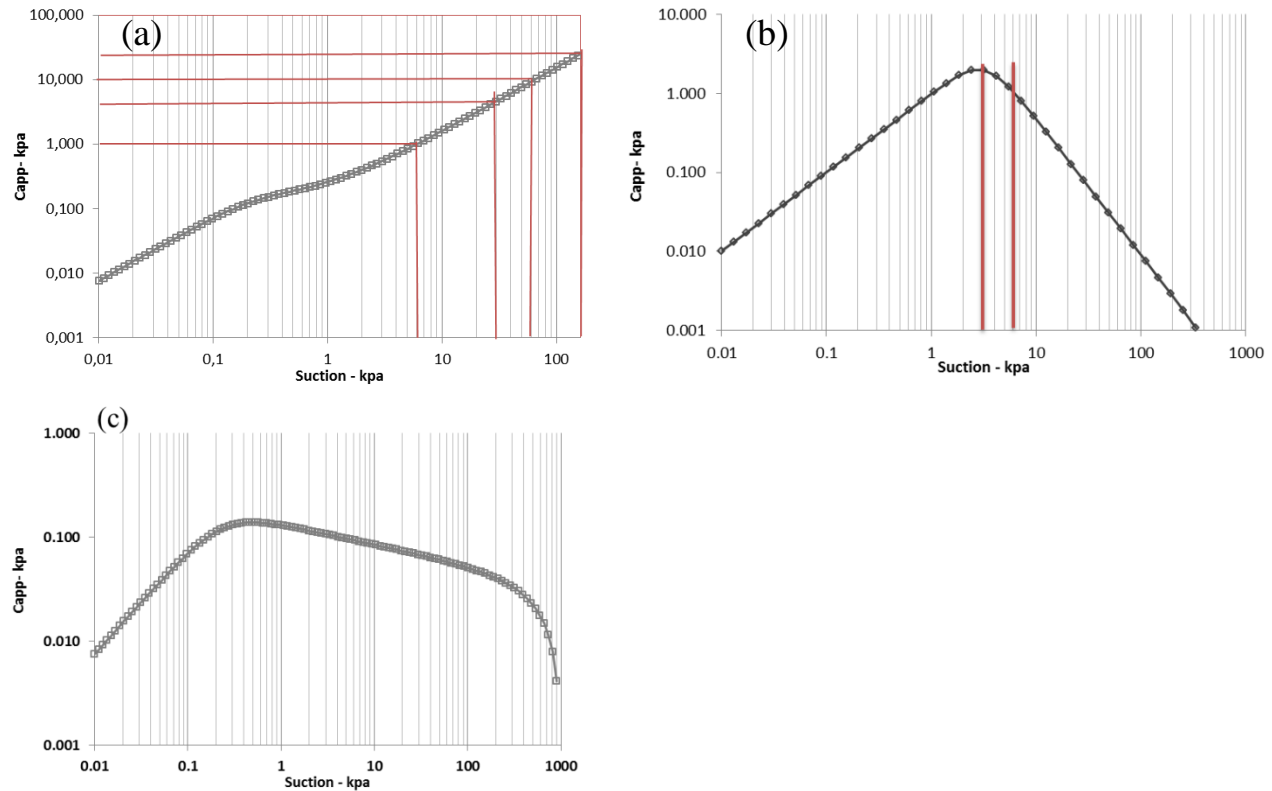
Figure 4-6: Values of c_{app} versus suction, based on Equation 4-1 (simplified version implemented in SIGMA/W); a) coarse waste rock (with $\phi' = 37°$); b) compacted, fine waste rock ($\phi' = 45°$) c) alternative for coarse waste rock (with $\phi' = 37°$) based directly on Eq. 4-1 (but not used in the calculations, as this function is not fully implemented in SIGMA/W)

As explained at the beginning of this section, SIGMA/W uses a simplified version of the Vanapalli et al. (1996) equation, by considering $\theta_r = 5\%$ θ_s. For compacted fine waste rock material, this equation appears to be realistic (with $\theta_r = 0.01 = 5\%$ $\theta_{s\,=\,}0.29$); but for the coarser waste rock material, the experimental and imposed values don't correspond ($\theta_r = 0.05 \neq 5\%$ $\theta_{s\,=\,}$ 0.21); this is why two different trends are seen here on Figure 4-6 (a and c).

Different values of c_{app} (= 1, 5, 10, 25 kPa) were applied to evaluate the effect of the (apparent) cohesion on the waste rock pile stability in a series of analyses.

As mentioned in Chapter 2, laboratory and field observations indicate that the effective cohesion c' of waste rock (from hard rock mines) is typically nil, while the apparent cohesion of coarse grained (humid) waste rock c_{app} is relatively small (given the low AEV = ψ_a and WEV = ψ_r). Based on the WRC, it can be inferred that the maximum (anticipated) c_{app} value would remain below about 5 (to 10) kPa for these materials, with typical values fairly close to 1 to 2 kPa. Although small, this value of c_{app} may still have an effect on the FS of the pile slope (as will be shown below).

Also, the existence of cohesion induced by cementation may lead to higher values of C. This explains (in part) why relatively large values (up to 25 kPa) were also considered here; these higher values also helped evaluate the tendencies. But such unrealistically high values of the cohesion are not deemed representative of what can be expected in most waste rock piles.

Also, it is recalled that, in practice, it can be non-conservative to include the apparent cohesion when performing stability analyses for the design of waste rock piles (because this value is highly uncertain and may vary over time and space).

4.7 Typical results from stability analyses under constant conditions

Detailed calculations for some base cases (Cases S1, S11, and S21, Table 4-4) are first shown here to illustrate numerical modeling process. Other results are then presented and discussed. Two types of slip surfaces are presented in this Chapter. First, the local slip surface covers less or equal to 50% H_t (pile total height), second, the global slip surface cover total pile height (100% H_t, passing at the toe).

4.7.1 Detailed calculations for Case S1

The effect of apparent cohesion on the pile stability is assessed in this section. For each simulation, the selected c_{app} is related to a specific suction imposed on the pile (Figure 4-7).

Figure 4-7 presents the pore water pressure within the waste rock pile simulated with SIGMA/W for c_{app} = 1 kPa. The negative pore pressure is constant along lines A and B; PWP ≈ - 6 kPa (for c_{app} = 1 kPa). It is assumed that the water table is deep and that the same suction exists in the foundation and pile.
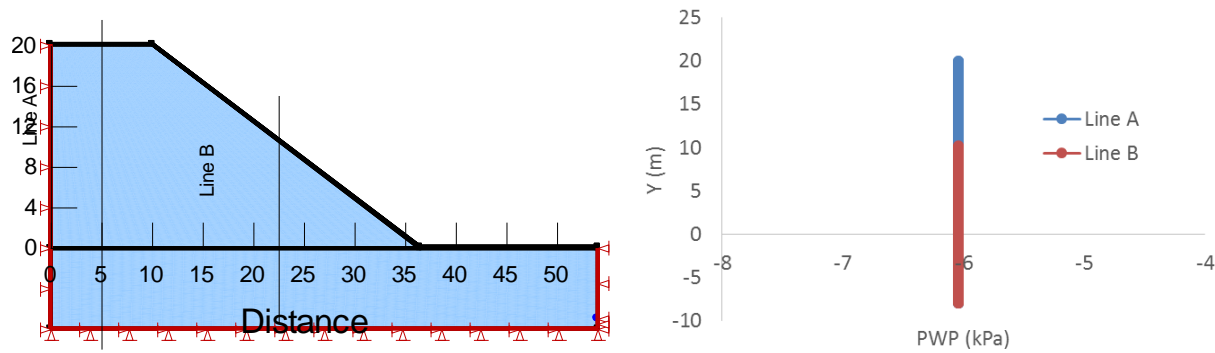
Figure 4-7: PWP distribution for Case S1 (c_{app} =1 kPa) along lines A and B obtained with SIGMA/W

The finite element stress analysis performed with SIGMA/W gives the value of σ_x, σ_y, and τ_{xy} within the pile. Figure 4-8 presents a typical contour plot of the total vertical stresses in the waste rock pile (Case S1). The vertical stresses are influenced by the overburden weight and tend to increase with depth. The contour for σ_y = 50 kPa is located at a varying distance from the ground surface, and it is closer to the surface along the inclined slope and near the toe area, which means that the overburden weight does not just influence the vertical stress, but it is also affected by the shear stresses induced the inclined surface.
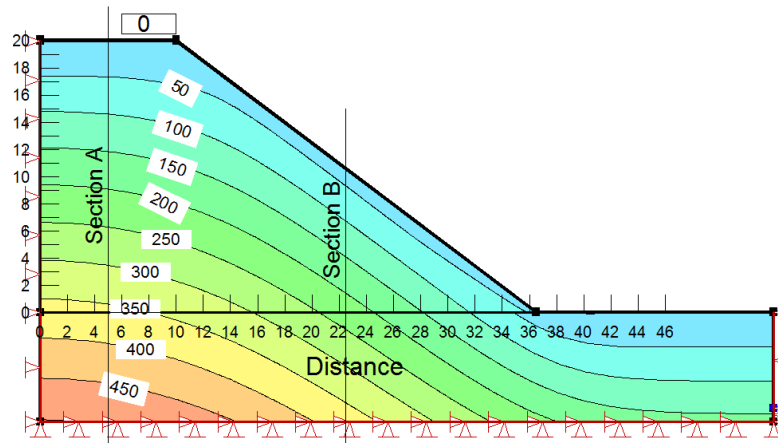
Figure 4-8: Total vertical stress σ_y contours (kPa) computed with SIGMA/W (Case S1, with c_{app} =1 kPa)

Figure 4-9 presents the vertical effective stresses σ'_y for Case S1, with c_{app}= 1 kPa. As illustrated, the value of effective stress on the ground surface is about 6 kPa, which is equal to the local negative PWP (= u; $\sigma' = \sigma - u = 0 - (-6$ kPa)).
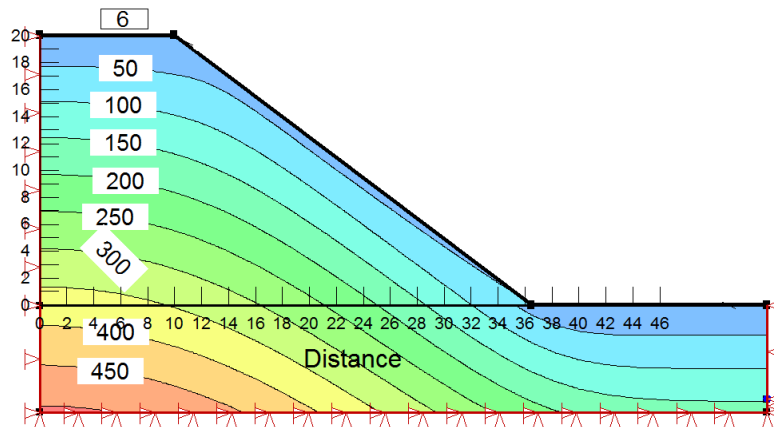
Figure 4-9: Vertical effective stress σ'$_y$ contours (kPa) computed with SIGMA/W (Case S1, with c$_{app}$ =1 kPa)

As explained in section 3-3, the stresses calculated with SIGMA/W (σ$_x$, σ$_y$, and τ$_{xy}$) are transferred into SLOPE/W to determine the value of the factor of safety FS of the slope (using the *FE stress-based* method). This approach differs from the usual limit equilibrium methods (available in SLOPE/W) to calculate FS (i.e. Bishop, Janbu, Morgenstern-Price (MP) methods of slices); details about these methods are given in section 2-4-1.

In these calculations, the *FE stress-based* method is applied for the stability analysis, both circular and non-circular (*Optimized*) surfaces. The suction values in the waste rock pile are used to calculate the stresses at mid-point at the base of each slice. A particular suction is thus imposed as the initial condition (with c' as zero). Other calculation methods, such as MP and simplified Bishop do not consider the effect (presence) of suction; for these methods, a value of c (equivalent to c$_{app,}$ without suction) is imposed on the material (for comparison purposes).

Figure 4-10 presents the relatively shallow critical slip surface and center of rotation obtained for Case S1 with different methods available in SLOPE/W, i.e. simplified Bishop, Morgenstern-Price (MP), circular *FE stress-based* method and *Optimized* (non-circular) *FE stress-based* method (for a minimum depth of 1 m for the deepest slice along the failure surface). It shows that the FS obtained with the *FE stress-based* method is somewhat higher compared to the Morgenstern-Price (MP) and Bishop Methods in this case; the slip surface is closer to the crest with the former. The *Optimized FE stress-based* method gives a lower factor of safety compare to *FE stress-based* method, in part due to the non-circular shape.
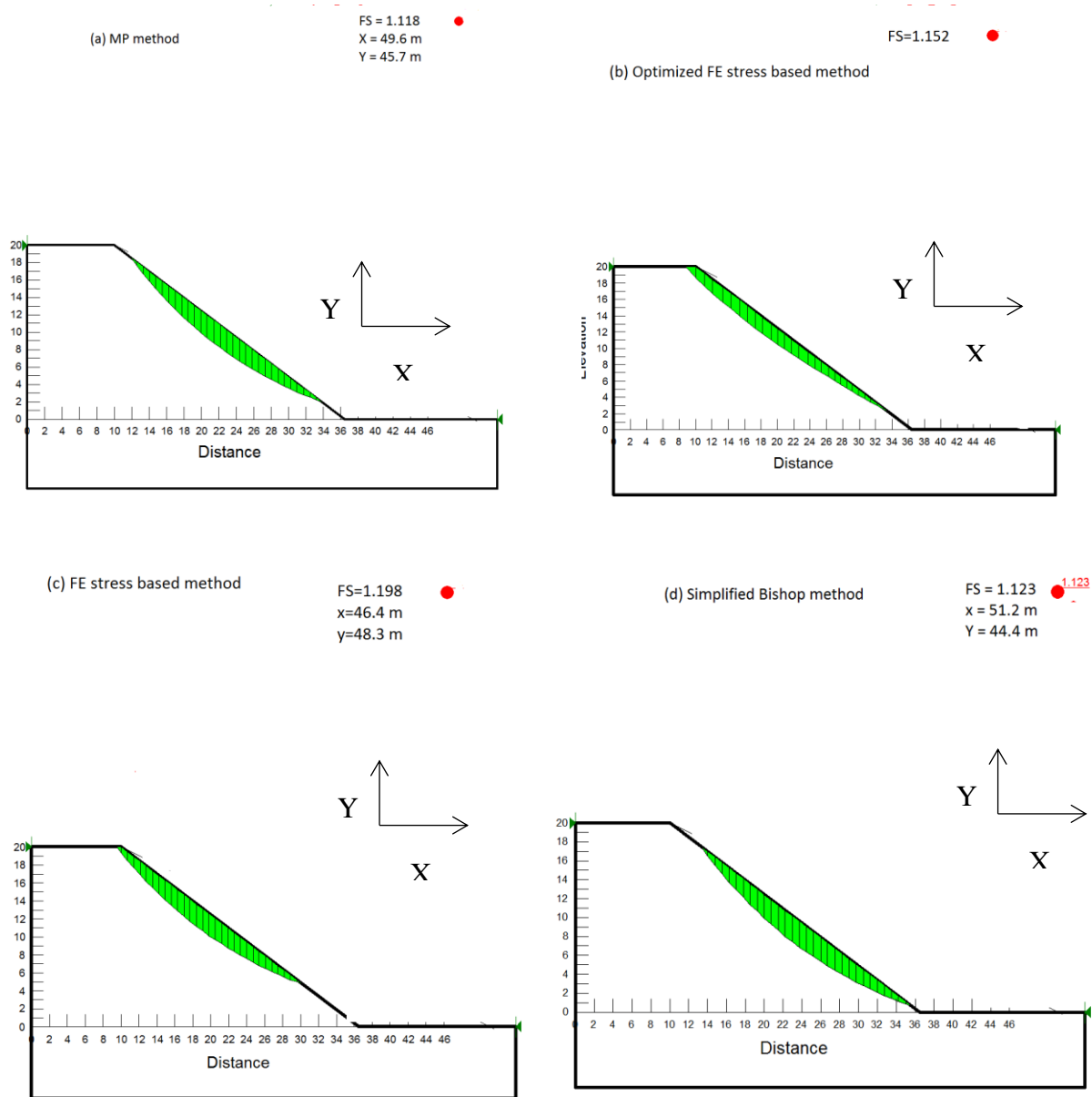
Figure 4-10: Relatively shallow critical slip surfaces, center of rotation, and FS obtained with SLOPE/W using different methods (Case S1, c_{app}=1 kPa; a) Morgenstern-Price (MP) method; b) *Optimized FS-stress* based method; c) *FE stress-based* method; d) Simplified Bishop method

Figure 4-11 presents the factor of safety and the center of rotation related to deeper slip surfaces. To obtain such deeper slip surfaces a minimum depth constraint for slip surface is defined in SLOPE/W to eliminate the shallower slip surfaces (see section 3-2-3). In these analyses, the *FE stress-based method* again gives a higher factor of safety compare to MP and Bishop Method

(1.318 versus 1.241 and 1.245 respectively). The non-circular slip (*Optimized*) surface also gives a lower factor of safety of 1.249, which is closer to the two standard methods.

It can be noted that increasing the depth of slip surface results in a higher factor of safety. For instance, an FS = 1.18 is obtained for shallow slip surface with the MP method; FS increases to 1.24 for deeper slip surface with the MP method (see Figures 4-10 and 4-11).
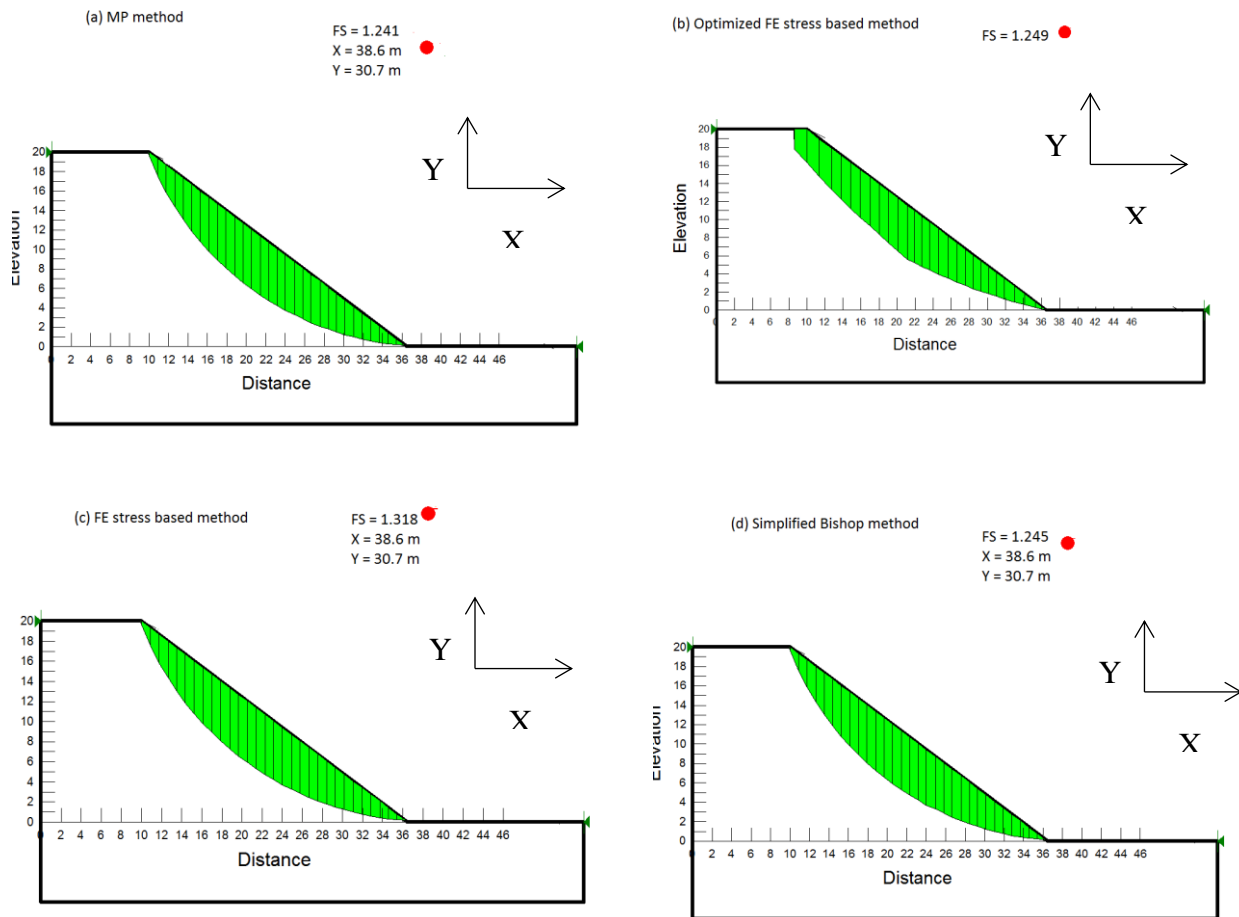
Figure 4-11: Relatively deep critical slip surfaces, center of rotation, and FS obtained with SLOPE/W using different methods (Case S1 c_{app}=1 kPa; a) Morgenstern-Price (MP) method; b) *Optimized FS-stress based* method; c) *FE stress-based* method; d) Simplified Bishop method

The stresses (and strength) distributions along the shallower slip surfaces (see Figure 4-10) for the different methods are presented in Figure 4-12.

Figure 4-12 (a) presents the shear stress mobilized along the slip surface. It is seen that for both *Optimized FE stress-based* and *FE stress-based* method, the mobilized shear stress values are higher near the toe of the slope. The values of shear strength are 25 kPa and 15 kPa for the circular *FE stress-based* and *Optimized FE stress-based* slip surfaces, while this value is close to zero for other methods.

Figure 4-12 (b) presents the shear strength distribution along the slip surface. It is seen that the shear strength distribution along the slip surface is very similar to simplified Bishop and MP method but different from *FE stress-based* (circular and *Optimized*) method. The *Optimized FE stress-based* method gives a lower peak value of the shear strength compared to the other methods, due in part to its non-circular shape (e.g. a peak value of about 20 kPa is obtained for the *Optimized FE stress-based* method while it is close to 25 kPa for the other methods).

These results indicate that the stress conditions computed by a limit equilibrium analysis may be different from that given by the finite element method. This difference is due to the localized shear stress concentrations that are not considered in the limit equilibrium method. The finite element stresses obtained with an FE analysis are thus considered more realistic for the cases analyzed here.
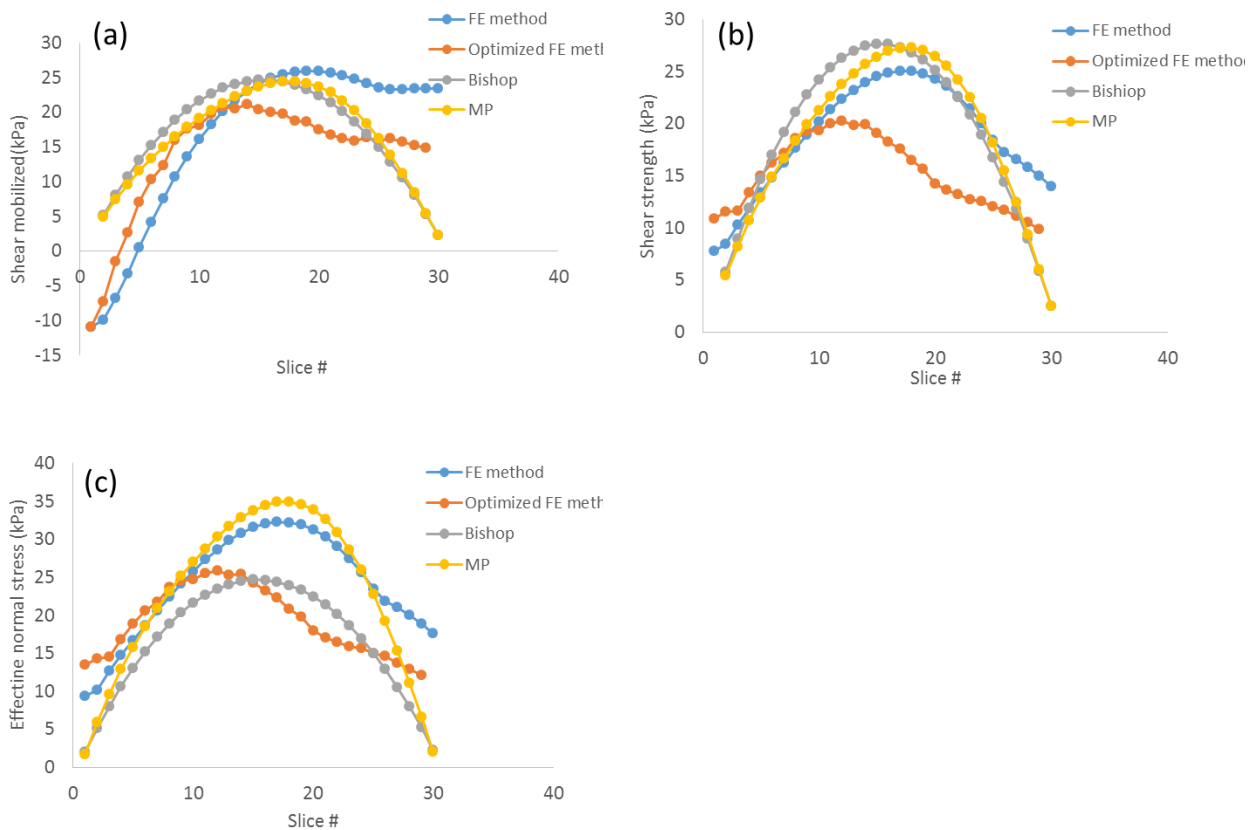
Figure 4-12: Distribution of the shear stress mobilized (a), shear strength (b) and effective normal stresses (c) along relatively shallow critical slip surface (see Figure 4-10) for different analysis methods (Case S1 c_{app}=1 kPa), obtained with SLOPE/W

The values of FS and the position of the center of the rotation are presented in Table 4-6. The values of FS can be somewhat different for each method because of the different hypotheses adopted (see more details in section 2-4-1). It is seen that the critical FS values from the different limit equilibrium methods (i.e. simplified Bishop, and Morgenstern–Price) are close to each other (with small differences due to different assumptions). The *FE stress-based* method gives higher FS. Other limit equilibrium methods (e.g. simplified Bishop, MP) do not consider the initial suction, for these cases C (= c_{app} + c') is imposed on the material. The *Optimized FE stress-based* method (where a slip surface that is not circular) often gives a lower value of FS than the circular *FE stress-based* method.

Table 4-6: FS and position of center of rotation for shallower slip surfaces (see Figure 4-10) obtained with different methods (Case S1 with c_{app} = 1 kPa)

Method	FS	Center of rotation (obtained with SLOPE/W)		
		X (m)	Y (m)	R (m)
Bishop simplified	1,123	51,2	44,4	46,47
Morgenstern-Price	1,118	49,6	45,7	46,48
FE stress-based method	1,198	46,4	48,3	46,49
Optimize FE stress-based method	1,152	N/A	N/A	N/A

With limit equilibrium methods of slices (such as simplified Bishop, MP), the assumption is that the value of FS does not change from one slice to another along the slip surface. However, with the *FE stress-based* methods, the value of local FS can vary from one slice to another (see section 3-2-3).

Figure 4-13 presents the local FS values for different calculations methods for Case S1 (c_{app} = 1 kPa). The value of FS for the different limit equilibrium methods is constant along the slip surface for all the slices, while it can change dramatically for the *FE stress-based* methods. The higher values are around 5 for the upper slices (close to crest), and the lower values (around 0.6) are for the slices near the toe.
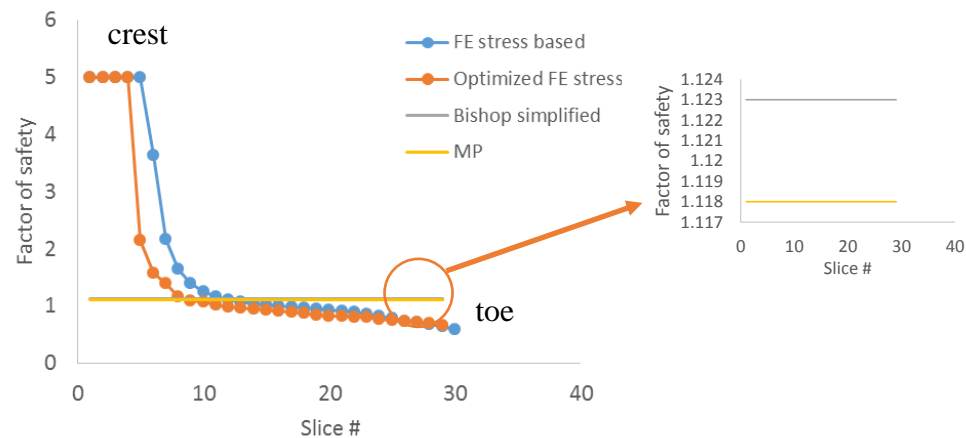
Figure 4-13: Local factor of safety per slice for the different analysis methods (*FE stress-based* method, *Optimized FE stress-based* method, simplified Bishop, MP), Case S1, c_{app}= 1 kPa

4.7.2 **Detailed calculations result for Case S11**

Figure 4-14 presents the pore water pressure distribution within Case S11 (homogeneous waste rock pile with two benches ($\alpha = 26°$, $\beta = 37°$), and waste rock as foundation material) simulated with SIGMA/W, with $c_{app} = 1$ kPa. The PWP along lines A, B, C, and D are constant (PWP $\approx$ -6 kPa); this value corresponds to $c_{app} = 1$ kPa within the pile.
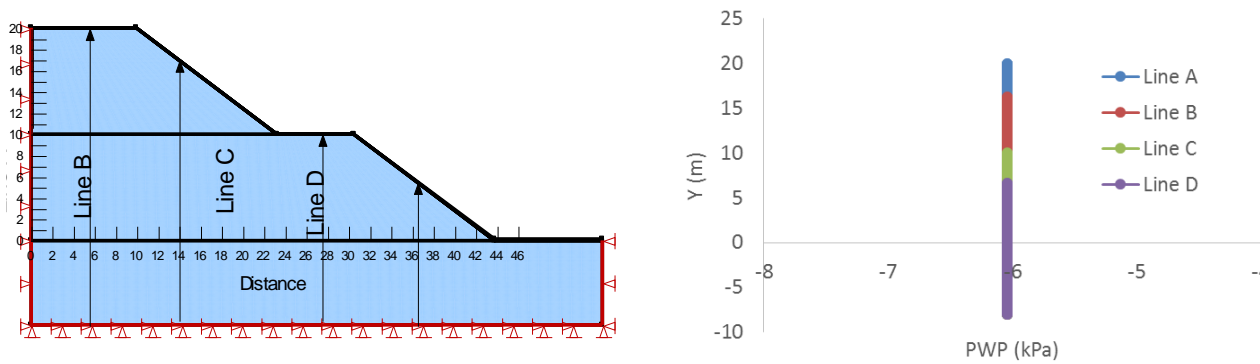
Figure 4-14: PWP distribution for Case S11 (c_{app} =1 kPa) along lines A, B, C, and D obtained with SIGMA/W

Figure 4-15 presents the contour plots of vertical total stress distribution within the waste rock pile (results from SIGMA/W). Like Case S1, the total stress on the ground surface is zero and increases with depth. Vertical stress contours are not always at a constant distance from the ground surface. For example, the 50 kPa contour is much closer to the ground surface near the slope and the toe of the waste rock pile. This indicates the influence of shear stress on the vertical stresses.
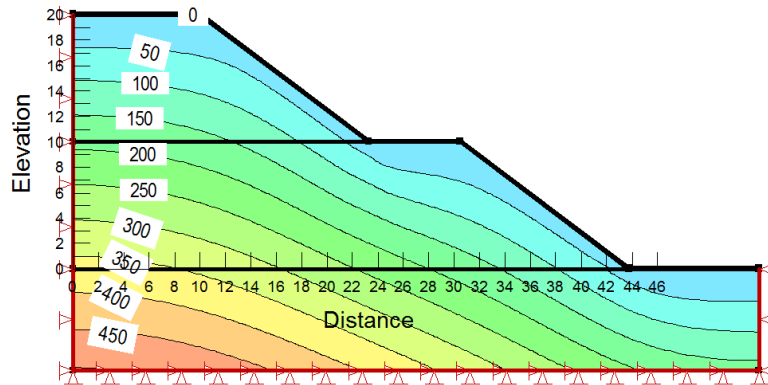
Figure 4-15: Total vertical stress σ_y contours (kPa) computed with SIGMA/W (S11) for c_{app} =1 kPa

Figure 4-16 shows vertical effective stresses σ'_y for Case S11 with c_{app}= 1 kPa. It is apparent that the value of effective stress on the ground surface is close to 6 kPa (representing initial PWP) and it satisfies the relation $\sigma' = \sigma - PWP$ (0- -6 kPa). It also shows that there is an increase in the vertical effective stresses in the depth of the pile due to the increase of vertical total stress.
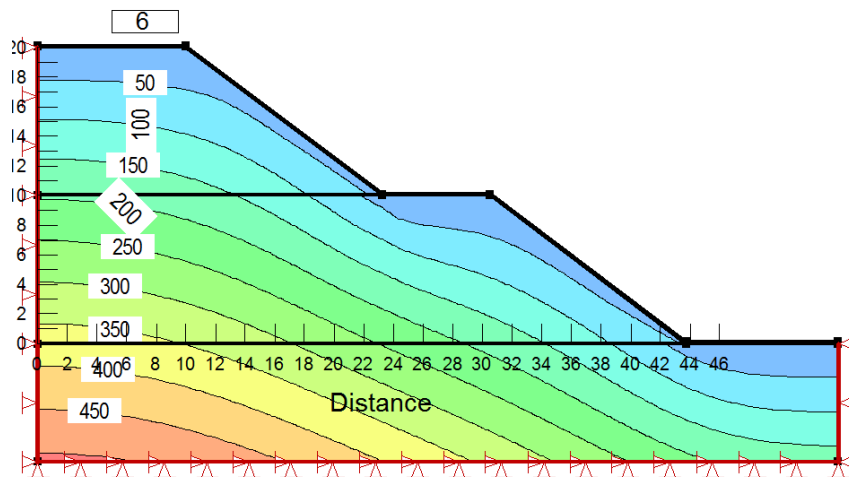
Figure 4-16: Vertical effective stress σ'_y contours (kPa) computed with SIGMA/W (Case S11, with c_{app} =1 kPa).

Figure 4-17 presents the slip surfaces, factors of safety and the centers of rotation of the slip surfaces for four different methods including Morgenstern-Price, simplified Bishop, *Optimized* and circular *FE stress-based* method. The slip surface for the *Optimized FE stress-based* method

is the shallowest of all the methods. It is seen that the slip surface is deeper near the crest of the pile for *FE stress-based* methods (circular and *Optimized*). The overall shape of slip surface is not significantly changing from one method to other, but the calculated FS is the smallest for MP method and largest for circular *FE stress-based method*.
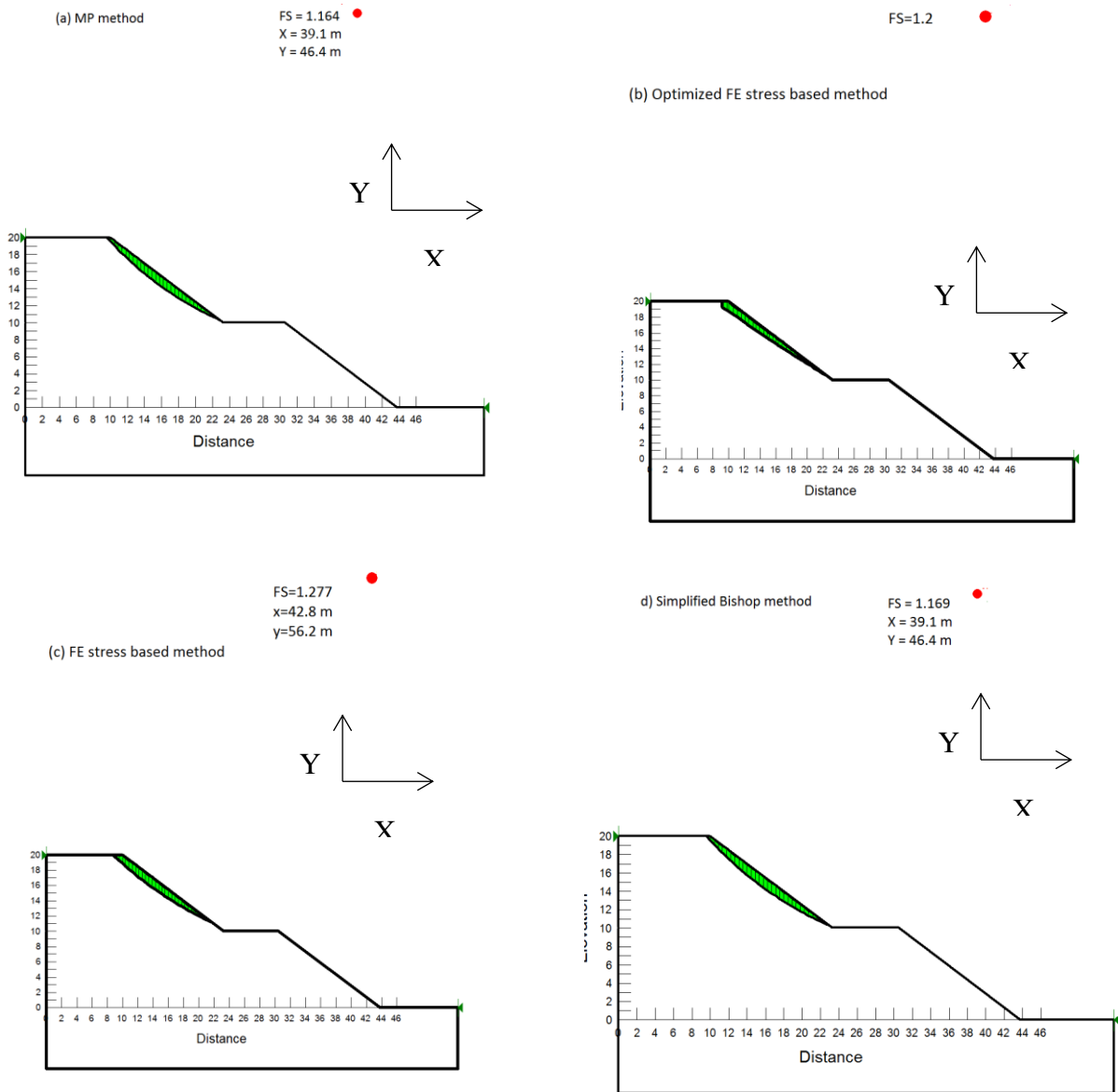
Figure 4-17: Relatively shallow critical slip surfaces, center of rotation and FS obtained with SLOPE/W using different methods (Case S11, c_{app}=1 kPa); a) Morgenstern-Price (MP) method; b) *Optimized FS stress-based* method; c) *FE stress-based* method; d) Simplified Bishop method

Figure 4-18 presents the global slip surfaces and related FS obtained with different methods. The slip surfaces enter the waste rock pile at some point in the crest and exit the pile from the toe. It shows a similar trend as local slip surface. The highest factor of safety is obtained with circular *FE stress-based* method and the lowest FS obtained with *Optimized FE stress-based* method, presenting a non-circular shape.
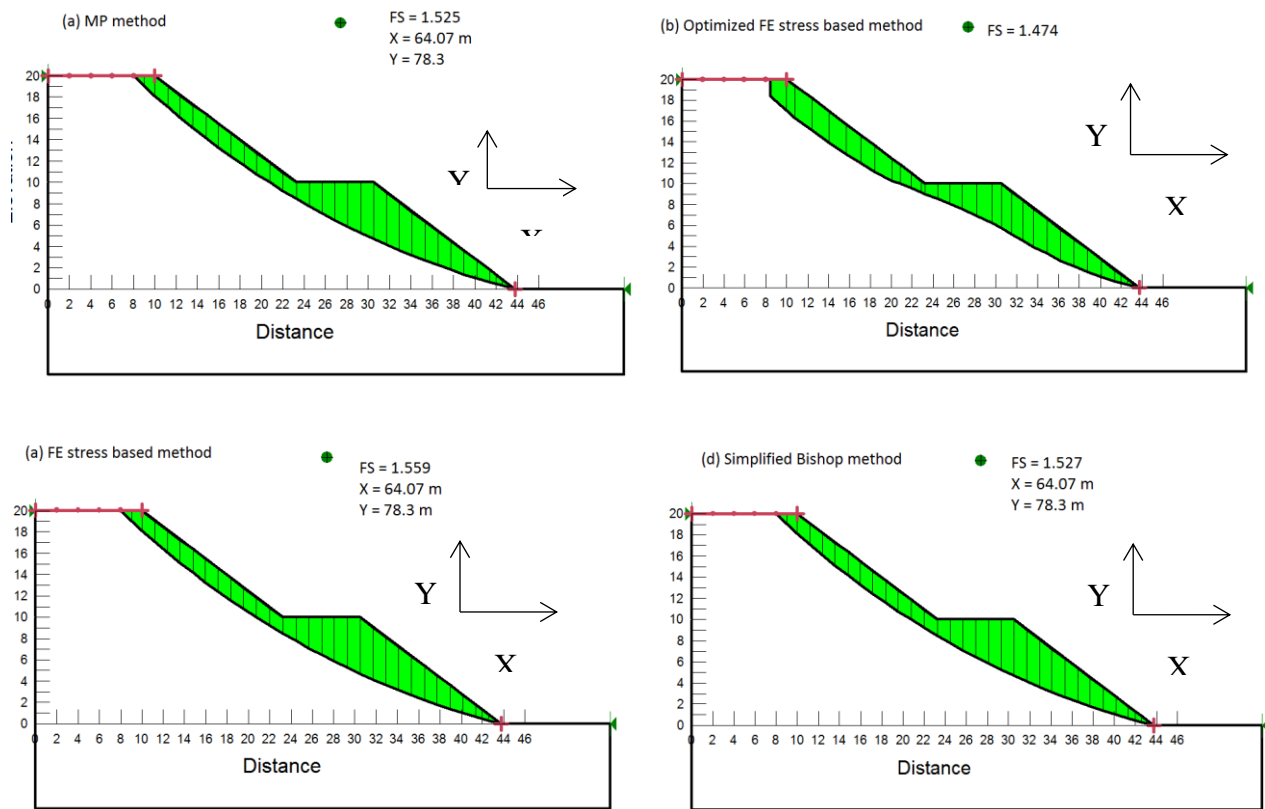
Figure 4-18: Relatively deeper critical slip surfaces (entering the crest and exiting the toe), related center of rotation obtained with SLOPE/W using different methods (Case S11, c_{app}=1 kPa); a) Morgenstern-Price method (MP); b) *Optimized FS stress-based* method; c) *FE stress-based* method; d) Simplified Bishop method

Figure 4-19 presents the shear mobilized (a) shear strength (b) and effective normal stress (c) distribution along the global critical slip surface.

The distribution of shear mobilized for limit equilibrium methods does not show significant changes from one method to another. Nonetheless it is different for the circular and *Optimized FE stress-based* methods. The shear mobilized is close to zero at the beginning and end of slip surface (i.e. slices no. 1 and 30) for limit equilibrium methods, whereas it has values close to 10 and 25 kPa for *Optimized* and circular *FE stress-based* methods, respectively (4-19, a).

This shows the shear strength distribution for limit equilibrium methods (e.g. simplified Bishop, MP) are similar yet differ from *FE stress-based* methods (circular and *Optimized*). In upper bench, the shear mobilized is higher for *FE stress-based* method (peak 30 kPa vs. 15 kPa for *FE stress-based* methods and limit equilibrium methods) while they are lower on the lower bench (peak 30 kPa vs. 40 kPa for *FE stress-based* methods and limit equilibrium methods). The peak value of shear mobilized in upper, and the lower bench is close in *FE stress-based* method while in other limit equilibrium methods a higher peak is observed for the lower bench (see Figure 4-19(b)). Likewise, the value of shear strength at the beginning and end of slip surface is close to zero for limit equilibrium methods; however, they have higher values for circular and *Optimized FE stress-based* methods (between 10 kPa to 25 kPa).

The distribution of effective normal stress for critical slip surface in Figure 4-19 (c) is similar to the shear strength distribution.
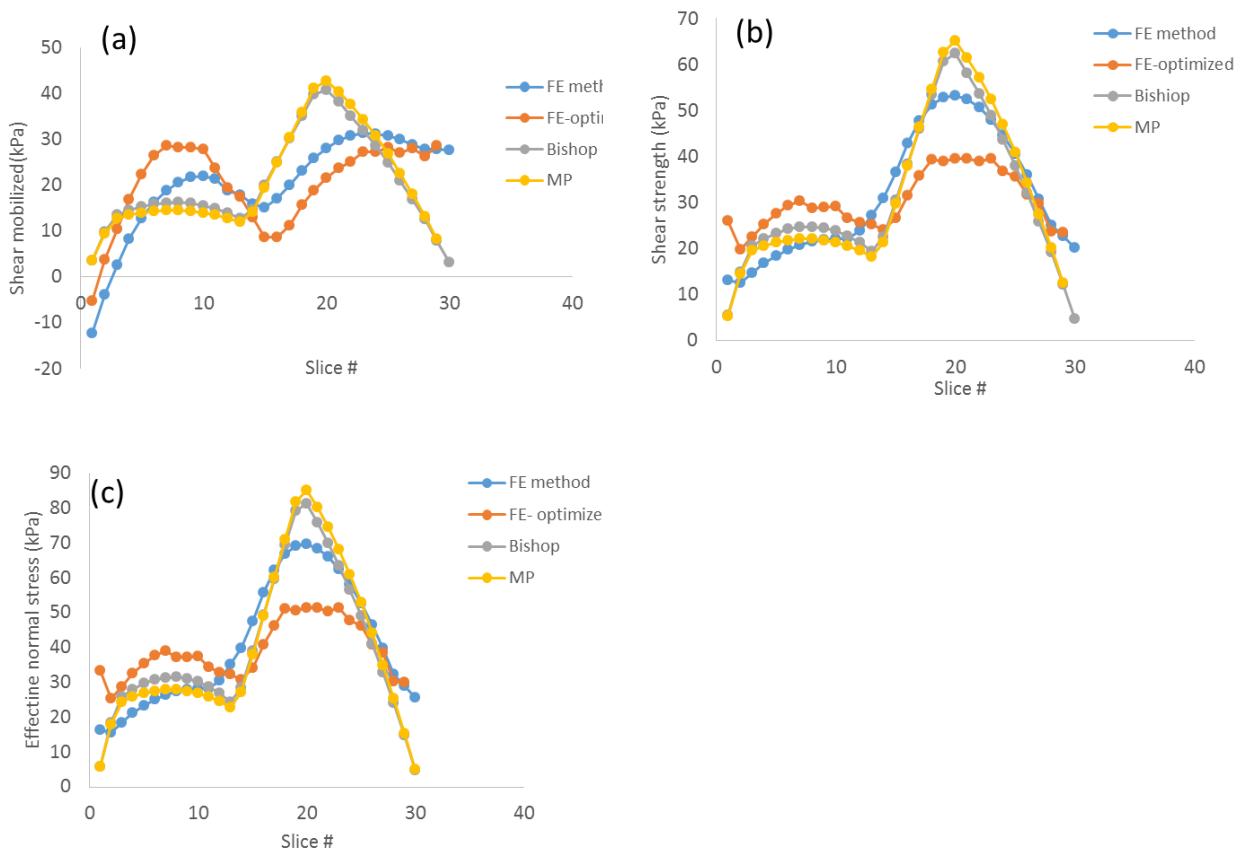
Figure 4-19: Distributions of the a) shear stress mobilized; b) shear strength; c) effective normal stresses; along critical slip surface for different analysis methods obtained with SLOPE/W (see also Figure 4-18)

Table 4-7 presents the FS and its related center of rotation for critical global slip surface in Figure 4-18. The FS is higher for the *FE stress-based* method compared to other methods. It is seen that the *Optimized FE stress-based* method (which does not have a circular shape) gives a lower factor of safety compare to *FE stress-based* method with a circular shape (Figure 4-18).

Comparing Tables 4-7 and 4-8 indicate that the values of FS for Case S11 are higher compared to Case S1 (from different methods). For both cases, the FS obtained with the *Optimized FE stress-based* method is lower compared to FS from *FE stress-based* method.

Table 4-7: FS and details of center of rotation for different method (Case S11), $c_{app} = 1$ kPa

Method	FS	Centre of rotation (obtained with SLOPE/W)		
		X (m)	Y (m)	R(m)
Bishop simplified	1,527	64,07	78,3	80,89
Morgenstern-Price	1,525	64,07	78,3	80,89
FE stress-based method	1,559	64,07	78,3	80,89
Optimize FE stress-based method	1,474	NA	NA	NA

It indicates the local FS starts from 5 for slices near the crest and decreases to a value close to 0.5 for the slice near the toe, with the FE stress-based methods. For slices, # 15 to 20 the local FS is different for *FE stress-based* and *Optimized FE-stress based* methods. These mid slices have higher local FS and smaller depth for *Optimized FE stress-based* method (see Figure 4-18).

For each slice, the local FS in *FE stress-based* methods is either higher or lower compared to global FS for limit equilibrium methods. It is seen that for a few slices, the local FS appears to be smaller than 1 even if this is not physically possible.

This suggests that the computed stressed in some zones are higher that the available soil strength. These unrealistic results appear to be due to some numerical convergence issues (as indicated in the Slope/W manual); as this situation is much localised, it is not expected to influence the outcome of the analysis significantly.
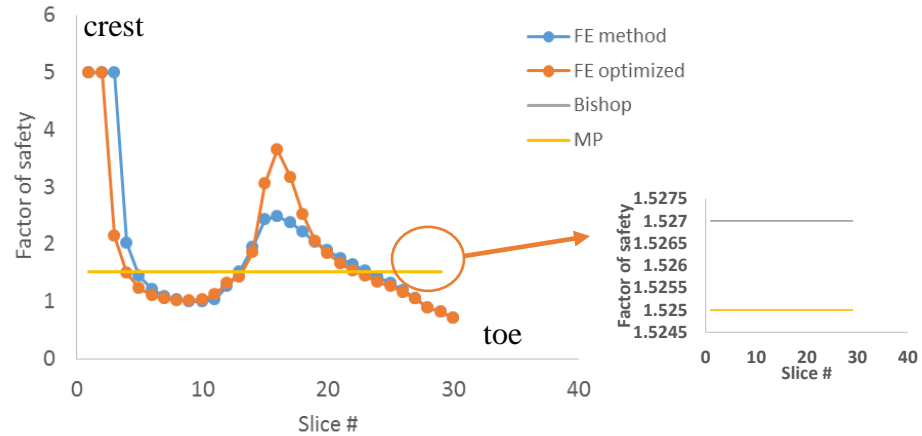
Figure 4-20: Local factor of safety per slice for different methods (*FE stress-based*, *Optimized FE stress-based*, simplified Bishop, MP), Case S11, c_{app} =1 kPa

4.7.3 **Detailed calculations result for simulation S21**

Figure 4-21 presents the PWP distribution within a waste rock pile (S21, with 2 benches and 2 horizontal compacted layers, $\alpha = 26°$, $\beta = 37°$) with $c_{app} = 1$ kPa. Along lines A, B, C, and D, the pore water pressure is constant in waste rock material ($\approx$ - 6 kPa), and it is also constant within the compacted waste rock layers ($\approx$ - 1 kPa).
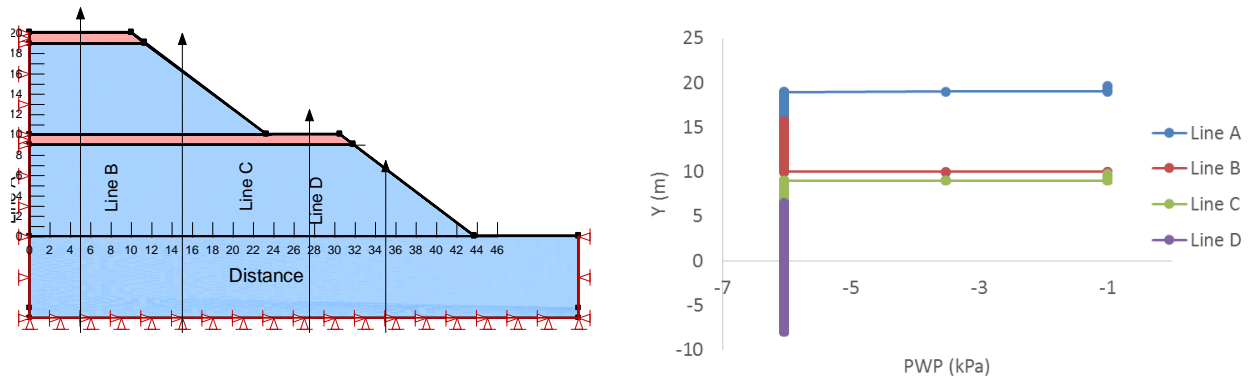
Figure 4-21: PWP distribution for Case S21, c_{app} =1 kPa, along lines A, B, C, and D obtained with SIGMA/W

SIGMA/W was used to calculate the vertical normal stresses distribution. As shown in Figure 4-22, the vertical stresses increase within depth. The distance of a given stress isocontour is not constant from the ground surface. These are somewhat closer to the ground surface near the toe of the pile, due to the effect of stress redistribution along the slope.
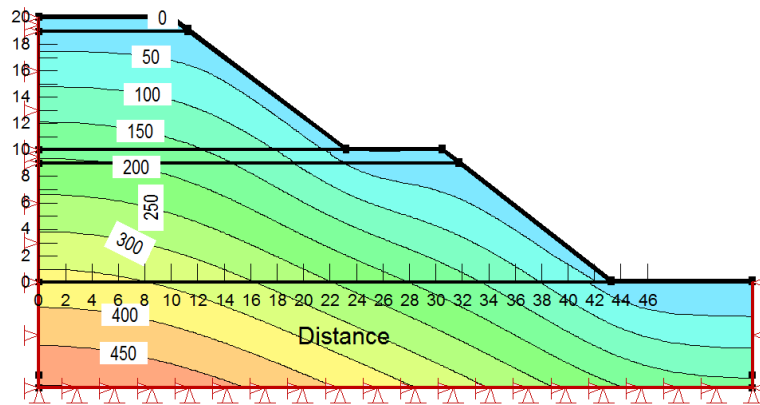
Figure 4-22: Total vertical stress σ_y contours (kPa) computed with SIGMA/W (S21, for $c_{app} = 1$ kPa)

Figure 4-23 shows vertical effective stresses σ'_y for Case S21 with $c_{app} = 1$ kPa. Effective stress on the ground surface in the layer is close to 1 kPa (representing initial PWP in the compacted layer), and it satisfies the relation $\sigma' = \sigma - PWP$ (0 – (-1kPa)). There is an increase in the vertical effective stresses at depth as a result of the increase in vertical load.
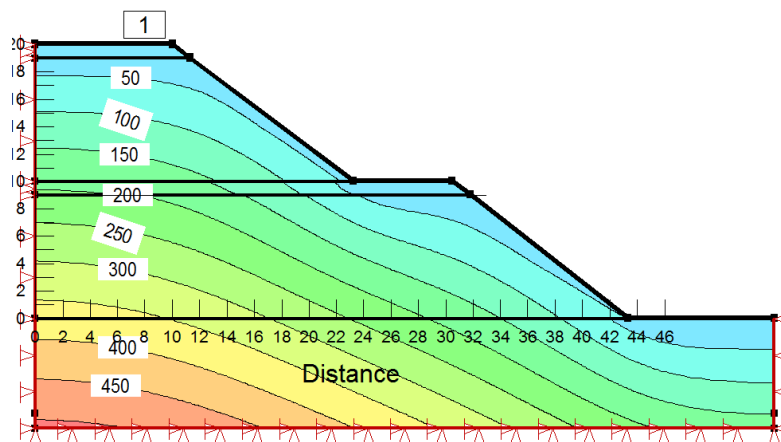
Figure 4-23: Vertical effective stress σ'_y contours (kPa) computed with SIGMA/W (Case S21, $c_{app} = 1$ kPa)

Figure 4-24 presents the distribution of shear mobilized, shear strength, and effective normal stresses along the local critical slip surface. Figure 4-24 (a) presents the distribution of shear mobilized along the critical slip surface. It is observed that *Optimized FE stress-based* and *FE stress-based* methods present higher shear mobilized near the toe.

The shear strength (kPa) at the beginning and end of a slip surface is close to zero for simplified Bishop and MP, whereas higher values (≈ 17 and 30 kPa at the beginning, and ≈ 10 kPa at the end) are observed for circular and *Optimized FE stress-based* methods (Figure 4-24 (b)). The distribution of effective normal stress is very similar to that of shear strength.
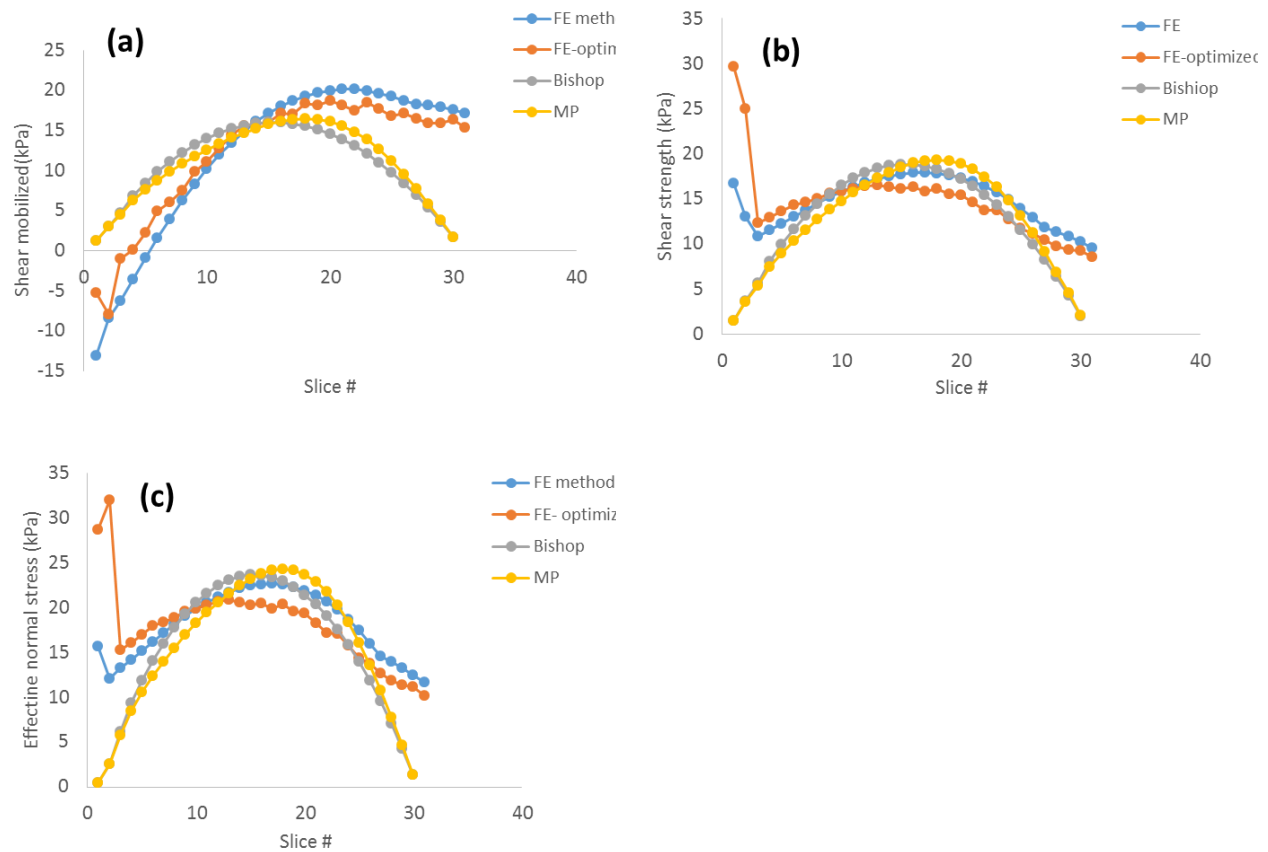
Figure 4-24: Distributions of the a) shear stress mobilized; b) shear strength; c) effective normal stresses, along local critical slip surface (Case S21, c_{app} =1 kPa) for different analysis methods obtained with SLOPE/W

Figure 4-25 presents the local FS per slice along the local critical slip surface. The local FS in not changing between slices in limit equilibrium methods, but it varies significantly in *FE stress based* methods. The FS is high for slices near the crest (SF = 5) and it is very low near the toe (FS ≈ 0.5)
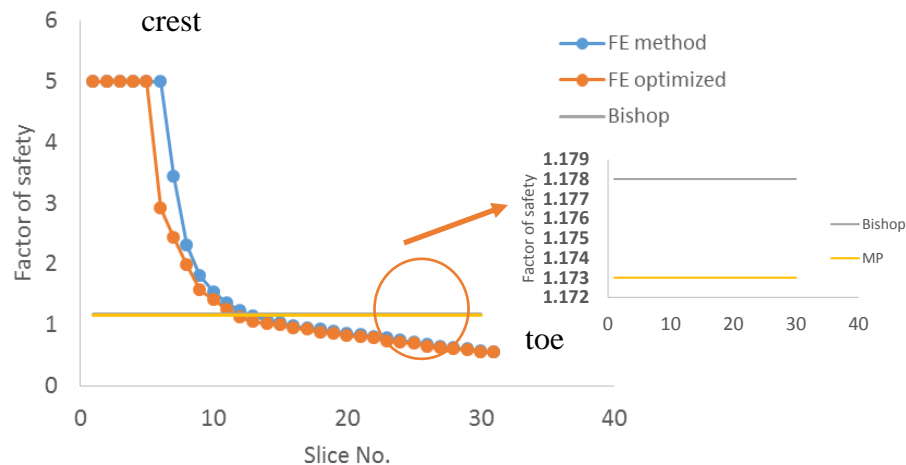
Figure 4-25: Local factor of safety per slice obtained with different methods (Case S21, c_{app} =1 kPa)

Table 4-8 presents the FS and the related center of rotation for local critical slip surface. The radius and FS are higher for the *FE stress-based* method compared to other methods. The *Optimized FE stress-based* method (which does not have a circular shape) gives a lower factor of safety compared to *FE stress-based* method with a circular shape.

Table 4-8: FS and centers of rotation for critical local slip surfaces with different methods (Case S21, c_{app} =1 kPa)

Method	FS	Centre of rotation		
		X (m)	Y (m)	R(m)
Local slip surface				
Bishop	1,178	30	32,9	23,79
Morgenstern-Price	1,173	30	32,9	23,79
FE stress-based method	1,284	37,2	46,2	38,73
Optimize FE stress-based method	1,245	NA	NA	NA

4.7.4 **Effect of c and ϕ' and comparisons with the Cousins charts**

As mentioned in section 2-4-2, the target value of FS for a large slope should be between 1.3 and 1.5 for waste rock piles during mining operations; FS = 1.5 is recommended for long-term behavior upon closure (Aubertin, 2013).

The analyses of a single bench waste rock pile like Case S1 can be performed in a simplified method by considering c', ϕ', and γ as constants. Graphical solutions can then be used to calculate the factor of safety, such as the charts developed by Cousins (1978). Figure 4-26 shows the geometry used for the Cousins' charts. It represents a single bench pile slope with a height of H, slope angle β and material parameters c', ϕ', and γ. This geometry is similar to that of Case S1 (Table 4-4).
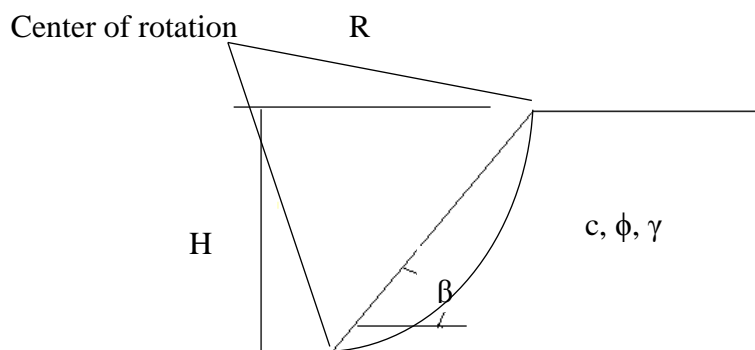
Figure 4-26: Slope geometry for Cousins' chart, adapted from Coduto (1999)

One of Cousins charts is presented in Figure 4-27. It is valid for a homogenous soil, with the ground water table well below the toe of the slope (i.e. PWP = u = 0). The first step to apply this chart is to calculate the value of $\lambda_{c\phi}$ from Equation 4-2.
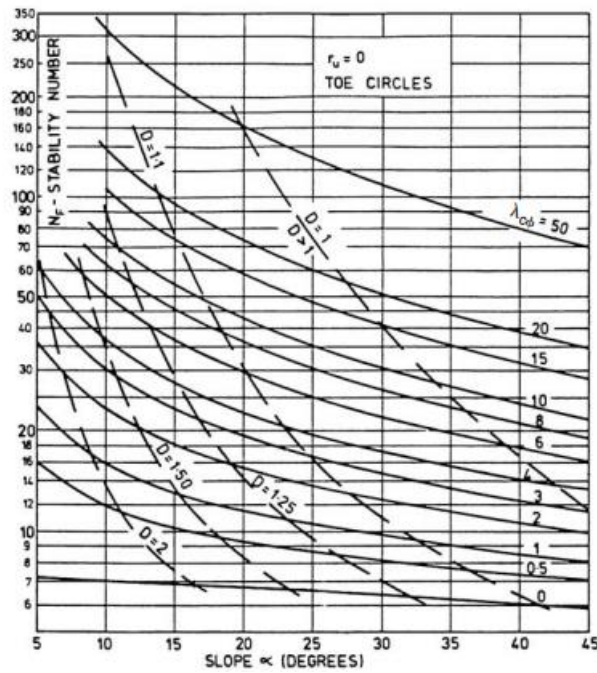
Figure 4-27: One of Cousins's (1978) charts for failure analysis through the toe of slopes with zero pore water pressure (adapted from American Society of Civil Engineers)

$$\lambda_{c\phi} = \frac{\gamma H \tan\phi}{c} \qquad\qquad [4\text{-}2]$$

The value of N_f can be retrieved from the graph (Figure 4-27). The value of N_f gives the value of factor of safety:

$$FS = N_f \, N_s \qquad\qquad [4\text{-}3]$$

Where $N_s = c / \gamma H$

Case S1 is used to help validate the stability analyses performed above with the code and with the Cousin's charts. The single bench pile height is 20 m and the deposition angle $\alpha = \beta = 37°$. Different values of the internal friction angle ϕ' ($= 30°$ to $50°$) and cohesion c' ($= 0$, 10, 25 and 50 kPa) are considered.

The limiting value of FS determined for the single bench pile made of a homogeneous material without cohesion is given by FS = tanϕ'/tanα (for a planar slip surface, dry case; (Caldwell and Moss, 1981)).

For cases with a non-zero cohesion (i.e. C = c_{app} > 0 for the unsaturated cases), the results are obtained with the graphical (charts) solutions provided by Cousins (1978) (see also (Coduto, 1999); these are presented in Figure 4-28 as *Analytic results*.

For the numerical analysis, two different approaches are considered. The first approach, identified as *Numerical with c_{app}* (see Figure 4-28), represents the situation when there is no cohesion (c' = 0), and the initial negative pore water pressure represents c_{app}. The second approach represents with the assumption that total cohesion is equal to the apparent cohesion plus effective cohesion (C = c' + c_{app} with c' = 0), and there is no suction within the material (identified as *Numerical with C*).

Figure 4-28 indicates that the results from these two different approaches are close to each other and also close to the values obtained with the Cousins (1978) charts. Hence, the results obtained with *FE stress-based* method give reasonable FS values (with the correct trends), confirming that this method is reliable.

These results indicate that the factor of safety increases with both ϕ' and C (as expected). For example, for C = 10 kPa, when ϕ' increase from 35° to 45° the FS increases from 1.4 to 1.7. For ϕ' = 37°, the FS increases from 1.4 to 1.7 when C increases from 10 kPa to 25 kPa (more results are presented in Appendix A).
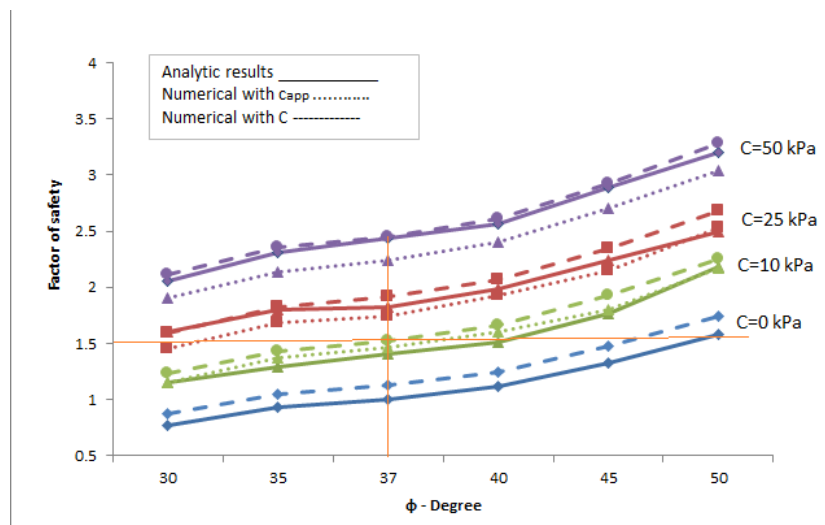
Figure 4-28: Factor of safety of a homogenous waste rock pile (Case S1, Table 4-4), for different ϕ' (= 30 to 50°) and C (= c_{app} = 0, 10, 25 and 50 kPa); obtained with SIGMA/W and SLOPE/W (*FE stress-based* method) compared with results from the Cousins' (1978) charts (for c > 0) and from the basic slope stability relationship (FS = $\tan\phi'/\tan\alpha$, for c = 0)

4.7.5 **Relationship between FS and apparent cohesion**

It is sometimes convenient to express the factor of safety FS as a function of the dimensionless ratio $c/\gamma H_t$ (or $c_{app}/\gamma H$, in this case, H_t is the waste rock pile height over the ground)

Different calculations were conducted (with SIGMA/W and then SLOPE/W) for the five main types of waste rock pile (Cases S1, S11, S21, S31, and S35; see Tables 4-4 and 4-5) to investigate the influence of ϕ' and c_{app}. The ϕ' for waste rock material is assumed to vary from 30° to 37° to 45°, and C = c_{app} can be equal to 1, 5, 10, or 25 kPa (c' value is zero). The foundation material is considered to be waste rock. The critical slip surfaces and their related factor of safety are obtained with the *Optimized FE stress-based* method.

The results are shown in Figure 4-29 (a, b, c, d, and e). They indicate that for a given ratio $c_{app}/\gamma H$, increasing the value of ϕ' raises the factor of safety of the waste rock piles. Also, as expected, a larger apparent cohesion enhances the value of FS. For instance, it is seen in Figure 4-29 (a) that for Case S1 with $c_{app}/\gamma H$= 0.04, FS increases from 1.1 to 1.4 to 1.7 when ϕ' goes from 30° to 37° to 45°, respectively. In Figure 4.29 (b), for Case S11 with ϕ' = 37°, increasing

$c_{app}/\gamma H$ from 0.012 to 0.025 to 0.065, increases FS from 1.2 to 1.3 to 1.6, respectively. The same trend is seen in Figures 4.29 (c) (Case S21), (d) (Case S31) and (e) (Case S35). For $c_{app}/\gamma H = 0.04$ it is seen for instance that the value of FS goes from 1.4 to 2 (Figure 4-29 c), 1.45 to 2.2 (Figure 4-29 d) and 1.4 to 2.15 (Figure 4-29 e) when ϕ' increases from 30° to 45°.
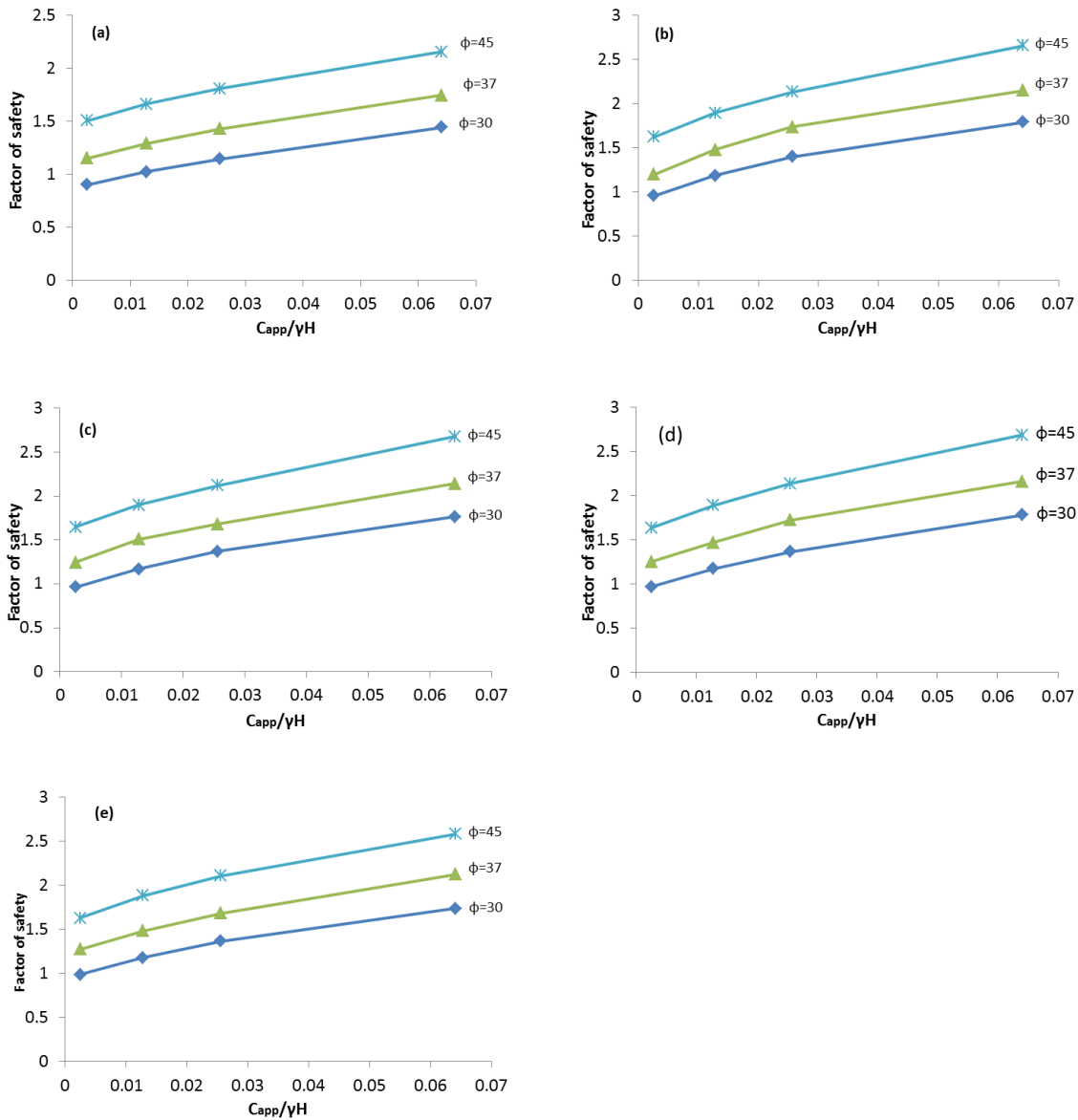
Figure 4-29: Relationship between the factor of safety FS and the dimensionless ratio $c_{app}/\gamma H_t$, for waste rock piles with $\phi' = 30°$, 37° and 45° and c_{app}= 1, 5, 10 and 25 kPa; a) Case S1; b) Case S11 ; c) Case S21 ; d) Case S31; e) Case S35 (see Tables 4-4 and 4-5 for details)

Figure 4-30 illustrates the detailed results for the shear strength, mobilized stress state, normal stress and local FS along the critical slip surfaces obtained with *FE stress- based* method for Case S1 (with c_{app} = 1, 5, 10 and 25 kPa). It is seen that the trends for shear strengths, shear stresses mobilized, and normal stresses distributions are similar for the different values of c_{app} (for Case S1).

The increase of c_{app} results in an increase of the normal stress, shear strength and mobilized (induced) shear stress along the critical slip surface (Figure 4-30 (a), (b) and (c) respectively). Figure 4-30 (d) show the local factor of safety (for each slice) along the slip surface.

It indicates that a lower c_{app} results in a lower factor of safety for most slices; for instance, the local FS for slices 8 to 30 is smaller or close to 1 for c_{app}=1 kPa, while it is close to 1.5 for c_{app}= 25 kPa.

Figure 4-30: Distribution a) shear strength; b) mobilized stress state; c) normal stress; d) local FS; along the critical slip surface, Case S1, c_{app} (= 1, 5, 10 and 25 kPa); results obtained with *Optimized FE stress-based* method

Figure 4-31 shows the changes of the global FS with the dimensionless ratio $c_{app}/\gamma H$, for the five main types of waste rock pile (Cases S2, S12, S22, S32, and S36). These calculations were conducted with SIGMA/W and then SLOPE/W with *Optimized FE stress-based* method to investigate the influence of ϕ' and c_{app} on the critical global slip surface obtained (see Figure 4-31 (f)).

The results shown in Figure 4-31 (from a to e) indicate, for a given ratio $c_{app}/\gamma H$, the factor of safety increases with ϕ'. As expected, a larger apparent cohesion also increases FS. For example, in Figure 4-31 (a) for Case S2 with $c_{app}/\gamma H= 0.032$, FS increases from 1.5 to 2.4 when ϕ' increases from 30° to 45°. In Figure 4-31 (b), when $c_{app}/\gamma H$ increases from 0.006 to 0.03, FS increases from 1.6 to 1.8 for Case S21 with $\phi' = 37°$.

This same trend is observed in Figures 4-31 (c) (Case S22), (d) (Case S32) and (e) (Case S36). For $c_{app}/\gamma H = 0.04$, the value of FS changes from 1.4 to 2 (Figures 4-31c), 1.45 to 2.2 (Figures 4-31d) and 1.4 to 2.15 (Figures 4-31e) when ϕ' increases from 30° to 45°.
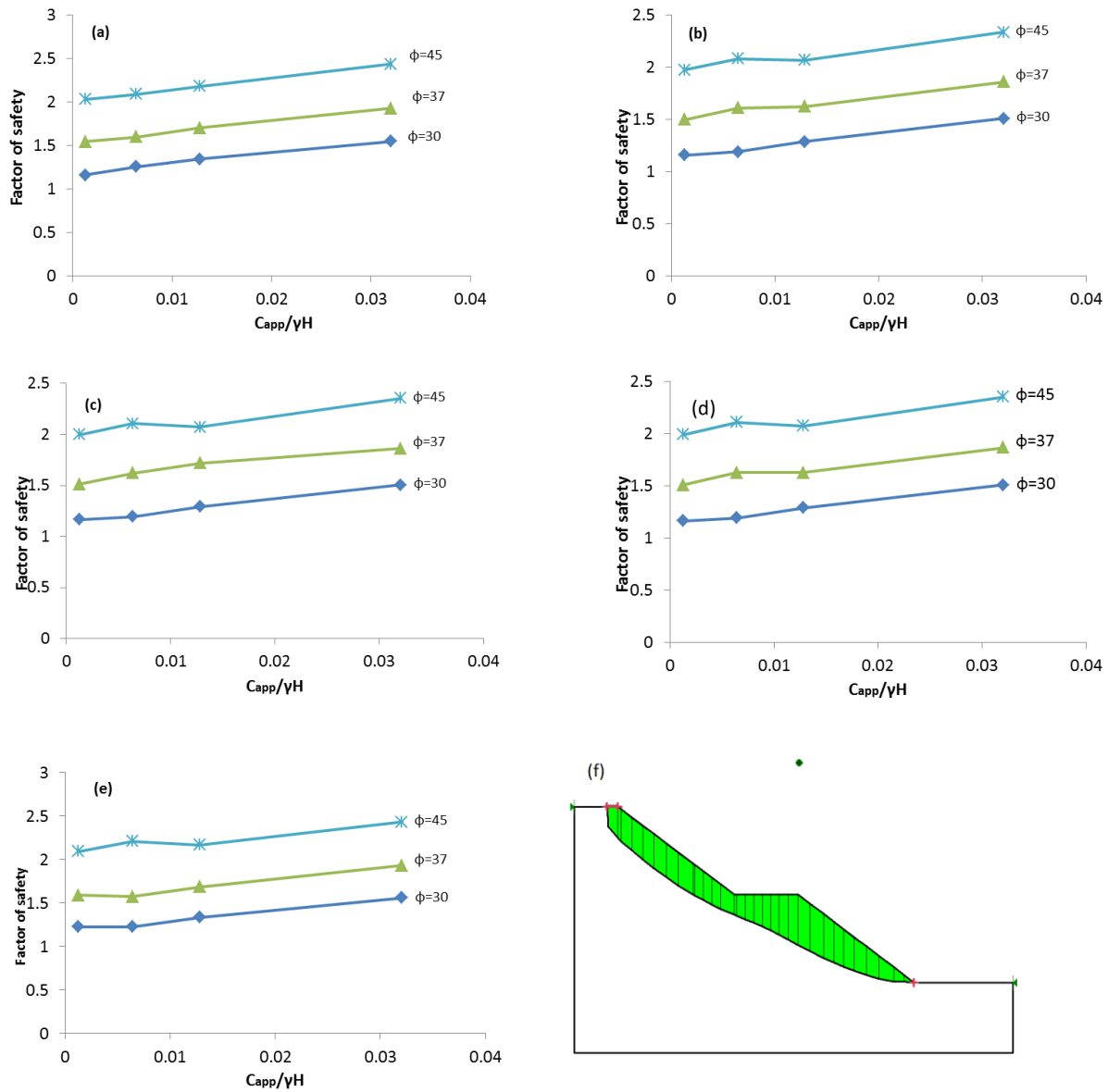
Figure 4-31: Relationship between the factor of safety FS and the dimensionless ratio $c_{app}/\gamma H_t$, for waste rock piles with $\phi' = 30°$, $37°$ and $45°$; $c_{app}= 1, 5, 10$ and 25 kPa; a) Case S2; b) Case S12; c) Case S22; d) Case S32; e) Case S36; f) typical global slip surface obtained with *Optimized FE stress-based* method

4.7.6 **Relationship between FS and height of the pile H_t**

The height of the pile H_t can affect the factor of safety FS. Calculations were conducted with various geometries for Group 1 (Cases S1 to S4, H_t = 20 m to 120 m), Group 2 (Cases S11 to S14, H_t = 20 m to 120 m), Group 3 (Cases S15 to S17, H_t = 40 m to 120 m), Group 4 (Cases S21 to S24, H_t = 20 m to 120 m), Group 5 (Cases S25 to S27, H_t = 40 m to 120 m) and Group 6 (Cases S31 to S34, H_t = 20 m to 120 m) (see Tables 4-4 and 4-5 for more details). The local slope angle β = 37°, ϕ' = 37°, different c_{app} (= 1, 5, 10 and 25 kPa) have been considered.

Figure 4-32 (a) illustrates the results obtained for a homogeneous pile with a single bench (Cases S1 to S4). These results indicate that a larger height results in a lower factor of safety for a given cohesion c_{app}. For a given height, a higher cohesion provides a larger factor of safety, the effect of height on FS appear to be more pronounced for larger c_{app} values.

Similar observations can be made for piles with two benches (Figure 4-32 (b), for Cases S11 to S14. A higher pile results in a lower factor of safety. For a given height, a larger apparent cohesion results in an increased FS. As an example, for c_{app}= 25 kPa, FS decreases from 2.1 to 1.5 when the height of pile increases from 20 m to 120 m.

Figure 4-32 (c, d, e, and f) present results obtained for the waste rock piles with two benches and compacted layers, two benches and compacted layers with 1% inclination, three benches and three benches with compacted layer respectively. The same patterns are observed for all these cases, indicating that regardless of the geometry, increasing the pile height results in decreasing FS. However, this effect seems more pronounced at lower values of H_t.
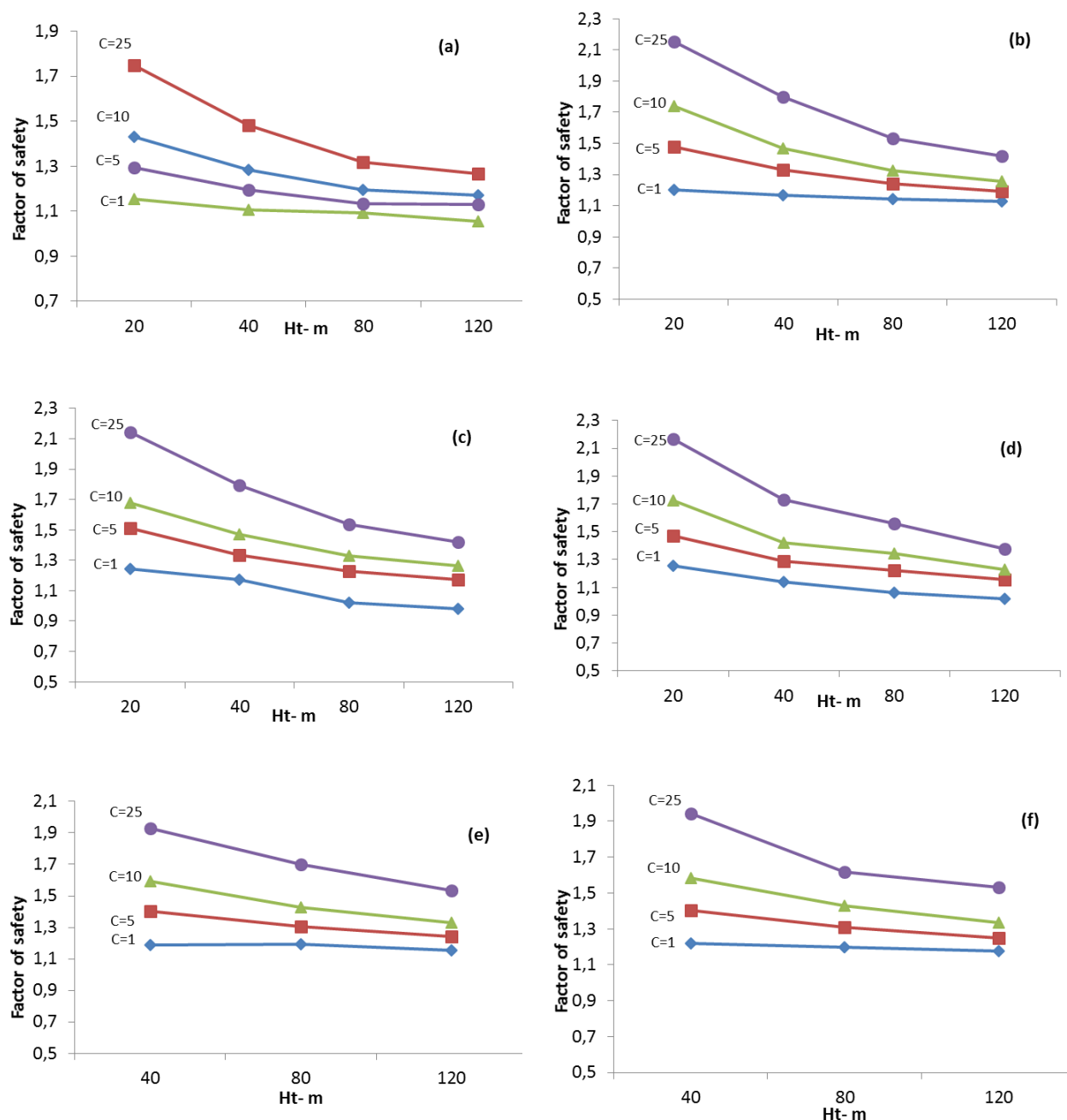
Figure 4-32: Relationship between the factor of safety FS and pile height H_t; a) Group 1(Cases S1 to S4, H_t = 20 m to 120 m); b) Group 2 (Cases S11 to S14, H_t = 20 m to 120 m); c) Group 4 (Cases S21 to S24, H_t = 20 m to 120 m); d) Group 6 (Cases S31 to S34, H_t = 20 m to 120 m); e) Group 3 (Cases S15 to S17, H_t = 40 m to 120 m); f) Group 5 (Cases S25 to S27, H_t = 40 m to 120 m); ϕ' = 37° and c_{app} = 1, 5, 10 and 25 kPa

4.7.7 **Relationship between FS and global slope angle α**

The effect of the overall slope angle (α, see Table 4-4) on the factor of safety FS was investigated for waste rock piles with one, two and three benches, for various values of c_{app} (=1, 5, 10 and 25 kPa) (with β = ϕ' = 37°) (Figure 4-33 d). Cases S2, S5, and S6, are considered as a base case, with α = β = 37°, 26°, and 30° respectively. Cases S1, S11 and S18, are considered to check the variation α (from 26° to 37°) for two bench waste rock and Cases S3, S16 and S19 are represented to evaluate the effect of α on three bench pile. Figure 4-33 (a, b and c) shows the effect of the global angle α and C (= c_{app}) on the factor of safety for these piles. More specifically, Figure 4-33 (a) shows that when c_{app} increases from 1kPa to 25 kPa, FS increases from 1.2 to 2.2 (for α=30°). For c_{app} = 25 kPa, FS decreases from 1.7 to 1.48 when α increases from 26° to 37°. Figure 4-33 (b) shows that for c_{app}=25 kPa the FS decrease from 1.8 to 1.4 when the global slope increase from 26° to 37°.
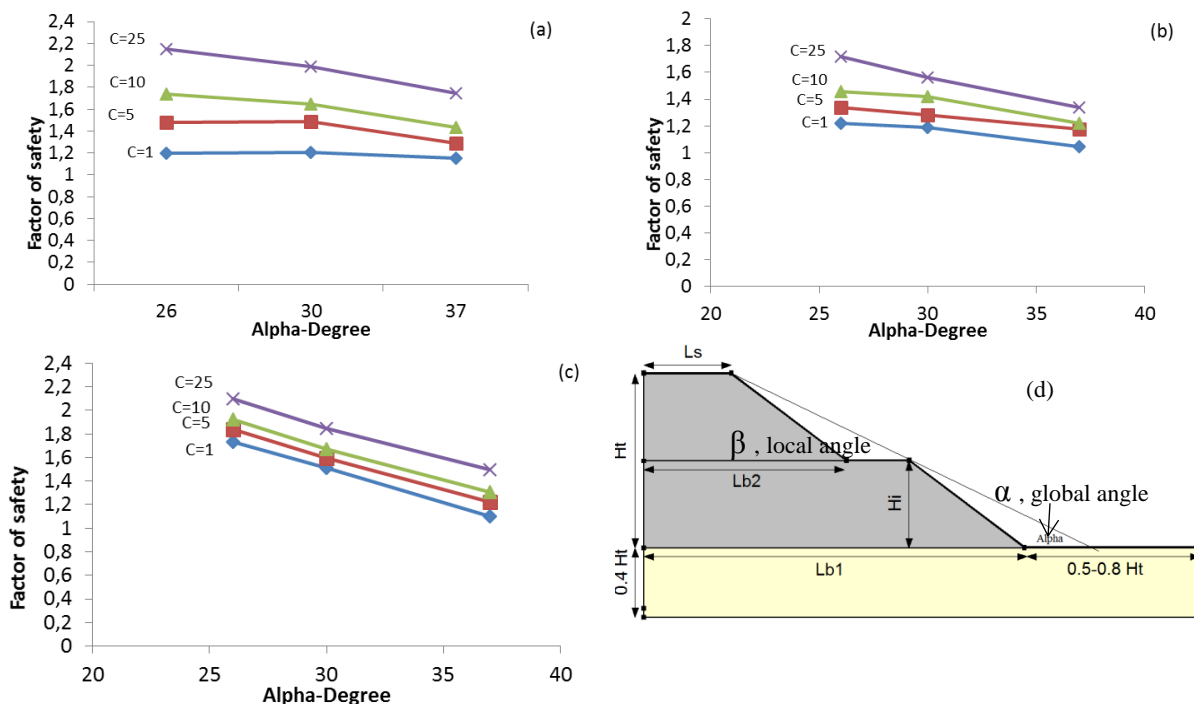
Figure 4-33: Relationship between FS and the global slope angle α (= 26, 30 and 37°) obtained with *Optimized FE stress-based* method; c_{app} = 1, 5, 10 and 25 kPa, (β = 37°), a) H= 20 m, (Cases S1, S11, S18); b) H=80 m, (Cases S3, S16, S19,); c) H=40 m, (Cases S2, S5, S6); c_{app} = 1, 5, 10 and 25 kPa; d) Typical two bench waste rock pile with local (β) and global (α) slope angle.

4.7.8 **Relationship between FS, global slope (α) and number of benches**

The effect of changing the number of benches in a waste rock pile was also investigated. For this purpose, three different Groups are considered. Group 1 (Cases S2 to S4, H_t = 40 m to 120 m) represents single bench pile; Group 2 (Cases S12 to S14, H_t = 40 m to 120 m) represents two bench piles, and Group 3 (Cases S15 to S17, H_t = 40 m to 120 m) represents three bench waste rock piles (ϕ' = 37° and c_{app} = 5, 10 and 25 kPa).

Cases from Group 1 have α = β = 37°. When benches are added (Group 2 and 3), the local slope remains at 37° (=β), but the global slope is changed to 26° (= α).

Figure 4-34 indicate that the factor of safety is larger for the two- and three-bench piles (Groups 2 and 3) compared with the single-bench (Group 1), for a given pile height. This increase is largely related to the lower global slope angle α (in Group 2 and 3 (α = 26°).

It is also observed that FS for Group 3 is larger than Group 2; this reflects the effect of the number of benches (3 versus 2, with α = 26° for both Groups). These results confirm the expected tendencies and also provide a quantitative evaluation of influence such factors.
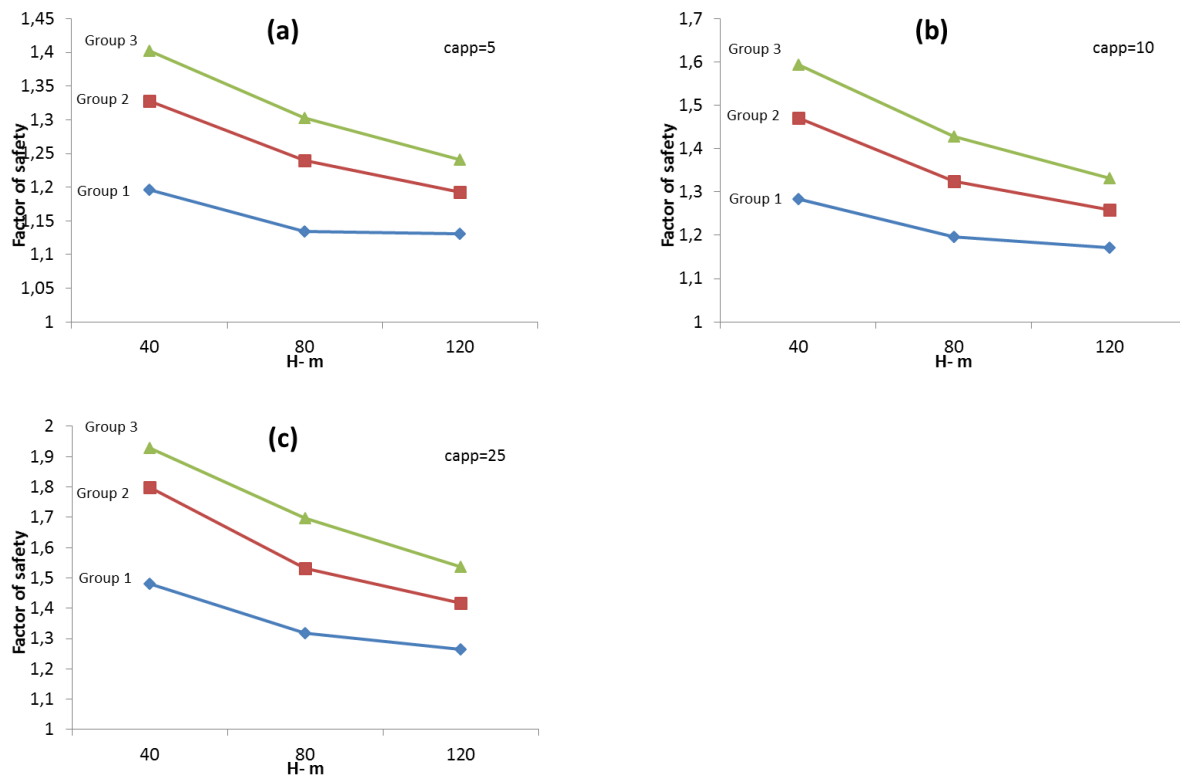
Figure 4-34: Relationship between the factor of safety FS and the number of benches, ($\alpha = 26°$, $\beta = 37°$) ; Group 1 (Cases S2 to S4), Group 2 (Cases S12 to S14) and Group 3 (Cases S15 to S17); a) $c_{app} = 5$ kPa; b) $c_{app} = 10$ kPa; c) $c_{app} = 25$ kPa

4.7.9 **Effect of compacted layers on FS**

It is recalled from section 2-1-2 that due to the method of construction, the internal geometry of a pile may include horizontal (or inclined) layers (e.g.(Aubertin et al., 2002b). In this section, the potential effect of these layers on the waste rock pile stability is investigated. The properties of these layers are given in section 4-3; the thickness is 1 m.

Horizontal layers

Figure 4-35 presents the result obtained with *FE stress-based* method. It shows the values of the factor of safety in Group 2 (Cases S11 to S14, pile with two benches) and Group 4 (Cases S21 to

S24, pile with two benches and two compacted layers), with $\phi' = 37°$ and $c_{app} = 0$ and 1 kPa (see Tables 4-1 and 4-3 for material properties).

Figure 4-35 (a) and (c) show FS for local slip surfaces. The addition of compacted layers increases FS slightly, especially for smaller piles. In larger piles, the effect of these layers is not significant (depending on the number of compacted layers).

A similar trend is observed in Figure 4-35 (b) and (d) for the global critical slip surfaces (that pass through the crest and toe). The addition of compacted layer increases FS slightly. This increase is more pronounced for smaller piles (when the layers are closer to each other, and their relative thickness is larger).
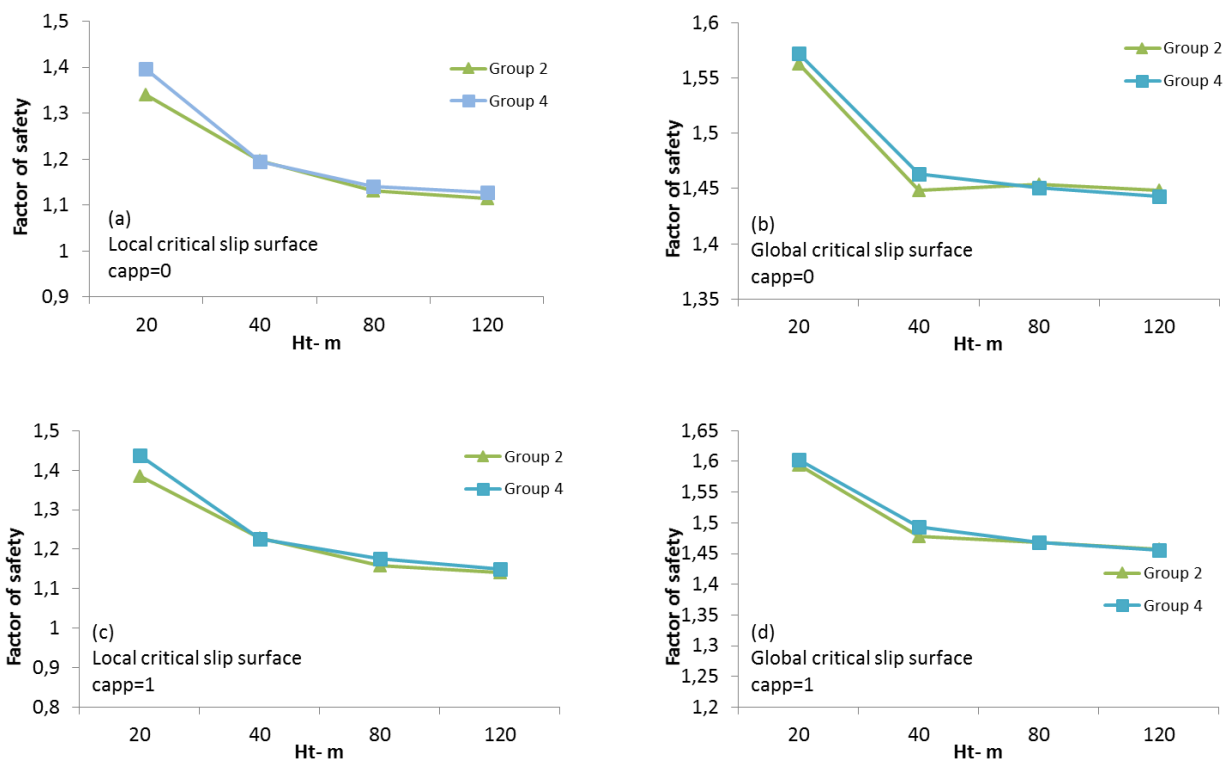
Figure 4-35: Relationship between FS and addition of compacted layers; Groups 2 (Cases S11 to S14, $H_t = 20$ m to 120 m) and Group 4 (Cases S21 to S24, $H_t = 20$ m to 120 m), $\phi' = 37°$; a) local critical surface, $c_{app} = 0$, b) global critical surface, $c_{app} = 0$; c) local critical surface $c_{app} = 1$ kPa; d) global critical surface, $c_{app} = 1$ kPa

Figure 4-36 presents the results obtained with *FE stress-based* method. It shows the comparison of a factor of safety FS for Group 3 (Cases S15 to S17, pile with three benches, H_t = 40 m to 120 m) and Group 5 (Cases S25 to S27, pile with three benches and three compacted waste rock layer, with ϕ' = 37° (waste rock) and 45° (compacted waste rock) and c_{app} = 0 and 1 kPa). Figure 4-36 (a) and (b) show FS for global slip surfaces (passing through the crest and toe) and indicate adding compacted layers tend to increase the global FS slightly, especially for smaller piles. For larger piles (e.g. H=80 m, 120 m), the effect is not significant
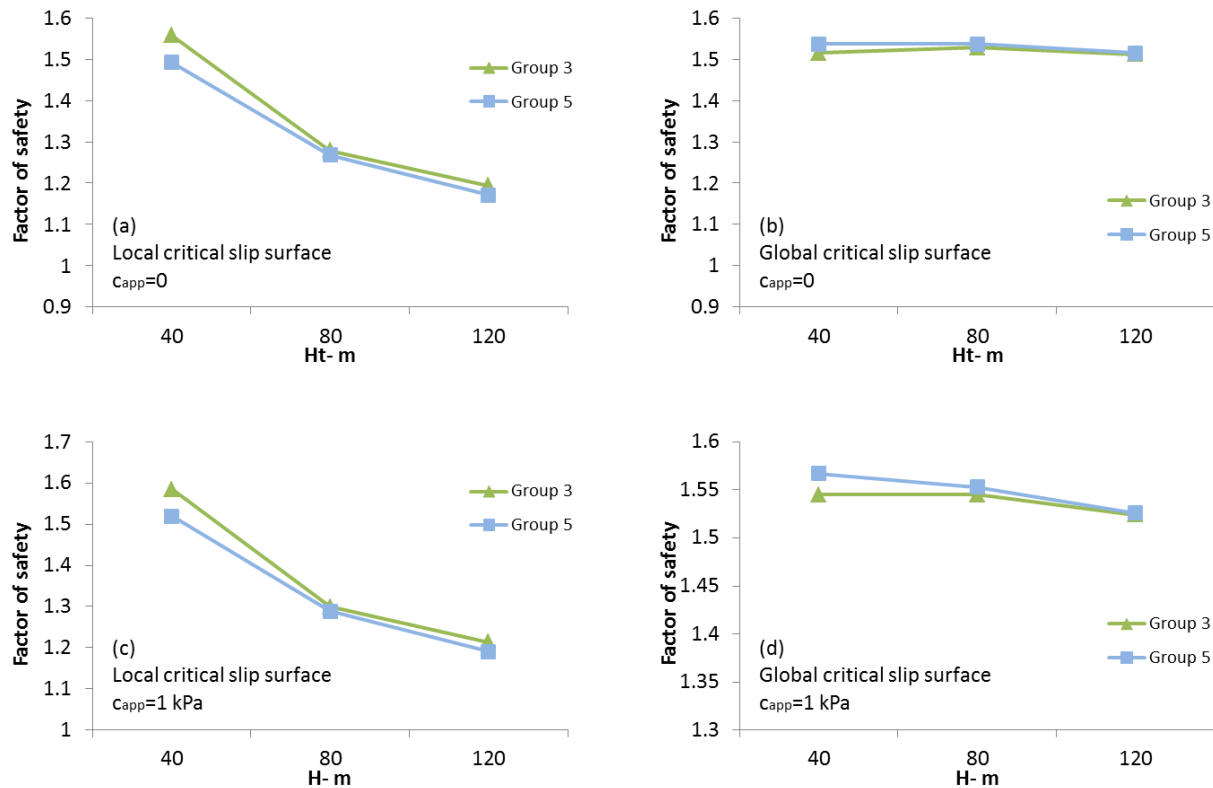
Figure 4-36: Relationship between FS, height and compacted layers obtained with *FE stress-based* method; Group 3 (Cases S15 to S17, H_t = 40 m to 120 m) and Group 5 (Cases S25 to S27, H_t = 40 m to 120 m), ϕ' = 37° (waste rock) and 45° (compacted waste rock); a) local slip surface, c_{app}= 0, b) global slip surface c_{app}= 0, c) local slip surface, c_{app}= 1 kPa; d) global slip surface, c_{app}= 1 kPa

Inclined compacted layers

Figure 4-37 presents FS obtained with *FE stress-based* method for relatively deep critical slip surface for Groups 4 (horizontally compacted layers), 6 and 7 (1% and 5% inclined compacted layers towards the outside of the pile). Figure 4-37 (a) and (c) presents FS for local slip surface with c_{app} = 0 and 1 kPa (respectively). It shows that the local FS is lower for Group 7 (5% inclination) in all cases. Figure 4-37 (b) and (d) shows the FS for global slip surface with c_{app} = 0 and 1 kPa (respectively). It shows that the global FS is higher for Group 7 (5% inclination) for both cases which is more significant for smaller piles (e.g. H = 20 m). It also indicates that increasing c_{app} results in an increase of FS (see Figure 4-37 (a) and (c)).
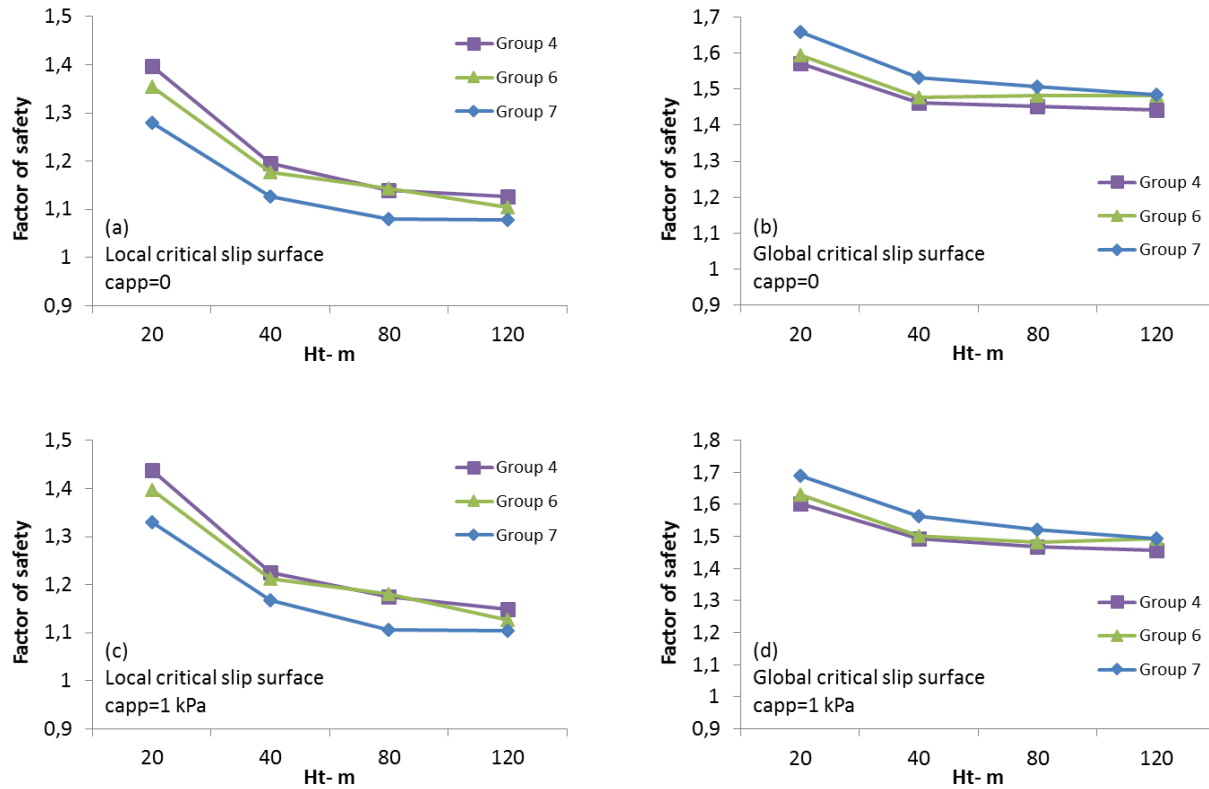
Figure 4-37: Relationship between FS, height and inclined compacted layers obtained with *FE stress-based* method; Group 4 (Cases S11 to S14, H_t = 20 m to 120 m), Group 6 (Cases S31 to S34, H_t = 20 m to 120 m) and Group 7 (Cases S35 to S38, H_t = 20 m to 120 m), ϕ' = 37° (waste rock) and 45° (compacted waste rock); a) local critical surface c_{app}=0, b) global critical surface c_{app}=0; c) local critical surface c_{app}=1 kPa; d) global critical surface c_{app}= 1 kPa

It should be recalled that the compacted layers (with lower hydraulic conductivity) in a pile (horizontal or inclined) may cause the diversion of water to the outside of the pile. This phenomenon is studied in the next Chapter.

Effect of horizontal and alternated layers (parallel to the slope)

Figure 4-38 presents the results related to Group 4 (Cases S21 to S24, H_t = 20 m to 120 m) and Group 8 (Cases S41 to S44, H_t = 20 m to 120 m). Figure 4-38 (a) and (c) shows FS of the local critical slip surfaces. It shows Group 8 gives higher FS compared to Group 4 (for both c_{app}= 0 and 1 kPa) due to the existence of alternate layers parallel to the external slope (with a higher value of ϕ' for half of these parallel layers).

Figure 4-38 (b) and (d) presents the global slip surface and related FS. For both c_{app}= 0 and 1 kPa, cases from Group 8 lead to higher FS, in the presence of alternate layers parallel to the external slope; this effect is more pronounced for smaller piles.

It can be concluded that having both horizontal layers and layers parallel to external slope affects the factor of safety; this effect can be more pronounced compared to cases when there are only horizontal compacted layers.
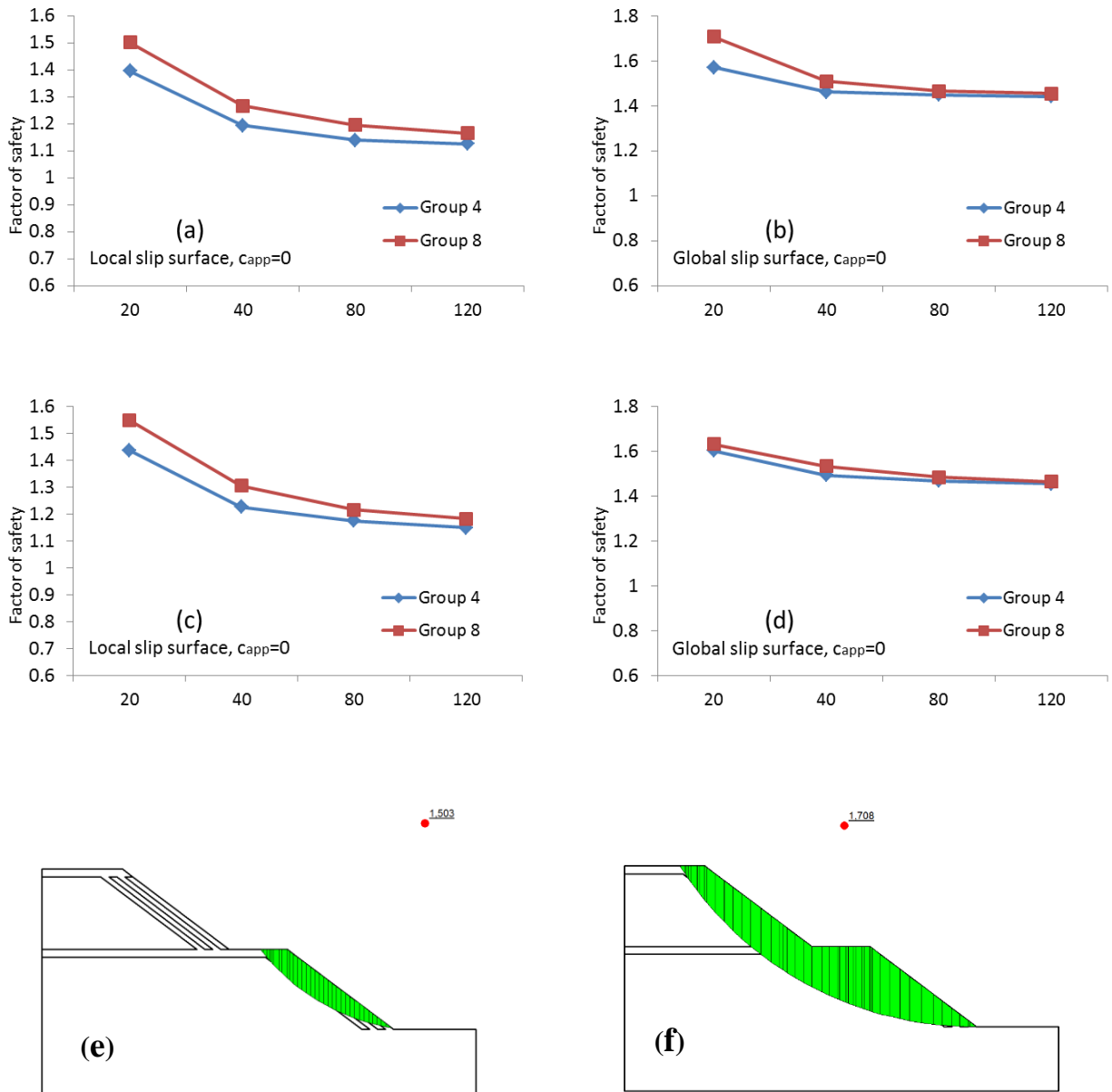
Figure 4-38: Effect of addition of alternate layers parallel to external slope on FS for piles from Group 4 (Cases S21 to S24, H_t = 20 m to 120 m) and Group 8 (Cases S41 to S44, H_t = 20 m to 120 m), ϕ' = 37° (loose) and 45° (compacted waste rock), α = 26°, β = 37°; a) local FS with c_{app}= 0 b) global FS with c_{app}= 0; c) local FS with c_{app}= 1 and d) global FS with c_{app}= 1; e) Typical local slip surface for Group 8 (with slices); f) Typical global slip surface for Group 9 (with slices).

4.7.10 **Effect of foundation material properties**

The geotechnical properties of the foundation material below the pile may also affect its stability. Analyses were conducted to investigate this factor explicitly. Four different Groups (Groups 1, 3, 4 and 5 for Cases S1, S21, S31, and S35, see Table 4-4) are utilized to investigate this aspect.

Analyses have been conducted for three foundation materials: waste rock, silty sand and silty clay (with c_{app} = 0 and 1 kPa, in the pile and foundation). The internal friction angle for these particular materials is 37°, 30°, 20° for the waste rock, silty sand, and silty clay respectively. Cohesion (c') was also changed from 0 to 15 kPa to 60 kPa when the foundation material changed from waste rock to silty sand to silty clay.

Figure 4-39 (a, b, c and d) illustrates the results for Groups 1, 3, 4 and 5 with the value of FS for the critical slip surface (not passing through the foundation) with the different foundation materials.

The factor of safety FS is changing with the value of ϕ' and c of the foundation material. It seems that the effect of ϕ' is more pronounced on the stability of waste rock pile. In all cases presented here, the FS is highest when the foundation material is the waste rock, and the silty clay foundation usually results in the lowest factor of safety. It is also seen that the difference between FS due to different foundations properties is more pronounced for higher piles (e.g. H=80 and 120 m).
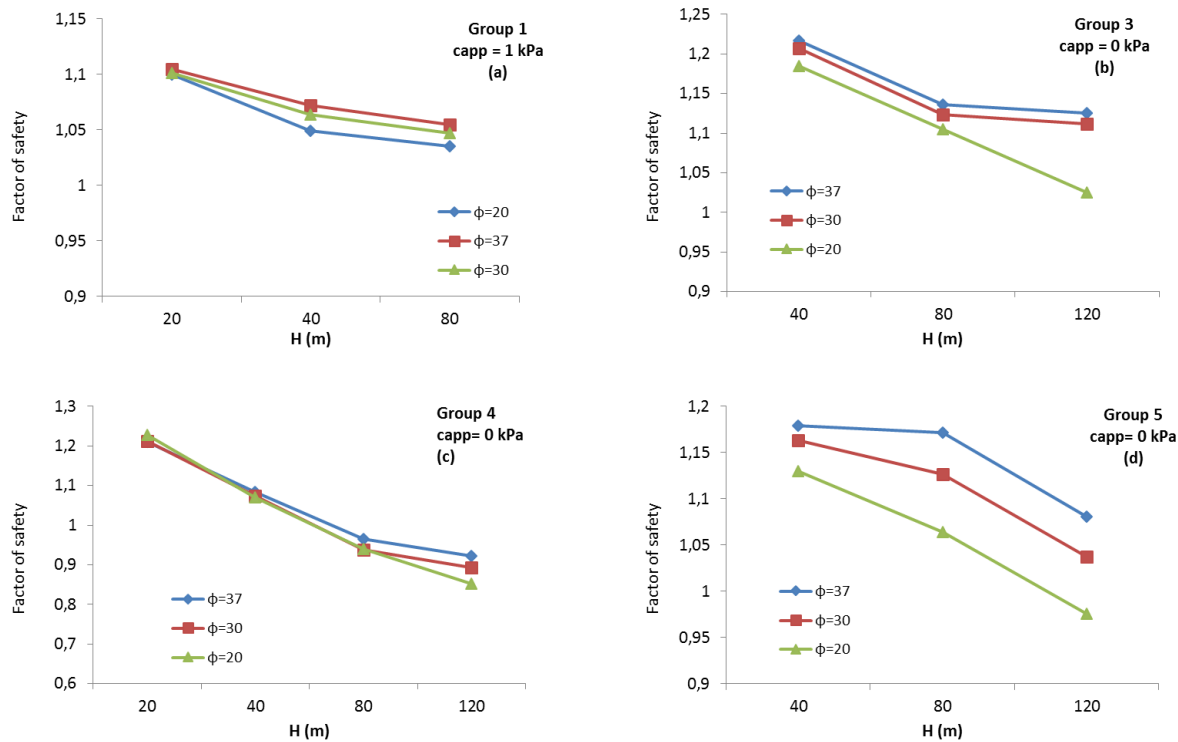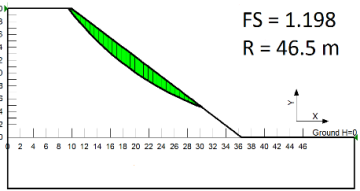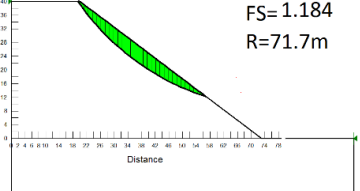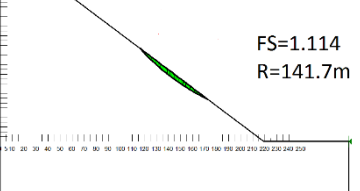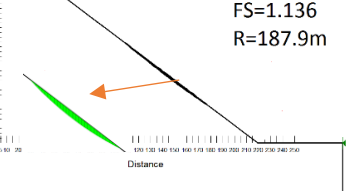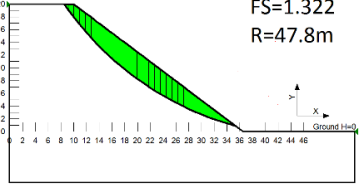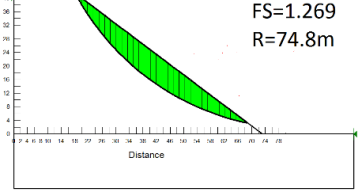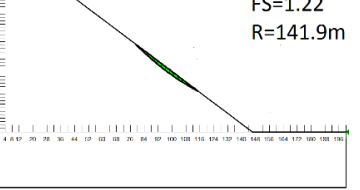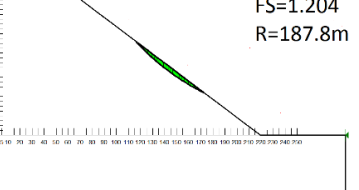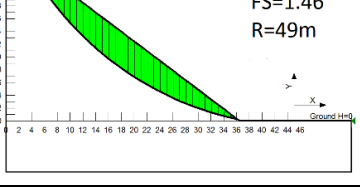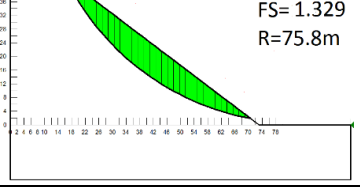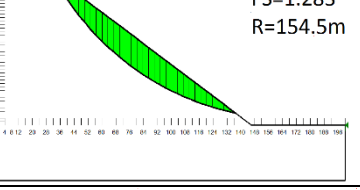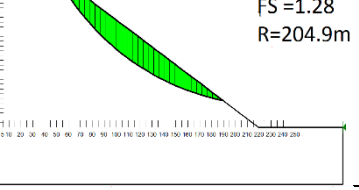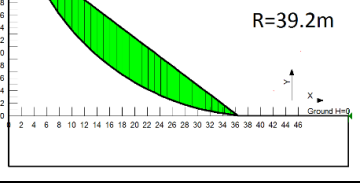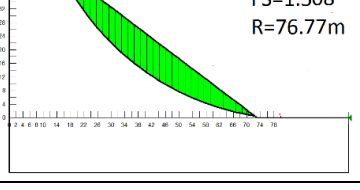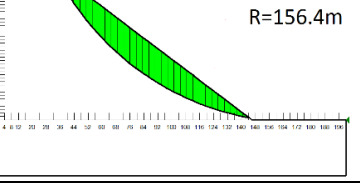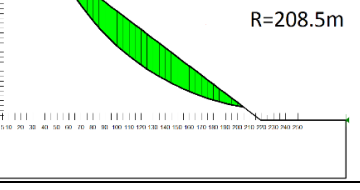
Figure 4-39: Relationship between FS and the properties of the foundation material (c and ϕ', waste rock, silty sand and silty clay), Groups 1, 3, 4 and 5 (Cases S1, S21, S31, and S35); a) Group 1(c_{app} = 1 kPa); b) Group 3 (c_{app} = 0); c) Group 4 (c_{app} = 0); d) Group 5 (c_{app} = 0)

4.7.11 **Effect of pile height and apparent cohesion and slope of slip surface**

As shown above, the factor of safety and its related slip surface can be affected by different parameters, including total pile height and the value of c_{app}. Table 4-9 presents the form and location of the critical slip surface (with minimum depth of 1 m) for Group 1 (Cases S1 to S4, H_t = 20 m to 120 m) for different c_{app} (= 1, 5, 10 and 25 kPa). For Case S1 (single bench, $\alpha = \beta =$ 37°), it is seen that by increasing c_{app}, the critical slip surface becomes deeper, moving towards the toe, while the value of FS increases (obtained with *FE stress-based* method). The same trend is also observed for Cases S2, S3, and S4. For a constant value of c_{app} increasing the pile height results in a decrease of FS. As an example for c_{app} = 25 kPa when the pile height increases from 20 m to 120 m, the FS decreases from 1.781 to 1.336.

Table 4-9: Effect of pile height H (m) and value of cohesion C = c$_{app}$ (kPa) on FS and the position of the critical slip surface with minimum depth of 1 m (for the deepest slice)

c$_{app}$ (kPa)	H=20 m (Case S1)	H=40 m (Case S2)	H=80 m (Case S3)	H=120 m (Case S4)
1	FS = 1.198 R = 46.5 m	FS= 1.184 R=71.7m	FS=1.114 R=141.7m	FS=1.136 R=187.9m
5	FS=1.322 R=47.8m	FS=1.269 R=74.8m	FS=1.22 R=141.9m	FS=1.204 R=187.8m
10	FS=1.46 R=49m	FS= 1.329 R=75.8m	FS=1.283 R=154.5m	FS =1.28 R=204.9m
25	FS=1.781 R=39.2m	FS=1.508 R=76.77m	FS=1.383 R=156.4m	FS = 1.336 R=208.5m

4.7.12 **Effect of variable internal friction angle ɸ' in the waste rock pile**

As mentioned in section 2-4, slope stability analyses carried out on waste rock piles assume a uniform friction angle for the entire waste rock pile, with a value of ɸ' close to its angle of repose (ɸ = β =37°). This assumption may not present the actual situation, and it cannot explain deep-seated failure mechanisms. This assumption is an oversimplification of the material strength distribution because of various data's show that there is a relation between the internal frictions angle, density and normal stress (e.g. (Marsal, 1967; Leps, 1970; Barton and Kjaernsli, 1981).

Leps (1970) has classified rockfill into three groups base on material density, particle strength and gradation: Weak (low-density, poorly graded), Average, and Strong (high density, well graded). Such types of results indicate that considering a single value of ɸ' may not represent the value of FS for waste rock piles where the density and stresses may vary significantly (see Figure 2-7).

This aspect was assessed based on a typical waste rock with a conservative value of the rock UCS (of 70 kPa) labeled as strong. The standard construction methods i.e. end or push dumping (see section 2-2-1), suggest the formation of a poorly graded structure with relatively low density. Hence, it was assumed that the function relating the friction angle to the normal stress would fall in the region of "weak" to "average" rockfill.

Barton (1981) proposed an empirical relationship to estimate the peak friction angle ɸ' of rockfill based. Equation 4-3 gives the friction angle of rockfill based on the uniaxial compressive strength of the rock, the mean particle size d_{50}, the particle roundness and material porosity. The Roughness R and equivalent strength S is also required (see Figure 2-6).

The peak drained friction angle ɸ' (°) can be calculated from the following Equation (Barton, 1981) (with R: roughness and S: equivalent stress).

$$\phi' = R. \log\left(\frac{S}{\sigma'_n}\right) + \phi_b \qquad [4\text{-}3]$$

The value of R can be retrieved from Figure 2-7. For example, for waste rock with a porosity of 35% (typical porosity of waste rock pile is between 30 % and 50 % (Morin et al., 1991; Aubertin

et al., 2002b; Hernandez, 2007) and a degree of roughness as "Talus", a value of 5 to 6 is obtained for R (as indicated in the figure).

The effect of variable ϕ' on the FS value was studied here using additional simulations conducted for Group 1 (Cases S1 to S4), Group 2 (Cases S11 to S14) and Group 3 (Cases S15 to S17). The foundation material is a waste rock for all the cases, with $c_{app} = 0$ kPa for the waste rock.

Internal friction angle (ϕ') is determined for different values of σ_n based on the contour plot of the vertical normal stresses obtained with SIGMA/W, using equation 4-3 with the $\phi_b = 25°$, $d_{50} = 10$ mm, UCS=70 kPa (it should be noted that density and strength could increase with depth for very strong rocks; this aspect is not considered here).

Some detailed results are first presented for Group 2, Case S11. Figure 4-40 (a) shows the normal stresses distribution in the pile. For each stress contour, the relevant value of ϕ' is calculated from equation 4-3. The contour values of ϕ' are shown in Figure 4-40 (b).

In this case, the normal stresses increase from 0 to 450 kPa (from the surface to the base, Figure 4-40 (a); the value of ϕ', which controls the shear strength of waste rock under effective stresses, decreases from 37.2° near the surface to 33.7° at depth.

Figures 4-40 (c) and (d) present a local and a global slip surface for Case S11. It is seen that the local slip surface pass through the layer with $\phi' = 37.2°$; global slip surface pass through two layers with $\phi' = 37.2°$ and 33.7°.
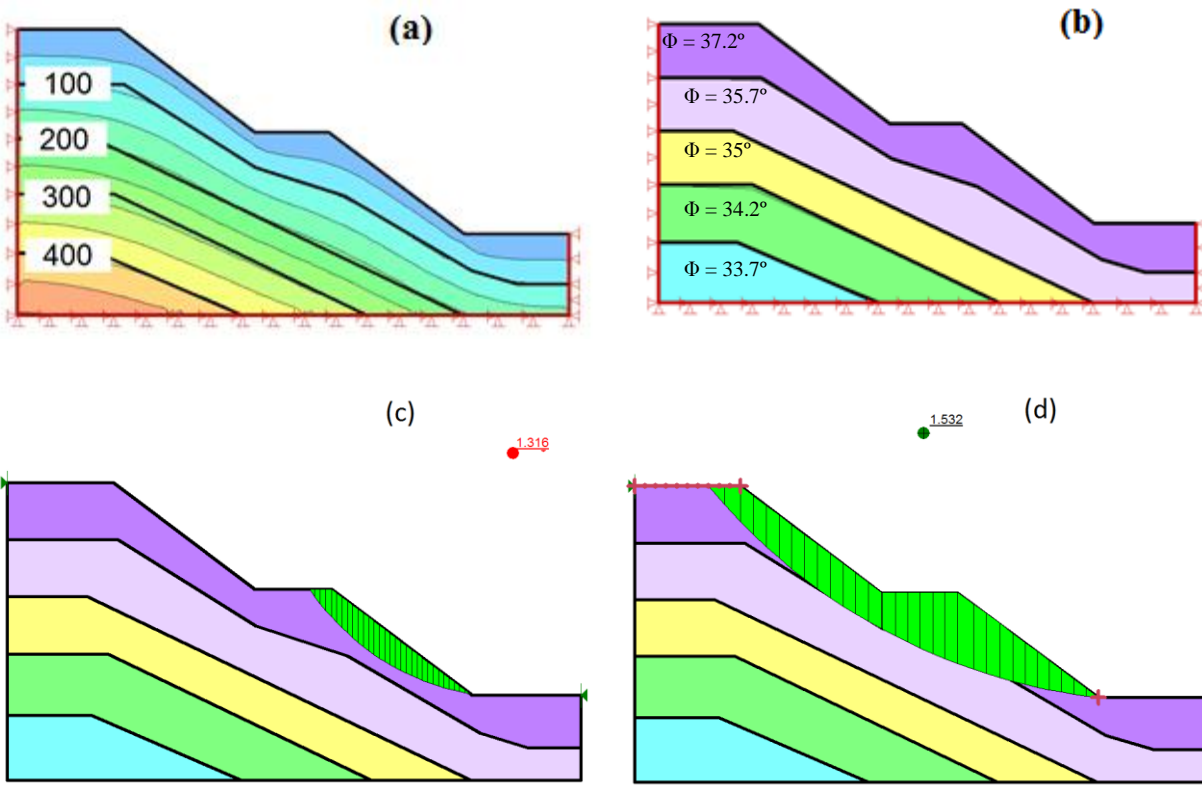
Figure 4-40: a) distribution of normal stresses (obtained with SIGMA/W), Case S11 (with c_{app} = 0 kPa), b) distribution of variable ϕ', c) factor of safety (1.316) and center of rotation for the local slip surface; d) factor of safety (1.522) and center of rotation for the global slip surface

Figure 4-41 presents the shear strength (a), shear mobilized (b) and effective normal stress (c) distribution along the global slip surface (see Figure 4-40 d), for Case S11 with variable and constant ϕ' (= 37°). The distribution pattern is similar for variable and constant ϕ' with higher values of shear strength for the variable ϕ' scenario.

Figure 4-41 (d) presents the local FS for each slice along the slip surface. The trend of FS distribution is close for both scenarios with higher FS for some slices in the case with constant ϕ'.
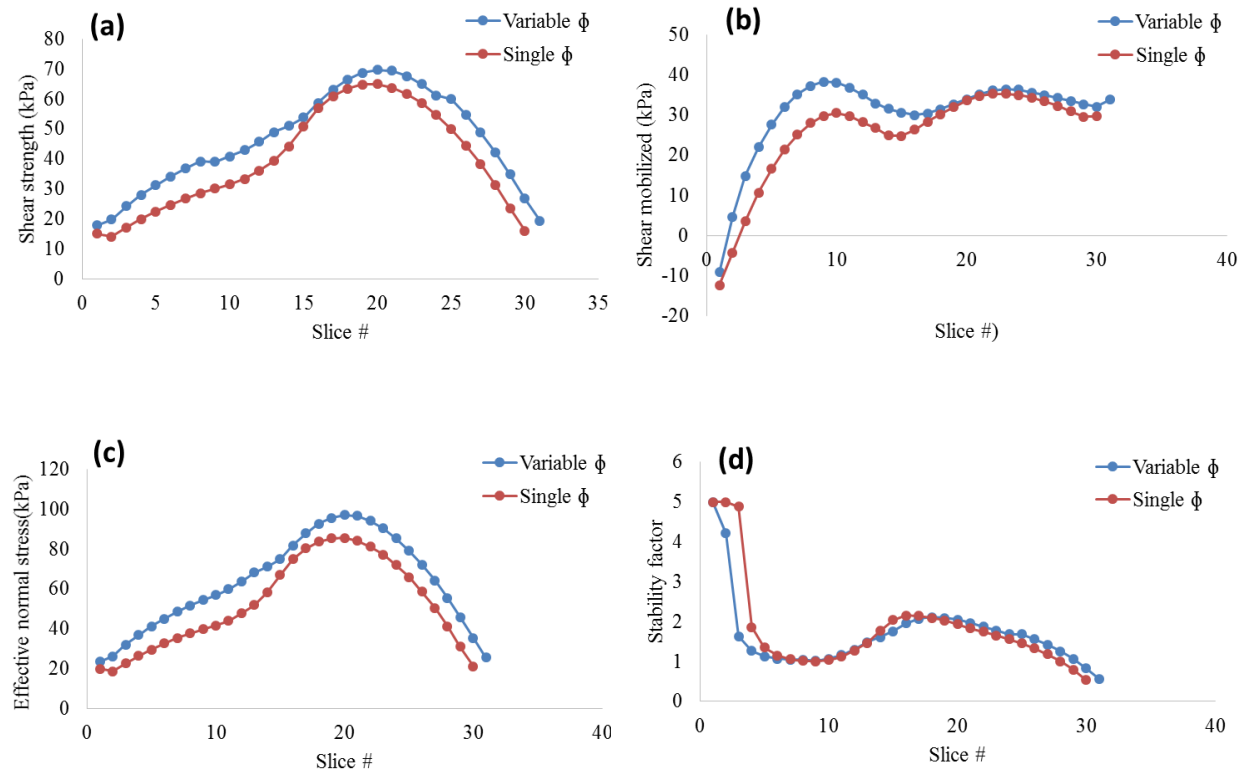
Figure 4-41: Distribution a) shear strength, b) shear mobilized, c) normal stress, d) local FS, along the surface for waste rock pile with c_{app} =0, Case S11, with variable ϕ' (37.2° and 33.7°) and constant $\phi' = 37°$, for global slip surface obtained with SLOPE/W

Figure 4-42 (b) presents the ϕ' distribution for Case S12, based on the normal stress distribution (Figure 4-42 (a)). In this case, the normal stress increases from 0 to 950 kPa (from the surface to base); the ϕ' value decreases from 37.2° to 32°, due to crushing and rounding of particles.

Figure 4-42 (c) and (d) present the local and global critical slip surface and the corresponding FS and the location of the center of rotation.
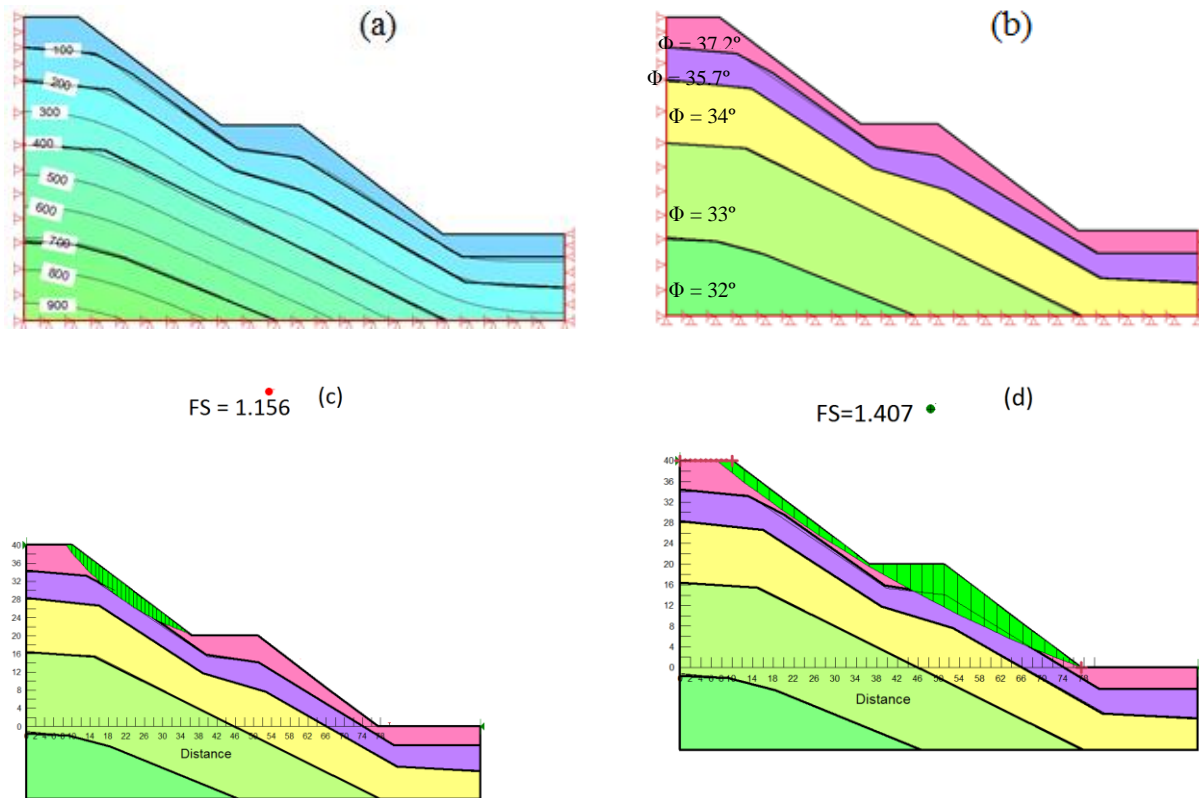
Figure 4-42: a) distribution of normal stress (obtained with SIGMA/W), Case S12 (with $c_{app} = 0$ kPa; b) distribution of variable ϕ'; c) factor of safety (1.156) and center of rotation for the local slip surface; d) factor of safety (1.407) and center of rotation for the global slip surface

Figure 4-43 presents the shear strength (a), shear mobilized (b) and effective normal stress (c) distribution along the global slip surface (see Figure 4-42 (d)) along the slip surface for Case S12 with variable and constant ϕ' (= 37°). The shear strength, shear mobilized and effective normal stresses are identical for slices 1 to 10 for both single and variable ϕ'. In Figure 4-43 (d) the slip surface passes first layer ($\phi' = 37.2°$ for slice 1 to 10) in the upper bench that may explain the similarity between properties of slip surface slices.

The shear strength presents slightly higher value for single ϕ' in slices 20 to 30) (slip surface enters layer with $\phi' = 35.7°$ in these slices). The same trend is seen for effective normal stress and an inverse trend for shear mobilized distributions.

Figure 4-43 (d) presents the local FS for each slice along the slip surface. The trend for the FS distribution is close for both scenarios with higher FS for some slices in the case with constant ϕ'.
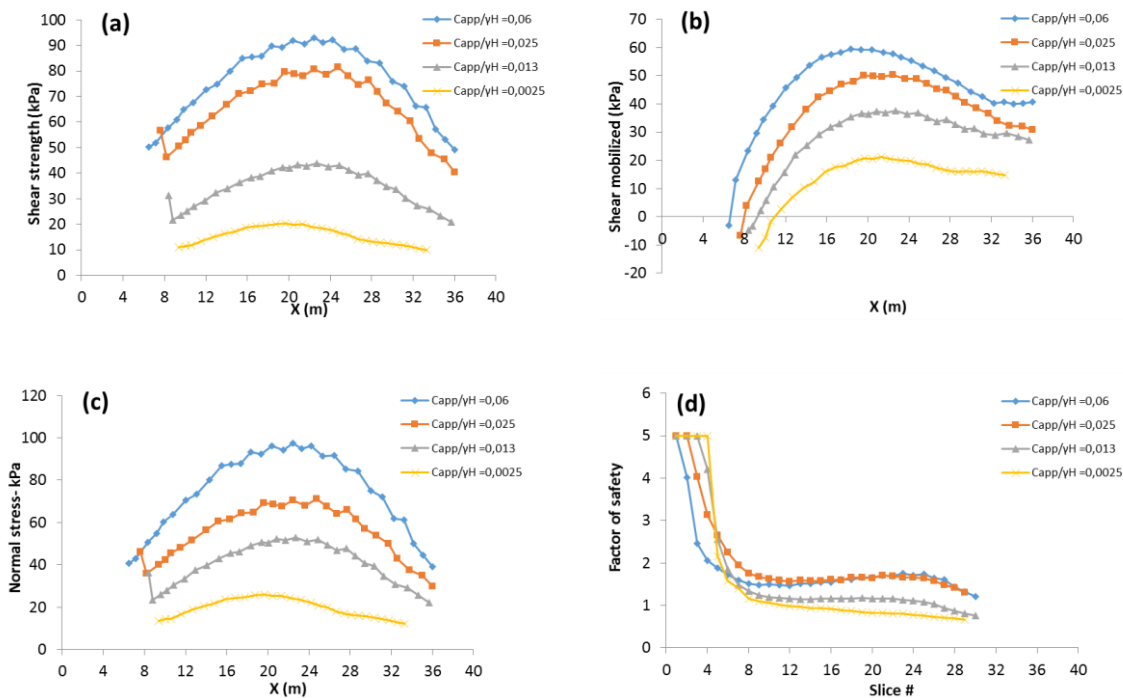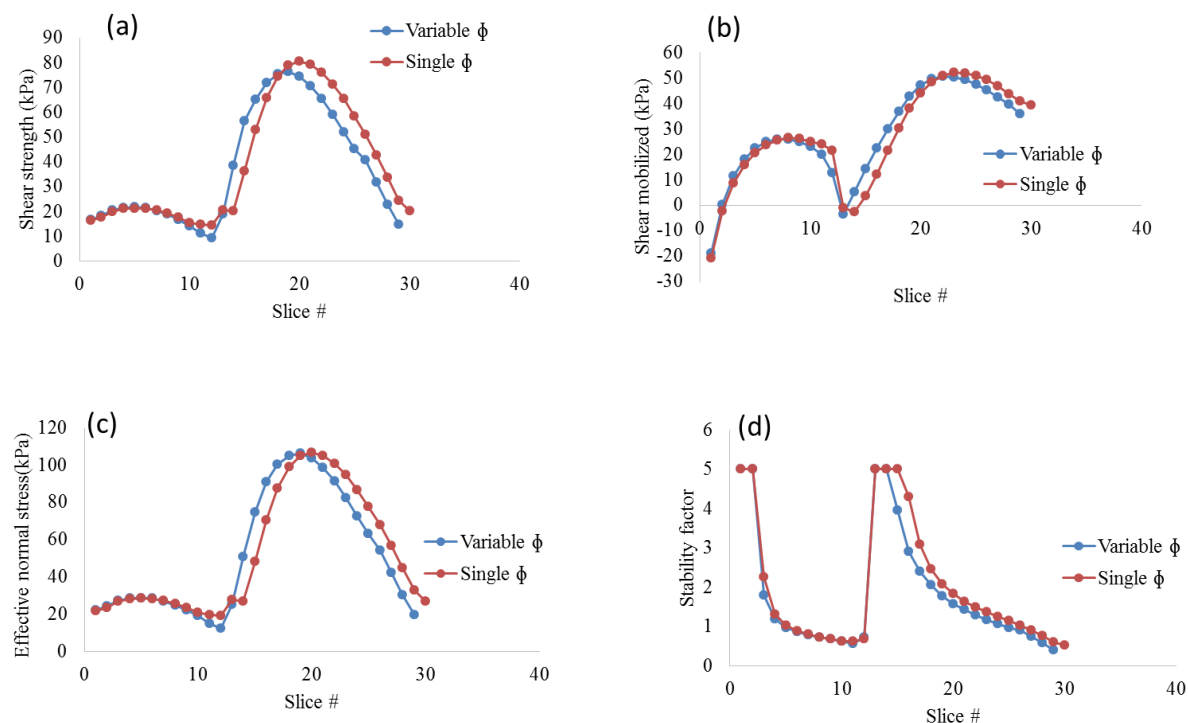

Figure 4-43: Distribution a) shear strength; b) shear mobilized; c) normal stress; d) local FS, along the global slip surface, $c_{app} = 0$, Case S12, variable ϕ' (37.2° to 32°) and constant $\phi' = 37°$, obtained with SLOPE/W

Figure 4-44 presents the values of FS obtained with analyses conducted on the various cases for Groups 1, 2 and 3 for both variable and constant ϕ'. Figures 4-44 (a), (b) and (c) show that a variable ϕ' usually results in a reduction of local and global FS for both Groups, 1 and 2. Figure 4-44 (d) and (e) indicates the same pattern for local and global FS of Group 3. The percentage of reduction for the factor of safety depends on the depth of the slip surface. For deeper slip surfaces (which pass more layers with lower ϕ') this reduction of FS appears to be more pronounced.
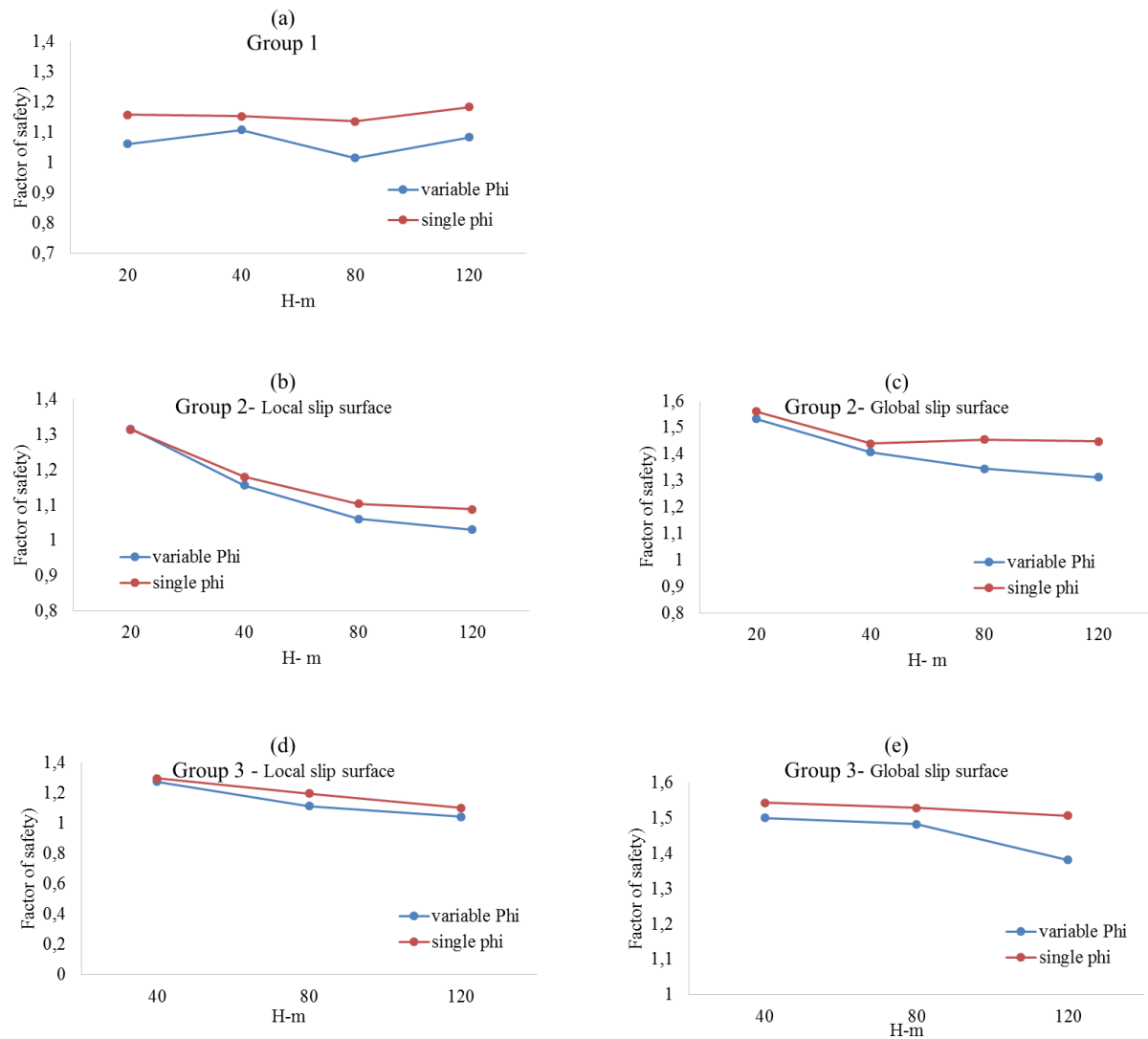
Figure 4-44: Variation of factor of safety due to variation of ϕ', a) Group 1 (Cases S1 to S4, H_t = 20 m to 120 m); b) Group 2 (Cases S11 to S14, H_t = 20 m to 120 m), local slip surface; c) Group 2, global slip surface; d) Group 3 (Cases S15 to S17, H_t = 40 m to 120 m), local slip surface; e) Group 3, global slip surface, c_{app} =0, single ϕ' = 37° and variable ϕ' between 37.2° to 32°)

It should be noted that the apparent cohesion might change with an increase in the soil's moisture, typically associated with rainfall. In the next chapter (Chap. 5), the impact of rainfall on the factor of safety and stability of the pile is being presented. The following chapter (Chap. 6) will also include analyses with statistically distributed material properties.

CHAPTER 5   STABILITY ANALYSIS OF WASTE ROCK PILES UNDER STEADY-STATE AND TRANSIENT FLOW CONDITIONS

5.1 Introduction

The effect of rainfall infiltration on the behavior of slopes of coarse-grained materials (such as waste rock) has not been investigated much. There have nonetheless been several investigations dealing with unsaturated water flow in waste rock piles (Aubertin et al., 2002b; Fala, 2002; Fala et al., 2005; Fala et al., 2006; Fala, 2008; Fala et al., 2008; Dawood and Aubertin, 2009; Dawood and Aubertin, 2012). The effect of precipitation and infiltration on slopes made of relatively fine-grained soils has also been studied (Ng and Shi, 1998; Collins and Znidarcic, 2004; Casagli et al., 2006; Rahimi et al., 2010; Bordoni et al., 2015; Acharya et al., 2016; Regmi and Jung, 2016).

This chapter presents the procedure developed and applied here to investigate the effect of moderate and relatively heavy rainfalls on the stability of waste rock piles. The goal is to determine how infiltration affects the pore water pressures in the piles and the slope stability.

Numerical calculations were used to study the stability of waste rock piles under a rainfall of different intensity and duration. A coupled approach was used to evaluate the minimum factor of safety and the corresponding critical slip surface based on the (total and effective) stresses distributions obtained with numerical simulations (using the general approach described in section 3-2). The simulations were also used to investigate the effect of internal geometry, hydraulic properties, initial pore water pressures, in addition to rainfall intensity and duration, on the minimum factor of safety.

5.2 Methodology

Pore water pressures (PWP) are not constant over time within a waste rock pile. These may change due to environmental conditions. This affects the suction and related apparent cohesion of the waste rock, which in turn influence the slope stability of the unsaturated pile. For example, a heavy rainfall may increase the degree of saturation in the waste rock pile, leading to a reduction of the apparent cohesion, whereas a more moderate rainfall may affect the apparent cohesion differently or in some parts only.

The initial pore water pressures, the rainfall intensity and hydraulic (hydrogeological) properties of the materials (water retention and hydraulic conductivity) are the main characteristics that affect the amount of infiltration and the water flow into the pile (Fredlund, 1984, 1989; Fredlund, 1995).

Numerical modeling can be used to determine the suction (negative PWP) distribution and its evolution due to infiltration. Due to the complexity of the process, it is preferable to use a coupled calculation approach. PWP and the stress distributions were calculated separately then combined to evaluate the effect on the factor of safety. These analyses are based on the finite element method.

The evaluation procedure, illustrated schematically in Figure 5-1, started with an estimate of the in situ stress state before the rainfall. The analysis using SIGMA/W gave the initial (equilibrium) stresses in the pile based on gravity (step 1). SEEP/W (step 2) was then used to solve the flow equations and evaluate the effects of rainfall (duration and intensity) and initial pore water pressure conditions. The resulting PWP were transferred to SIGMA/W to calculate the stresses (and strains, not shown here) over time (step 3). The shear stresses are also assessed to calculate the minimum factor of safety with SLOPE/W (step 4). Additional details on the calculation procedure are given in section 3-3 (Krahn, 2007b, 2007c, 2007d).
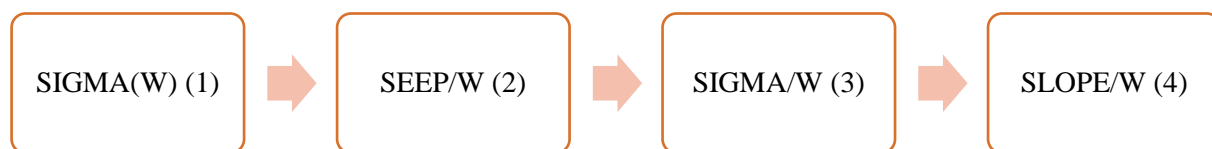
Figure 5-1: Steps used to conduct the simulation process for slope analysis of the waste rock piles based on Krahn (2007 b, c, d)

Ponding on the ground surface was not allowed, and the simulations did not permit pore water pressure development above 0 kPa; thus, excess water that didn't infiltrate was assumed to be (non infiltrating) runoff (which doesn't contribute to the recharge)

The results, which include pore water pressure distributions during and after rainfall and the associated factors of safety for slope stability, are presented below. These results among other findings indicate that in some cases the factor of safety FS may not reach its minimum value during or immediately after the end of rainfall because water continues to seep downwards. This minimum factor of safety may be achieved sometime after the rainfall stops.

5.3 Geometry, boundary conditions, and material properties

Cases from Groups 2, 4, 7, 8 and 9 are considered for the numerical stability analyses (see Tables 4-4 and 4-5); specific details about the simulated cases are presented below. The simulated piles included coarse and fine waste rock materials and a silty sand or silty clay foundation material. The hydraulic and geotechnical properties of these materials are given in Tables 4-1 and 4-3 and Figures 4-1 and 4-2.

The mesh configuration for these simulations is presented and discussed in Section 3-3-1. A mesh sensitivity analysis presented in Appendix B-1 showed that an unstructured mesh configuration leads to better results. The element size (for those located along the slope surface) close to the waste rock AEV (about 12 cm) are used it gives acceptable results.

Boundary and initial conditions

The boundary conditions defined in SEEP/W and SIGMA/W include the stresses and displacements, and hydraulic conditions.

A relatively deep initial water table is imposed for transient and steady-state simulations with SIGMA/W; it is located seven meters below the ground (i.e. below the base of the waste rock pile) for step 1. For the following calculations with SEEP/W, SIGMA/W and SLOPE/W (step 2, 3 and 4), this boundary condition (location water table) is implemented as an input (from step 1). Figure 5-2 illustrates two different cases (Cases S1 and S21) with this water table located 7 m below the ground. A free drainage condition was applied at the right side of the waste rock pile

model, in the foundation, to prevent a rise of the water table; the position of the water table is thus maintained constant at this location in the calculations.
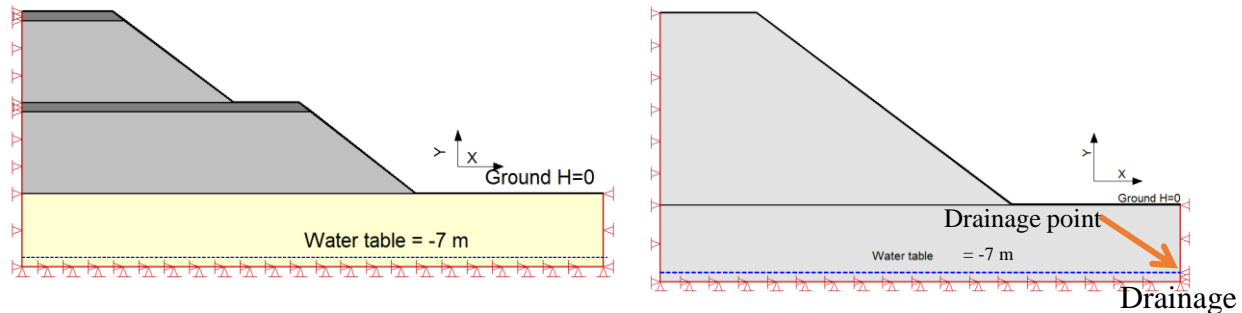
Figure 5-2: Model used with SIGMA/W, water table position (-7 m from the base) (step 1) for different cases of waste rock piles (Case S1 on the right, S21 on the left; details in Tables 4-4 and 4-5),

Figure 5-3 shows a typical initial pore water pressure distribution and the vertical profile imposed within the silty sand foundation. Below the phreatic surface (horizon of zero pore pressure), the pore pressure is positive and increases hydrostatically with depth; above it, the water pressure is negative due to capillary action. This negative pore water pressure increases uniformly from the groundwater level up to the top of the capillary zone, initially entered into the simulations using SEEP/W and SIGMA/W; considering the assumed maximum suction in the foundation. The negative pore pressures increased the effective stresses and thus the shear strength increasing stability.

During infiltration, the volumetric water content may increase as water accumulates at specific locations such as just above the interface between two materials (i.e. waste rock and silty sand). In the latter case, water may accumulate until the local suction approaches the WEV of the lower material, which corresponds (on the water retention curve) to the suction at which water starts to penetrate significantly into the material on a wetting path, e.g. (Aubertin et al., 2009).

In these simulations, the residual water content θ_r (and the corresponding residual suction Ψ_r) was used to establish the maximum initial suction within the foundation; for the silty sand soil, the residual suction is around 50 kPa ($\approx \Psi_r = $ WEV).

Figure 5-3 shows that the suction value reaches a maximum of 50 kPa below the ground. It then decreases near the interface between the foundation and waste rock pile until it reaches the initial suction imposed within the waste rock pile (around 1.2 kPa).
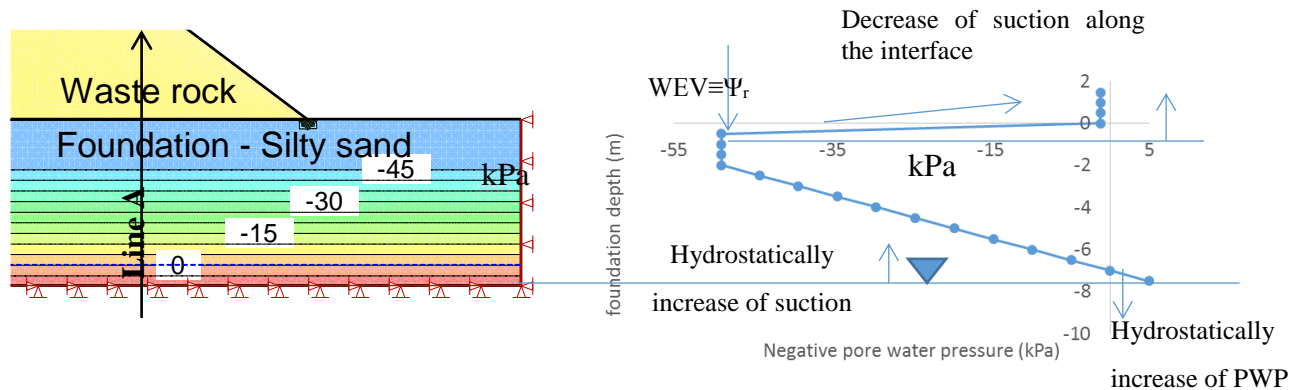
Figure 5-3: Pore water pressure distribution in the silty sand foundation (Case S1) before the rainfall; isocontours on the left and distribution along Line A on the right

As was mentioned in Section 4-6, the selected c_{app} is related to a specific suction which is imposed in the pile (above the ground surface); here, this suction corresponds to the WEV of the waste rock ($\Psi_r \approx 1.2$ kPa). The level of the initial water table and negative pore water pressures were defined in SIGMA/W as *in situ* conditions.

Rainfall

Surface infiltration corresponded to the recharge, i.e. the portion of rainfall or snowmelt that enters the waste rock pile by downward flow through the surface. During infiltration, changes may occur in water content, PWP, and strength within a pile (including its slope).

SEEP/W boundary condition was applied to the pile (with the option potential *seepage face review*) and foundation surface with a unit flux (q) having a constant rate (m/s or cm/s); the no ponding option was used with constant rainfall intensity. Figure 5-4 shows a typical waste rock pile (Case S11) under a constant rainfall boundary condition; i.e. recharge q (m/s).
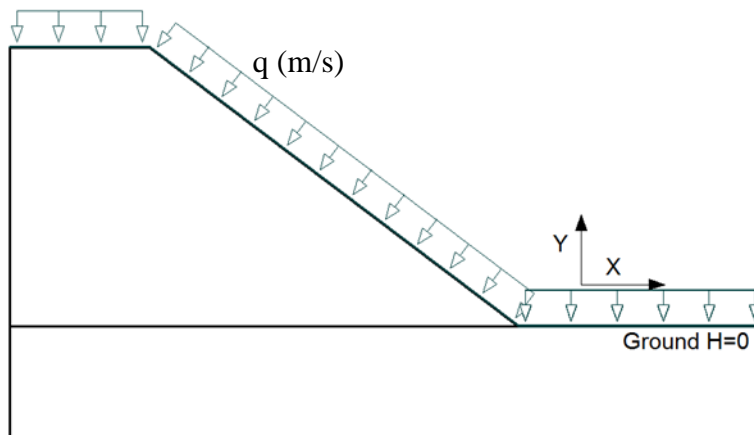
Figure 5-4: Infiltration boundary condition with a constant rate (m/s) applied on the waste rock pile and foundation (presented with SEEP/W)

The mechanical boundary conditions for the analysis with SIGMA/W are presented in section 4-5 and Figures 5-2 and 5-3. These boundary conditions block the movement in the horizontal direction along the two sides of the model and the x and y directions at the base. These boundary conditions were imposed for all the simulations.

5.4 Rainfall intensity and duration

Natural rainfall patterns have a high uncertainty and can be highly variable. Their introduction of engineering analyses is generally based on probabilistic forecasts. One of the parameters often used in the design of dams and dikes, spillways and reservoirs is the Probable Maximum Precipitation (PMP), established statistically for a given length of time such as 6 or 24 hours (section 2-4-2-1). Other conditions considered are often associated with a specific a return period (such as 100 or 1000 years) or a fraction of the PMP, for a specific duration (Aubertin et al., 2002a).

Although there is no steady-state condition in reality, such a condition is useful to assess a model response under a long period of rain (or to consider an average condition during an extended period). Performing a transient analysis with constant conditions over a long period can lead to similar results as a steady-state analysis. To avoid the additional difficulties in simulating a steady-state condition for the infiiltration within a waste rock pile, two transient conditions (i.e. pseudo steady-state) were applied for an extended period (365 days), with a relatively low

intensity of 3.16×10^{-9} m/s (total 10 cm) and 1.17×10^{-8} m/s (total 37 cm), which would be fairly close to a typical rainfall in the eastern region of the province of Québec. Other transient analyses were also conducted for shorter periods.

Simulations were carried out to assess how infiltration varies over time on the applied rainfall and initial PWP distribution for these transient analyses. The focus was mainly placed on short-duration rainfall events (less than or equal to 24 hours) with relatively high intensities because these are considered the most critical for slope stability of coarse grained materials (see section 2-4-2). For the first set of the scenarios (Cases S11, S21, S35, S41 and S51), five rainfall total value considered a duration of 24 hrs: 5 cm and 10 cm (low intensity); 15 cm (moderate intensity); 30 cm and 37 cm (high intensity), close to the PMP (Aubertin et al., 2011).

The second set of scenarios (Cases S11, S21, S35, S41, and S51) simulates the effect of rainfall duration on the slope stability of waste rock pile considering a constant amount of rainfall (15 cm) for three different durations (t): 6, 12 and 24 hours.

The characteristics of the precipitation events with different total rainfall amounts and their respective durations are given in Table 5-1.

Table 5-1: Different rainfalls imposed in this study (duration and intensity)

Rainfall	Duration			
	6 hrs	12 hrs	24 hrs (1st set)	365 days
Total (cm)	Transient			Pseudo steady- state
5	-	-	5.78×10^{-7} m/s (0.05 m/day) (R1)	-
10	-	-	1.157×10^{-6} m/s (0.1 m/day) (R2-1)	3.16×10^{-9} m/s (2.7×10^{-4} m/day) (R2-2)
15 (2nd set)	6.94×10^{-6} m/s (0.6 m/day) (R3-1)	3.47×10^{-6} m/s (0.3 m/day) (R3-2)	1.736×10^{-6} m/s (0.15 m/day) (R3-3)	-
30	-	-	3.47×10^{-6} m/s (0.3 m/day) (R4)	-
37	-	-	4.28×10^{-6} m/s (0.37 m/day) (R5-1)	1.17×10^{-8} m/s (0.001 m/day) (R5-2)

The results presented here mainly focus on the time during and immediately after the rainfall, which was followed by two days without precipitation (for transient analyses).

5.5 Slip surface specifications

The shape of a sliding plane mainly depends on the material properties, moisture content and pore water pressure, and geometry of the slope.

In the analyses presented below, the trial slip surfaces were assumed to be circular. Two types of sliding surfaces are considered; i.e. a local slip surface related to one bench and a global slip surface covering two benches (the surface enters along the crest and exit at the toe of the pile, see Figure 5-5). The slip surfaces are relatively deep; shallow slip surfaces were not considered as they may not lead to a significant failure (or impact). They were defined to meet a minimum specific depth for at least one slice along the slip surface; for local (one bench) and global (two benches) slip surfaces, the specific slip surface depth was assumed to be 3 m and 6 m respectively (see section 3-2-3).
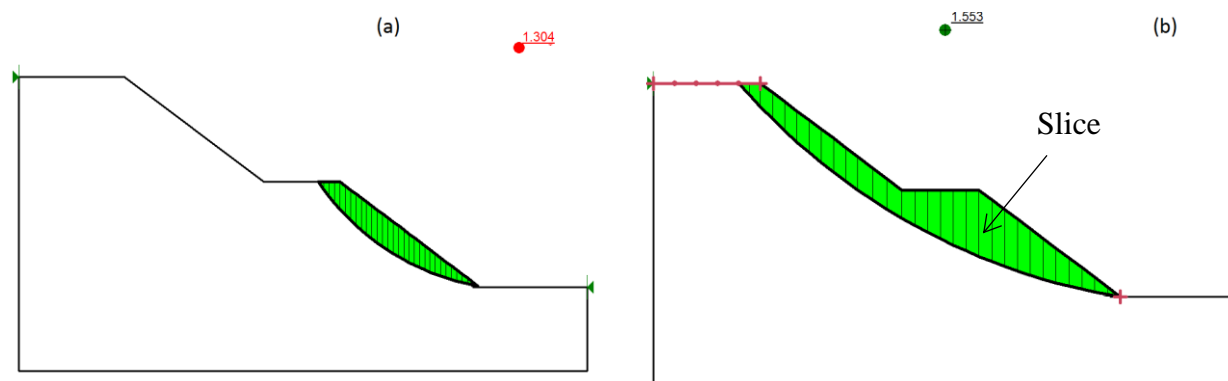
Figure 5-5: Typical slip surfaces exiting at the toe for Case S11 (see Table 4-4) with SLOPE/W; a) local slip surface (one bench, 3 m deep); b) global slip surface (two benches, 6 m deep)

5.6 Results from SEEP/W for extended transient conditions

Results from simulations conducted with SEEP/W are presented here, in relation with infiltration following a very long transient (pseudo steady-state) period. These results show an expansion of the wetting front with changes in volumetric water content, for different initial suctions and rainfall rates. The factors of safety of the piles are presented in section 5.7.

Five different cases are analysed here (see Tables 4-4 and 4-5): S11 (two benches, homogenous waste rock), S21 (two benches with horizontally compacted layers), S35 (two benches with 5% inclined compacted layers), S41 (2 benches with horizontal compacted layers and alternate layers parallel to the slope) and S51 (two benches with 5% inclined compacted layers and alternate layers parallel to the slope); results related to single bench pile are presented in Appendix II. The pseudo steady-state analysis is simulated with an extended transient analysis (over a period of 365 days) with a rainfall intensity, q of 3.16×10^{-9} m/s (2.7×10^{-4} m/d) applied on the crest slope and natural ground surface (see Figure 5-4).

The materials included the coarse (pile body for all cases) and compacted fine waste rock layers (added for Cases S21, S35, S41, and S51). A silty sand foundation was used for all cases (see Table 4-3 and Figures 4-1 and 4-2 for materials properties). As stated above, the initial water table was fixed at -7 m below the ground surface (Figure 5-3); ponding over the surface is not allowed.

5.6.1 **Case S11**

Infiltration during and following rainfall tends to fill the pores of the waste rock from the surface downward and lateraly. The added moisture forms a wetting front that increases the pore water pressure (decrease suction) as it spread downward. Figure 5-6 illustrates the pore water pressure distributions in the waste rock pile at different times under the relatively low-intensity rainfall of 3.16×10^{-9} m/s (2.7×10^{-4} m/d) (R 2-2) for Case S11 (Tables 4-4 and 4-5).

Figure 5-6 (a) shows the initial pore water pressure distribution, which is uniform (constant) within the waste rock pile (PWP = -6 kPa). It is seen in Figure 5-6 (b) that the wetting front reduced the negative pore pressures after 90 days of rainfall, down to a depth of approximately 4 meters (the suction was changed from 6 kPa to 5 kPa). As expected, the rainwater that infiltrated into the unsaturated zone increased the pore-water pressure (i.e. reduced suction).

The rate of development of the wetting front depends on the initial conditions, material properties and rainfall intensity and duration– see section 5-7). Figure 5-6 (c) and (d) presents the wetting front after 180 and 270 days respectively for this extended recharge period. As the rainwater percolates down, the matric suction decreases at depth; the expansion of the wetting front

continues until the end of the simulation (365 days) (Figure 5-6 (e)). It is also seen that water moves and accumulates above the interface of the waste rock and foundation, where there is a progressive increase of the degree of saturation.
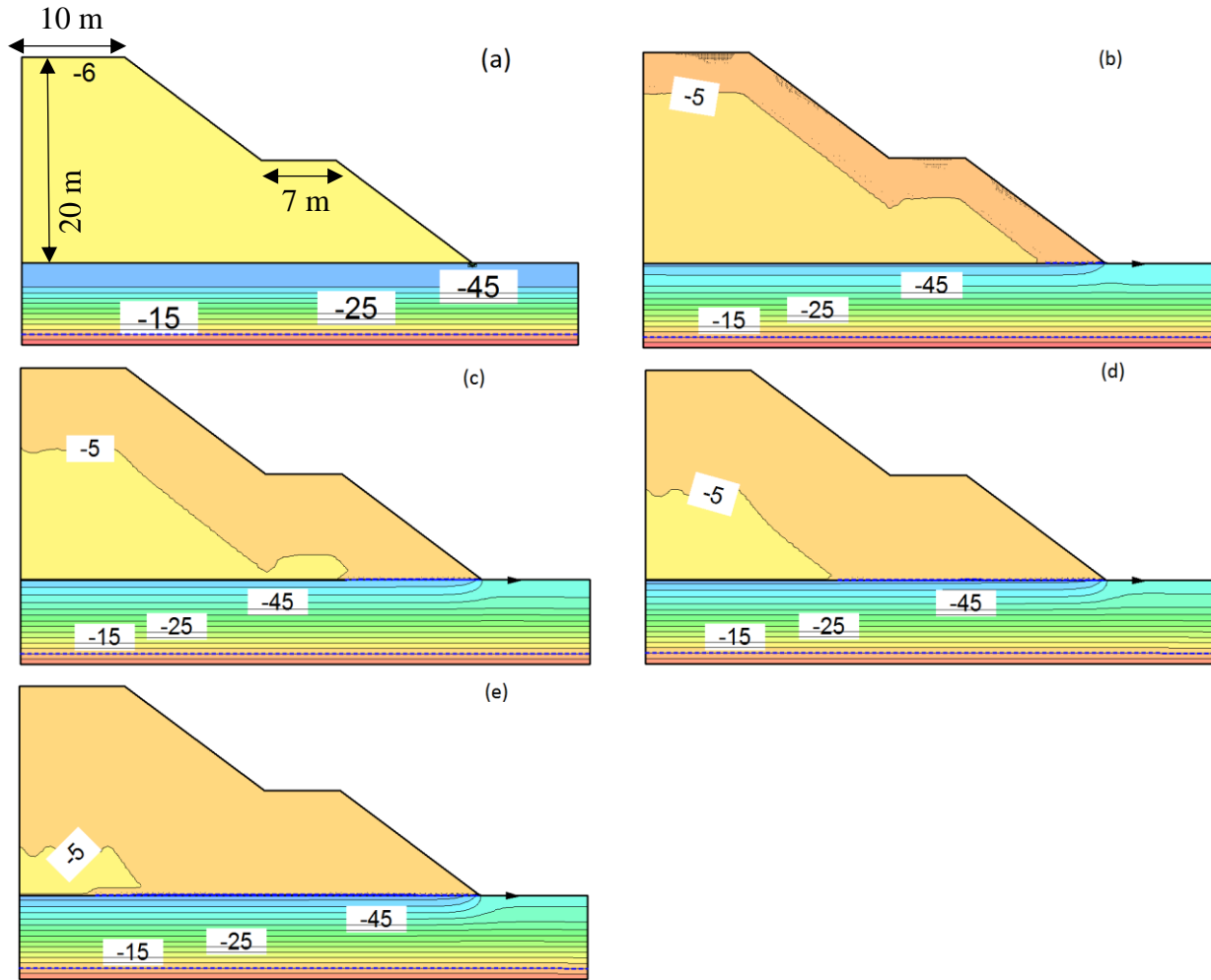
Figure 5-6: Evolution of the pore water pressures (kPa) with the development of a wetting front, Case S11 under a constant rainfall 3.16×10^{-9} m/s (2.7×10^{-4} m/d, R2-2, Table 5-1); a) before rainfall; b) after 90 days; c) after 180 days; d) after 270 days; e) after 365 days

Figure 5-7 (a to d) shows the changes of PWP along different lines over the year (i.e. Lines A, B, C, and D, shown in Figure 5-7 (e)). The initial distribution of PWP within the foundation is same as in Figure 5-3. For the waste rock pile, the PWP has a constant value equal to the residual suction (-1.2 kPa).

It is seen that the rainfall infiltrates differently into the waste rock pile from the surface along different lines (based partly on the effect of the PWP). For example, along line A, after 90 days of infiltration into the pile, the PWP change reaches a depth of 5 m after 365 days, it reaches a depth of 15 m (see Figure 5-7 (a)).

Along line A (going to the top of the pile) Figure 5-7 (a) indicates that suction reaches 2 kPa at depth 3.5 m after 90 days. After 180 days, the suction at depth 7 m is 2 kPa; after 270 days, suction 2 kPa is obtained at a depth of 11 m, while at the end of 365 days, the suction equals 2 kPa in depth 15 m. A similar pattern (with different rate and depth of infiltration) is obtained for other lines. For line D (shallow depth), the water infiltrates and it changes the suction over 90 days and then stays constant afterward.
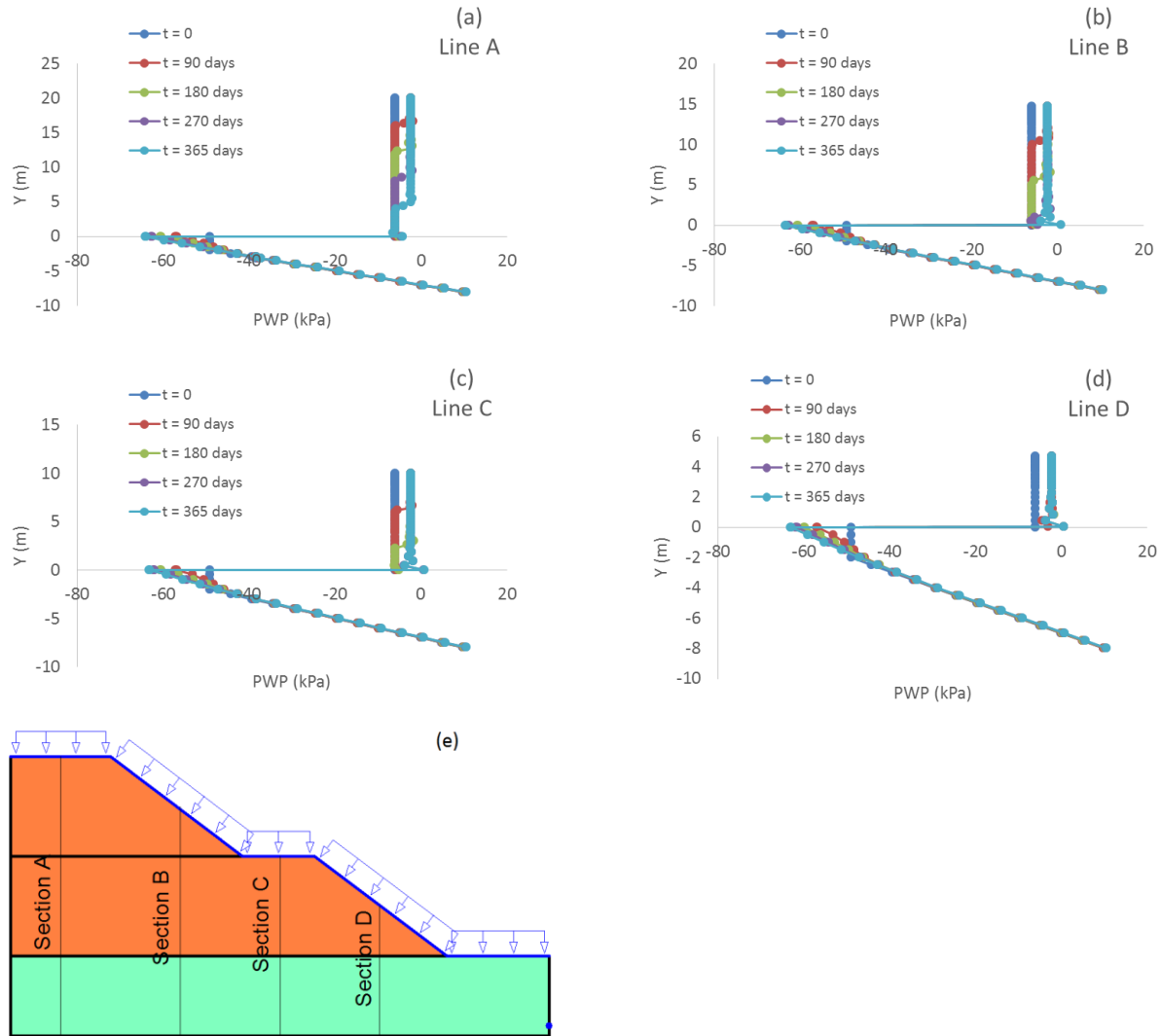
Figure 5-7: Evolution of the pore water pressures (kPa) under rainfall 3.16×10^{-9} m/s (2.7×10^{-4} m/d , R 2-2), Case S11, after 90, 180, 270 and 365 days along; a) line A; b) line B; c) line C; d) line D; e) location of lines A, B, C, and D

Figure 5-8 (a to d) displays the volumetric water content during the relatively low rainfall intensity of 3.16×10^{-9} m/s (2.7×10^{-4} m/d; R 2-2, Table 5-1, Case S11). The initial VWC is about 0.05 within the waste rock pile. VWC changes (increase) due to infiltration. It follows the trend corresponding to the PWP distribution, with the change of VWC (wetting front) expanding inside the pile over time.
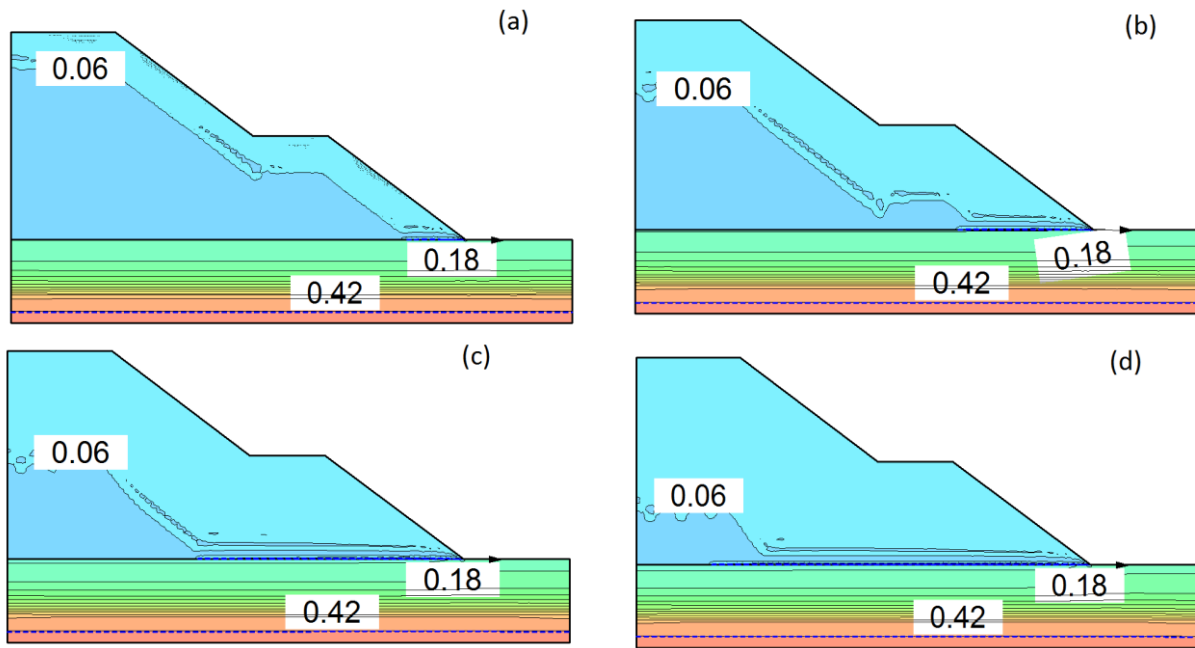
Figure 5-8: Evaluation of the volumetric water content distribution under rainfall 3.16×10^{-9} m/s (2.7×10^{-4} m/d, R 2-2), Case S11 with initial VWC ≈ 0.05; a) after 90 days; b) after 180 days; c) after 270 days; d) after 365 days

Comparing Figure 5-7 and 5-8 indicate that the PWP is more sensitive to the infiltration than the VWC.

Figure 5-9 shows the evolution of the VWC along lines A, B, C, and D (see Figure 5-7e). It is seen that the value of volumetric water content tends to increase due to infiltration, although the change is not very significant. For example, along line A, there is an increase in the VWC to a depth of 5 m after the 90 days (θ_w ≈ 0.055) and 15 m after the 365 days (θ_w ≈ 0.06) (Figure 5-9 (a)). A similar pattern (with different rate and depth) is observed along the other lines.
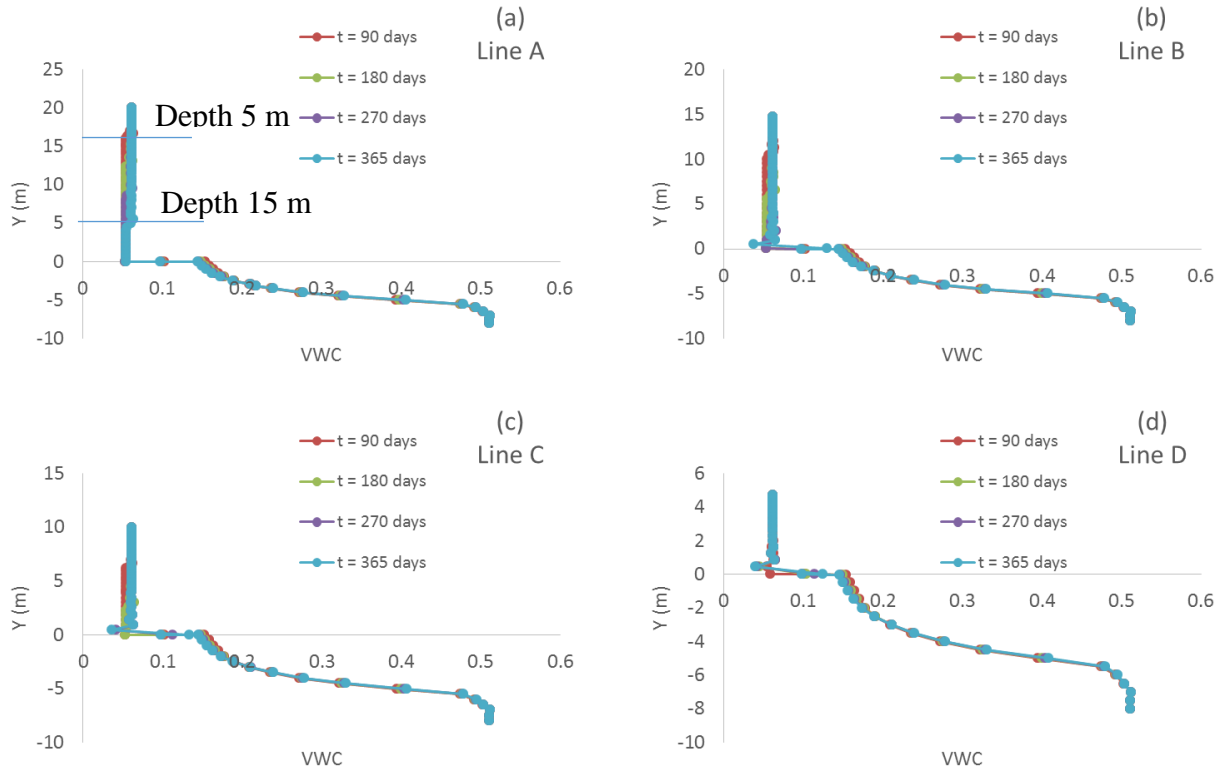
Figure 5-9: Evolution of the volumetric water content distribution under rainfall 3.16×10^{-9} m/s (2.7×10^{-4} m/d, R 2-2), Case S11, after 90, 180, 270 and 365 days along; a) line A; b) line B; c) line C; d) line D

5.6.2 Case S21

Figure 5-10 (a) shows the initial pore water pressure distribution for Case S21 (waste rock pile with two benches and compacted horizontal layers, Tables 4-4 and 4-5) subjected to the relatively low-intensity rainfall. Figure 5-10 (b), (c), (d) and (e) display the contour plots of negative pore water pressures and the wetting front advancement during the rainfall at 90, 180, 270 and 365 days respectively. Moving from Figure 5-10 (a) to 5-10 (e) indicate that the wetting front penetrates deeper within the waste rock pile from slope surface similar to Case S11. With time and infiltration the value of negative pore water pressure decrease (from -6 kPa to -5 kPa and higher) from slope surface, also it shows that compacted waste rock does not prevent water from infiltrating to the bottom and towards the center of the pile.

Infiltration also changes the pore water pressure distribution in the foundation. Infiltrated water accumulates along the interface between waste rock and silty sand due to the differences in the hydraulic properties of the two materials. More details about the evolution of infiltration in depth are discussed in Figure 5-11.
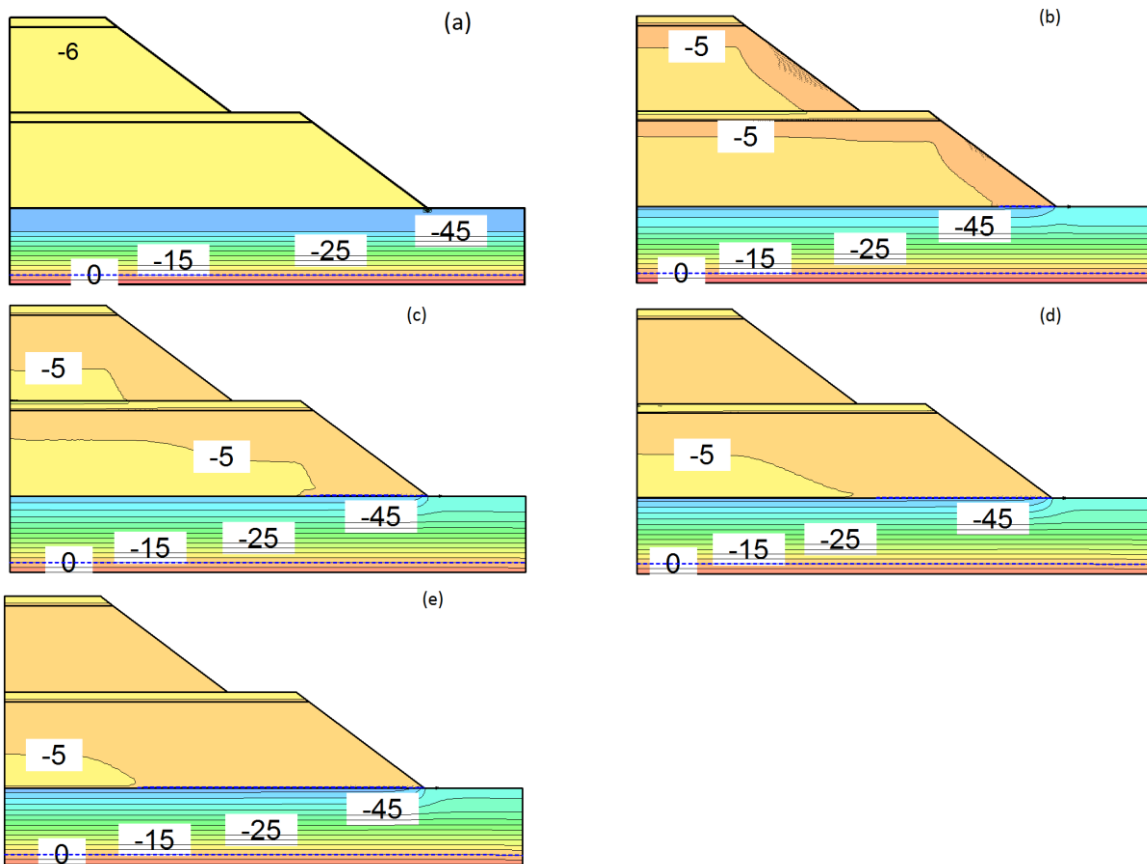
Figure 5-10: Evaluation of pore water pressure (kPa) with the development of a wetting front, Case S21 under rainfall 3.16×10^{-9} m/s (2.7×10^{-4} m/d, R2-2); a) before rainfall; b) after 90 days; c) after 180 days; d) after 270 days; e) after 365 days

Figure 5-11 shows the infiltration in depth along lines A, B, C, and D (see Figure 5-7 (e)). It indicates the value of suction decrease for waste rock along different lines by time. With initial suction 6 kPa, the hydraulic conductivity of compacted layer is in order of 10^{-8} and waste rock 10^{-11}. As the rainfall starts, an increase of suction is observed within the compacted layer, but by continuing rainfall, the suction decreases again (see Figure 5-11 (e)). It can be due to downward movement of water from top to the bottom of the layer. Figure 5-11 (a) indicate that after 90

days, the suction reaches 2.6 kPa at depth 3 m. After 180 days the suction at depth 6.8 m is 2 kPa; after 270 days, suction 2 kPa is seen at a depth of 10 m; at the end of 365 days, suction 2 kPa reaches depth 17 m. a similar pattern is observed for the evolution of PWP distribution along Lines B, C and D. Comparing Figures 5-7 and 5-11 shows that the expansion of the wetting front is affected by the compacted layer within the waste rock pile.
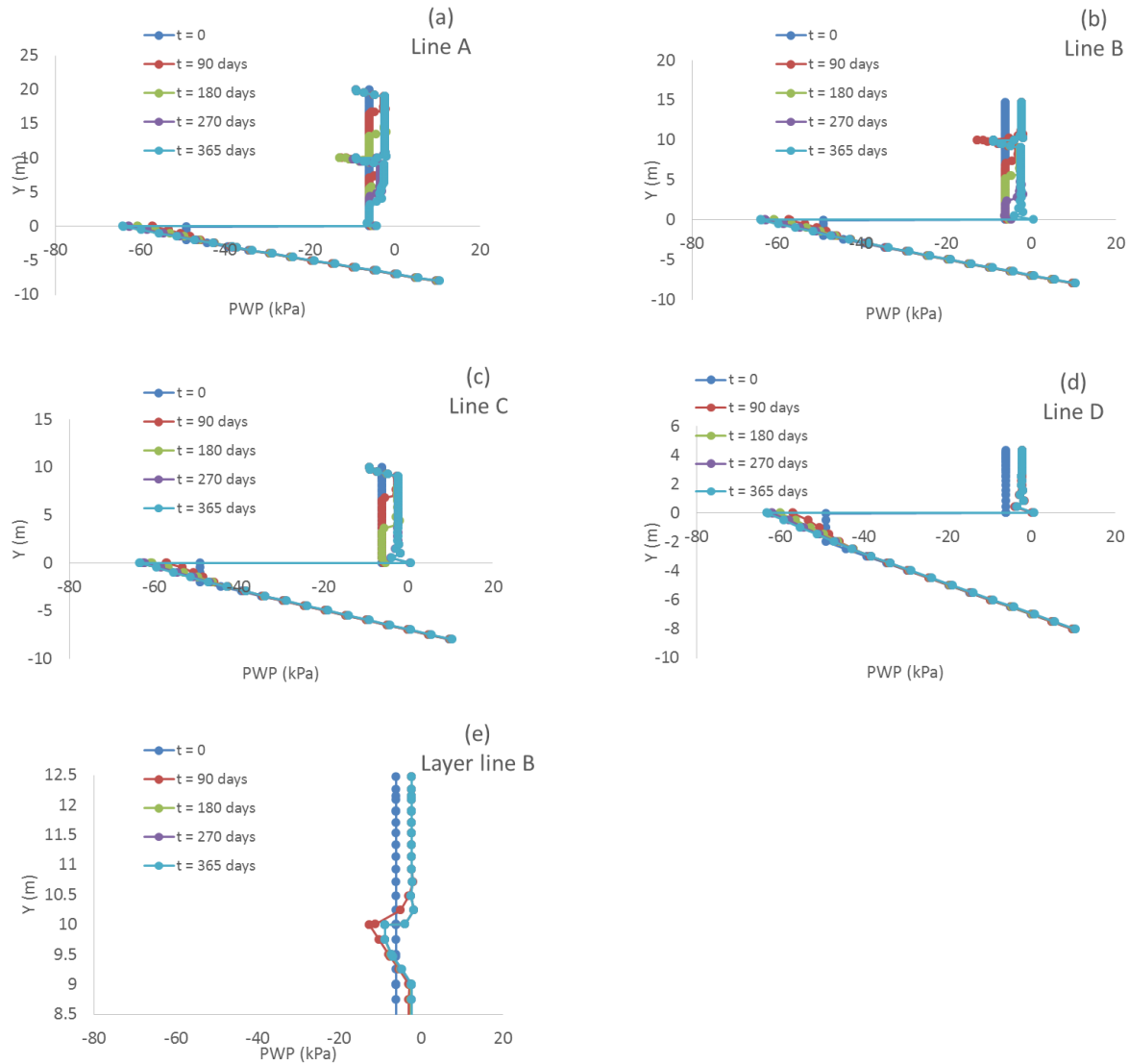
Figure 5-11: Evolution of the pore water pressure under rainfall 3.16×10^{-9} m/s (2.7×10^{-4} m/d, R2-2), Case S21, after 90, 180, 270 and 365 days along; a) line A; b) line B; c) line C; d) line D; e) compacted layer along line B

Figure 5-12 (a) to (d) present the changes in volumetric water content due to the infiltration resulting from rainfall 3.16×10^{-9} m/s (2.7×10^{-4} m/d, R2-2) in Case S21. The initial volumetric water content in the waste rock material is around 0.05 in suction 6 kPa and increases due to infiltration from 0.05 to 0.06. It follows almost the same trend as the pore water distribution and with time, the changes of volumetric water content go deeper inside the pile (see Figure 5-12 (b), (c) and (d)).

Figure 5-12 (d) shows volumetric water content 0.12 along the interface of waste rock and silty sand. It presents the water accumulation and a local water table at that point.
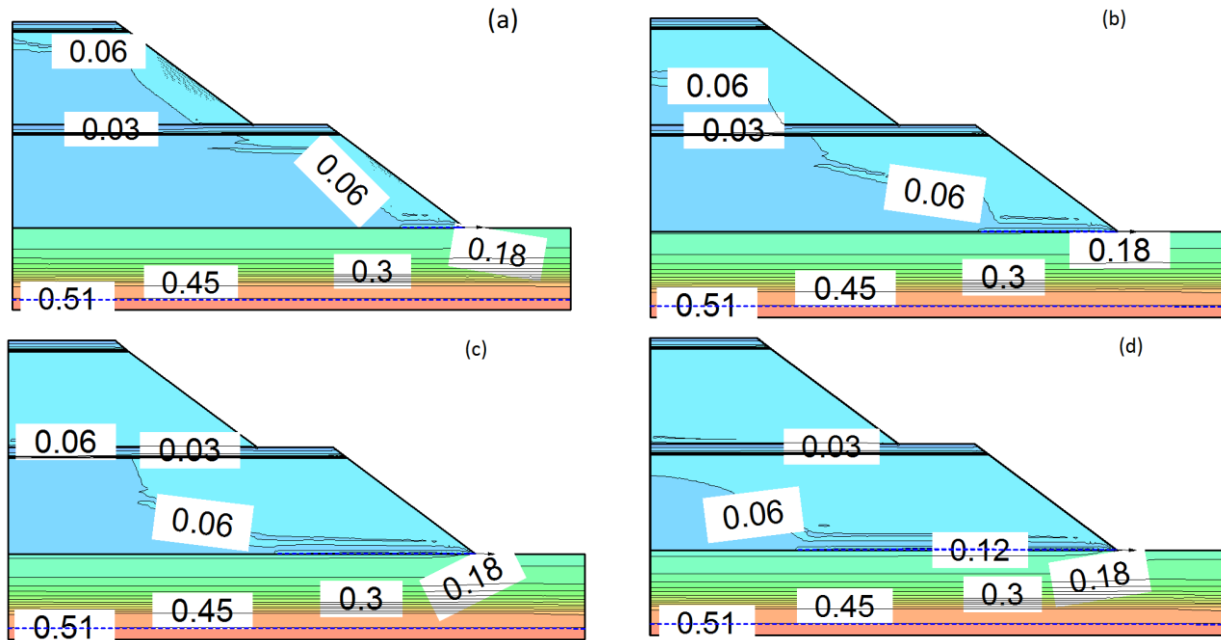
Figure 5-12: Evolution of the volumetric water content distribution under rainfall 3.16×10^{-9} m/s (2.7×10^{-4} m/d, R2-2), for Case S21; a) after 90 days; b) after 180 days; c) after 270 days; d) after 365 days

Figure 5-13 presents the difference between infiltration in Cases S11 and S12 along line A, B, and C, under rainfall R 2-2 after 365 days. Case S11 shows homogenous expansion of wetting front whereas in Case of S21, due to the existence of the compacted layers, the wetting front expansion is not homogenous and the disruption (an increase of suction) is being observed.
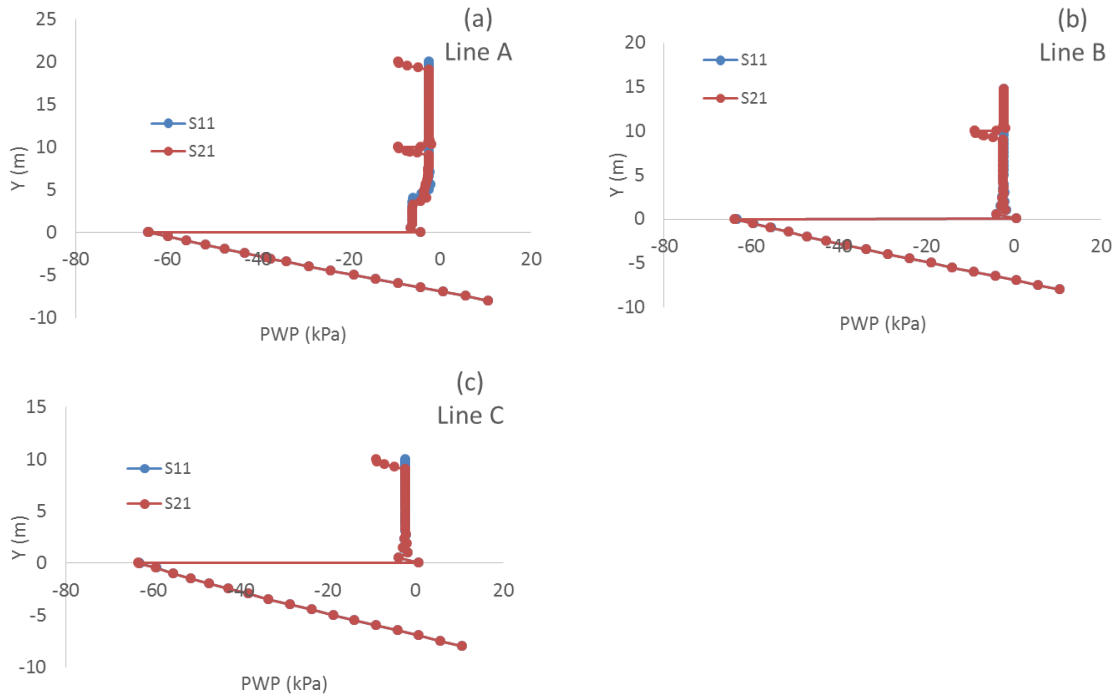
Figure 5-13: Evolution of the pore water pressure under rainfall 3.16×10^{-9} m/s (2.7×10^{-4} m/d, R2-2), for Cases S11 and S21, after 365 days along; a) line A; b) line B; c) line C

5.6.3 Case S35

Figure 5-14 shows the wetting front development (PWP distribution) for Case S35 (two bench waste rock pile with 5% inclined compacted layers, Tables 4-4 and 4-5), under a relatively low-intensity rainfall of 3.16×10^{-9} m/s (2.7×10^{-4} m/d, R2-2).

It indicates as the rainfall infiltrates into the pile, the initial suction (around 6 kPa) is reduced. The wetting front penetrates deeper in the pile until it covers most of the inside space (see Figure 5-14 (b) to (e)). Comparing Figure 5-14 with Figure 5-10 shows that the inclined compacted layers tend to limit deep infiltration; these direct the flow and accumulation of water toward the edge.

It is seen that compacted layer can cause an accumulation of water, which flows downward, causing the appearance of more localised flow zones in the pile. This feature has been observed and studied before (e.g. Fala 2002; Dawood et al., 2009; Dawood and Aubertin, 2014)

The water accumulates along the interface between waste rock and silty sand due to the difference in the hydraulic conductivity. This causes the reduction of suction at the interface, from 45 kPa to 25 kPa (see Figure 5-14 (a) and (e)).
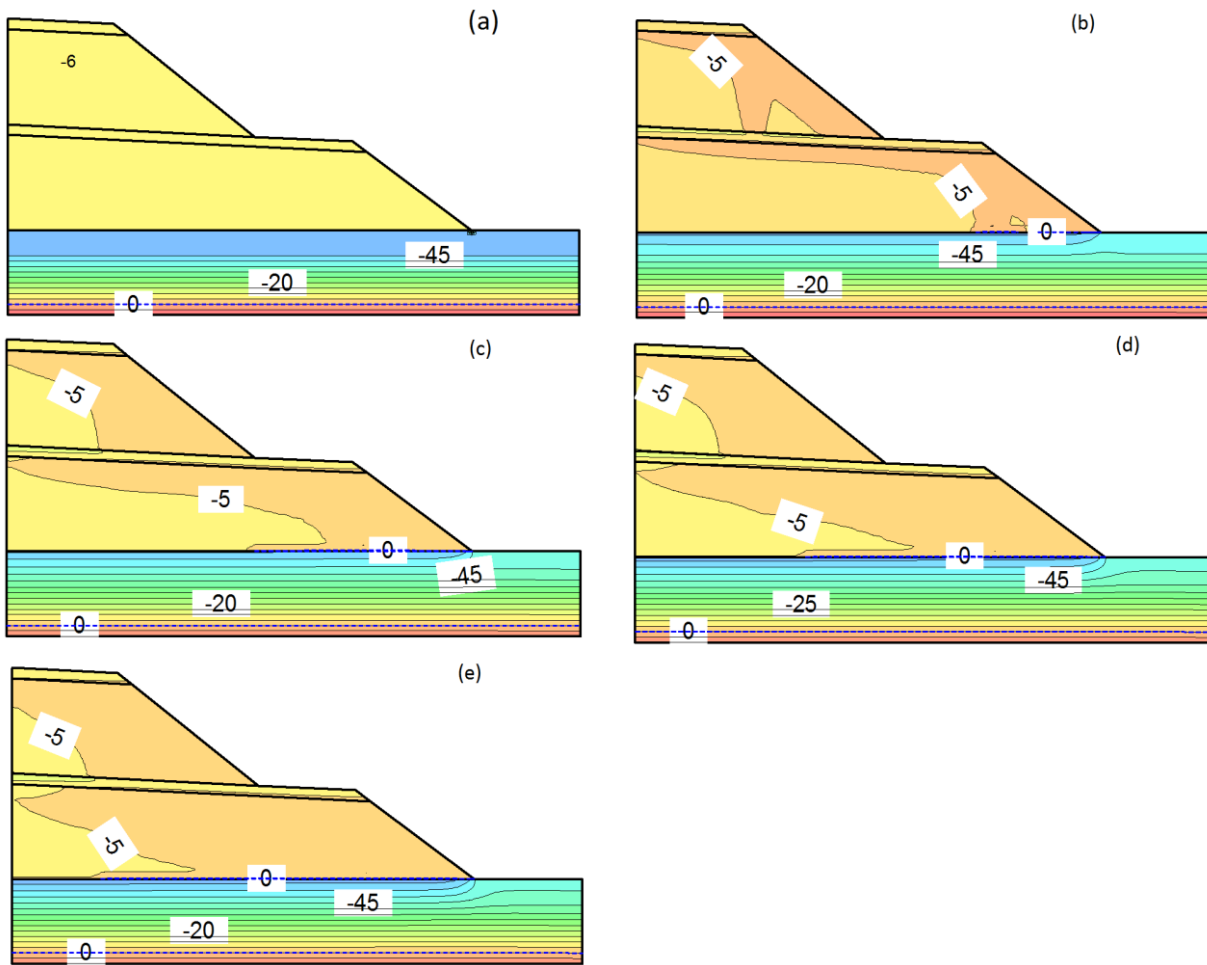
Figure 5-14: Evolution of pore water pressure (kPa) with the development of a wetting front, Case S35 under rainfall 3.16×10^{-9} m/s (2.7×10^{-4} m/d, R 2-2); a) before rainfall; b) after 90 days; c) after 180 days; d) after 270 days; e) after 365 days

Figure 5-15 shows the distribution of PWP in different times along lines A, B, C and D for Case S21, under rainfall 3.16×10^{-9} m/s (2.7×10^{-4} m/d, R2-2) (see Figure 5-7(e) for lines). It indicates the decrease of suction by time within the waste rock along different lines and at the same time the downward seepage in layers from top to bottom (Figure 5-15 (e)) that results in the increase of suction within the layers.
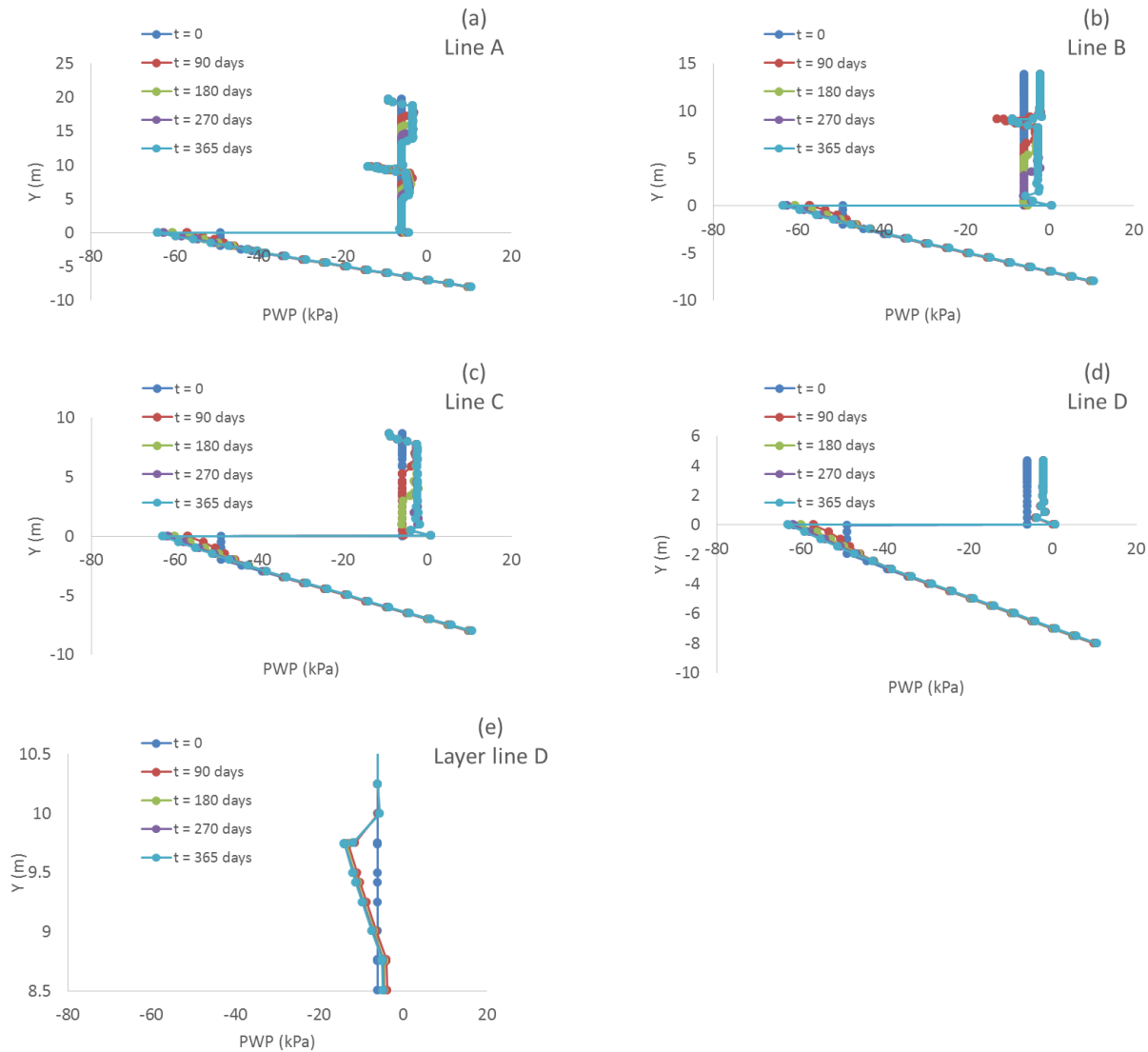
Figure 5-15: Evolution of the pore water pressure under rainfall 3.16×10^{-9} m/s (2.7×10^{-4} m/d, R 2-2), Case S35, after 90, 180, 270 and 365 days along; a) line A; b) line B; c) line C; d) line D; e) compacted layer along line D

Figure 5-16 presents the distribution of volumetric water content in waste rock pile for Case S35, during the rainfall 3.16×10^{-9} m/s (2.7×10^{-4} m/d, R 2-2) at different time steps. The volumetric water content value tends to increase at depth (compare Figure 5-16 (a), (b), (c) and (d)). The volumetric water content in the foundation is also changing.
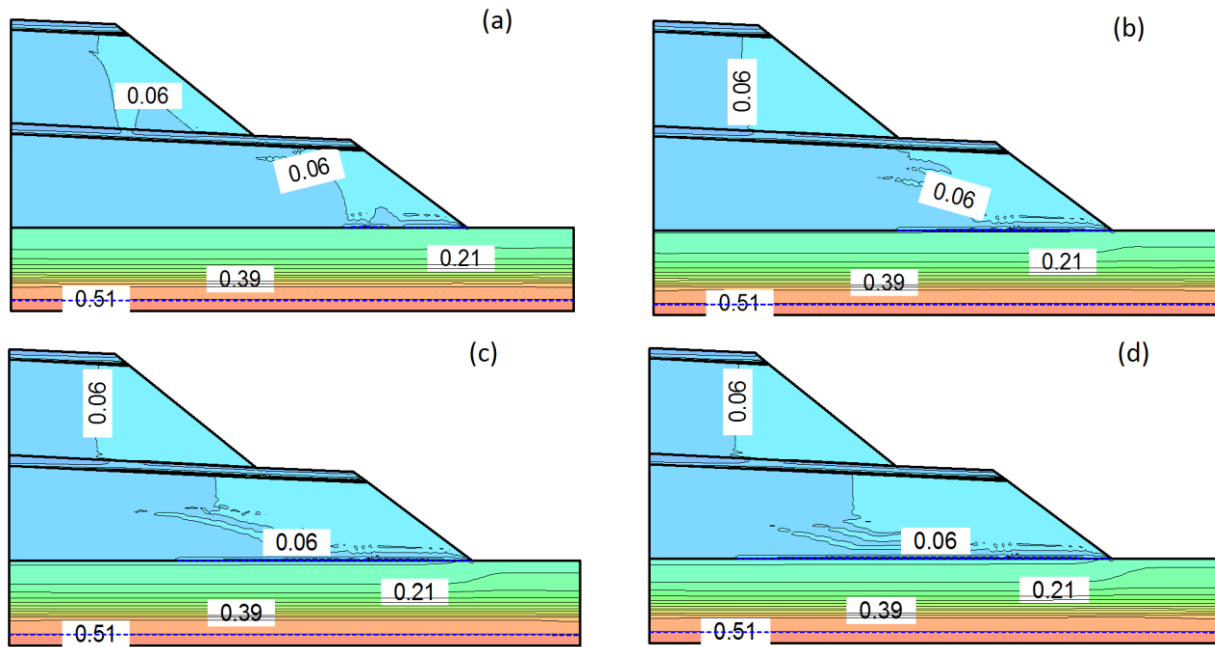
Figure 5-16: Evolution of volumetric water content distribution under rainfall 3.16×10^{-9} m/s (2.7×10^{-4} m/d, R 2-2), for Case S35; a) after 90 days; b) after 180 days; c) after 270 days; d) after 365 days

Figure 5-17 presents the infiltration and suction along lines A and B for Cases S21 and S35 after rainfall 3.16×10^{-9} m/s (2.7×10^{-4} m/d) for 365 days. The differences are not very significant though along line A the suction reached a lower value (more decreased) for Case S21 that presents less infiltration in Case S35 due to the inclination of the layer and outward movement of water.
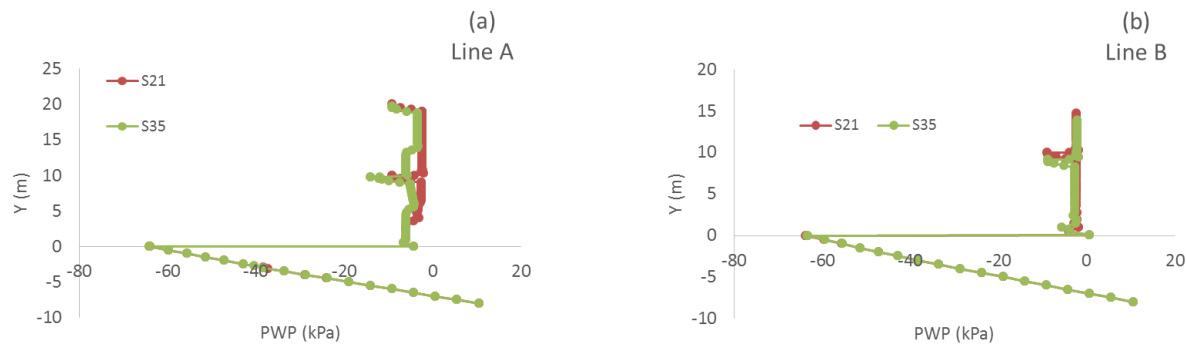
Figure 5-17: Evolution of the pore water pressure under rainfall 3.16×10^{-9} m/s (2.7×10^{-4} m/d, R 2-2, Table 5-1), for Cases S21 and S35, after 365 days along; a) line A; b) line B

5.6.4 Case S41

Figure 5-18 presents the wetting front development for Case S41 (two bench waste rock pile with horizontally compacted layers and alternate layers parallel to the slope, Tables 4-4 and 4-5), under a relatively low-intensity rainfall 3.16×10^{-9} m/s (2.7×10^{-4} m/d**,** R 2-2) at different time steps. Figure 5-18 (b) indicated that the wetting front starts developing from the alternate layers (parallel to the slope) and below the horizontal layers, resulting in a decrease in suction (PWP from -6 kPa to -5 kPa and less). The first and third layers parallel to slope contain loose waste rock while the second and forth consist crushed (finer) waste rock. The rainfall infiltrates to the loose waste rock layer and decreases the suction, but it does not move into adjacent layer (crushed waste rock) significantly.

The development of the wetting front below the layer may be due to the difference in hydraulic conductivity of loose and compacted waste rock at the initial suction of 6 kPa. At this specific suction, the hydraulic conductivity is close to 10^{-7} m/s for the compacted waste rock and about 10^{-11} m/s for loose waste rock.

The water also tends to accumulate along the interface between waste rock and silty sand forming a local water table; it then infiltrates into the foundation, resulting in a decrease of suction from 45 to 35 kPa in the silty sand near the interface (see Figure 5-18 (c) and (e)).

The rainfall that infiltrates tends to move downward in the layers parallel to the slope. The water then enters the foundation. Hence, a decrease in suction is shown along the interface of layers

parallel to slope and foundation (local effect). The suction decreases from 45 kPa to 35 kPa in the silty sand foundation and in time the isocontour of 35 kPa goes deeper in the silty foundation (see Figures 5-18 (a) to (c)).
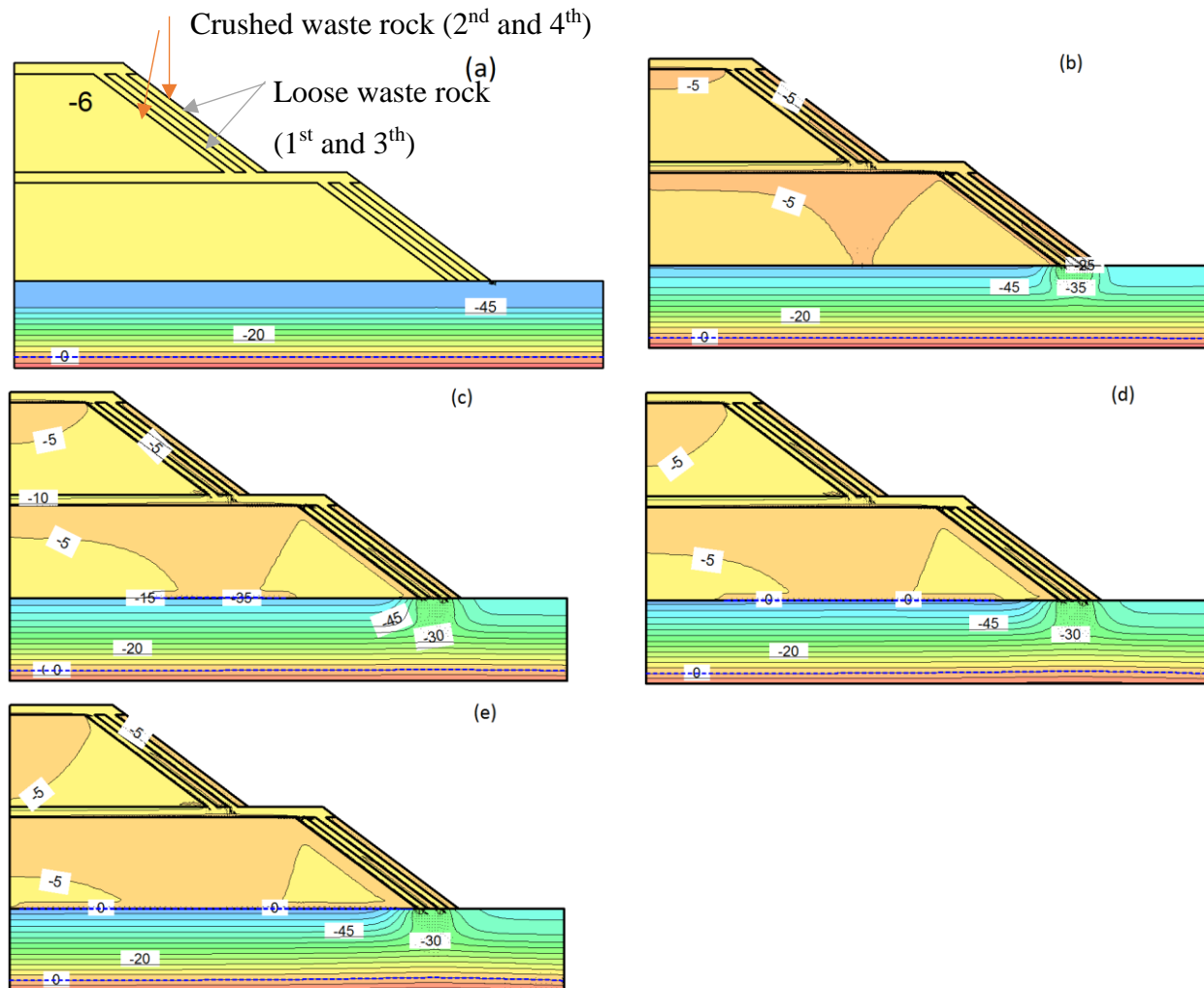
Figure 5-18: Evolution of pore water pressure (kPa) with the development of a wetting front, Case S41, under rainfall 3.16×10^{-9} m/s (2.7×10^{-4} m/d, R 2-2); a) before rainfall; b) after 90 days; c) after 180 days; d) after 270 days; e) after 365 days

Figure 5-19 presents the development of infiltration within the waste rock pile (Case S41) under rainfall 3.16×10^{-9} m/s (2.7×10^{-4} m/d) at different times along lines A, B, C, and D (see Figure 5-7 (e)). Infiltration results in a decrease of suction in the waste rock that goes deeper inside the pile

over time. As an example, along line C, the reduction of suction appears at depth 3 m and 7 m from the surface after 90 and 365 days respectively. Lines B and D represent the layers parallel to the slope. It is seen the suction decreases on the first layer (loose waste rock) and becomes close to zero while for other layers the oscillation in suction value is viewed. The suction value increases close to the interface between layers.
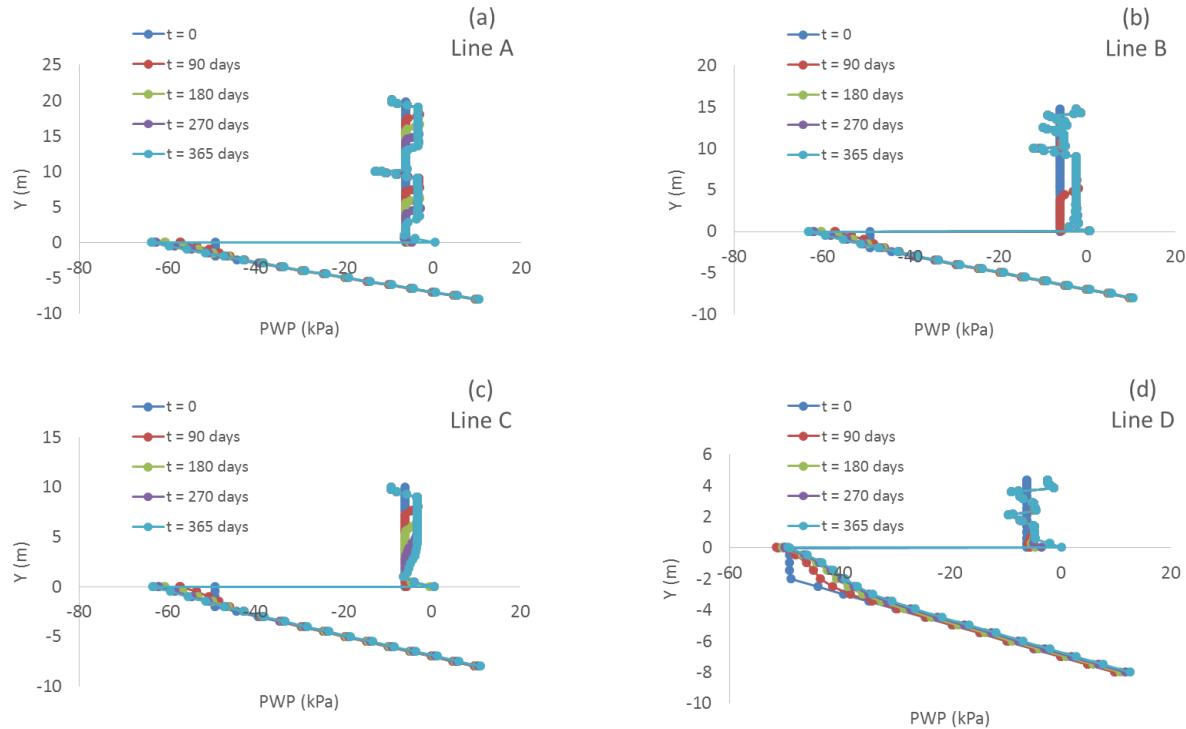
Figure 5-19: Evolution of the pore water pressure under rainfall 3.16×10^{-9} m/s (2.7×10^{-4} m/d, R 2-2), Case S41, after 90, 180, 270 and 365 days along; a) line A; b) line B; c) line C; d) line D

Figure 5-20 presents the volumetric water content for Case S41 under constant rainfall 3.16×10^{-9} m/s (for 365 days). The volumetric water content is approximately 0.03 and 0.05 for the compacted and loose waste rock materials (see Figure 5-20 (a)). The value of the volumetric water content is increasing below the compacted layer (specifically below the intersection of the first bench with compacted layer) and extends deeper with the development of wetting front during the rainfall.
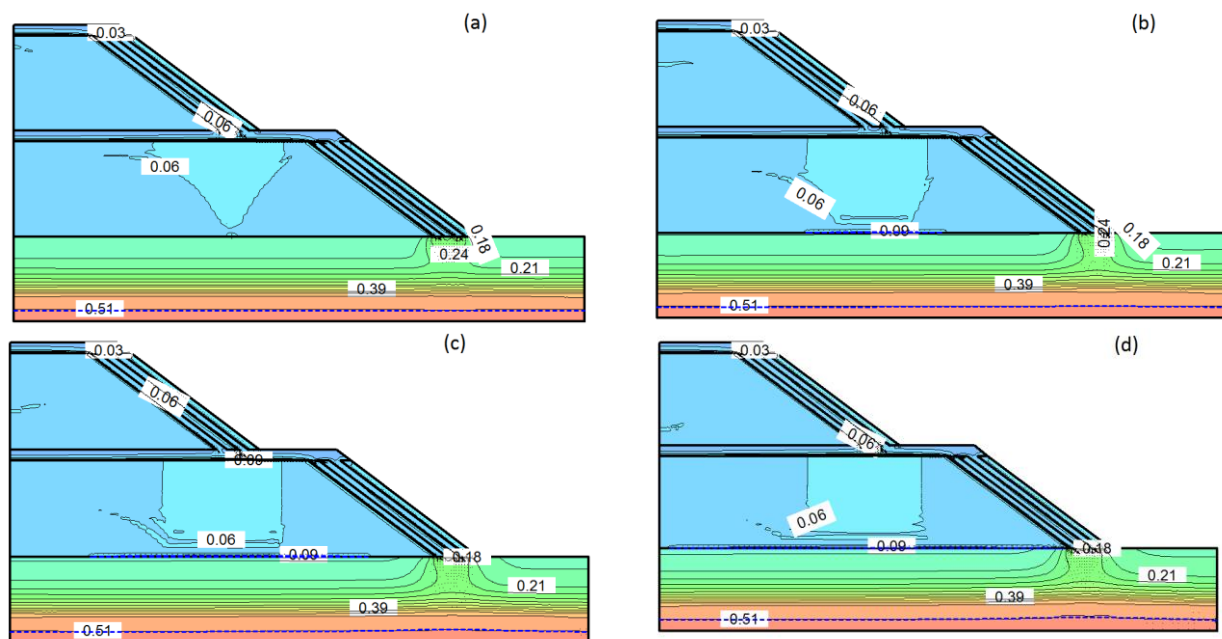
Figure 5-20: Evolution of volumetric water content distribution under rainfall 3.16×10^{-9} m/s (2.7×10^{-4} m/d, during 365 days), Case S35; a) after 90 days; b) after 180 days; c) after 270 days; d) after 365 days

5.6.5 Case S51

Figure 5-21 shows the wetting front development for Case S51 (two benches with 5% inclined compacted layers and alternate layers parallel to the slope, Tables 4-4 and 4-5), under transient relatively low-intensity rainfall (2.7×10^{-4} m/d, R 2-2) for different time steps.

Figure 5-21 (b) shows the development of wetting front starting with the layers parallel to the slope and below the horizontal layers, resulting in a decrease in suction (from 6 kPa to 5 kPa and less). The development of a wetting front parallel to the slope is due to the rainfall infiltration that decreases the suction, and also below the compacted layers (due to the higher hydraulic conductivity of the layer at this particular suction (e.g. 6 kPa) compare to the loose waste rock material. The wetting front then expands deeper as the rainfall continues. Comparing Case S41 to S51 shows that the wetting front goes deeper in Case S41 compared to Case S51 (see Figure 5-18 (e) and 5-21 (e)). This is due to the inclination of compacted layer that forwards the water to the

outside of the pile. The infiltrated rainfall then accumulates along the interface of waste rock, and silty sand is forming a local water table due to differences in hydraulic conductivity and AEV of two materials. The water infiltrates to foundation and results in a decrease of suction to 35 kPa in some part (see Figure 5-21 (c) and (e)).
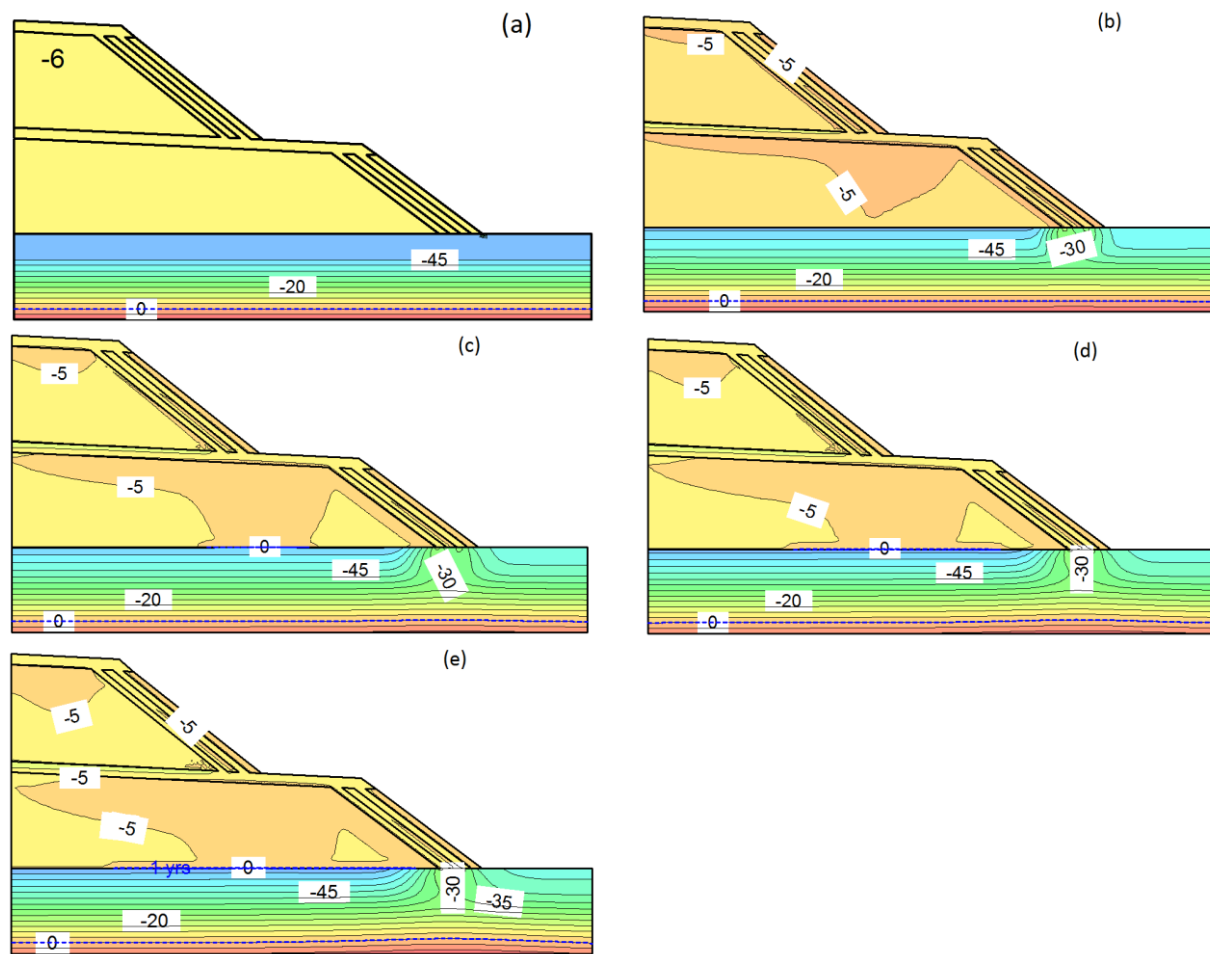
Figure 5-21: Evolution of pore water pressure (kPa) with the development of a wetting front, Case S51 under rainfall 3.16×10^{-9} m/s (2.7×10^{-4} m/d, R 2-2); a) before rainfall; b) after 90 days; c) after 180 days; d) after 270 days; e) after 365 days

Figure 5-22 presents the evolution of negative pore water pressure due to infiltration in depth along lines A, B, C and D for Case S51, under rainfall 3.16×10^{-9} m/s for 365 days. It shows the decrease of suction due to rainfall infiltration along different lines in the pile. Like Case S41, the changes of suction on the layers parallel to the slope is oscillating and shows an increase of

suction near the interface of layers. This process is illustrated in Figure 5-22 (e) more clearly. The suction value decreases in the layers of loose waste rock while it shows a non-significant increase in layers of crushed waste rock.
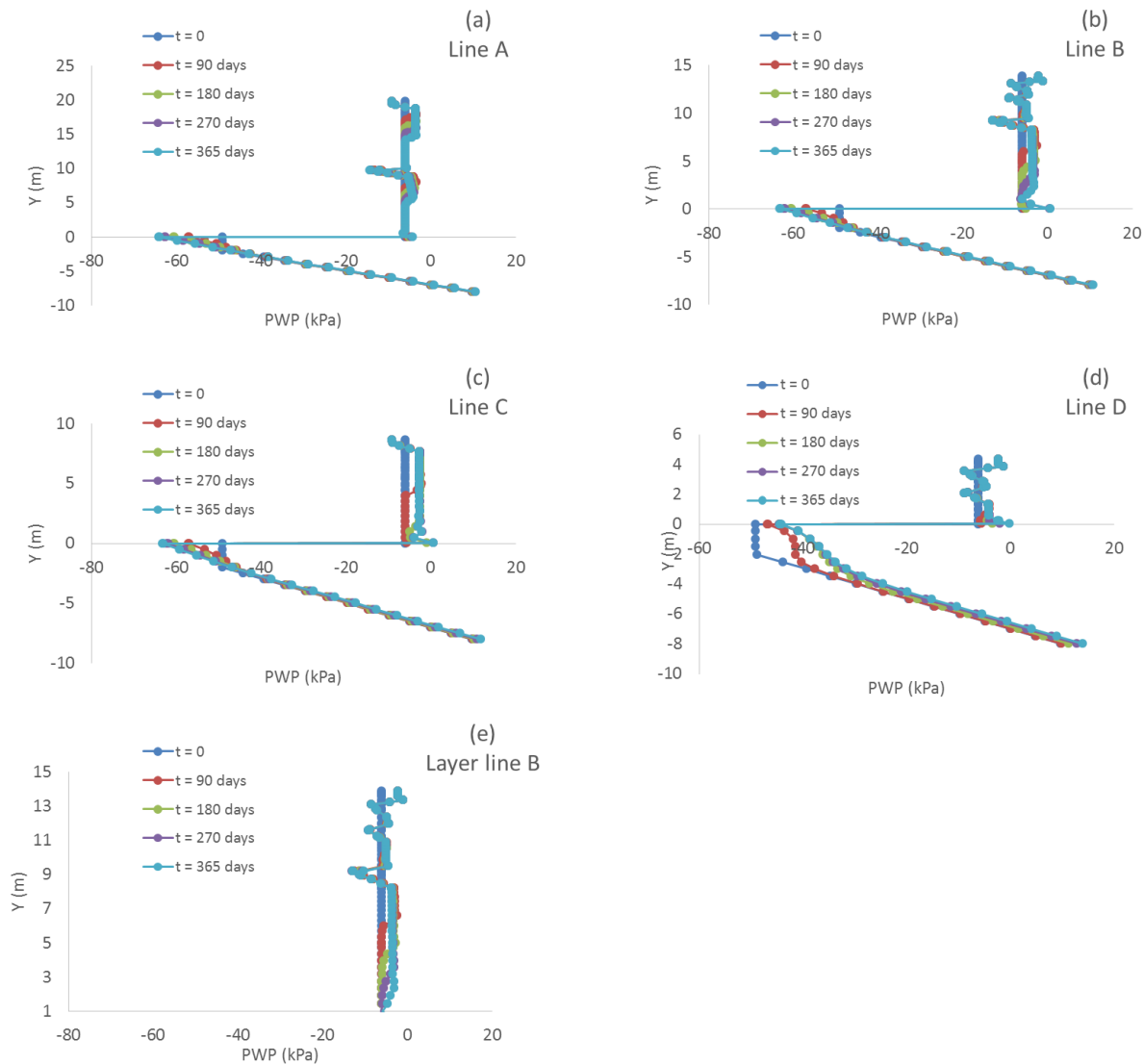
Figure 5-22: Evolution of the pore water pressure under rainfall 3.16×10^{-9} m/s (2.7×10^{-4} m/d, R 2-2), Case S51, after 90, 180, 270 and 365 days along; a) line A; b) line B; c) line C; d) line D; e) Layer line B

Figure 5-23 presents the volumetric water content for Case S51 (constant rainfall 3.16×10^{-9} m/s for 365 days). The initial volumetric water content of compacted waste rock is close to 0.03 while for loose waste rock it is near 0.05 (see Figure 5-23 (a)). The value of volumetric water content is

increasing below the compacted layer and extends deeper and get close to the interface of the waste rock pile and the foundation, following a similar path compare to the development of wetting front (see Figure 5-23 (b), (c) and (d)).
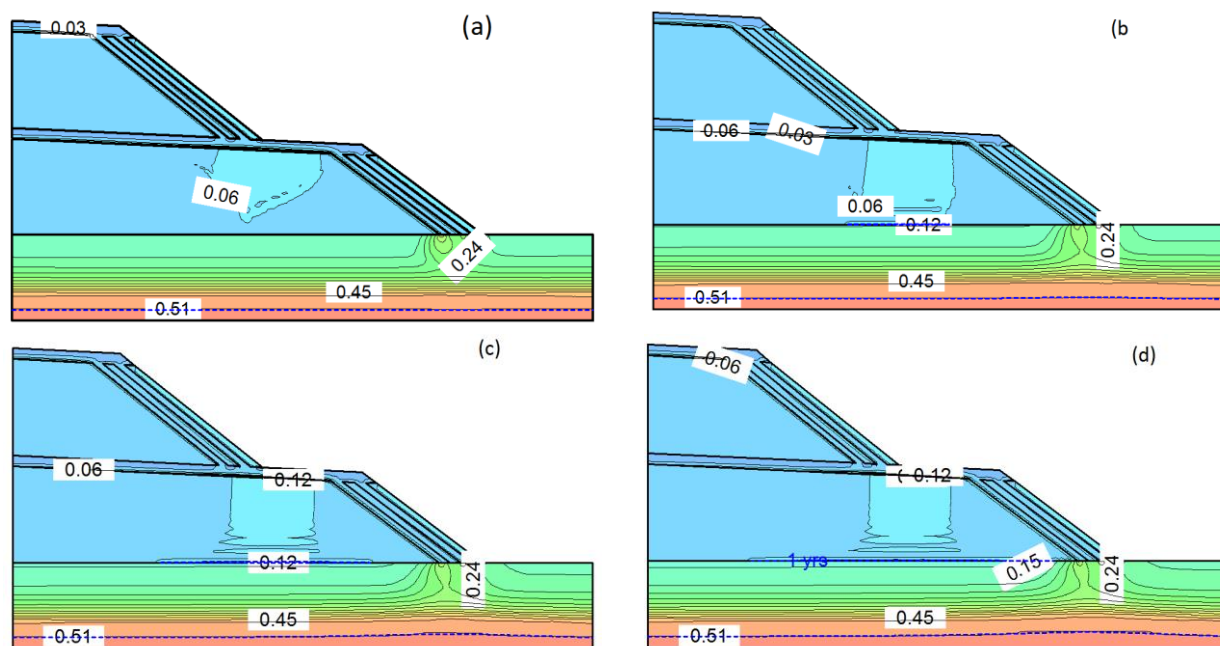
Figure 5-23: Evolution of volumetric water content distribution under rainfall 3.16×10^{-9} m/s (2.7×10^{-4} m/d, R 2-2), Case S51; a) after 90 days; b) after 180 days; c) after 270 days; d) after 365 days

Figure 5-24 presents a comparison of infiltration under rainfall 3.16×10^{-9} m/s after 365 days along line B for different cases. Figure 5-24 (a) compares infiltration for Cases S41 and S51 and indicate a lower suction after rainfall for Case S41. That reduction of infiltration for Case S51 is due to the inclined compacted layers making the water movement outward the pile. Figure 5-24 (b) shows the difference in infiltration for Cases S21 and S41 and indicates the effect of layers parallel to the slope. When the layers are presented a higher suction is viewed, compare to the case with no layer parallel to the slope. Figure 5-24 (c) also shows the effect of parallel layers in Case S51 compare to Case S35 with no parallel layers. It shows a less decrease of suction and expansion of wetting front for the case with layers parallel to the slope (Case S51).
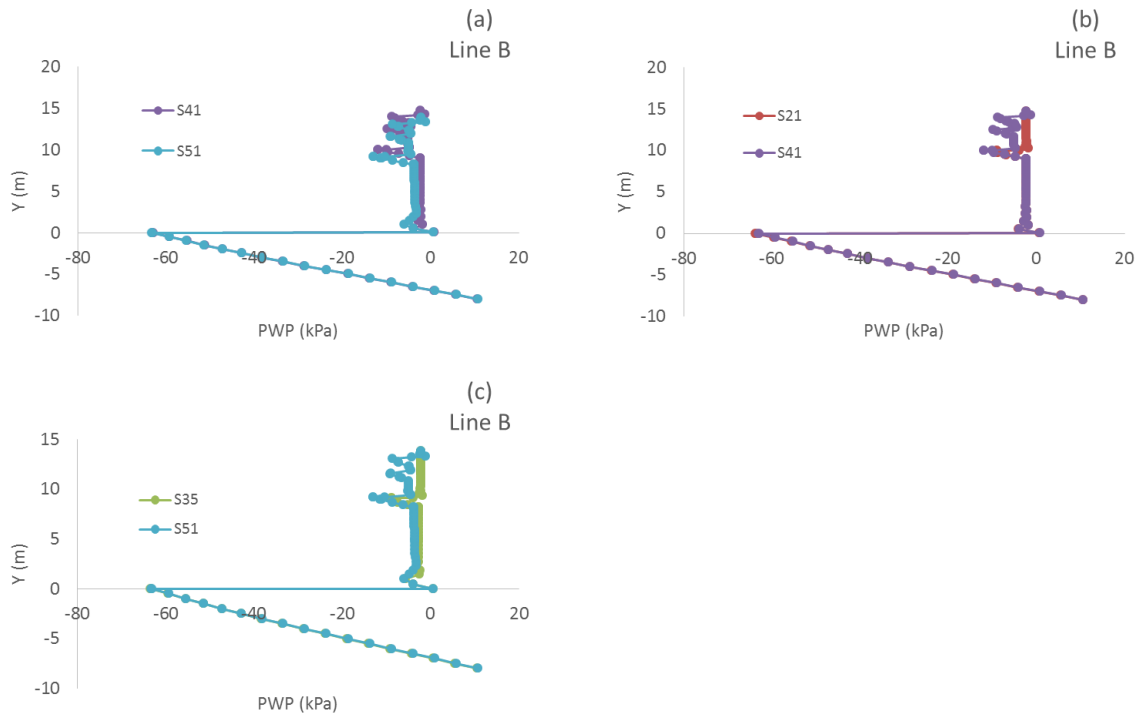
Figure 5-24: Evolution of the pore water pressure under rainfall 3.16×10^{-9} m/s (2.7×10^{-4} m/d, R 2-2), after 365 days along Line B; a) Cases S41 and S51; b) Cases S21 and S41; c) Cases S35 and S51

5.6.6 **Effect of prolonged rainfalls**

The results presented in Figure 5-25 (a to h) illustrate the effect of infiltration simulated using pseudo steady-state rainfall on the minimum factors of safety for Cases S11, S21, S35, S41, and S51. Figure 5-25 (g) (Case S11) shows a typical local slip surface that covers one bench exiting at the toe. A similar type of slip surface was obtained for Cases S21 and S41. For Cases S35 and S51, the local slip surface is located on the upper bench (see Figure 5-25 (h)) due to a larger height of this upper bench because of inclination inside the pile.

These piles are submitted to a prolonged simulated rainfall 3.16×10^{-9} m/s (2.7×10^{-4} m/d, R 2-2, for 365 days). Due to infiltration and PWP variation (given by SEEP/W) variations of a factor of safety is observed. For Cases, S11, S21, and S35, the factor of safety tends to decrease for the first 100 days approximately and then stays more or less constant (after reaching a constant suction value).

For example, the minimum local factor of safety for Case S11 changes between 1.335 (initial condition) and 1.315 (minimum FS reached during rainfall) (Figure 5-25 (a)). For Case S21, this reduction goes from 1.4 (initial condition) to 1.38 (minimum FS reached during rainfall), which is very small. For Case S35, the minimum local factor of safety decreases from 1.31 (initial condition) to 1.28 (minimum FS reached during rainfall) and stays constant afterwards. For Cases S41 and S51, the factor of safety fluctuates during the rainfall. The range of this fluctuation is very small compared to other Cases (S11, S21, and S35) with a small decrease and an increase of FS (which is not significant).

Figure 5-25 (f) displays a comparison between Cases S11, S21, S35, S41, and S51 under rainfall R 2-2, showing the variation of the minimum local factor of safety. It is seen that the lowest minimum factor of safety relates to Case S35 (5% inclined compacted layers) and the highest to Case S41 (horizontally compacted layer and alternate layer parallel to external slope). The results also indicate that the change of the minimum local factor of safety due to this prolonged rainfall for Cases S41 and S51 is very small (negligible).

Figures 5-25 (g) and (h) show typical local slip surface for Cases S11 and S35. For Case S11 (and also S21 and S41, see Tables 4-4 and 45) $H_1 = H_2$, while for Case S35 (and S51) $H_1 > H_2$ (due to layers inclination). In section 4-7-6, it was indicated that increasing the height of the pile often results in a lower factor of safety. This is confirmed by the lower critical local FS for Case S35. It was also concluded that alternate layers parallel to the slope may increase the FS (mainly due to the higher internal friction angle of crushed waste rock); this is also the case for higher FS in Case S51, compare to Cases S11, S21, and S35. It suggests that alternate layers parallel to slope may have a significant impact on FS; on the other hand, the inclination of the compacted layers appears to have a limited effect for these cases.

The addition of compacted layers nonetheless tends to increase the minimum factor of safety (compare Cases S21 vs. S11). However, inclined compacted layers may decrease the minimum local factor of safety (see Cases S51 and S35 with 5% inclined compacted layers, vs. S41 and S21 with horizontally compacted layers respectively). For cases with inclined compacted layers, adding alternate layers parallel to outer slope tend to increase the minimum factor of safety (due to the higher value of ϕ' for crushed waste rock, see Cases S51 vs. S35).
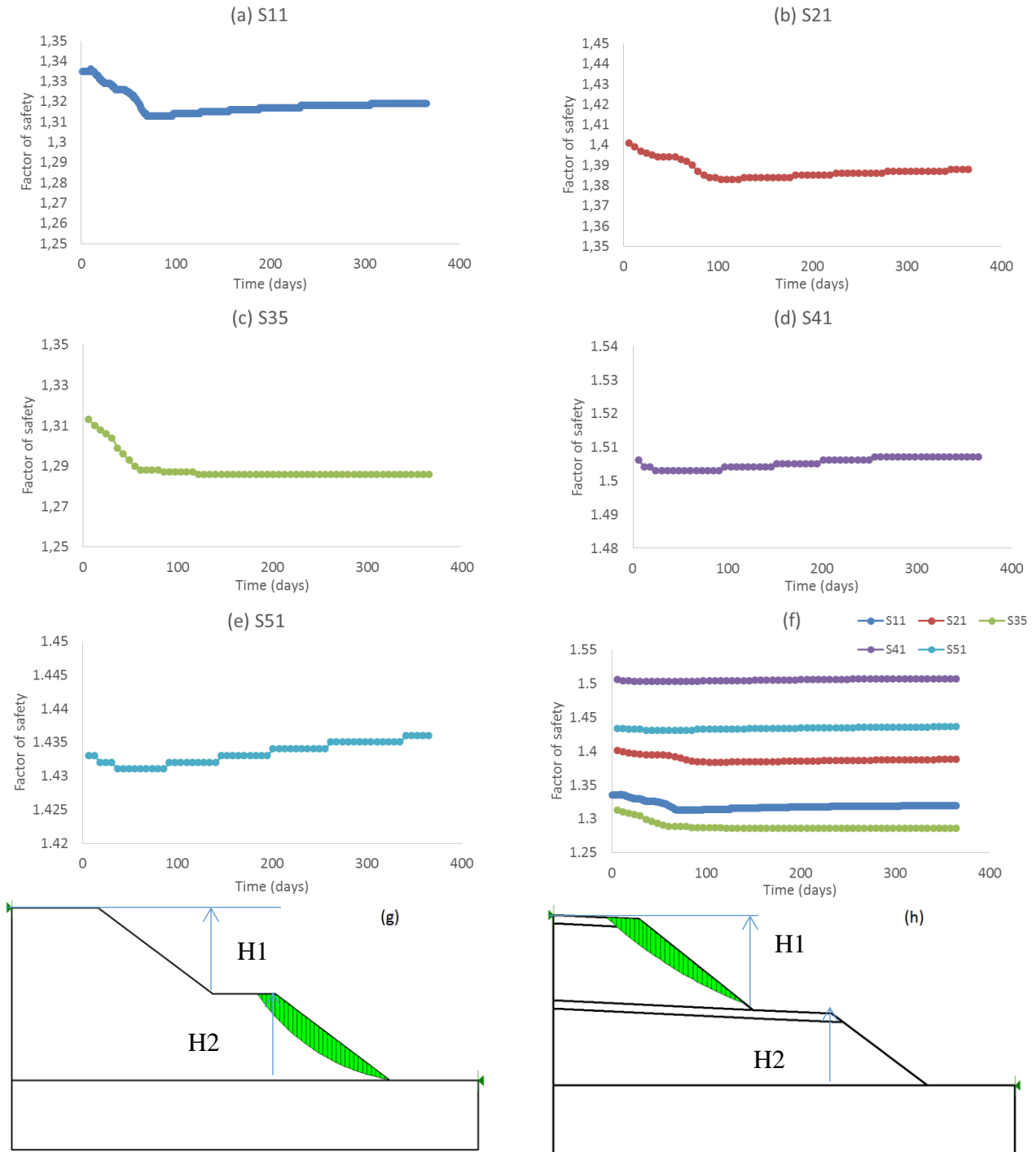
Figure 5-25: Evaluation of local minimum factor of safety under rainfall R 2-2; a) Case S11; b) Case S21; c) Case S35; d) Case S41; e) Case S51; f) Cases S11, S21, S35, S41, and S51; g) typical local slip surface Case S11; h) typical local slip surface Case S35

Figure 5-26 shows the variation of the minimum global factor of safety over time for Cases S11, S21, S35, S41 and S51 under rainfall R 2-2 (see Figure 5-26 (g) for a typical slip surface). In all cases, the factor of safety tends to decrease after infiltration starts. In general, the factor of safety decreases for about 150 days and then stays relatively constant (after the suction becomes almost constant).

For example, the minimum global factor of safety for Case S11 goes from 1.57 to 1.56 (a), while for Case S21 it goes from 1.58 to 1.57. There is not a significant change for critical global FS during the imposed rainfall, and it stays almost constant for all these cases (Cases S11, S21, S35, S41, and S51; see Figure 5-26 f). It should be noted that the minimum global factor of safety for the pile is usually higher compared to a local slip surface involving only one bench (i.e. compare Figure 5-25 (a) and 5-26 (a)).

Figure 5-26 (f) presents a comparison between the variation of the minimum global factor of safety for Cases S11, S21, S35, S41 and S51 under rainfall R 2-2. The lower minimum global FS is related to Case S11. This indicates adding compacted layers within the pile (Cases S21, S35, S41, and S51) increase the global FS. Higher global FS for Case S41 (compare to S21) and S51 (compare to S35) indicate that addition of alternate layers parallel to the external slope increases the global FS (as was concluded in section 4-7-9). The highest global FS belongs to Cases S35 and S51; these results show that the inclination of compacted layers may have positive effects on global FS. The differences between FS of Cases S41 and S51 to Cases S21 and S35 show the positive effect of alternate layers parallel to the external slope on the pile stability under rainfall. It is also seen that alternate layers have a more pronounced effect when the compacted layer is horizontal. The inclination of compacted layer increase global FS more significantly compared to the addition of alternate layers.
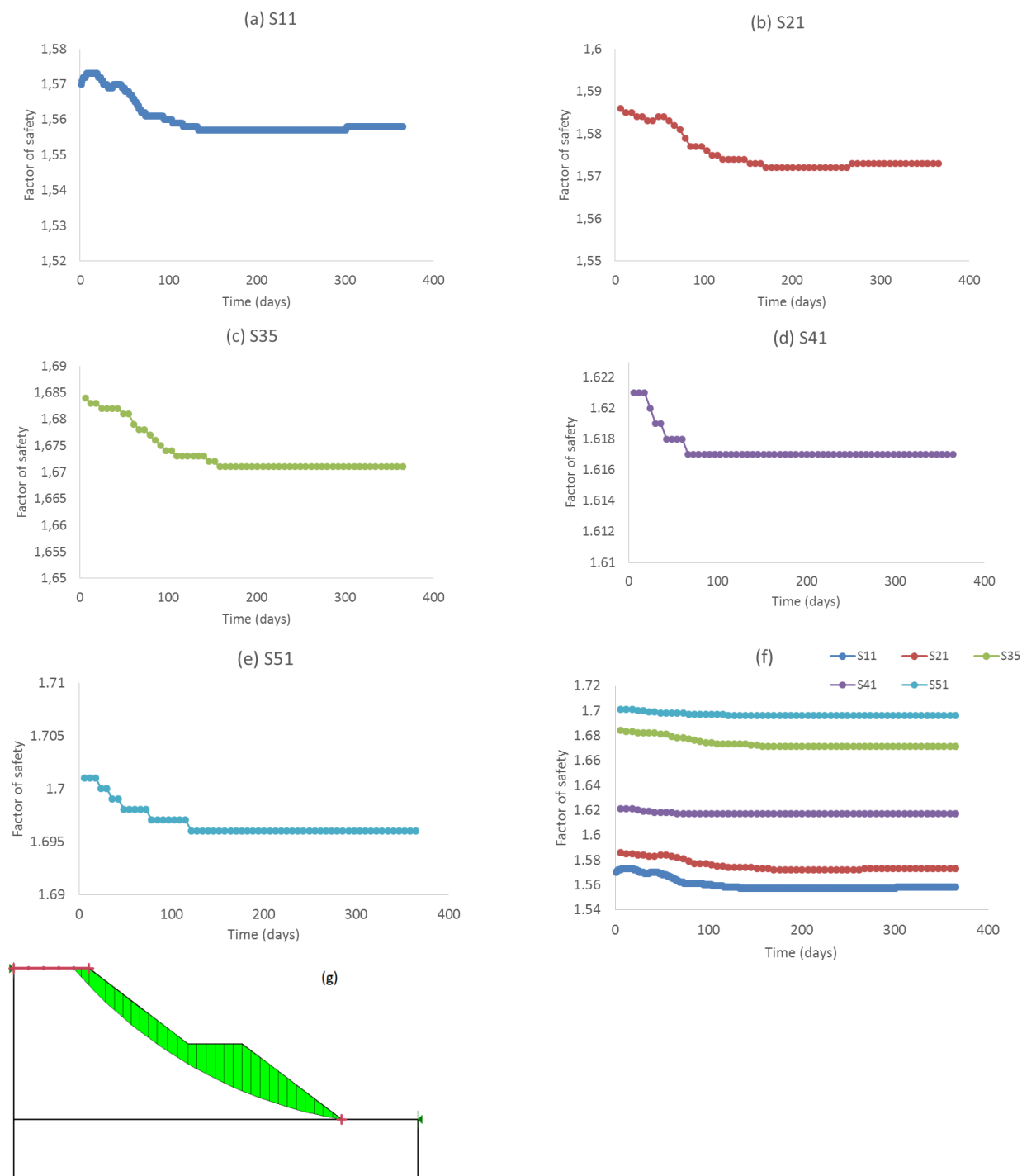
Figure 5-26: Variation of minimum factor of safety of Global slip surface under rainfall R 2-2; a) Case S11; b) Case S21; c) Case S35; d) Case S41; e) Case S51; f) Cases S11, S21, S35, S41, and S51; g) typical global slip surface for Case S11

Table 5-2 gives a summary of the minimum local factor of safety obtained under rainfall R 2-2. For local slip surfaces the prolonged rainfall produces the largest change of FS for Case S35 (2%) and the minimum change for Cases S41 and S51 (0.2%). It seems that the prolonged rainfall is not large enough to produce significant changes of FS in these cases.

Table 5-2: Minimum local factor of safety during rainfall (2.7×10^{-4} m/d, R 2-2) for different cases

Cases	S11	S21	S35	S41	S51
Initial	1.335	1.401	1.313	1.506	1.433
Minimum FS during rainfall	1.313	1.383	1.286	1.503	1.431
Final after 365 days	1.319	1.388	1.286	1.507	1.436
Max reduction of minimum FS (%)	1.65	1.28	2.06	0.2	0.14

For the global (deeper) slip surfaces, the maximum change occurred for Cases S11 and S21 with a 0.88% reduction of a global factor of safety under this rainfall. The FS related to a global slip surface is usually less susceptible to the rainfall infiltration compare to a local slip surface for these cases.

Table 5-3: Minimum global factor of safety during rainfall (2.7×10^{-4} m/d, R 2-2) for different cases

Cases	S11	S21	S35	S41	S51
Initial	1.572	1.586	1.684	1.621	1.701
Minimum FS during rainfall	1.557	1.572	1.671	1.617	1.696
Final after 365 days	1.558	1.573	1.671	1.617	1.696
Max reduction of minimum FS (%)	0.83	0.88	0.77	0.25	0.29

A comparison between different cases indicates that the minimum local and global FS for Case S11 increase 5% and 0.6% compare to Case S21 (representing the effect of the addition of compacted layers). There is a 9% and 3% increase for local and global FS between Cases S21 and S41 (the effect of alternate layers parallel to slope). The minimum local and global FS during rainfall show 7% decrease and 6% increase when Cases S21 and S35 are compared (decrease of local FS when the compacted layers are inclined). Comparing the FS changes due to pile

configuration and FS changes due to rainfall indicated that the effect of geometry is more significant on the changes of FS.

Effect of relatively high-intensity, prolonged (pseudo steady-state) rainfall

Additional calculations have been conducted for Cases (S11, S21, S35, S41 and S51) under rainfall 1.17×10^{-8} m/s (0.001 m/d, R 5-2 over 365 days). Figure 5-27 presents the results of these simulations. Figure 5-27 (a) and (b) show the changes in the local and global factor of safety for the five different Cases (S11, S21, S35, S41, and S51). A similar trend is observed here (compare to rainfall R 2-2) for both local and global slip surfaces.
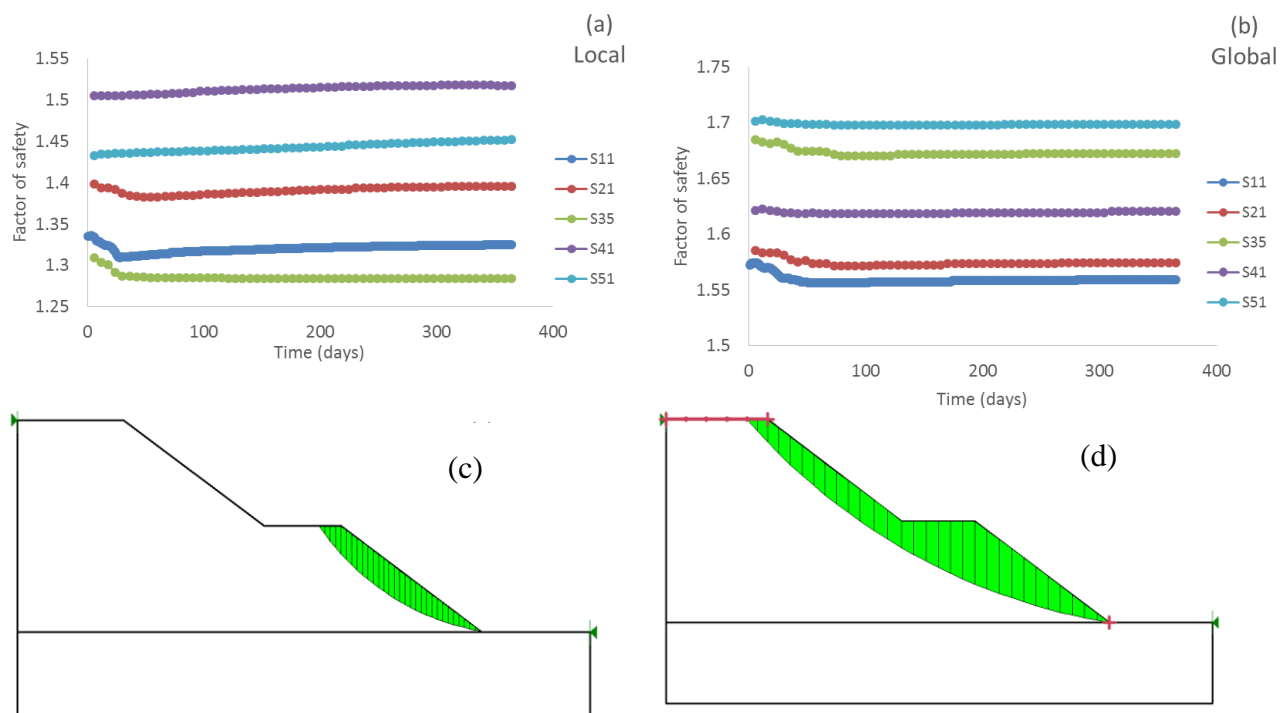
Figure 5-27: Variation of minimum factor of safety (local and global slip surface) obtained for different cases (S11, S21, S35, S41, S51) during rainfall R 5-2; a) local FS; b) global FS; c) typical local slip surface for Case S11; d) typical global slip surface for Case S11

Table 5-4 presents the minimum local factor of safety and the maximum reduction of the factor of safety (%) under rainfall 1.17×10^{-8} m/s (0.001 m/d, R 5-2) for five different cases (S11, S21, S35, S41 and S51, initial suction = 6 kPa). The smallest changes are related to Cases S41 and

S51. The maximum reduction of FS is around 2% for Cases S11 and S35 (which is not significant). These results indicate that for the specific initial conditions, the global stability of waste rock pile is not very sensitive to prolonged rainfall with such low intensity.

Table 5-4: Minimum local factor of safety during rainfall R 5-2 (0.001 m/d) for different cases

Cases	S11	S21	S35	S41	S51
Initial	1.335	1.398	1.309	1.505	1.432
Minimum FS during rainfall	1.309	1.382	1.284	1.505	1.432
Final after 365 days	1.325	1.395	1.284	1.517	1.452
Max reduction of minimum FS (%)	1.95	1.14	1.91	0.00	0.00

Table 5-5 shows a summary of the minimum global factor of safety obtained during rainfall R (0.001 m/d) with SLOPE/W. The maximum reduction of the minimum FS (due to rainfall) occurs in Case S11 whereas the minimum reduction is related to Cases S41 and S51 (cases with alternate layers parallel to the slope).

Table 5-5: Minimum global factor of safety during rainfall R (0.001 m/d) for different cases

Cases	S11	S21	S35	S41	S51
Initial	1.572	1.585	1.684	1.621	1.701
Minimum FS during rainfall	1.556	1.571	1.67	1.618	1.697
Final after 365 days	1.559	1.574	1.672	1.62	1.698
Max reduction of minimum FS (%)	1.02	0.88	0.83	0.19	0.24

5.7 Results for short term transient rainfalls

This section presents the results of slope stability analyses for five different Cases: S11, S21, S35, S41 and S51 (with loose and compacted waste rock and a silty sand foundation, see Table 4-3 and Figures 4-1 and 4-2). These are subjected to the transient rainfalls defined in Table 5-1 (Cases R 1, R 2-1, R 3-1, R 3-2, R 3-3, R 4 and R 5-1).

The analyses included two main components. The first addressed the wetting front development and changes of volumetric water content and PWP during rainfall. The second component considers the effects of different parameters (such as initial PWP, rainfall intensity and duration, groundwater level, k anisotropy, and foundation material properties) on the minimum local and

global factor of safety, during and after rainfall. The water table is usually fixed at z = -7 m (below the ground; see Figure 5-1). It is assumed that silty sand foundation material is initially subjected to a pore water pressure distribution with a maximum suction value of 50 kPa (see Figure 5-2). Several rainfalls (Table 5-1) are applied (at a constant rate) over the crest, slope, and the ground (for 6, 12 or 24 hours) to assess the effect of infiltration on slope stability; no ponding is allowed over the surface.

5.7.1 **Effect of initial matric suction on infiltration and stability**

The initial suction may have a significant role on the stability of the waste rock pile through its effect on the apparent cohesion. One of the important aspects to consider is the effect of initial condition on infiltration rate. The conditions that produce the highest pore water pressures may be the most susceptible to failure.

When the rainfall starts and water infiltrates, the factor of safety may change. Analyses were done to assess the effect of initial suction on the infiltration rate and factor of safety.

In the first scenario, the initial suction is set to close to the residual condition (i.e., suction equal to water entry value, WEV, or ψ_r). For the coarse waste rock, this value is around 1.2 kPa; for compacted waste rock, it is around 7 kPa (see Figure 4-1).

Other scenarios are considered with suction values equal to twice the WEV (2 residual; i.e. initial suction 2.4 kPa and 14 kPa for loose and compacted waste rock respectively) and three times the WEV (3 residual; i.e. initial suction 3.6 kPa and 21 kPa for loose and compacted waste rock respectively).

Figure 5-28 shows the obtained FS for the local, and global slip surfaces (covering one and two benches respectively) for Cases S21, S35, S41 and S51 during and after rainfall R 2-1 (0.1 m/d, or 1.157×10^{-6} m/s). It is seen that there may be a slight change in the factor of safety during the rainfall. As was mentioned before (see Figures 5-11 (e), 5-15 (e)), the reduction of suction in the compacted layers may result in an increase of FS (based on the c_{app} versus suction relationship). For low initial suctions (e.g. 1.2 kPa (WEV, Figure 5-28 a,b), 3.4 kPa (2WEV, Figure 5-28 c,d), the rainfall does not seem to have a significant effect on the factor of safety. The results tend to indicate that when initial suction is larger, the changes of the factor of safety become more

visible. For all the cases presented here (with different initial suctions) the factor of safety is not changing significantly after the rainfall stops.
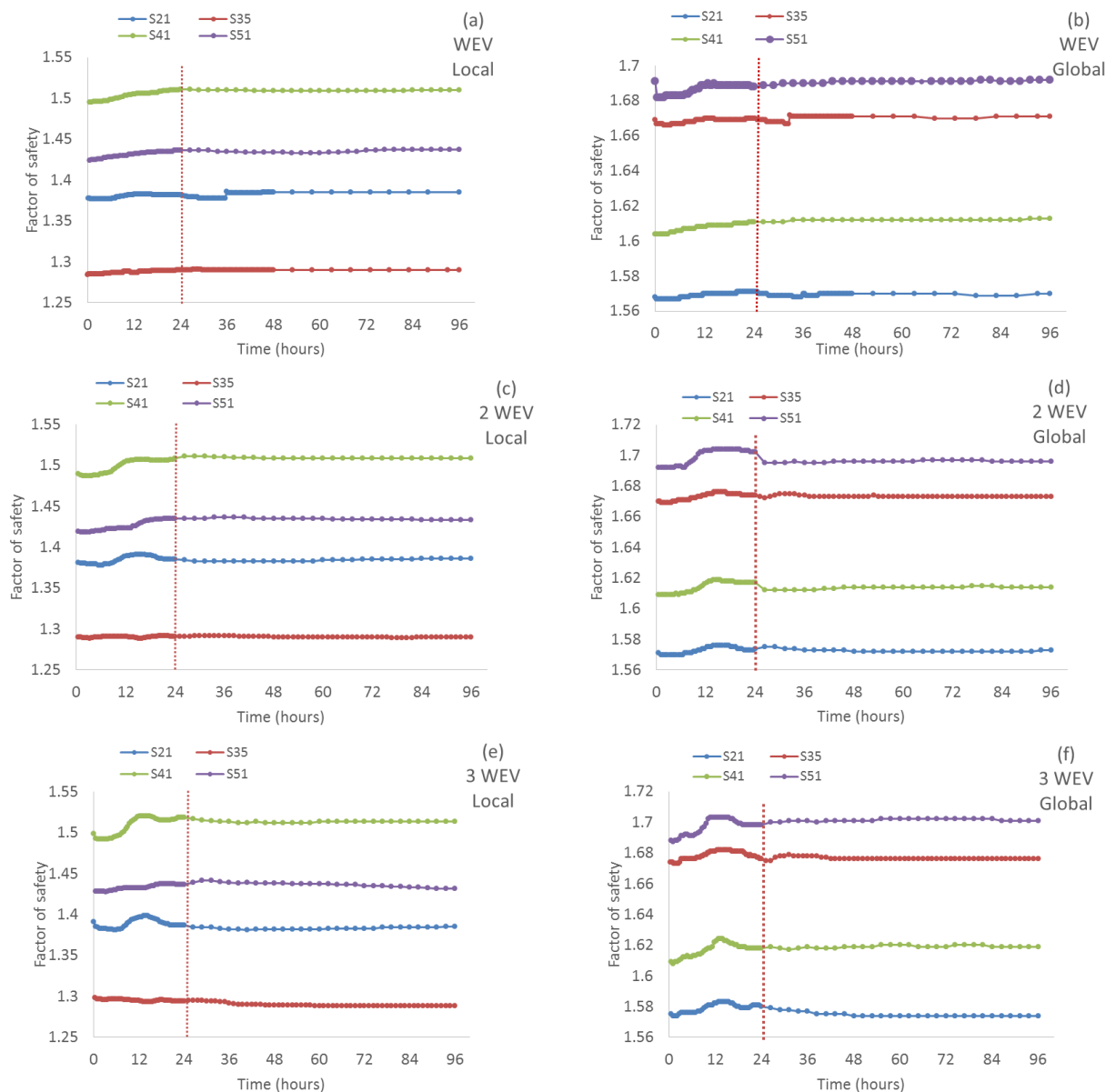
Figure 5-28: Variation of factor of safety for local and global slip surfaces during and after a 24-hour rainfall 1.157×10^{-6} m/s (0.1 m/d, R 2); Cases S21, S35, S41, and S51 (see Tables 4-4 and 4-5); a) local slip surface, initial suction equal to WEV; b) global slip surface, initial suction equal to WEV; c) local slip surface, initial suction of 2 WEV; d) global slip surface, initial suction of 2 WEV; e) local slip surface, initial suction of 3 WEV; f) global slip surface, initial suction of 3 WEV

Table 5-6 presents the initial and minimum factor of safety obtained with SLOPE/W during and right after the rainfall R 2-1. It is seen that the maximum decrease of the factor of safety is less than 1%. It can thus be considered that factor of safety is not significantly influenced by these different values of the initial suction.

Table 5-6: Initial and the minimum factor of safety FS for a local slip surface for different cases with the imposed rainfall R 2-1

Cases	Residual (WEV)			2 Residual (2WEV)			3 Residual (3WEV)		
	Initial FS	Minimum FS	Decrease FS (%)	Initial FS	Minimum FS	Decrease FS (%)	Initial FS	Minimum FS	Decrease FS (%)
S21	1,38	1,377	0,22	1,385	1,378	0,51	1,391	1,381	0,72
S35	1,284	1,284	0,00	1,29	1,288	0,16	1,298	1,293	0,39
S41	1,495	1,495	0,00	1,491	1,487	0,27	1,498	1,492	0,40
S51	1,424	1,424	0,00	1,418	1,418	0,00	1,427	1,427	0,00

Table 5-7 presents the initial and minimum factor of safety for four different Cases (S12, S35, S41 and S51), with three different initials suctions (WEV, 2WEV, 3WEV) during and right after rainfall (R 2-1). The maximum reduction of a global factor of safety is 0.5% (not significant). Comparing Tables 5-6 and 5-7 indicate that with these initial conditions the local factor of safety is more susceptible to changes in rainfall compare to the global factor of safety.

Table 5-7: Initial and the minimum factor of safety for a global slip surface for different cases under rainfall R 2-1

Cases	Residual (WEV)			2 Residual (2WEV)			3 Residual (3WEV)		
	Initial FS	Minimum FS	Decrease FS (%)	Initial FS	Minimum FS	Decrease FS (%)	Initial FS	Minimum FS	Decrease FS (%)
S21	1,568	1,567	0,06	1,572	1,57	0,13	1,577	1,574	0,19
S35	1,669	1,666	0,18	1,672	1,669	0,18	1,676	1,673	0,18
S41	1,604	1,604	0,00	1,61	1,609	0,06	1,611	1,608	0,19
S51	1,691	1,682	0,53	1,693	1,692	0,06	1,69	1,687	0,18

Figure 5-29 shows the time variation of the factor of safety for the local slip surface during and after rainfall R 2-1, considering four different Cases (S21, S35, S41 and S51, see Tables 4-4 and 4-5) with three different initial suction (WEV, 2WEV, and 3WEV). The initial suction may

change the initial factor of safety. For example, in Figure 5-29 (b), the initial factor of safety tends to increase with the initial suction (e.g. when the initial suction change from WEV to 2WEV to 3 WEV), although the differences are small. The variation of the factor of safety during the rainfall for different initial suction follows a similar path for all the cases. The factor of safety may increase a bit after the rainfall starts, but the increase is limited to about 1.5% of FS. The results also indicate that the largest change is related to the initial suction equal to 3WEV (three times water entry value).
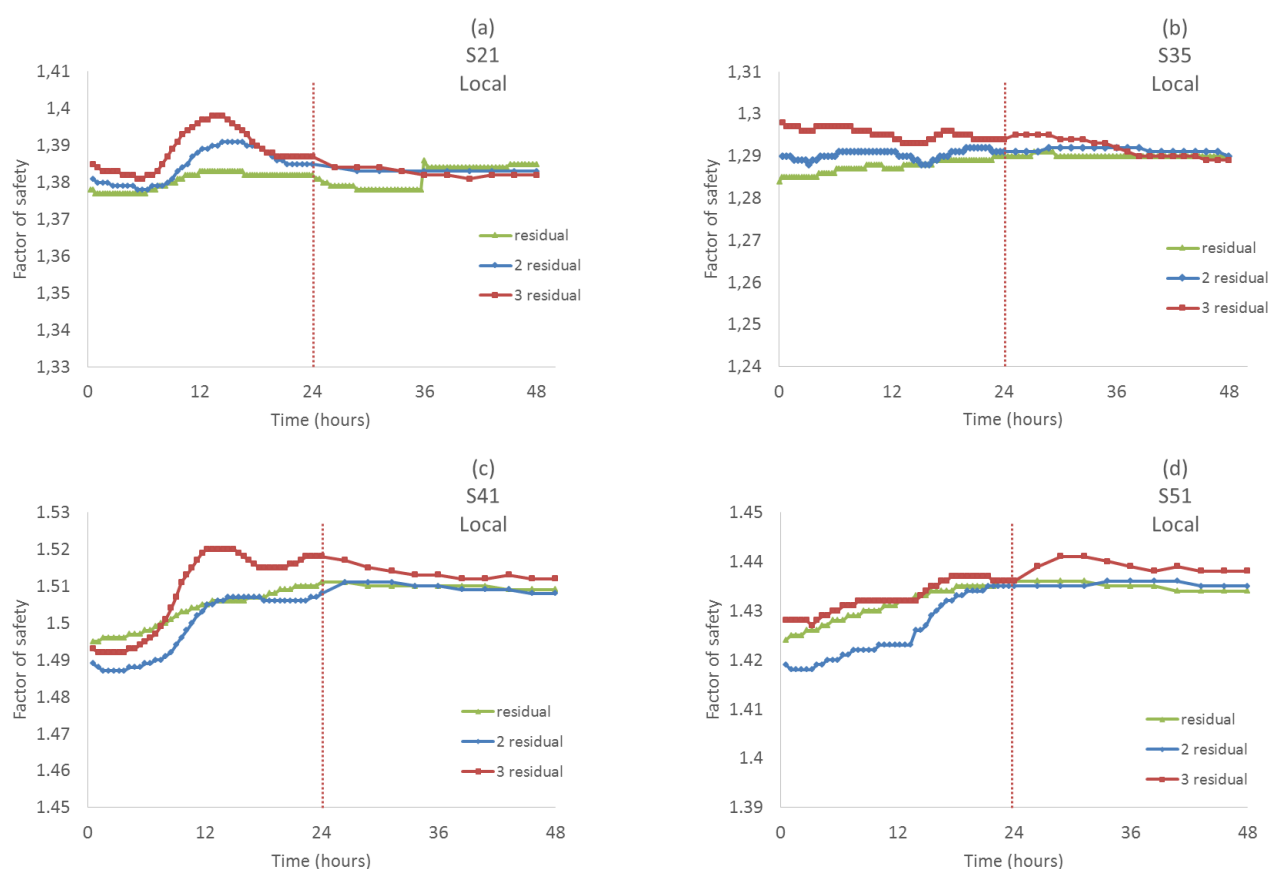
Figure 5-29: Variation of the factor of safety for local slip surfaces during rainfall R 2-1, with 3 different initial suction (WEV or residual, 2WEV or 2 residual, and 3WEV or 3 residual); a) Case S21; b) Case S35; c) Case S41; d) Case S51.

Table 5-8 presents the initial and maximum increase of the factor of safety during rainfall R 2-1 for different cases, for both local and global slip surfaces. It is seen the maximum increase is less

than 1.5%, which is due to the relation between suction and apparent cohesion for compacted waste rock layer (see section 4-6).

Table 5-8: Initial and the maximum factor of safety for a global slip surface for different cases under rainfall R 2-1

Case	Local slip surface								
	Initial FS	Max FS	Increase FS (%)	Initial FS	Max FS	Increase FS (%)	Initial FS	Max FS	Increase FS (%)
S21	1,38	1,383	0,22	1,385	1,39	0,43	1,391	1,40	0,50
S35	1,284	1,29	0,47	1,29	1,29	0,16	1,298	1,30	0,00
S41	1,495	1,511	1,07	1,491	1,51	1,14	1,498	1,52	1,47
S51	1,424	1,436	0,84	1,418	1,44	1,20	1,427	1,44	0,70
	Global slip surface								
S21	1,568	1,57	0,19	1,572	1,58	0,25	1,577	1,58	0,38
S35	1,669	1,67	0,06	1,672	1,68	0,24	1,676	1,68	0,36
S41	1,604	1,61	0,44	1,61	1,62	0,56	1,611	1,62	0,81
S51	1,691	1,69	0,00	1,693	1,70	0,65	1,69	1,70	0,77

Figure 5-30 presents the results related to four different Cases (S21, S35, S41, and S51) under rainfall R 2-1. For each case, three different initial suction is considered. Residual suction related to residual condition 1.2 kPa and 7 kPa for loose and compacted waste rock respectively. 2 residual relates to 2.4 kPa and 14 kPa for loose and compacted waste rock and 3 residual relates to 3.6 kPa and 21 kPa for loose and compacted waste rock.

Different initial suction results in a different initial factor of safety though the differences are not very significant (due to low value of c_{app}). The variation of a global factor of safety has a similar trend to a local factor of safety for different initial suction for each case. It is noted that the lower global factor of safety belongs to the waste rock piles with initial residual suction, due to the lower suction and its related apparent cohesion.
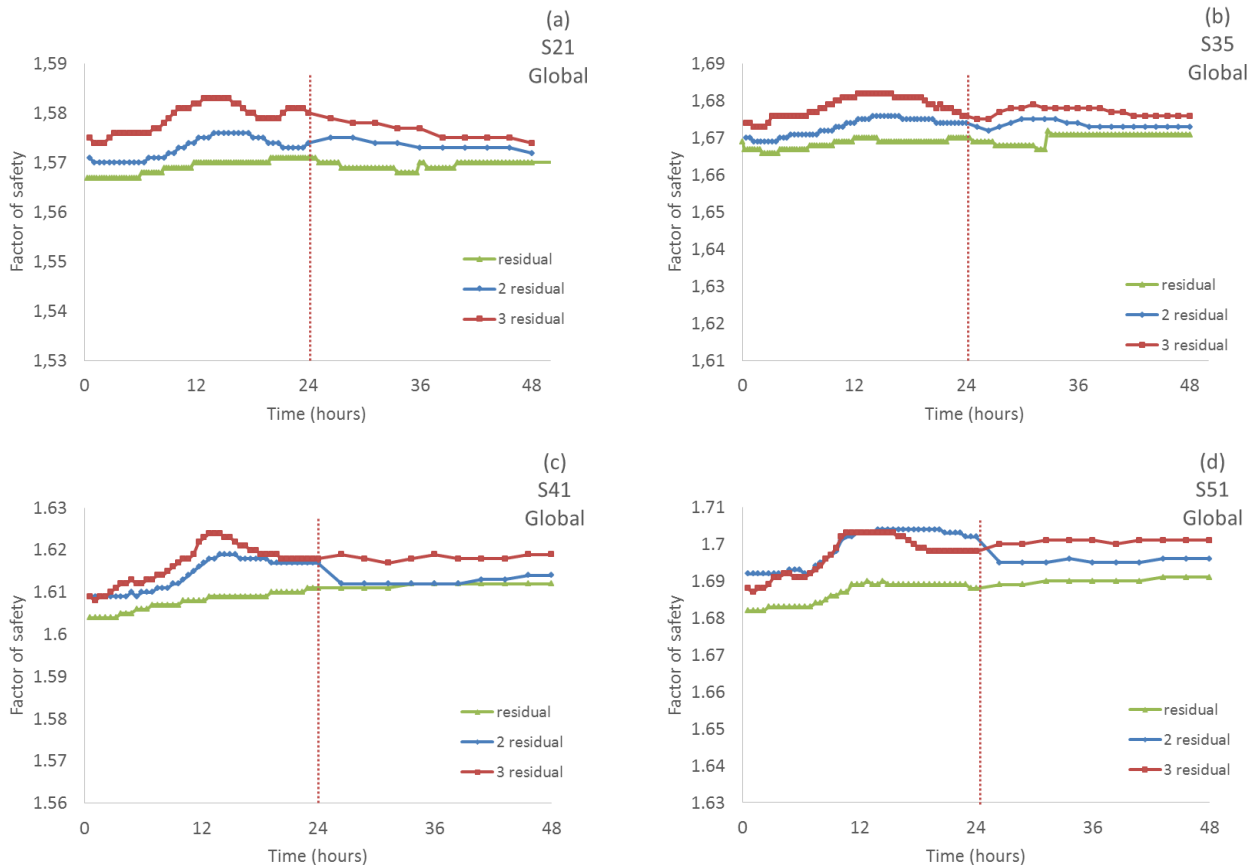
Figure 5-30: Variation of factor of safety for Global slip surface with respect to time during and after rainfall R 2-1, with 3 different initial suction WEV or residual, 2WEV or 2 residual, and 3WEV or 3 residual); a) Case S21; b) Case S35; c) Case S41; d) Case S51

Detailed results for Case S21 with an initial suction of 2WEV

 Figure 5-31 presents the distribution of different parameters along a local slip surface for Case S21, with an initial suction 2 WEV (2 residual) under rainfall R 2-1. The initial condition shows suction 14 kPa at the base of slices 1 and 2 (at mid-point, located in compacted layer); the suction is 2.4 kPa for the other slices (located in coarser (loose) waste rock).

After 12 hours of rainfall, the suction at the base of slice 1 is reduced to 6 kPa. After 18 hours, the suction at the base of slices 15 to 31 tends toward zero (from 2.4 kPa). After 24 hours, there is no suction at the base of all the slices along the slip surface.

Figure 5-31 (b) presents the strength at the base (mid-point) of the slices. This strength is initially close to 0.5 kPa for slices in the coarse waste rock and close to zero for compacted waste rock. After infiltration starts, the strength (related to suction) tends to decrease.

Figure 5-31 (c) and (d) presents the shear mobilized and shear strength at the base (mid-point) of the slices, indicating that there is not a significant change due to the rainfall.

Figure 5-31 (e) gives the factor of safety after 6 hours, 12 hours, 18 hours and 24 hours during rainfall. It is seen that the factor of safety does not change much, in agreement with the small changes in matric suction and its related strength. It can be inferred that the small value of initial suction (e.g. 1.2 kPa, 2.4 kPa) does not have a meaningful role in the variation of the factor of safety during rainfall.
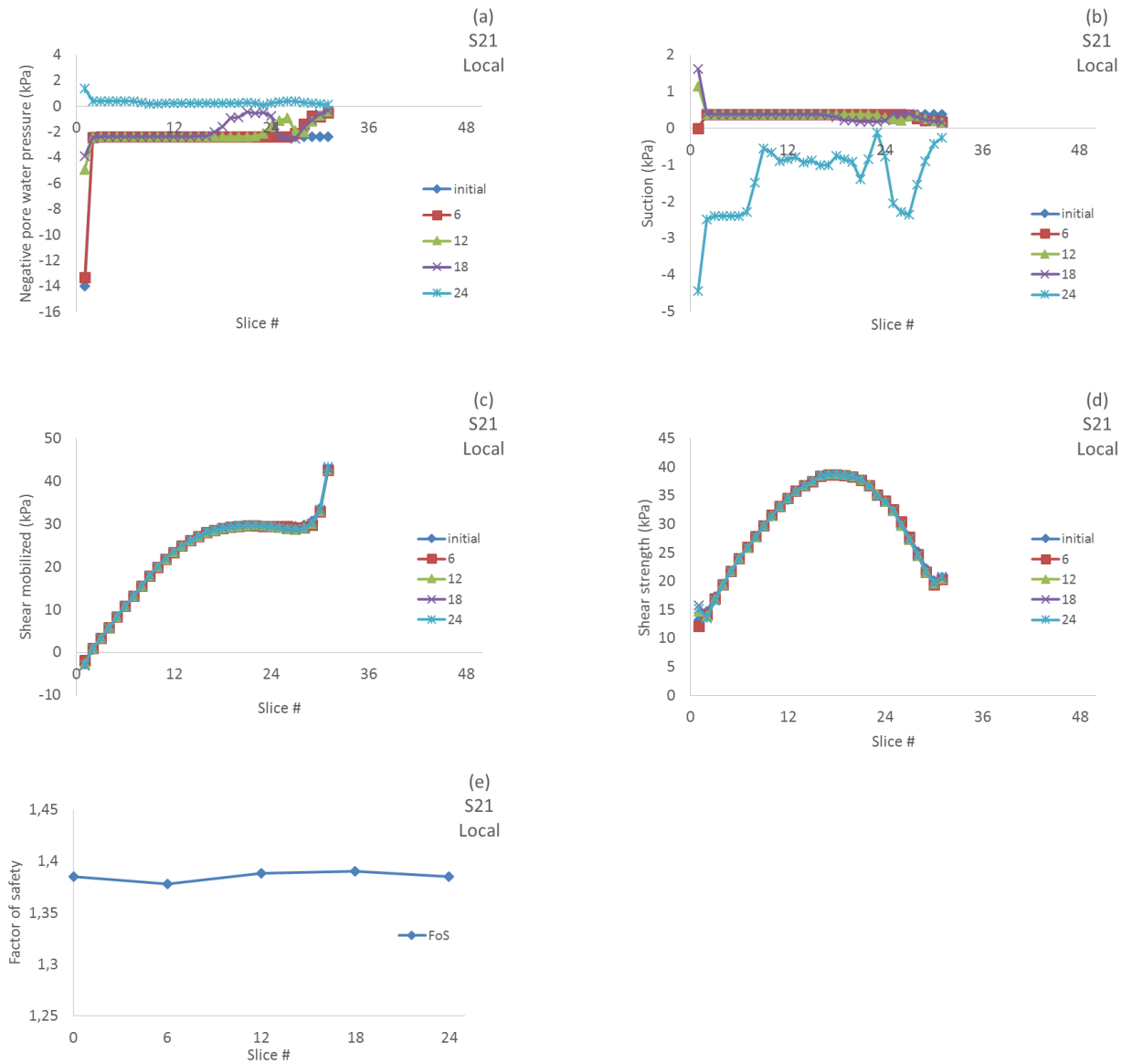
Figure 5-31: Variation of different parameters along the local slip surface, with respect to time (6, 12, 18, 24 hours) under a rainfall of 1.157×10^{-6} m/s (0.1 m/d, R 2-1), Case S21, initial suction 2WEV; a) negative pore water pressure; b) strength due to apparent cohesion; c) shear mobilized; d) shear strength; e) factor of safety

Effect of higher suctions

The effect of higher initial suctions in a pile on infiltration rate, and factor of safety was also assessed for Case S11 (two benches waste rock pile, see Tables 4-4 and 4-5); three different initial suction were imposed to obtain c_{app} = 1 kPa, 5 kPa, and 10 kPa (6, 32 and 64 kPa).

Figure 5-32 presents the variation of the factor of safety during and after rainfall R 2-1 (q = 1.157×10^{-6} m/s). Figure 5-32 (a) indicates that there is an increase of the initial factor of safety with an initial suction (i.e. with a larger c_{app}). A higher initial suction (or c_{app}) leads to a smaller variation of a factor of safety. The same trend is seen for the FS of the global slip surfaces (see Figure 5-32 (b)).
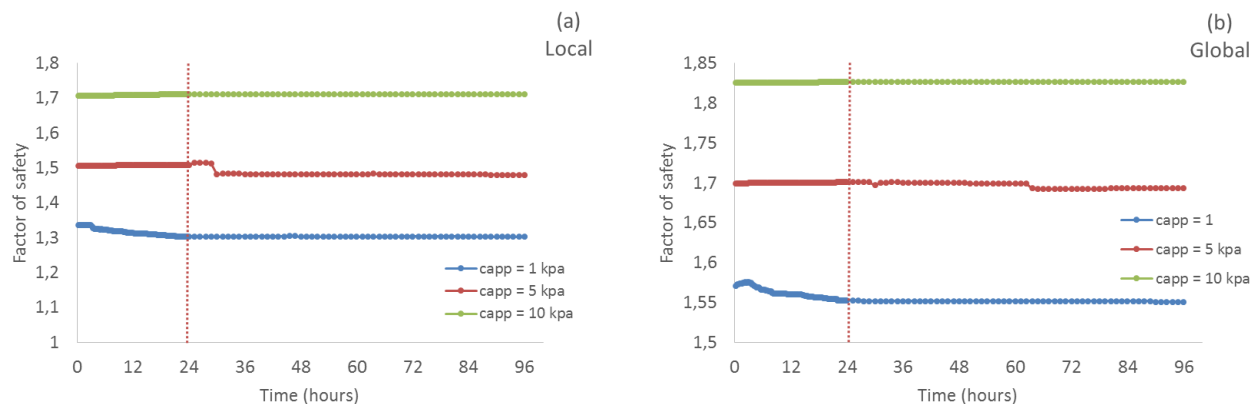
Figure 5-32: Evaluation of factor of safety during and after rainfall R 2-1, for three different initial apparent cohesion (c_{app} = 1, 5 and 10 kPa), Case S11; a) local slip surfaces; b) global slip surfaces

Table 5-9 presents the initial and minimum factor of safety reached during rainfall R 2-1 for Case S11. It shows that increase of suction (going from c_{app} = 1 kPa to c_{app} = 10 kPa) results in the increase of an initial factor of safety (from 1.339 to 1.719 and from 1.569 to 1.826 for a local and a global slip surface respectively). On the other hand, increasing the suction leads to a less variation of a factor of safety due to infiltration, the decrease of FS is around 2.4% for c_{app} =1 kPa, while it is 0.7% for c_{app} = 10 kPa (for local slip surface).

Table 5-9: Initial and minimum factor of safety for local and global slip surface, Case S11 with c_{app} = 1, 5 and 10 kPa, rainfall R 2-1

Case	Local slip surface			Global slip surface		
	Initial FS	Min FS	Decrease FS (%)	Initial FS	Min FS	Decrease FS (%)
c_{app} =1	1,336	1,304	2,40	1,569	1,553	1,02
c_{app} = 5	1,508	1,506	0,13	1,693	1,693	0,00
c_{app} = 10	1,719	1,707	0,70	1,828	1,826	0,11

Figure 5-33 illustrates the changes of negative pore water pressure along the local slip surface (at mid-base of slices) during 24 hours of rainfall R 2-1. Figure 5-33 (a) presents the initial suction 6 kPa (representing c_{app} = 1 kPa), the initial suction starts to decrease from slices close to toe and the crest, and after 24 hours most of the slices have a reduction in matric suction to a value around 1.5 kPa.

Figure 5-33 (b) and (c) illustrate the changes of the suction along the local slip surface for initial suction 32 kPa (representing c_{app} = 5 kPa) and 64 kPa (representing c_{app}=10 kPa). For both cases when the rainfall starts, the slice near toe lost its suction at mid-point of slice due to infiltration, but the rest of slices do not see changes of matric suction on their base mid-point.

It indicates that more water is needed to allow the seepage more easily through the waste rock in deeper depth. In these cases the shallow layer close to the surface lost the suction more rapidly and became closer to saturated condition hence, the water passes more easily on that layer downward the slope.
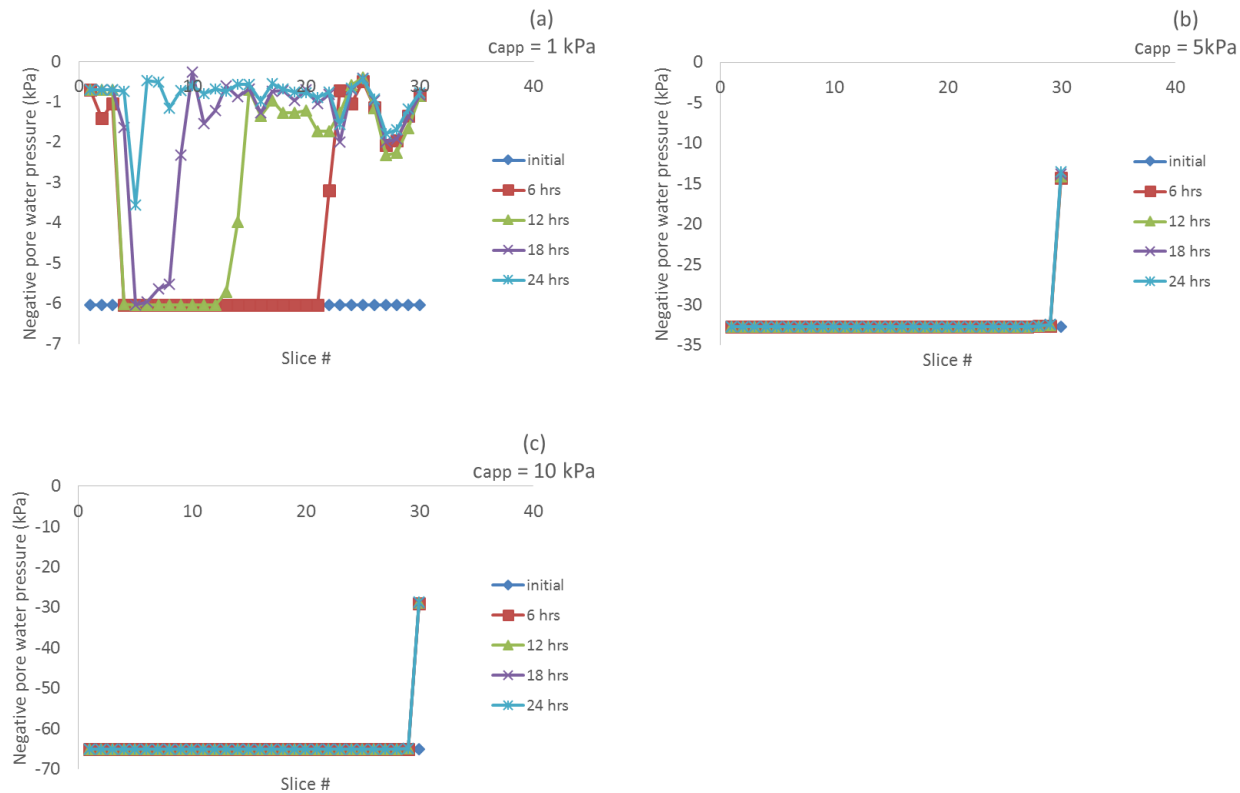
Figure 5-33: Variation of the PWP along local slip surface under rainfall R 2-1, Case S11; a) c_{app} = 1 kPa; b) c_{app} = 5 kPa; c) c_{app} = 10 kPa

Figure 5-34 presents the changes of suction due to infiltration with respect to time under rainfall R 2-1 for Case S11 along a global slip surface (mid-point for each slice base) for different initial suctions. Figure 5-34 (a) shows that during the rainfall, the water infiltrates deep for initial c_{app} = 1 kPa. In the beginning, the initial suction is 6 kPa, after 12 hours slices 1 to 3 and 15 to 30 show suctions around 2 kPa, and after 24 hours all of the slices show a reduction of suction.

In Figure 5-34 (b) and (c) the initial suctions are 32 kPa and 64 kPa (related to c_{app} = 5 and 10 kPa respectively). During the rainfall, there are no changes in the suction at mid-point of slices bases along slip surface (except for slices near the toe that are small and close to the surface). The decrease of the factor of safety was attributed to the reduction in suctions, and not many changes are observed here; hence, the reduction of a factor of safety is not significant here.
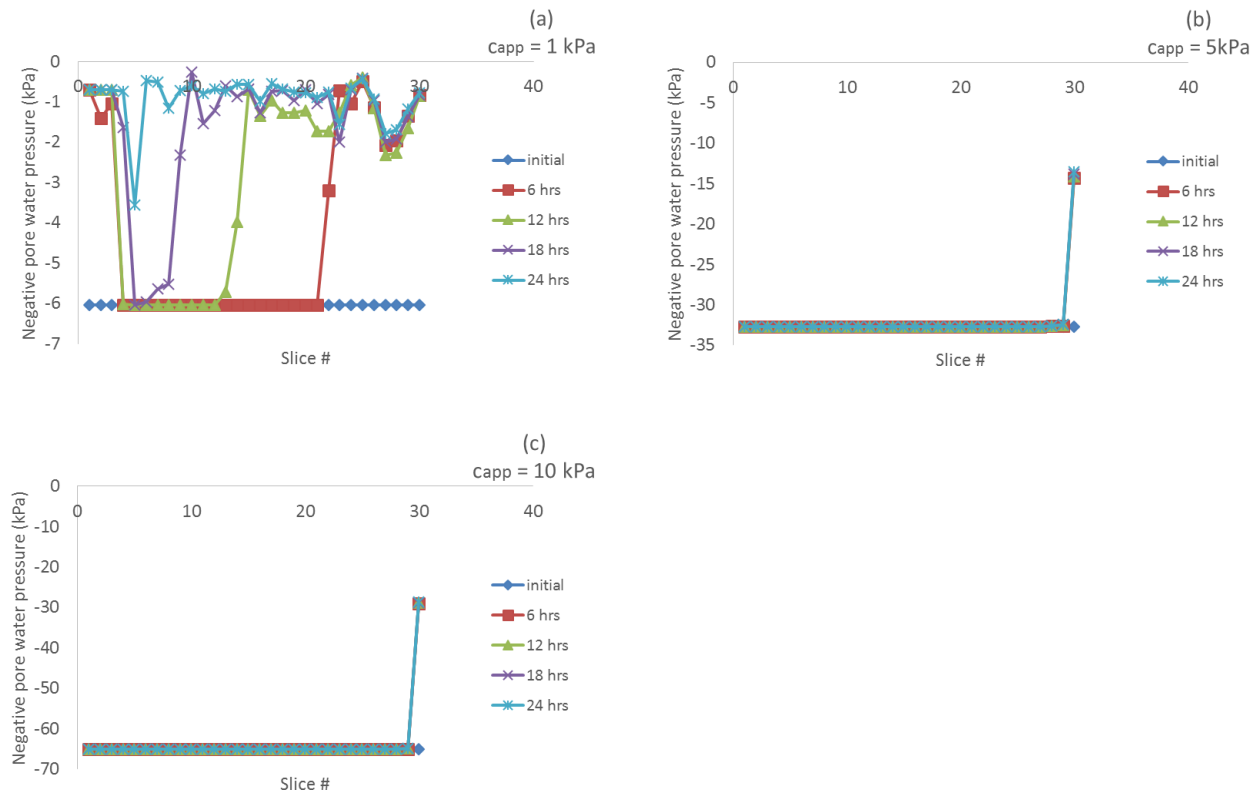
Figure 5-34: Variation of the PWP along global slip surface under rainfall R 2-1, Case S11; a) $c_{app} = 1$ kPa; b) $c_{app} = 5$ kPa; c) $c_{app} = 10$ kPa

5.7.2 Effect of transient rainfall rate on the factor of safety

Five different cases are simulated in the following: S11 (2 benches), S21 (2 benches with compacted horizontal layer), S35 (2 benches with 5 % inclined compacted layers), S41 (2 benches, horizontal compacted layer, alternate layers parallel to the slope) and S51 (2 benches, 5 % inclined compacted layer, alternate layers parallel to slope). In all cases, the initial suction is 6 kPa (both loose and compacted layers), and four different rainfalls are considered i.e. R 1, R 2-1, R 3-3, R 4 and R 5-1 followed by 2 dry days (see Table 5-1).

5.7.2.1 Pore water pressure distribution

Figure 5-35 shows typical results for the wetting front development obtained with SEEP/W, for Case S11 under transient rainfall R 3-3 (1.736×10-6 m/s, 0.15 m/day) for 24 hours.

In the beginning, the suction is 6 kPa everywhere (all lines). After 6 hours, the infiltration reduces suction from the ground surface to a depth about 0.25 m; close to the slope surface, the suction tends to be zero, showing the saturation of the ground (i.e. lines A and B). The depth of infiltration and wetting front progressively move down, and after 24 hours the suction reaches about 0.5 kPa for 5 m below the surface (Figure 5-35 (a), (b), and (c)).

Figure 5-35 (a) shows that the depth of infiltration is around 5 m after 24 hours; along line D, infiltration expands to the total depth. As rainwater infiltrates into the waste rock, it can generate positive pore water pressures and create a perched water table locally, as is sometimes the case along the interface between waste rock and silty sand foundation at lines B, C, and D.

The variation of hydraulic conductivity with soil suction is particularly critical as it is largely control water flow in the unsaturated piles. For waste rock, increasing suction can dramatically decrease the hydraulic conductivity (shown in sections 2-3-2 and 4-3-1). This very low hydraulic conductivity may produce a local perched water table in the waste rock (as stated above).
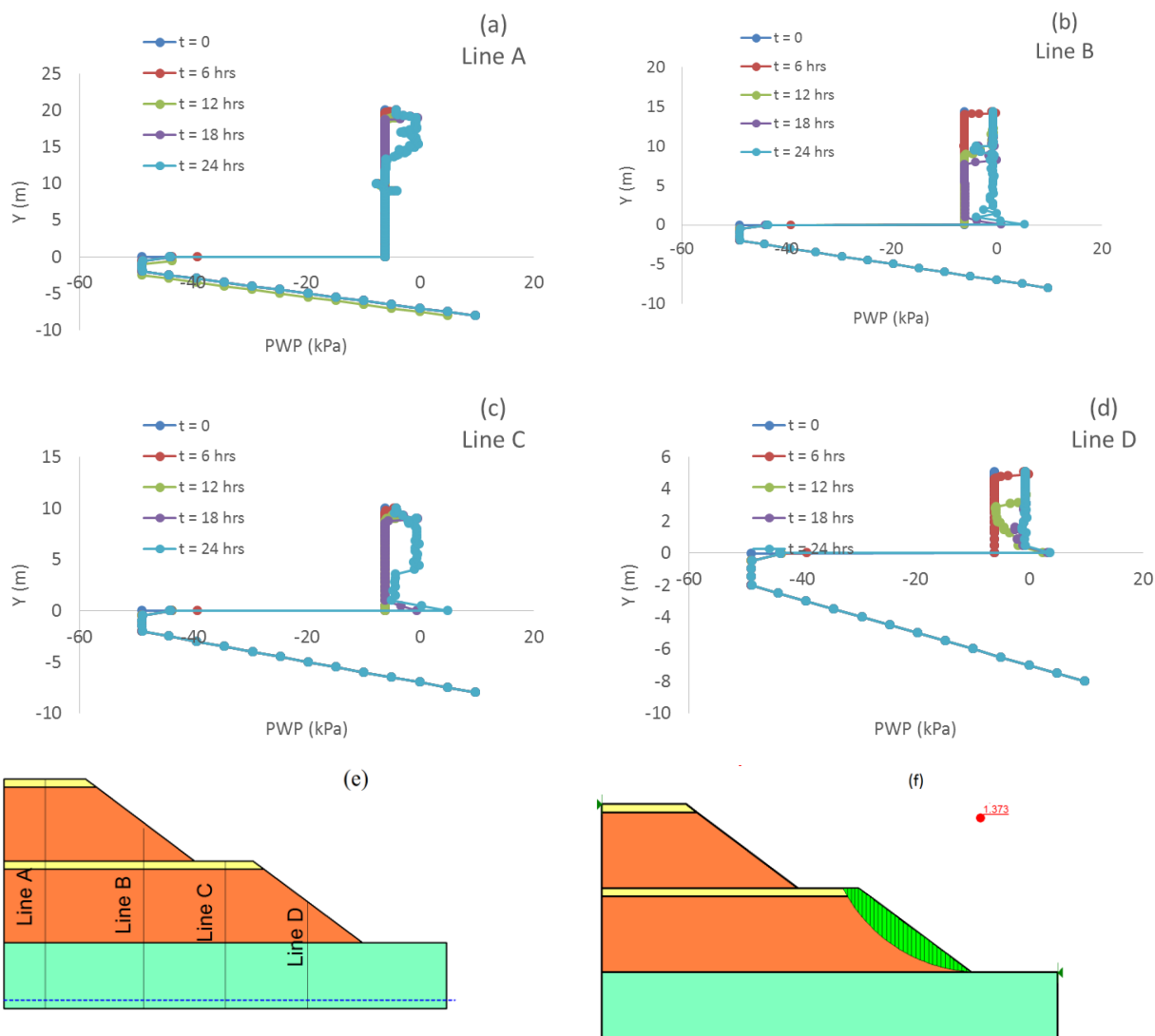
Figure 5-35: Variation of the PWP with the wetting front in Case S21 under rainfall $1.736{\times}10^{-6}$ m/s (0.15 m/d, R 3-3, Table 5-1) at different time steps (t=0, 6, 12, 18 and 24 hrs); a) line A; b) line B; c) line C; d) line D; e) pile with location of lines A, B, C and D; f) typical local slip surface for Case S21

Figure 5-36 presents the changes in the volumetric water content inside the pile for Case S11 during rainfall R 3-3. This distribution of volumetric water content is related to the distribution of suction shown in Figure 5-35.

For initial suction 6 kPa, the water content is around 0.06 (= Θ_r) for the waste rock. Rainfall tends to increase pore water pressure close to the surface; at that time the volumetric water content also

increases to 0.08. The volumetric water content close to the slope surface increases with water infiltration and reduction of suction, (i.e. $\Theta_r = 0.11$ at time 6 hrs; see Figure 5-36 (d) line D). The volumetric water content follows a similar trend as the distribution of PWP and increases progressively as the wetting front goes deeper. Along the interface between the waste rock and silty sand foundation, the volumetric water content increases more dramatically due to the accumulation of water and formation of the local water table.
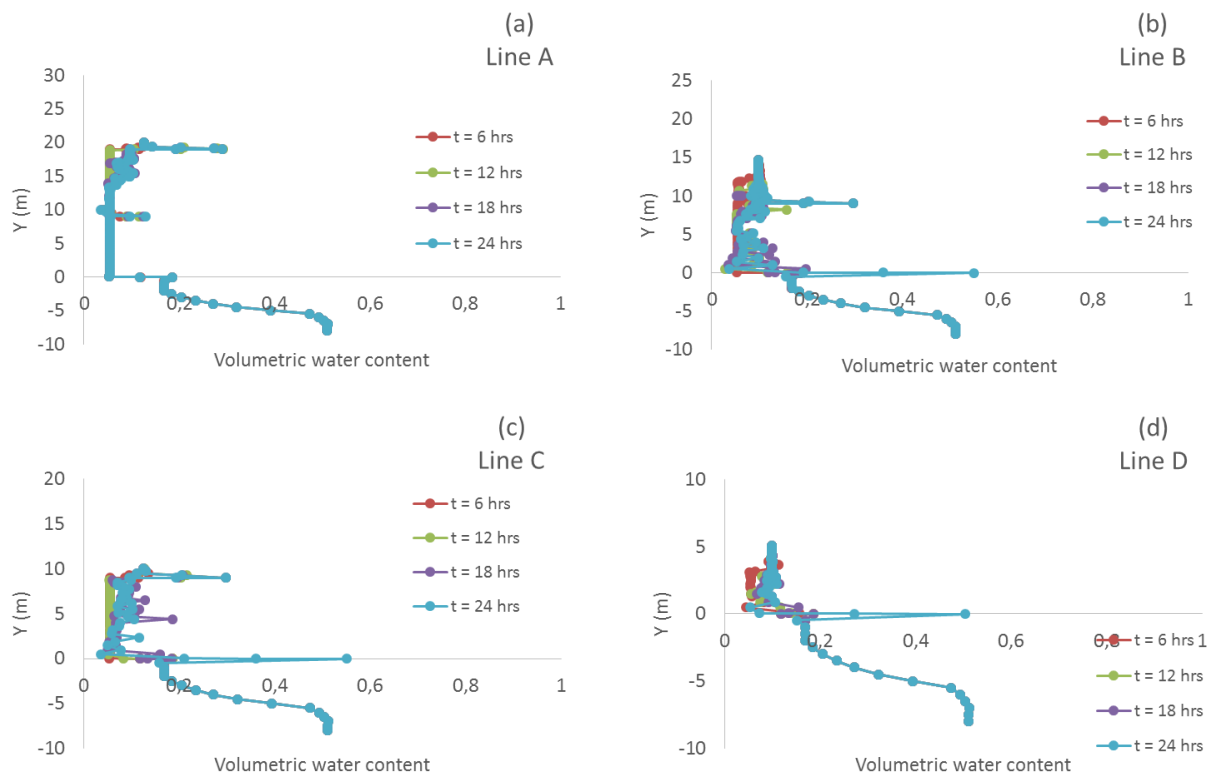
Figure 5-36: Evolution of the volumetric water content distribution, Case S21, under rainfall 1.736×10^{-6} m/s (0.15 m/d, R 3-3) at different time steps; a) line A; b) line B; c) line C; d) line D (see other details in Figure 5-35 and Table 5-1)

Figure 5-37 presents the variation of the minimum factor of safety for local slip surface with respect to time during and after constant rainfall 5.78 $\times 10^{-7}$ m/s (0.05 m/d, R 1) for 24 hours. Figure 5-37 (a), (b) and (c) show the factor of safety decreases slightly when the rainfall starts.

The initial minimum factor of safety is 1.336 for Case S11. During the rainfall, FS reaches the minimum value 1.315 (1.57% reductions). For Case S21, the FS value changes from 1.406 to minimum 1.389 (1.21% reduction); for Case S35, it goes from 1.318 to 1.297, (1.59% reduction) (see Figure 5-37 (a), (b), (c) and Table 5-10).

Figures 5-37 (d) and (e) show 2% maximum change in the factor of safety during rainfall related to Cases S41 and S51. Figure 5-37 (f) shows the local factor of safety for different cases under same initial and boundary conditions. The highest and lowest initial factor of safety belongs to Cases S41 and S35 respectively. The outcome of these results indicates that the changes of FS due to waste rock pile configuration is more pronounced compared to changes of FS due to rainfall.
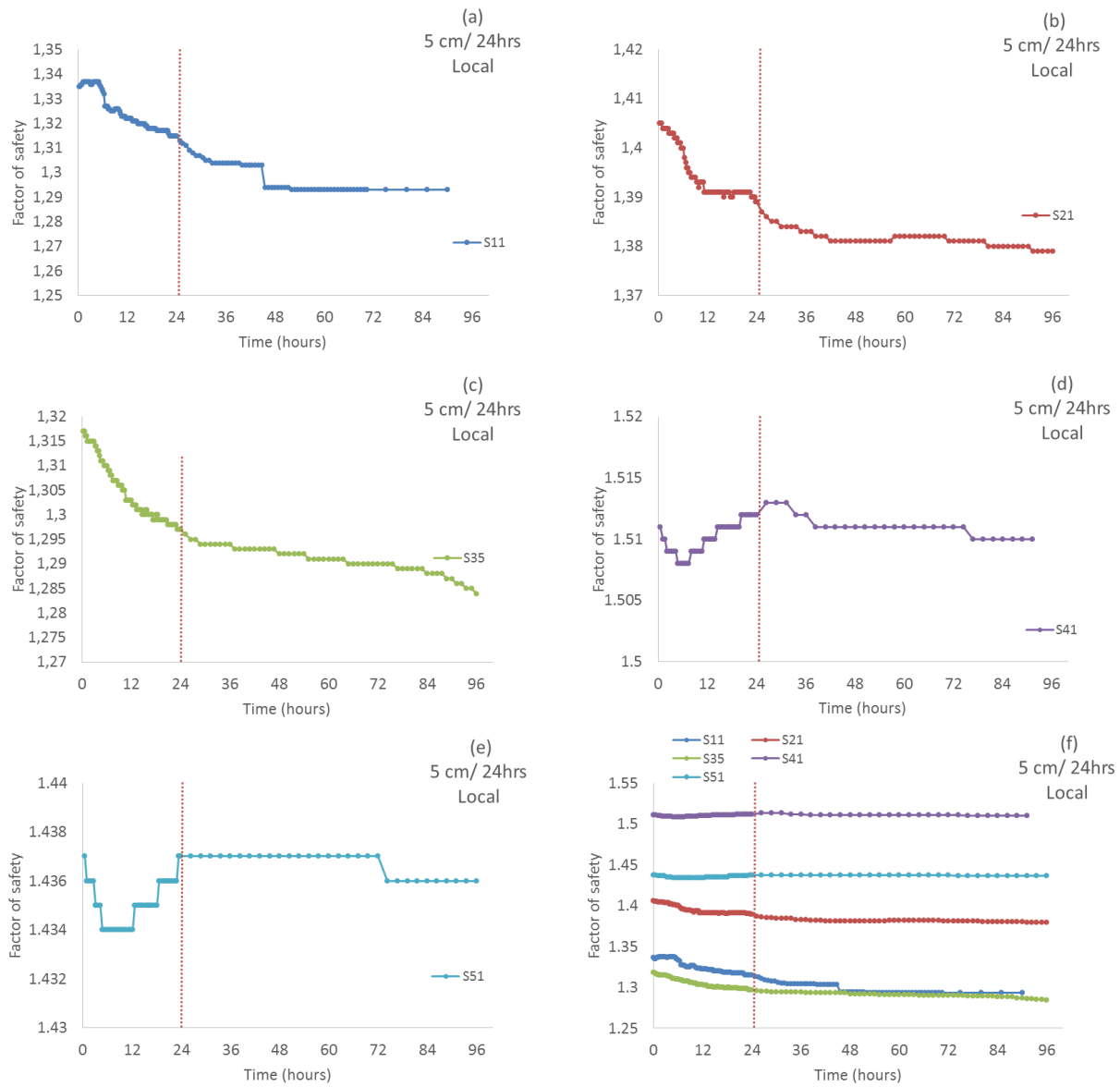
Figure 5-37: Variation of the local factor of safety over time during and after rainfall 5.78×10^{-7} m/s (0.05 m/d, R 1); a) Case S11; b) Case S21; c) Case S35; d) Case S41; e) Case S51; f) Cases S11, S21, S35, S41 and S51

Table 5-10: Initial and the minimum factor of safety for local slip surface during rainfall R 1

Case	Initial FS	Minimum FS during rainfall	Decrease (%) of FS
S11	1,336	1,315	1,57
S21	1,406	1,389	1,21
S35	1,318	1,297	1,59
S41	1,511	1,508	0,20
S51	1,437	1,434	0,21

For Cases, S11, S12, and S35, the factor of safety continues to decrease after the rainfall stops. After rainfall, matric suction tends to increase at shallow depth; while the wetting front keeps moving downwards and the minimum safety factor keeps decreasing for some time.

Figure 5-38 presents the changes of a global factor of safety for five different Cases (S11, S21, S35, S41 and S51) with respect to time under rainfall 5.78×10^{-7} m/s (0.05 m/d, R 1). The initial suction within the pile has a constant value 6 kPa.

The factor of safety starts decreasing with minor oscillation when the rainfall continues for Cases S11, S21, and S35 (see Figure 5-38 (a), (b) and (c)). During the rainfall pore water pressure in the slope moved gradually towards positive values and results in the reduction of the factor of safety. For these cases, the maximum decrease of the factor of safety during the rainfall is around 0.5% for Cases S11 and S21, which is low (see Table 5-11).

For two Cases S41 and S51, when the rainfall starts the factor of safety starts oscillation (increasing and decreasing), showing a maximum reduction of 0.06% during the rainfall (see Table 5-11). Figure 5-38 (f) show the effect of rainfall on the minimum factor of safety related to a global slip surface for different cases. A similar trend to the prolonged rainfall is observed here; FS variation under rainfall R 1 for different cases is not significant.

The results show the minimum global factor of safety is related to Case S11 (2 bench pile), and the addition of compacted layers increase the minimum factor of safety (see Cases S21, S35, S41, and S51). Also, the addition of alternate layers parallel to the slope increases the minimum factor of safety (compare Cases S41 with S21 and S51 with S35). The addition of inclined compacted layer has a positive effect on the global factor of safety unlike the local FS (compare Cases S35 with S21 and S51 with S41).
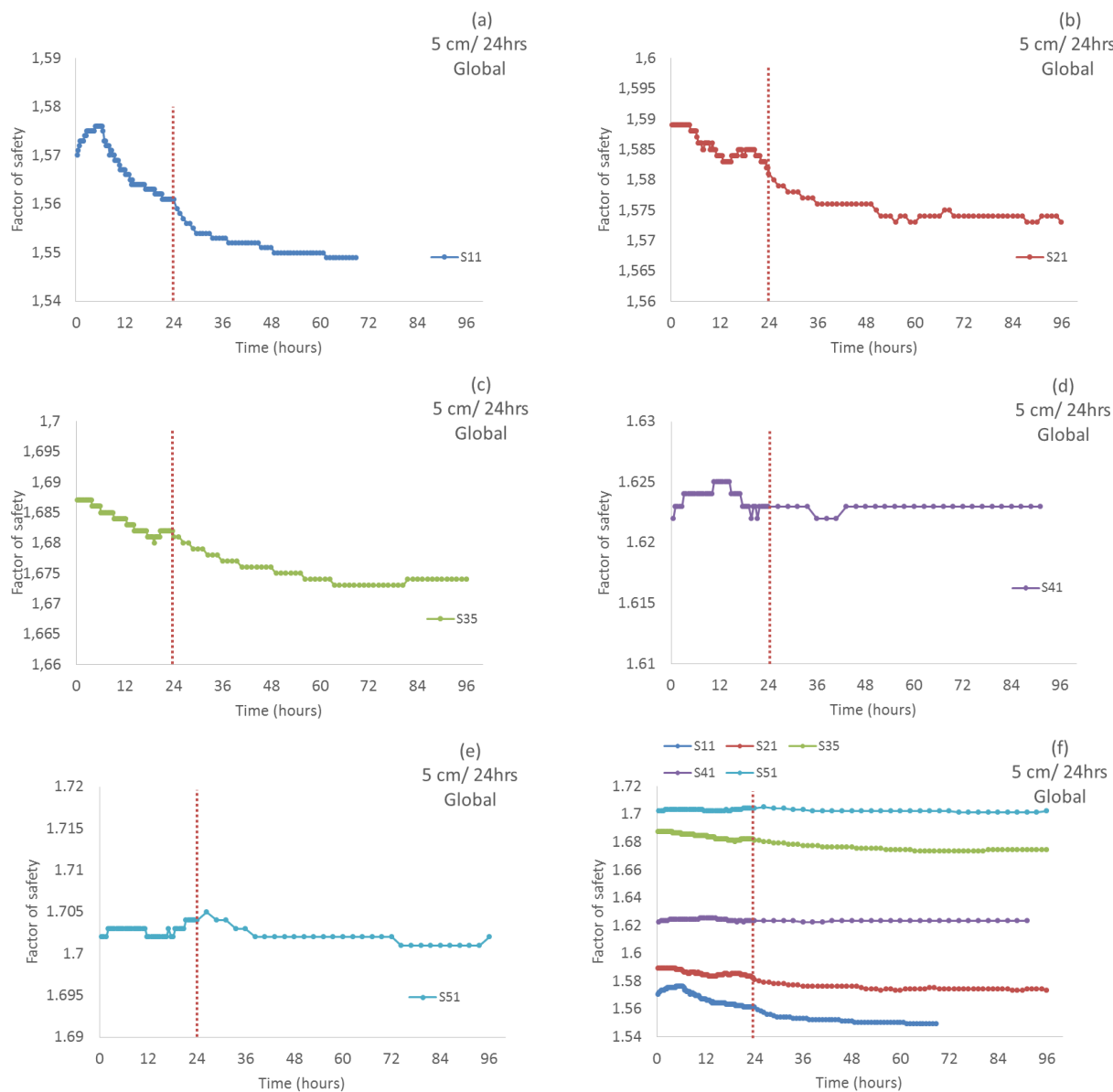
Figure 5-38: Variation of the global factor of safety over time during and after rainfall 5.78×10^{-7} m/s (0.05 m/d, R 1) for a global slip surface; a) Case S11; b) Case S21; c) Case S35; d) Case S41; e) Case S51; f) Cases S11, S21, S35, S41 and S51

Table 5-11 presents the initial and minimum of the global factor of safety for different cases under rainfall 5.78×10^{-7} m/s (0.05 m/d, R 1). It shows the highest reduction of the factor of safety is related to Cases S11, S21, and S35 that is not significant.

Table 5-11: Initial and the minimum factor of safety for a global slip surface under rainfall R 1

Case	Initial FS	Minimum FS	Decrease %
S11	1,569	1,561	0,51
S21	1,589	1,581	0,50
S35	1,688	1,68	0,47
S41	1,623	1,622	0,06
S51	1,703	1,702	0,06

Comparing results in Tables 5-10 and 5-11 indicate that the initial global FS is greater than 1.5. During the rainfall, the reduction of FS in not very significant and the values of FS remain higher than 1.5. Case S41 presents a FS higher than 1.5 for local slip surface and during the rainfall, it stays higher than 1.5, however for other Cases (S11, S21, S35, and S51) the initial FS is below 1.5.

Figure 5-39 presents local and global factor of safety with respect to time under different rainfalls (Cases S11, S21, S35, S41, and S51). Figure 5-39 (a) shows the local factor of safety for all the cases under rainfall R 2. After the rainfall starts Cases S11, S21 and S35 face a reduction of the factor of safety, for Cases S41 and S51, the change is very small. The same trend is seen for the other rainfalls R 3-3, R 4 and R 5 (see Figure 5-39 (a), (c), (e) and (g)). In all the graphs, the lowest factor of safety belongs to Case S35, and the highest belongs to Case S41. As discussed before, the inclination of compacted layer results in a minor decrease of the local factor of safety (compare Cases S35 with S21 and S51 with S41). Existences of alternate layers parallel to the slope, increase the factor of safety (compare S51 with S35 and S41 with S21). Figures 5-39 (a), (c), (e) and (g) indicate that for local slip surface factor of safety is lower than 1.5 except for Case S41; hence, these piles are not on the safe side.

Similar trends are obtained for the global slip surfaces, for all the rainfalls. For Cases S11, S21 and S35, there is a reduction of the factor of safety due to rainfall, for Cases S41 and S51 the changes in FS are not significant. Similar to prolonged rainfalls (pseudo steady-state), the highest global factor of safety results from cases with inclined compacted layers (see Figure 5-39 (b), (d), (f) and (h)). Figures 5-39 (b), (d), (f) and (h) indicate that the global factor of safety for all cases is above 1.5 (in the safe zone according to Table 2-8) for the initial condition. There is a variation

of FS during the rainfall, but the minimum value of FS is still above 1.5. It is thus considered that for global slip surfaces, the rainfall does not put the waste rock pile stability at risk. It is also observed, again, that the waste rock piles are more susceptible to local slip surfaces compare to global slip surface (with the former showing a lower local factor of safety).

The FS value may stay constant or slightly decreases after the rainfall starts. As was discussed before, the matric suction may increase the pile strength. Infiltration may cause matric suction to decrease from the ground surface to the deeper part of the pile. After the rainfall stops, the wetting front may still be extending deeper in the pile and result in FS reduction.
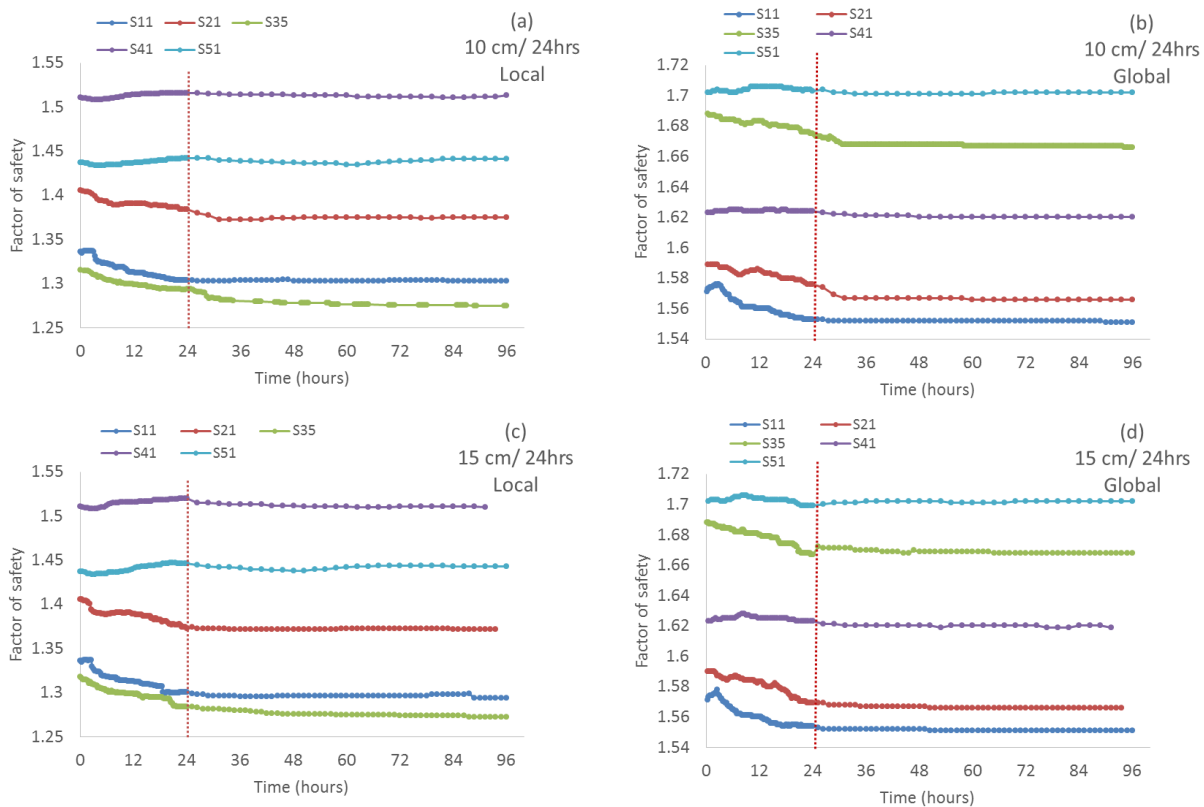
Figure 5-39: Variation of factor of safety with respect to time during and after different rainfalls for a local and a global slip surface; a) rainfall R 2, local slip surface; b) rainfall R 2, global slip surface; c) rainfall R 3-3, local slip surface; d) rainfall R 3-3, global slip surface; e) rainfall R 4, local slip surface; f) rainfall R 4, global slip surface; g) rainfall R 5, local slip surface; h) rainfall R 5, global slip surface
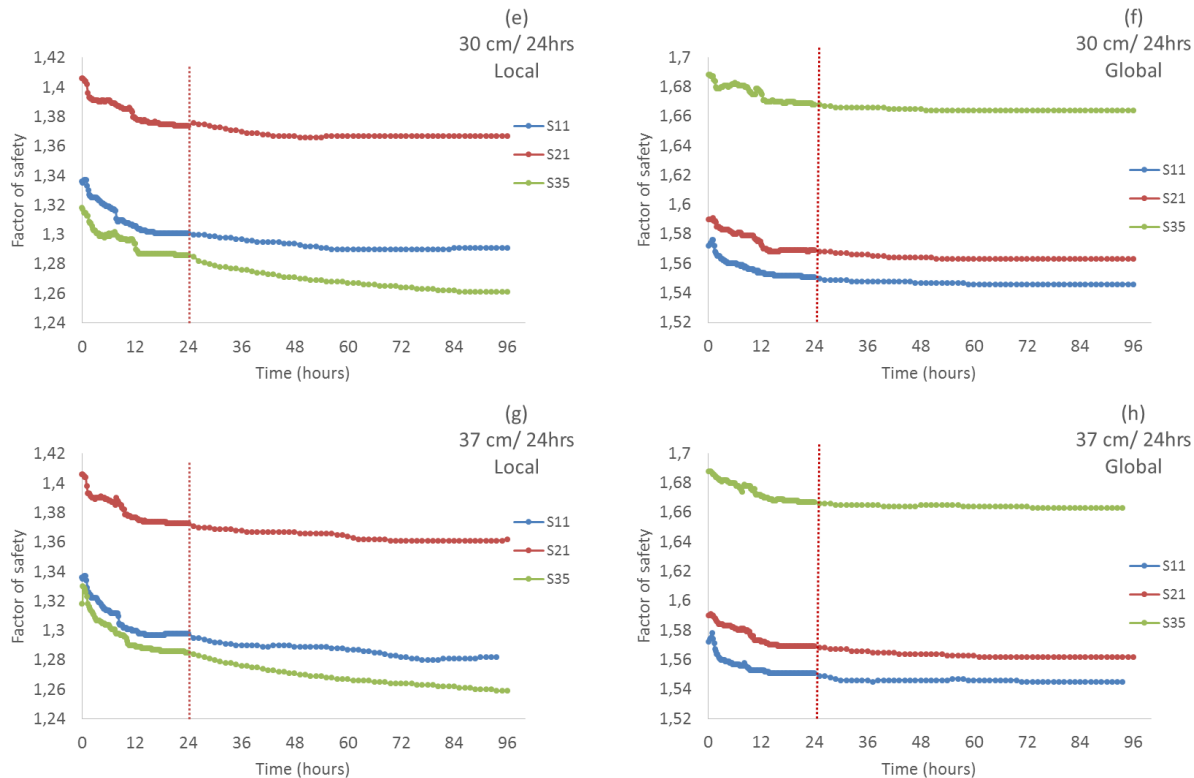
Figure 5-39 (continued): Variation of factor of safety with respect to time during and after different rainfalls for a local and a global slip surface; a) rainfall R 2, local slip surface; b) rainfall R 2, global slip surface; c) rainfall R 3-3, local slip surface; d) rainfall R 3-3, global slip surface; e) rainfall R 4, local slip surface; f) rainfall R 4, global slip surface; g) rainfall R 5, local slip surface; h) rainfall R 5, global slip surface

Table 5-12 presents the initial and minimum factor of safety obtained with SLOPE/W for Cases S11, S21, S35, S41 and S51 (Tables 4-4 and 4-5) under several rainfalls (i.e. R 2-1, 3-3, 4 and 5). It shows that in all cases, the factor of safety decreases during the rainfall due to increasing PWP and a reduction of strength (though the decrease is small, between 0.2 to 2.9%). As previously stated, relatively larger decreases are seen for Cases S11, S21, and S35; Cases S41 and S51 (with alternate layers parallel to slope) show less significant changes of the factor of safety due to rainfall. The variation of FS is more pronounced due to the geometry and configuration of waste rock pile than the rainfall infiltration (for the cases considered here).

The results also show how the magnitude of the rainfall affects the value of FS. As an example, in Case S11, when the rainfall changes from R 2-1 (10 cm/24 hrs) to R 3-3 (15 cm/24 hrs) to R 4

(30 cm/24 hrs) to R 5 (37 cm/24 hrs), the factor of safety is reduced by 2.4 % , 2.69% , 2.62% and 2.92%. The decrease is thus slightly higher when the rainfall rate increases.

Table 5-12: Initial and minimum factor of safety for the local slip surface for different rainfalls

Case	Initial FS	Minimum FS							
		R 2-1	Decrease (%)	R 3-3	Decrease (%)	R 4	Decrease (%)	R 5	Decrease (%)
S11	1,336	1,304	2,40	1,3	2,69	1,301	2,62	1,297	2,92
S21	1,406	1,384	1,56	1,373	2,35	1,374	2,28	1,373	2,35
S35	1,318	1,293	1,90	1,284	2,58	1,286	2,43	1,285	2,50
S41	1,511	1,508	0,20	1,508	0,20	-	-	-	-
S51	1,437	1,434	0,21	1,434	0,21	-	-	-	-

Some additional results are presented below to improve the understanding of how the changes of PWP and related strength parameters along the slip surfaces can affect the factor of safety.

5.7.2.2   PWP distribution along the slip surface

Figure 5-40 presents a plot of the suction (negative PWP) variation with time along a local slip surface (mid-base each slice, for five different Cases (S11, S21, S35, S41, and S51) under rainfall 1.736×10^{-6} m/s for 24 hours (R 3-3).

The initial suction is 6 kPa for all the cases. The water level is fixed at -7m (below the ground surface), the rise of the water table is prevented during rainfall, and no ponding is allowed.

When the rainfall starts, the water infiltrates from the surface and tends to accumulate near the toe. This results in a decrease of suction along the base of slices near the toe (slices # 20 to 30), slices near the crest (slices # 1 to 5) also drop suction more rapidly. The negative pore water pressure decrease gradually until it reaches 0.5 kPa for most of the slices (at the base mid-point of each slice, see Figure 5-40 (a)). Over time most of the slices in the slip surface (base mid-point) are exposed to infiltration and diminishing the suction.

Similar patterns are observed for Cases S21 and S35 (Figure 5-40 (b) and (c)). It worth noting that for Cases S11 and S21, the suction fluctuates near the toe of waste rock pile (interface between waste rock and foundation) due to the accumulation of water. For Case S35, no

significant fluctuation is seen. The critical local slip surface in Case S35 is located on the upper bench (due to inclination the upper bench has a higher height compare to lower bench, see Figure 5-40 (h)). The infiltrated water does not accumulate near the toe of the upper bench, as it moves outward for Case S35. Figure 5-40 (d) and (e) displays the suction profiles along the local slip surface for Cases S41 and S51 respectively. Case S41 shows that for slices 1 to 5 and 24 to 30 there are significant changes in suction due to infiltration, whereas it stays unchanged for slices 6 to 15 (the wetting front is not going that deep in the pile). Case S51 follows a similar pattern for the suction distribution.
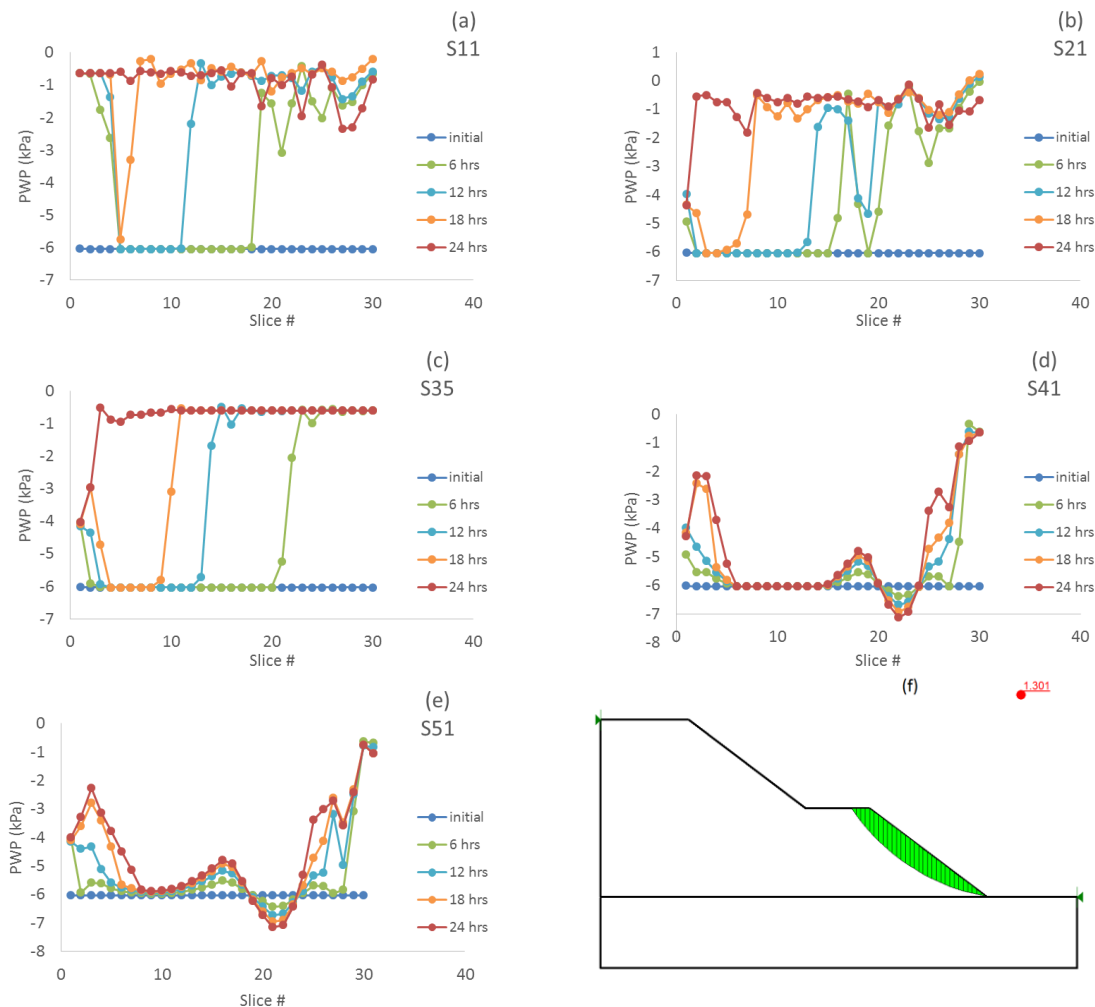
Figure 5-40: Pore water pressures distribution along a local slip surface (at midpoint of each slice at the base) under rainfall 1.73×10^{-6} m/s (R 3-3); a) Case S11; b) Case S21; c) Case S35; d) Case S41; e) Case S51; f) typical local slip surface for Case S11

5.7.2.3 Distribution of shear strength along slip surface

Figure 5-41 displays the variation of the additional strength (produced by suction, effective cohesion is zero everywhere) obtained with SLOPE/W along a local slip surface (base of each slice, mid-point) for five different Cases (S11, S21, S35, S41, and S51). Initial matric suction is 6 kPa, cases are under rainfall 1.73×10^{-6} m/s (0.15 m/d, R 3-3).

Case S11 indicates when the rainfall starts the water infiltrates and the strength due to suction decrease gradually for the slices near the crest and the toe; after 24 hours the strength reaches to 0.2 kPa from 0.8 kPa at the mid-point of slices base along the slip surface. Cases S21 and S35 follow the same path except for the slices in compacted layer (slice 1) that shows an increase of strength while suction decrease due to the path of c_{app} versus suction obtained with Equation 4-1 (section 4-6).

Like suction profile, the strength (due to suction) is not changing significantly for slices 5 to 20 in Cases S41 and S51 (see Figure 5-41(d) and (e).

Figure 5-41 (f) presents the variation of a factor of safety (with respect to time) for all the cases. The results indicate the decrease of a factor of safety with time in Cases S11, S21 and S35 due to a decrease of negative pore water pressure and decrease of strength. Variation of a factor of safety is negligible for Cases S41 and S51 due to the minor influence of rainfall on the expansion of wetting front.

The lowest minimum local factor of safety belongs to Case S35 due to the inclination of compacted layer. The addition of compacted layers increases the minimum factor of safety (Case S11 vs. S21). The combination of compacted layer and alternate layers parallel to the slope increase the minimum factor of safety (compare S21 with S41 and S51).

.
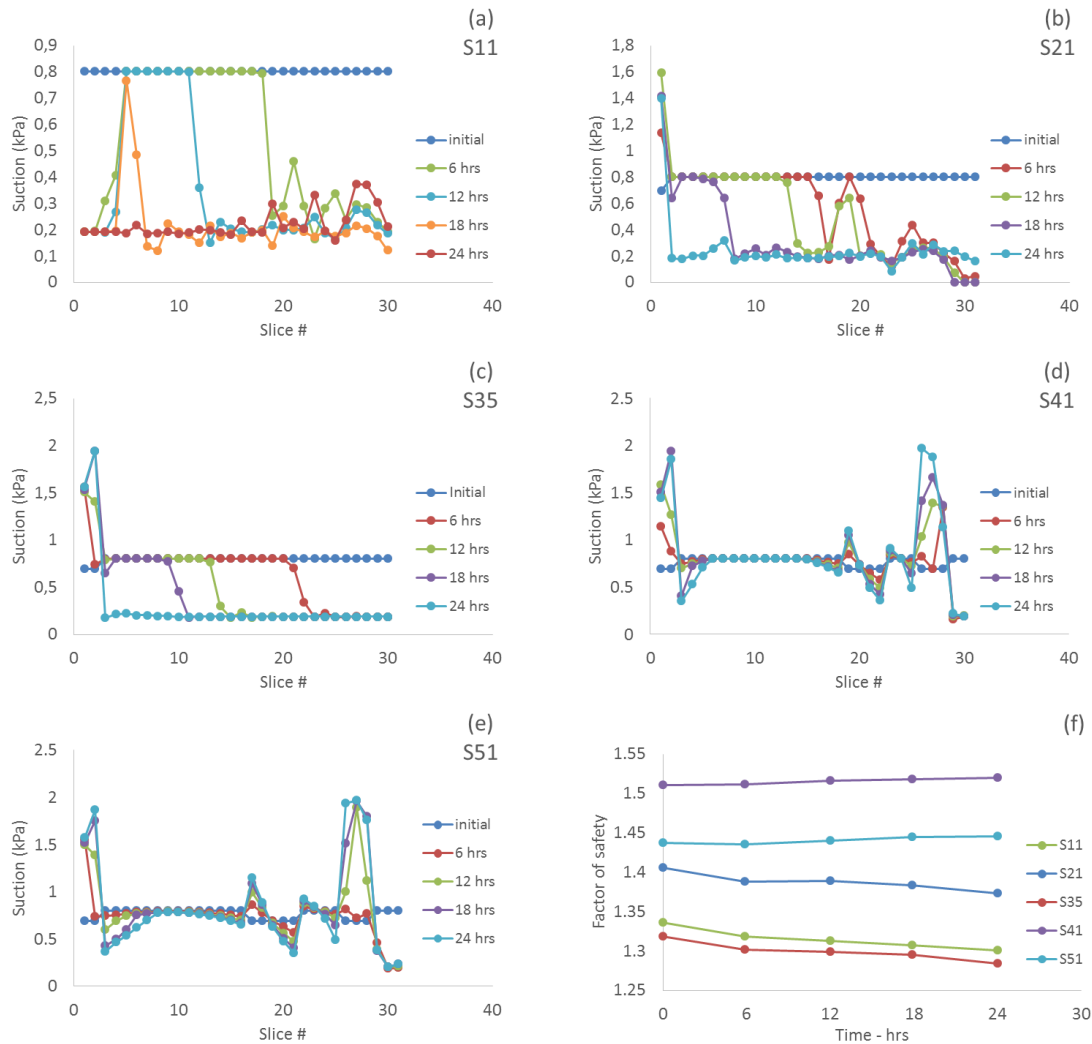
Figure 5-41: Variation of strength due to the suction (kPa) along a local slip surface at the midpoint of each slice, under rainfall 1.73×10^{-6} m/s (0.15 m/d, R 3-3), for different time steps; a) Case S11; b) Case S21; c) Case S35; d) Case S41; e) Case S51; f) variation of FS over time for all cases

5.7.3 **Effect of increasing rainfall on slope stability**

Figure 5-42 presents the factor of safety for different rainfalls (R 1, R 2-1, R 3-3, R 4 and R 5-1, Table 5-1) on different waste rock piles (Cases S11, S21, S35, S41, and S51) for a local slip surface.

Figure 5-42 (a) shows that for different rainfalls, the infiltration reduces the factor of safety for Case S11. The larger decrease is due to the rainfall with higher intensity (R 5-1), and the lower reduction belongs to rainfall with lower intensity (R 1).

The reduction rate is faster for higher intensity rainfall compare to lower intensity rainfall, meaning the minimum factor of safety is reached earlier when the rainfall intensity is higher. The same trends are seen for Cases S21 and S35 (see Figure 5-42 (b) and (c)).

For Cases S41 and S51, the rainfalls produce a small decrease of FS followed by a small increase. Comparing the results for cases with and without alternate layers parallel to the slope, shows that piles with such layers are less sensitive to infiltration.
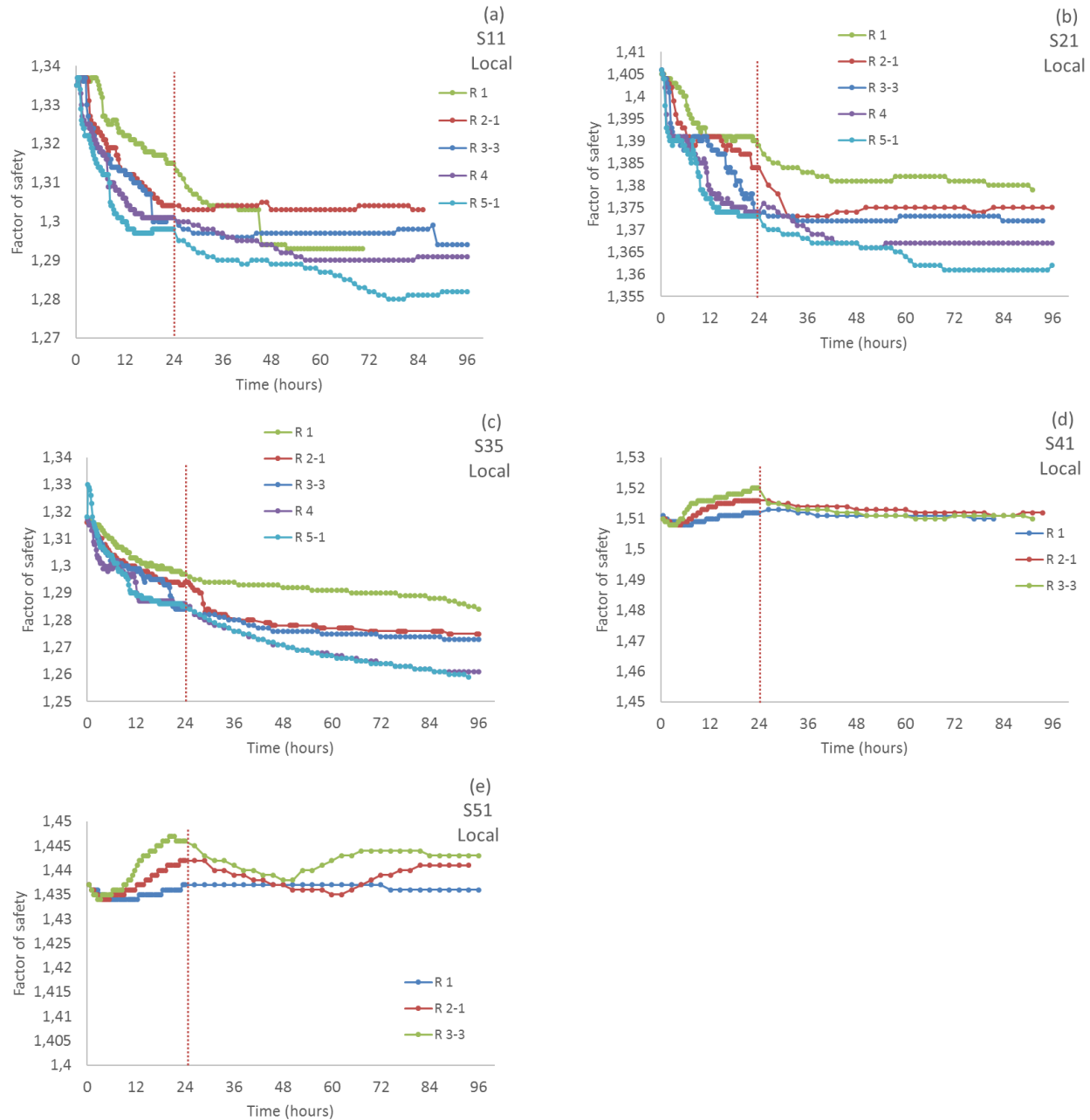
Figure 5-42: Variation of the factor of safety during and after different rainfalls (R 1, R 2-1, R 3-3, R 4 and R 5-1), for local slip surfaces; a) Case S11; b) Case S21; c) Case S35; d) Case S41; e) Case S51

Figure 5-43 illustrates the changes of a global factor of safety with respect to time, during and after different rainfalls. Results are related to Cases S11, S12, S35, S41 and S51 under rainfalls R 1, R 2-1, R 3-3, R 4 and R 5-1. Comparison of these results with those of local slip surfaces (Figure 5-43) indicates that the responses to the infiltration and the suction changes follow a similar pattern. For Cases S11, S12 and S35, infiltration results in a reduction of strength and factor of safety. As the rainfall intensity increases, the reduction of the factor of safety accelerates and it is achieved sooner. A lower intensity increases the time to reach the minimum factor of safety during the rainfall.

The minimum factor of safety (reached during different types of rainfall) for these cases do not change considerably when rainfall changes from R 2-1 to R 5; the difference is more significant between rainfall R 1 and R 2-1.

The results illustrate that the impact of rainfall intensity on waste rock pile stability is not very significant with these initial conditions. For Cases S41 and S51 the rainfalls results in the oscillation of factor of safety which is not very significant (see Figure 5-43 (d) and (e)).
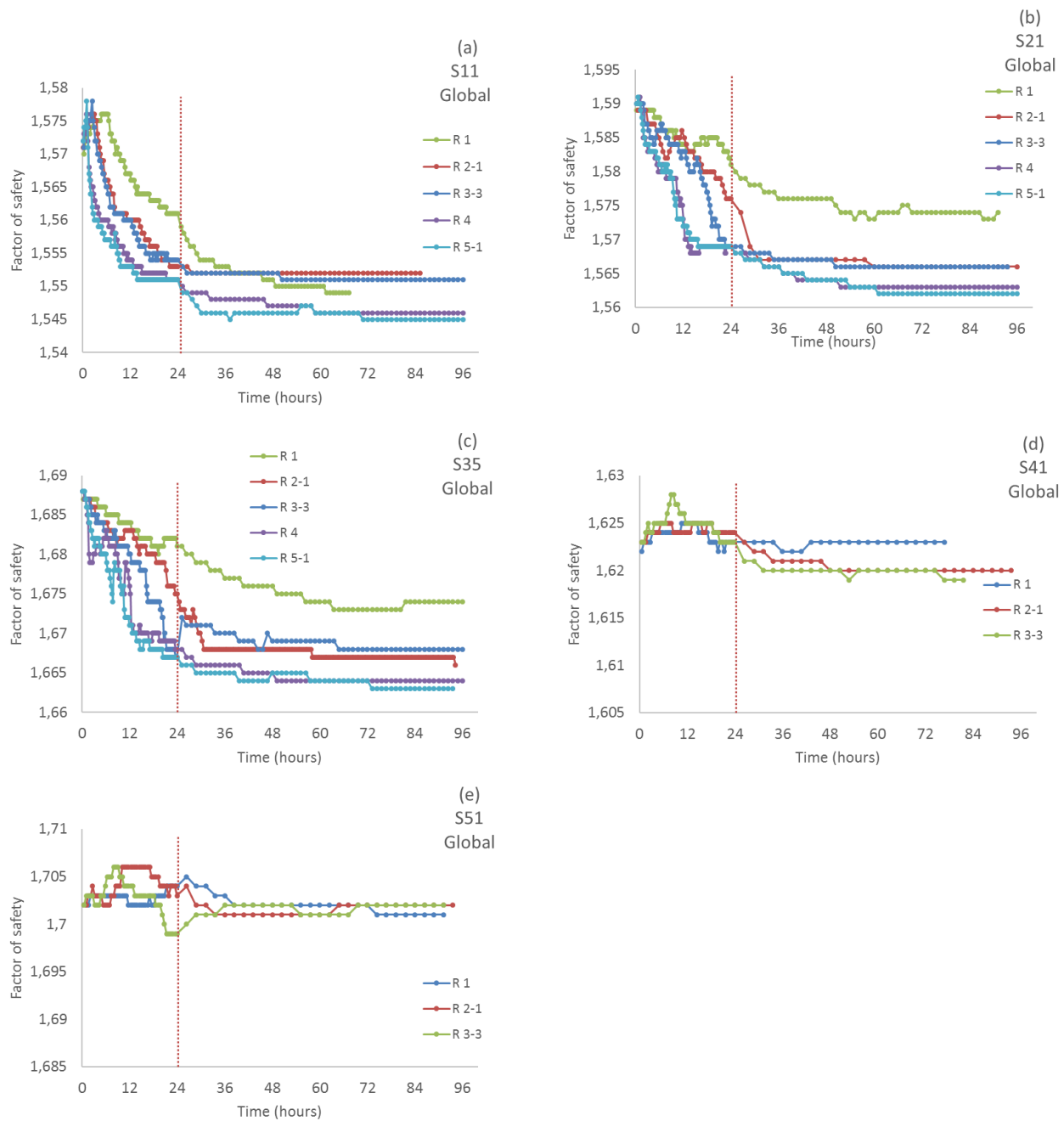
Figure 5-43: Variation of factor of safety during and after different rainfalls (R 1, R 2-1, R 3-3, R 4 and R 5-1), for a global slip surface; a) Case S11; b) Case S21; c) Case S35; d) Case S41; e) Case S51

5.7.4 **Effect of rainfall duration on slope stability**

The influence of rainfall durations on the stability behavior has been studied. For that purpose, three different durations 6 hours (rainfall R 3-1, 6.94×10^{-6} m/s, 0.6 m/d), 12 hours (rainfall R 3-2, rainfall 3.47×10^{-6} m/s, 0.3 m/d) and 24 hours (rainfall R 3-3, rainfall 1.736×10^{-6} m/s, and 0.15 m/d) are considered. Four different Cases S12, S35, S41, and S51, are studied.

The initial suction for all the cases is 6 kPa. For each case when the rainfall stops the dry period continues for 48 hours (i.e. the 6 hours rainfall is followed by 42 hours dry period, 12 hours rainfall with 36 hours and for 24 hours it is 24 hours).

Figure 5-44 presents the variations of FS for a local slip surface under three different rainfalls (R 3-1, R 3-2 and R 3-3 respectively) with respect to time.

For Cases S21 and S35, the factor of safety decreases when the rainfall starts. The reduction of FS follows a similar pattern for three rainfall durations (6, 12 and 24 hrs), but the decrease is faster for shorter rainfall duration because of the higher intensity. It indicates that when the rainfall duration increases, it takes longer to achieve the minimum factor of safety. The differences between the factor of safety under different type of rainfalls, for Case S21, is less pronounced after 48 hours (see Figure 5-44 (a))

Cases S41 and S51 show a similar pattern for the variation of FS due to an increasing rainfall duration. This variation is less significant for cases with layers parallel to the slope compare to cases without these layers, as stated before. These results indicate that the rainfall duration influences the reduction of a minimum factor of safety values for all cases. It also has a significant impact on the advancement of the wetting front in the waste rock.
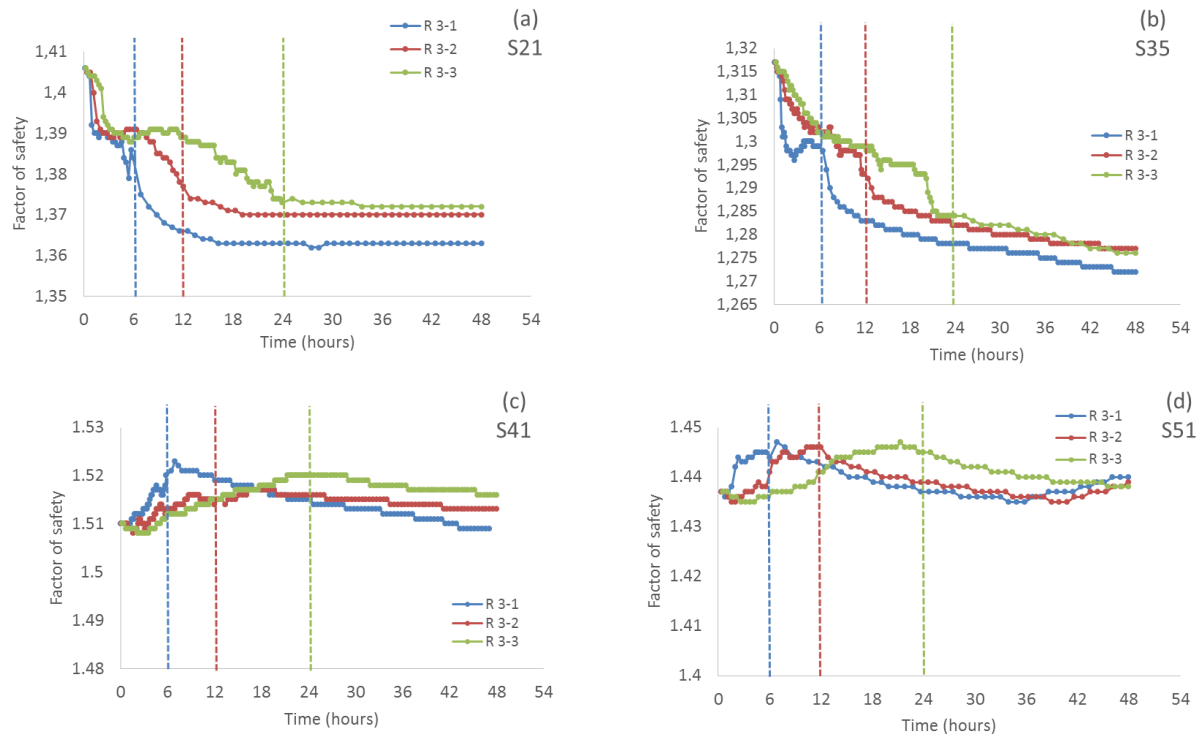
Figure 5-44: Variation of factor of safety for local slip surface under rainfall R 3-1, R 3-2, and R 3-3; a) Case S21; b) Case S35; c) Case S41; d) Case S51

Figure 5-45 presents the variation of FS for three different rainfall durations (R 3-1 (6 hrs), R 3-2 (12hrs) and R 3-3 (24 hrs) respectively).

The trend for the global factor of safety is very similar to that of the local factor of safety. With other factors fixed, the longer the duration, the later the minimum FS is achieved. Longer time (e.g. 24 hours) results in a delay on the occurrence of a minimum factor of safety.
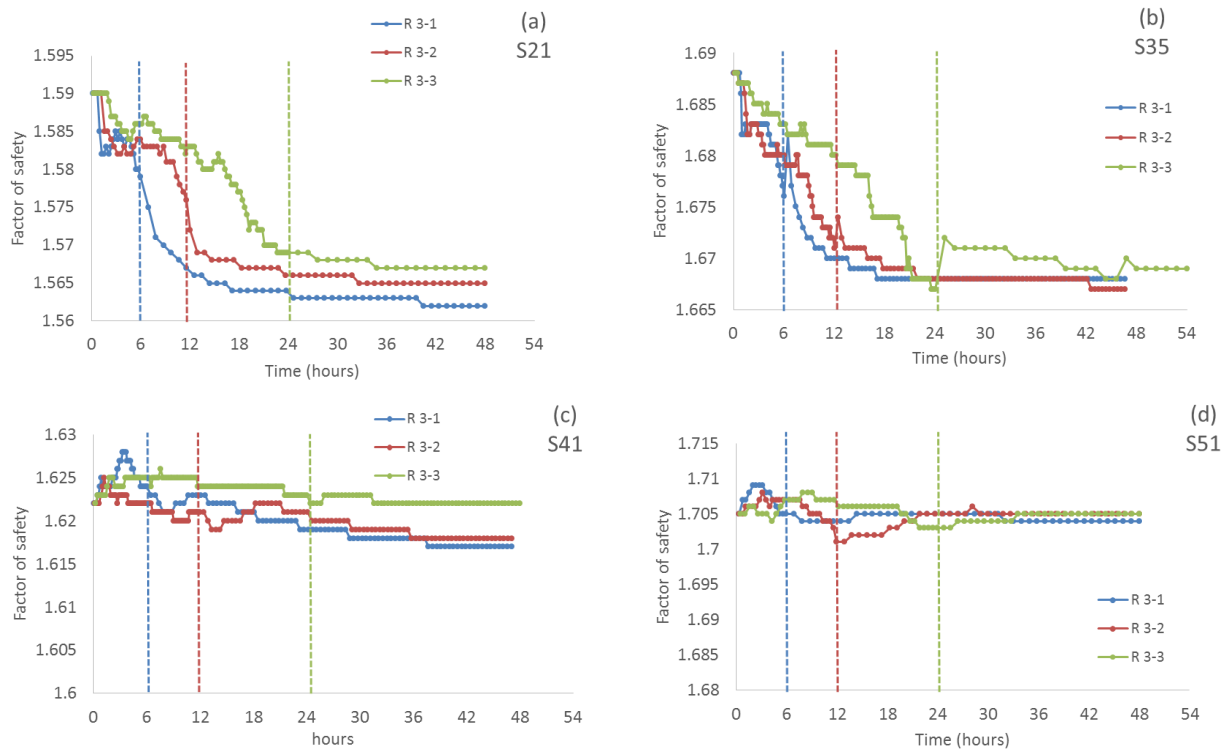
Figure 5-45: Variation of factor of safety for Global slip surface under rainfall R 3-1 (6 hrs), R 3-2 (12 hrs) and R 3-3 (24 hrs); a) Case S21; b) Case S35; c) Case S41; d) Case S51

Table 5-13 shows the reduction (percentage) of the factor of safety for different cases under rainfalls durations (R 3-1, R 3-2 and R 3-3). It is seen that reduction (percent) of FS is approximately constant under different rainfall durations. The significant difference is seen to be the time to reach the minimum factor of safety. Increasing the duration (reduction of intensity) may produce a delay in reaching a minimum factor of safety.

Table 5-13: Initial and minimum factor of safety for a local slip surface, under different rainfalls R 3-1, R 3-2 and R 3-3

Case	Initial FS	6 hours (R 3-1)		12 hours (R 3-2)		24 hours (R 3-3)	
		Min FS	Decrease FS (%)	Min FS	Decrease FS (%)	Min FS	Decrease FS (%)
S21	1,406	1,362	3,13	1,37	2,56	1,372	2,42
S35	1,318	1,272	3,49	1,277	3,11	1,276	3,19
S41	1,51	1,508	0,13	1,508	0,13	1,508	0,13
S51	1,438	1,435	0,21	1,435	0,21	1,435	0,21

Table 5-14 shows that the rainfall duration does not affect the reduction (%) of global FS significantly. It follows a similar trend as Table 5-13. The minimum factor of safety is fairly changing when the duration of rainfall increase. Moreover, it was shown in Figure 5-45 that this minimum value might reach later in time when the duration increases.

Table 5-14: Initial and minimum factor of safety for a global slip surface, under different rainfall R 3-1, R 3-2, and R 3-3

Case	Initial FS	6 hours		12 hours		24 hours	
		Min FS	Decrease FS (%)	Min FS	Decrease FS (%)	Min FS	Decrease FS (%)
S21	1,589	1,562	1,70	1,565	1,51	1,566	1,45
S35	1,688	1,668	1,18	1,667	1,24	1,667	1,24
S41	1,623	1,617	0,37	1,618	0,31	1,622	0,06
S51	1,704	1,704	0,00	1,701	0,18	1,703	0,06

5.7.5 Effect of groundwater level on infiltration and slope stability

To evaluate the effect of ground water table on the infiltration rate and changes in the factor of safety a study is conducted here. Three different Cases S11 (2 benches), S21 (2 benches and horizontally compacted layer) and S35 (2 benches and 5% inclined compacted layer) are considered with initial suction 6 kPa, under rainfall R 2-1. The groundwater level is located in

three different depths below the ground including 7 m, 3 m, and 1 m. Water level location affects the pore-water pressure distribution and defines the thickness of unsaturated zone.

Figure 5-46 presents the changes of the factor of safety with respect to time for three different Cases (S11, S21, and S35) under rainfall R 2-1 with various groundwater levels (i.e. 7 m, 3m and 1m below the ground). The initial suction within the waste rock piles is 6 kPa for all the cases. Results are presented for both a local and a global slip surface.

The results indicate that after the rainfall starts, the factor of safety related to global slip surfaces follows similar patterns of reduction for different groundwater level. With this particular initial conditions, the global slope surface changes do not show significant differences when the groundwater level increases from -7 m to -1 m (see Figure 5-46 (b), (d) and (f)).

For local slip surface, the same trend is seen. It should be noted that for a shallower groundwater level (-1 m below the ground) in the long term the factor of safety reaches lower value compare to deeper groundwater level.

As discussed before, the local slip surface for Case S35 is located on the upper bench. Hence, that may be the reason the changes of FS is very similar when the groundwater level is deeper.
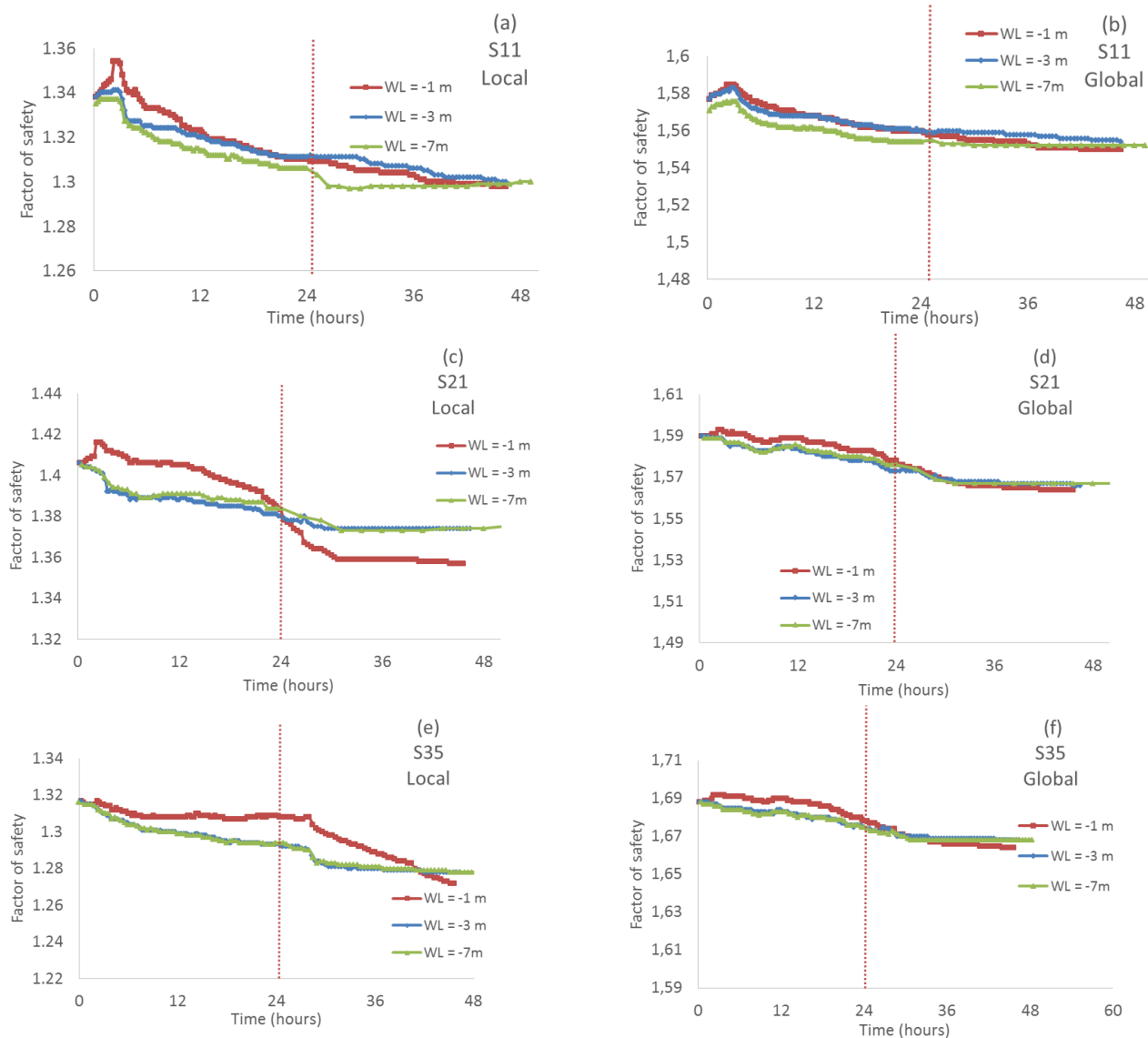
Figure 5-46: Variation of the factor of safety for local and global slip surfaces under rainfall R 2-1, different groundwater levels (located 1, 3 and 7 m below the ground surface); a) local slip surface, Case S11; b) global slip surface, Case S11; c) local slip surface, Case S21; d) global slip surface, Case S21; e) local slip surface, Case S35; f) global slip surface, Case S35

5.7.6 Effect of minimum depth of critical slip surfaces

SLOPE/W can define the minimum depth of the slip surface, based on the height of at least one slice, which must be equal or greater than the specified depth. For example, a slip surface with a

minimum depth 3 m means there is at least one slice with a depth of 3 m (or higher) in the critical slip surface. To see the effect of slip surface depth on the factor of safety, a study is conducted.

Case S21 is presented here, with rainfall R 1 (Table 5-1), and initial matric suction 6 kPa and a water level fixed at 7 m below the ground. Figure 5-47 presents the variation of the factor of safety for different minimum depths, for the local and global slip surfaces.

For local slip surfaces (depth up to 3 m) with a very shallow slip surfaces (e.g. 0.1, 0.5 and 1 m), the changes of the factor of safety are similar; for a deeper slip surface, of 2 m and 3 m, the initial factor of safety increases by about 4% and 11% respectively. It indicates that deeper slip surface is related to a higher FS compared to shallower slip surfaces (see Figure 5-47 (a)). For different depths of slip surfaces, the changes of a factor of safety due to rainfall follow a similar path.

For global slip surface, an increase of 2 % is seen in the initial factor of safety when the minimum depth of slip surface reaches 6 m (see Figure 5-47 (b)).
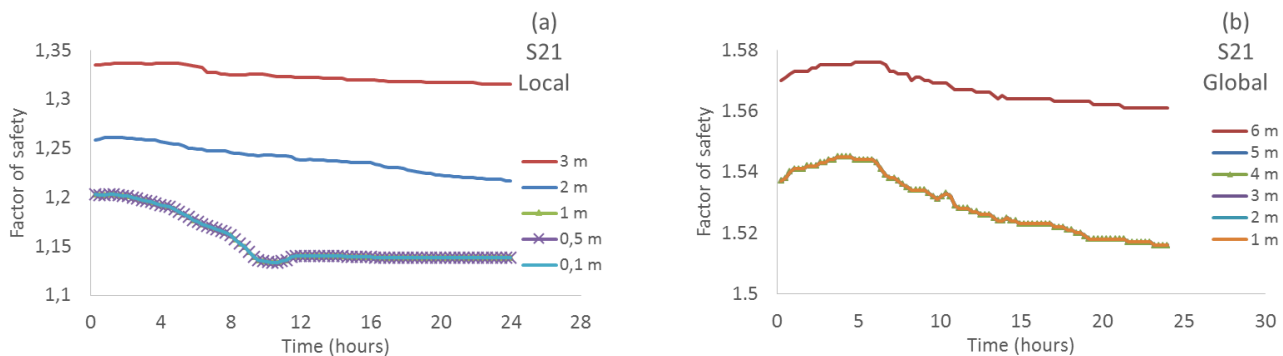
Figure 5-47: Variation of factor of safety for local and global slip surface under rainfall R 1 for Case S21; a) local slip surface with different depth (3, 2, 1, 0.5 and 0.1 m; b) global slip surface with different depth (6, 5, 4, 3, 2 and 1 m)

Table 5-15 presents the reduction (%) of local and global slip surfaces with different minimum depth with respect to time. It shows the shallower local slip surfaces (minimum depth 0.1, 0.5 and 1 m) are more susceptible to changes due to rainfall compared to deeper slip surfaces (depth 2 and 3 m). When the depth of local slip surface goes from 1 m to 2 m to 3 m; the reduction of the factor of safety during rainfall decreases from 5.8% to 3.3% to 1.5% respectively. That indicates

in waste rock piles; the rainfall infiltration affects shallow local slip surfaces more. In this thesis, depth 3 m is considered for local slip surface.

It is noted that compared to local slip surface, the reduction of the global factor of safety is less. As an example, a local slip surface with minimum depth 2 m shows a maximum reduction of 3.26% during the rainfall whereas a global slip surface with same depth shows a reduction 1.37%. For global slope surface, the changes happen when the depth of slip surface reaches 6 m. In this study, the depth is considered to be 6 m.

Table 5-15: Reduction (%) of local and global factor of safety comparing different depths of slice surface, Case S21, rainfall R 1

Minimum depth	Initial FS	Min FS	Reduction (%)
Local slip surface			
0.1	1.203	1.133	5.82
0.5	1.203	1.133	5.82
1	1.203	1.133	5.82
2	1.258	1.217	3.26
3	1.335	1.315	1.50
Global slip surface			
1	1.537	1.516	1.37
2	1.537	1.516	1.37
3	1.537	1.516	1.37
4	1.537	1.516	1.37
5	1.537	1.516	1.37
6	1.57	1.561	0.57

5.7.7 Effect of k_{xy} anisotropy on infiltration and slope stability

One of the factors that affect the infiltration and water flow and distribution is the hydraulic conductivity of the waste rock. The hydraulic conductivity in the horizontal (k_x) and vertical (k_y) directions is often assumed to be similar for simplicity, but in reality, these may be different (e.g. (Fala, 2008). In SEEP/W, the conductivity ratio k_y/k_x can be controlled. A ratio of 10 means the

hydraulic conductivity in the y-direction is 10 times greater than x-direction. Three Cases (S11, S21, and S35; with initial suction 6 kPa) were analyzed with rainfall R 2-1 (1.157×10^{-6} m/s, 0.1 m/d) to evaluate the effect of k_{xy} anisotropy (in loose and compacted layers) on infiltration and factor of safety

Figure 5-48 shows the development of the wetting front (PWP changes, kPa) inside the pile after 24 hours of rainfall for different k anisotropy for Case S21. It is seen that when k_y are smaller than k_x (ratio =0.01, Figure 5-48 (a)), the infiltration rate is very low. As the ratio increase (e.g. ratio =100, Figure 5-48 (e)) the depth of infiltration increases significantly. This shows the increase of k in y-direction has a significant effect on the rate of infiltration (as observed by Fala, 2008).
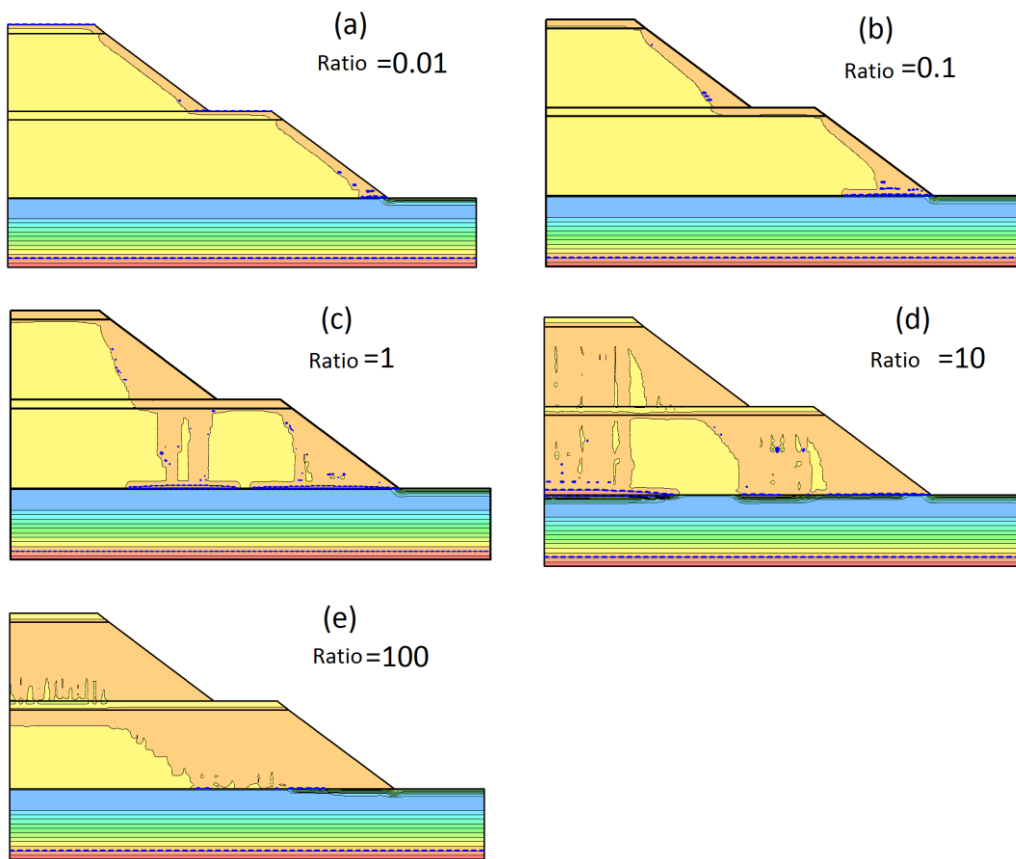
Figure 5-48: Variation of Wetting front (PWP changes, kPa) for Case S21 after 24 hours , under different k anisotropy under rainfall R 2-1 for 24 hours; a) $k_y/k_x = 0.01$; b) $k_y/k_x = 0.1$; c) $k_y/k_x = 1$; d) $k_y/k_x = 10$; $k_y/k_x = 100$

Figure 5-49 presents the variation of the local factor of safety for three different waste rock piles (Cases S11, S21, and S35) under rainfall R 2-1 for 24 hours, followed by 24 hours of the dry period. The initial suction is 6 kPa for all cases. The results indicate that for all cases the factor of safety decreases when the rainfall starts. Due to different k_y / k_x ratio, the minimum factor of safety and needed time to reach it are changing.

As the ratio k_y / k_x increase the infiltration rate increases too. The wetting front expands faster and deeper, and the factor of safety decreases at a higher rate. As an example, the minimum local factor of safety is reached after approximately 3 hours of rainfall for ratio 100 whereas it is reached after 24 hours for ratio 0.01. It is also noted that when the rainfall stops, the factor of safety starts to increase rapidly for a ratio of 100, while it decreases slightly or stays constant for smaller ratios.
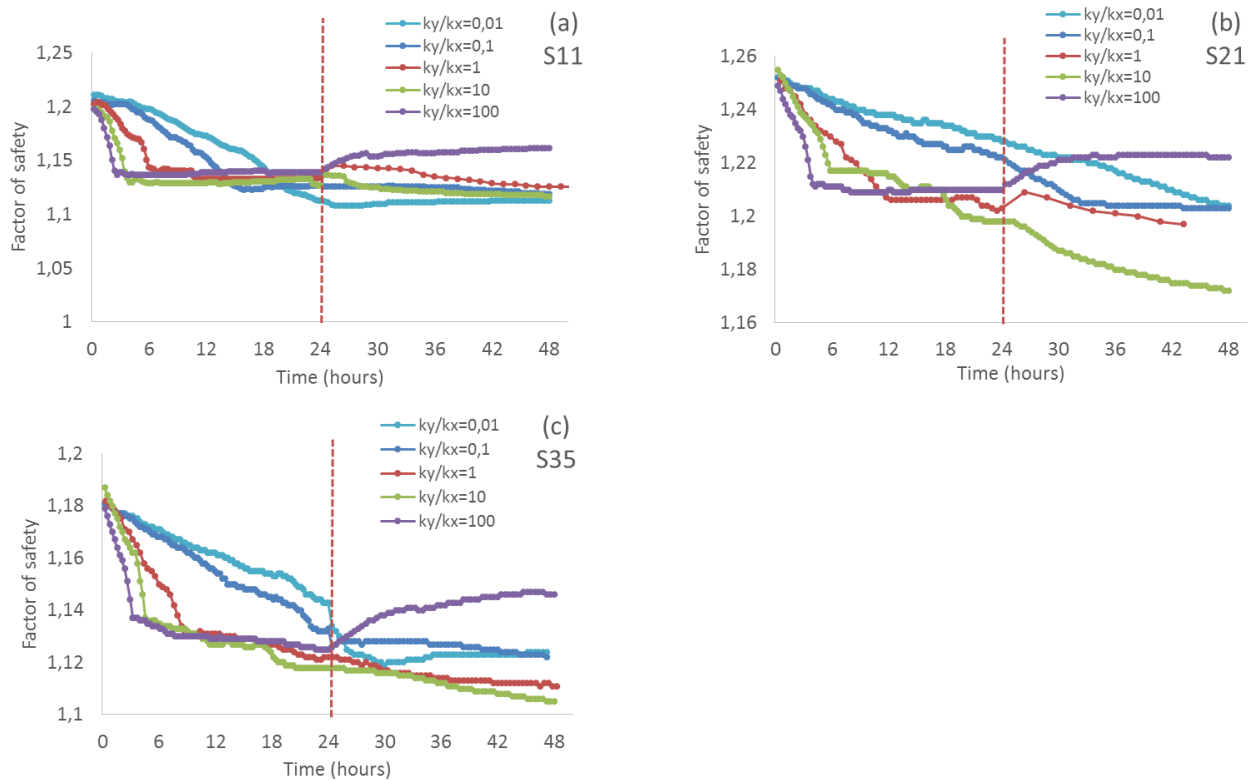
Figure 5-49: Changes of factor of safety during and after rainfall R 2-1 for local slip surface, different k_{xy} anisotropy 0.01, 0.1, 1, 10 and 100; a) Case S11; b) Case S21; c) Case S35

Figure 5-50 presents the variation of the global factor of safety for slip surfaces with minimum depth 1 m, for three Cases S11, S21, and S35 under rainfall R 2-1 followed by 24 hours of the dry period. The similar trend as the local factor of safety is observed for the global factor of safety. FS magnitude and reduction between ratios 1, 10 and 100 are not very significant, whereas for ratio 0.01 and 0.1 the minimum factor of safety is higher and it is reached with a delay in time compare to other ratios.
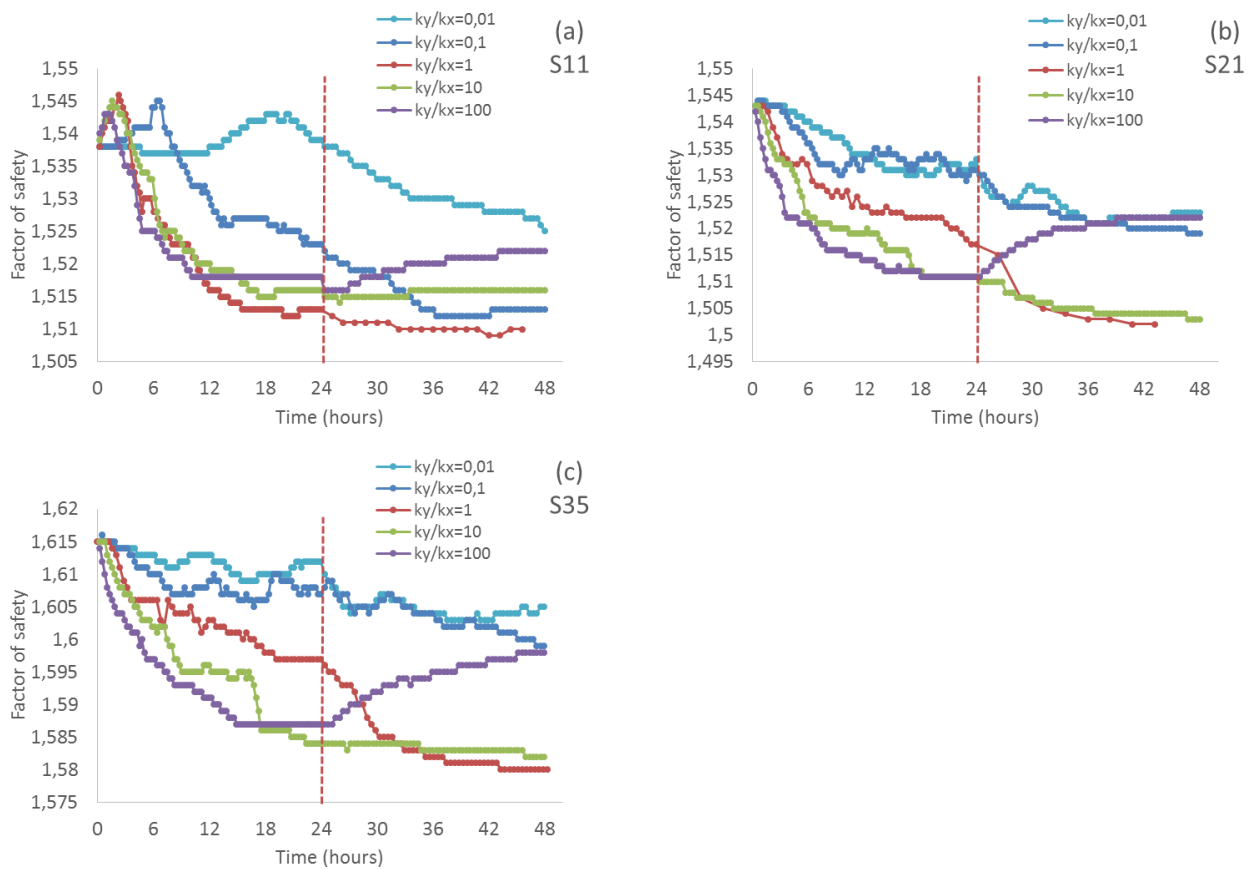
Figure 5-50: Variation of factor of safety during and after rainfall R 2-1 for global slip surface and different k_{xy} anisotropy 0.01, 0.1, 1, 10 and 100; a) Case S11; b) Case S21; c) Case S35

5.7.8 **Effect of foundation material properties**

This section includes the results of numerical simulations to represent water movement, pore water pressure distribution and the FS of waste rock piles located on different foundation materials.

Figure 5-51 presents the changes of the factor of safety for local (covering one bench) and global slip surfaces (covering two benches, passing the toe) with respect to time for Case S11 under rainfall R 2-1. It is seen that the factor of safety for a foundation with waste rock and silty sand is similar, and it decrease by rainfall with the similar path.

The factor of safety for silty clay foundation is lower compare to waste rock and silty sand foundations, but it follows the similar path of the reduction in rainfall. Both local and global slip surfaces are inside the pile, and they are not passing the foundation.
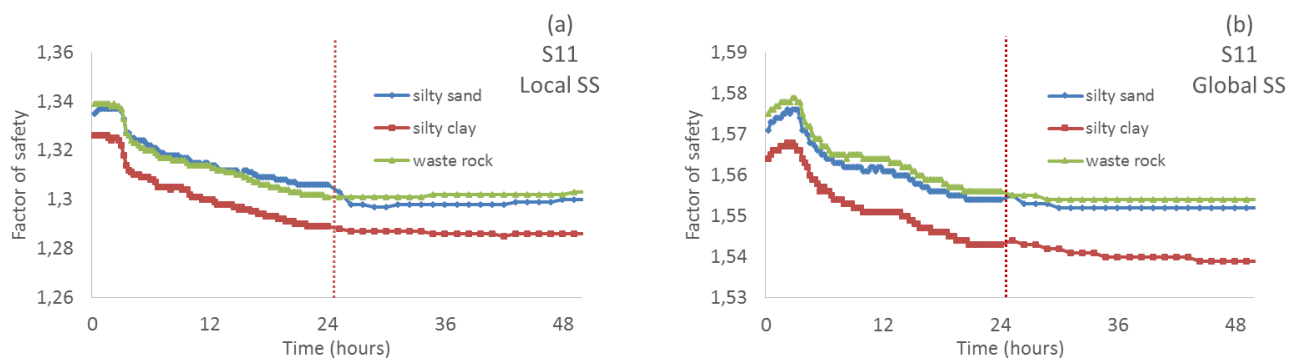
Figure 5-51: Variation of factor of safety with time during and after rainfall R 2-1 for local and global slip surface, Case S11, foundation silty sand, silty clay and waste rock, initial suction 6 kPa; a) local slip surface; b) global slip surface

5.7.9 **Effect of pile size**

Figure 5-52 presents the variation of the local and global factor of safety for four Cases S21, S22, S23 and S24 (waste rock piles with two benches and compacted waste rock layer with height 20, 40, 80 and 120 m respectively; see Tables 4-4 and 4-5). All the cases have initial suction 6 kPa (c_{app} = 1 kPa) and are under rainfall R 1 (5.78 $\times 10^{-7}$ m/s, Table 5-1) followed by 24 hours of the dry period.

The higher initial factor of safety is obtained for Case S21 (smallest pile). Increasing the height leads to a decrease of the initial factor of safety (section 4-7-6). When the rainfall starts, the factor of safety tends to decrease slightly for all cases. The trend is similar for both local and global slip surfaces. Smaller piles always have a larger FS in these cases (as expected).
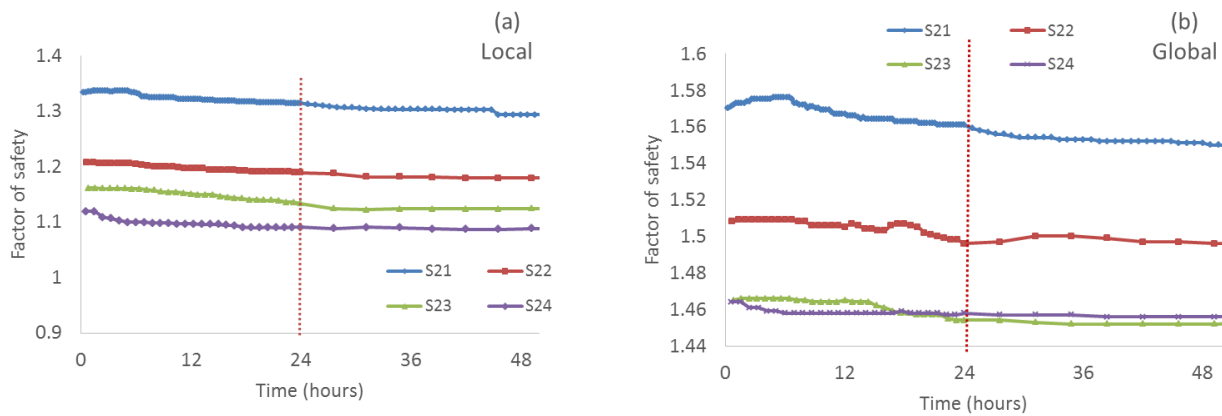
Figure 5-52: Changes of factor of safety during and after rainfall R 2-1 for Cases S21, S22, S23, and S24; a) local slip surface; b) global slip surface

The results presented in Chapters 4 and 5 assumed a single value for material properties (c_{app}, ϕ') within the pile for all the analyses. It was mentioned in section 2-4-3, that these types of consideration might not be close to the reality. The construction methods and internal features of waste rock piles affect the material properties distribution. Numerical analyses based on material properties distribution are being conducted, and the effect of material properties distribution is on the waste rock pile stability is illustrated.

CHAPTER 6   ADDITIONAL RESULTS AND DISCUSSION

6.1 Introduction

The purpose of the work presented in this chapter is (6 part) to evaluate the impact of uncertainties on the stability and reliability of waste rock piles. These uncertainties may include geotechnical (i.e. internal friction angle, cohesion), geological/hydrogeological (i.e. groundwater level, pore water pressure) or geometric (i.e. layer thickness) characteristics.

To achieve this goal, the probabilistic approach (based on Monte-Carlo simulations) implemented in SLOPE/W was used. These Monte-Carlo simulations generate various scenarios and apply statistical techniques to identify the likelihood of the slope's stability.

In the following sub-sections, a group of preliminary results is first presented to help provide a better understanding of the input parameters of Monte-Carlo simulations. This section is followed by a presentation of the main results used to evaluate the influence of different factors through probabilistic analyses, including the pile geometry and properties of the waste rock.

6.2 Methodology

The numerical simulations were used to evaluate the uncertainty of waste rock piles stability, using the probabilistic analyses implemented in SLOPE/W.

As described in section 2-4-3, a probabilistic analysis may cover different types of uncertainties such as geotechnical strength parameters, hydrological characteristics, and geometric conditions (Li and Lumb, 1987).

Figure 6-1 presents a framework for the probabilistic analyses presented in this Chapter. The application of the probabilistic analysis to evaluate the mean factor of safety ($\overline{FS}$), reliability index (RI) and the probability of failure (PoF), may involve uncertainty in the values of internal friction angle (ϕ), apparent cohesion (c_{app}), groundwater level (z_w) and layer thickness (L_t).
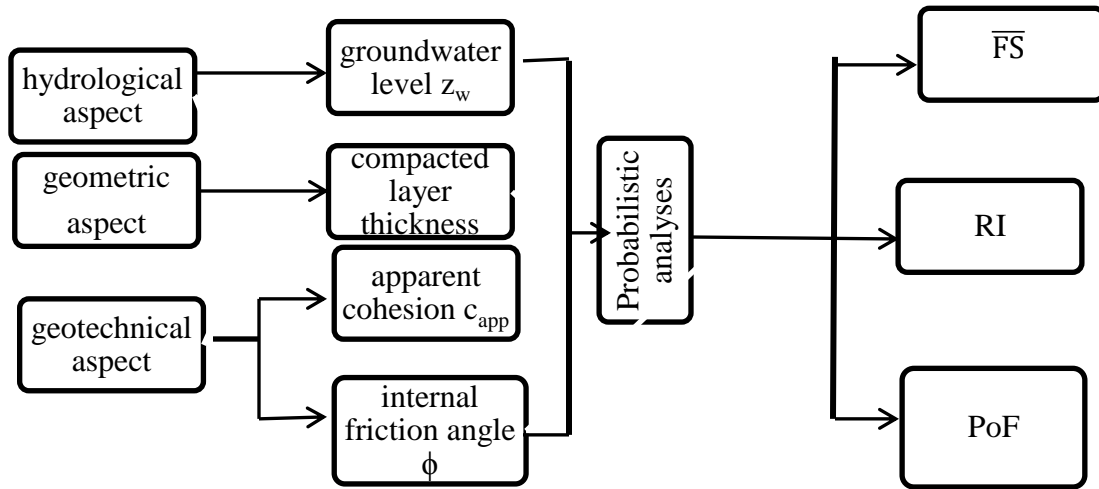
Figure 6-1: Flow chart of the framework used for probabilistic analyses

The geometry and initial boundary conditions are first defined with SIGMA/W (GeoSlope International Ltd, 2008) to evaluate the stress state in a pile. The code SLOPE/W (Geoslope International Ltd; Krahn, 2007c) is then used to analyze the slope stability with *finite element stress-based* method. Monte-Carlo simulations were used to conduct probabilistic analyses considering a normal distribution of geotechnical properties of the waste rock along the failure plane. The corresponding results for the critical slip surface(s) include the mean factor of safety ($\overline{FS}$), reliability index (RI), and the probability of failure (PoF).

Several cases are included in the numerical analyses which will be described later. As mentioned before (section 4-3), three different materials have been considered in the conceptual models of waste rock piles: a coarse waste rock, a compacted fine waste rock, and silty sand for the foundation. The hydraulic properties of these materials are given in Table 4-1 and Figures 4-1 and 4-2. These geotechnical properties are listed in Table 4-3. In SLOPE/W, the internal friction angle (ϕ') can have a normal distribution instead of a single value (see section 6.4.1 for details). In some cases, a normal distribution is applied for the total cohesion values (i.e. $C = c' + c_{app}$, for suction equals to zero, i.e. $c_{app} = 0$; see Section 6.5.1 for details). The initial conditions used with SIGMA/W were presented in Sections 4-5 and 4-6.

6.3 Shapes and positions of typical slip surface

The results presented in this chapter can be grouped according to five different circular slip surface locations. Figure 6-2 presents the typical forms of these slip surfaces in this section. Figure 6-2 (a) and 6-2 (e) present two extreme cases with local (depth ≤ 50% H_t) and a global (H_t, through the toe) slip surfaces. Figure 6-2 (b), (c) and (d) represent slip surfaces involving approximately 60%, 70% and 90% of pile height (H_t) respectively. The slip surface can start from any point on the crest and exit at a specific point that can be located at 60%, 70%, 90% or 100% of H_t).
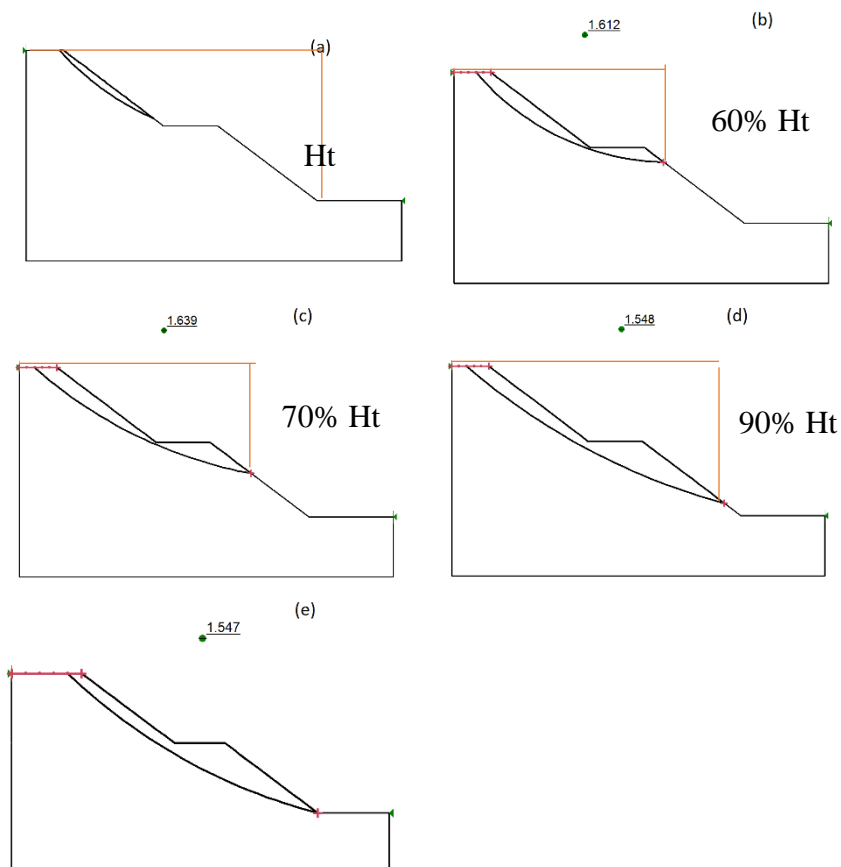
Figure 6-2: Various slip surfaces for a two bench pile (Group 2); a) local slip surface involving ≤ 50% H_t); b) slip surface involving 60% H_t; c) slip surface involving 70% H_t; d) slip surface involving 90% H_t; e) global slip surface, 100% H_t through the toe

6.4 Preliminary results from probabilistic parametric studies

Some initial results are first presented to illustrate the effect of input parameters on the results obtained with a probabilistic stability analysis of waste rock piles (using the Monte-Carlo method implemented in SLOPE/W see details in section 2-4-3).

6.4.1 Probability density function of geotechnical properties

Generating a probabilistic analysis of slope stability includes sampling the strength properties. The most commonly used probability density function is a normal distribution defined by two indices, i.e. the mean value and standard deviation.

Figure 6-3 (a) presents the selected probability density function (normal distribution) for the internal friction angle (ϕ') for loose and dense waste rock with COV 10%, and 15% (see section 2-4-3). The distributions are represented by a plot of the value of the friction angle on the X-axis and the likelihood of occurrence of that value on the Y axis. It is seen that a higher COV corresponds to a higher standard deviation (wider distribution) and a lower probability of occurrence. For example, for $\phi' = 37°$, increasing the COV from 10% to 15% increases the standard deviation from 3.7° to 5.55° and decreases the probability of occurrence 10% to 7% for loose waste rock.

Figure 6-3 (b) shows the sampling function for coarse and fine waste rock material with COV 10% and 15%. It can be observed that for a higher COV%, the sampling number is greater for random numbers between 0.5 and 1, while it is lower for random numbers between 0 and 0.5 (generating sample numbers at random from any probability distribution given its cumulative distribution function).

SLOPE/W integrates the area under the probability density function to establish a cumulative distribution function which is inverted to form an inverse distribution function (or a percent point function). The inverse distribution function is called a sampling function in SLOPE/W. The X-axis covers the range of possible random numbers. Each time a random number is obtained, the parameter is "sampled" using this function.

Figure 6-3 (c) and (d) shows the normal distribution of unit weight (γ) for COV 10% and its sampling function, respectively.
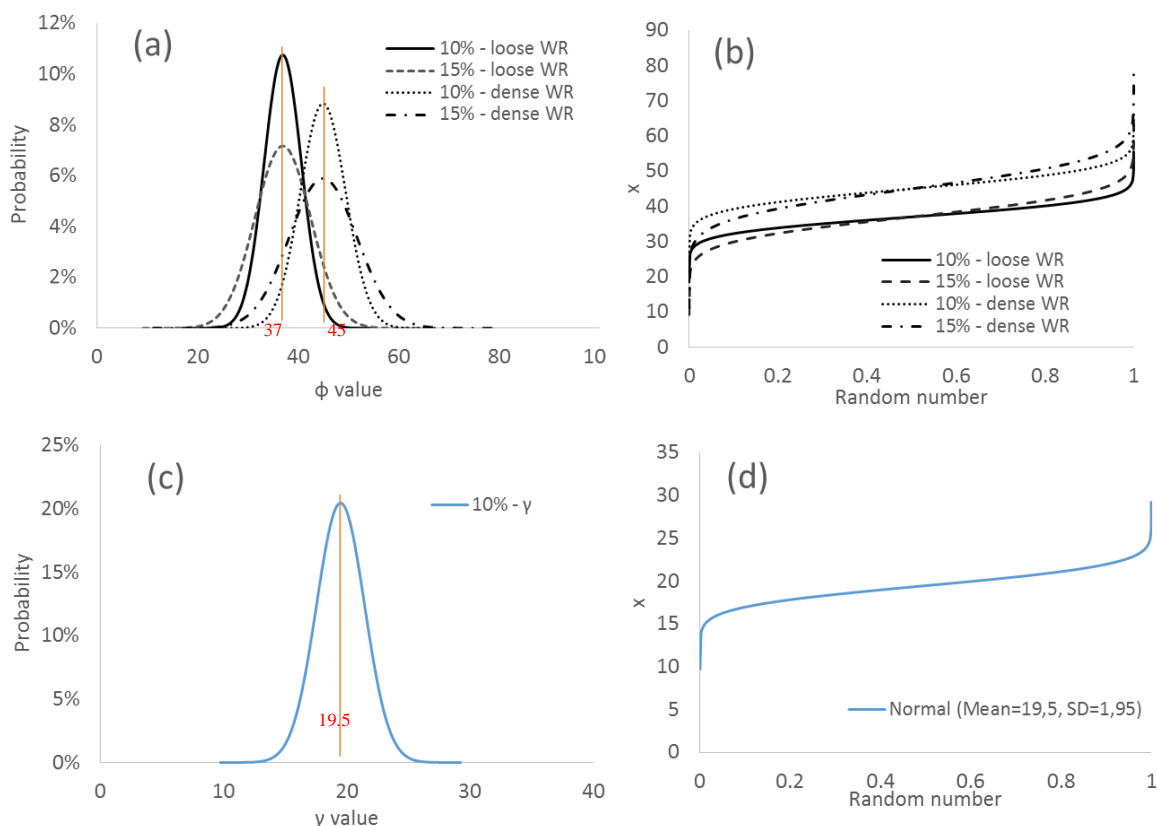
Figure 6-3: a) Probability density function for φ' (loose and compacted waste rock, COV 10% and 15%); b) Sampling function for φ' (loose and compacted waste rock, COV 10% and 15%); c) Probability density function for γ (loose and dense waste rock, COV 10%); d) Sampling function for γ (loose and dense waste rock, COV 10%)

Table 6-1 presents the values for the mean and standard deviation for the unit weight and cohesion of loose and dense waste rock materials. COV 10% and 15% are selected (see section 2-4-33). The mean internal friction angles (φ') are 37° and 45° for loose and dense waste rock, respectively; the unit weight is 19.5 kN/m³ for loose and dense waste rock (later in this section it is shown that unit weight is not a significant factor in the probabilistic analysis). The c_{app} (due to suction) is not presented in a normal distribution (because of the SIGMA/W limitations). For this

reason, some additional results are presented with total cohesion (with zero suction) in a normal distribution (e.g. 5, 10 and 15 kPa instead of c_{app}).

Table 6-1: Mean and standard deviation values for ϕ' and γ and c

Waste rock	Parameter	Mean	COV 10% Standard deviation	COV 15% Standard deviation
Loose	ϕ' (°)	37	3.7	5.55
	γ (kN/m³)	19.5	1.95	-
Dense	ϕ' (°)	45	4.5	6.75
	γ (kN/m³)	19.5	1.95	-
Loose and dense	c' (kPa)	5	-	0.75
		10	-	1.5
		15	-	2.25

A sensitivity analysis was conducted to evaluate the effect of using a probability density function for ϕ' and γ on the probabilistic stability analysis of waste rock pile. The results related to Case S11 are presented here (other results in Appendix C). For each slip surface, two probabilistic analyses were conducted; the first involves the normal distribution of ϕ' and the second, involves a normal distribution for both ϕ' and γ. Table 6-2 gives the results obtained for two locations of the slip surface corresponding to Figure 6-2 (a) local and (e) global. It can be observed that addition of unit weight probability distribution does not cause significant changes to the values of the $\overline{FS}$, RI and PoF for both slips surfaces. The impact of COV of γ on PoF for the global slip surface, rounded to 6 decimal, is not visible (see Table 6-2).

Table 6-2: Results obtained with Monte-Carlo slope stability analyses, using a COV 10% for ϕ', or ϕ' and γ values; Case S11 (Chapter 4, Table 4-4), local and global slip surfaces

Slip Surface	COV (%)	$\overline{FS}$	RI	PoF
Local	(ϕ')	1.19	1.61	4.5
	(ϕ') & (γ)	1.18	1.62	4.4
Global	(ϕ')	1.56	5.73	0.00
	(ϕ') & (γ)	1.56	5.74	0.00

Figure 6-4 presents the distribution of FS related to the probability analysis for Case S11, considering the local and global slip surfaces with the normal distribution of ϕ' or ϕ' and γ. Since

the variability of the friction angle and unit weight is normally distributed, the probability density function of FS is also normally distributed. It is observed that using a normal distribution for the unit weight has no significant influence on the normal distribution of FS. Figure 6-4 (a) shows that the normal distribution of local FS is similar for both cases; regardless of unit weight distribution (normal distribution or single value). A similar trend is seen for the global slip surface with mean FS = 1.6

Other researchers have also shown that the uncertainty in the unit weight does not have a significant impact on FS compared to strength parameters (Matsuo and KURODA, 1974; Alonso, 1976; El-Ramly, 2001). Thus, the probabilistic distribution of the unit weight will not be considered in the rest of this study.
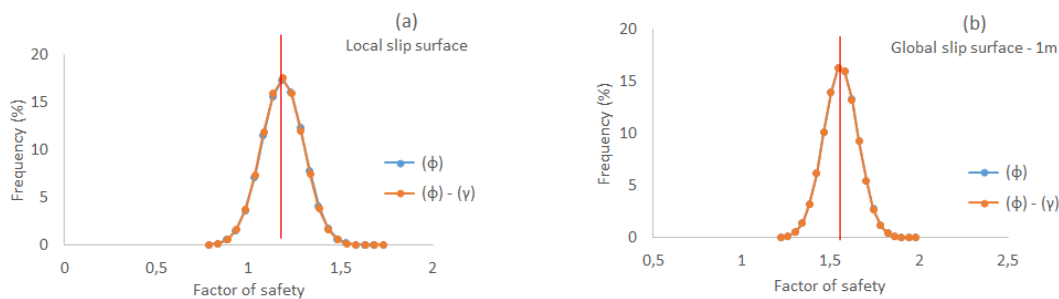
Figure 6-4: Normal distribution of the factor of safety for COV% = 10 (ϕ', ϕ' and γ), Case S11 (see Tables 4-4 and 4-5), for sampling distance = 8 m; a) local slip surface (see Figure 6.2 (a)); b) global slip surface (Figure 6.2 (b))

6.4.2 Spatial variability for different sampling distances

SLOPE/W is based on the limit equilibrium method of slices. As stated in section 2-4-3-2. The spatial variability defined at the mid-point of each slice is used for calculating the probabilistic factor of safety. Probabilistic stability analyses were conducted for different sampling distances.

Figure 6-5 presents the results related to Cases S11 and S21 (Tables 4-4 and 4-5); with both local and global slip surfaces. The normal distribution of FS is evaluated for COV 10% on ϕ' with a uniform suction 6 kPa (representing c_{app} = 1 kPa). Different sampling distances (SD, used to define the spatial variability in SLOPE/W, see section 2.4.3.1) have been considered. The simulated cases include a different random numbers for the SD : i.e. no spatial variation (no

sampling distance), 1, 3, 5, 8, 12, and 15 m, and also one sampling per slice. The results indicate that an increase of the sampling distance results in an increase of the variance of normal distribution. It is also seen (Fig. 6-5) that the lowest standard deviation is linked to the one sampling per slice, and the highest standard deviation is obtained when there is no spatial variation (no sampling distance).

The $\overline{FS}$ value is not influenced significantly by sampling distance for local slip surface; in global slip surface the no spatial variability presents the higher frequency of occurrence (Figure 6-5 (a), (c) and (b), (d)). It is also observed that the sampling distances between 3 m to 12 m have the most effect on the spatial variability analyses; other sampling distances are close to either case sample per slice or no spatial variation.
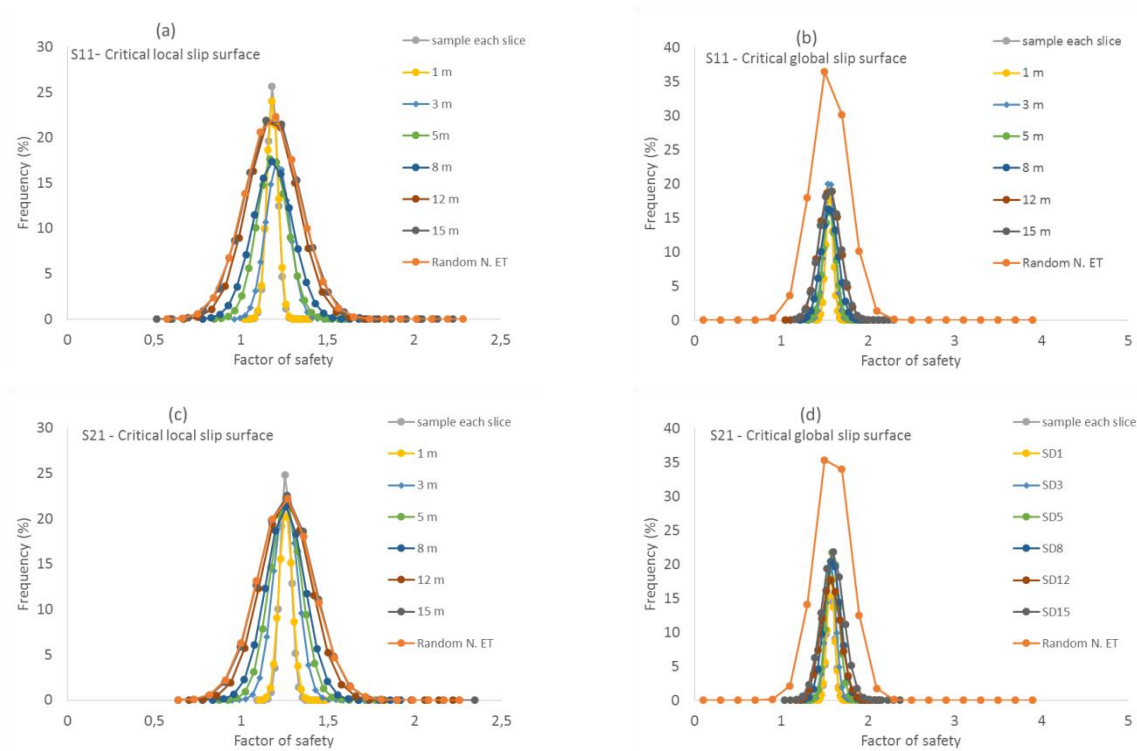
Figure 6-5: Normal distribution of FS obtained with Monte-Carlo simulations (SLOPE/W), COV = 10% on ϕ', c_{app} = 1 kPa; sampling distances (SD): 1 m, 3 m, 5 m, 8 m, 12 m, 15 m, per slice and random number each time a) critical local slip surface, Case S11 (two bench pile); b) critical global slip surface, Case S11; c) critical local slip surface, Case S21 (two benches with compacted layers); d) critical global slip surface for Case S21

Figure 6-6 summarizes the outputs of the probabilistic analyses, $\overline{FS}$, RI and PoF, for Cases S11 and S21, for both local and global slip surfaces. It is observed that $\overline{FS}$ has no significant changes when sampling distance increases from sample per slice (approximately 30 slices) to approximately 10 m and then it show some changes. It is also observed that for local slip surface, the PoF increases as the sampling distance increases, the highest PoF occurs when there is no spatial variability (Figure 6-6 (e)), for global slip surface the PoF has values very small close to zero (not shown here).

It is observed for both Cases S11 and S12 the RI decreases for local and global slip surfaces (i.e. decreasing from 13 to 3 for global slip surface Case S11). When the sampling distance increases, a more unstable waste rock pile is observed (with the decrease of RI below 3; Figure 6-6 (f)). The lowest RI corresponds to the highest PoF which presents the no spatial variability sampling distance case.
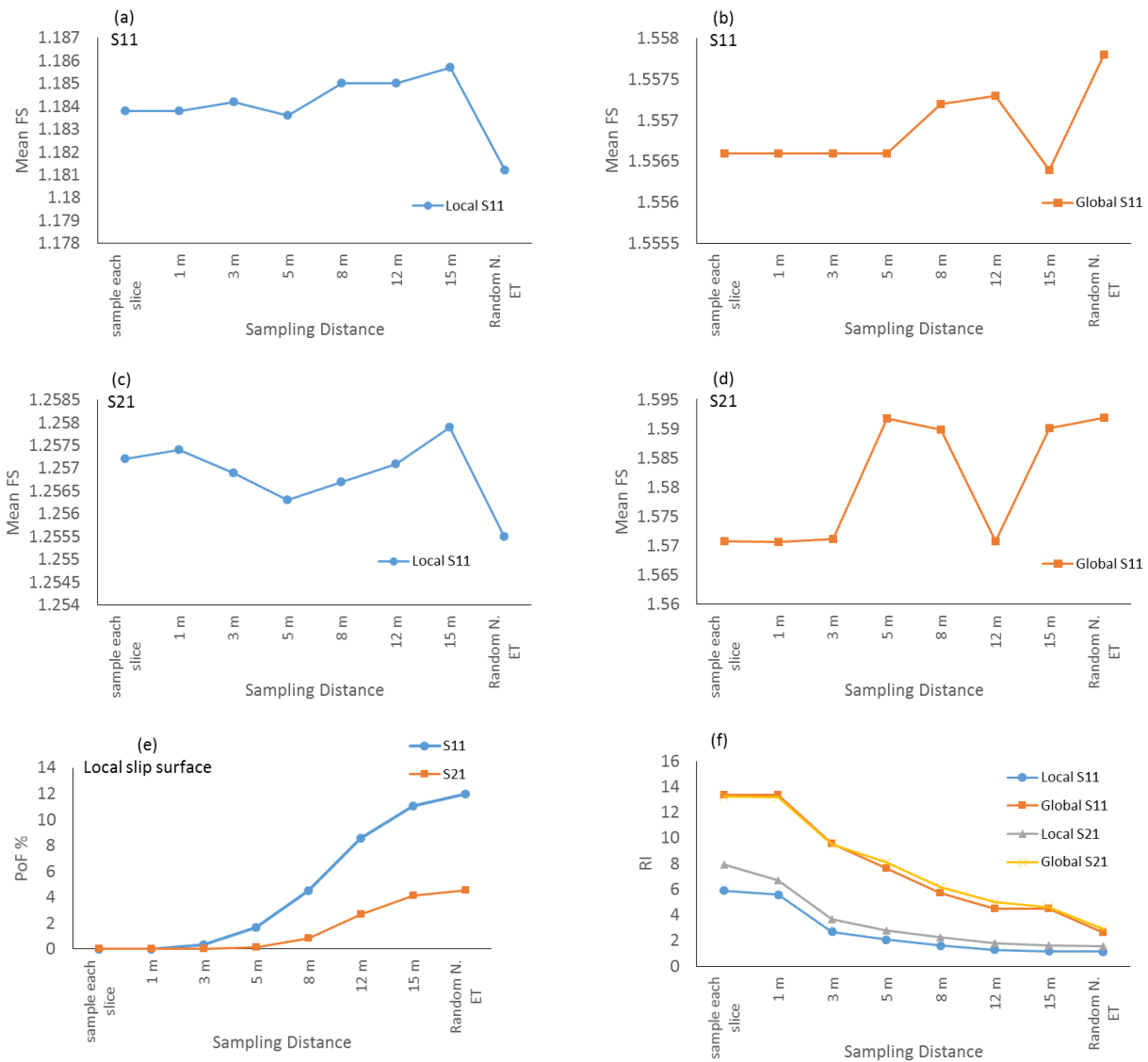
Figure 6-6: $\overline{FS}$, RI and PoF distribution for different sampling distance (sampling once; 1, 3, 5, 8, 12 and 15m; sampling per slice), COV 10%, obtained with SLOPE/W; a) $\overline{FS}$ for local slip surface, Case S11; b) $\overline{FS}$ for global slip surface, Case S11; c) $\overline{FS}$ for local slip surface, Case S21; d) $\overline{FS}$ global slip surface Case S21; e) PoF for local slip surfaces, Cases S11 and S21; f) RI for local and global slip surfaces, Cases S11 and S21

These results indicate that the sampling distance has more significant effects on PoF and RI rather than $\overline{FS}$. It is important to select an appropriate sampling distance; hence, a detailed understanding of the material and statistical characteristics is required using sufficient data.

In this study, the size of the waste rock pile is changing for different cases (H_t =20 m to H_t = 120 m). It was decided to consider a sampling distance expressed as a ratio of total height (H_t) of the waste rock pile. For Cases S11 and S21 (H_t = 20 m), a sampling distance of 10 m (=½ H_t) seems appropriate based on the distribution presented in Figure 6-6. A sampling distance of ½ H_t is also considered for the other cases.

6.4.3 **Effect of the COV**

Based on the values given in section 2-4-3-3, values COV equal to 10% and 15% is considered for the variation of ϕ'. A sensitivity analysis is conducted for these two values (10% and 15%) to see their effect on the FS normal distribution obtained with the Monte-Carlo simulations with SLOPE/W. Figure 6-7 (a), (b), (c) and (d) present the results for Group 1 (Cases S1, S2, S3, and S4, Tables 4-4 and 4-5). The distribution of FS is related to the slip surface that approximately involves 60% H_t; the sampling distance is 1/2 H_t.

It shows a larger COV (15%) gives a distribution of factor of safety with a larger standard deviation (a larger dispersion), resulting in more factor of safety ≤ 1. However, the changes in $\overline{FS}$ is not very significant when going from COV= 10% to COV = 15%. For a given factor of safety, the frequency (%) of occurrence increases with a larger COV.

Figure 6-7: Normal distribution of FS for slip surface involving 60% H_t obtained with Monte-Carlo method of SLOPE/W for different COV (10%, 15%); a) Case S1; b) Case S2; c) Case S3; d) Case S4

Figure 6-8 presents the $\overline{FS}$ (a), RI (b), and PoF (c) and the standard deviation SD (d) obtained from the Monte-Carlo method with SLOPE/W for Group 1 (Cases S1, S2, S3, S4, see Tables 4-4 and 4-5), for COV 10% and 15% (ϕ') and slip surface involving 60% H_t.

It indicates that $\overline{FS}$ does not change much, while the PoF and standard deviation are higher for COV = 15% compared to COV = 10% for all cases. Figure 6-8 (b) shows a reduction of the RI for COV = 15% compared to COV = 10%. That indicates a lower COV results in a higher RI and a lower PoF. It is observed for these cases the RI value for COV 15% is below 3; this is below average performance (see section 2-4-3-4), for COV 10%, except Case S1, other cases show a performance below the average level.
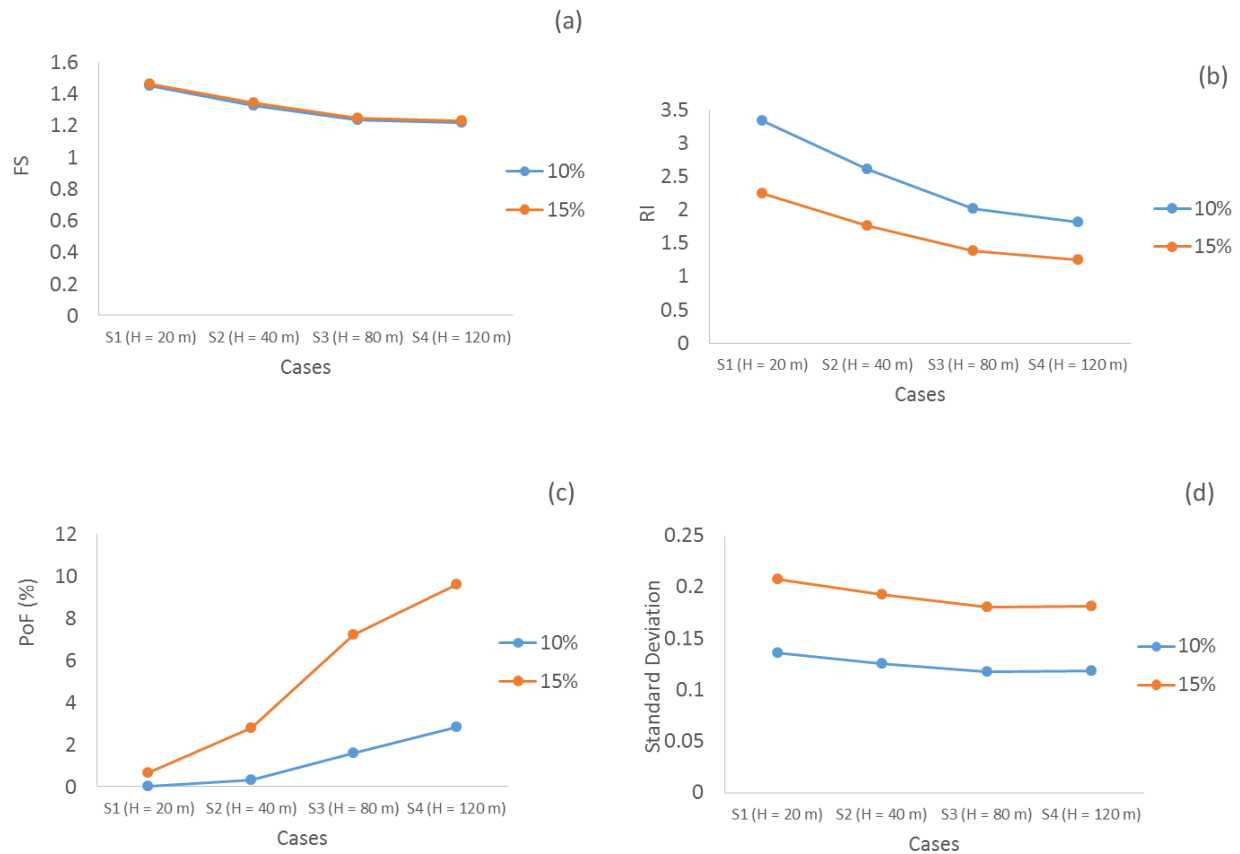
Figure 6-8: Effect of COV% (10%, 15%) on $\overline{FS}$, RI, PoF and Standard deviation for a slip surface involving 60% H_t, obtained with Monte-Carlo method (SLOPE/W), Group 1 (Cases S1, S2, S3, and S4); a) $\overline{FS}$; b) RI; c) PoF (%); d) Standard deviation

Figure 6-9 presents the $\overline{FS}$ (a), RI (b), PoF (c) and the Standard deviation (d) related to Monte-Carlo with SLOPE/W for Group 2 (Cases S11, S12, S13, S14) for COV 10% and 15% (ϕ') and slip surface involving 60% H_t.

It is seen that the $\overline{FS}$ is slightly higher for COV 15%, whereas there is a reduction in the RI for COV 15% compared to 10% (b). The PoF increases slightly for COV 15%, and the same trend is observed for a standard deviation (d) (however, the impact of this increase on the PoF rounded to 6 decimal points is not visible, as shown in Figure 6-5 (c) for Cases S11 and S12).

A similar trend is seen for both Groups 1 and 2 due to the variation of COV%. A higher coefficient of variation (ϕ') usually results in lower RI (less stable waste rock piles).
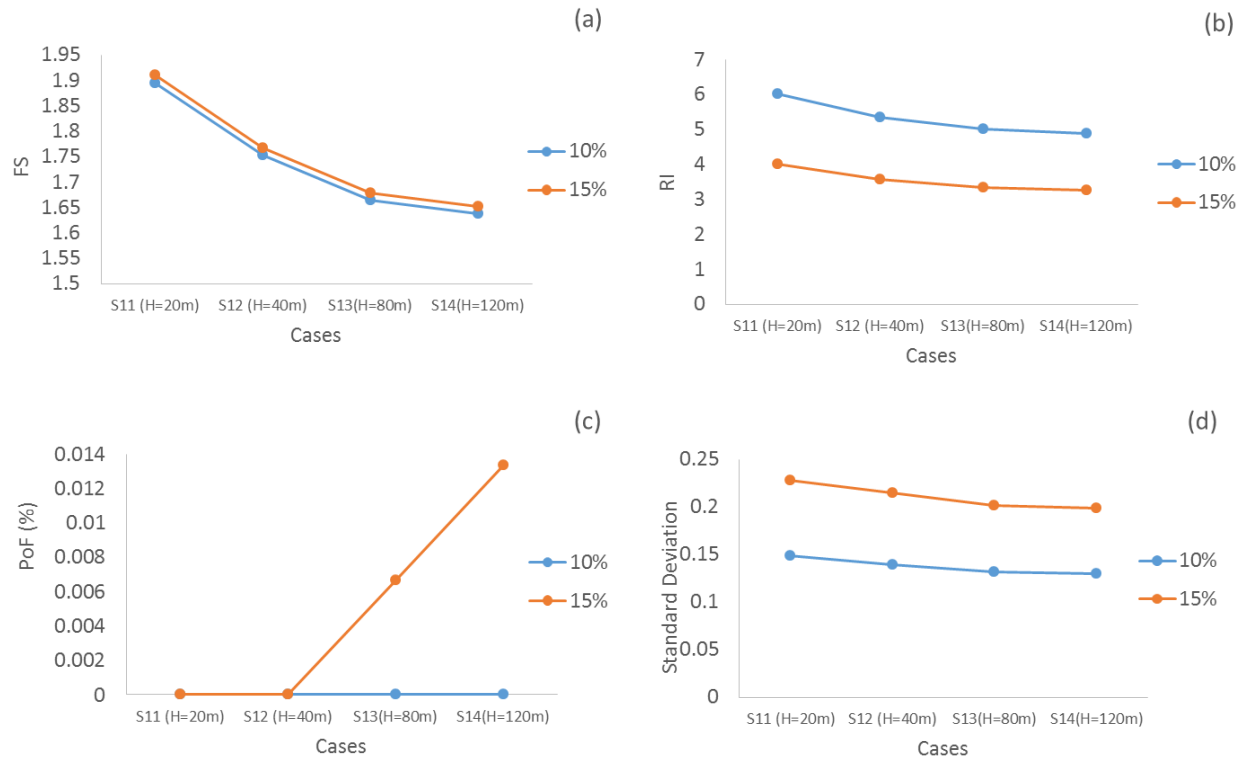
Figure 6-9: Effect of COV% (10%, 15%) on $\overline{FS}$, RI, PoF and Standard deviation for a slip surface involving 60% H_t, obtained with Monte-Carlo (SLOPE/W), Group 2 (Cases S11, S12, S13, and S14); a) $\overline{FS}$; b) RI; c) PoF (%); d) Standard deviation

6.4.4 **Number of iterations for Monte-Carlo method**

A practical method for determining the optimum number of iterations for Monte-Carlo simulations is to run the calculations a few times with similar variable values (i.e. ϕ') and increase the number of iterations. The output can then be plotted versus the iterations number which can be used to evaluate the optimal iteration number. The optimum number of iterations can be defined as the minimum number of iterations where the output quantity is stable.

The parametric study conducted for this purpose and the results related to Case S21 (which represents a relatively typical waste rock pile) are presented here.

Figure 6-10 presents the normal distribution of the factor of safety for Case S21 with COV = 10% and 15% (ϕ'). Sampling distance is 8 m, slip surfaces involve 60% H_t (see Figure 6-6 (a) and (b)), and five different iterations number (2000, 5000, 10000, 15000 and 20000, for Monte-Carlo method) resulted in the below normal distribution of FS. It shows the normal distribution of FS is not very sensitive to the number of iterations of Monte-Carlo method.
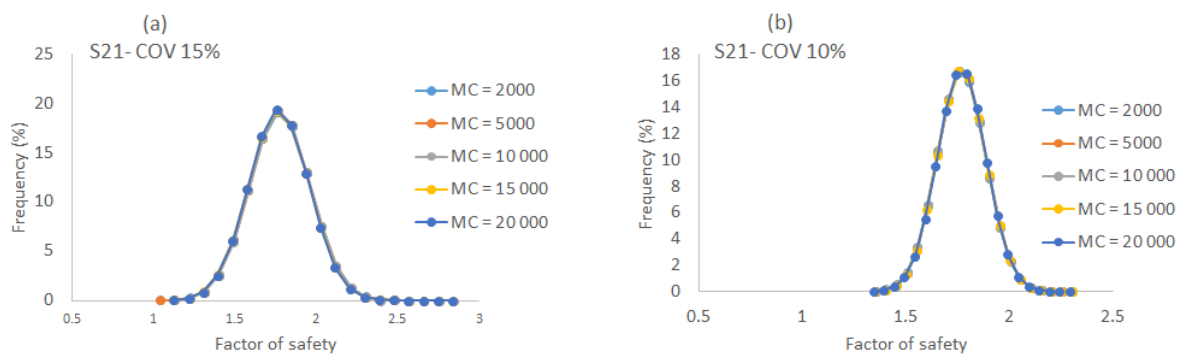
Figure 6-10: Normal distribution of FS based on different iterations numbers, Case S21, slip surface involving 60% H_t; a) COV 15%; b) COV 10%

Figure 6-11 presents the output values related to the probabilistic stability analyses of Case S21. As demonstrated the RI and standard deviation do not show significant changes due to the number of iteration (See Figure 6-11 (b) and (c)). The $\overline{FS}$ changes due to the variation of some iteration which is not very significant. The maximum changes appear between iteration numbers 10 000 and 15 000.
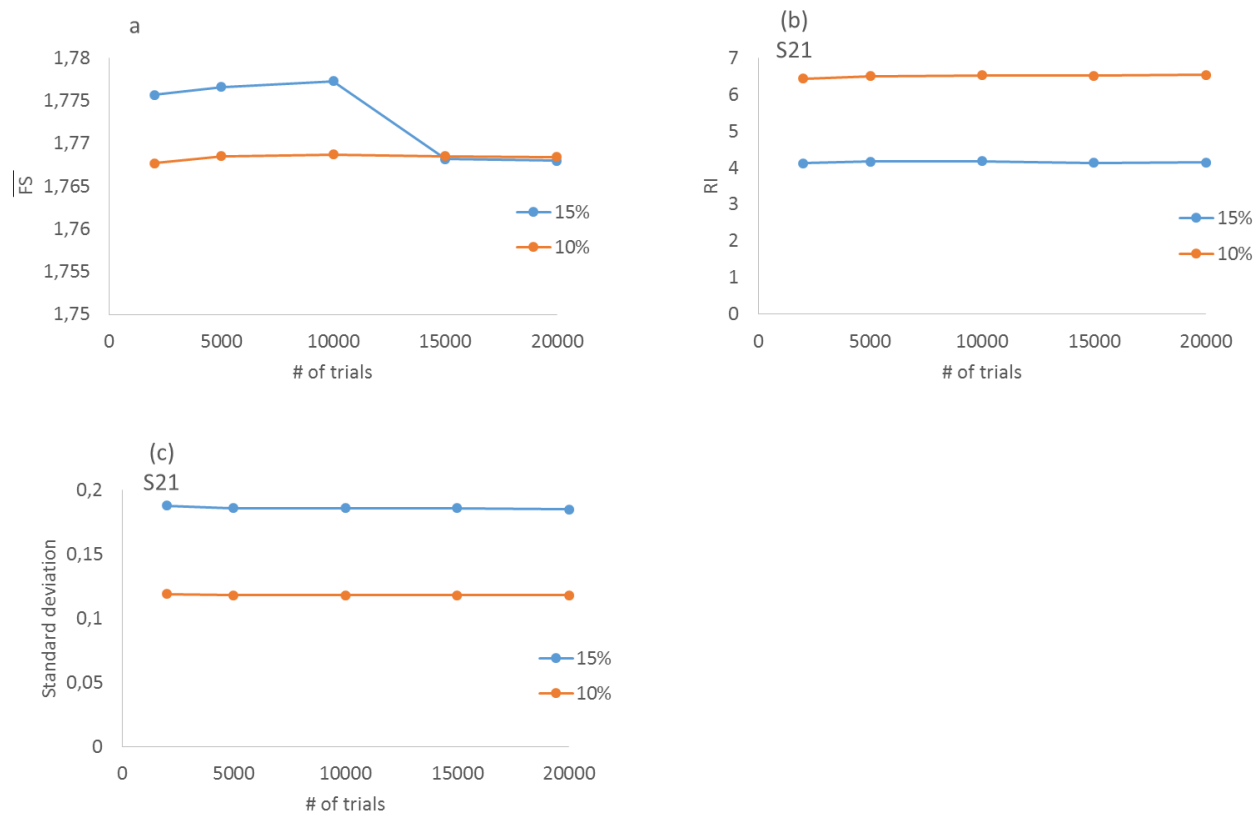
Figure 6-11: Distribution of $\overline{FS}$, RI and standard deviation due to different iteration numbers, obtained with Monte-Carlo method (SLOPE/W), slip surface involving 60%H_t, COV 10% and 15%; a) $\overline{FS}$; b) RI; c) Standard deviation

6.5 Selected results from probabilistic slope stability analyses

The stability analyses result presented in this section focus on slip surfaces in piles presented in Figure 6-2.

Detailed calculations are presented for various scenarios to assess the effect of the various parameters i.e. the apparent cohesion c_{app}, the number of benches, presence of compacted layers (e.g., horizontal, inclined, parallel to slope, layer thickness), groundwater level and rainfall.

The Monte-Carlo number of iterations is 15 000 with COV 10% or 15% (ϕ'). The spatial variability (sampling distance) is defined as a ratio to the pile height, 1/2 H_t (see section 6-.4-2).

6.5.1 **Relationship between FS, ф and apparent cohesion c_{app} and H_t**

Different calculations were conducted (with SIGMA/W and then SLOPE/W using the Monte-Carlo method) for Groups 1 (Cases S1, S2, S3 and S4), 2 (Cases S11, S12, S13 and S14) and 3 (Cases S15, S16 and S17) (see Tables 4-4 and 4-5).

The mean ϕ' is 37° for waste rock material; COV is 15% (ϕ'). Effective cohesion (c') is zero. Apparent cohesion (c_{app}) is presented in two forms: a) presented by its equivalent suction in SIGMA/W (single value, see details in section 4-6), b) presented as C (c'+c_{app}) with values 5, 10, and 25 kPa (normal distribution). The foundation material is waste rock. The critical slip surfaces and their related $\overline{FS}$, RI and PoF are evaluated with *FE stress-based* method.

6.5.1.1 **Normal distribution of ф' and single value of c_{app}**

Figure 6-12 (a, b, c and d) presents the normal distribution of FS related to a slip surface covering approximately 60% H_t for Groups 1 (Cases S1 and S2) and 2 (Cases S15 and S16) (see Tables 4-4 and 4-5 for details). c_{app} is presented by its equivalent suction in SIGMA/W.

The results indicate that when c_{app} increases, the FS with the highest probability of occurrence increases. As an example Figure, 6-12 (a) shows that FS (with the highest probability of occurrence) increases from 1.5 to 1.7 to 2.25 when the c_{app} increase from 5 to 10 to 15 kPa (Case S1).

These results also illustrate that the variation of highest probability of occurrence for FS due to the variation of c_{app} is more significant for smaller waste rock piles. As an example in Figure 6-12 (a) the highest probability of occurrence decreases from 37.8% to 33.9% to 26.8% for c_{app} increasing from 5 to 25 kPa, and it decreases from 21.05% to 20.5% to 19.6% in Figure 6-12 (d).
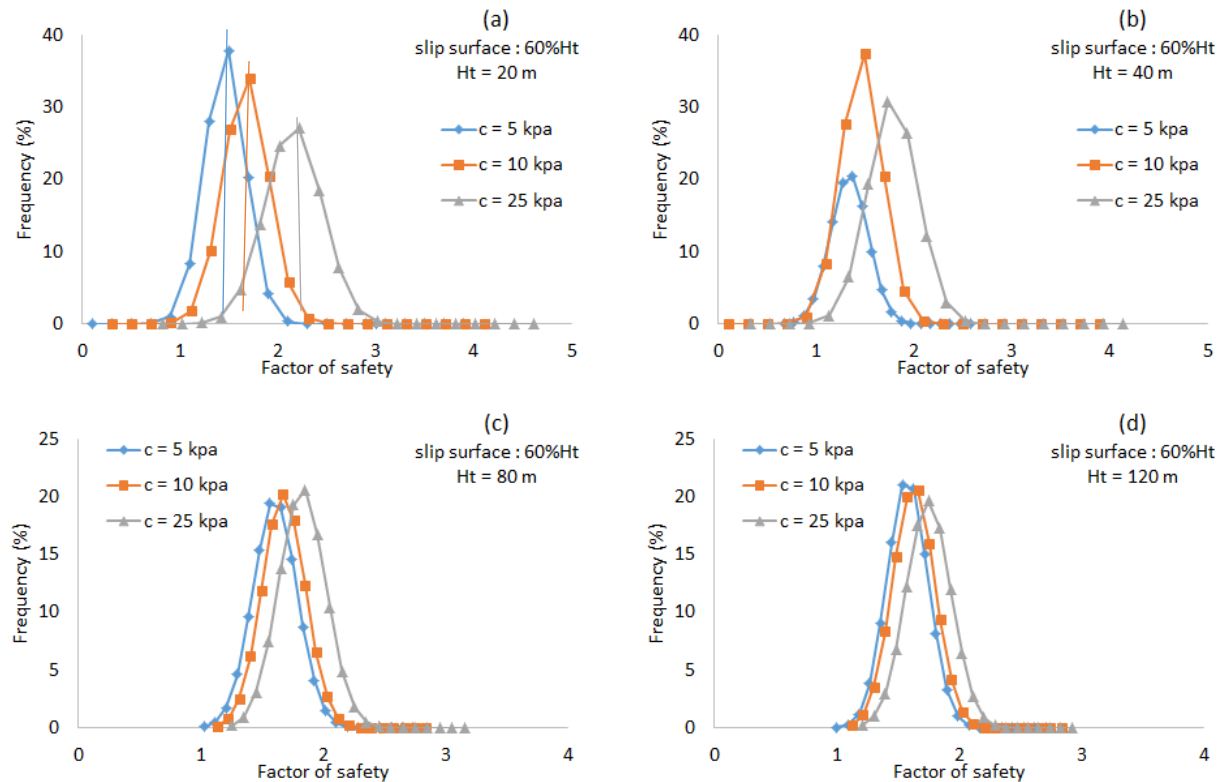
Figure 6-12: Distribution functions of FS produced with Monte-Carlo method, COV = 15% for selected slip surface involves 60% H_t; c_{app}= 5, 10 and 25 kPa, a) Case S1; b) Case S2; c) Case S15; d) Case S16 (see Tables 4-4 and 4-5 for details)

Figure 6-13 shows the normal distribution of FS for Group 1 (Cases S1, S2, S3, and S4) for slip surfaces involving 60%, 70%, and 90% H_t respectively.

Figure 6-13 (a) presents the slip surface for 60% H_t for Group 1 with three different values of c_{app} (= 5 kPa, 10 kPa, 25 kPa, imposed as suction). It shows that (as stated in section 4-5-7) $\overline{FS}$ tends to decrease when the height of the pile increases. As an example, $\overline{FS}$ decreases from 2.16 to 1.41 (for c_{app} = 25 kPa) when H_t increases from 20 m to 120 m (Case S1 to Case S4). It indicates that when the height of the pile increases the $\overline{FS}$ decreases even below target FS = 1.5.

Figure 6-13 (b) and (c) presents $\overline{FS}$ for slip surface 70% and 90% H_t. The trend for the $\overline{FS}$ is similar for different c_{app} (Group 1) with slip surface involving 60% H_t. A lower c_{app} also results in a lower $\overline{FS}$. As an example for Case S2, the $\overline{FS}$ decreases from 1.8 to 1.3 when c_{app} decrease from 25 kPa to 5 kPa (see Figure 6-13 (b)).
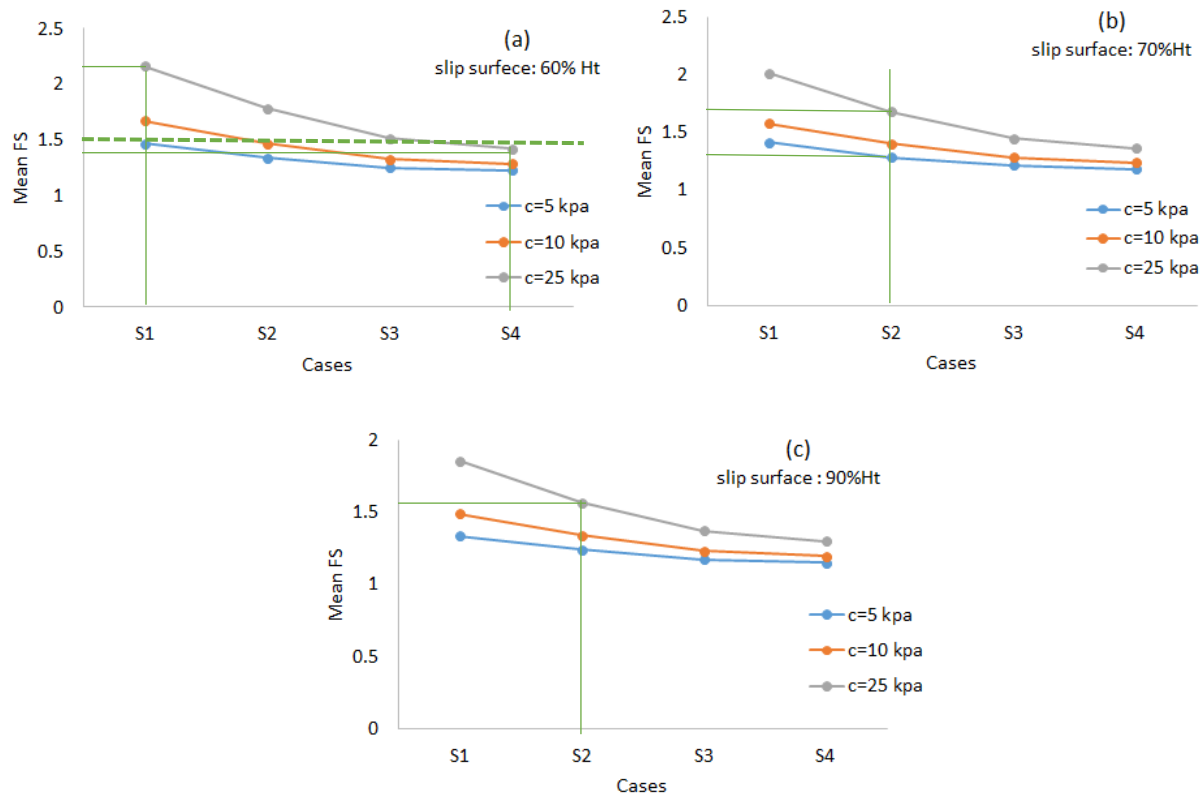
Figure 6-13: $\overline{\text{FS}}$ with Monte-Carlo method, COV = 15%, for different c_{app} (= 5, 10 and 25 kPa, imposed as suction), Group 1, a) slip surface involving 60% H_t; b) slip surface involving 70% H_t; c) slip surface involving 90% H_t

Figure 6-14 (a), (b) and (c) show the changes in RI due to variation of c_{app} and COV = 15% (ϕ') for the Monte-Carlo method with SLOPE/W for Group 1 (Cases S1, S2, S3, S4) for different slip surfaces (= 60%, 70% and 90% H_t). It was mentioned in section 2-4-3-4 that RI $\geq$ 3 represents an above average performance for structures like waste rock piles.

Results indicate that an increase in H_t results in a decrease in the RI. For instance, in Figure 6-14 (b), (for c_{app} = 10 kPa) an increase of H_t from 20 m to 120 m (Cases S1 to S4) decreases RI from 2.89 to 1.55. This trend is observed for all the cases.

The results show that the increase of c_{app} results in the increase of RI (Figure 6-14 (a), (b) and (c) respectively) that is more pronounced for smaller waste rock piles. For example, Figure 6-14 (c)

indicates that in Case S4, an increase of c_{app} from 5 kPa to 10 kPa to 25 kPa results in an increase in the RI from 1.07 to 1.38 to 1.96 for slip surfaces involving 90% H_t.

Comparison between Figures 6-13 and 6-14 indicate that $\overline{FS}$ and RI has a direct relationship, and they both decrease due to the increase of pile height and decrease of c_{app} value.
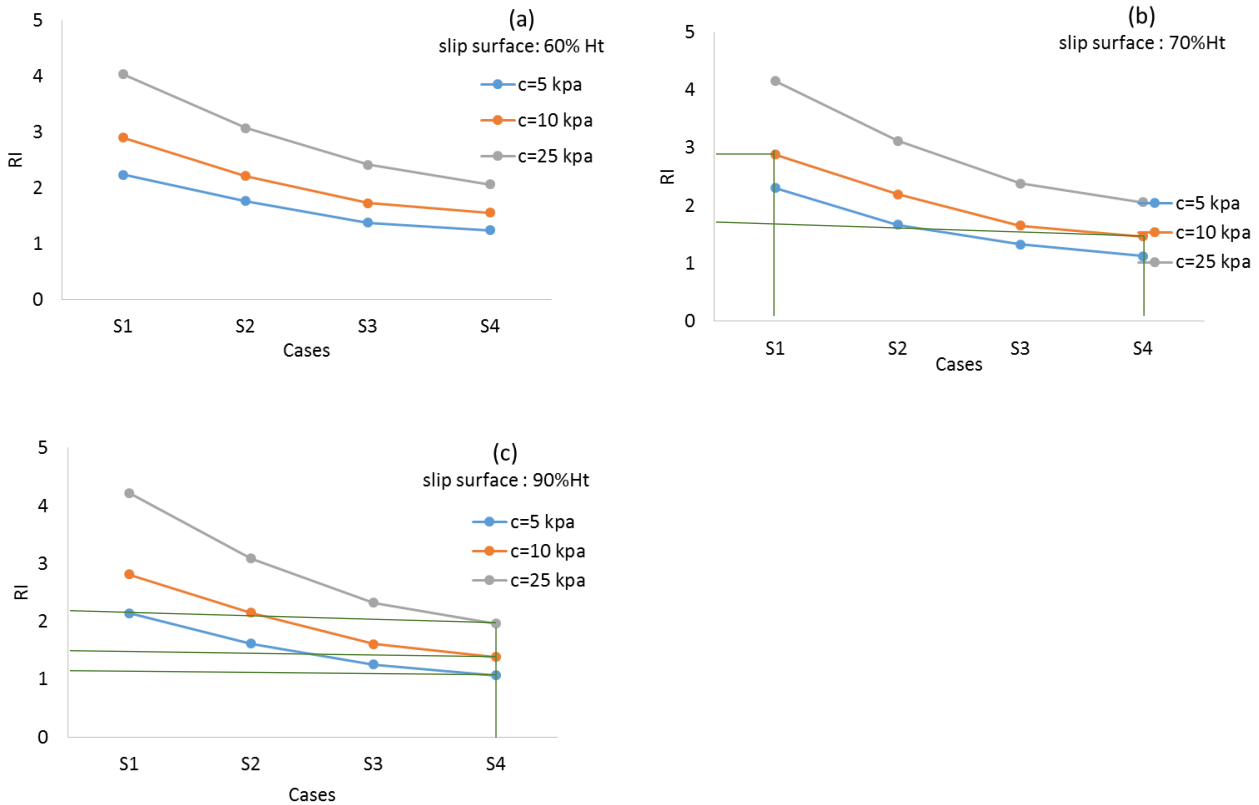
Figure 6-14: RI distribution for COV 15% (ϕ'), different c_{app} (= 5, 10 and 25 kPa), Group 1, a) slip surface involving 60% H_t; b) slip surface involving 70% H_t; c) slip surface involving 90% H_t

Figure 6-15 shows the relationship between PoF, $c_{app,}$ and H_t of waste rock piles for Group 1. The trend shows an increase in PoF due to an increase in H_t (Figure 6-15 (a), (b) and (c)). For instance, in Figure 6-15 (a) for c_{app} = 10 kPa, the PoF increases from nearly zero to 4.8 when H_t goes from 20 to 120 m (Case S1 to S4).

This figure also presents the trend for the PoF as a function of c_{app}. For instance, in Figure 6-15 (b) Case S3 shows that with c_{app} increases from 5 kPa to 10 kPa to 25 kPa, the PoF decreases from 8 to 3.7 to 0.5 for a slip surface involving 70% H_t.

Comparison between Figures 6-13, 6-14 and 6-15 indicate that the PoF has in inverse relationship to RI and $\overline{FS}$; decrease of $\overline{FS}$ and RI results in the increase of PoF.
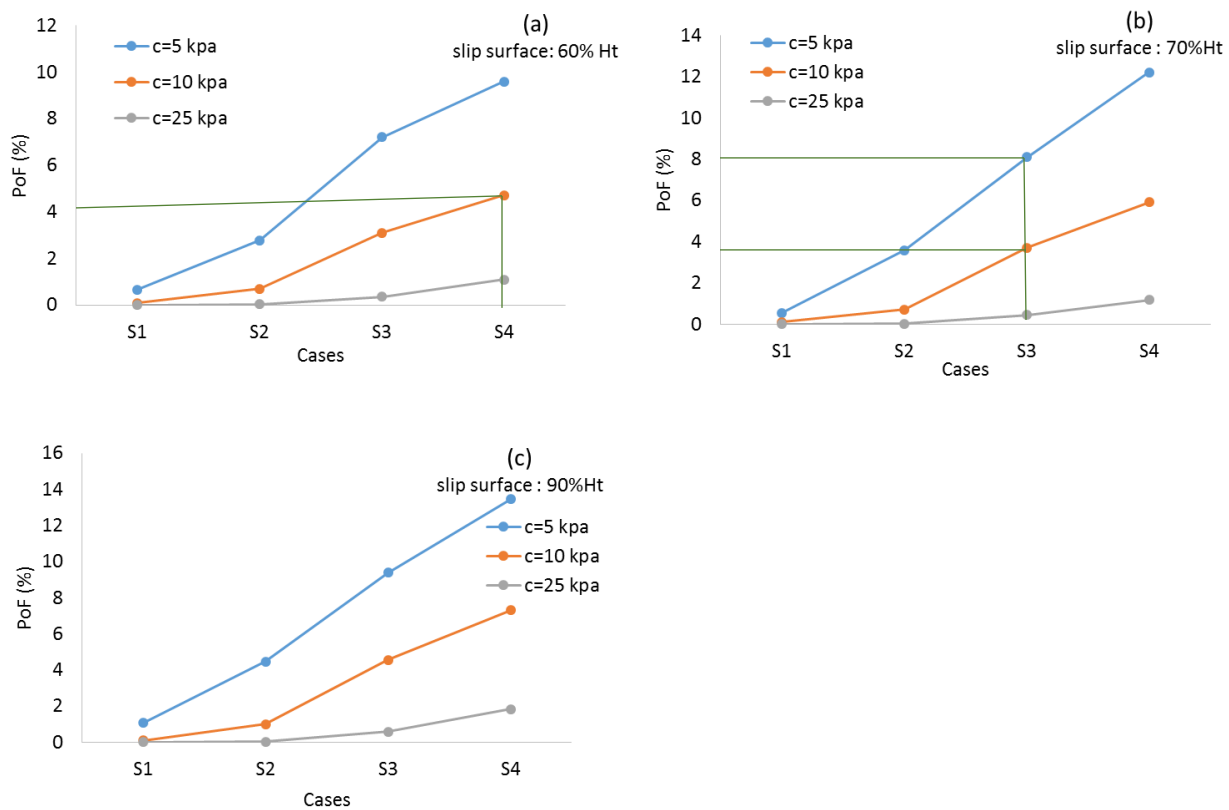
Figure 6-15: PoF (%) distribution for COV 15%, different c_{app} (= 5, 10 and 25 kPa), Group 1, a) slip surface involving 60% H_t; b) slip surface involving 70% H_t; c) slip surface involving 90% H_t

Figure 6-16 shows the variation of $\overline{FS}$ (related to normal distribution of factor of safety) for Group 2 (Cases S11, S12, S13, S14) and Group 3 (S15, S16, S17). Different c_{app} (= 5 kPa, 10 kPa and 25 kPa); with COV = 15% (ϕ', sampling distance ½ H_t) is also applied.

The results are represented for the slip surfaces involving 60%, 70% and 90% H_t (see Figure 6-16 (a), (b), (c), (d), (e), (f), (g) and (h)).

Results in Figure 6-16 (a), (c), (e) and (g) indicate that, increasing c_{app} results in an increase in the $\overline{FS}$, this trend is more pronounced for smaller waste rock piles; as an example, for Case S12, $\overline{FS}$ increases from 1.8 to 2.5 where c_{app} changes from 5 to 25 kPa (Figure 6-16 (a)).

For a given c_{app} an increase of H_t results in a reduction in the $\overline{FS}$. For instance, for $c_{app} = 25$ kPa, H_t increase from 20 m to 120 m (going from S11 to S14) the $\overline{FS}$ decreases from 2.6 to 1.9 (Figure 6-16 (a)).

The results also indicate that increasing c_{app} results in an increase in the RI (see Figure 6-16 (b), (d), (f) and (h)). The increase of pile height results in the reduction of the RI. As an example, the value of the RI decreases from 5.7 to 4.5 when the pile height increases from 20 m (Case S11) and 120 m (Case S14), in Figure 6-16 (b) (for $c_{app} = 25$ kPa).

The values of $\overline{FS}$ and RI is also changing for different Groups of waste rock piles. Figures 6-16 (c), 6-16 (c) and 6-16 (g) are used for comparisons. For $c_{app} = 25$ kPa Cases S4, S14, and S17 present the $\overline{FS}$ 1.3, 1.7 and 1.8 respectively. This indicates $\overline{FS}$ increases due to the addition of benches in the pile (for a slip surface involves 90% Ht). Figure 6-16 (c), 6-16 (d) and (h) show that RI increased from 1.94 to 4 to 4.3 for Cases S4, S14 and S17 respectively ($c_{app} = 25$ kPa). It indicates the improvement of waste rock pile performance from poor to the above average by the addition of benches.
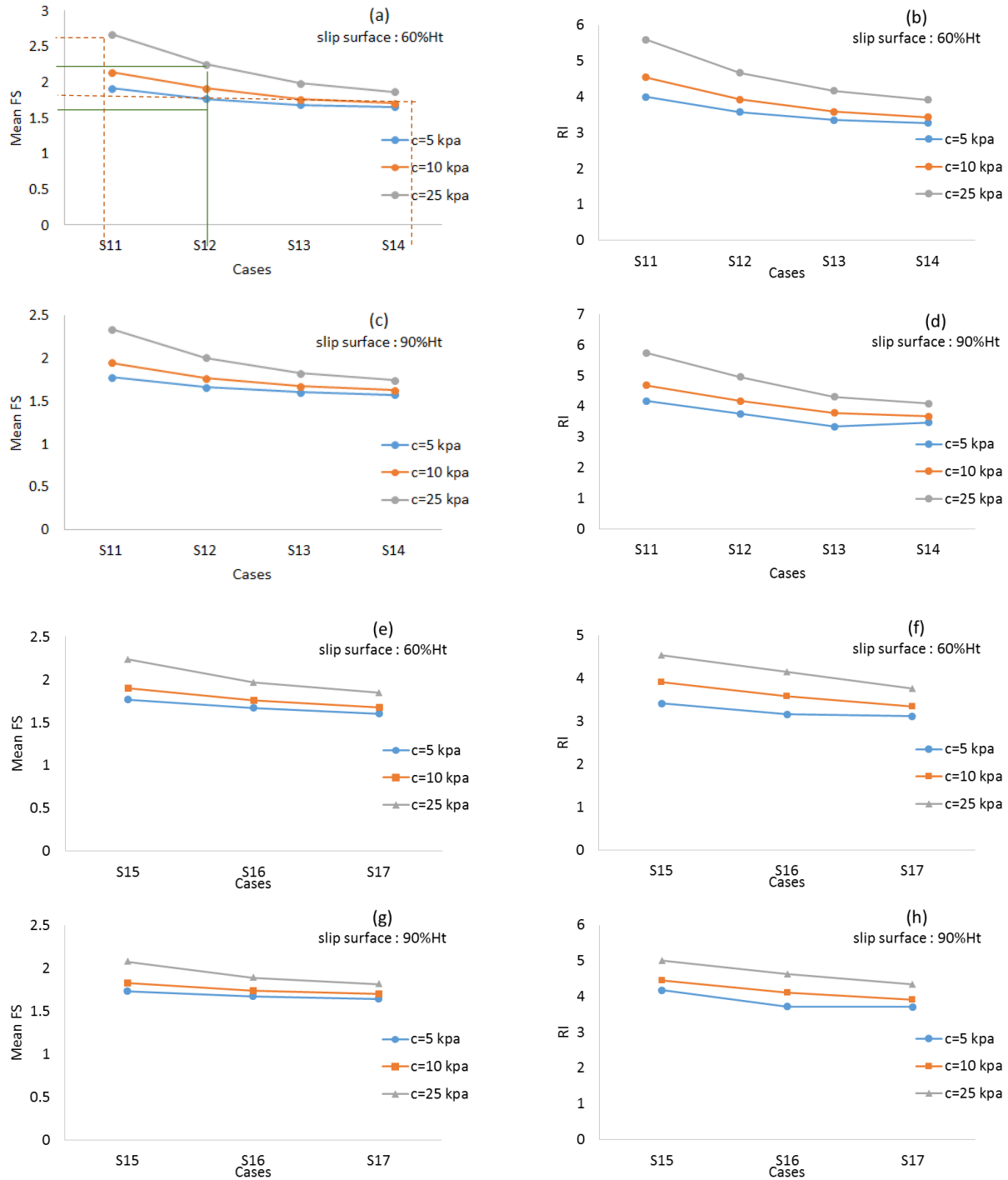
Figure 6-16: $\overline{FS}$ and RI distribution, COV 15% (ϕ'), different c_{app} (= 5, 10 and 25 kPa), for slip surfaces involving 60% and 90% H_t; a) $\overline{FS}$, Group 2 (Cases S11, S12, S13, S14, H_t 20, 40, 80, 120 m); b) RI, Group 2; c) $\overline{FS}$, Group 2; d) RI, Group 2; e) $\overline{FS}$, Group 3 (Cases S15, S16, S17, H_t 40, 80, 120 m; f) RI, Group 3; g) $\overline{FS}$, Group 3; h) RI, Group 3

6.5.1.2   Normal distribution for both ϕ' and c_{app}

It was shown (section 4-7-5) that FS of a pile largely depends on the c_{app}. SIGMA/W cannot perform normal distribution for input/output data (it only accepts a single value of properties such as cohesion). Additional calculations were conducted with SIGMA/W (and then SLOPE/W) for scenarios with zero suction in the waste rock pile and an imposed C (= c_{app}+ c'). In this case, the value of c_{app} (=c) can be represented by a normal distribution instead of using a single value. As mentioned in Section 4-6, the maximum (anticipated) c_{app} value should be lower than about 5 (to 10) kPa for waste rock, with an average realistic value closer to 1 or 2 kPa (for most waste rocks from hard rock mines). However, considering the potential existence of cohesion induced by cementation, and also our need to assess the trends and tendencies, a few unrealistically high values of cohesion have also been included in the analyses.

Figure 6-17 represents the normal distribution of FS obtained with Monte-Carlo method (SLOPE/W) for Group 2 (Cases S11, S12, S13, and S14, H_t = 20 m to 120 m) to investigate the effect of the probabilistic distribution of c_{app} and height of the waste rock pile. Effective internal friction angle ϕ' = 37° for waste rock, with COV = 15% (ϕ' and c). The results indicate that as C (= c'+c_{app}) increase $\overline{FS}$ increase. As an example Figure, 6-17 (a) shows that when c_{app} changes from 5 to 10 to 25 kPa (with some unrealistically high values for the apparent cohesion, as stated above and also in Section 4-6), $\overline{FS}$ changes from 2.03 to 2.27 to 2.5. It worth noting, in this case, the probability of occurrence for $\overline{FS}$ is changing from 19% to 35.5% when C goes from 5 to 15 kPa. It is observed for larger piles (Figure 6-17 (c) and (d)), the difference between the normal distribution of FS due to C values is less pronounced compared to smaller piles (Figure 6-17 (a) and (b)). However, in all cases, a higher C results in a higher $\overline{FS}$.
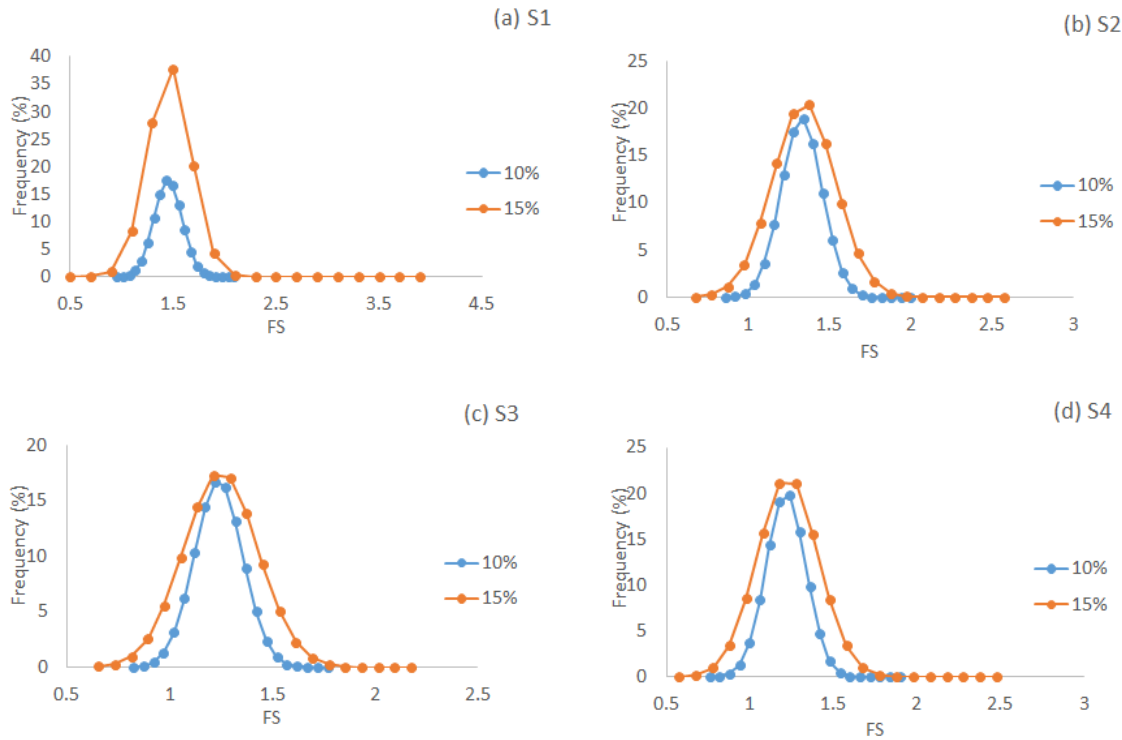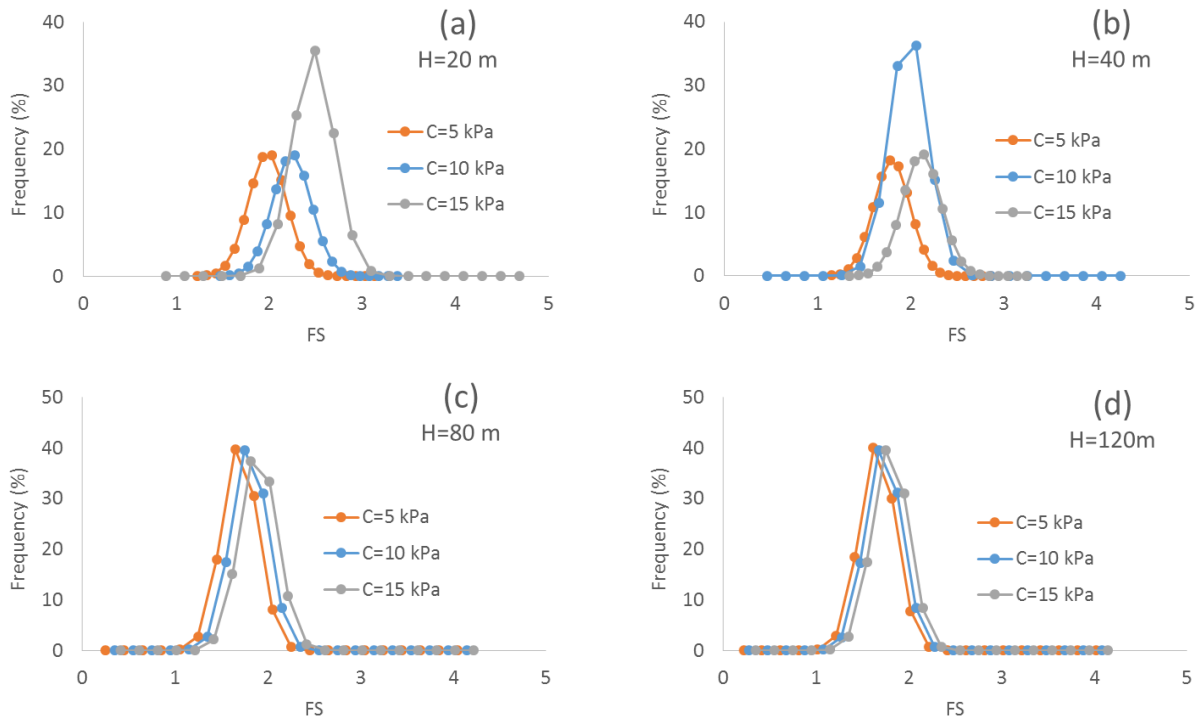
Figure 6-17: Normal distribution of FS for slip surface involving 60% H_t obtained with Monte-Carlo method (SLOPE/W), COV= 15%, C (=5, 10 and 15 kPa); a) Case S11; b) Case S12; c) Case S13; d) Case S14

Figure 6-18 presents $\overline{FS}$, RI and the PoF obtained with SLOPE/W for Group 2 (Cases S11, S12, S13, and S14, two benches pile, H_t= 20, 40, 80 and 120 m respectively). The COV = 15% (ϕ' and C), with a sampling distance ½ H_t. It is observed that $\overline{FS}$ for each case increases with the increase of C. As an example, for Case S11, increasing the C from 5 kPa to 15 kPa results in an increase of $\overline{FS}$ from 2 to 2.5 (Figure 6-18 (a)). RI also increases due to increase of C (Figure 6-18 (b)). As stated before, a larger RI means a lower PoF, which corresponds to the trend presented in Figure 6-18 (c).
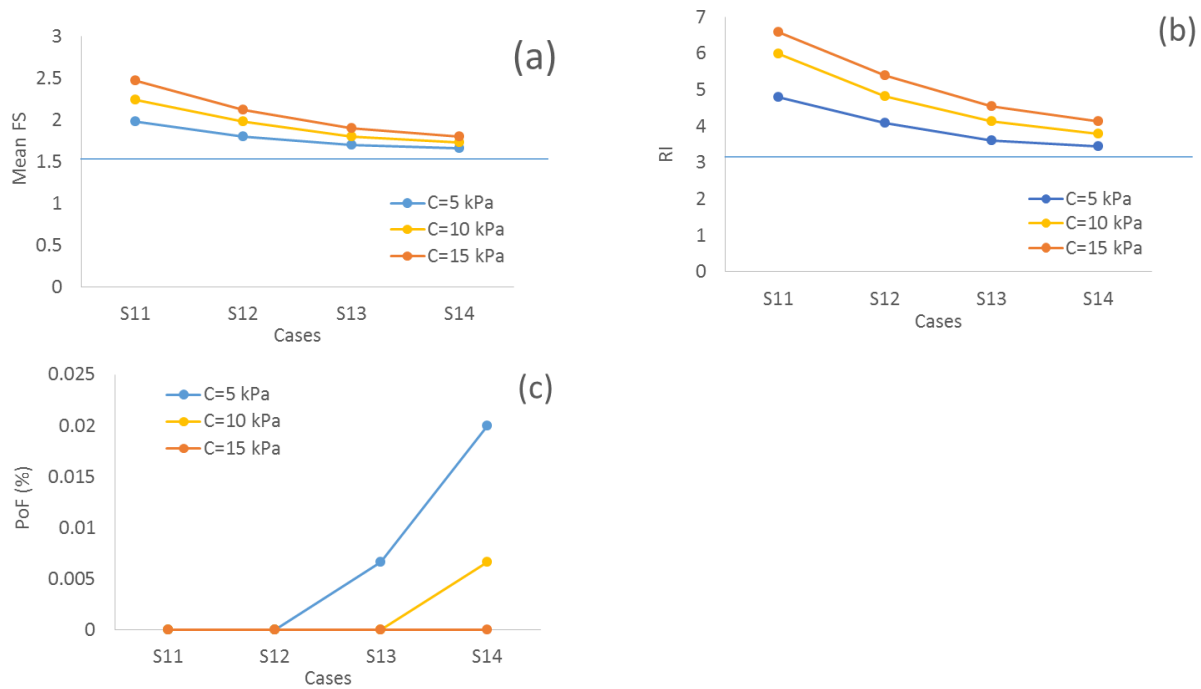
Figure 6-18: Distribution of $\overline{FS}$, RI and PoF obtained with the Monte-Carlo (SLOPE/W), COV = 15% (ϕ' and C), C = 5, 10 and 15 kpa, Group 2 (Cases S11, S12, S13, S14, H_t = 20, 40, 80, 120 m); a) $\overline{FS}$; b) RI; c) PoF

Figure 6-19 presents the normal distribution of the factor of safety calculated with Monte-Carlo method (SLOPE/W) for Group 4 (Cases S21, S22, S23 and S24, H_t = 20 m to 120 m) to investigate the effect of probabilistic distribution for c_{app} (C= 5, 10 and 25 kPa) with COV 15%, with ϕ'= 37° for a critical local slip surface.

It is observed that by increasing C, the $\overline{FS}$ increases and the normal distribution of FS tend to move to the right (with an increase of $\overline{FS}$). The probability of occurrence though does not present a specific trend.
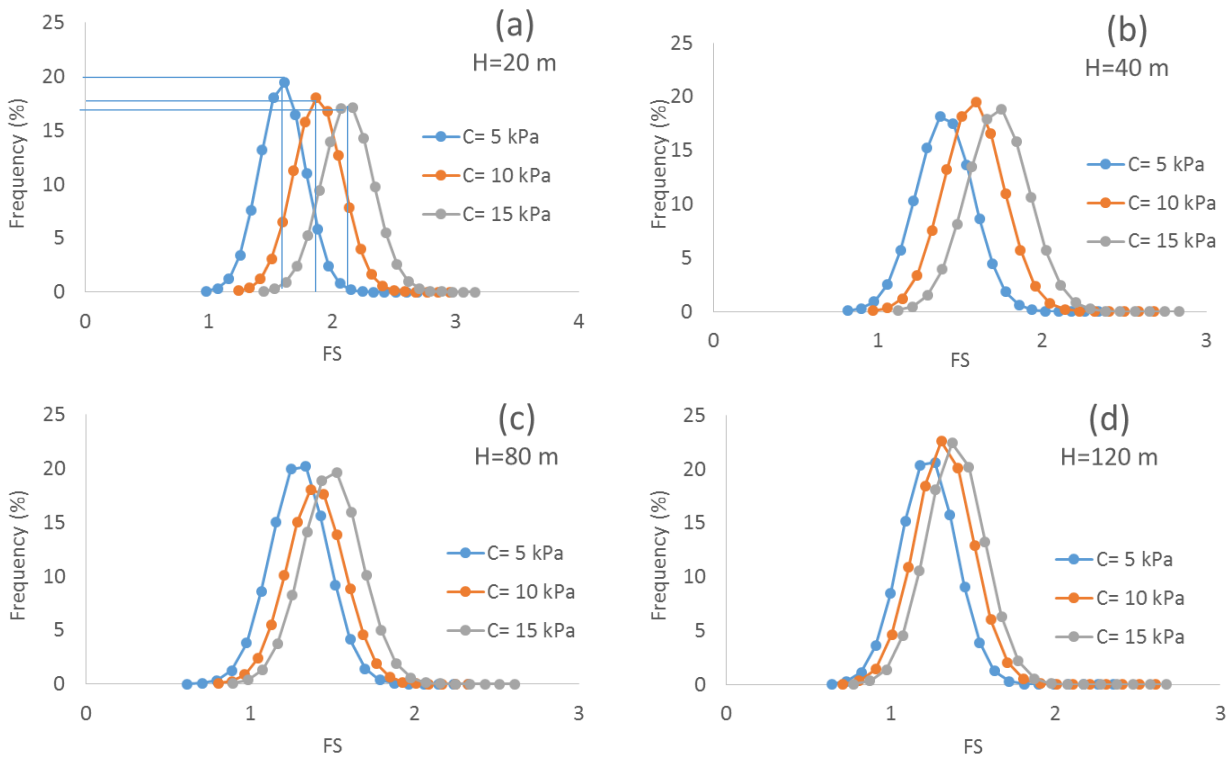
Figure 6-19: Normal distribution of FS for local slip surface obtained with Monte-Carlo method (SLOPE/W), COV 15% (φ' and C), C (=5, 10 and 15 kPa); a) Case S21; b) Case S22; c) Case S23; d) Case S24

Figure 6-20 illustrates $\overline{FS}$, RI and the PoF calculated with SLOPE/W for COV = 15% (φ' and C, sampling distance ½ Ht). Figure 6-20 (a) shows that $\overline{FS}$ for each case decreases when the C decrease. As an example in Case S21, reduction of C from 15 kPa to 5 kPa results in the decrease of $\overline{FS}$ from 2.3 to 1.6.

Figure 6-20 (b) indicates that a reduction of C results in the fall in the RI, Figure 6-20 (c) also shows that a decrease in C results in the increase of PoF. As an example, when C decreases from 15 kPa to 5 kPa for Case S24, RI also decreases 2.5 to 1.5, where the PoF increases from nearly zero to almost 8%. It is noted that an increase of the pile height results in a decrease of FS and RI and an increase of PoF. The increase of FS due to an increase of C is more pronounce for smaller piles (compare Case S21 and S24 in Figure 6-20 (a)).
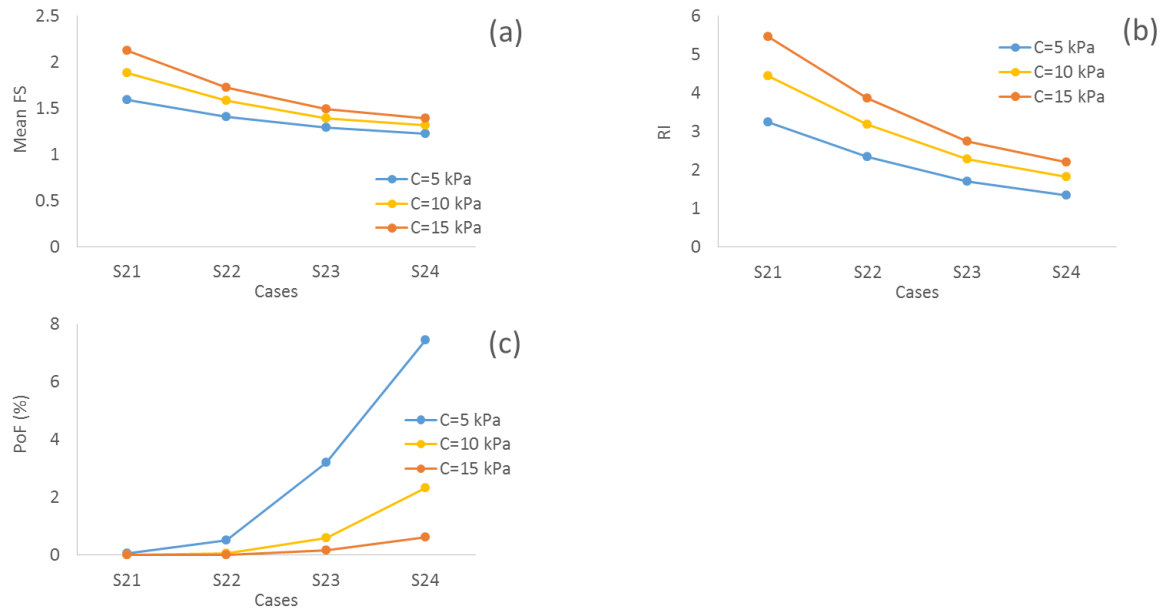
Figure 6-20: Distribution of $\overline{FS}$, RI and PoF obtained with Monte-Carlo (SLOPE/W), COV = 15% (ϕ' and C = 5, 10 and 15 kpa), Group 2 (Cases S21, S22, S23, S24); a) $\overline{FS}$; b) RI; c) PoF

6.5.2 Effect of the number of benches (pile geometry)

Probabilistic analyses were also conducted to study the effect of adding benches into a waste rock pile. For this purpose, three different Groups are considered. Group 1 (Cases S1, S2, S3, S4; H_t = 20 m to 120 m) represents single bench pile (with $\beta = \alpha = 37°$); Group 2 (Cases S11, S12, S13, S14; H_t = 20 m to 120 m) represents two bench piles (with $\beta = 37°$, $\alpha = 26°$); Group 3 (Cases S15, S16, S17; H_t = 40 m to 120 m) represents three bench piles (with $\beta = 37°$, $\alpha = 26°$, see details in Tables 4-4 and 4-5) with ϕ' = 37°, COV = 15%, c_{app} = 5 kPa (single value, imposed by suction; this value of c_{app} is considered as an upper bound for realistic conditions in waste rock; see above and Section 4.6) and sampling distance ½ H_t. The results are shown for three different slip surfaces involving 60%, 70% and 90% of H_t.

Figure 6-21 (a) and (c) show that $\overline{FS}$ is larger for the two-bench piles (Group 2) compared with the single-bench piles (Group 1) and in Figure 6-21 (e) the $\overline{FS}$ for the three-bench piles (Group 3) are larger compared to single-bench (Group 1) and two benches (Group 2) at a given height, though the difference is more pronounced between Group 1 and Group 2 (or 3, due to lower global slope angle in Group 2 and 3, $\alpha = 26°$ versus $\alpha = 37°$). RI also increases due to the

addition of benches. Figure 6-21 (b), (d) and (f) show that for different slip surface configurations (involving 60%, 70% and 90% H_t), the RI for Group 3 is larger compared to Group 2 and Group 1. When waste rock pile consist of benches, both $\overline{FS}$ and RI increase (more stable).
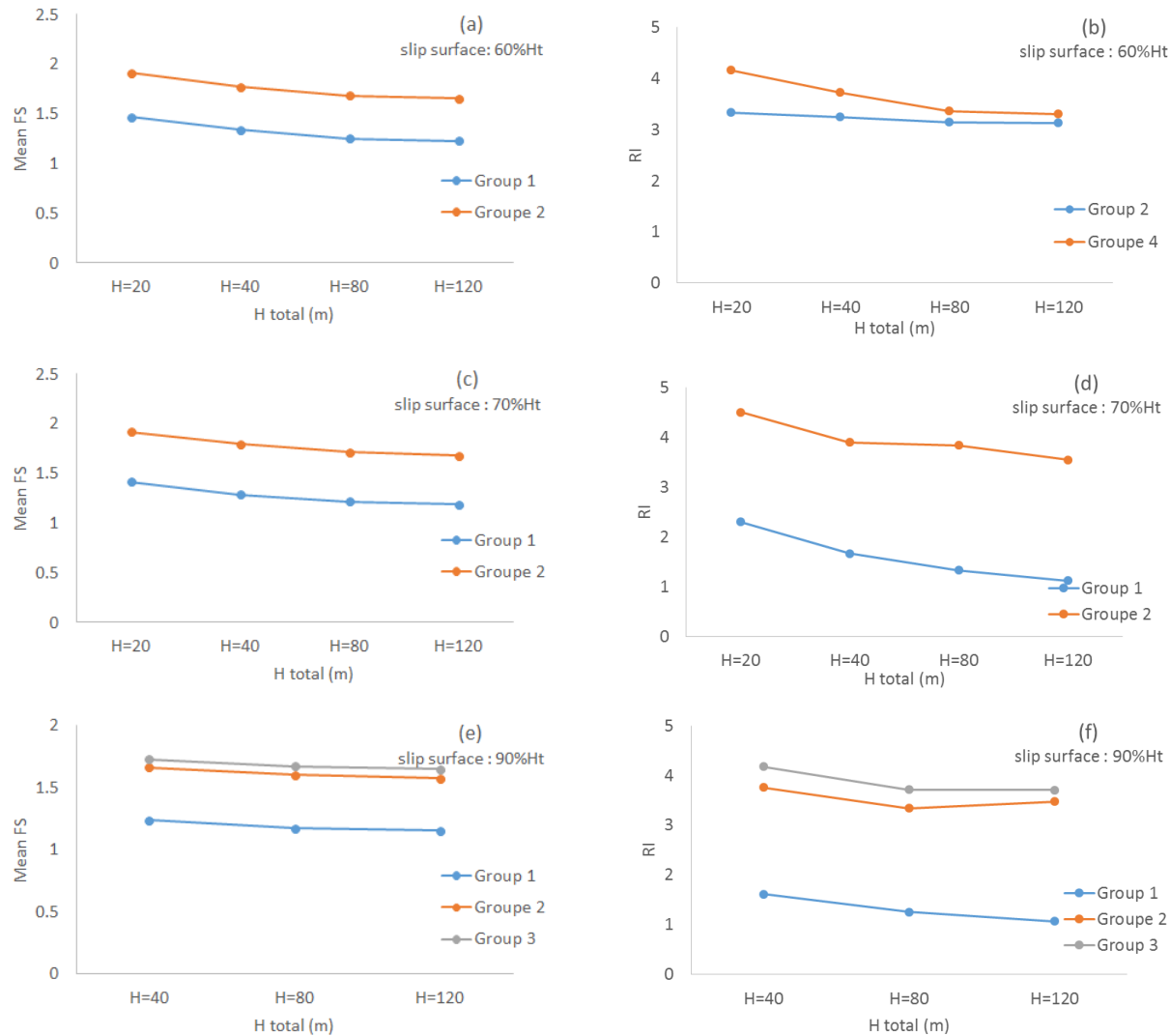
Figure 6-21: Effect of number of benches on $\overline{FS}$ and RI, COV = 15% (ϕ'), sampling distance ½ H_t, c_{app}= 5 kPa, Group 1 (Cases S1, S2, S3, S4, H_t = 20, 40, 80, 120 m), Group 2 (Cases S11, S12, S13, S14, H_t = 20, 40, 80, 120 m), Group 3 (Cases S15, S16, S17, H_t = 40, 80, 120 m); a) $\overline{FS}$, slip surface 60% H_t, Groups 1 and 2; b) RI, slip surface 60% H_t, Groups 1 and 2; c) $\overline{FS}$, slip surface 70% H_t, Groups 1 and 2; d) RI, slip surface 70% H_t, Groups 1 and 2; e) $\overline{FS}$, slip surface 90% H_t Groups 1, 2 and 3; f) RI, slip surface 90% H_t, Groups 1, 2 and 3

6.5.3 **Effect of compacted layers**

It was mentioned in section 2-1-2 that due to the method of construction of waste rock piles, the internal geometry might include layers that are horizontal, slightly inclined or even parallel to the slope. In this section, different configurations of these layers (see Tables 4-4 and 4-5 for details) within the pile are studied through probabilistic analyses to show their effect on the stability of the waste rock pile.

Piles with two benches without and with horizontally compacted layers

Figure 6-22 shows the normal distribution of FS obtained with the Monte-Carlo simulations (SLOPE/W, *FE stress-based* method) for slip surfaces involving 60% H_t, with COV = 15% (ϕ'), sampling distance ½ H_t and c_{app} = 1 kPa. Two groups of waste rock piles are presented here: Group 2 (pile with two benches, Cases S11, S12, S13, S14; H_t = 20 m to 120 m) and Group 4 (pile with two benches and two horizontally compacted layers, Cases S21, S22, S23, S24; H_t = 20 m to 120 m, see Tables 4-4 and 4-5 for more details).

The results show that for any given case from Group 2, addition of compacted layer(s) results in a slight increase of $\overline{FS}$ and its related probability of occurrence (Figure 6-22 (a), (b), (c) and (d)). Such as increase of $\overline{FS}$ from 1.69 to 1.79 and probability of occurrence from 19.6% to 21.3% (Figure 6-22 (a)).
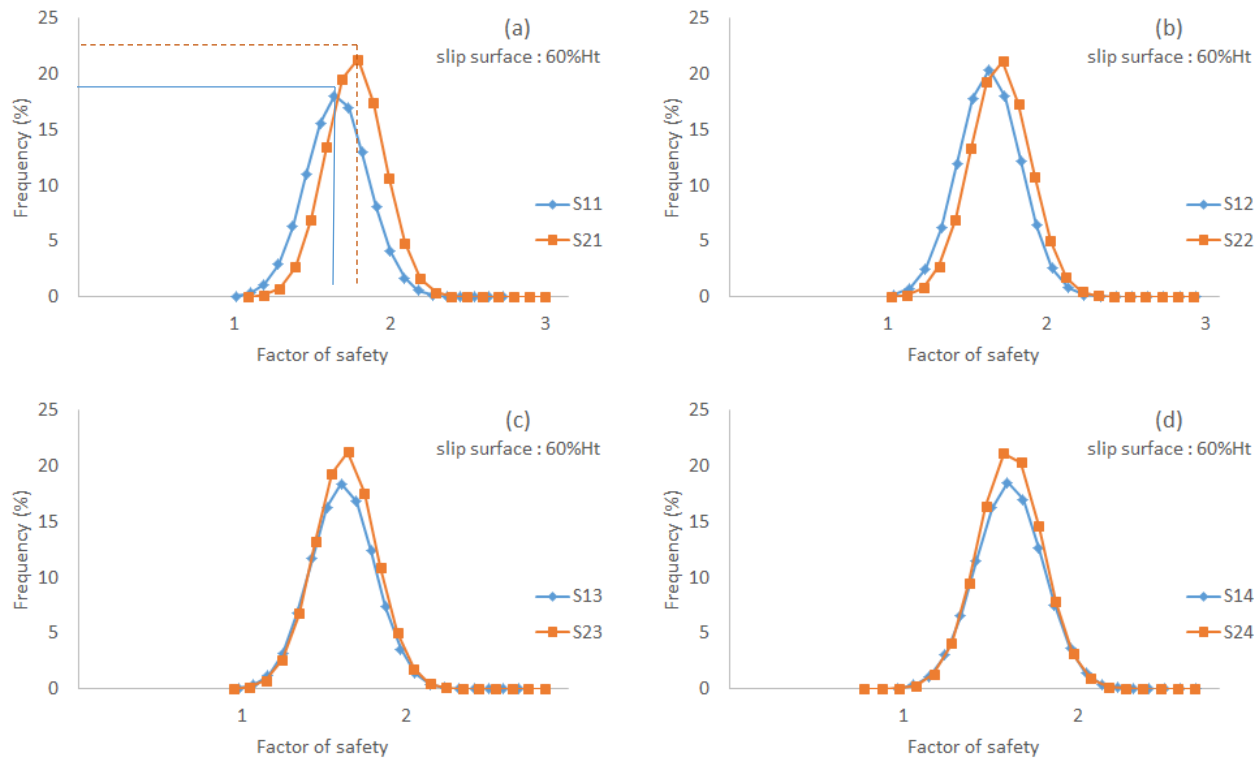
Figure 6-22: Effect of horizontal layers on the normal distribution of FS, COV 15% (ϕ'), slip surface involving 60% H_t, c_{app}= 1 kPa, Group 2 (Cases S11, S12, S13, S14, H_t = 20 m to 120 m), Group 4 (Cases S21, S22, S23, S24, H_t = 20 m to 120 m); a) Cases S11 vs S21; b) Cases S12 vs S22; c) Cases S13 vs S23; d) Cases S14 vs S24

Figure 6-23 presents the results obtained ($\overline{\text{FS}}$ and RI) from probabilistic analyses (Monte-Carlo method) with SLOPE/W (*FE stress-based* method) COV= 15% (ϕ'), sampling distance ½ H_t and slip surfaces involving 60%, 70% or 90% H_t for Group 2 (Cases S11, S12, S13, S14; H_t = 20 m to 120 m; pile with two benches) and Group 4 (Cases S21, S22, S23, S24; H_t = 20 m to 120 m; piles with two benches and two compacted waste rock layers). Figure 6-23 (a), (c) and (e) represents the changes in $\overline{\text{FS}}$ for slip surfaces involving 60%, 70%, and 90% H_t. Results indicate that addition of compacted layers increases $\overline{\text{FS}}$. This effect is more pronounced for smaller piles and for slip surfaces with lower heights (e.g., H_t = 20 m and slip surface = 60% H_t). In larger piles, the effect of compacted layers is less significant.

Increasing the total height of the pile decreases $\overline{FS}$. This effect is more pronounced for smaller piles. It is also noted that for slip surface involved a higher portion of H_t, the difference of $\overline{FS}$ between Group 2 and 4 decreases; this means that the effect of compacted layers addition is more pronounced for smaller slip surfaces.

Figure 6-23 (b), (d) and (f) show the changes in RI when horizontally compacted layers are added to the pile. It can be observed that adding these layers (Group 4) results in a higher RI (i.e. more stable piles). This increase is more pronounced for slip surfaces involving 60% H_t compare to deeper (larger) slip surfaces. The changes in RI are less significant for higher slip surfaces. The PoF for these cases is very close to zero, and it is not presented here.
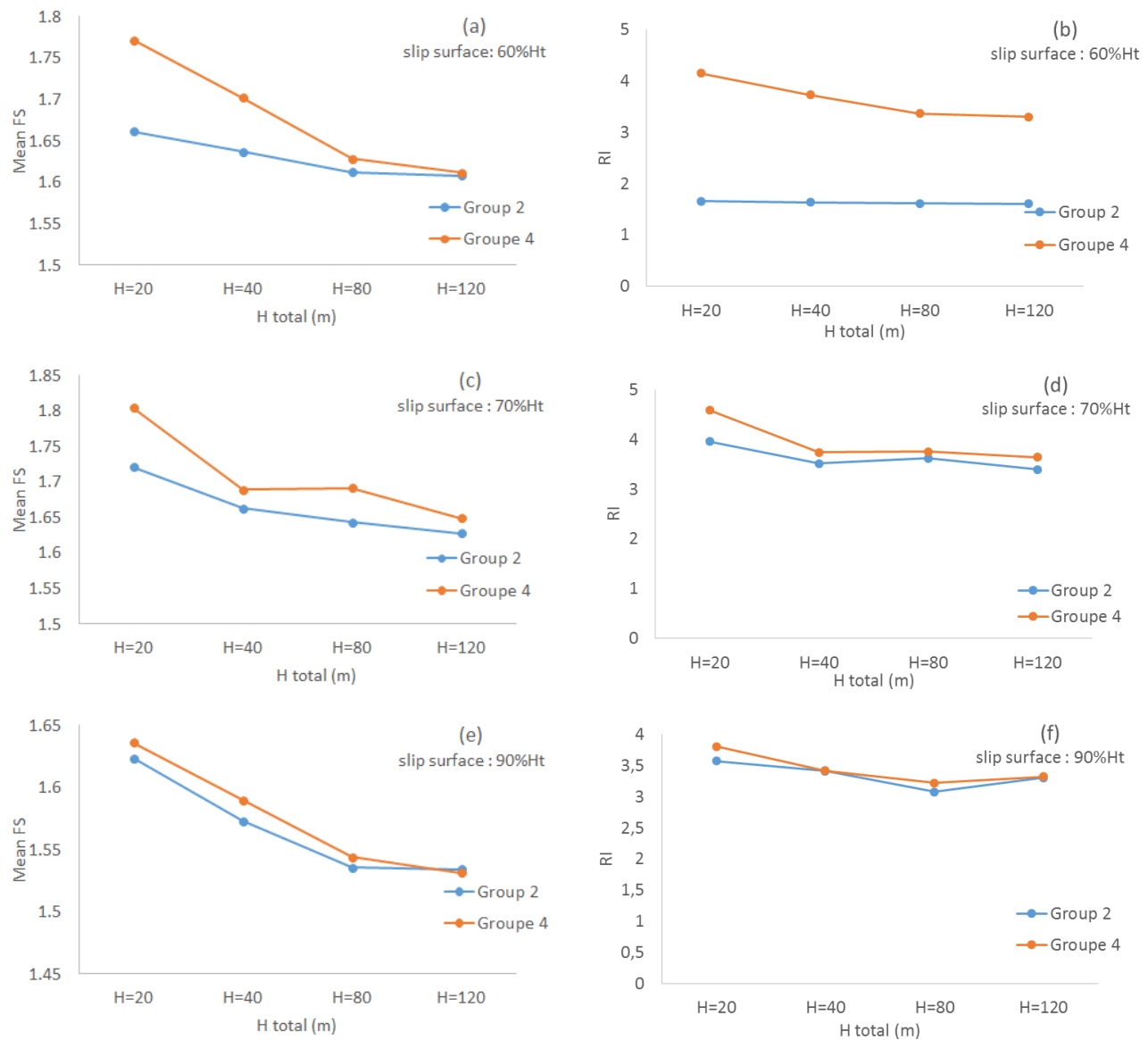
Figure 6-23: Effect of addition of compacted layers on $\overline{FS}$ and RI, COV 15% (ϕ'), c_{app}= 1 kPa, slip surface involving 60%, 70% and 90% H_t, c_{app}= 1 kPa, Group 2 (Cases S11, S12, S13, S14, H_t = 20, 40, 80, 120 m), Group 4 (Cases S21, S22, S23, S24, H_t = 20, 40, 80, 120 m); a) $\overline{FS}$, slip surface 60% H_t; b) RI, slip surface 60% H_t; c) $\overline{FS}$, slip surface 70% H_t; d) RI, slip surface 70% H_t; e) $\overline{FS}$, slip surface 90% H_t; f) RI, slip surface 90% H_t

Pile with three benches without and with horizontally compacted layers

Figure 6-24 shows the normal distribution of FS obtained with Monte-Carlo simulations (SLOPE/W, *FE stress-based* method) for Group 3 (Cases S15, S16, S17; H_t = 40 m to 120 m; piles with three benches) and Group 5 (Cases S25, S26, S27; piles with three benches and horizontal compacted layers). COV = 15% (ϕ') and sampling distance is ½ H_t and slip surfaces involve 60%, 70% or 90% H_t. The results indicate that addition of compacted layers results in a slight increase in $\overline{FS}$ moreover, its related probability of occurrence (Figure 6-24 (a), (b) and (c)).
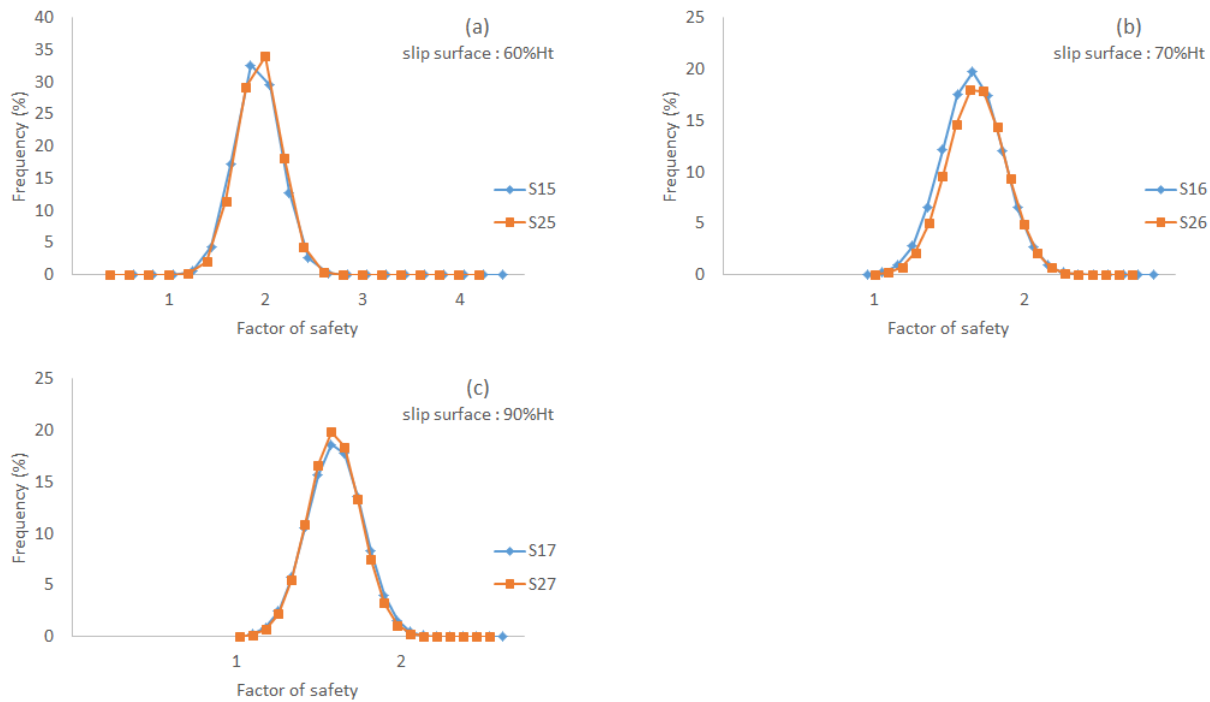
Figure 6-24: Effect of horizontal compacted layers on normal distribution of FS, COV 15% (ϕ'), c_{app}= 1 kPa and 2.5 kPa for loose and compacted waste rock, Group 3 (Cases S15, S16, S17, H_t = 40, 80, 120 m), Group 5 (Cases S25, S26, S27, H_t = 40, 80, 120 m); a) slip surface involving 60% H_t, Cases S15 vs. S25; b) slip surface involving 70% H_t, Cases S16 vs. S26; c) slip surface involving 90% H_t, Cases S17 vs. S27

Figure 6-25 presents the results obtained with the Monte-Carlo method (SLOPE/W, *FE stress-based* method), with COV = 15% (φ') and sampling distance ½ H_t for slip surfaces involving 60%, 70%, and 90% H_t. The results show the calculated values for $\overline{FS}$ and RI of Group 3 (Cases S15, S16, S17; H_t = 40, 80, 120 m, pile with three benches) and Group 5 (Cases S25, S26, S27; H_t = 40, 80, 120 m, piles with three benches and compacted waste rock layers).

Figure 6-25 (a), (c) and (e) present the variation of $\overline{FS}$ for slip surfaces involving 60%, 70%, and 90% H_t respectively. The trend is similar to results represented for Groups 2 and 4 (see Tables 4-4 and 4-5 for details). Addition of compacted layers to a three bench pile increases $\overline{FS}$; this effect is more pronounced for smaller piles and larger slip surfaces.

As an example, waste rock pile with H_t = 40 m and slip surfaces of 70% and 90% H_t show more significant changes. Figure 6-25 (b), (d) and (f) presents the changes in RI when the horizontally compacted layers are added. Group 4 leads to a higher RI (i.e. more stable piles) compared to Group 3. This increase is more pronounced for slip surfaces involving 70% or 90 % H_t.
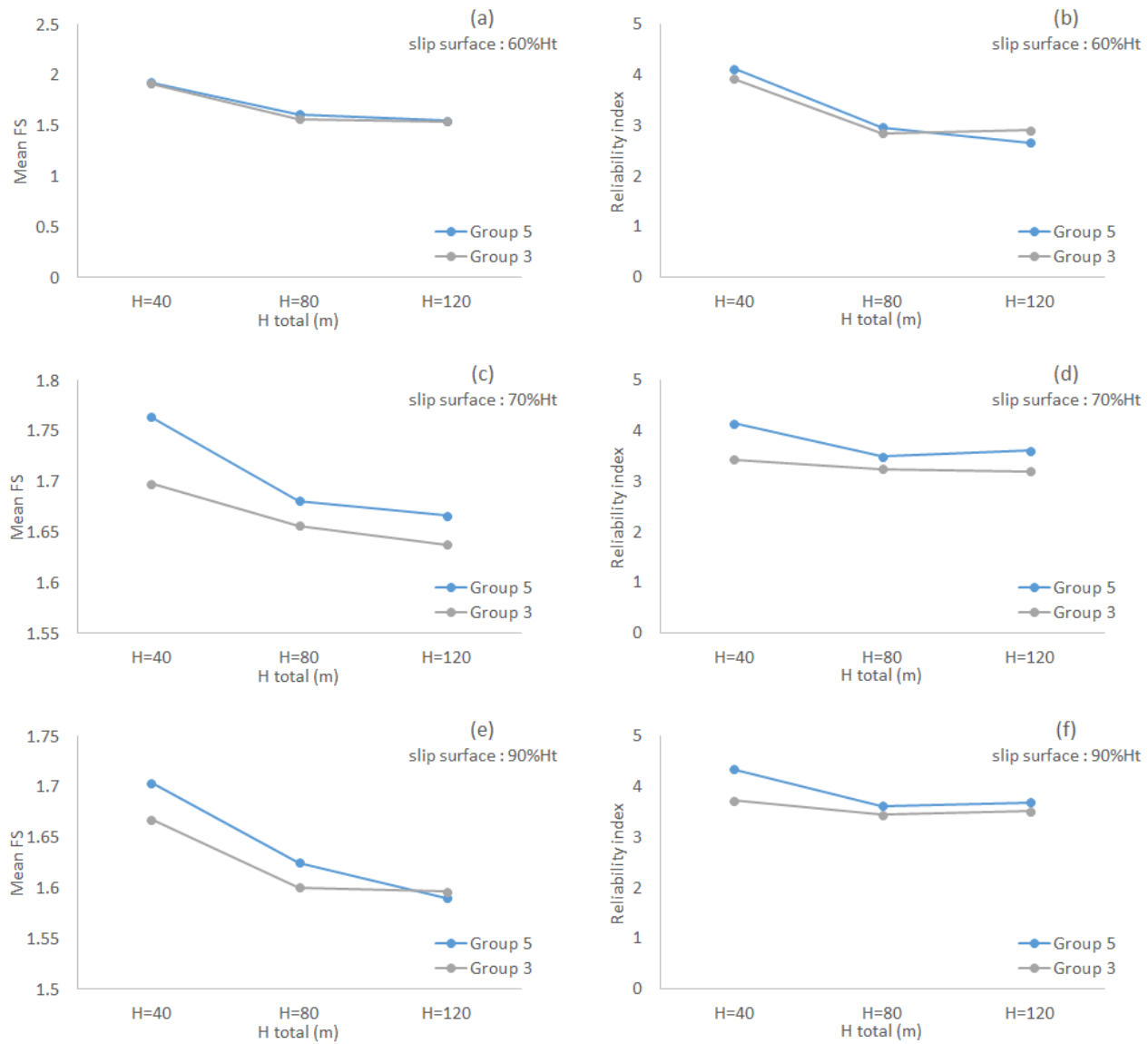
Figure 6-25: Effect of compacted layers on $\overline{FS}$ and RI, COV 15% (ϕ'), sampling distance ½ H_t, c_{app}= 1 kPa and 2.5 kPa for loose and compacted waste rock, Group 3 (Cases S15, S16, S17, H_t = 40, 80, 120 m), Group 5 (Cases S25, S26, S27, H_t = 40, 80, 120 m); a) $\overline{FS}$, slip surface involving 60% H_t; b) RI, slip surface involving 60% H_t; c) $\overline{FS}$, slip surface involving 70% H_t; d) RI, slip surface 70% H_t; e) $\overline{FS}$, slip surface involving 90% H_t; f) RI, slip surface involving 90% H_t

Horizontal versus 5% inclined compacted layers

Group 6 (Cases S35, S36, S37, S38, H_t = 20, 40, 80, 120 m) represents waste rock piles with 5% inclined compacted layers towards the outside of the pile; Group 4 (Cases S21, S22, S23, S24, H_t = 20, 40, 80, 120 m) represents piles with horizontal compacted layers. COV is 15% (ϕ', $\overline{\phi'}$ = 37° and 45° for loose and compacted waste rock respectively) and c_{app} = 1 kPa.

Figure 6-26 (a), (c) and (e) present $\overline{FS}$ obtained (Monte-Carlo method) with SLOPE/W (*FE stress-based* method) for slip surfaces involving 60%, 70% and 90% H_t for Groups 4 and 6.

They show that, for a relatively small slip surfaces (e.g. 60% and 70% H_t), $\overline{FS}$ is higher for the cases in Group 4 compared to Group 6, while for deeper slip surfaces (e.g. 90% H_t), $\overline{FS}$ is higher for cases in Group 6.

A similar trend is obtained for RI. Figure 6-26 (b), (d) and (e) gives a higher RI for Group 4 compared to Group 6 when the slip surface is 60% and 70% of H_t; RI is lower for Group 4 compared to Group 6 for slip surface 90% H_t.

This suggests that an inclined layer may slightly reduce the stability of a waste rock pile for the local slip surfaces; as the slip surfaces tend to become larger, the stability of a pile with inclined layers may be improved (at least when there is no water infiltration).
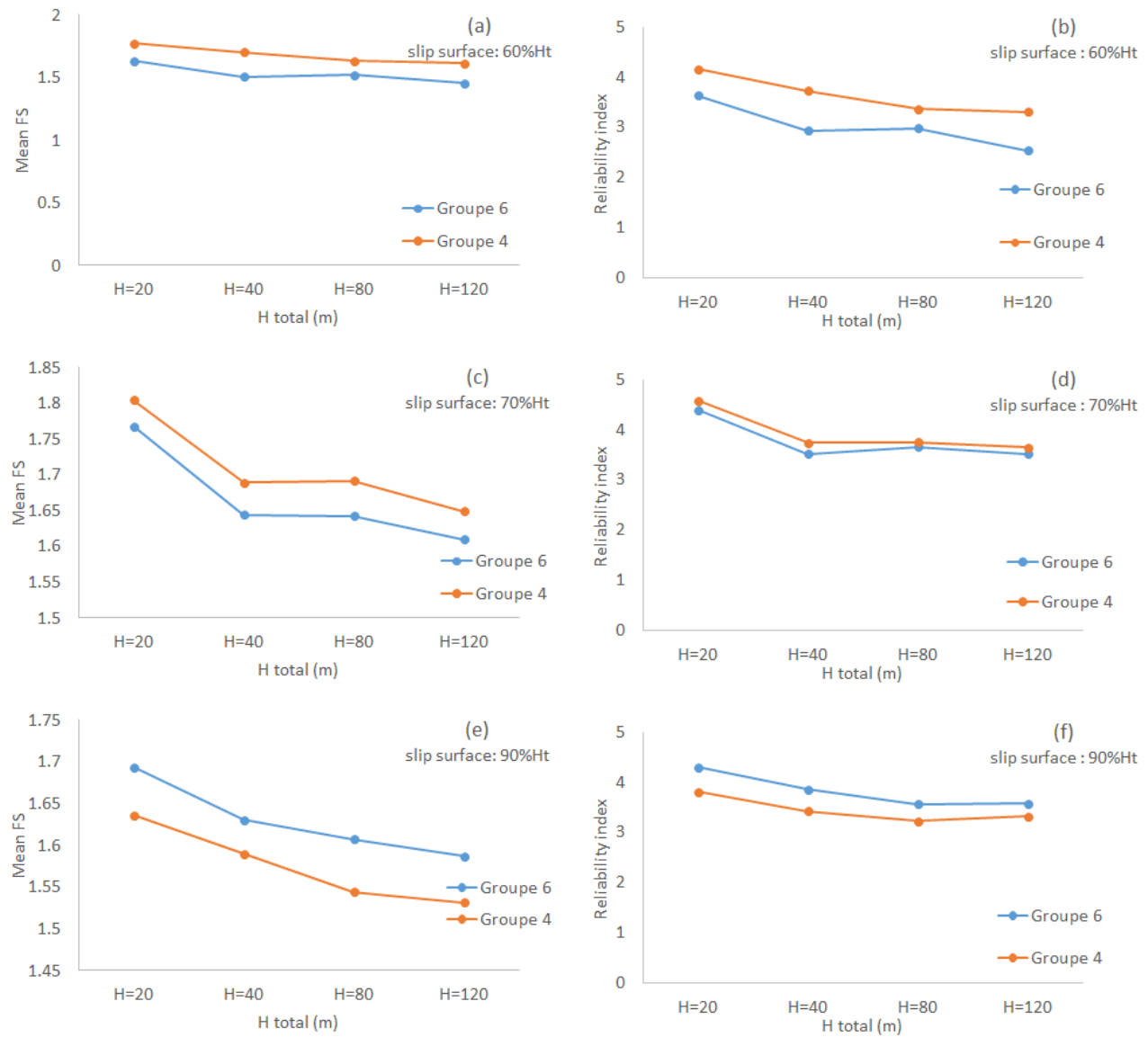
Figure 6-26: Effect of inclined layers on $\overline{FS}$ and RI, COV 15% (ϕ'), sampling distance ½ H_t, $c_{app}=$ 1 kPa, Group 4 (Cases S21, S22, S23, S24, H_t = 20, 40, 80, 120 m), Group 6 (Cases S35, S36, S37, S38, H_t = 20, 40, 80, 120 m); a) $\overline{FS}$, slip surface involving 60% H_t; b) RI, slip surfaces involving 60% H_t; c) $\overline{FS}$, slip surface involving 70% H_t; d) RI, slip surface involving 70% H_t; e) $\overline{FS}$, slip surface involving 90% H_t; f) RI, slip surface involving 90% H_t

Alternate layers parallel to the slope

Probabilistic analyses were conducted with the Monte-Carlo method in SLOPE/W to assess the effect of alternate layers parallel to the slope. The COV is 15% for ϕ' ($\overline{\phi'}$ = 37° and 45° for loose and compacted waste rock respectively) and c_{app} = 1 kPa (which is considered a realistic average value for waste rock).

Results related to Group 4 (Case S21; horizontally compacted layers), Group 6 (Case S35, 5% inclined compacted layers), Group 8 (Case S41, horizontal and alternate layers), Group 9 (Case S51, 5% inclined and alternate layer) are presented and compared in Figure 6-27. It can be observed that for the different slip surfaces (involving 60%, 70% or 90% H_t), $\overline{FS}$ is higher for Group 8 (Case S41) compared to Group 4 (S21) (see Figure 6-27 (a)).

A similar trend is noted while comparing Group 6 (Case S35) and Group 9 (Case S51); for instance, for a slip surface involving 70% H_t, $\overline{FS}$ increases from 1.76 to 1.87 for the pile with inclined compacted layer and pile with inclined compacted and alternate layer (see Figure 6-27 (c)).

RI presents similar trend to $\overline{FS}$. Figure 6-27 (b) and (d) show that RI increases when alternate layers are added (Cases S41, S51). Having either horizontal or inclined 5% layers with alternated layers within a pile may increase the $\overline{FS}$ and RI compared to cases with only horizontal or slightly inclined compacted layers.
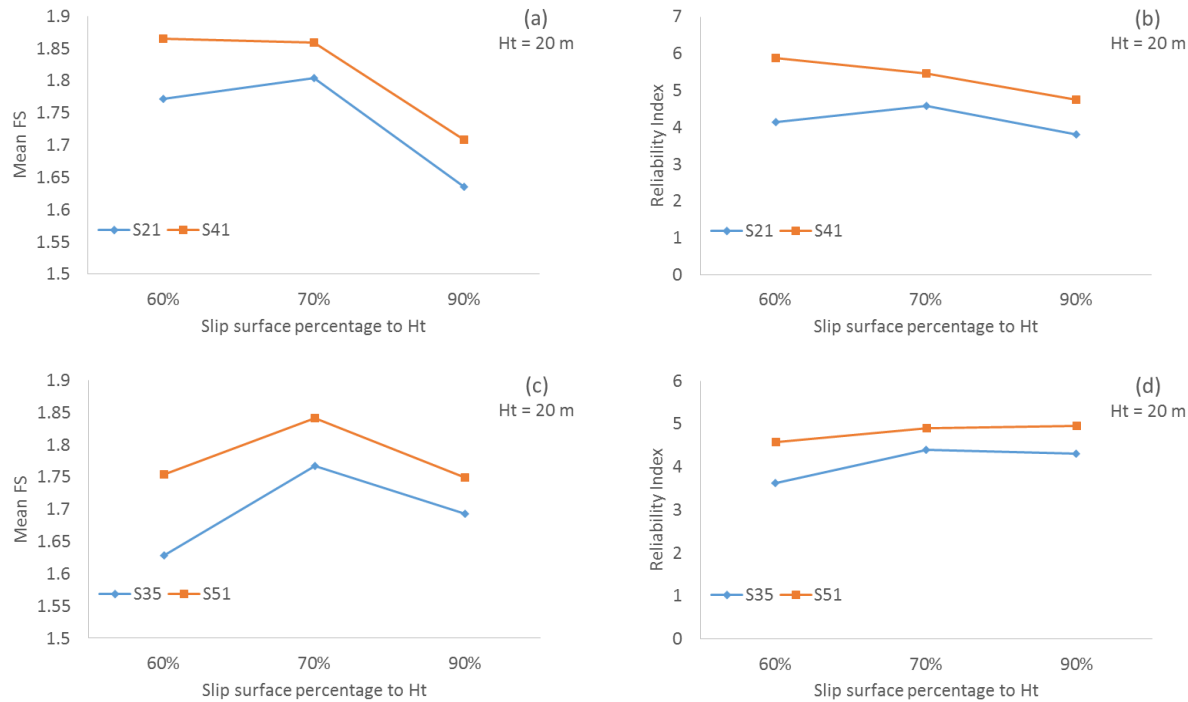
Figure 6-27: Effect of alternate layers on $\overline{FS}$ and RI, COV 15% (φ'), sampling distance ½ H_t, slip surface involving 60%, 70% and 90% H_t, c_{app}= 1 kPa, Group 4 (Case S21), Group 6 (Case S35), Group 8 (Case S41), Group 9 (Case S51); a) $\overline{FS}$ Cases S21 vs. S41; b) RI Cases S21 vs. S41; c) $\overline{FS}$ Cases S35 vs. S51; d) RI Cases S35 vs. S51

Figure 6-28 presents $\overline{FS}$, and RI obtained with the Monte-Carlo simulation (SLOPE/W, *FE stress-based* method) for COV = 15% (φ'), sampling distance ½ H_t (= 20 m). Figure 6-28 (a) presents the result of Group 4 (Case S22), Group 6 (Case S36), Group 8 (Case S42) and Group 9 (Case S51). It can be seen that regardless the depth of the slip surface (involving height 60%, 70% or 90% H_t), $\overline{FS}$ is higher for Group 8 (Case S42) compared to Group 4 (S22), which is the trend in Figure 6-27 (a).

For a slip surface involving 60% H_t, $\overline{FS}$ Increases from 1.7 to 1.73 for cases S22 and S42, (see Figure 6-28 (a)). A similar pattern is seen for Group 6 (Case S36) and Group 9 (Case S51). RI also presents identical pattern. For instance, for a slip surface involving 90% H_t, RI increases

from 3.4 to 5.3 when alternating layers are added to the waste rock pile (Case S22 to S42) (see Figure 6-28 (b)).
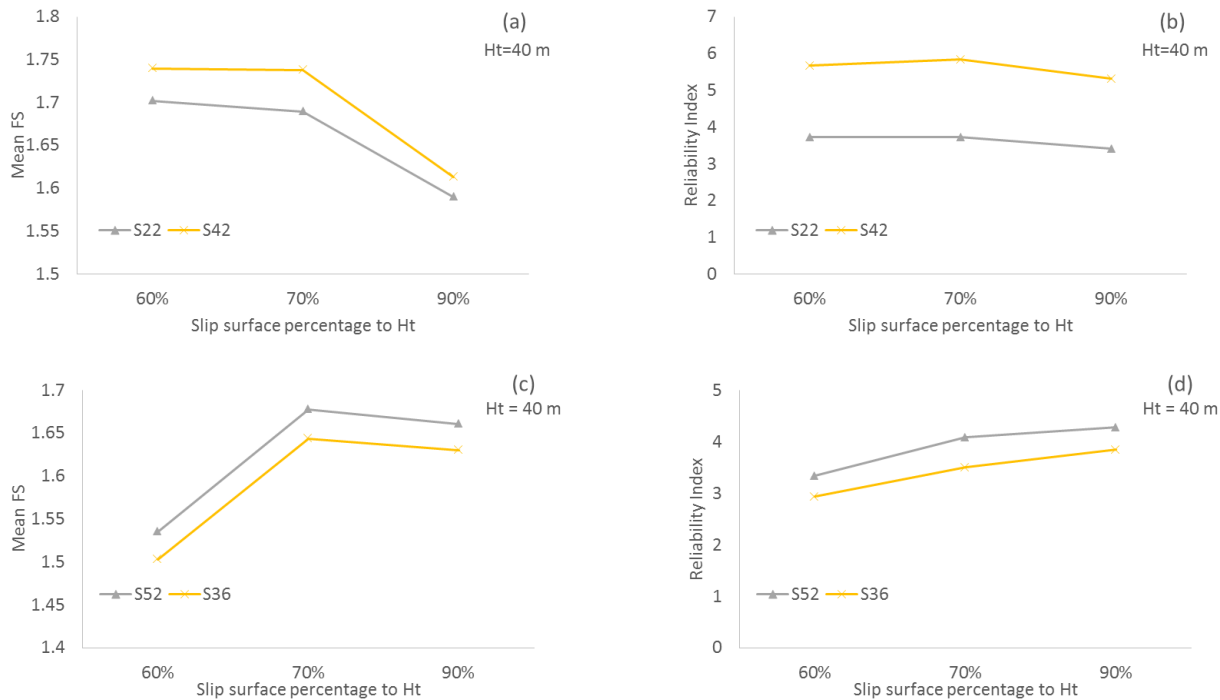
Figure 6-28: Effect of alternate layers on $\overline{FS}$ and RI, COV 15% (ϕ'), sampling distance ½ H_t, slip surface involving 60%, 70% and 90% H_t, c_{app}= 1 kPa, Group 4 (Case S22), Group 6 (Case S36), Group 8 (Case S42), Group 9 (Case S51); a) $\overline{FS}$ Cases S21 vs. S41; b) RI Cases S21 vs. S41; c) $\overline{FS}$ Cases S35 vs. S51; d) RI Cases S35 vs. S51

Relationship between FS and thickness of compacted layers

A sensitivity analysis was performed to assess the relative impact of the compacted layers thickness on stability. Since a variable layer thickness can not be regarded statistically in slope, this effect is reviewed by looking at various configurations and potential slip surfaces.

These analyses are conducted on a waste rock pile (Case 22) with horizontally compacted layers with variable thickness; i.e. 1 m, 2 m, 3 m and 4 m (presented here as the ratio to H_t, (e.g. 0.025, 0.05, 0.075 and 0.1).

The results related to Case S22 are presented for a global slip surface passing through the toe, Figure 6-29 (e)). Figure 6-29 shows the normal distribution of factor of safety Figure 6-29 (a), $\overline{FS}$ 6-29 (b), RI 6-29 (c) and PoF 6-29 (d). $\overline{FS}$ tends to increases when the layer is thicker. For example, when the layer thickness changes from 0.025 to 0.1 H_t, FS increases from approximately 1.54 to 1.59 (see Figure 6-29 (b).

It is indicated the normal distribution of FS is not very sensitive to layer thickness; the standard deviation and maximum probability of occurrence of a factor of safety do not show significant changes.

The same trend is shown for RI. When the layer thickness increases from 0.025 to 0.1 H_t, RI increases from 3.2 to 3.55 (see Figure 6-29 (c)).

Increasing the layer thickness decreases the PoF; for an increase in layer thickness from 0.025 to 0.1, PoF decreases from 0.014% to nearly zero. The impact of such an increase on the PoF rounded to 6 decimal points is not visible.
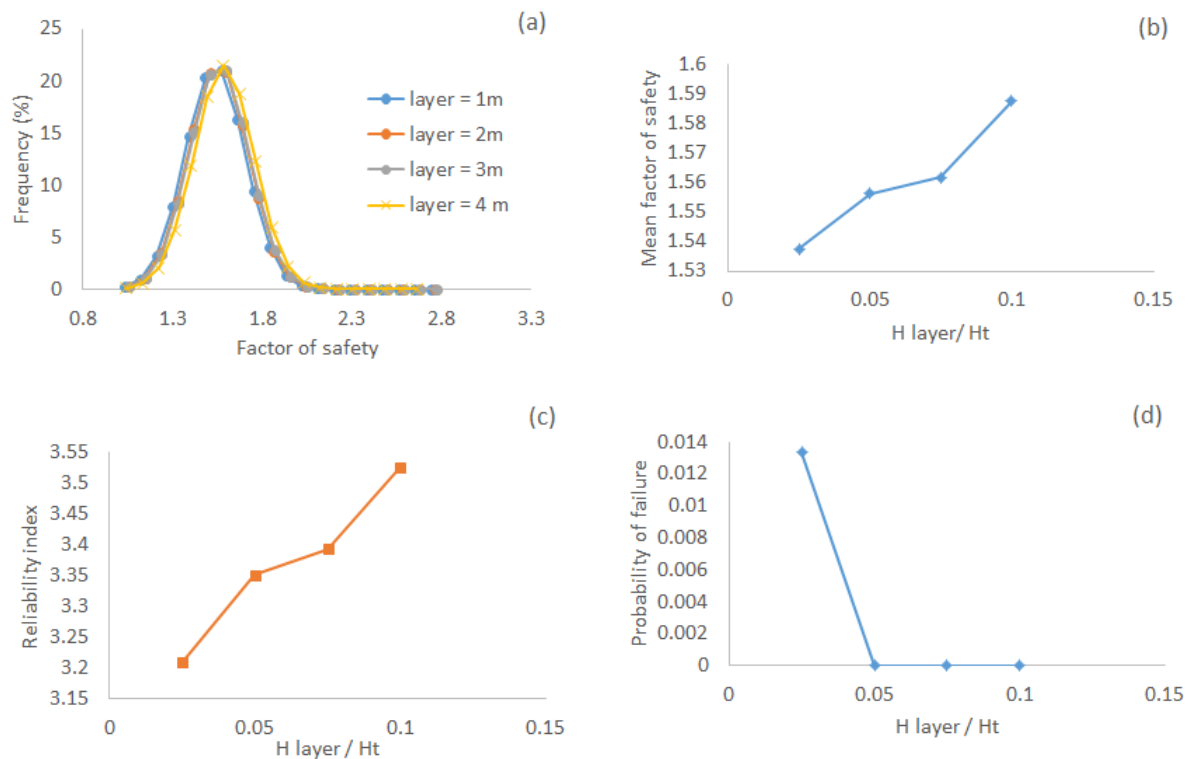
Figure 6-29: The effect of horizontal layer thickness on the slope stability obtained with Monte-Carlo method (SLOPE/W), COV 15% (ϕ'), sampling distance ½ H_t, global slip surface, c_{app}= 1 kPa, Case S22; a) FS normal distribution; b) $\overline{FS}$; c) RI; d) PoF

6.5.4 Effect of the groundwater level and rainfall

Another addressed issue is the effect of the elevation of the phreatic surface on slope stability. A sensitivity analysis was conducted to evaluate the effect of the groundwater level on the output variables from stability analyses. The results are related to Case S11 with c_{app} =1 kPa (i.,e. realistic average value for waste rock) and three groundwater level -7 m, -3 m and -1 m below the base of the pile.

Figure 6-30 presents that increasing the depth of underground water results in a slight decrease in $\overline{FS}$ and RI (see Figure 6-30 (a) and (b)), whereas the standard deviation and PoF remain almost unchanged.
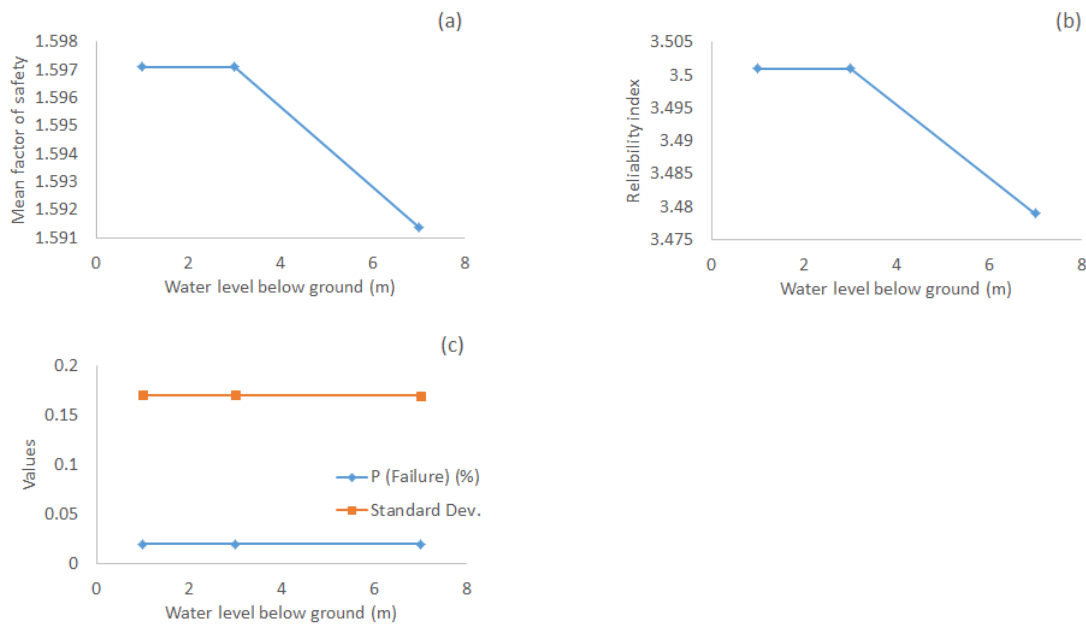
Figure 6-30: Effect of the groundwater level on the probabilistic analysis of slope stability, COV 15% (ϕ'), sampling distance ½ H_t, global slip surface, c_{app}= 1 kPa, foundation silty sand, Case S11; a) $\overline{FS}$; b) RI; c) PoF and standard deviation

Effect of rainfall

Rainfall infiltration has been one of the leading causes of landslides. The effect of infiltration and expansion of the wetting front on PoF of a waste rock pile is presented in this section.

Three different Cases S11, S21, and S35 are presented with the initial matric suction of 6 kPa under three different rainfalls (R 1, R 2-1, R 3-3, Table 51). The foundation material is the silty sand, and the groundwater level is 7 m below the ground.

Figure 6-31 (a), (b) and (c) represent the changes in PoF under rainfalls with different intensities for a critical local slip surface. It shows the lower PoF belongs to case S21 (two benches with horizontally compacted layers). The PoF tends to increase under the rainfall (due to a decrease of FS and reduction of suction) for all the cases.
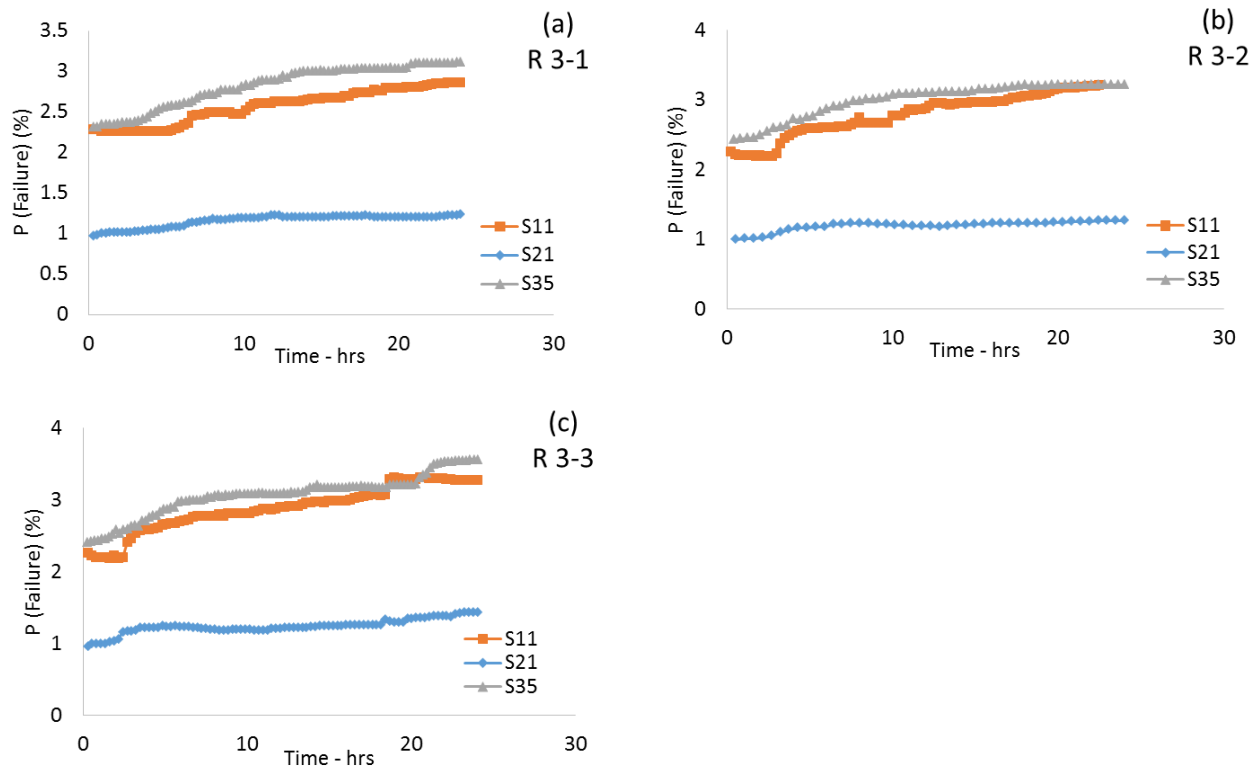
Figure 6-31: Effect of rainfall infiltration on PoF of local slip surface, COV 15% (ϕ'), Cases S11, S21, S35; a) Rainfall R 3-1; b) Rainfall R 3-2; c) Rainfall R 3-3

6.5.5 **Summary and complimentary remarks**

The results from the probabilistic analyses indicate that not all of the parameters' uncertainties have an effect on the pile stability and related indicators (i.e. $\overline{FS}$, PoF, RI). For instance, it has been observed that the unit weight does not significantly affect $\overline{FS}$ and its normal distribution function.

The results also indicated that decreasing sampling distance leads to a decrease of PoF. A higher coefficient of variation (COV) for strength properties results in a lower RI and a higher PoF; the COV does not affect $\overline{FS}$ significantly.

Apparent cohesion has a positive effect on the stability of the pile (as shown in section 4-5-7). Results shown here indicate that an increase of apparent cohesion (normal distribution, instead of a single value) may result in an increase of $\overline{FS}$ and RI and a decrease of PoF. As water infiltration

may affect the apparent cohesion (increase or decrease), it can also affect the PoF of waste rock piles (when considering the stochastic distribution of hydrogeological properties; Fala, 2008). Increasing the height of the pile results in a decrease in $\overline{FS}$ and RI and increase the PoF

The results also showed that adding benches can increase the value of $\overline{FS}$ and RI and decrease that of the PoF.

Compacted layers (horizontal or inclined) can also impact the factor of safety. These usually increase the values of $\overline{FS}$ and RI; this effect is more pronounced for smaller piles. Inclined layers may, however, have a negative impact on the stability of the pile when considering local (shallow) slip surfaces (contrary to deeper slip surfaces). The increase of layer thickness results in an increase of RI. Alternated layers along the external slope may help increase $\overline{FS}$. Combinations of both horizontal and alternate layers usually result in more stable piles (for the conditions assessed here).

6.6 General synthesis and discussion

The original purpose of this study was to develop and apply a systematic procedure to assess the stability of unsaturated waste rock piles and to better understand slope behavior under various climatic conditions. This further understanding of the influence factors should lead to improved design of waste rock piles.

This thesis specifically investigated (analyzed) the effect of internal features and external geometry of waste rock piles, material properties (geotechnical and hydraulic), and boundary conditions (with transient or quasi-stationary recharge), on pile stability.

The failure of waste rock piles can be a relatively complex process because of their complex nature. Numerical models were used with typical data (properties and characteristics) to assess the response of idealised piles, which are in many ways similar to existing waste rock piles (such as those described by: (Fala, 2002, 2008; Anterrieu et al., 2010; Dawood et al., 2011; Dawood and Aubertin, 2014).

One of the main limitations of this study is the lack of experimental data and field validation. Nonetheless, some validation of the calculations have been performed by comparing the results obtained with the codes for single bench waste rock piles with the Simplified Bishop Method

and the graphical solution (Charts) proposed by Cousins (1978) – see Appendix A-1 ; a few other comparative analyses for the slope stability of different cases are also presented in Appendix A-1.

The main objectives of the research project are listed in Chapter 1. Results presented in the thesis (particularly in Chapters 4, 5 and 6) indicate that these objectives have been met. The following recalls and briefly discusses the main outcomes from the various components of the project.

Chapter 2 presented a fairly extensive review of previous work on waste rock piles. This information was used to determine the range of waste rock properties and pile characteristics to be employed in the parametric analyses. The models used here assumed that the waste rock piles are constructed by push or end dumping methods and that they remain under unsaturated conditions (with a water table below the natural ground surface). Waste rocks have a wide grain size distribution and are heterogeneous. The pile construction methods often lead to a complex internal geometry that may include layers with different grain sizes and degrees of compaction. Sub-horizontal layers are formed by the passage of heavy equipment in the core of the pile; this feature is taken into account in the analyses performed in the thesis.

Chapter 3 describes the methodology applied based on numerical analyses. These make use of three Geostudio 2007 codes: SEEP/W, SIGMA/W, and SLOPE/W (GeoSlope International Ltd, 2008) to conduct partly coupled analyses. For cases under constant (unchanging) conditions, a combined FEM stress distribution-slope stability analysis procedure has been adopted. For cases with transient rainfalls (short term and long term), the analyses involved the combined use of two-dimensional finite-element seepage, stress distribution, and slope stability analysis. In these transient analyses, the solution is obtained by solving the seepage equations first and then entering the results into the stress state and slope stability calculations

Appropriate material properties, boundary conditions, time-steps and mesh size have been considered. The study is based on 2D-analyses of slopes for circular or optimised (quasi-circular) local and global slip surfaces; as mentioned, it combines limit equilibrium and finite element stress analyses. The results first deal with simple waste rock piles, and progressively address increasing complexity.

Chapter 4 presents a fairly extensive parametric study carried out to determine the effects of internal and external geometry (including slope angle, pile height, the number of benches and compacted layers) and waste rock properties (i.e. internal friction angle and apparent cohesion) on the slope stability of waste rock piles. A combination of finite element stress analyses and limit equilibrium analyses was used to assess slope stability. These calculations have led to the following results and observations:

- The increase of the internal friction angle ϕ' has a positive effect on the stability of waste rock piles; increasing the value of ϕ' results in an increase in the factor of safety FS of the slope.

- Unsaturated soil mechanics principles and theory are used to assess the stability of unsaturated piles. These indicate that an evolving matric suction may increase the effective stress, σ' and the available shear strength. This effect enables slopes to remain stable at angles close to (and even in excess of) their internal friction angle (ϕ'). The analyses specifically showed how the apparent cohesion c_{app} might have a positive effect on the stability of a waste rock pile, by increasing the value of the factor of safety FS; this applies to various waste rock pile configurations (i.e. simple bench or multiple benches, with or without compacted layers). The analyses also indicate that a higher value of c_{app} may result in a deeper slip surface, with the sliding plane moving toward the toe of the pile.

- As expected, the results indicate that the pile geometry also has a significant impact on the factor of safety. Increasing the height of the pile results in a decrease of FS, while decreasing the slope angle increases the factor of safety. The results also confirmed that smaller piles with flatter slope are more stable. These geometrical effects are more pronounced for waste rock with a higher apparent cohesion (c_{app}).

- When different than the local angle β (for a single bench), the overall slope angle α of the pile (for two or more benches) can also affect the factor of safety. Increasing the overall slope angle α results in a decrease of the factor of safety FS.

- The results specifically showed the major influence of pile height, with an increase resulting in the decrease of FS. However, this effect can be partly offset by breaking down the pile into

(two, three or more) benches, which tends to increase of a factor of safety. This positive effect of adding benches is largely related to the decrease of global slope angle α.

- Another feature that can impact the factor of safety is the existence of compacted layers (horizontal or inclined) within the waste rock pile. The outcomes of this investigation showed that horizontally compacted layers usually increase the FS; this effect is more pronounced for smaller piles (due to the higher ratio of layer thickness to the total pile height). Slightly outward inclined layers (5%) can also increase the value of FS for global (deep) slip surfaces. Alternated layers parallel to the slope may also increase FS.

- Analyses that consider the effect of the normal stress on the value of ϕ' (which may then decrease with depth due to particle crushing) indicate that using a single and constant value of ϕ' for the entire pile may not be conservative (as this can lead to a larger FS). The effect of an increased density (and strength) with depth in the pile has not been considered here.

Chapter 5 investigated the variation of the apparent cohesion and factor of safety during and after rainfalls. The results indicate slopes may fail due to heavy rainfalls because of an increase of the degree of saturation that may cause a decrease of matric suction and the related additional shear strength due to c_{app}. The suction in the unsaturated pile is directly affected by infiltration due to rainfall on the surface. The results illustrate how the rate of infiltration and development of the wetting front are impacted by hydraulic properties of waste rock (i.e. WRC and hydraulic conductivity function). Several transient, two-dimensional finite-element seepage simulations were conducted to determine the distribution of pore water pressures and the effect on the pile stability, using a combination of analyses performed with SEEP/W, SIGMA/W and SLOPE/W.

Varying rainfall intensities were considered with five different geometries, under short-term transient and (pseudo) steady-state conditions. The results conducted from these simulations were compared to determine the general effects of each parameter on the stability of the slope. The obtained results illustrated the complexity of unsaturated flow in waste rock piles and helped identify key trends. The main results and observations from this part of the study can be summarised as follows:

- The rate of rainfall infiltration relates to the initial water content and suction in the waste rock, together with material hydrogeological properties.

- When the effective cohesion of waste rock is close to zero ($c' = 0$), as is usually the case, only c_{app} contributes to total cohesion C, as part of the material shear strength. A reduction of this apparent cohesion (with infiltration) then favours the development of shallow slip surfaces (with a reduction of FS). Rainfall infiltration reduces the suction near the surface; in turn, the apparent cohesion can approach zero, and shallow slips may then occur. For a given rainfall (constant intensity and duration), a low to moderate initial suction tends to dissipate more rapidly compare to a high suction in the waste rock (in part due to the smaller unsaturated hydraulic conductivity of the latter). These results suggest that rainfalls may preferentially lead to shallow landslides along the slope of waste rock piles (at least in the short term).

- Rainfall infiltration and its effect on matric suction and strength decrease in the waste rock typically has a fairly limited effect on the stability of the slope. In most cases (considered here), the decrease of FS is not very significant (compare to other influence factors).

- Results also showed that horizontal, inclined and alternate layers can help control the expansion of the wetting front (compared to homogeneous piles). Slightly inclined (5%) compacted layers may be more beneficial for the global (deep slip) stability, compared to horizontally compacted layer (more efficient to prevent shallow slips), because the former favors the movement of infiltrated water outward instead of inside the pile.

- It was observed that for a given set of characteristics (i.e. waste rock initial water content, slope geometry, water table position), the factor of safety of the slope tends to decrease (evolve) more rapidly as rainfall intensity increases.

- The anisotropic conductivity ratio (k_x / k_y) (in SEEP/W presented as k_x / k_y) has an impact on the factor of safety due to its effect on rainfall infiltration. Decreasing the ratio (k_x / k_y) results in an increase in water infiltration rate and expansion of the wetting front deep in a pile, and a decrease of the factor of safety.

- The external geometry of the waste rock pile has more influence on the factor of safety compare to other parameters (such as the amount of rainfall). Homogenous waste rock piles with a single bench usually give the lowest factor of safety. Adding benches can increase the

value of FS very significantly. Compacted layers may help increase the factor of safety and so are alternate layers parallel to slope; their effect on the factor of safety is however much more limited compared to that of external geometry and global slope angle.

Chapter 6 includes analyses carried out to demonstrate that assessing only the "classical" factor of safety of a pile may not be sufficient. Waste rock properties may vary widely in a pile, and this creates uncertainty for slope stability; it was deemed important to consider these uncertainties in the investigation. The main results in this chapter can be summarized as follows:

- The value of the coefficient of variation (COV), applied to geotechnical properties, has a significant impact on the safety of a pile. A larger COV results in a higher standard deviation, lower Reliability Index (RI) and a higher Probability of failure (PoF) for the waste rock pile.

- Varying the sampling distance also evaluated the importance of spatial variability; an increase of this sampling distance tends to reduce the factor of safety and increase the probability of failure.

- As was observed in Chapter 4, increasing the total height of pile results in a reduction of the mean FS, and also of the reliability index (RI). Adding benches to the pile results in the increases in the mean FS and reliability index (RI) and a reduction in the probability of failure (PoF).

- The tendencies briefly described above apply to the effect of the COV for both the internal friction angle and apparent cohesion.

Despite the valuable information gathered from the many analyses performed and presented in this thesis, some notes of caution should be kept in mind when considering these results. Some of these limitations are recalled briefly here.

This study used a 2D (plane strain), finite element stress distribution combined with analyses performed in the framework of a limit equilibrium evaluate slope stability. 3D effects on pile geometry and critical slip surface are neglected here.

The results of these analyses only indicate whether these failures have a chance to occur, not if they will develop. The approach also neglects how this process evolves, including the potential for progressive failure. The effects progressive construction, stress history, and evolving strains (and displacements) in the waste rock pile are not addressed in this study.

These models are using simplified geometry, and tend to ignore the heterogeneity and segregation within the slope profile (except in Chap. 6, to some extent). The analyses also neglect groundwater fluctuation and its potential rise due to rainfall infiltration. Spatial variability of flow paths (due to spatial variability of material, hydraulic conductivity) and uncertainties in boundary conditions are not taken into account either.

It was assumed the only process that affects seepage within the pile is infiltration; evaporation is not explicitly considered (although its effect can be included in the imposed recharge). Also, no case with positive pore water pressure within the pile was considered. The effect of water accumulation inside a pile over many years was not addressed either.

It was also seen that for some simulations, the local FS was smaller than 1 due to some numerical convergence issues. In such cases, the neighboring slices usually have a higher local FS that compensates for the lower ones. All mobilized and resisting shear forces are then tailed along the slip surface and local irregularities are smoothed out with little effect on the total forces. Hence, local safety factors that are less than unity can be ignored without affecting the results significantly (see SLOPE/W Manual).

The work presented in this thesis includes the following original and significant contributions to the current state of engineering knowledge and practice:

- Increase understanding of the slope stability behavior of the waste rock piles.

- Effect of geometric features and their impact on waste rock pile stability (i.e. number of benches, compacted layers, slope angle)

- Material geotechnical properties and their effect on waste rock pile stability

- Effect of apparent cohesion (due to suction) on stability (usually neglected)

- Effect of rainfall infiltration on waste rock pile stability due to various initial boundary conditions and, rainfall patterns.

- Effect of probabilistic distribution of strength parameters on stability.

It can be expected that many of the results presented here can help improve the analysis and design of waste rock piles, based on guidelines proposed by the author of this thesis and collaborators (e.g. Aubertin et al. 2013).

CHAPTER 7   CONCLUSION AND RECOMMENDATIONS

This thesis aimed at expanding our understanding of the slope stability and behavior for the case of unsaturated waste rock piles. This research was conducted by performing numerical analyses with the finite element method, limit equilibrium methods, and Monte-Carlo probabilistic simulations. The information gained from these activities has been combined to explain features related to the waste rock piles stability.

The investigation focussed on parametric analyses that covered different aspects of slope stability, for a variety of conditions that are deemed relevant for actual piles in the field. Local and global slip surfaces with both circular and non-circular (optimized) shapes are considered in the analyses. The results presented here lead to the following conclusions:

- Different parameters such as material strength (i.e. apparent cohesion and internal friction angle) and pile geometry (i.e. height, number of benches, existence of compacted layers, global slope angle) can affect the factor of safety of unsaturated waste rock piles

- The significance of the various factors is not the same, as the stability of unsaturated waste rock pile is more sensitive to some parameters compare to others. The apparent cohesion and some geometric components (i.e. addition of benches, adding compacted layers) may have a very positive contribution to the factor of safety of waste rock pile. Overall, the factor of safety is more sensitive to the external geometric configuration of the pile.

- Single bench waste rock piles (still commonly used often lead to the lower factor of safety. The results of this study indicate that an acceptable factor of safety (particularly for higher piles) can be attained by using multiple bench geometry, due to the increased overall slope angle. Such benches may also lead to an increase of the reliability index (RI) and a decrease of the probability of the failure (PoF). This information can be used for developing more stable waste rock pile design with a lower risk of failure.

- The presence of compacted layers (horizontal or inclined) within the waste rock pile may also have a positive impact on the factor of safety and reliability index. This aspect should also be considered in designing stable waste rock piles. The behavior of these compacted layers should be checked to avoid producing a local perched water table during and after rainfall.

- Probabilistic analyses of slope stability indicate that a single value of factor of safety might not be sufficient to evaluate the stability of waste rock pile. The outcomes of probabilistic analysis, including the reliability index (RI) and the probability of failure (PoF), can be very useful (as complementary parameters) for evaluating the stability and risk of failure of waste rock piles.

- Apparent cohesion can be effective for increasing the shear strength in unsaturated waste rock piles, but it is safe to neglect this contribution in the slope stability analysis. As shown here, rainfall infiltration may result in a decrease of suction and apparent cohesion, which in turn results in a decrease of shear strength and factor of safety. This aspect requires a good knowledge and understanding of hydraulic properties of waste rock and the internal geometric features in a pile (can be difficult in practice).

- The results of this research project are thus deemed useful to improve the approaches being used to analyze and design stable waste rock piles.

Recommendations for future study

This study has focused on developing the concepts and understanding the waste rock pile slope stability regarding different parameters. Future research work could take into consideration the following additional components and factors:

- Performing the slope stability analysis with three-dimensional models

- Consider different configurations for the piles and compacted layers; also consider the effect of water table increase due to precipitation.

- Water retention curve and hydraulic conductivity functions are essential factors in modeling water flow under unsaturated conditions. Probabilistic analyses should be conducted with spatial variation of this hydraulic conductivity during rainfall infiltrations in waste rock piles (as was done by Fala, 2008).

- The physical behavior of waste rock pile is controlled by different parameters including grain size distribution (that controls the hydraulic conductivity and flow path within the pile).

Further analyses to consider changes in the grain size distribution would be valuable in evaluating the long-term slope stability of waste rock piles.

- This thesis covers only the geotechnical aspects of the waste rock pile stability. However, geochemical aspects also must be considered in the design of waste rock piles.

- Continued work in this area could focus on developing methods to assess the effect of strain-softening, and weathering on strength, stability and settlements (and potential collapse),

BIBLIOGRAPHY

Abramson, L. W., Lee, T. S., Sharma, S., & Boyce, G. M. (2002). *Slope stability and stabilization methods* (Second ed.). USA: John Wiley & Sons.

Acharya, K. P., Bhandary, N. P., Dahal, R. K., & Yatabe, R. (2016). Seepage and slope stability modelling of rainfall-induced slope failures in topographic hollows. *Geomatics, Natural Hazards and Risk, 7*(2), 721-746.

Adamczyk, E. (Réalisateur). (2016). Landslide at Myanmar jade mine kills12 people.

Adams, R., Ahlfeld, D., & Sengupta, A. (2007). Investigating the potential for ongoing pollution from an abandoned pyrite mine:. *Mine Water and the Environment, 26*(1), 2-13.

Agaiby, S., Kulhawy, F., & Trautmann, C. (1996). On large-scale model testing of laterally loaded drilled shafts in sand. *ASTM geotechnical testing journal, 19*(1), 32-40.

Alonso, E. E. (1976). Risk analysis of slopes and its application to slopes in Canadian sensitive clays. *Geotechnique, 26*(3), 453-472.

Anderson, D. L., & Anderson, O. L. (1970). The bulk modulus volume relationship for oxides. *Journal of Geophysical research, 75* 3494–3500.

Anderson, L. R., Sharp, K. D., Bowles, D. S., & Canfield, R. V. (1984). *Application of methods of probabilistic characterization of soil properties.* Communication presented at Probabilistic Characterization of Soil Properties (p. 90-105).

Anderson, S. A., & Sitar, N. (1995). Analysis of rainfall-induced debris flows. *Journal of Geotechnical Engineering, 121*(7), 544-552.

Anterrieu, O., Chouteau, M., & Aubertin, M. (2010). Geophysical characterization of the large-scale internal structure of a waste rock pile from a hard rock mine. *Bulletin of engineering geology and the environment, 69*(4), 533-548.

Au, S. (1998). Rain-induced slope instability in Hong Kong. *Engineering Geology, 51*(1), 1-36.

Aubertin, M. (2013). *Waste rock disposal to improve the geotechnical and geochemical stability of piles.* Communication presented at Proceedings of the world mining congress, Montreal, Canada.

Aubertin, M., Bussière, B., Aachib, M., Chapuis, R. P., & Crespo, J. R. (1996). Une modélisation numérique des écoulements non saturés dans des couvertures multicouches en sols. *Hydrogéologie, 1* 3-13.

Aubertin, M., Bussiere, B., & Bernier, L. (2002a). *Environnement et gestion des rejets miniers*.

Aubertin, M., Cifuentes, E., Apithy, S., Bussière, B., Molson, J., & Chapuis, R. (2009). Analyses of water diversion along inclined covers with capillary barrier effects. *Canadian Geotechnical Journal, 46*(10), 1146-1164.

Aubertin, M., Fala, O., Bussière, B., Martin, V., Campos, D., Gamache-Rochette, A., . . . Chapuis, R. P. (2002b). *Analyse des écoulements de l'eau en conditions non saturées dans les haldes à stériles.* Communication presented at Symposium 2002 sur l'Environnement et les Mines, [CD-ROM], Rouyn-Noranda, Canada.

Aubertin, M., Fala, O., Molson, J., Chouteau, M., Anterrieu, O., Hernandez, M. A., Lefebvre, R. (2008). *Caractérisation du comportement hydrogéologique et géochimique des haldes à stériles.* Communication presented at Symposium Rouyn-Noranda:L'Environnement et les Mines, Rouyn-Noranda, Proc. on CD-ROM, CIM.

Aubertin, M., Fala, O., Molson, J., Gamache-Rochette, A., Lahmira, B., Martin, V., WILSON, G. W. (2005). *Évaluation du comportement hydrogéologique et géochimique des haldes à stériles.* Communication presented at Symposium Rouyn-Noranda: L'Environnement et les Mines, mai 2005,, Rouyn-Noranda, Proc. on CD-ROM, CIM. (p. 15-18).

Aubertin, M., Mbonimpa, M., Bussière, B., & Chapuis, R. P. (2003). A model to predict the water retention curve from basic geotechnical properties. *Canadian Geotechnical Journal, 40*(6), 1104-1122.

Aubertin, M., Ricard, J., & Chapuis, R. (1998). A predictive model for the water retention curve: application to tailings from hard-rock mines. *Canadian geotechnical journal, 35*(1), 55-69.

Ayres, B., Landine, P., Adrian, L., Christensen, D., & O'Kane1, M. (2006). Cover and final landform design for the B-zone waste rock pile at Rabbit Lake Mine. *Uranium in the Environment* 739-749.

Azam, S., Wilson, W. G., Herasymuik, G., Nichol, C., & Barbour, L. S. (2007). Hydrogeological behaviour of an unsaturated waste rock pile: A case study at the Golden Sunlight Mine, Montana, USA. *Bulletin of Engineering Geology and the Environment, 66*(Compendex), 259-268. Tiré de http://dx.doi.org/10.1007/s10064-006-0077-7

Baecher, G. (1987). *Statistical Analysis of Geotechnical Data*. DTIC Document.

Baecher, G., & Christian, J. (2003). *Geotechnical reliability: playing cards with the universe.* Communication presented at Proceedings of 12th Pan-American Conference on Soil Mechanics and Geotechnical Engineering. Cambridge: Massachusetts, America.

Baecher, G. B. (1987). *Geotechnical risk analysis user's guide*. Rep. No. FHWA/RD-87-011,: Federal Highway Administration, McLean, Va.

Bao, C., Gong, B., & Zhan, L. (1998). *Properties of unsaturated soils and slope stability of expansive soils. Keynote Lecture, UNSAT 98*.

Barbour, S., Hendry, M., Smith, J., Beckie, R., & Wilson, G. (2001). A research partnership program in the mining industry for waste rock hydrology. *University of Saskatchewan, Canada*.

Barbour, S. L., Hendry, M. J., Smith, J. L., Beckie, R. D., & Wilson, G. W. (2001). *A research partnership program in the mining industry for waste rock hydrology. Workshop Notes(unpublished)*. NSERC CRD Project. University of Saskatchewan, Canada.

Barker, R., Duncan, J., Rojiani, K., Ooi, P., Tan, C., & Kim, S. (1991). Manuals for the design of bridge foundations. *NCHRP Report, 343*.

Barton, N. (1981). *Shear strength investigations for surface mining.* Communication presented at 3rd International Conference on stability surface mining, Vancouver.

Barton, N., & Kjaernsli, B. (1981). Shear strength of rockfill. *Journal of the Geotechnical Engineering Division, 107*(7), 873-891.

Barton, N. R. (2008). *Shear Strength of rockfill, interfaces and rock Joints and their points of contact in rock dump design; in A. Fourie, ed.,*. Communication presented at Rock Dumps 2008: Australian Centre for Geomechanics, Perth (p. 3-17).

Basile, A., Mele, G., & Terribile, F. (2003). Soil hydraulic behaviour of a selected benchmark soil involved in the landslide of Sarno 1998. *Geoderma, 117*(3-4), 331-346.

Becker, D. E. (1997). Limit states design for foundations. Part II. Development for the national building code of Canada. *Canadian Geotechnical Journal, 33*(6), 984-1007.

Becker, E., Chan, C. K., ., & Seed, H. B. (1972). *Strength and deformation characteristics of rockfill materials in plane strain and triaxial compression tests*. Dept. of civil Eng., Univ. of California, Berkeley, CA.

Benda, L. E., & Cundy, T. W. (1990). Predicting deposition of debris flows in mountain channels. *Canadian Geotechnical Journal, 27*(4), 409-417.

Bergado, D. T., & Anderson, L. R. (1985). Stochastic analysis of pore pressure uncertainty for the probabilistic assessment of the safety of earth slopes. *Soils and Found, 25*(2), 87-105.

Bian, Z., Dong, J., Lei, S., Leng, H., Mu, S., & Wang, H. (2009). The impact of disposal and treatment of coal mining wastes on environment and farmland. *Environmental geology, 58*(3), 625-634.

Billam, J. (1971). *Some aspects of the behaviour of granular materials at high pressures.* Communication presented at Proceeding of Roscoe memorial symposium on stress-strain behavior of soils, Cambridge University (p. 69-80).

Bishop, A., . (1954). The use of pore pressure coefficients in practice. *Geotechnique, 4*(4), 148-152.

Bishop, A. W. (1954). The use of pore-pressure coefficients in practice. *Geotechnique, 4*(4), 148-152.

Blight, G. (2010). *Geotechnical engineering for mine waste storage facilities*: CRC Press.

Boakye, K. (2008). *Large in Situ Direct Shear Tests on Rock Piles at the Questa Mine, Taos County, New Mexico.* (M. Sc. Thesis, Socorro, New Mexico).

Bordoni, M., Meisina, C., Valentino, R., Lu, N., Bittelli, M., & Chersich, S. (2015). Hydrological factors affecting rainfall-induced shallow landslides: From the field monitoring to a simplified slope stability analysis. *Engineering Geology, 193* 19-37.

Borja, R. I., & White, J. A. (2010). Continuum deformation and stability analyses of a steep hillside slope under rainfall infiltration. *Acta Geotechnica, 5*(1), 1-14.

Bowles, J. E. (1984). *Physical and Geotechnical Properties of Soils (London: McGraw-Hill)*

Bowles, J. E. (1996). *Foundation analysis and design*: 5th ed. McGrawHill, NewYork.

Brooks, R. H. (1964). Hydraulic properties of porous media.

Brooks, R. H., & Corey, A. T. (1964). Hydraulic properties of porous media and their relation to drainage design. *Transactions of the ASAE, 7*(1), 26-0028.

Brooks, S., Richards, K., & Anderson, M. (1993). Shallow failure mechanism during the Holocene: utilisation of a coupled slope hydrology-slope stability model. *Landscape Sensitivity* 149-175.

Burnley, R. B. (1993). *Mine reclamation and waste dump stability.* (M. Sc. Thesis, University of Nevada, Reno, Reno, United States).

Buscarnera, G., & Whittle, A. J. (2012). Constitutive modelling approach for evaluating the triggering of flow slides. *Canadian Geotechnical Journal, 49*(5), 499-511.

Bussière, B. (1999). *Étude du comportement hydrique de couvertures avec effets de barrières capillaires inclinées à l'aide de modélisations physiques et numériques.* (Ph. D. Thesis, École Polytechnique de Montréal, Que.).

Bussière, B. (2007). Hydro-geotechnical properties of hard rock tailings from metal mines and emerging geo-environmental disposal approaches. *Canadian Geotechnical Journal, 44*(9), 1019-1052.

Bussière, B., & Aubertin, M. (1999). *Clean tailings as cover material for preventing acid mine drainage: an in situ experiment.* Communication presented at In: Goldsack D, Belzile N, Yearwood P, Hall G (eds) Proc Sudbury'99 Conf Mining and the Environment II, September 13–17, Sudbury, Canada, (vol. 1, p. pp 19–28).

Bussière, B., Demers, I., Dawood, I., Plante, B., Aubertin, M., Peregoedova, A., . . . Benzaazoua, M. (2011). *Comportement géochimique et hydrogéologique des stériles de la mine Lac Tio.* Communication presented at Proceedings of the Symposium sur l'Environnement et les Mines, Rouyn-Noranda. CIM.[CD-ROM].

Cai, F., & Ugai, K. (2004). Numerical analysis of rainfall effects on slope stability. *International Journal of Geomechanics, 4* 69.

Caldwell, J. A., & Moss, A. S. E. (1981). *The simplified analysis of mine waste embankments.* Communication presented at Symposium on design of non-impounding mine waste embankments., Denver USA. AIME Fall Meeting.

Campbell, G. S. (1974). A simple method for determining unsaturated conductivity from moisture retention data. *Soil science, 117*(6), 311-314.

Casagli, N., Dapporto, S., Ibsen, M., Tofani, V., & Vannocci, P. (2006). Analysis of the landslide triggering mechanism during the storm of 20th–21st November 2000, in Northern Tuscany. *Landslides, 3*(1), 13-21.

Chapuis, R. (2010). *Stockage géologique des déchets- Note des cours*. Ecole polytechnique Montreal:

Chapuis, R., Chenaf, D., Bussière, B., Aubertin, M., & Crespo, R. (2001). A user's approach to assess numerical codes for saturated and unsaturated seepage conditions. *Canadian geotechnical journal, 38*(5), 1113-1126.

Chapuis, R. P. (2004). Predicting the saturated hydraulic conductivity of sand and gravel using effective diameter and void ratio. *Canadian Geotechnical Journal, 41*(5), 787-795.

Chapuis, R. P., & Aubertin, M. (2003). On the use of the Kozeny–Carman equation to predict the hydraulic conductivity of soils. *Canadian Geotechnical Journal, 40*(3), 616-628.

Chapuis, R. P., Gill, D. E., & Baass, K. (1989b). Laboratory permeability tests on sand: influence of the compaction method on anisotropy. *Canadian Geotechnical Journal, 26* 614-622.

Charles, J. (1990). *Laboratory compression tests and the deformation of rockfill structures.* Communication presented at in Advances in Roekfill Structures, Maranha das Neves, E., Proc of NATO Advanced Science. , London: Kluwer (p. 72-95).

Chen, H., Lee, C., & Law, K. (2004). Causative mechanisms of rainfall-induced fill slope failures. *Journal of geotechnical and geoenvironmental engineering, 130*(6), 593-602.

Cheng, Y. M., & Lau, C. K. (2014). *Slope stability analysis and stabilization: new methods and insight (2nd ed.)*: CRC Press.

Cherubini, C. (1997). *Data and considerations on the variability of geotechnical properties of soils.* Communication presented at Proceedings of the international conference on safety and reliability, ESREL (vol. 97, p. 1583-1591).

Cherubini, C. (2000). Reliability evaluation of shallow foundation bearing capacity on c'φ'soils. *Canadian Geotechnical Journal, 37*(1), 264-269.

Cherubini, C., Giasi, C., & Rethati, L. (1993). The coefficients of variation of some geotechnical parameters. *Probabilistic methods in geotechnical engineering. Editado por KS Li y S.-CR Lo. AA Balkema, Rotterdam* 179-184.

Cho, G. C., Dodds, J., & Santamarina, J. C. (2006). Particle shape effects on packing density, stiffness, and strength: Natural and crushed sands. *Journal of Geotechnical and Geoenvironmental Engineering, 132*(5), 591-602. Tiré de http://dx.doi.org/10.1061/(ASCE)1090-0241(2006)132:5(591)

Cho, S. E. (2007). Effects of spatial variability of soil properties on slope stability. *Engineering Geology, 92*(3), 97-109.

Cho, S. E. (2010). Probabilistic assessment of slope stability that considers the spatial variability of soil properties. *Journal of geotechnical and geoenvironmental engineering, 136 (7)* 135-146.

Cho, S. E., & Lee, S. R. (2001). Instability of unsaturated soil slopes due to infiltration. *Computers and Geotechnics, 28*(3), 185-208.

Christian, J. T. (2004). How well do we know what we are doing? *Journal of geotechnical and geoenvironmental engineering, 130*(10), 985-1003.

Christian, J. T., Ladd, C. C., & Baecher, G. B. (1994). Reliability applied to slope stability analysis. *Journal of Geotechnical Engineering, 120(12)* pp. 2180–2207.

Claridge, F. B., Nichols, R. S., & Stewart, A. F. (1986). Mine waste dumps constructed in mountain valleys. *CIM Bulletin, 892* 79-87.

Coduto, D. (1999). Geotechnical engineering: principles and practices Prentice-Hall International London: Abt, Alan.

Collins, B. D., & Znidarcic, D. (2004). Stability analyses of rainfall induced landslides. *Journal of Geotechnical and Geoenvironmental Engineering, 130*(4), 362-372.

Cornforth, D. (2005). *Landslides in practice: investigation, analysis, and remedial/preventative options in soils*. Hoboken, NJ: Wiley.

Dai, F., Deng, J., Tham, L., Law, K., & Lee, C. (2004). A large landslide in Zigui County, Three Gorges area. *Canadian Geotechnical Journal, 41*(6), 1233-1240.

Das, B. (2003). *Principles of foundation engineering (5th edition), .* PWS, Boston, MA Cengage learning.

Das, B. M. (1983). *Advanced Soil Mechanics*: New York, McGraw-Hill Book Company.

Dawood, I., & Aubertin, M. (2009). *A numerical investigation of the influence of internal structure on the unsaturated flow in a large waste rock pile*. Communication presented a t GeoHalifax2009, Halifax.

Dawood, I., & Aubertin, M. (2012). *Influence of internal layers on water flow inside a large waste rock piles. Technical Report EPM-RT-2012-001*

Montreal, Quebec, Canada: École Polytechnique de Montreal.

Dawood, I., & Aubertin, M. (2014). Effect of Dense Material Layers on Unsaturated Water Flow Inside a Large Waste Rock Pile: A Numerical Investigation. *Mine Water and the Environment, 33*(1), 24-38.

Dawood, I., Aubertin, M., Intissar, R., & Chouteau, M. (2011). *A combined hydrogeological–geophysical approach to evaluate unsaturated flow in a large waste rock pile*. Communication presented a t Pan-Am CGS Geotechnical Conference Toronto, Canada.

Dawson, E., Roth, W., & Drescher, A. (1999). Slope stability analysis by strength reduction. *Geotechnique, 49*(6), 835-840.

Delleur, J. W. (2006). *The handbook of groundwater engineering*: CRC press.

Deng, Q., Zhu, Z., Cui, Z., & Wang, X. (2000). Mass rock creep and landsliding on the Huangtupo slope in the reservoir area of the Three Gorges Project, Yangtze River, China. *Engineering geology, 58*(1), 67-83.

Duncan, J. M. (1996). State of the art: limit equilibrium and finite-element analysis of slopes. *Journal of Geotechnical engineering, 122*(7), 577-596.

Duncan, J. M. (2000). Factors of safety and reliability in geotechnical engineering. *Journal of geotechnical and geoenvironmental engineering, 126*(4), 307-316.

Duncan, J. M., & Wright, S. G. (2005). *Soil strength and slope stability*: Wiley, Hoboken, N.J.

Duncan, J. M., Wright, S. G., & Brandon, T. L. (2014). *Soil strength and slope stability*: John Wiley & Sons.

Dye, H. B., Houston, S. L., & Welfert, B. D. (2009). Influence of Unsaturated Soil Properties Uncertainty on Moisture Flow Modeling. *Geotechnical and Geological Engineering* 1-9.

El-Ramly, H., Morgenstern, N., & Cruden, D. (2002). Probabilistic slope stability analysis for practice. *Canadian Geotechnical Journal, 39*(3), 665-683.

El-Ramly, H. M. F. (2001). *Probabilistic analyses of landslide hazards and risks: bridging theory and practice.* (Ph.D. Thesis, Univ. of Alberta, Alberta, Canada).

El Mkadmi, N. (2012). *Simulations du comportement géotechnique des remblais dans les chantiers miniers: effets du drainage et de la consolidation.* (M. Sc. Thesis, École Polytechnique de Montréal, Canada).

Espinoza, R. D. (1999). *Infiltration. The Handbook of Groundwater Engineering (Jack W. Delleur, ed.),* . CRC Press. Boca Raton, Fl.

Fala, O. (2002). *Étude des écoulements non saturés dans les haldes à stériles à l'aide de simulations numériques.* (M. Sc. Thesis, École polytechnique Montréal, Montréal, Québec, Canada).

Fala, O. (2008). *Analyses des conditions d'ecoulement non sature dans les haldes a steriles.* (Ph. D. Thesis, Ecole Polytechnique Mnotreal).

Fala, O., Aubertin, M., Bussière, B., Chapuis, R., & Molson, J. (2008). *Stochastic numerical simulations of long term unsaturated flow in waste rock piles.* Communication presented at GeoEdmonton 2008. Proc. Can. Geot. Conf., (p. pp. 1492-1498.).

Fala, O., Molson, J., Aubertin, M., Bussière, B., & Chapuis, R. P. (2006). *Numerical simulations of long term unsaturated flow and acid mine drainage at waste rock piles* Communication presented at In Procedings of the 7th international Conference on Acid Rock Drainage (ICARD) and the 23rd Annual Meetings of the Amercian Society of Mining and Reclamation, St. Louis, R.I. Barnhisel (ed.). (p. pp. 582-597.).

Fala, O., Molson, J. W., Aubertin, M., & Bussiere, B. (2005). Numerical modelling of flow and capillary barrier effects in unsaturated waste rock piles. *Mine Water and the Environment, 24*(4), 172-185.

Fourie, A. (1996). *Predicting rainfall-induced slope instability.* Communication presented at Proc. Instn Civ.Engrs Geotech. Engng, (vol. Vol. 119,, p. pp. 211-218).

Fredlund, D. G. (1984). *Analytical methods for slope stability analysis, State-of-the-Art.* Communication presented at Proc. 4th Int. Symp. Landslides, 1, Toronto (p. 229-250).

Fredlund, D. G. (1989). *Negative pore water pressures in slope stability.* Communication presented at Proceeding Simposio Suramericano de Deslizamientos, Paipa, Columbia.

Fredlund, D. G. (1995). *The stability of slopes with negative pore water pressures.* Communication presented at Proceedings, Ian Boyd Donald Symposium on Modern Developements in Geomechanics, Monash university, Melbourne, Australia (p. pp. 99-116).

Fredlund, D. G. (2000a). The 1999 RM Hardy Lecture: The implementation of unsaturated soil mechanics into geotechnical engineering. *Canadian Geotechnical Journal, 37*(5), 963-986.

Fredlund, D. G. (2000b). Slope stability analysis involving unsaturated soils,From Theory to Practice of Unsaturated Soil Mechanics, Session 12, . Dans. CGS, Montreal.

Fredlund, D. G., Morgenstern, N. R., & Widger, R. A. (1978). The shear strength of unsaturated soils. *Canadian Geotechnical Journal, 15*(3), 313-321.

Fredlund, D. G., & Rahardjo, H. (1993). *Soil mechanics for unsaturated soils*: Wiley-Interscience.

Fredlund, D. G., & Xing, A. (1994). Equations for the soil-water characteristic curve. *Canadian geotechnical journal, 31*(4), 521-532.

Fredlund, D. G., Xing, A., Fredlund, M. D., & Barbour, S. L. (1996). The relationship of the unsaturated soil shear to the soil-water characteristic curve. *Canadian Geotechnical Journal, 33*(3), 440-448.

Freeze, R. A., & Cherry, J. A. (1979). *Groundwater*: Prentice-Hall, Englewood Cliffs, NJ.

Gamache-Rochette, A. (2004). *Une étude de caractérisation en laboratoire et sur le terrain des écoulements de l'eau dans les roches stériles.* (École Polytechnique de Montréal.).

Garven, E. A., & Vanapalli, S. K. (2006). *Evaluation of empirical procedures for predicting the shear strength of unsaturated soils.* Communication presented at Proceedings of the Fourth International Conference on Unsaturated Soils,, Carefree, Arizona, (vol. 147(2):, p. 2570–2581).

Gasmo, J., Rahardjo, H., & Leong, E. C. (2000). Infiltration effects on stability of a residual soil slope. *Computers and Geotechnics, 26*(2), 145-165.

Gavin, K., & Xue, J. (2010). Design Charts for the Stability Analysis of Unsaturated Soil Slopes. *Geotechnical and Geological Engineering, 28*(1), 79-90.

GeoSlope International Ltd. (2008). *Stress-deformation Modeling with SIGMA/W 2007*.

Gerscovich, D., Vargas, E., & De Campos, T. (2006). On the evaluation of unsaturated flow in a natural slope in Rio de Janeiro, Brazil. *Engineering Geology, 88*(1), 23-40.

Godt, J., Baum, R., & Lu, N. (2009). Can landslides occur under unsaturated soil conditions. *Geophys Res Lett, 36* L02403.

Gofar, N., & Kassim, K. A. (2007). *Introduction to Geotechnical Engineering*: Prentice Hall/Pearson Education South Asia.

Griffiths, D., & Fenton, G. A. (2004). Probabilistic slope stability analysis by finite elements. *Journal of Geotechnical and Geoenvironmental Engineering, 130*(5), 507-518.

Griffiths, D., Huang, J., & Fenton, G. A. (2009). Influence of spatial variability on slope reliability using 2-D random fields. *Journal of Geotechnical and Geoenvironmental Engineering, 135*(10), 1367-1378.

Griffiths, D., & Lane, P. (1999). Slope stability analysis by finite elements. *Geotechnique, 49*(3), 387-403.

Griffiths, D. F., GA. (2007). Probabilistic methods in geotechnical engineering Dans: SpringerWienNewYork.

Guan, G. S., Rahardjo, H., & Choon, L. E. (2010). Shear Strength Equations for Unsaturated Soil under Drying and Wetting. *Journal of Geotechnical and Geoenvironmental Engineering, 136* 594-606.

Gui, S., Zhang, R., Turner, J. P., & Xue, X. (2000). Probabilistic slope stability analysis with stochastic soil hydraulic conductivity. *Journal of Geotechnical and Geoenvironmental Engineering, 126*(1), 1-9.

Gutierrez, L. (2006). *The influence of mineralogy, chemistry and physical engineering properties on shear strength parameters of the goathill north rock pile material, Questa molybdenum mine, New Mexico,.* (M. Sc. Thesis, Socorro, New Mexico).

Guzzetti, F., Peruccacci, S., Rossi, M., & Stark, C. P. (2007). Rainfall thresholds for the initiation of landslides in central and southern Europe. *Meteorology and Atmospheric Physics, 98*(3-4), 239-267.

Haldar, A., & Mahadevan, S. (2000). *Probability, reliability, and statistical methods in engineering design*: John Wiley & Sons, Incorporated.

Harr, M. E. (1987). Reliability-Based Design in Civil Engineering: New York: McGraw-Hill.

Hawley, P. M. (2000). Site Selection:, Characterization, and Assessment. Dans M. K. M. a. D. J. A. v. Z. In: W.A. Hustrulid (Édit.), *Slope Stability in Surface Mining* (p. 267-274): Society for Mining Metallurgy.

Herasymuik, G. M. (1996). *Hydrogeology of a sulphide waste rock dump.* (M. Sc. Thesis, University of Saskatchewan, Saskatoon, Saskatchewan, Canada).

Hernandez, M. A. (2007). *Une étude expérimentale des propriétés hydriques des roches stériles et autres matériaux à granulométrie étalée.* (M. Sc. Thesis, École Polytechnique de Montréal).

Hicks, M. A., & Samy, K. (2002). Influence of heterogeneity on undrained clay slope stability. *Quarterly Journal of Engineering Geology and Hydrogeology, 35*(1), 41-49.

Hockley, D. E., Noel, M., Rykaart, E. M., Jahn, S., & Paul, M. (2003). *Testing of soil covers for waste rock in the ronneburg WISMUT mine closure*. Communication presented a t 6th ICARD,, Cairns, Australia.

Höeg, K., & Murarka, R. P. (1974). Probabilistic analysis and design of a retaining wall. *Journal of the Geotechnical Engineering Division, 100*(3), 349-366.

Holtz, R. D., Kovacs, W. D., & Sheahan, T. C. (2010). *An introduction to geotechnical engineering* (second edition^e éd.): Pearson.

Hribar, J., Dougherty, M., Ventura, J., & Yavorskyu, P. (1986). *Large scale direct shear tests on surface mine spoil:*. Communication presented at International symposium on geotechnical stability in surface mining, , Calgery, November (p. p. 295-303.).

Huat, B. B., Ali, F. H., & Low, T. (2006). Water infiltration characteristics of unsaturated soil slope and its effect on suction and stability. *Geotechnical & Geological Engineering, 24*(5), 1293-1306.

Hughes, T. J. (2012). *The finite element method: linear static and dynamic finite element analysis*: Courier Corporation.

Hustrulid, W. A., McCarter, M. K., & Van Zyl, D. J. A. (2000). *Slope stability in surface mining*: Society for Mining Metallurgy.

Hutchinson, J. (1988). *General report: Morphological and geotechnical parameters of landslides in relation to geology and hydrogeology:*. Communication presented at 5th International symposium on landslides, , Switzerland, (vol. 1, p. p. 3-35.).

Huyakorn, P. S. (2012). *Computational methods in subsurface flow*: Academic Press.

Igo, M. (2006). *Two-dimensional parametric study of rainfall infiltration into slopes.* (M. Sc. Thesis, TUFTS UNIVERSITY).

Indrawan, I. G. B., Rahardjo, H., & Leong, E. C. (2006). *Study of Infiltration Characteristics in the Field.* Communication presented at ASCE Conf. Proc., Carefree, Arizona, USA (vol. v. 189, p. pp. 9-9).

Iverson, R. M. (2000). Landslide triggering by rain infiltration. *Water resources research, 36*(7), 1897-1910.

Janbu, N. (1959). *Stability analysis of slopes with dimensionless parameters*: Harvard University, Division of Engineering and Applied Physics.

Janbu, N. (1975). *Slope stability computations: In Embankment-dam Engineering. Textbook. Eds. RC Hirschfeld and SJ Poulos. JOHN WILEY AND SONS INC., PUB., NY, 1973, 40P.* Communication presented at International Journal of Rock Mechanics and Mining Sciences & Geomechanics Abstracts (vol. 12, p. 67).

Jia, G., Zhan, T. L., Chen, Y., & Fredlund, D. (2009). Performance of a large-scale slope model subjected to rising and lowering water levels. *Engineering Geology, 106*(1), 92-103.

Jones, F. O., Embody, D. R., Peterson, W. L., & Hazlewood, R. M. (1961). *Landslides along the Columbia River valley, northeastern Washington, with a section on seismic surveys* (Rapport nᵒ 2330-7102). US Govt. Print. Off.

Kesimal, A., Yilmaz, E., & Ercikdi, B. (2004). Evaluation of paste backfill mixtures consisting of sulphide-rich mill tailings and varying cement contents. *Cement and Concrete Research, 34*(10), 1817-1822.

Kézdi, Á., & Rétháti, L. (1974). *Handbook of soil mechanics* (vol. 1): Elsevier Amsterdam.

Khalili, N., & Khabbaz, M. H. (1998). A unique relationship for the determination of the shear strength of unsaturated soils. *Geotechnique, 48*(5), 681-687.

Kim, J., Jeong, S., & Regueiro, R. A. (2012). Instability of partially saturated soil slopes due to alteration of rainfall pattern. *Engineering Geology*.

Kingpaiboon S.; Netwong T. (2004). *Relation of Probable Maximum Precipitation Depth-Area-Duration Using GIS*. Communication presented a t 24th Annual ESRI International User Conference.

Kirkby, M. (1987). General models of long-term slope evolution through mass movement. *Slope Stability: Geotechnical Engineering and Geomorphology. John Wiley and Sons New York. 1987. p 359-379, 11 fig, 25 ref.*

Klohn Leonoff Ltd. (1991). *Mined rock and overburden piles: Operating and monitoring manual*. Victoria; British Columbia: Prepared for British Columbia Mine Dump Committee and Ministry of Energy and Mines.

Kovacs, G. (1981). *Seepage Hydraulics.*: Elsevier Science Publishers, Amsterdam.

Krahn, J. (2007a). *Limit Equilibrium, Strength Summation and Strength Reduction Methods for Assessing Slope Stability.* Communication presented at Proceeding, 1st Canada-US Rock Mechanics Symposium, Vancouver, BC May (p. 27-31).

Krahn, J. (2007b). *Seepage Modeling with Seep/W*.

Krahn, J. (2007c). *Stability modeling with Slope/W*.

Krahn, J. (2007d). *Stress-deformation modeling with SIGMA/W 2007*.

Kulhawy, F. H. (1993). *On the evaluation of static soil properties.* Communication presented at Stability and performance of slopes and Embankments II (p. 95-115).

Kulkarni, B. (2002). Generalized physical approach of estimating areal probable maximum precipitation (PMP) for plain region of the Godavari river basin (India). *Journal of Spatial Hydrology, 2*(2).

L-Bolduc, F. (2012). *Une étude sur l'utilisation des roches stériles comme inclusions drainantes dans les résidus miniers.* (M. Sc. Thesis, École Polytechnique de Montréal).

Lacasse, S., & Nadim, F. (1997). Uncertainties in characterising soil properties. *Publikasjon-Norges Geotekniske Institutt, 201* 49-75.

Lacasse, S. N. (1996). *Uncertainties in characterizing soil properties.* Communication presented at Proceedings of ASCE GED Special Conference on Uncertainty in the Geologic Environment: From Theory to Practice, Madison, Wisconsin (vol. 49, p. 75).

Laloui, L., Ferrari, A., & Eichenberger, J. (2010). Effect of climate change on landslide behaviour. *Geo-Strata – Geo Institute of ASCE, 14(5)*(September/October 2010), 36-41.

Lane, K. (1966). *Stability of reservoir slopes.* Communication presented at The 8th US Symposium on Rock Mechanics (USRMS).

Lane, P., & Griffiths, D. (2000). Assessment of stability of slopes under drawdown conditions. *Journal of Geotechnical and Geoenvironmental Engineering, 126*(5), 443-450.

Lee, I. K., White, W., & Ingles, O. G. (1983). *Geotechnical Engineering*: Pitmans Books Limited.

Lee, I. M., Sung, S. G., & Cho, G. C. (2005). Effect of stress state on the unsaturated shear strength of a weathered granite. *Canadian Geotechnical Journal, 42*(2), 624-631.

Lee, L. M., Kassim, A., & Gofar, N. (2011). Performances of two instrumented laboratory models for the study of rainfall infiltration into unsaturated soils. *Engineering Geology, 117*(1), 78-89.

Leps, T. M. (1970). Review of shearing strength of rockfill. *Journal of the Soil Mechanics and Foundations Division, 96*(4), 1159-1170.

Lessard, G. (2011). *Essais d'infiltration sur la halde à stériles Petit-Pas de la mine Tio, Havre-St-Pierre.* (M. Sc. Thesis, École Polytechnique de Montréal, Québec, Canada).

Li, A. G., Yue, Z. Q., Tham, L. G., Lee, C. F., & Law, K. T. (2005). Field-monitored variations of soil moisture and matric suction in a saprolite slope. *Canadian Geotechnical Journal, 42*(1), 13-26.

Li, K., & Lumb, P. (1987). Probabilistic design of slopes. *Canadian Geotechnical Journal, 24*(4), 520-535.

Li, M. (2000). *Unsaturated flow and transport observations in large waste rock columns.* Communication presented at in Proceedings fifth international conference on acid rock drainage: (p. pp 247-256).

Lim, T. T., Rahardjo, H., Chang, M. F., & Fredlund, D. G. (1996). Effect of rainfall on matric suctions in a residual soil slope. *Canadian Geotechnical Journal, 33*(4), 618-628.

Linero, S., Palma, C., & Apablaza, R. (2007). *Geotechnical characterisation of waste material in very high dumps with large scale triaxial testing:.* Communication presented at Proceedings of international symposium on rock slope stability in open pit mining and civil engineering, 12-14 September 2007, Perth, Australia (p. p. 59-75).

Lu, N., & Likos, W. J. (2004). *Unsaturated soil mechanics*: Wiley, Hoboken, NJ.

Lu, N., Şener-Kaya, B., Wayllace, A., & Godt, J. W. (2012). Analysis of rainfall-induced slope instability using a field of local factor of safety. *Water Resources Research, 48*(9).

Lumb, P. (1966). The variability of natural soils. *Canadian Geotechnical Journal, 3*(2), 74-97.

Lumb, P. (1974). Application of statistics in soil mechanics. *Soil Mechanics New Horizons. IK Lee, ed, 1974*.

Lumb, P. (1975). Slope failures in Hong Kong. *Quarterly Journal of Engineering Geology & Hydrogeology, 8*(1), 31-65.

Manoliu, I., & Marcus, A. *years of utilization of the limit state concept in the Romanian Code for geotechnical design.* Communication presented at Proceedings of the International Symposium on Limit State Design in Geotechnical Engineering. Copenhagen, may (p. 26-28).

Marachi, N. D., Chan, C. K., Seed, H. B., & Duncan, J. M. (1969). *Strength and deformation characteristics of rockfill materials: .* Dept. of Civil Eng., Univ. of California, Berkeley, California.

Marasal, R. J. (1965). *Soil properties, shear strength and consolidation:.* Communication presented at Proceedings 6th international conference on soil mechanics and foundation engineering, (vol. Vol. 3, p. pp. 310-316).

Marescotti, P., Carbone, C., De Capitani, L., Grieco, G., Lucchetti, G., & Servida, D. (2008). Mineralogical and geochemical characterisation of open-air tailing and waste-rock dumps from the Libiola Fe-Cu sulphide mine (Eastern Liguria, Italy). *Environmental Geology, 53*(8), pp. 1613-1626.

Marsal, R. J. (1967). Large-scale testing of rockfill materials. *Journal of the Soil Mechanics and Foundations Division, 93*(2), 27-43.

Martin, V. (2004). *Étude des propriétés non saturées des stériles miniers.* (M. Sc. Thesis, École Polytechnique de Montréal, Montreal).

Matsuo, M., & KURODA, K. (1974). Probabilistic approach to design of embankments. *Soils and foundations 14*(2).

Mbonimpa, M., Aubertin, M., Chapuis, R. P., & Bussière, B. (2002). Practical pedotransfer functions for estimating the saturated hydraulic conductivity. *Geotechnical and Geological Engineering, 20*(3), 235-259.

McCarter, M. K. (1990). Design and operating considerations for mine waste embankments. Dans *in surface mining* (p. pp. 890-899): Society of mining, metallurgy and expliration: Littleton CO United States.

McCarthy, D. F. (2007). *Essentials of Soil Mechanics and Foundations-Basic Geotechnics*: Prentice-Hall International

McLemore, V. T., Donahue. K.M., Walsh, P., Tachie-Menson, S., Phillips, E. H., Guitierrez, L. A. F., & Shannon, H. R. (2005). Trench Sampling of the Molycorp Goathill Northrock

piles, Questa Rock Pile Stability Study, New Mexico. *National Meeting of the American Society of Mining and Reclamation, .*

McLemore, V. T., Fakhimi, A., van Zyl, D., Ayakwah, G. F., Anim, K., Boakye, K., . . . S., V., V.C. (2009). *Literature review of other rock piles: characterization, weathering, and stability: New Mexico Bureau of Geology and Mineral Resources* New Mexico Bureau of Geology and Mineral Resources.

Meyerhof, G. G. (1995). Development of geotechnical limit state design. *Canadian Geotechnical Journal, 32*(1), 128-136.

Moffitt, K. (2000). *Mine waste dump instability.* (M. Sc. Thesis, University of british columbia).

Molson, J. W., Fala, O., Aubertin, M., & Bussiere, B. (2005). Numerical simulations of pyrite oxidation and acid mine drainage in unsaturated waste rock piles. *Journal of Contaminant Hydrology, 78*(4 Issue date:August 2005), 343-371. doi: 10.1016/j.jconhyd.2005.06.005

Moregenstern, N. (1963). Stability charts for earth slopes during rapid drawdown. *Geotechnique, 13*(2), 121-131.

Morgenstern, N. (1995). *Managing risk in geotechnical engineering.* Communication presented at Memorias del 10mo Congreso Panamericano de Mecánica de Suelos e Ingeniería de Fundaciones (vol. 4).

Morgenstern, N., & Price, V. E. (1965). The analysis of the stability of general slip surfaces. *Geotechnique, 15*(1), 79-93.

Morin, K. A., Gerencher, E., Jones, C. E., & Konasewich, D. E. (1991). *Critical review of acid drainage from waste rock*. MEND Report 1.11.1.

Mualem, Y. (1976). A new model for predicting the hydraulic conductivity of unsaturated porous media. *Water Resources Research, 12* 513-522.

Mukhlisin, M., Kosugi, K. i., Satofuka, Y., & Mizuyama, T. (2006). Effects of soil porosity on slope stability and debris flow runout at a weathered granitic hillslope. *Vadose Zone Journal, 5*(1), 283-295.

Muntohar, A. S., & Liao, H.-J. (2009). Analysis of rainfall-induced infinite slope failure during typhoon using a hydrological–geotechnical model. *Environmental geology, 56*(6), 1145-1159.

Na, Y. M., Choa, V., Teh, C. I., & Chang, M. F. (2005). Geotechnical parameters of reclaimed sandfill from the cone penetration test. *Canadian Geotechnical Journal, 42*(1), 91-109.

Napolitano, E., Fusco, F., Baum, R. L., Godt, J. W., & De Vita, P. (2015). Effect of antecedent-hydrological conditions on rainfall triggering of debris flows in ash-fall pyroclastic mantled slopes of Campania (southern Italy). *Landslides* 1-17.

Narvaez, Y. B. (2013). *Étude expérimentale de la résistance en traction de résidus miniers non saturés à l'aide d'essais de flexion.* (M.Sc. Thesis, École Polytechnique de Montréal, Montreal).

Nash, D. (1987). Comparative review of limit equilibrium methods of stability analysis. *Slope Stability: Geotechnical Engineering and Geomorphology. John Wiley and Sons New York. 1987. p 11-75, 43 fig, 6 tab, 70 ref.*

Navfac, D. (1974). Design manual-soil mechanics, foundations, and earth structures. *US Government Printing Office, Washington, DC*.

Navfac, D. (1982). Design Manual-Soil Mechanics, Foundations, and Earth Structures. *US Department of the Navy, Washington, DC*.

Nelson, J. D., & McWhorter, D. B. (1985). Water Movement *Design of non-impounding mine waste dumps* (p. 99): Society for Mining Metallurgy.

Neumann-Mahlkau, P. (1993). Acidification by pyrite weathering on mine waste stockpiles, Ruhr District, Germany. *Engineering Geology, 34*(3-4), 125-134.

Ng, C., & Shi, Q. (1998). A numerical investigation of the stability of unsaturated soil slopes subjected to transient seepage. *Computers and geotechnics, 22*(1), 1-28.

Nichols, R. (1986). *Rock segregation in waste dumps.* Communication presented at In: Flow-through rock drains :Proceedings of the International symposium convened at the Inn of the South, Cranbrook, B.C., September 8-11.

Noriah, A., & Rakhecha, P. (2001). Probable maximum precipitation for 24 h duration over southeast Asian monsoon region—Selangor, Malaysia. *Atmospheric research, 58*(1), 41-54.

Nunoo, S. (2009). *Geotechnical evaluation of Questa mine material, Taos County, New Mexico.* (M. Sc. Thesis, New Mexico institute of mining and technology).

O'Kane, M. A., Ayres, B., Christensen, D., & Meiers, G. (2002). *CANMET–CETEM Manual on Cover System Design for Reactive Mine Waste*.

Öberg, A. L., & Sällfors, G. (1997). Determination of shear strength parameters of unsaturated silts and sands based on the water retention curve. *ASTM Geotechnical Testing Journal, 20*(1), 40-48.

Obrzud, R., & Truty, A. (2012). The hardening soil model-a practical guidebook z soil: PC.

Oka, Y., & Wu, T. H. (1990). System reliability of slope stability. *Journal of Geotechnical Engineering, 116*(8), 1185-1189.

Pedroni, L. (2011). *Étude expérimentale et numérique de la sédimentation et de la consolidation des boues de traitement des eaux acides.* (Ph. D. Thesis, École Polytechnique de Montréal, Montreal).

Peregoedova, A. (2012). *Étude expérimentale des propriétés hydrogéologiques des roches stériles à une échelle intermédiaire de laboratoire.* (M. Sc. Thesis, École Polytechnique de Montréal, Montreal).

Pernichele, A. D., & Kahle, M. B. (1971). Stability of waste dumps at Kennecott s Bingham Canyon mine. *Society of mining engineers, AIME, Transactions, v. 250* pp. 363-367.

Phoon, K.-K. (1995). *Reliability-based design of foundations for transmission line structures*. Electric Power Research Institute, Palo Alto, California.

Phoon, K.-K., & Kulhawy, F. H. (1999). Characterization of geotechnical variability. *Canadian Geotechnical Journal, 36*(4), 612-624.

Phoon, K. K., & Kulhawy, F. H. (1996). *On quantifying inherent soil variability.* Communication presented at Uncertainty in the Geologic Environment (GSP 58) (p. 326-340).

Pirone, M., Papa, R., Nicotera, M. V., & Urciuoli, G. (2015). In situ monitoring of the groundwater field in an unsaturated pyroclastic slope for slope stability evaluation. *Landslides, 12*(2), 259-276.

Piteau Associates Engineering. (1991). *Mined rock and overburden piles: Investigation and design manual*: Prepared for British Columbia Mine Dump Committee and Ministry of Energy and Mines.

Piteau Associates Engineering Ltd. (1991). *Mined rock and overburden piles: Investigation and design manual*: Prepared for British Columbia Mine Dump Committee and Ministry of Energy and Mines.

Powrie, W. (2004). *Soil mechanics: concepts and applications*: Spon Pr.

PRAT, M., BISCH, P., Millard, A., Mestat, P., & PIJAUDIER-CALOT, G. (1995). *La modélisation des ouvrages*.

Quine, R. L. (1993). *Stability and deformation of mine waste dumps in north-central Nevada.* (M. Sc. Thesis, University of Nevada, Reno).

Rahardjo, H., Lee, T. T., Leong, E. C., & Rezaur, R. B. (2005). Response of a residual soil slope to rainfall. *Canadian Geotechnical Journal, 42*(2), 340-351.

Rahardjo, H., Li, X. W., Toll, D. G., & Leong, E. C. (2001). The effect of antecedent rainfall on slope stability. *Geotechnical and Geological Engineering, 19*(3), 371-399.

Rahardjo, H., Lim, T., Chang, M., & Fredlund, D. (1996). Shear-strength characteristics of a residual soil. *Canadian geotechnical journal, 32*(1), 60-77.

Rahardjo, H., Nio, A. S., Leong, E. C., & Song, N. Y. (2010). Effects of groundwater table position and soil properties on stability of slope during rainfall. *Journal of geotechnical and geoenvironmental engineering, 136*(11), 1555-1564.

Rahardjo, H., Ong, T., Rezaur, R., & Leong, E. C. (2007). Factors controlling instability of homogeneous soil slopes under rainfall. *Journal of Geotechnical and Geoenvironmental Engineering, 133*(12), 1532-1543.

Rahimi, A., Rahardjo, H., & Leong, E.-C. (2010). Effect of antecedent rainfall patterns on rainfall-induced slope failure. *Journal of Geotechnical and Geoenvironmental Engineering, 137*(5), 483-491.

Rakhecha, P., & Clark, C. (1999). Revised estimates of one-day probable maximum precipitation (PMP) for India. *Meteorological Applications, 6*(4), 343-350.

Rassam, D. W., & Cook, F. (2002). Predicting the shear strength envelope of unsaturated soils. *ASTM geotechnical testing journal, 25*(2), 215-220.

Rassam, D. W., & Williams, D. J. (1999). 3-dimensional effects on slope stability of high waste rock dumps. *International Journal of Surface Mining, Reclamation and Environment, 13* 19-24.

Ray, R.L., & De Smelt, F. (2008). Slope stability analysis on a regional scale using GIS: a case study from Dhading, Nepal. *Environmental Geology*

Regmi, R. K., & Jung, K. (2016). Application of dynamic programming to locate the critical failure surface in a rainfall induced slope failure problem. *KSCE Journal of Civil Engineering, 20*(1), 452-462.

Richards, L. (1931). Capillary conduction of liquids through porous mediums. *Physics, 1*(5), 318-333.

Robertson, A. M. (1982). *Deformation and Monitoring of Waste Dump Slopes* (p. p.16).

Robertson, A. M. (1985). Mine Waste Disposal: An Update on Geotechnical and Geohydrological Aspects.

Robertson, A. M., & Clifton, A. W. (1987). *Design consideration for the long term containment of tailings*. Communication presented a t 40th Canadian Geotechnical Conference, Regina, October.

Sassa, K., Fukuoka, H., Wang, F., & Wang, G. (2007). Landslides induced by a combined effect of earthquake and rainfall. Dans *Progress in landslide science* (p. 193-207): Springer.

Savci, G., & Williamson, A. L. (2002). *Hydrologic assessment of waste tock stockpiles: A case study from Ajo mine, Arizona:*. Communication presented at SME proceedings, Phoenix.

Schultze, E. (1975). *Some aspects concerning the application of statistics and probability to foundation structures.* Communication presented at Proceeding of the 2nd International Conference on the Applications of Statistics and Probability in Soil and Structure Engineering, Aachen, Germany (p. 15-18).

Selby, M. J. (1982). Hillslope materials and processes. *Hillslope materials and processes.*

Sheets, R., & Bates, E. (2008). *Gold Quarry North Waste Rock Facility Slide Investigation and Stabilization.* Communication presented at Proceedings of the 12th International Conference on Tailings and Mine Waste, Vail, Colorado, CRC Press/Balkema, Taylor & Francis Group, London, pgs (p. 409-421).

Shen, Z., & Yu, S. (1996). *The problems in the present studies on mechanics for unsaturated soils.* Communication presented at Proceeding of the symposium on geotechnical aspects of regional soils, China. In chinese.

Singh, A. (1972). *How reliable is the factor of safety in foundation engineering?* Communication presented at International Conference on Application of Statistics and Probability to Soil and Structural Engineering, Hong Kong (1971).

Skempton, A. W. (1975). Long-term stability of clay slopes. *Geotechnique, v. 14* pp. 75-101.

Smith, L., Lopez, D. L., Beckie, R., Dawson, R., & Price, W. (1995). *Hydrogeology of waste rock dumps*. Report for Dep. of Natural Resources Canada, Ontario, Canada.

SNC-LAVALIN. (2004). *Estimation des conditions hydrométéorologiques conduisant aux crues maximales probables (CMP) au Québec*. Rapport final, Ministère de l'environnement, Centre d'expertise hydrique du Québec.

Song, Y.-S., Chae, B.-G., & Lee, J. (2016). A method for evaluating the stability of an unsaturated slope in natural terrain during rainfall. *Engineering Geology, 210* 84-92.

Spencer, E. (1967). A method of analysis of the stability of embankments assuming parallel inter-slice forces. *Geotechnique, 17*(1), 11-26.

Statham, I. (1974). The relationship of porosity and angle of repose to mixture proportions in assemblages of different sized materials. *Sedimentology, 21*(1), 149-162.

Stormont, J. C., & Farfan, E. (2005). Stability evaluation of a mine waste pile. *Environmental and Engineering Geoscience, 11*(1), 43.

Strang, G., & Fix, G. J. (1973). *An analysis of the finite element method* (vol. 212): Prentice-Hall Englewood Cliffs, NJ.

Sun, G., Zheng, H., & Jiang, W. (2012). A global procedure for evaluating stability of three-dimensional slopes. *Natural hazards, 61*(3), 1083-1098.

Sveinsdóttir, B. Ö. (2011). *Pavement behaviour evaluation during spring thaw based on the falling weight deflectometer method.* (Stockholm).

Tachie-Menson, S. (2006). *Characterization of the acid-producing potential and investigation of its effect on weathering of the Goathill North Rock Pile at the Questa Molybdenum Mine, New Mexico.* (M. Sc. Thesis, New Mexico institute of mining and technology, Socorro, NM).

Tang, W. H. (1984). *Principles of Probabilistic Characterizations of Soil Properties.* Communication presented at Probabilistic Characterization of Soil Properties (p. 74-89).

Tang, Y., Xue, Q., Li, Z., & Feng, W. (2015). Three modes of rainfall infiltration inducing loess landslide. *Natural Hazards, 79*(1), 137-150.

Tekinsoy, M. A., Keskin, M. S., & Söylemez, M. (2004). An equation for predicting shear strength envelope with respect to matric suction. *Computers and Geotechnics, 31*(7), 589-593.

Terzaghi, K. (1950). Geologic aspects of soft-ground tunneling.

Toll, D. G., Rahardjo, H., & Leong, E. C. (1999). *Landslides in Singapore.* Communication presented at Proc. 2nd international conference on landslides, slope stability and the safety of infra-structures

Singapore (p. pp. 269-276.).

Upadhyay, O., Sharma, D., & Singh, D. (1990). Factors affecting stability of waste dumps in mines. *International Journal of Surface Mining, Reclamation and Environment, 4*(3), 95-99.

URS Corporation. (2003). *Mine rock pile erosion and stability evaluations, Questa mine: .* Unpublished Report to Molycorp, Inc. 4 volumes.

Vallerga, B. A., Seed, H. B., Monismith, C. L., & Cooper, R. S. (1957). Effect of shape, size and surface roughness of aggregate particles on the strength of granular materials. *Special Technical Publication, No. 212*(ASTM.).

Van Genuchten, M. T. (1980). A closed-form equation for predicting the hydraulic conductivity of unsaturated soils. *Soil science society of America journal, 44*(5), 892-898.

Vanapalli, S. K., Fredlund, D. G., Pufahl, D. E., & Clifton, A. W. (1996). Model for the prediction of shear strength with respect to soil suction. *Canadian Geotechnical Journal, 33*(3), 379-392.

Vanmarcke, E. (1983). *Random fields: analysis and synthesis*: MIT Press, Cambridge, MA.

Vanmarcke, E. H. (1977a). Probabilistic modeling of soil profiles. *Journal of the geotechnical engineering division, 103*(11), 1227-1246.

Vanmarcke, E. H. (1977b). Reliability of earth slopes. *Journal of the Geotechnical Engineering Division, 103*(11), 1247-1265.

Vilar, O. M. (2006). A simplified procedure to estimate the shear strength envelope of unsaturated soil. *Can. Geotech. J., , v. 43,* pp. 1088–1095.

Wahler, W. A. (1979). *A perspective - Mine waste disposal structures - Mine dumps, and mill and plant impoundments* Communication presented at Proceeding 6th Panamerican Conf. Soil Mech., Lima, Peru (vol. Vol.III.).

Walker, W. K., & Johnsonf, M. J. (2000). Observational engineering for open-pit geotechnics: A case study of predictions versus performance for the stability of a high overburden embankment over a soft/deep soil foundation at PT freeport Indonesia's Grasberg open-pit mine. Dans *Slope Stability in Surface Mining* (p. pp. 329-344): Society for Mining Metallurgy.

Wang, B.-H. (1998). *Report on review of PMP estimates for Hong Kong*. Wang Reidel & Associates Inc:

Wang, Y., Cao, Z., & Au, S.-K. (2010). Practical reliability analysis of slope stability by advanced Monte Carlo simulations in a spreadsheet. *Canadian Geotechnical Journal, 48*(1), 162-172.

Wang, Z., & Cao, L. Influence of Rainfall to the Stability of Foundation Pit.

Ward, R. C., & Robinson, M. (1967). *Principles of hydrology*. McGraw-Hill New York.

White, D. J., Yang, H., Thompson, M. J., & Schaefer, V. R. (2005). Innovative solutions for slope stability reinforcement and characterization: Vol. I.

Whitman, R. V. (2000). Organizing and evaluating uncertainty in geotechnical engineering. *Journal of Geotechnical and Geoenvironmental Engineering, 126*(7), 583-593.

Wickland, B. E., & Wilson, G. W. (2005). Self-weight consolidation of mixtures of mine waste rock and tailings. *Canadian Geotechnical Journal, 42*(2), 327-339.

Wickramasuriya, S. S. F., W. C. D. K., . (2011). *Investigation of probable maximum precipitation for disaster risk reduction in Sri Lanka.* Communication presented at International Conference on Building Resilience, Books of abstracts, p. 75.

Williams, D. J. (2000). Assessment of embankment parameters. Dans *Slope Stability in Surface Mining* (p. pp. 275-284): Society for Mining Metallurgy.

Williams, D. J., & Rohde, T. K. (2008). *Rainfall infiltration into and seepage from rock dumps-A review.* Communication presented at First International Seminar on the Management of Rock Dumps, Stockpiles and Heap Leach PAds, Australia (p. pp. 79-89).

Wilson, G. (2000). Embankment Hydrology and Unsaturated Flow in Waste Rock. Dans *Slope stability in surface mining* (p. 305): Society for Mining Metallurgy.

Wilson, J. A. (2003). *Numerical modelling of unsaturated flow in vertical and inclined waste rock layers using the seep/w model.* (M. Sc. Thesis, University of Saskatchewan, Saskatoon).

WMO. (1986). *Manual for estimation of probable maximum precipitation (2nd edition) (World Meterorological Organization)* (vol. Publ. no. 232). Geneva.

Wong, T. T., Fredlund, D. G., & Krahn, J. (1998). A numerical study of coupled consolidation in unsaturated soils. *Canadian Geotechnical Journal, 35*(6), 926-937.

Xue, J., & Gavin, K. (2008). Effect of rainfall intensity on infiltration into partly saturated slopes. *Geotechnical and Geological Engineering, 26*(2), 199-209.

Yang, H., Rahardjo, H., & Leong, E.-C. (2006). Behavior of unsaturated layered soil columns during infiltration. *Journal of Hydrologic Engineering, 11*(4), 329-337.

Yellishetty, M., & Darlington, W. J. (2011). Effects of monsoonal rainfall on waste dump stability and respective geo-environmental issues: a case study. *Environmental Earth Sciences, 63*(6), 1169-1177.

Zhan, G. (2000). *Experimental and theoretical studies on leach pad hydraulics and transport behavior during rinsing.* (Ph. D. Thesis University of Nevada, Reno, USA).

Zhan, T. L., Zhang, W., & Chen, Y. (2006). *Influence of reservoir level change on slope stability of a silty soil bank.* Communication presented at Unsaturated Soils 2006 (p. 463-472).

Zhang, L. (2005). Probabilistic study of slope stability under rainfall condition.

Zhang, L., Zhang, J., Zhang, L., & Tang, W. H. (2011). Stability analysis of rainfall-induced slope failure: a review. *Proceedings of the ICE-Geotechnical Engineering, 164*(5), 299.

Zhou, Z., Wang, H.-g., Fu, H.-l., & Liu, B.-c. (2009). Influences of rainfall infiltration on stability of accumulation slope by in-situ monitoring test. *Journal of Central South University of Technology, 16* 297-302.

Zienkiewicz, O. C., Taylor, R. L., Zienkiewicz, O. C., & Taylor, R. L. (1977). *The finite element method* (vol. 3): McGraw-hill London.

APPENDICES

Appendix A – Additional results for Chapter 4

This appendix presents some numerical analyses related to single bench waste rock piles, obtained with the Simplified Bishop Method and the graphical solution proposed by Cousins (1978). It also presents some back analyses for slope stability of different cases presented in the literature. Some additional results related to sections 4-3-2 and 4-7-10 are also included. The last part presents the Plate Loading testing to assess the Young modulus (E) of waste rocks, with the obtained results.

A-1 Comparison between results obtained with the Simplified Bishop slope stability analysis method and Cousin's Charts

Slope stability analyses of a single bench waste rock pile (Figure A-1) were conducted with the Simplified Bishop Method (available in Slope/W) and with the graphical solution given by the Cousins (1978) charts. The results shown below indicate that there is generally a very good agreement between the two approaches; this supports the use of the Slope/W software in this investigation.
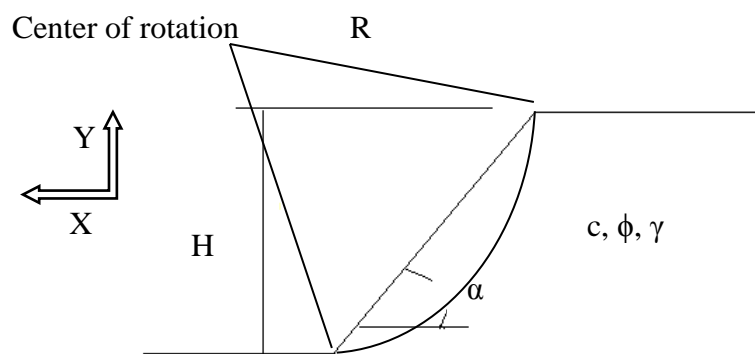

Figure A-1: Slope geometry for Cousins' charts, adapted from Coduto (1999)

Figures A-2 to A-6 present the comparison between results obtained with Simplified Bishop method (available in SLOPE/W) and from the Cousin's charts.
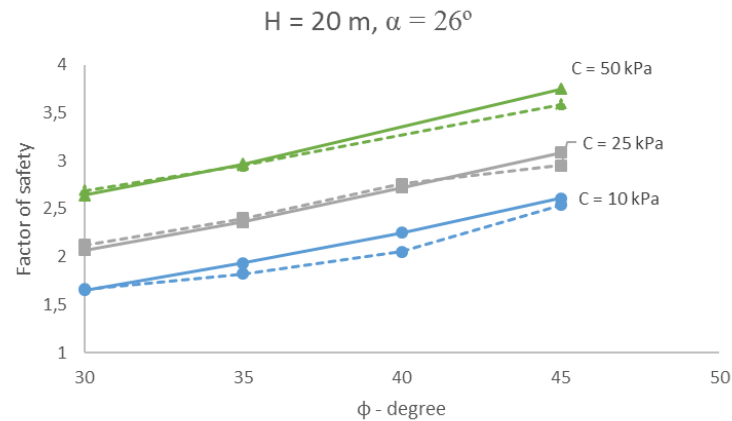
Figure A-2: Factor of safety of a single bench homogenous waste rock pile (H = 20 m, α = 26°), for different values of ϕ' (= 30 to 45°) and C (= 10, 25 and 50 kPa); results obtained with SLOPE/W (Simplified Bishop Method) and from the Cousins' (1978) charts

Figure A-3: Factor of safety of a single bench homogenous waste rock pile (H = 20 m, α = 37°), for different values of ϕ' (= 30 to 45°) and C (= 10, 25 and 50 kPa); results obtained with SLOPE/W (Simplified Bishop Method) and from the Cousins' (1978) charts

Figure A-4: Factor of safety of a single bench homogenous waste rock pile (H = 40 m, α = 30°), for different values of ϕ' (= 30 to 45°) and C (= 25 and 50 kPa); results obtained with SLOPE/W (Simplified Bishop Method) and from the Cousins' (1978) charts

Figure A-5: Factor of safety of a single bench homogenous waste rock pile (H = 40 m, α = 37°), for different values of ϕ' (= 30 to 45°) and C (= 25 and 50 kPa); results obtained with SLOPE/W (Simplified Bishop Method) and from the Cousins' (1978) charts

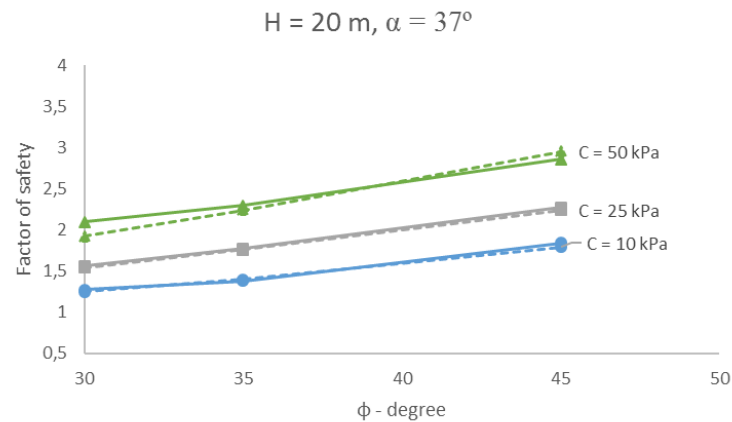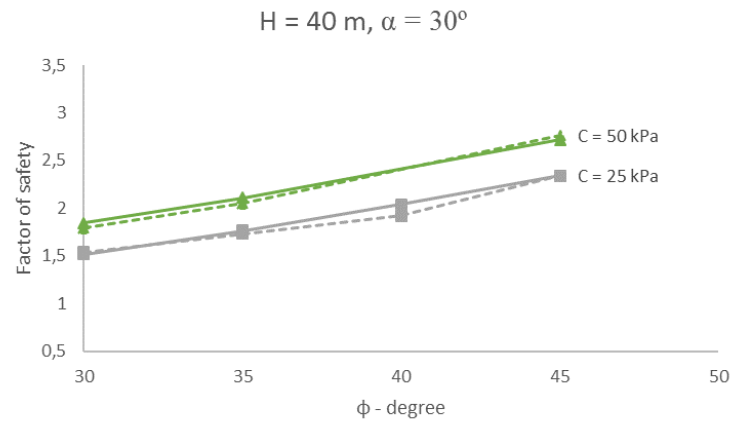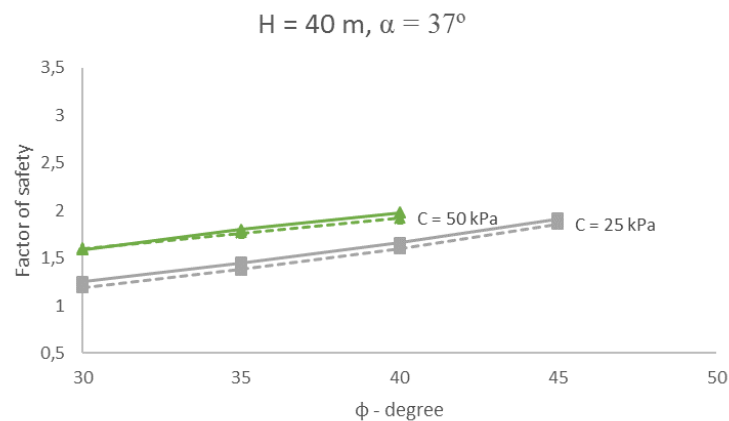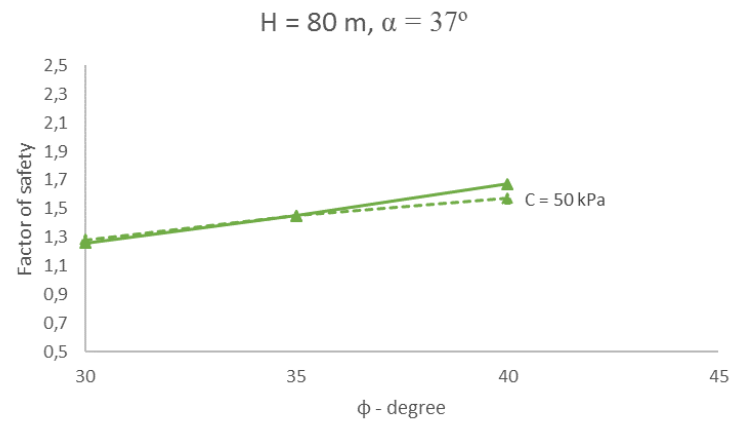Figure A-6: Factor of safety of a single bench homogenous waste rock pile (H = 50 m, β = 37°), for different values of ϕ' (= 30 to 40°) and C (= 50 kPa); results obtained with SLOPE/W (Simplified Bishop Method) and from the Cousins' (1978) charts

Table A-1: Factor of safety and center of rotation of single bench homogenous waste rock piles with different values of H (= 20 m, 40 m, 80 m); C (=10 kPa, 25 kPa, 50 kPa); α (= 26°, 30°, 37°); and φ (= 30°, 35°, 40°, 45); results obtained with SLOPE/W (Simplified Bishop Method) and from the Cousins' (1978) charts (see Figures A-2 to A-6)

No.	Properties				Obtained with Cousin's Chart			Obtained with SLOPE/W Simplified Bishop Method			
	H (m)	α (°)	φ (°)	C (kPa)	FS	Y/H(tana)	X/H(tana)	FS	X	Y	R
1	20	26	30	10	1.66	1.4	0	1.65	61.1	65.7	57.7
2	20	26	30	25	2.12	1.18	0.12	2.07	52.8	43.5	44
3	20	26	30	50	2.69	0.95	0.27	2.64	50.2	39.5	41
4	20	26	35	10	1.82	1.4	0	1.936	60.8	57.5	57
5	20	26	35	25	2.4	0.15	1.2	2.36	45	60.2	52.3
6	20	26	35	50	2.95	1.05	0.25	2.97	52.8	47.5	48
7	20	26	40	10	2.05	1.45	-0.04	2.25	61.2	59.5	59
8	20	26	40	25	2.76	1.3	0.18	2.72	55.5	47.5	48
9	20	26	45	10	2.54	1.55	-0.07	2.61	60.8	57.5	57
10	20	26	45	25	2.95	1.25	0.1	3.086	59.5	55.7	55.7
11	20	26	45	50	3.59	1.15	0.18	3.75	52.8	45.5	46
12	40	26	30	10	1.44	1.62	-0.1	1.475	136	136	118
13	40	26	30	25	1.89	1.25	0.1	1.724	128	128	110
14	40	26	30	50	2.11	1.18	0.18	2.2	78	56	59.8
15	80	26	30	25	1.44	1.5	-0.05	1.52	216.5	253.5	253.5
16	80	26	30	50	1.8	1.3	0.08	1.9	137	123	109
17	80	26	35	25	1.73	1.6	-0.13	1.794	222	263	263
18	80	26	35	50	1.93	1.3	0.1	2.2	137	123	109
19	80	26	40	50	2.18	1.4	0.02	2.326	206.5	234	234
20	40	30	30	10	1.27	1.65	-0.22	1.28	117.5	101	101
21	40	30	30	25	1.54	1.37	-0.02	1.519	117	105	105.2
22	40	30	30	50	1.79	1.18	0.09	1.845	105.7	90	89.75
23	40	30	35	25	1.73	1.4	-0.1	1.763	111.6	97	96
24	40	30	35	50	2.05	1.22	0.08	2.108	104	87	86.5
25	40	30	40	25	1.92	1.4	-0.05	2.038	115.5	102.5	102
26	40	30	45	25	2.34	1.49	-0.1	2.342	120	108.2	108.6
27	40	30	45	50	2.76	1.32	0	2.716	110.5	94.7	94.7
28	80	30	45	50	2.21	1.45	-0.1	2.364	226	193	191
29	80	30	30	50	1.53	1.36	-0.02	1.52	220	221	187.6

Table A-1: Factor of safety and center of rotation of a single bench homogenous waste rock pile with H (= 20 m, 40 m, 80 m); C (=10 kPa, 25 kPa, 50 kPa), α (= 26°, 30°, 37°) and φ (= 30°, 35°, 40°, 45); results obtained with SLOPE/W (Simplified Bishop Method) and from the Cousins' (1978) charts (see Figures A-2 to A-6) (continued)

	Properties				Obtained with Cousin's Chart			Obtained with SLOPE/W Simplified Bishop Method			
	H (m)	α (°)	φ (°)	C (kPa)	FS	Y/H(tana)	X/H(tana)	FS	X	Y	R
30	20	37	30	10	1.25	1.5	-0.22	1.27	44.2	27	26.9
31	20	37	30	25	1.54	1.4	-0.05	1.558	49.5	41.7	35.7
32	20	37	30	50	1.92	1.22	0.1	2.1	45	35.7	32.5
33	20	37	35	10	1.4	1.6	-0.3	1.38	42	43	43
34	20	37	35	25	1.76	1.4	-0.08	1.77	36.5	45	37
35	20	37	35	50	2.24	1.18	0.11	2.3	32.7	41.15	33.17
36	20	37	45	10	1.79	1.71	-0.4	1.841	56.8	44.8	45.8
37	20	37	45	25	2.24	1.42	-0.17	2.27	49	37	36.7
38	20	37	45	50	2.95	1.33	0	2.857	47.5	37	37
39	40	37	30	10	1.01	1.78	-0.42	1.033	119	100	103
40	40	37	30	25	1.19	1.5	-0.18	1.25	82	98	83
41	40	37	30	50	1.6	1.3	0	1.59	72.4	93	77.4
42	40	37	35	25	1.38	1.45	-0.21	1.452	87.5	86	87
43	40	37	35	50	1.76	1.35	-0.05	1.8	69	56	55
44	40	37	40	25	1.6	1.6	-0.3	1.66	86.1	103	88.6
45	40	37	40	50	1.92	1.4	-0.12	1.977	108.4	72	72
46	40	37	45	25	1.86	1.62	-0.31	1.913	115.5	96.5	99
47	80	37	30	50	1.28	1.5	-0.14	1.26	214.5	175	176.6
48	80	37	35	25	1.3	1.73	-0.45	1.27	210	154	155
49	80	37	35	50	1.45	1.5	-0.25	1.45	22.4	157.5	158.8
50	80	37	40	50	1.57	1.6	-0.27	1.672	212	163	164

A-2 Comparing the value of the factor of safety and center of rotation between previously presented cases by Fredlund (2000) and numerical simulations (calculations performed with Sigma/W and Slope/W)

This section presents some additional cases that are used for validation purposes. Figure A-7 presents critical slip surface related to two relatively flat slopes with a high water table, with and without considering the effect of negative pore water pressure; they were presented by Fredlund (2000)). Flat slope height is 20 m high; the slope angle $\alpha = 30°$, $\gamma = 18.5$ kN/m³, C= c = 20 kN/m² and $\phi' = 24°$. The water table covers 2/3 of the slip surface. For $\phi^b = 0$ and 15, FS = 1.278 and 1.319, respectively.
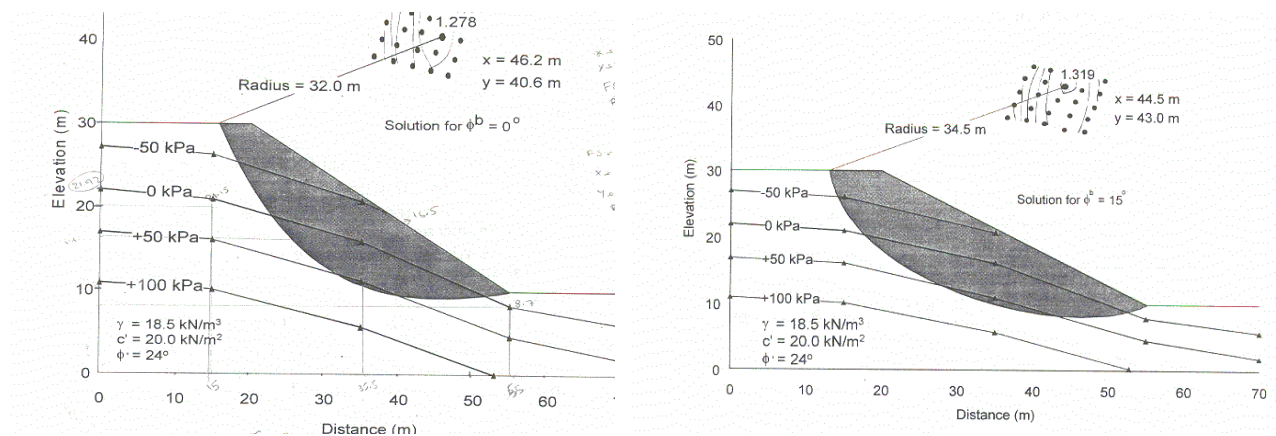

Figure A-7: Critical slip surface for a relatively flat slope when negative pore-water pressure are ignored (right) and taken into consideration (left) (taken from (Fredlund, 2000b)

To simulate these cases, two different methods are used: the Morgenstern-Price method (available in SLOPE/W) and FE stress-based method (coupling of SIGMA/W and SLOPE/W; see section 3-2-3). The effect of negative pore water pressures on the slope stability is considered by using two different methods (available in SLOPE/W): the first method, using a constant value of ϕ^b (based on equation proposed by Fredlund (1978) Equation), and the second method using the material water retention curve (WRC) (based on the equation proposed by Vanapalli et al., 1996).

It should be noted that in the second method, the material property in the original case by Fredlund is not clarified, so two different materials are considered here, sand and clayey silt (adapted from Fredlund, 1994, see Figure A-8).
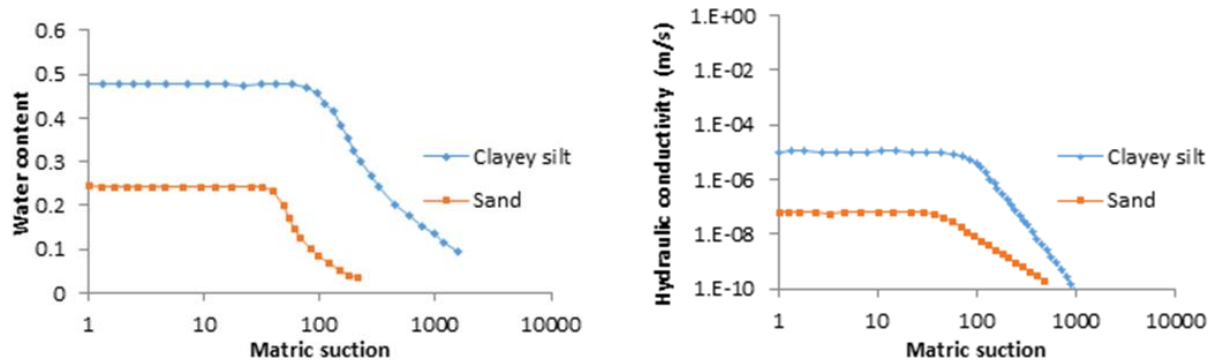

Figure A-8: WRCs and hydraulic conductivity functions for sand and clayey silt (Fredlund et al., 1994)

Table A-2: Description of different scenarios, geometry and material properties for a relatively flat slope with high water table, with and without considering negative pore water pressures

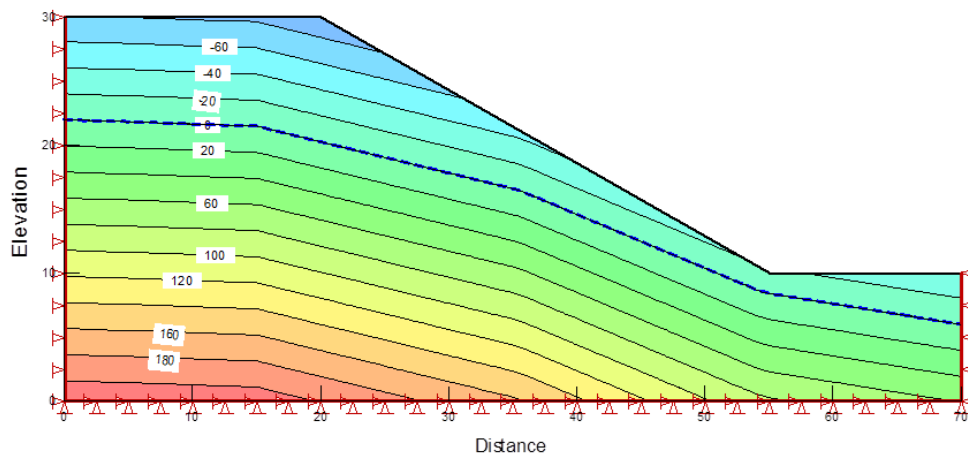| Simulations	H (m)	α (°)	γ (kN/m³)	c (kPa)	φ (°)	φᵇ (°)	Simulation methods
F1						0	Morgenstern-Price method
F1S						0, Sand	FE stress-based method
F1C						0, Clay	FE stress-based method
F2	20	30	18.5	20	24	15	Morgenstern-Price method
F2S						15, Sand	FE stress-based method
F2C						15, Clay	FE stress-based method
F3S						WRC, Sand	FE stress-based method
F3C						WRC, Clay	FE stress-based method

Figure A-9: PWP distribution within the flat slope with high water table obtained with SIGMA/W
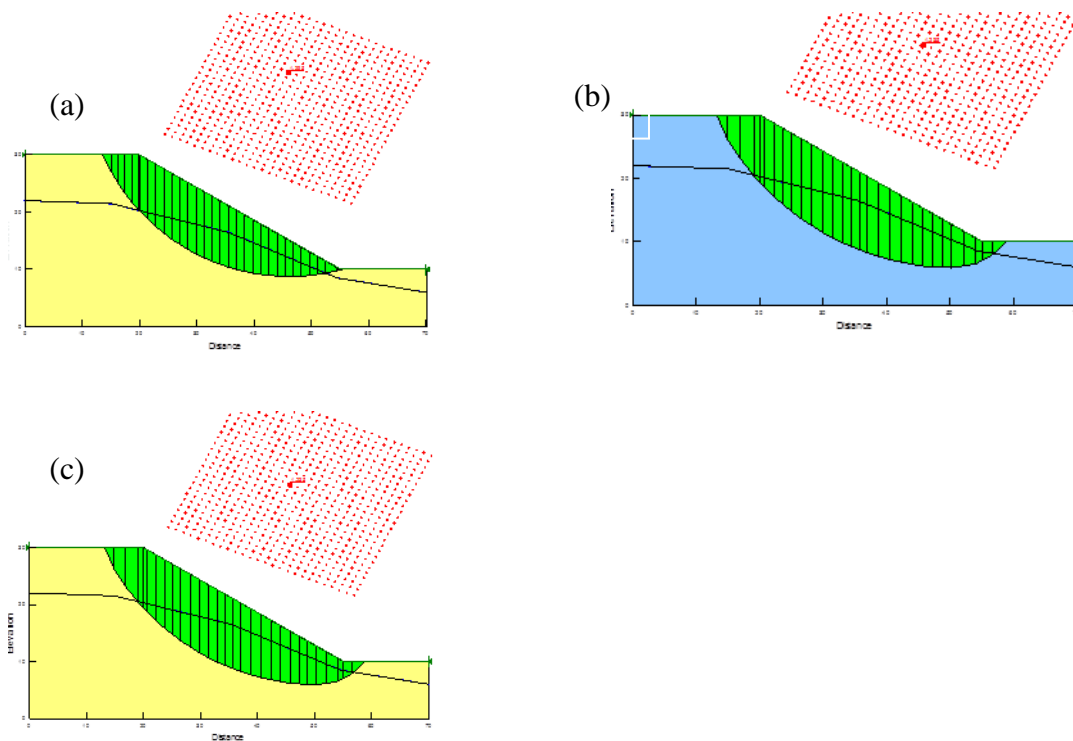

Figure A-10: Critical slip surface for simulations F1 (a), F1C (b) and F1S (c) (see Table A-2) obtained with SLOPE/W; the location of the center of rotation is also shown for the critical slip surface.
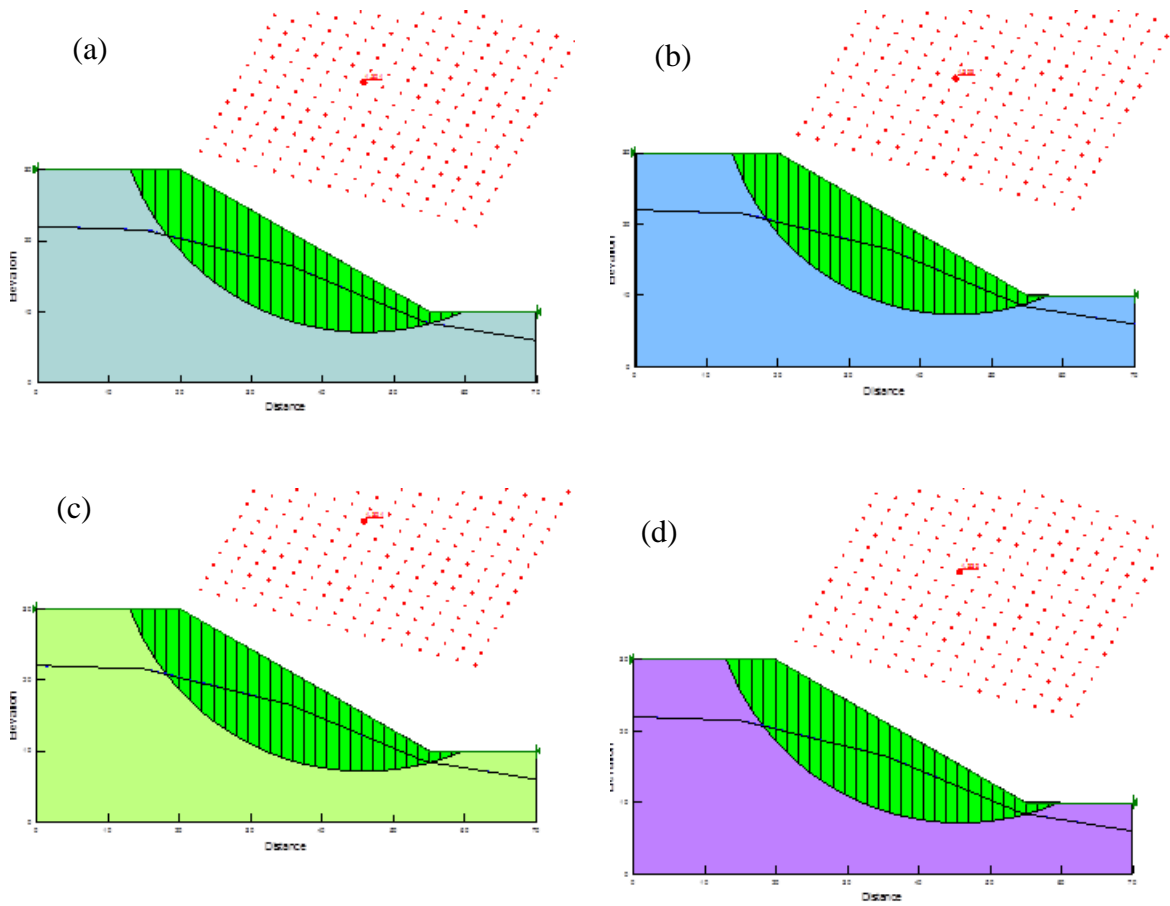
Figure A-11: Critical slip surface for simulations F2C (a), F2S (b), F3C (c) and F3S (d) (see Table A-3) obtained with SLOPE/W

Table A-3: Factor of safety and location of the center of rotation obtained with SLOPE/W (Morgenstern-Price and FE stress based methods) for different simulations presented in Table A-2, compared with FS obtained by Fredlund (2000, shown in figure A-7)

Simulation		FS	x (m)	y(m)	Radius (m)
Flat slope	Fredlund (F1)	1.278	46.2	40.6	32
	F1	1.296	46.14	44.38	35.61
	F1S	1.259	45.82	40/96	34.05
	F1C	1.259	45.82	40/96	34.05
	Fredlund (F2)	1.319	44.5	43	34.5
	F2	1.333	45.86	42.16	33.69
	F2C	1.301	45.86	42.16	35.03
	F2S	1.301	45.86	42.16	35.03
	F3C	1.309	44.93	40.43	33.09
	F3S	1.33	45.86	42.16	35.03

Figure A-12 presents critical slip surface related to two relatively steep slopes with a deep water table, with and without considering the effect of negative pore water pressure; that presented by Fredlund (2000). Steep slope height is 30 m, the slope angle $\alpha = 50°$, $\gamma = 18$ kN/m^3, C= c = 10 kN/m^2 and $\phi' = 34°$. Most of the slip surface is located above the water table. For $\phi^b = 0$ and 15°, FS = 0.901 and 1.088, respectively.
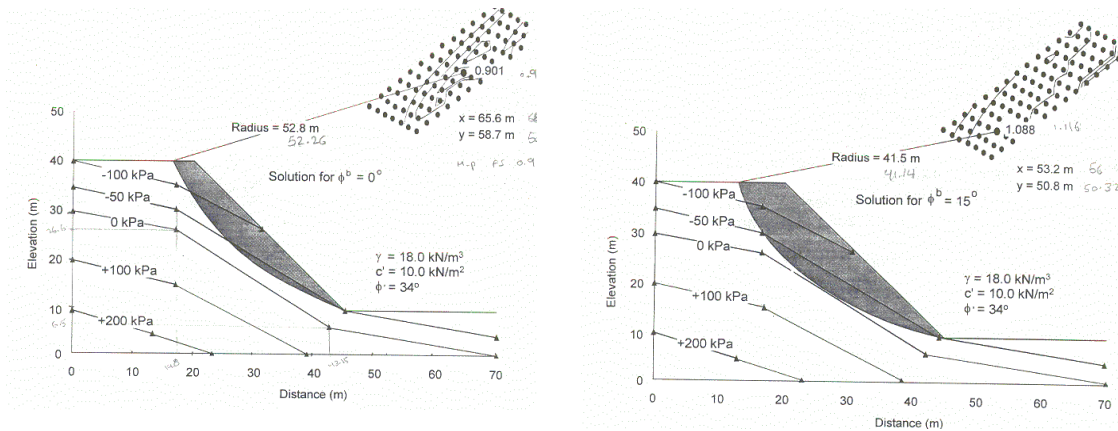
Figure A-12: Critical slip surface for a steep slope when negative pore-water pressure are ignored (right) and taken into consideration (left) (taken from Fredlund, 2000)

Table A-4: Descriptions of different scenarios, geometry and material properties for a relatively steep slope with deep water table, with and without considering negative pore water pressure

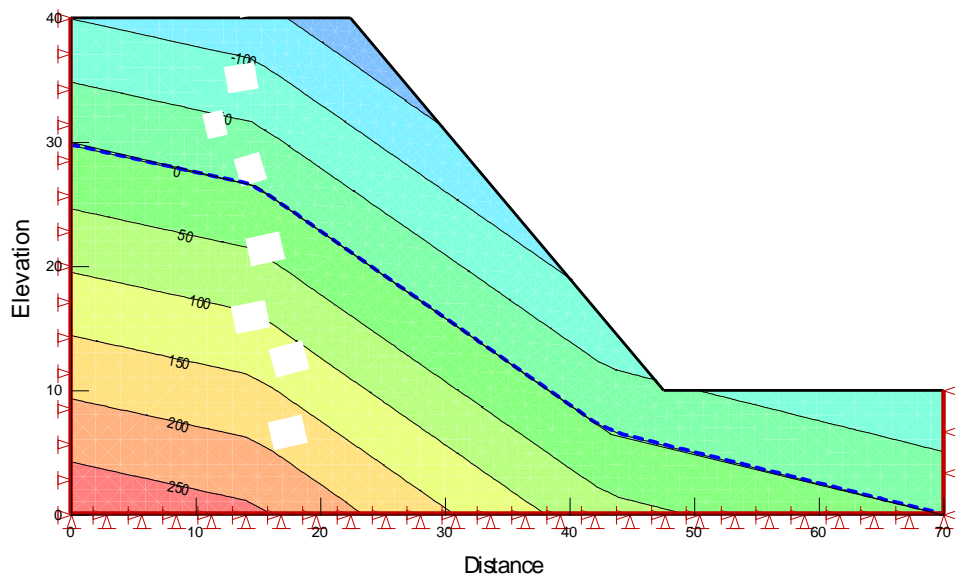| Simulations	H (m)	α (°)	γ (kN/m³)	c (kPa)	φ (°)	φᵇ (°)	Simulation methods
S1						0	Morgenstern-Price method
S1S						0, Sand	FE stress-based method
S1C						0, Clay	FE stress-based method
S2	30	50	18	10	34	15	Morgenstern-Price method
S2S						15, Sand	FE stress-based method
S2C						15, Clay	FE stress-based method
S3S						WRC, sand	FE stress-based method
S3C						WRC, clay	FE stress-based method

Figure A-13: PWP distribution within the steep slope with deep water table obtained with SIGMA/W
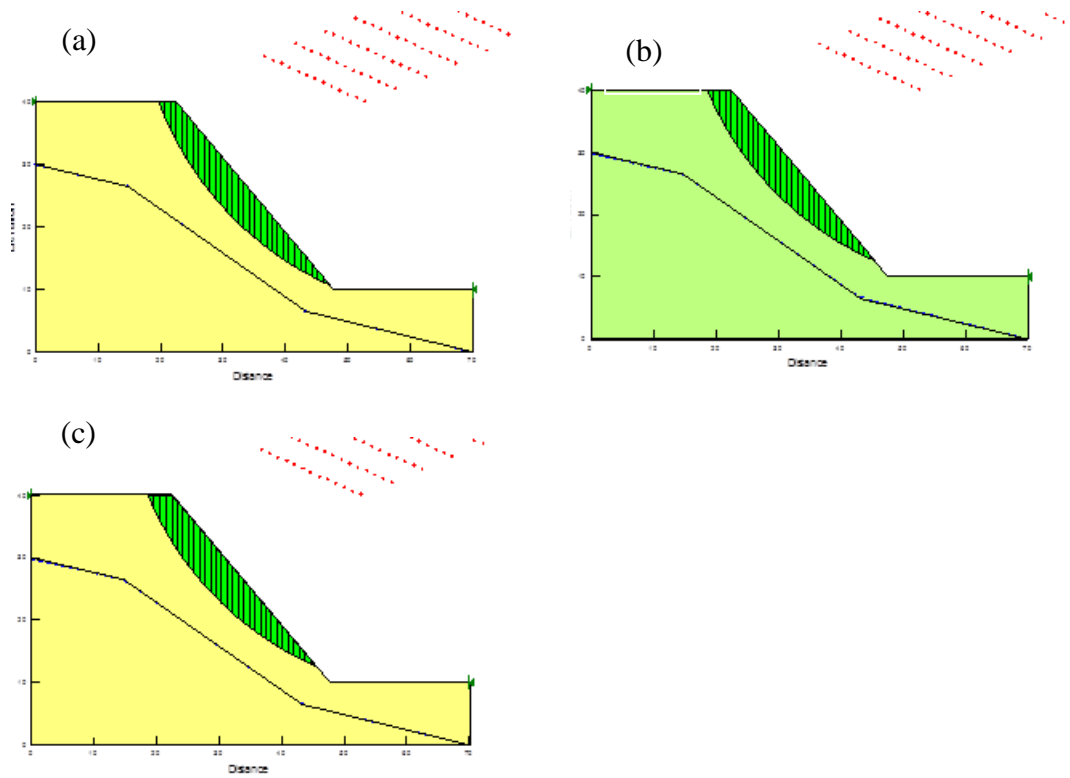
(a)

(b)

(c)

Figure A-14: Critical slip surface for simulations S1 (a), S1C (b) and S1S (c) (see Table A-3) obtained with SLOPE/W; the location of the center of rotation is also shown for the critical slip surface.
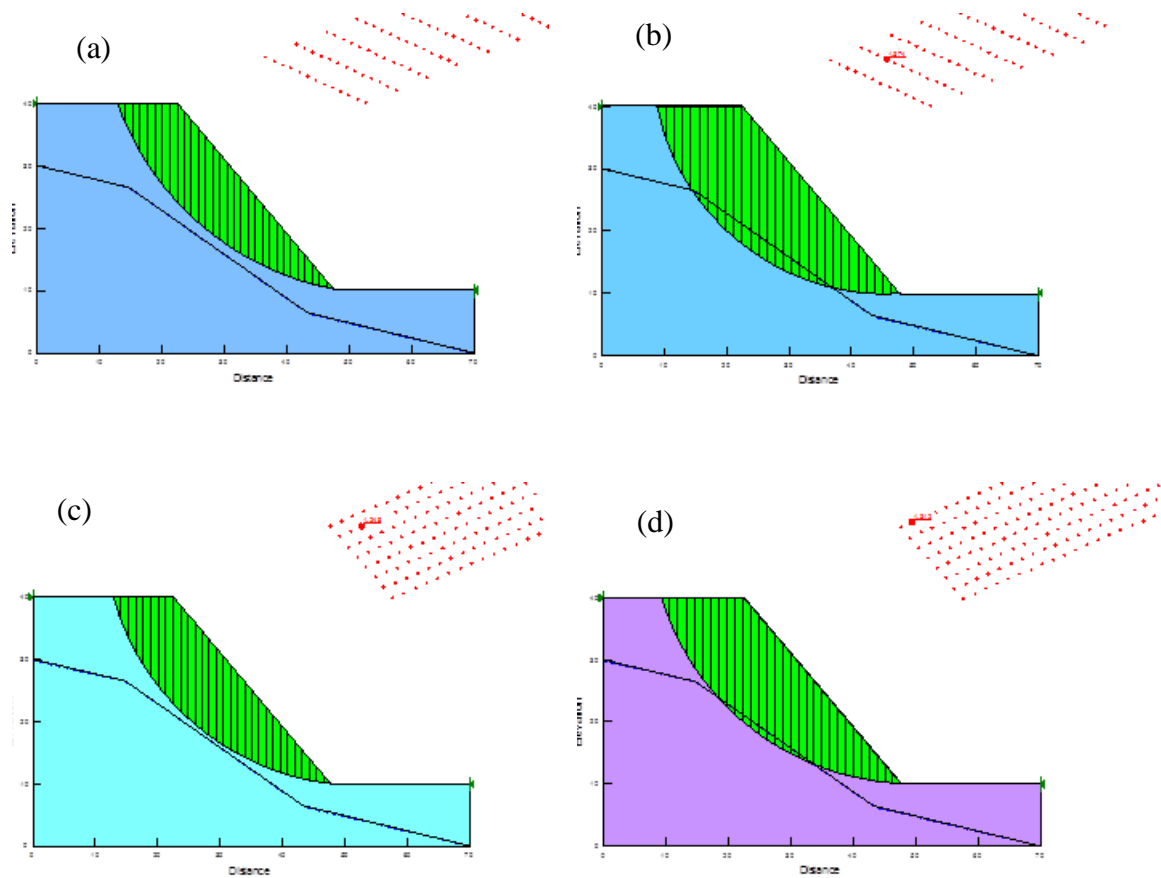
Figure A-15: Critical slip surface for simulations S2C (a), S2S (b), S3C (c) and S3S (d) (see Table A-2) obtained with SLOPE/W; the location of the center of rotation is also shown for the critical slip surface

Table A-5: Factor of safety and location of center of rotation obtained with SLOPE/W (Morgenstern-Price and FE stress-based method) for different simulations presented in Table A-4, compared with FS obtained by Fredlund (2000, shown in figure A-7)

Simulation		FS	x (m)	y (m)	Radius (m)
Steep slope	Fredlund (S1)	0.901	65.6	58.7	52.8
	S1	0.901	68.66	58.29	52.26
	S1S	0.975	66	59.5	51.17
	S1C	0.975	66	59.5	51.17
	Fredlund(S2)	1.088	53.2	50.8	41.5
	S2	1.112	56	50.32	41.14
	S2C	1.245	56.25	55.41	46
	S2S	1.248	52.77	51.17	41.46
	S3C	1.374	45.62	47.47	37.55
	S3S	1.312	49.54	52.03	41.95

A-3 Additional results related to Section 4-3-2: effect of dilatation angle ψ

To verify the effect of dilatation angle on the slope stability of waste rock pile (cases presented in this study), some sensitivity analyses have been conducted.

Table A-6: Effect of variation of dilatation angle ψ on slope stability for cases in Group 2, local slip surface, $C = c_{app} = 1$ kPa

Dilatation angle ψ (°)	Factor of safety (FS)			
	Case S11	Case S12	Case S13	Case S14
0	1.277	1.204	1.159	1.109
24	1.277	1.204	1.159	1.109

A-4 Additional results related to Section 4-7-10: Effect of alternate layers parallel to the slope

Figure A-16 shows a waste rock pile with two benches and alternate layers parallel to the slope, (see Section 4-7-10 and Tables 4-4 and 4-5). A sensitivity analysis was conducted to evaluate the effect of alternate layer's thickness on the critical factor of safety (obtained with FE stress-based method). Two different thicknesses (0.5 m and 1 m) are considered.

Figure A-16: Waste rock pile with two benches and alternate layers (parallel to the slope) with different thicknesses (0.5 and 1 m), defined based on height Ht, Hi1, Hi2 (m), length at the base Lb1, Lb2 (m) and length at the top Ls (m), thickness of layer Lt (m) and the angles ($\alpha = 26°$ and $\beta = 37°$).

Figures A-17 (a) and (b) show that the thickness of layer affects the critical local FS obtained by FE stress-based method. As the thickness increases from 0.5 m to 1 m, the FS increases. For example, $\phi' = 37°$ and $c_{app} = 1$ kPa, FS increase from 1.2 to 1.35 when the thickness changes from 0.5 m to 1 m.

Figures A-17 (c) and (d) present the FS for the global critical slip surface (going through the crest and toe). The difference in FS due to layer thickness is not significant for the global critical slip surfaces.

Figure A-17: Relationship between the local and global factor of safety and the ϕ' value for piles with alteration layer, H_t=20 m, α = 26°, β = 37° (layer thickness 0.5 and 1 m respectively); a) local FS with c_{app} = 0 kPa; b) local FS with c_{app} = 1 kPa; c) global FS with c_{app} = 0 kPa; a) global FS with c_{app} = 1 kPa.

Figure A-18 presents the waste rock pile with two benches and alternate layers parallel to the slope. The properties of material are changing in alternate layers (shown in different colors). Unlike Figure A-16, Figure A-18 shows the material in alternate layers are changed in both vertical and horizontal directions in each bench (for each bench, the alternate layers are divided into two section vertically, the material properties of the upper part are different from lower part). This configuration is presented to see its effect on the waste rock pile stability.
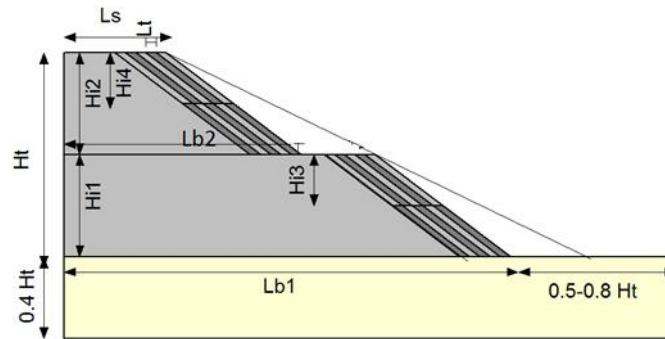
Figure A-18: Waste rock pile with two benches and horizontal and vertical alternate layers, parallel to the slope, horizontally and vertically with thicknesses 0.5 and 1 m, defined based on height H_t, H_{i1}, H_{i2} (m), length at the base L_{b1}, L_{b2} (m) and length at the top L_s (m), thickness of layer L_t (m) and the angles ($\alpha = 26°$ and $\beta = 37°$).

The results in Figure A-19 show that if alternate layers change in both directions (horizontally and vertically) there is a slight increase of FS (both local and global critical slip surfaces).
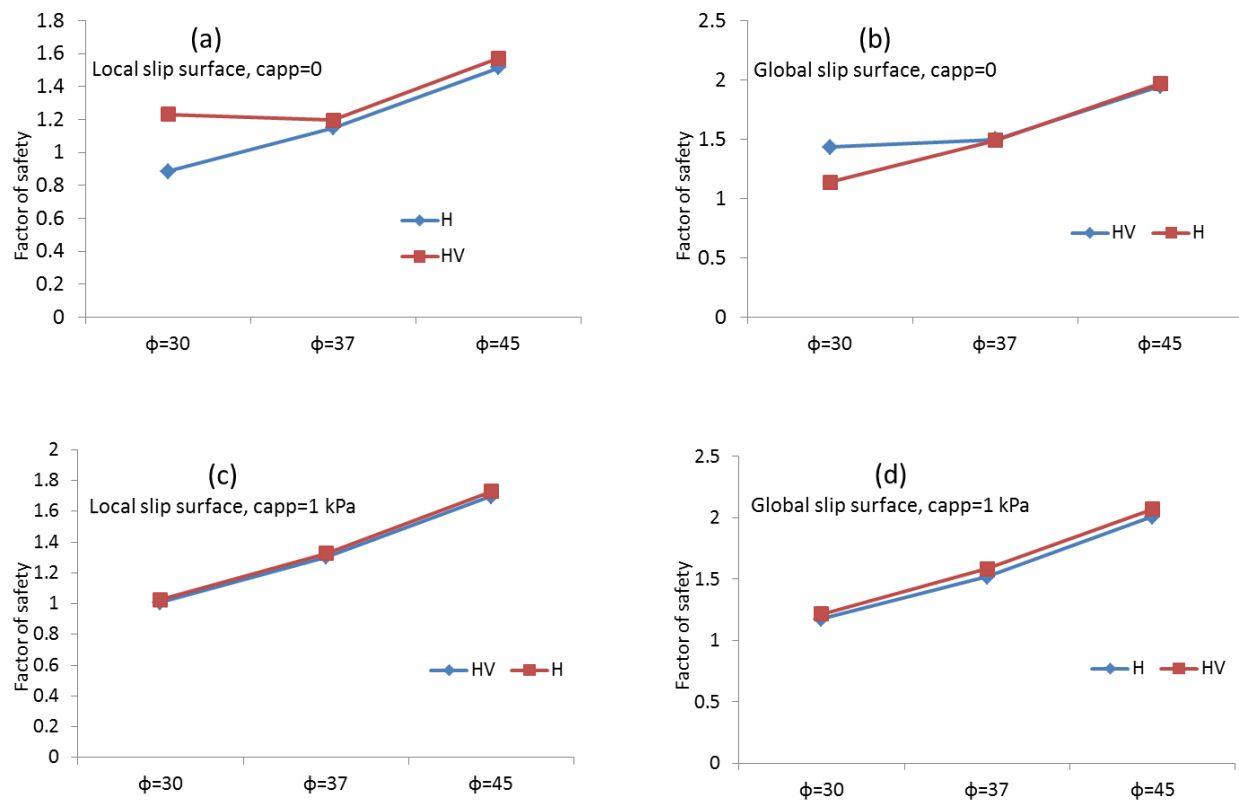
Figure A-19: Relationship between the factor of safety FS of piles with alternate layer; a) and b) layer thickness 0.5 m, horizontal (H), horizontal-vertical (HV), $c_{app} = 0$, local critical slip surface; c) and d) layer thickness 1 m, horizontal (H), horizontal-vertical (HV), $c_{app} = 1$ kPa, Global critical slip surface

A-5 Plate loading tests to assess the Young modulus (E) of waste rock

There is a paucity of results available to evaluate the modulus of elasticity (Young's modulus) E [FL^{-2}] of waste rock, which represents the material stiffness or its resistance to straining. This value of E is expected to depend on various factors, including material density and effective confining stresses.

There was thus a need for conducting experiments to obtain representative values of E. Plate loading tests were conducted in the laboratory to measure the vertical subgrade reaction, K_s (e.g. McCarthy, 2007):

$$K_s = \frac{Pressure}{Settlement} \quad [A\text{-}4\text{-}1]$$

The elastic theory provides a relationship (for a semi-infinite isotropic soil) between the vertical subgrade reaction K_s and modulus E, for a plate of diameter D and an applied uniform pressure (Teodoru et al. 2009):

$$K_s = \frac{4E}{\pi D(1 - v^2)} \quad [A\text{-}4\text{-}2]$$

A-5-1 Test description

The tests were performed in a large circular rigid (steel) tank (with D = 92 cm and H = 90 cm) filled with waste rock. The apparatus consist of a rigid plate, several rigid disks, and instrument to measure the applied loads and resulting settlements.

When the tank is filled with waste rock, the relatively coarse material is removed so that a 75 cm diameter plate is fully in contact with the soil and four gauges are placed and fixed on this plate to capture the displacement. After that, a rigid disk is added to the center of the first plate. The settlement reading is noted. Rigid disks have diameters of either 46 cm or 22 cm. The rigid disks were added step by step and the corresponding displacements were measured until there was no perceptible increase in settlement. The average of the four (or three) gauges settlement reading

was taken as the average settlement of the plate corresponding to the applied load. Each plate was 8 kg.

.
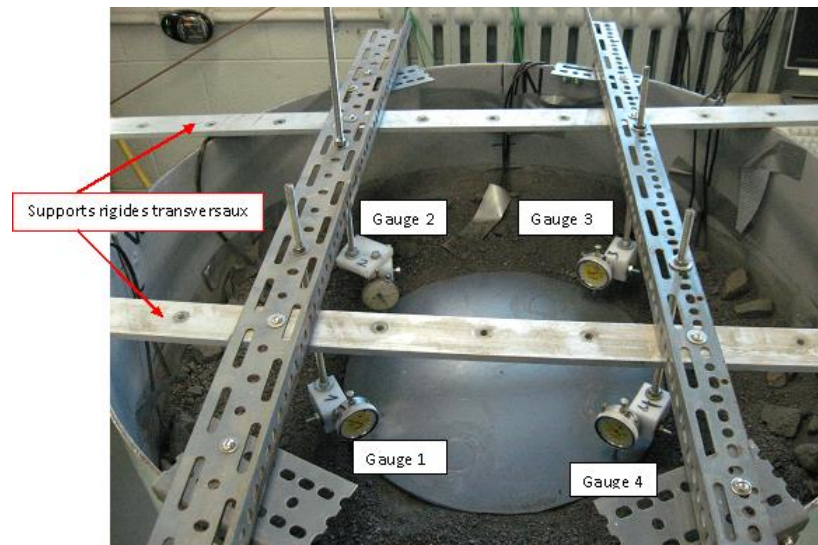
Figure A-20: Pilot apparatus in Laboratory for plate loading test.

A-5-2 Plate loading test results

Figure A-21 presents the results that are obtained through 6 plate loading tests. Tests 1 to 4 were performed with rigid plates with D = 46 cm, tests 5 and 6 were conducted by application of rigid plates with D = 22 cm.
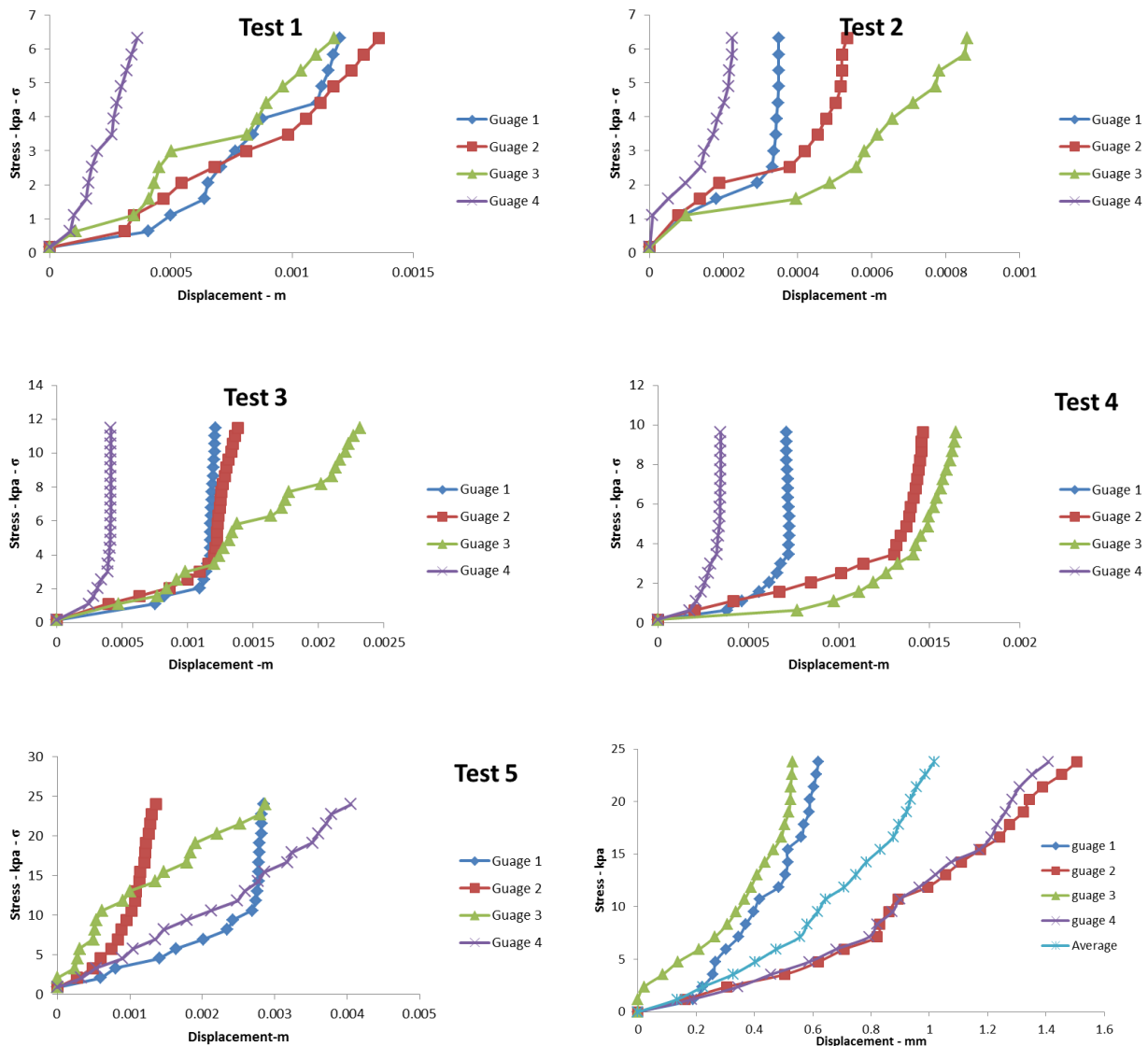

Figure A-21: Results for plate load tests No.1, 2, 3, 4, 5 and 6

The estimated values of E based on Equation A-4-2 (assuming a Poisson's ratio = 0.285, based on ϕ' and on Jaky's assumption for K_o) obtained from these tests are presented in Tables A-7 to A11.

Table A-7: Generated E modulus from Figure A-21, Test 1

$E_s= \pi D/4(1-v^2) K_s$ (kPa)		
Test 1	**first slope (soft)**	**second slope (stiff)**
gauge 1	338.55	1,208.09
gauge 2	238.64	506.03
gauge 3	304.53	481.21
gauge 4	1,177.11	1,561.48

Table A-8: Generated E modulus from Figure A-21, Test 2

Test 2	**first slope (soft)**	**second slope (stiff)**
gauge 1	592.35	16,479.60
gauge 2	755.68	1,447.04
gauge 3	658.17	737.47
gauge 4	1,177.11	3,732.31

Table A-9: Generated E modulus from Figure A-21, Test 3

Test 3	**first slope (soft)**	**second slope (stiff)**
gauge 1	956.41	8,970.42
gauge 2	447.44	3,317.61
gauge 4	805.39	40,806.63

Table A-10: Generated E modulus from Figure A-21, Test 4

Test 4	first slope (soft)	second slope(stiff)
gauge 1	1,133.52	45,907.46
gauge 2	1,133.52	2,518.93
gauge 3	523.16	1,669.36
gauge 4	755.68	18,362.99

Table A-11: Generated E modulus from Figure A-21, Test 6

Test 6	first slope (soft)	second slope(stiff)
gauge 1	1 150,8	1 712,6
gauge 2	481,8	673,8
gauge 3	825,1	1 566,9
gauge 4	456,8	767,1

A-5-3 Numerical simulation of the plate loading tests

The plate load tests results were also assessed using FE analyses with an axis-symmetric model. The simulation configuration is presented in Figure A-22. The waste rock elevation (thickness) was 65 cm; the width was 45 cm and the loading surfaces were $(0.23)^2\pi$ and $(0.11)^2\pi$ for tests 1 to 4 and 5 to 6 respectively. The displacement boundary condition is fixed X-Y in the bottom, fixed X on left and right. The stiff interface was considered on the right, bottom and below the load and step by step loading was 8 kg for each step.
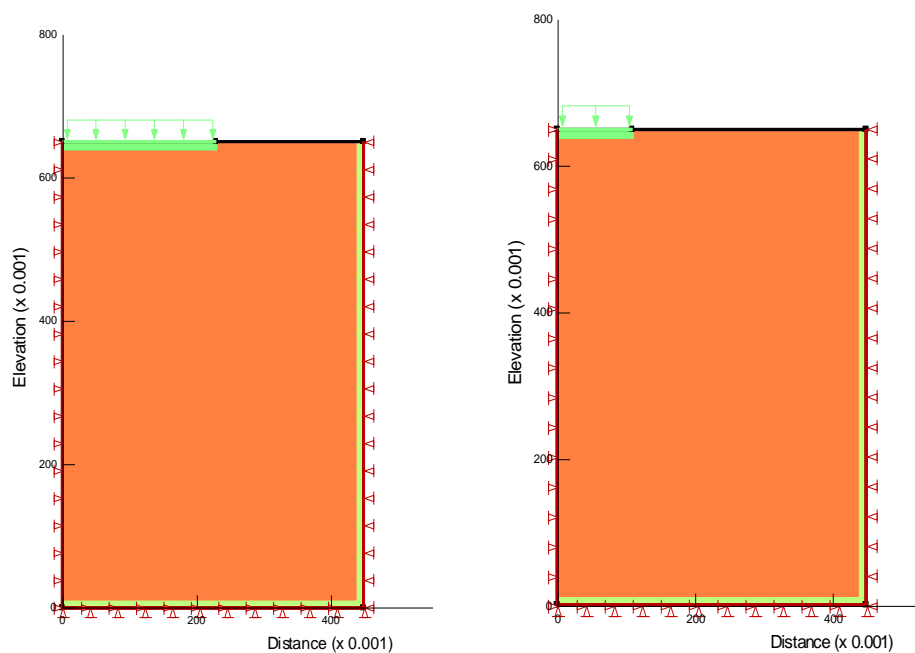
Figure A-22: Simulation configuration test 1-4 (left) test 5 and 6 (right)

Table A-12: Material properties for simulation

Material	Category- model	Total E modulus (kPa)	Unit weight (kN/m³)	Poisson's ratio	φ (°)
Waste material		From Tables 2 to 5	19.5	0.285	37
Interface 1 (right and bottom)	Total stress parameters Linear elastic	1e8	19.5	0.45	
Interface 2 (load surface)		2.3e6	19.5	0.45	

Figures A-23 to A-27 present the comparison between the simulation results and the results obtained from different tests. The simulation results are shown for all the tests (1 to 6). The experiments results present a graph with two different slopes (soft part, first par vs. stiff part, second part). The obtained results from SIGMA/W are closer to the experiment results related to the stiff part; here only the second part (stiff part) is shown.
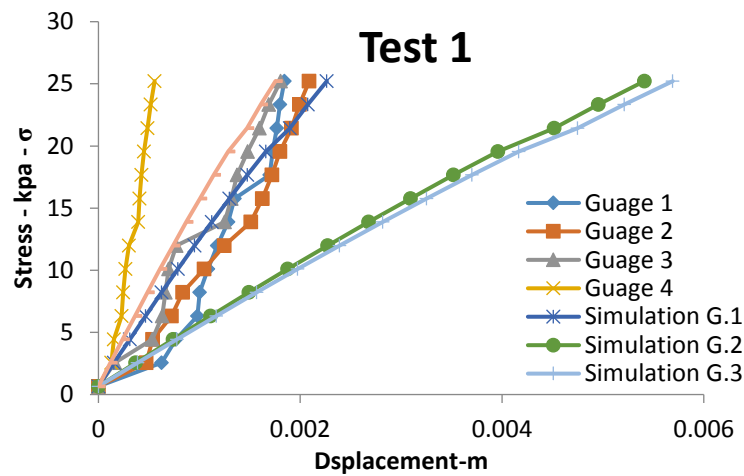
Figure A-23: Comparison of simulation and test results for Test No.1
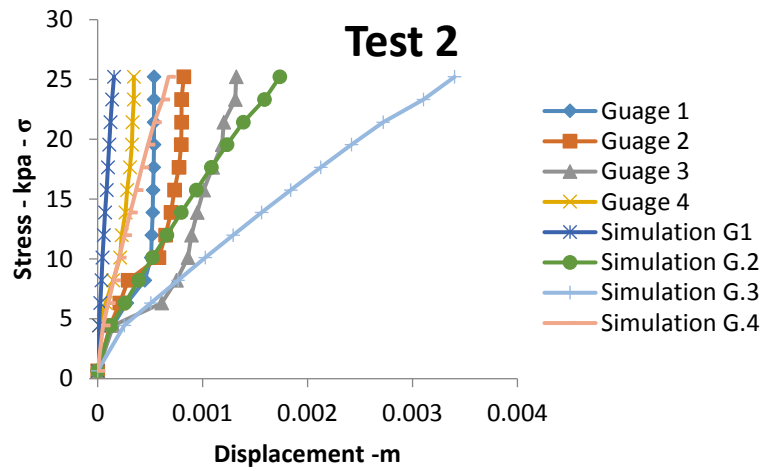
Figure A-7: Comparison of simulation and test results for Test No.2
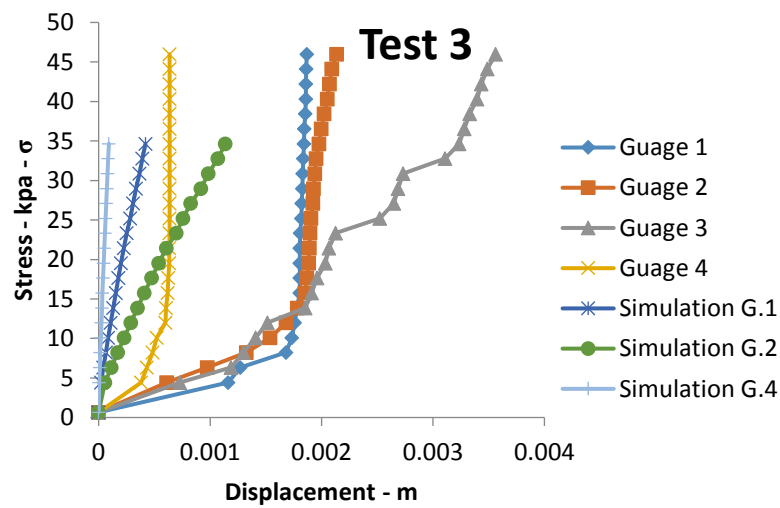
Figure A-25: Comparison of simulation and test results for Test No.3
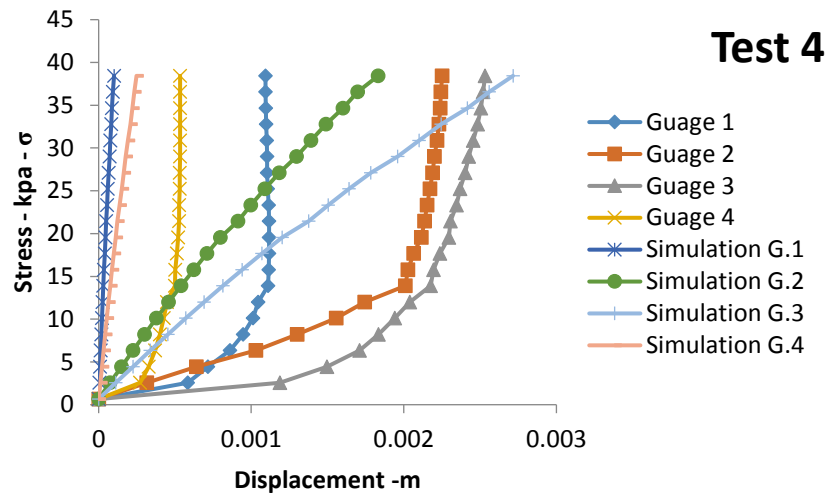
Figure A-26: Comparison of simulation and test results for Test No.4
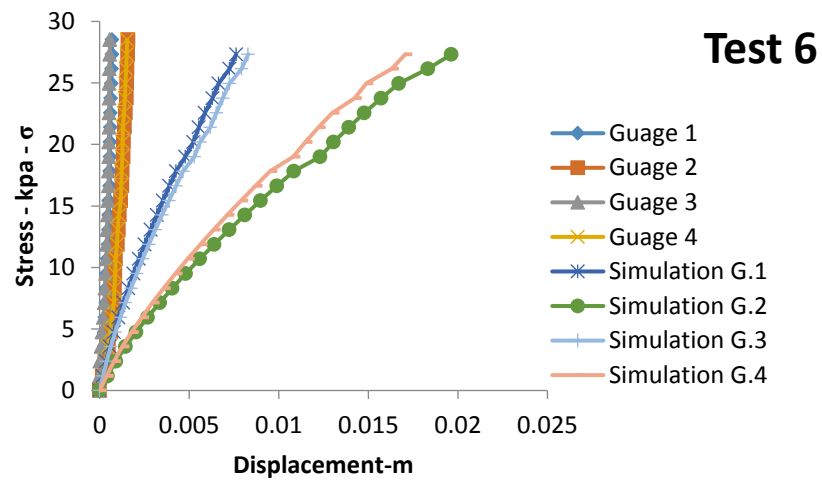
Figure A-27: Comparison of simulation and test results for Test No.6

The comparison between the simulation results and the results obtained from different tests (shown in Figures A-22 to A-27) indicate that in most cases higher displacement in tests was achieved. There is a need for higher E values in simulations to get more precise displacement values (comparing to test results),. Table A-13show the range of E-values from 6 test results (excluding test result 5) varied from 0.5MPa to 40 MPa.

Table A-13: Average E values obtained

Range of E (stiff part) – kPa				
	Gauge 1	**Gauge 2**	**Gauge 3**	**Gauge 4**
Test 1	1,208.09	506.03	481.21	1,561.48
Test 2	16,479.60	1,447.04	737.47	3,732.31
Test 3	8,970.42	3,317.61		40,806.63
Test 4	45,907.46	2,518.93	1,669.36	18,362.99
Test 6	1 712,6	673,8	1 566,9	767,1

Sensitivity analysis of E values (=5000, 10000, 20000 and 30000 kPa) in the simulation of Test 6 is shown in Figure A-28. The results indicate a value of E between 10000 to 20000 kPa is very close to the test results.
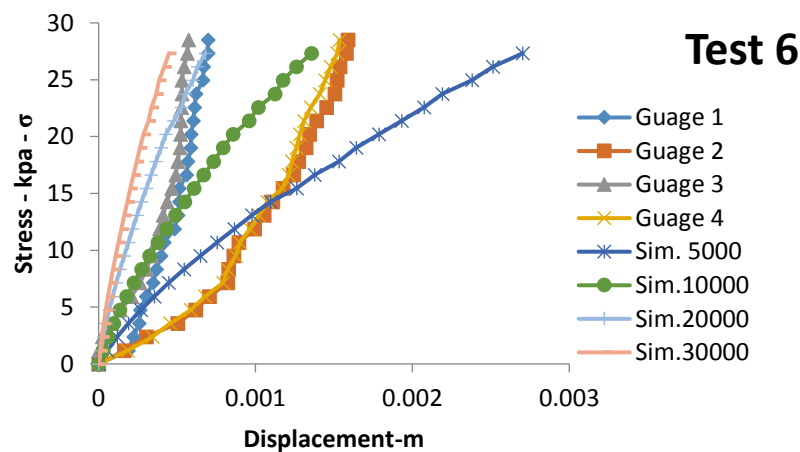
Figure A-28: Comparison of simulation and test results for Test No.6

Densified or compacted waste rocks are expected to show a larger modulus than in these laboratory tests. Bases on literature review and data presented in Table 4-2 (section 4-3-2) a value E= 80 MPa was used for the main analyses on homogeneous piles was presented in this thesis. For the compacted layers introduced in some simulations $\phi' = 45°$ and E = 240 MPa were used (see Table 4-2 and Section 2-2).

Appendix B – Additional results for Chapter 5

This appendix includes the mesh sensitivity analysis, some additional results related to sections 5-6-6, 5-7-2, 5-7-2-3 and a sensitivity analysis related to the WRC and its effect on infiltration and slope stability.

B - 1 Mesh sensitivity analysis

A sensitivity analysis has been conducted to select appropriate mesh size for simulations carried out with SEEP/W. This process is illustrated in the following. Figure B-1 presents a small waste rock pile with a height H = 10 m, with two benches. The water table is located at -4 m from the ground surface and foundation material is silty sand; the initial pore water pressure is fixed at -1.2 kPa in the waste rock material (based on ψ_r). A rainfall of 2.314×10^{-6} m/sec is applied for 6 hours over the surface.
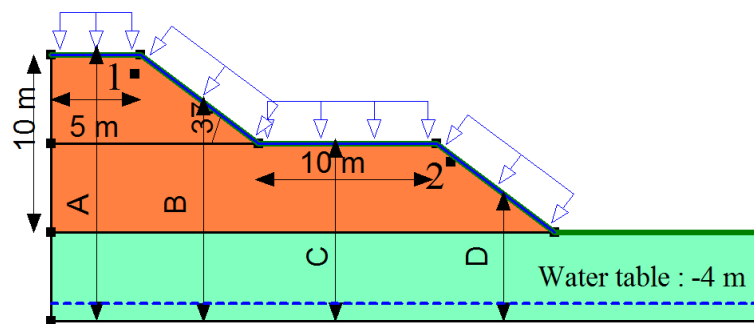
Figure B-1: Typical pile geometry used for mesh sensitivity analyses, four different sections (A, B, C and D) and two points have been pointed to evaluate the infiltration in the pile due to various mesh sizes

B-1-1 Mixed quad and triangle unstructured mesh

Figure B-2 shows a typical non-structured mesh (square and triangle, see Figure 3-3 for mesh configuration). Three different mesh sizes with different element sizes along the slope surface (length along the line edge of 0.2m, 0.15m, and 0.1 m).
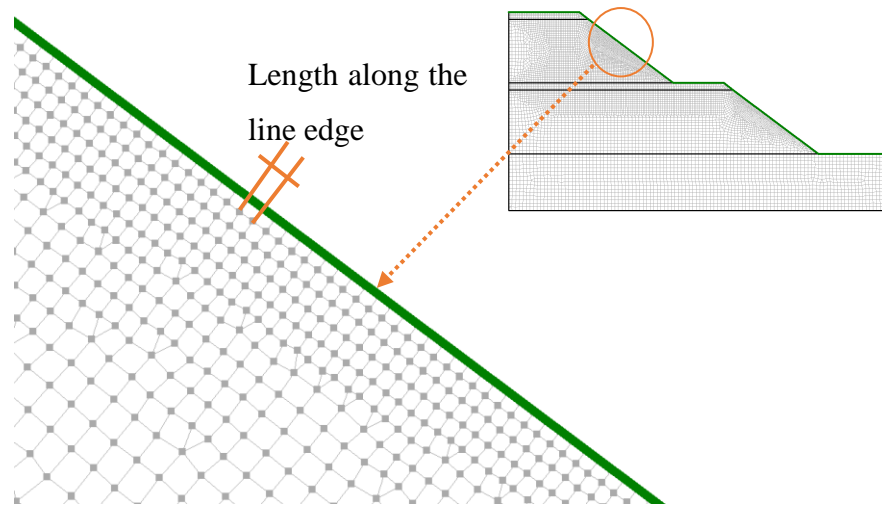
Figure B-2: Typical non-structured mesh

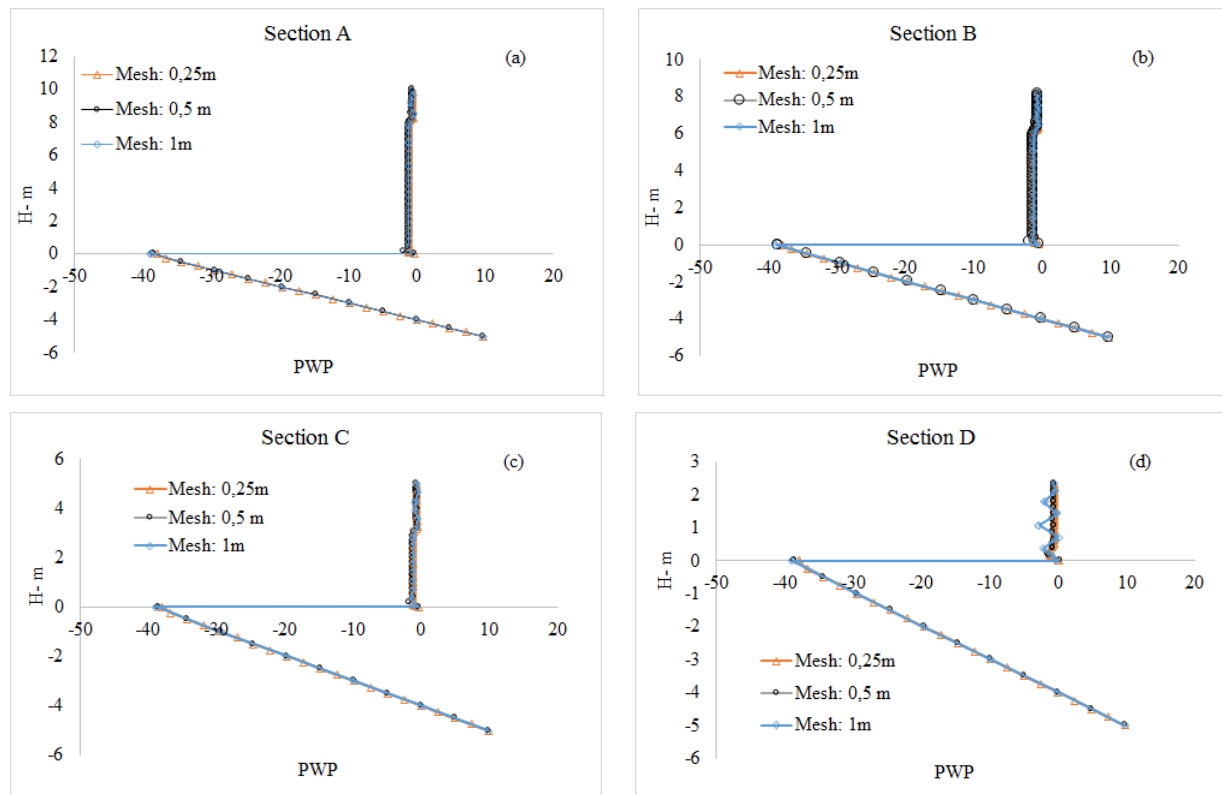Figure B-3 shows the infiltration along sections A, B, C and D.
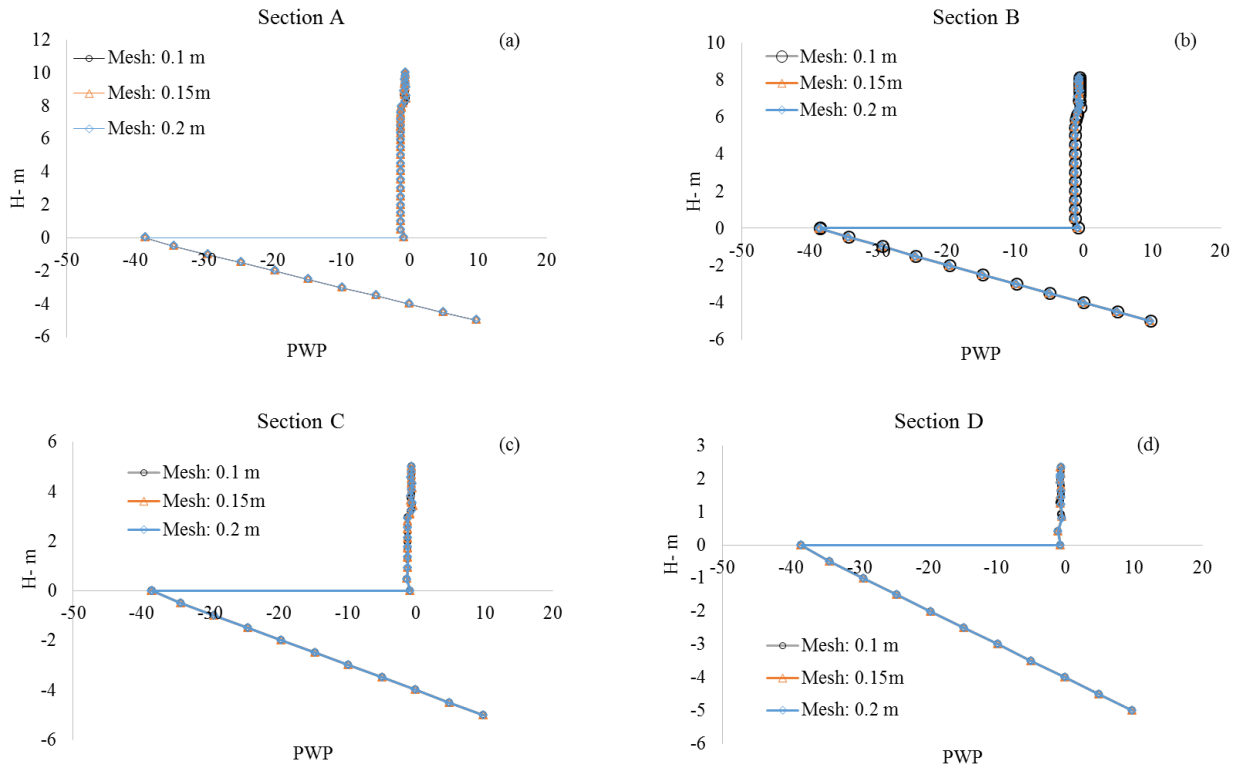
Figure B-3: PWP distribution after 6 hours for a rainfall of 2.314×10^{-6} m/sec along lines (sections) A, B, C and D (Fig. B-1) for different mesh sizes

Figure B-4 presents the change of PWP during the 6 hours of rainfall (with an intensity of 2.314 x 10^{-6} m/sec) at points 1 and 2 (Figure B-1). It shows that the PWP changes at point 1 are relatively similar for three different mesh sizes. For point 2, the pattern of infiltration during rainfall are relatively close for mesh sizes 0.15 and 0.1 m, but it is different for a mesh size 0.2 m. Point 2 in much closer to the surface compared to point 1 and PWP fluctuation at point 2 is better presented with smaller mesh size.
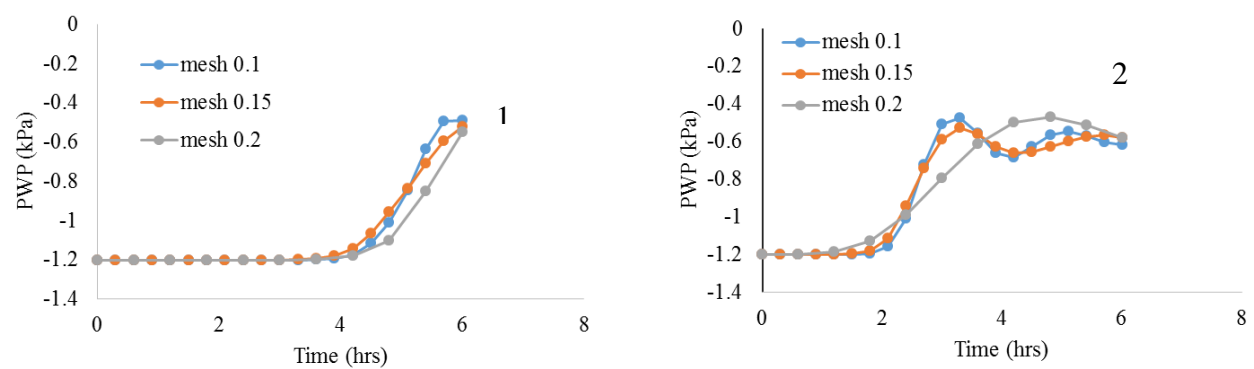
Figure B-4: PWP evaluation due to infiltration at points 1 and 2 for three mesh sizes (0.2m, 0.15m and 0.1), under a precipitation of 2.314×10^{-6} m/sec, for 6 hours.

B-1-2 Structured mesh (Rectangular grid of quads)

To evaluate the effect of mesh size on infiltration, SEEP/W configured a specify mesh density (global element size) as a real length unit (m). In this study, three different global mesh densities (1 m, 0.5 m, and 0.25 m) are defined for this particular simulation.
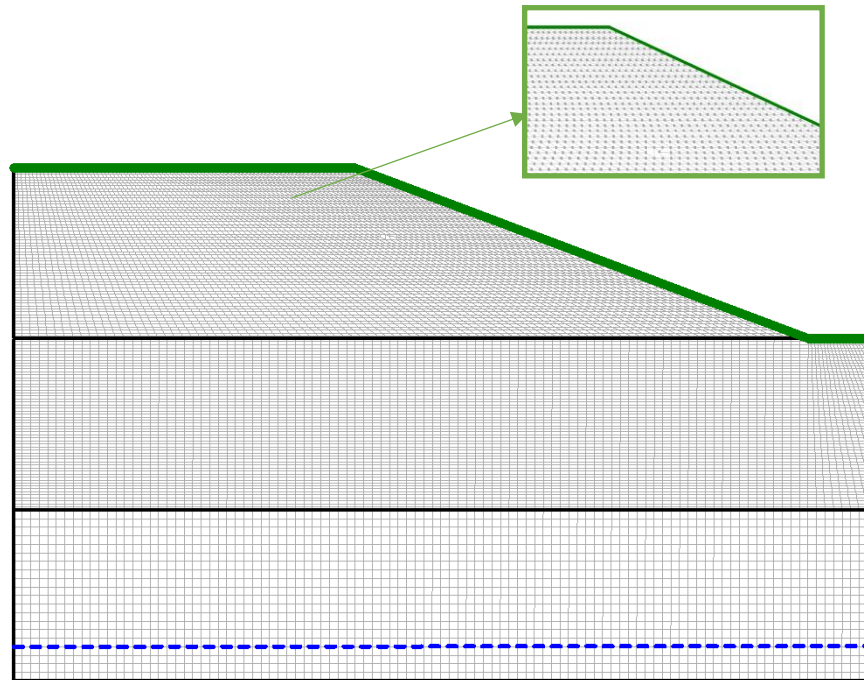
Figure B-5: Structured mesh (square) configuration for model simulation presented in Figure B-1 (in SEEP/W and SIGMA/W), Case S21

It is observed that after the rainfall, there is infiltration and a reduction of suction for all sections with all of the mesh sizes. It is seen that the infiltration of mesh size of 0.5 and 0.25 is smoother (more regular) compared to a mesh size of 1 m; the suction reduction is slightly higher for a mesh size of 0.5 and 0.25 m. It is also observed that for a mesh size of 1m, there is more oscillation in the PWP distribution compared to the other two mesh sizes; this phenomenon is more significant along section D.

Figure B-6: PWP distribution after 6 hours for a rainfall of 2.314×10^{-6} m/sec along lines (sections) A, B, C and D (Fig. B-1) for different mesh size

Figure B-7 presents the change of PWP during the time of rainfall for points 1 and 2. In this particular case, with the same time steps, the mesh of 0.25 and 0.5 m present approximately similar results.

At point 1, mesh sizes = 0.25 and 0.5 show a similar trend for PWP variation, whereas the mesh = 1 m presents a decrease in PWP with slower rate after 4 hours, compared the two other mesh sizes (0.25 and 0.5m). PWP reaches the value -0.6 kPa after 5 hours of rainfall for mesh 0.25m and 0.5 m, while this value is reached for mesh 1m after 6 hours of rainfall.

At point 2, the PWP variation over the time does not show significant changes from one mesh size to the other. However, again, the rate of PWP decrease is smoother for mesh =1 m. After 3 hours of rainfall, mesh = 1 m gives a higher suction (-0.7 kPa) compare to mesh sizes = 0.25 m, 0.5 m (-0.6 kPa). Also after 6 hours of rainfall, a higher suction (around -0.85 kPa) for mesh= 1 m is observed.
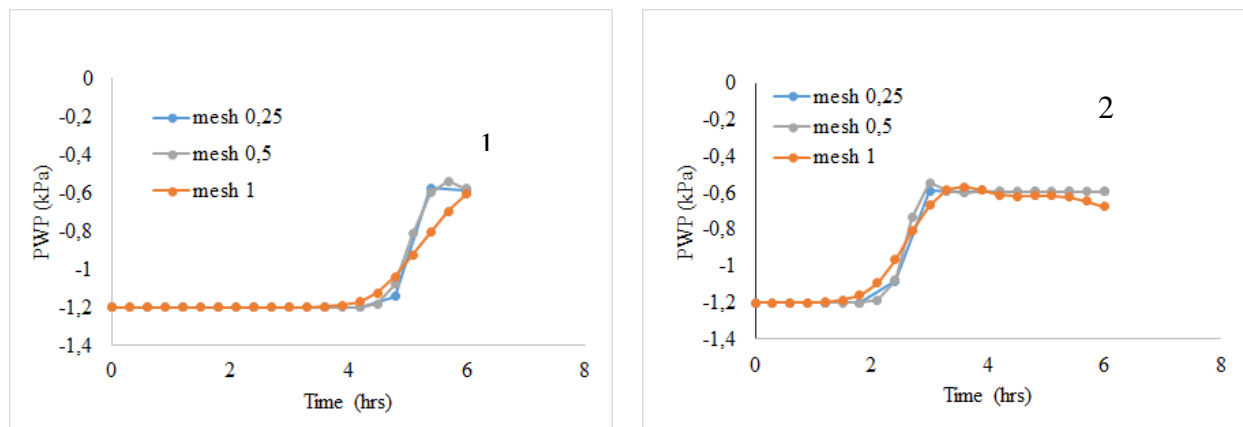
Figure B-7: PWP evaluation due to infiltration at points 1 and 2 for three mesh sizes (0.25, 0.5 and 1m), under a precipitation of 2.314×10^{-6} m/sec, for 6 hours.

B – 2 Additional results related to effect of prolonged rainfalls (see section 5-6-6)

- Variation of negative pore water pressures along the slip surface
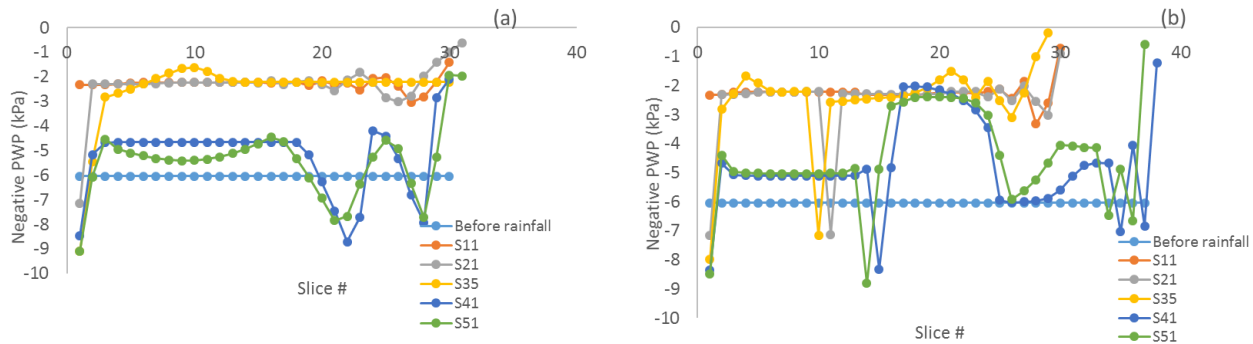
Figure B-8: Variation of negative pore water pressure along the local and global slip surface, before and at the end of rainfall Type R 2-2, for different cases S11, S21, S35, S41 and S51, initial suction WEV; a) local slip surface; b) global slip surface
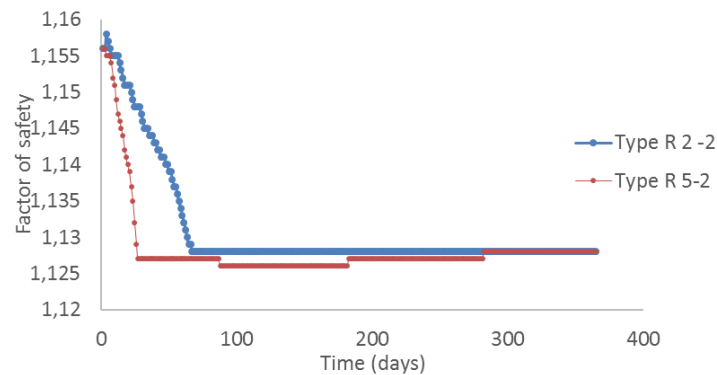
- Variation of FS for Case S1, under rainfall R 2-2

Figure B-9: Evaluation of minimum critical factor of safety under rainfalls R 2-2 and R 5-2, Case S1, $c_{app} = 1$ kPa (suction 6 kPa)

B – 3 Additional results presenting evolution of PWP and volumetric water content related to Section 5-7-2

- Case S11, PWP, and volumetric water content distribution under rainfall Type R 3-3
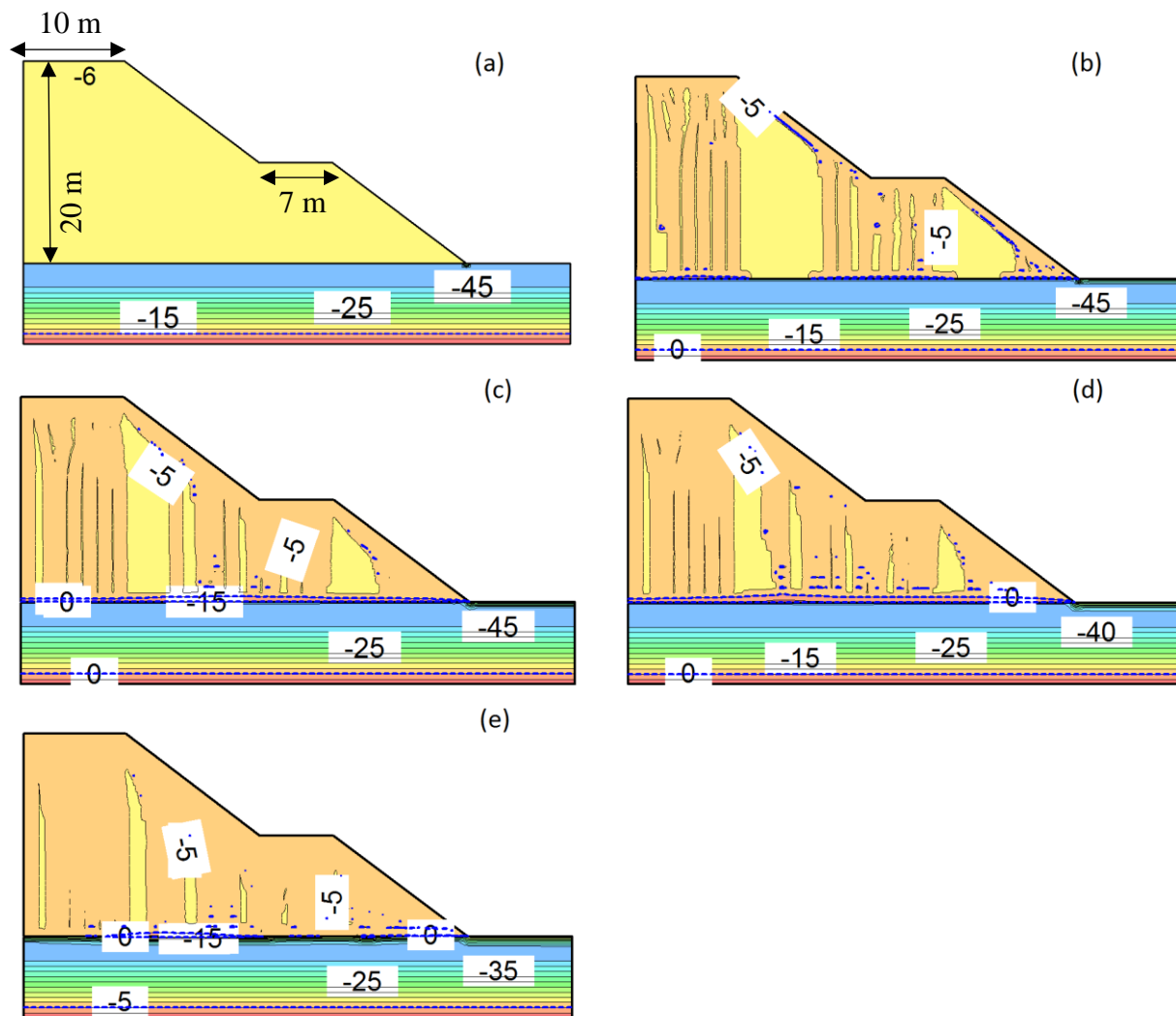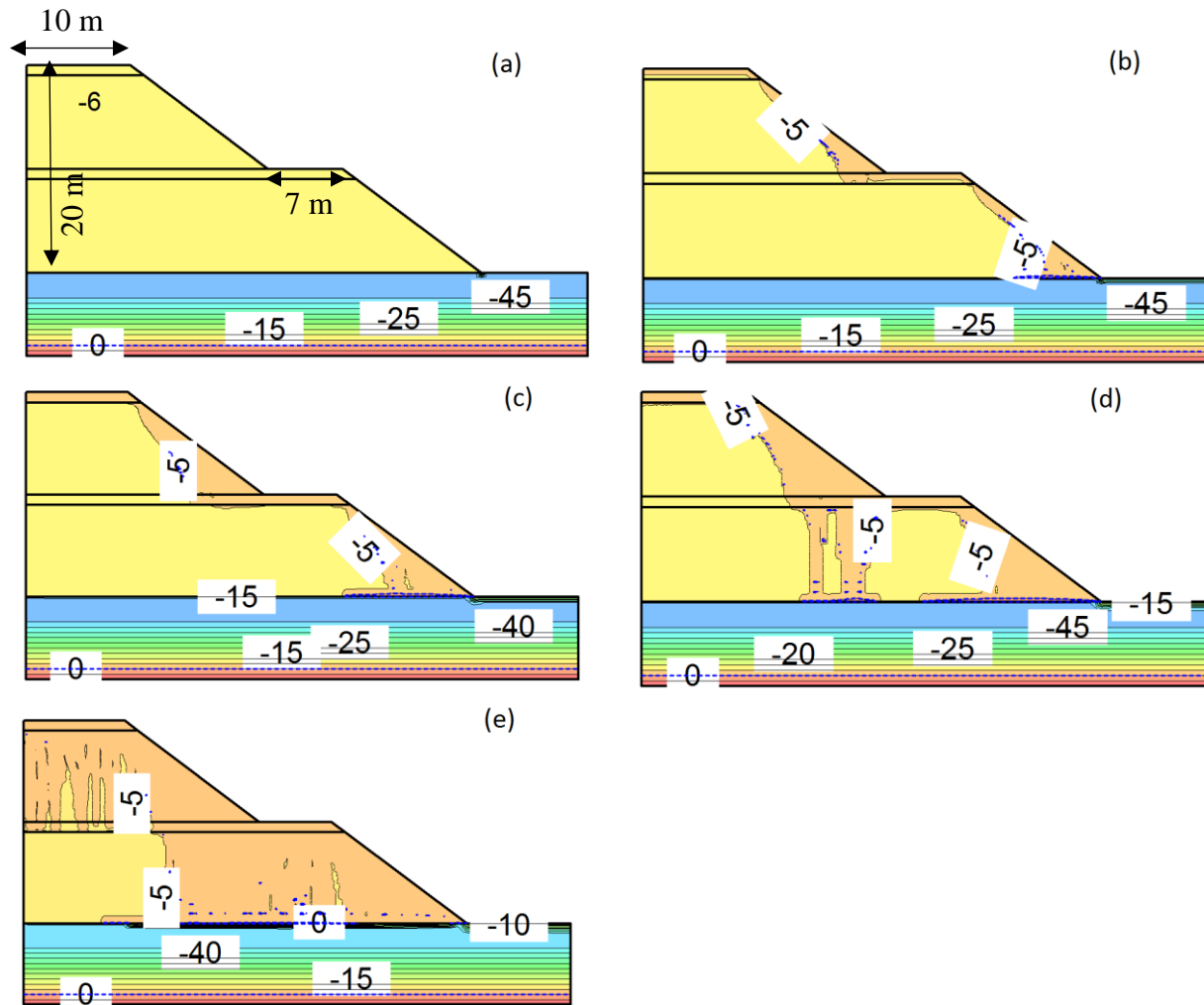

Figure B-10: Evolution of the pore water pressures (kPa) with the development of a wetting front, Case S11 under a constant rainfall 1.736×10^{-6} m/s (0.15 m/d, R 3-3); a) before rainfall; b) after 6 hrs; c) after 12 hrs; d) after 18 hrs; e) after 24 hrs
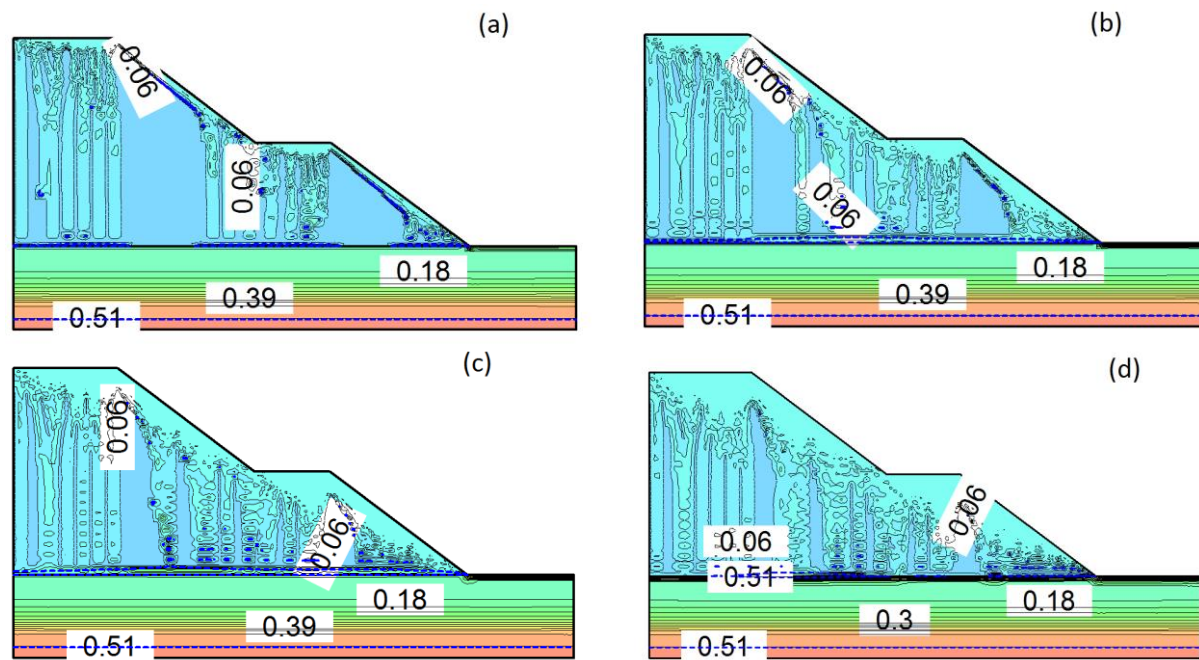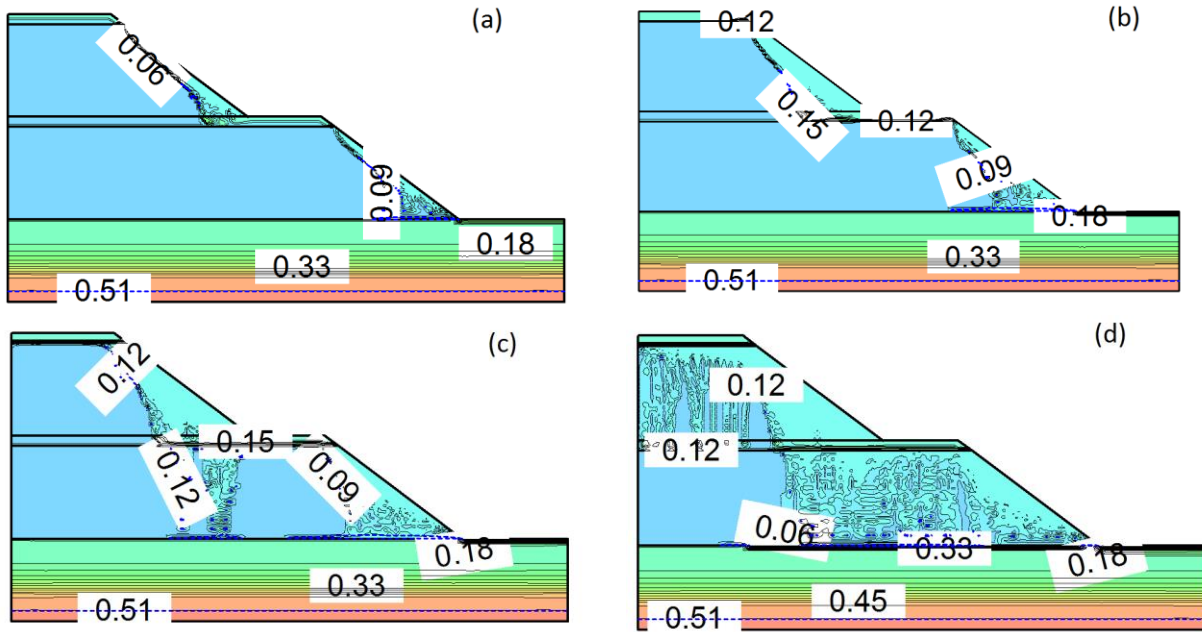
Figure B-11: Evolution of the volumetric water content distribution under rainfall 1.736×10^{-6} m/s (0.15 m/d, R 3-3); Case S11 with initial VWC ≈ 0.05; a) after 6 hrs; b) after 12 hrs; c) after 18 hrs; d) after 24 hrs

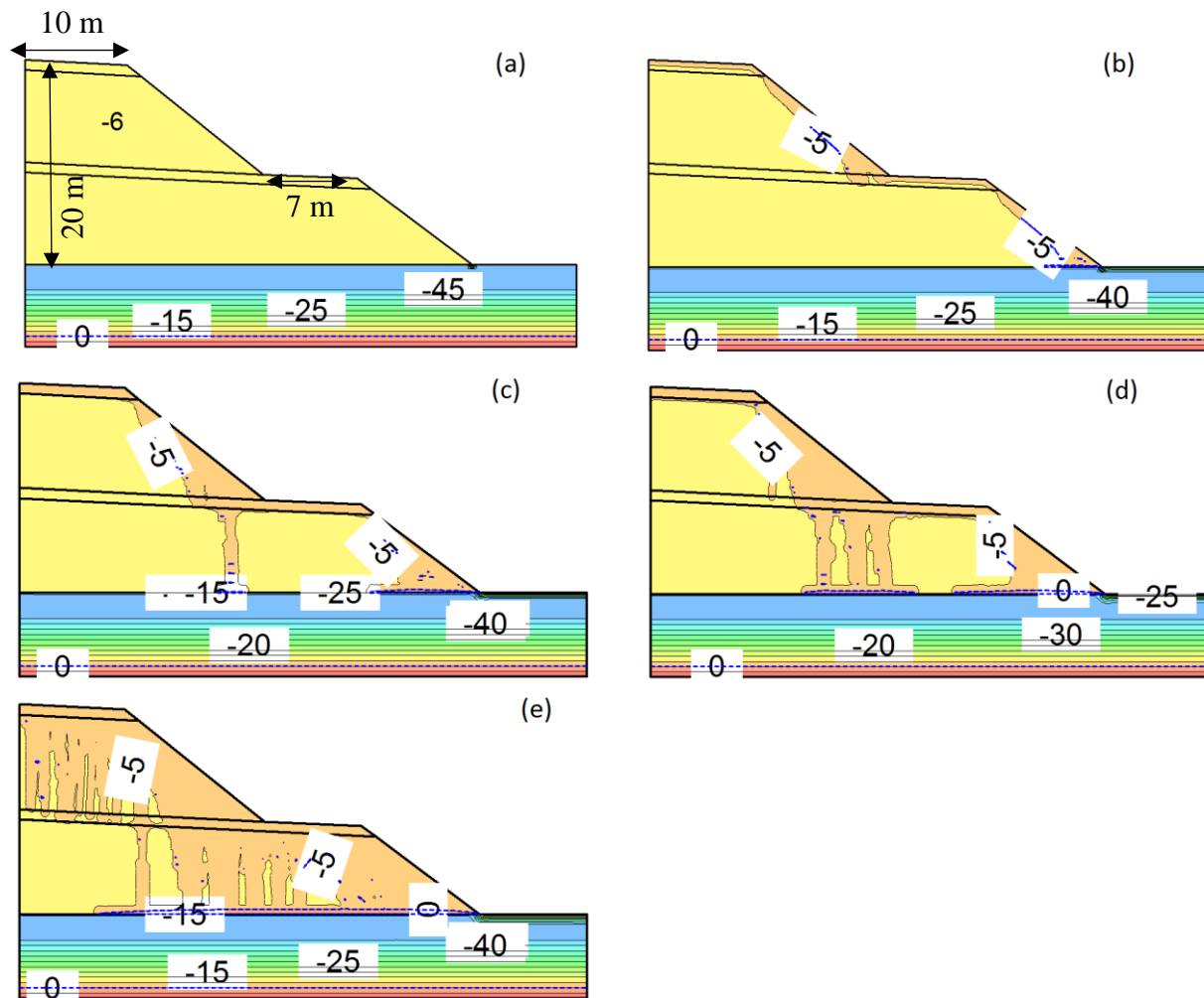- Case S21, PWP, and volumetric water content distribution under rainfall Type R 3-3

Figure B-12: Evolution of the pore water pressures (kPa) with the development of a wetting front, Case S21 under a constant rainfall 1.736×10^{-6} m/s (0.15 m/d, R 3-3); a) before rainfall; b) after 6 hrs; c) after 12 hrs; d) after 18 hrs; e) after 24 hrs
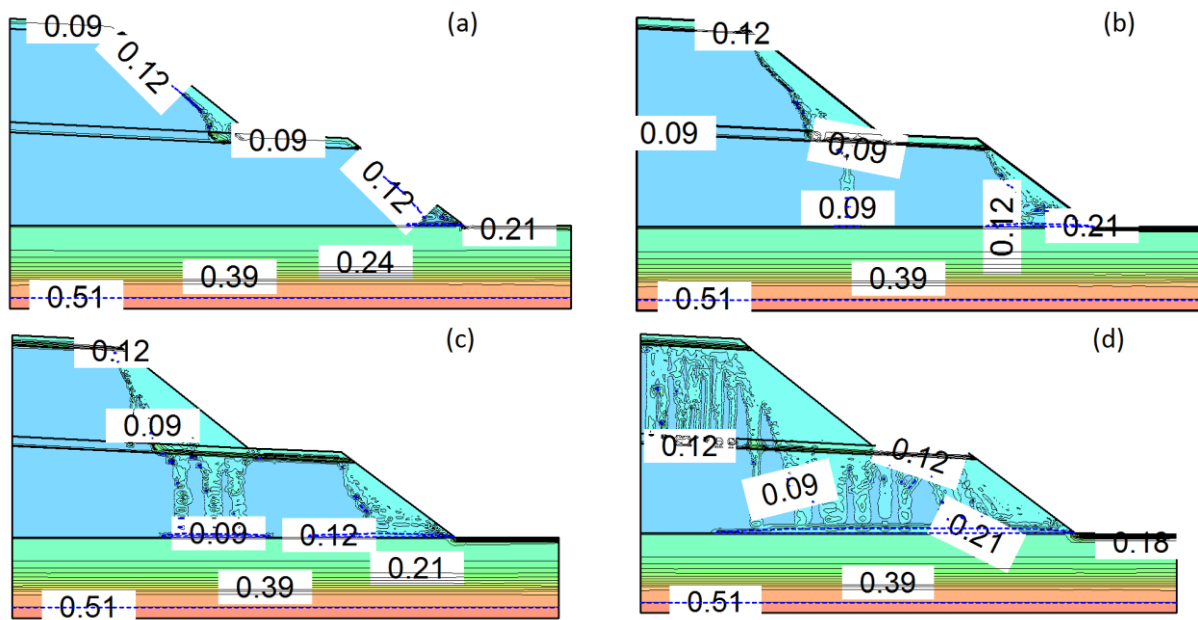
Figure B-13: Evolution of the volumetric water content distribution under rainfall 1.736×10^{-6} m/s (0.15 m/d, R 3-3), Case S21 with initial VWC ≈ 0.05; a) after 6 hrs; b) after 12 hrs; c) after 18 hrs; d) after 24 hrs

- Case S35, PWP, and volumetric water content distribution under rainfall Type R 3-3

Figure B-14: Evolution of the pore water pressures (kPa) with the development of a wetting front, Case S35 under a constant rainfall 1.736×10^{-6} m/s (0.15 m/d, R 3-3); a) before rainfall; b) after 6 hrs; c) after 12 hrs; d) after 18 hrs; e) after 24 hrs

Figure B-15: Evolution of the volumetric water content distribution under rainfall 1.736×10^{-6} m/s (0.15 m/d, R 3-3), Case S35 with initial VWC ≈ 0.05; a) after 6 hrs; b) after 12 hrs; c) after 18 hrs; d) after 24 hrs.

B - 4 Additional results related to the effect of increasing rainfall on slope stability (see section 5-7-3)
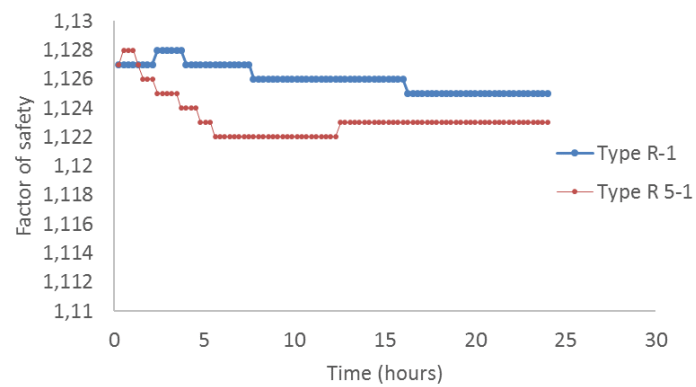
Figure B-16: Evaluation of minimum critical factor of safety under rainfalls R 1 and R 5-1, Case S1, initial condition residual suction

B - 5 Additional results related to section 5-7-2-3, variation of negative pore water pressure along global slip surface
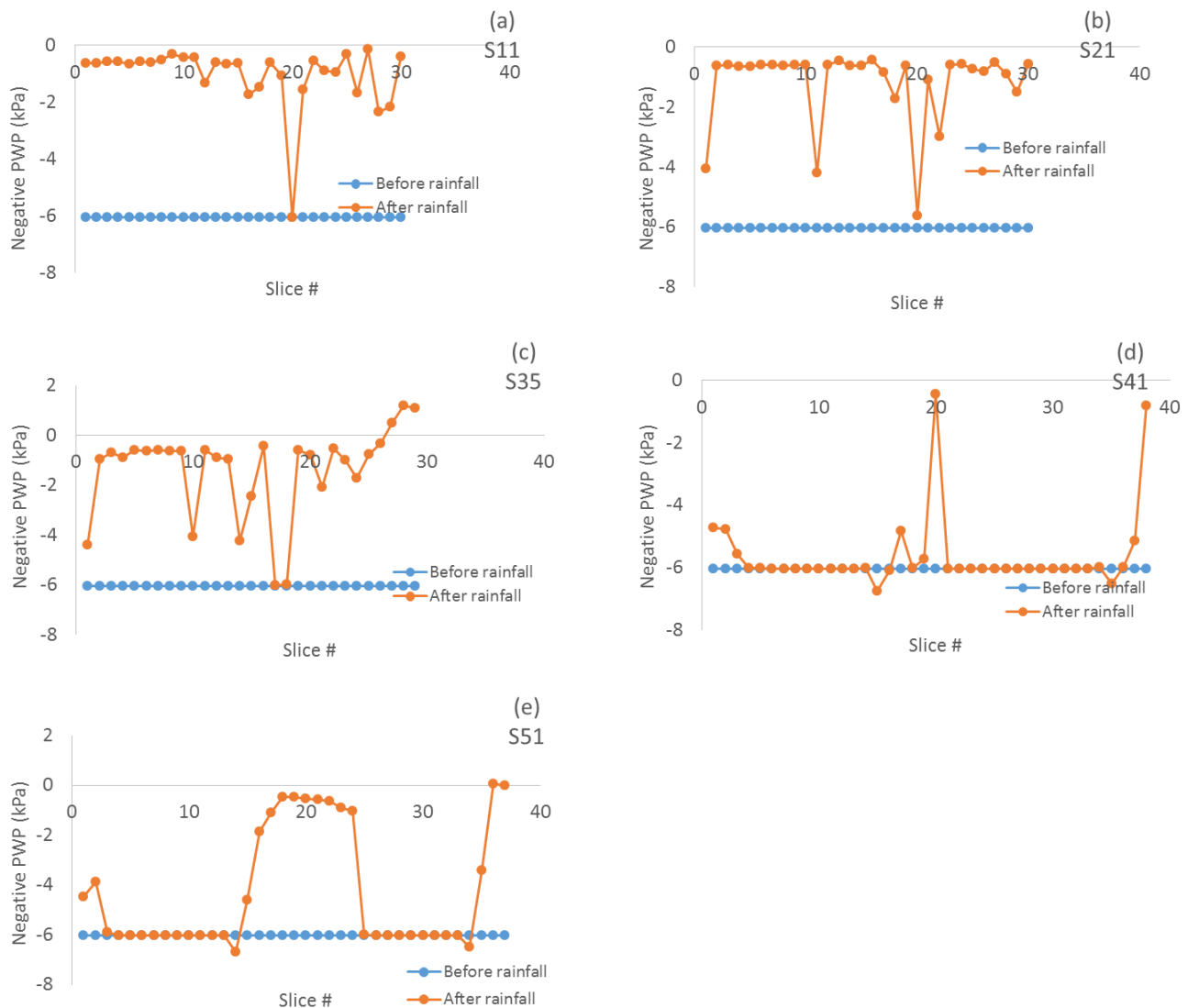
Figure B-17: Variation of negative pore water pressure along the global slip surface, before and after rainfall 1.736×10^{-6} m/s (0.15 m/d, R 3-3), initial suction 6 kPa; a) Case S11; b) Case S21; c) Case S35; d) Case S41; e) Case S51.

B - 6 Additional results to evaluate the effect of AEV and WEV of material WRC in transient analysis

The volumetric water content inside a waste rock pile is not expected to change much from one year to the next, once a (pseudo) steady-state is established (Fala et al., 2006). However, infiltration episodes due to major climatic events (such as snow melt and large precipitation) may modify the water distribution inside a pile (e.g. Dawood et al. 2011; Dawood and Aubertin 2012) temporarily.

For such changing conditions, the factor of safety can be determined by the shear strength, based on the degree of saturation and local suction. These relationships are incorporated into SIGMA/W and SLOPE/W. To examine the stability of slopes during and after rainfalls, infiltration and groundwater flow were first modeled using SEEP/W (Geoslope International Inc.) to obtain the distribution of pore water pressure and volumetric water content inside the pile. Then the total and effective stresses distributions were determined with SIGMA/W, followed by a stability analysis performed with SLOPE/W. The value of FS is shown for the conditions at the end of the rainfalls (i.e. t = 6 hours or 12 hours for the simulations presented here). Five different water retention curves WRC (with different air entry values AEV and water entry values WEV - see Figure B-18 and Table B-1) have been considered for the waste rock materials (the other parameters are taken as constant, in these simplified calculations).
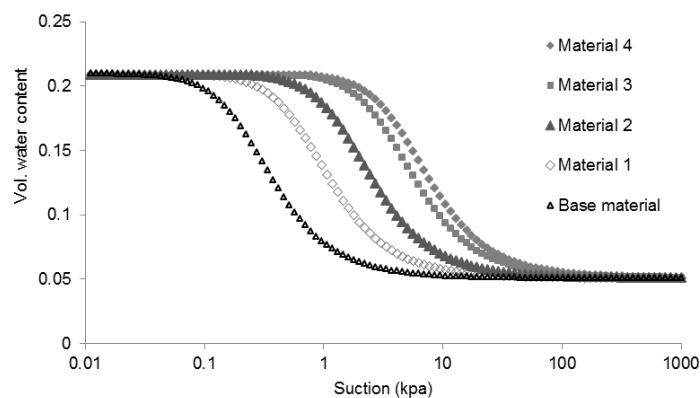

Figure B-18. Different water retention curves for different waste rock materials

Table B-1: Air entry values AEV and water entry values WEV for materials with different WRC

Type	AEV (kPa)	WEV (kPa)
Base material	0.1	1.2
Material 1	0.35	3.5
Material 2	0.8	8
Material 3	2	18
Material 4	2.5	20

Three precipitation rates are considered for the single bench pile (H = 20 m, α = β = 37°); the values of recharge applied on the surface are q_s (m/s) = 4.28e-007, 2.14e-006 and 4.28e-006. Table B-2 represents the different scenarios simulated; evaporation is not taken into account here. In all cases, the waste rock is initially at the residual water content (and suction). The water table level is located 7 m below the ground. The material below the pile has similar properties as the in the pile.

Table B-2: Rainfall (recharge) scenarios

Scenarios	Description
1.1	6 hrs of rainfall
1.2	Five days of drainage following 6 hrs of rainfall
2.1	12 hrs of rainfall
2.2	Five days of drainage following 12 hrs of rainfall
3.1	6 hrs of rainfall, followed by one day of drainage, followed by 6 hrs of rainfall
3.2	Five days of drainage following scenario 3.1

Figures B-19 and B-20 shows the computed distributions of pore-water pressure (PWP) and volumetric water content (VWC) obtained with SEEP/W, for a vertical section located near the crest of the slope; these are varying with depth after 6 hours of rainfall (scenario 1.1, qs=4.28e-006 m/s)

Figure B-19 presents the PWP distribution for different materials (different WRC with different AEV and WEV). The position of the wetting front (with reduced suction) can be seen in all cases. The effect of the different WRC (and different hydraulic conductivity functions – not shown here) on the infiltration is seen in this figure. It is seen that the variation of suction along the vertical profile is more pronounced for materials with a higher AEV and WEV.
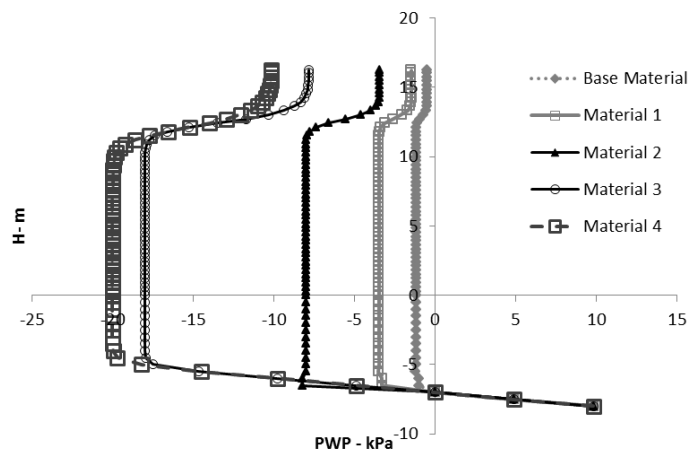
Figure B-19: Suction profiles for different materials with different WRC; scenario 1.1 (q_s=4.28e-006 m/s).

Figure B-20 shows the volumetric water content profile for scenario 1.2. As the general shape of the WRC is the same for the different materials, the VWC distribution is relatively similar in all cases, with some local differences due to the different AEV and WEV. The volumetric water content profiles show an increased magnitude at an elevation of about 12 m, due to infiltration at the wetting front.
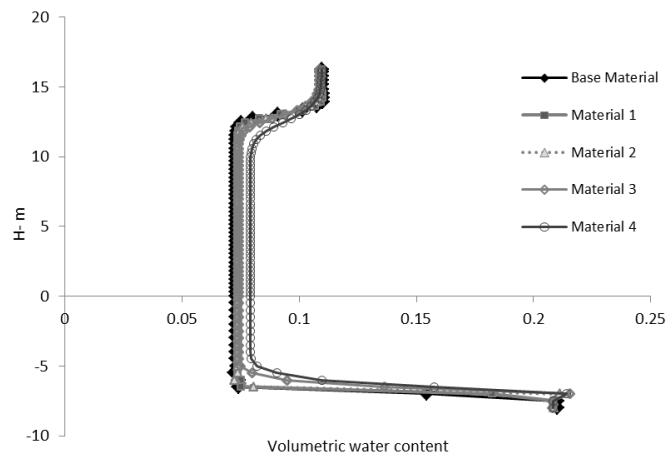

Figure B-20: Volumetric water content profiles for different materials (with different WRC) for scenario 1.1 ($q_s = 4.28e$-006 m/s).

Figure B-21 presents the PWP distribution for different scenarios for the Base material (Figure and Material 3 (Figure B-17). The pattern of PWP distribution is similar for both materials, with a decrease of suction near the surface due to infiltration, followed by an increase of suction during drainage (dry period). There are differences in the rate of infiltration and the magnitude of the PWP. This illustrates how the PWP distribution is influenced by the rainfall and material properties.
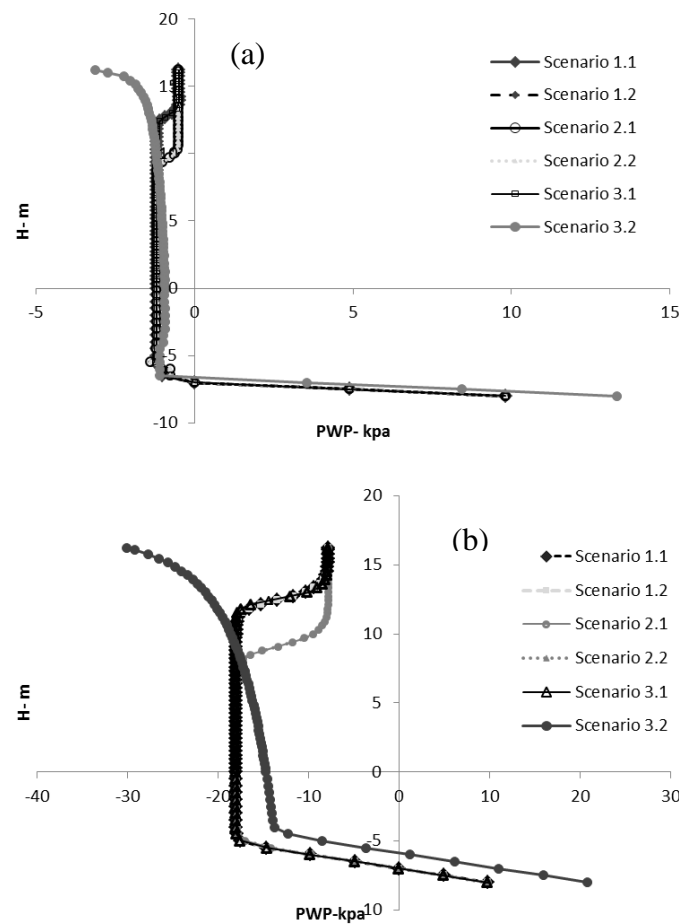

Figure B-21: Pore water pressure profiles for the different recharge scenarios (see Table 3); single bench pile; H=20 m; (q_s=4.28e-006 m/s); a) Base material, b) Material 3.

Figures B-22 to B-25 show some of the key results obtained from the stability analyses for transient cases, for different recharge scenarios. It is seen that the factor of safety can be influenced significantly by the rainfall and material properties, through their effect on the degree of saturation (and suction) in the pile.

Figure B-22 indicates that when the waste rock in the pile is close to the residual condition (for VWC and PWP), two groups can be identified: group 1 for materials 3 and 4 and group 2 for the base material, materials 1 and 2. It is seen that group 1 shows a higher FS due to the larger residual suction (giving a larger c_{app}). Also, when suction is reduced due to the rainfall infiltration, the factor of safety tends to decrease. This reduction of the factor of safety is mainly due to a decrease of the apparent (capillary) cohesion when the matric suction decreases.
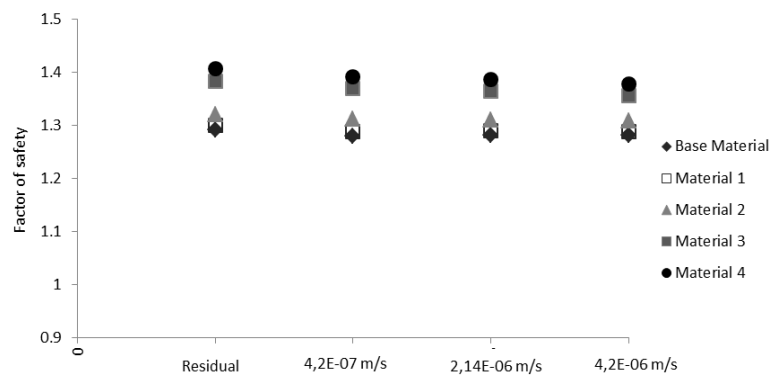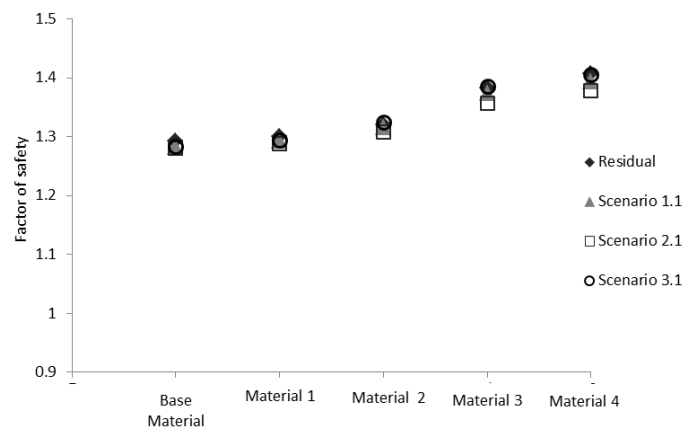

Figure B-22: Factor of safety of a single-bench pile, for waste rock having different WRCs (given in Figure 6) for varying rainfall (q_s=4.28e-007; 2.14e-006; 4.28e-006 m/s), scenario 2.1.

Figure B-23 show that the differences between the values of FS for different WRCs, following infiltration, are more pronounced for materials with a larger AEV. The factor of safety obtained for different materials for the three scenarios tends to indicate that the stability of the waste rock pile depends on internal configuration, the degree of saturation and infiltration rate. For a medium rate recharge (qs= 4.28e-6 m/s) with durations of 6 hrs and 12 hrs, an increase of the AEV produces more significant changes in the factor of safety; the most significant changes occur in material 4. The fact that Scenario 2.1 leads to lower values of FS, compare to scenario 1.1, also shows that longer rainfall duration produces a lower FS. The larger factor of safety obtained for scenario 3.1, compare to scenario 2.1 and also illustrates the effect of an increased recharge.

Figure B-23: Factor of safety of the single-bench pile, for waste rock having different WRC (given in Figure 6) for varying WRC applied for q_s=4.28e-006 m/s – scenarios 1.1, 2.1, 3.1.

Figure B-24 shows the calculations results obtained for 3 different scenarios (no 1.2, 2.2 and 3.2) for qs=4.28e-006 m/s. A higher factor of safety is obtained for scenario 3.2 compare to scenario 2.2, indicating the rainfall pattern (including precedent rainfall) may also affect the pile stability.
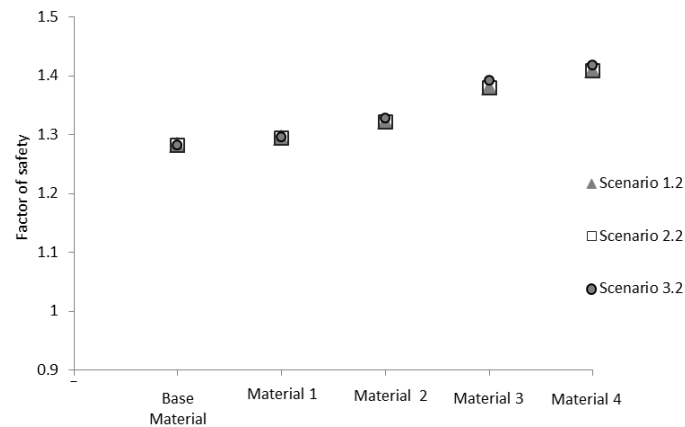

Figure B-24: Factor of safety of a single-bench pile, for waste rock having different WRC (given in Fig. 9) for q_s=4.28e-006 m/s for scenarios 1.2, 2.2 and 3.2.

Figure B-25 shows the values of FS for material 3, for different recharge scenarios. It is seen that when the rainfall is relatively small (q_s=4.28e-007 m/s), the value of FS does not change much for the various recharge rates, as suction and VWC do not vary significantly. As the rainfall intensity increases (up to q_s=4.28e-006 m/s), the differences in the value of FS between the different scenarios become somewhat more pronounced, due to the effect of recharge on suction (and VWC).
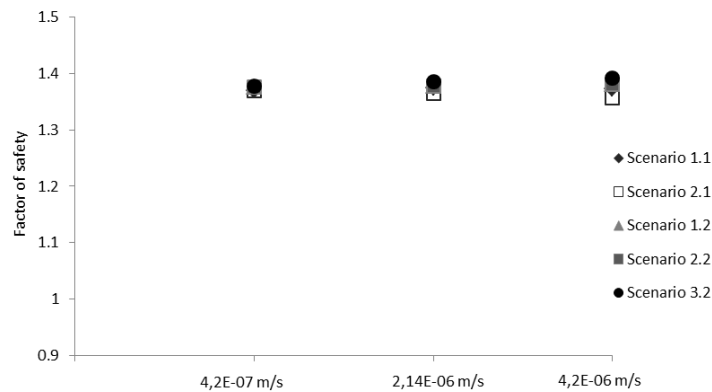

Figure B-25: Factor of safety of the single-bench pile, for Material 3 for varying rainfall intensities (for scenarios 1.1, 2.1, 1.2, 2.2 and 3.2).

Appendix C – Additional results for Chapter 6

This appendix presents some complementary results related to sections 6-4-1, 6-4-2, 6-4-3 and 6-4-4.

C-1 Additional results related to section 6-4-1

This section presents the sensitivity analysis to evaluate the effect of using a probability density function for ϕ' and γ on the probabilistic stability analysis of waste rock pile for cases S1, S21, S35

Table C-1: Results obtained with Monte-Carlo slope stability analyses, using a COV 10% for ϕ', or ϕ' and γ values; Case S1 (Chapter 4, Table 4-4), local and global slip surfaces.

Slip Surface	COV (%)	$\overline{FS}$	RI	PoF
	(ϕ')	1.31	3.19	0.0467
	(ϕ') & (γ)	1.31	3.18	0.06

Table C-2: Results obtained with Monte-Carlo slope stability analyses, using a COV 10% for ϕ', or ϕ' and γ values; Case S21 (Chapter 4, Table 4-4), local and global slip surfaces.

Slip Surface	COV (%)	$\overline{FS}$	RI	PoF
Local	(ϕ')	1.27	2.13	0.9733
	(ϕ') & (γ)	1.27	2.15	0.92
Global	(ϕ')	1.61	5.98	0.0000
	(ϕ') & (γ)	1.61	6.08	0.0000

Table C-3: Results obtained with Monte-Carlo slope stability analyses, using a COV 10% for ϕ', or ϕ' and γ values; Case S35 (Chapter 4, Table 4-4), local and global slip surfaces.

Slip Surface	COV (%)	$\overline{FS}$	RI	PoF
Local	(ϕ')	1.13	1.19	10.97
	(ϕ') & (γ)	1.13	1.2	10.77
Global	(ϕ')	1.59	5.1	0.0000
	(ϕ') & (γ)	1.59	5.17	0.0000

Figure C-1 to C-3 present the normal distribution of the factor of safety distribution related to the probability analysis for Cases S1, S21 and S35 considering the local and global slip surfaces with the normal distribution of ϕ' or ϕ' and γ
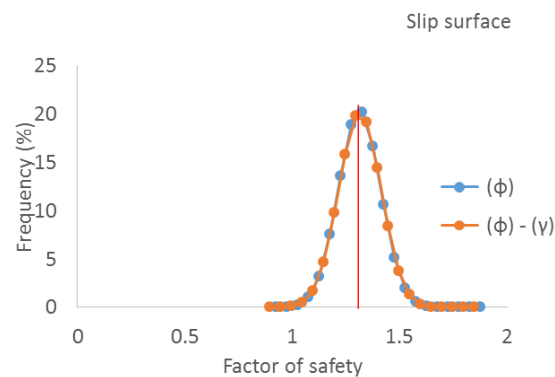
Figure C-1: Normal distribution of the factor of safety for COV% = 10 (ϕ', ϕ' and γ), Case S1 (see Tables 4-4 and 4-5), for sampling distance = 10 m.
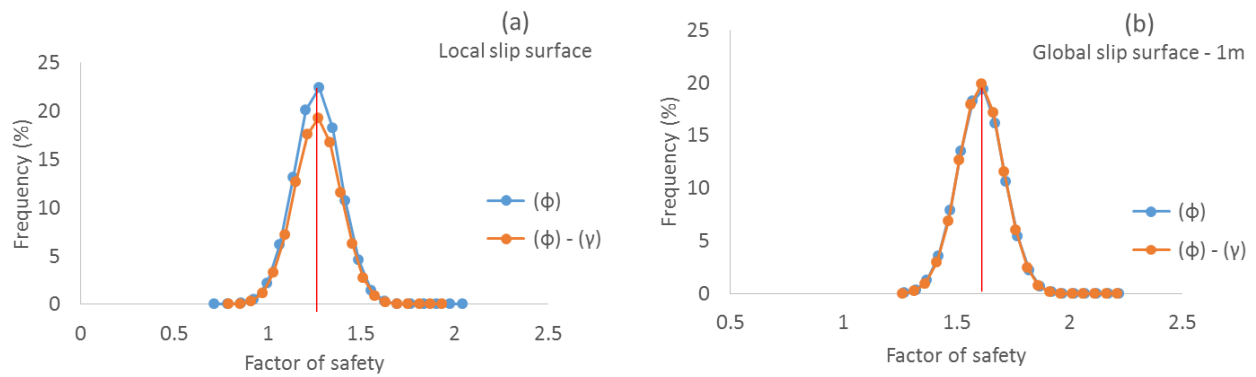
Figure C-2: Normal distribution of the factor of safety for COV% = 10 (ϕ', ϕ' and γ), Case S21 (see Tables 4-4 and 4-5), for sampling distance = 10 m; a) local slip surface; b) global slip surface.
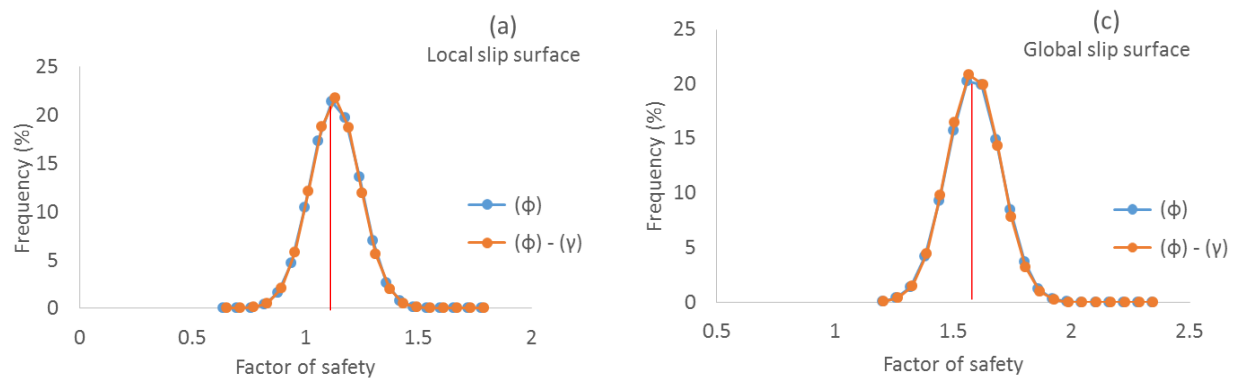

Figure C-3: Normal distribution of the factor of safety for COV% = 10 (ϕ', ϕ' and γ), Case S35 (see Tables 4-4 and 4-5), for sampling distance = 10 m; a) local slip surface; b) global slip surface.

C-2 Additional results related to section 6-4-2

The normal distribution of FS is evaluated for COV 15% on ϕ' with a uniform suction 6 kPa (representing c_{app} = 1 kPa) and different sampling distances (SD) (including random number each time (no spatial variation), 1, 3, 5, 8, 12 and 15 m, and sample per slice) for cases S11 and S21.
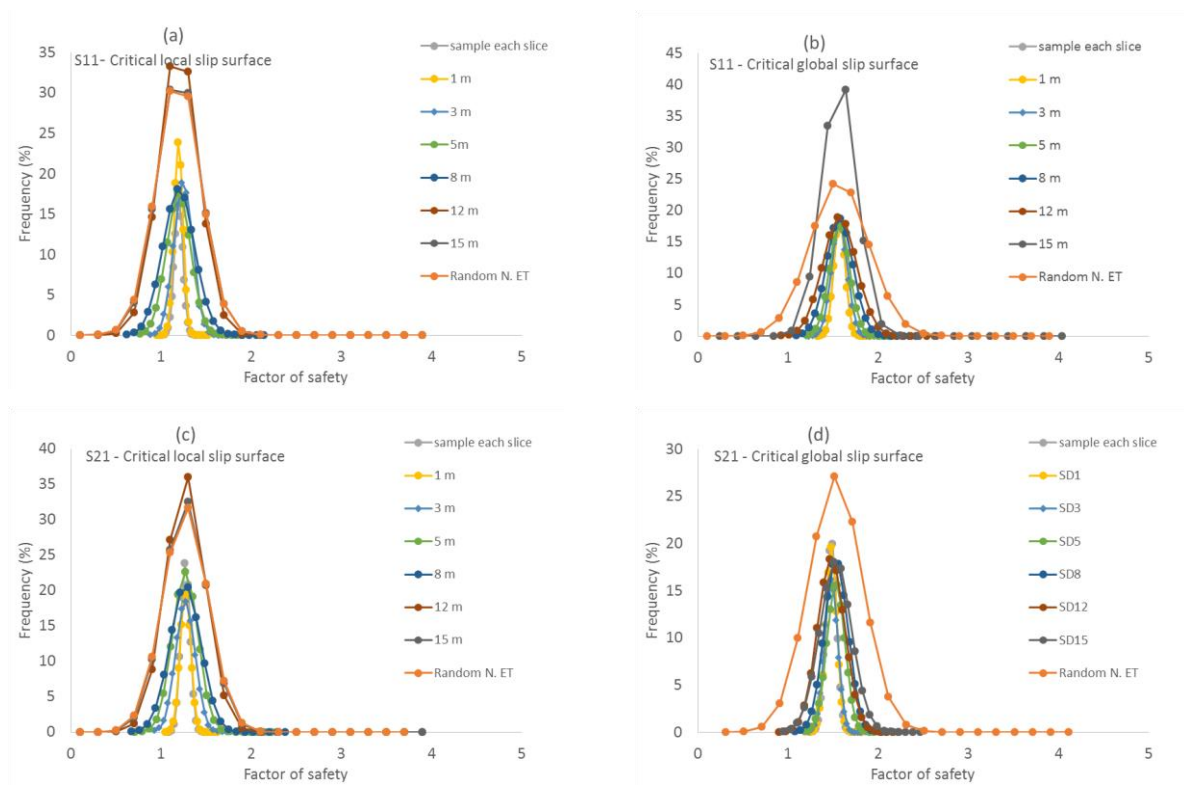

Figure C-4: Normal distribution of FS obtained with Monte-Carlo simulations (SLOPE/W), COV = 15% on ϕ', c_{app} = 1 kPa; sampling distances (SD): 1 m, 3 m, 5 m, 8 m, 12 m, 15 m, per slice and random number each time a) critical local slip surface, Case S11 (two bench pile); b) critical global slip surface, Case S11; c) critical local slip surface, Case S21 (two benches with compacted layers); d) critical global slip surface for Case S21.

Figure C-5 summarizes the outputs of the probabilistic analyses; $\overline{FS}$, RI and PoF, for Cases S11 and S21, for both local and global slip surfaces with COV 15%.
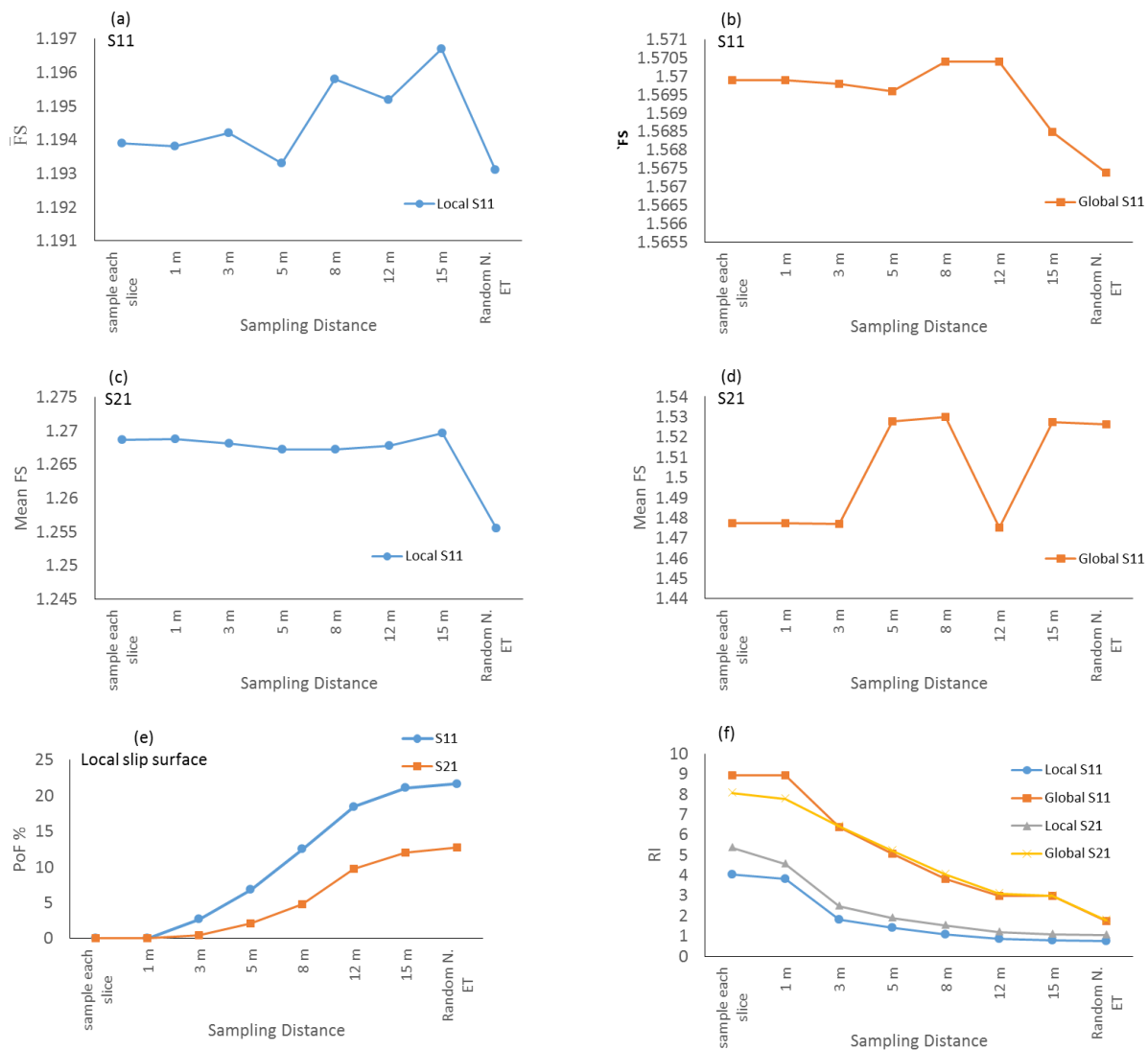

Figure C-5: $\overline{FS}$, RI and PoF distribution for different sampling distance (sampling once; 1, 3, 5, 8, 12 and 15m; sampling per slice), COV 15%, obtained with SLOPE/W; a) $\overline{FS}$ for local slip surface, Case S11; b) $\overline{FS}$ for global slip surface, Case S11; c) $\overline{FS}$ for local slip surface, Case S21; d) $\overline{FS}$ global slip surface Case S21; e) PoF for local slip surfaces, Cases S11 and S21; f) RI for local and global slip surfaces, Cases S11 and S21.

C-3 Additional results related to section 6-4-3

A sensitivity analysis is conducted for these two values (10% and 15%) to see their effect on the FS normal distribution obtained with the Monte-Carlo simulations with SLOPE/W. For cases S21, S22, S23 and S23 (see Tables 4-4 and 4-5).
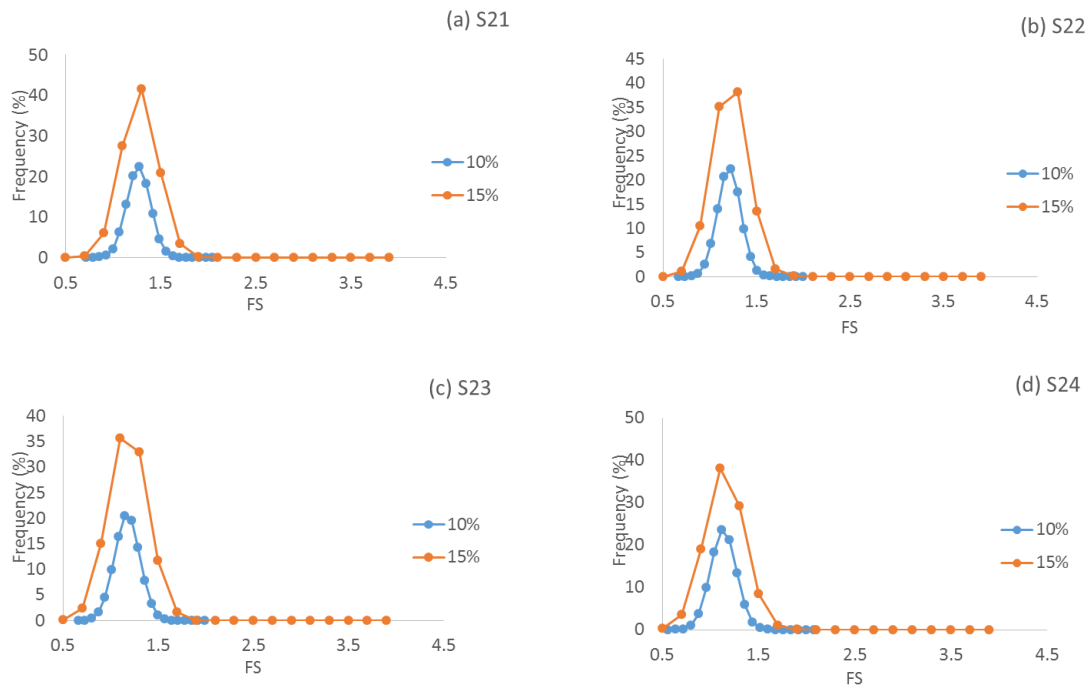

Figure C-6: Normal distribution of FS for local slip surface obtained with Monte-Carlo method of SLOPE/W for different COV (10%, 15%); a) Case S21; b) Case S22; c) Case S23; d) Case S24.

Figure C-7 presents the $\overline{FS}$ (a), RI (b), and PoF (c) and the standard deviation SD (d) related to a local slip surface, obtained from the Monte-Carlo method with SLOPE/W for Group 3 (Cases S21, S22, S23, S24, see Tables 4-4 and 4-5), for COV 10% and 15% (φ') and slip surface involving 60% H_t.
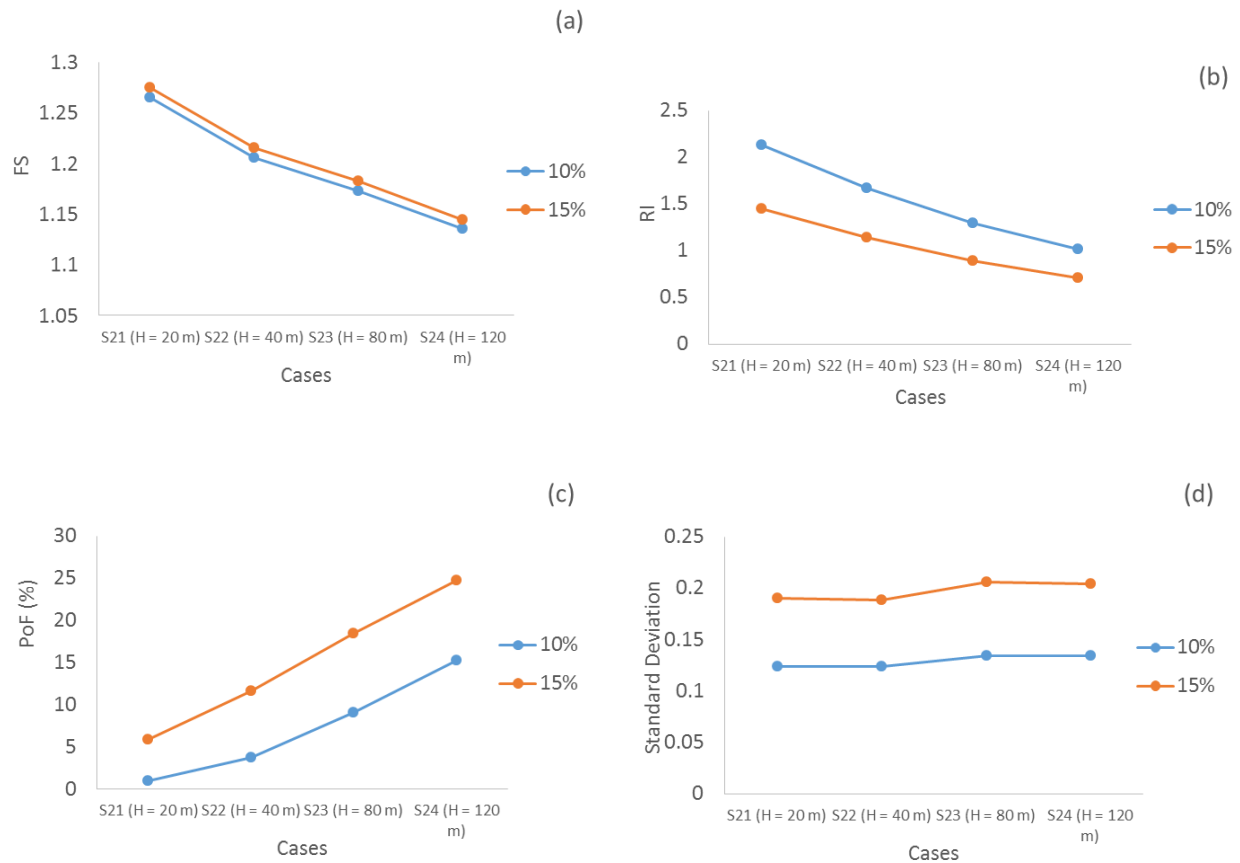

Figure C-7: Effect of COV% (10%, 15%) on $\overline{FS}$, RI, PoF and Standard deviation for a local slip surface obtained with Monte-Carlo method (SLOPE/W), Group 3 (Cases S21, S22, S23, and S24); a) $\overline{FS}$; b) RI; c) PoF (%); d) Standard deviation.
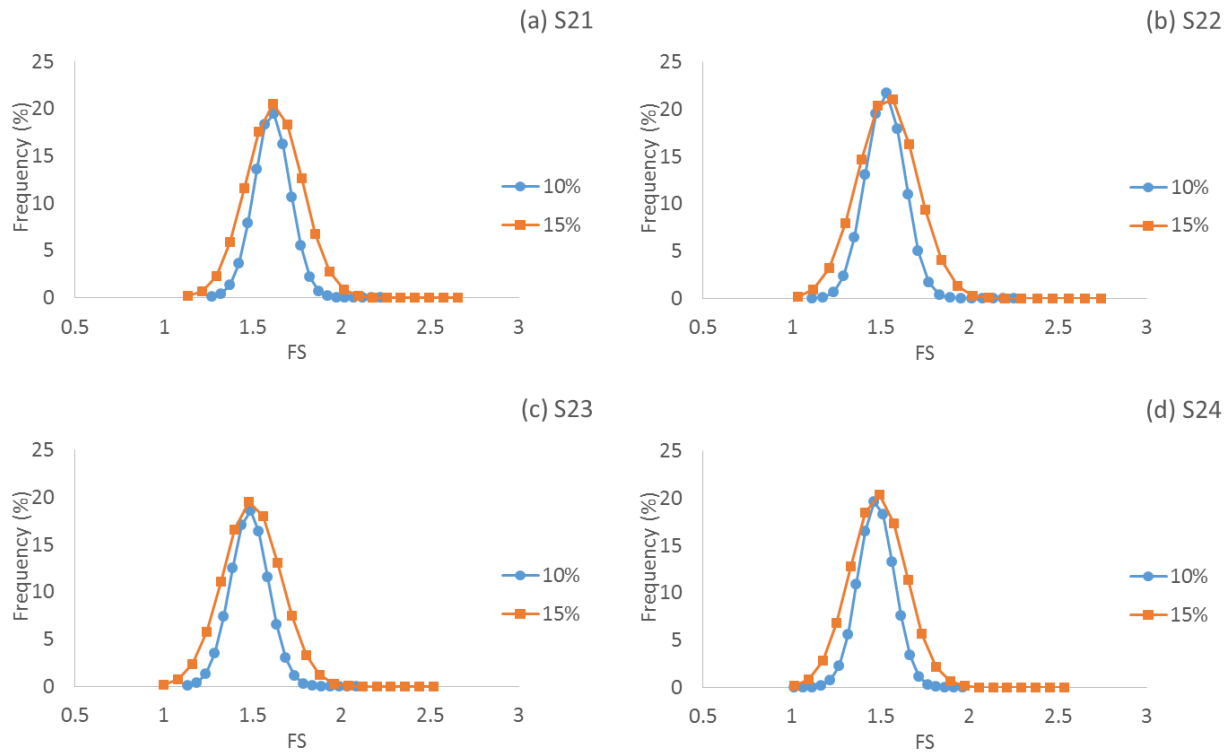
Figure C-8: Normal distribution of FS for global slip surface obtained with Monte-Carlo method of SLOPE/W for different COV (10%, 15%); a) Case S21; b) Case S22; c) Case S23; d) Case S24.
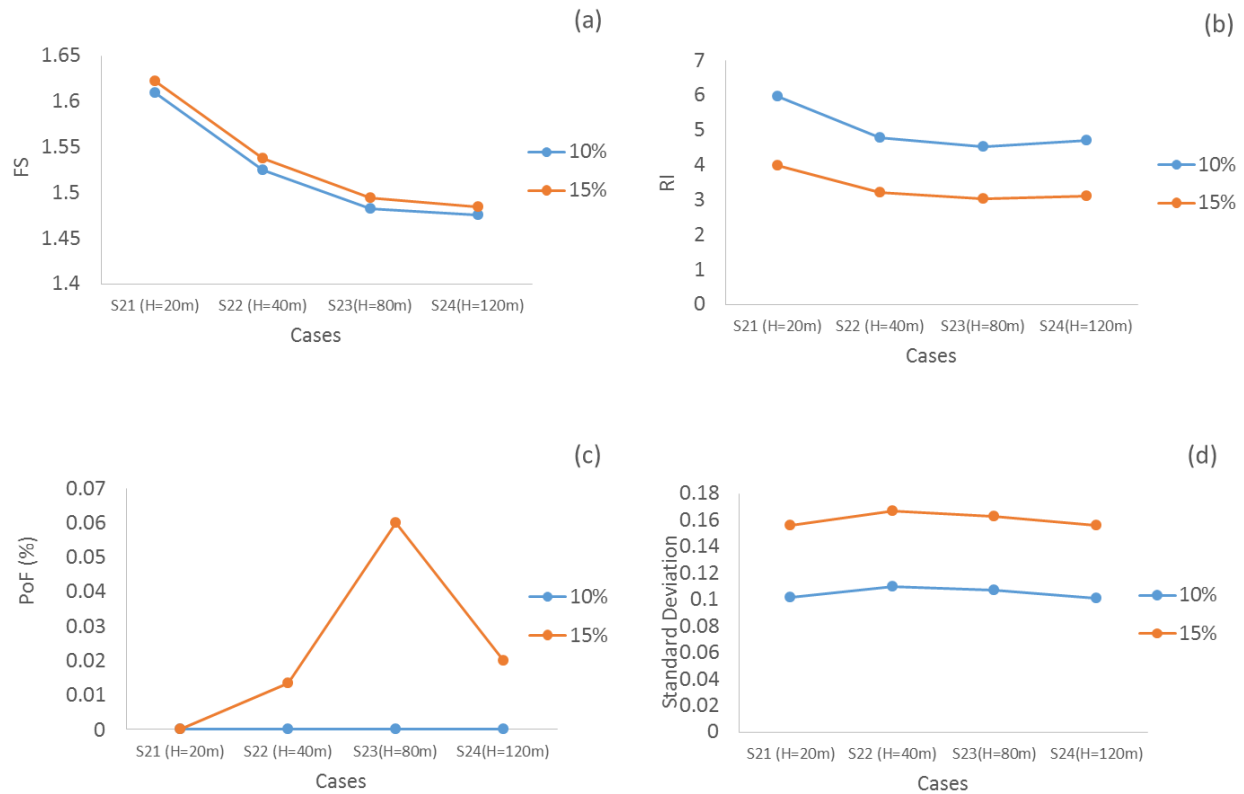
Figure C-9: Effect of COV% (10%, 15%) on $\overline{FS}$, RI, PoF and Standard deviation for a global slip surface obtained with Monte-Carlo method (SLOPE/W), Group 3 (Cases S21, S22, S23, and S24); a) $\overline{FS}$; b) RI; c) PoF (%); d) Standard deviation.

C-4 Additional results related to section 6-4-4

Effect of the number of iterations for Monte-Carlo method on the probabilistic stability analysis of waste rock pile has been shown in Figure C-10.
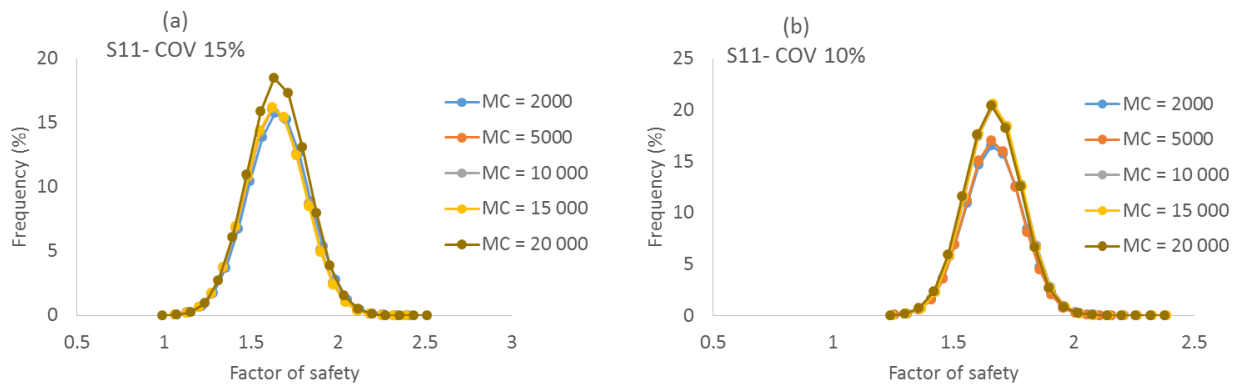

Figure C-10: Normal distribution of FS based on different iterations numbers, Case S11, slip surface involving 60% H_t; a) COV 15%; b) COV 10%.
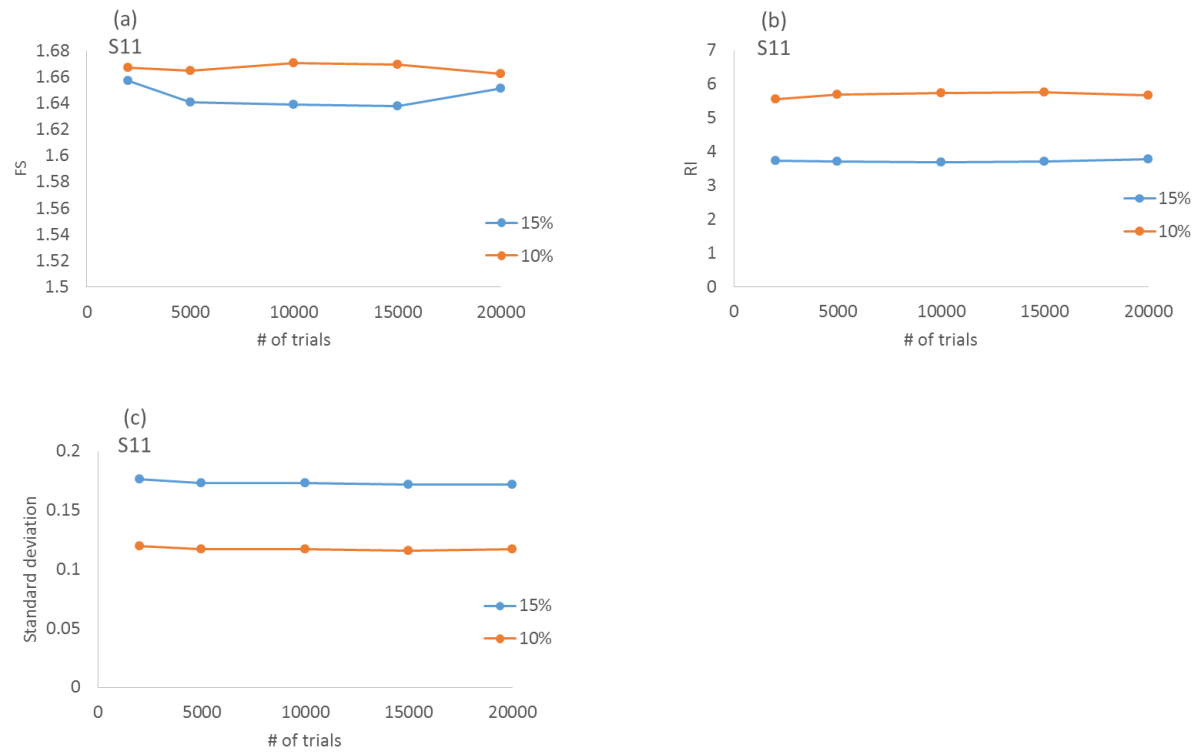
Figure C-11: Distribution of $\overline{FS}$, RI and standard deviation due to different iteration numbers, obtained with Monte-Carlo method (SLOPE/W), Case S11, slip surface involving 60%H_t, COV 10%, and 15%; a) $\overline{FS}$; b) RI; c) Standard deviation.